Zebrafish models of cystic kidney disease related ciliopathies

Roslyn Jane Simms

Thesis submitted in partial fulfilment of the requirements for the degree of Doctor of Philosophy

Newcastle University

Faculty of Medical Sciences

Institute of Genetic Medicine

March 2013

Abstract

Cystic kidney diseases are a fascinating cluster of discrete conditions and an important, common cause of established renal failure. Both isolated and syndromic inherited cystic kidney diseases are known to be linked by their pathogenesis involving ciliary dysfunction. Interestingly to date, all mutated genes which have been related to cystic kidney disease, encode proteins which are located on cilia, the basal body or centrosomes and are required for ciliary function. To date, over 50 causal genes have been identified and are capable of causing additional disease phenotypes, such as neurological disorders and blindness, often of variable severity. Understanding this clinical heterogeneity may considerably guide appropriate genetic counselling and screening of patients for relevant complications.

Zebrafish are a well-recognised animal model, their advantages of: transparency; conserved genome; representative kidney and rapid external development; make them useful for studying organogenesis in the context of disease. Furthermore the ability to perform combined gene knockdown in zebrafish, to study the effect of oliogenicity, which was proposed to influence clinical phenotypes in cystic kidney disease related ciliopathies, was of interest.

Using zebrafish models, this work studied the impact of four key genes, independently and in combination: *ahi1, cc2d2a, nphp6* and *mks3* on the development of cystic kidney disease and ciliopathy phenotypes, to resemble the human diseases nephronophthisis (NPHP), Joubert syndrome (JBTS) and Meckel Gruber syndrome, (MKS). A frequent finding in zebrafish morphants was a reduction in the number of cilia, which was usually associated with abnormal development of left-right body patterning and cystic kidney disease. Additionally, combined gene knockdown of: *nphp6* and *cc2d2a*; *ahi1* and *cc2d2a*; *ahi1* and *nphp6* was associated with a synergistic increase in disease phenotypes, suggesting an interaction between these genes.

In conclusion, zebrafish are a powerful developmental model to study and ideally improve understanding of cystic kidney disease related ciliopathies.

Dedication

For my fabulous sister and wonderfully supportive parents,

If it were easy, it would not be worth doing,

often the trick is the determination to try,

supported by encouragement, love and laughter

Thank you

Acknowledgements

Many people have supported me throughout this journey from beginning research in the laboratories of the IGM to finally completing my thesis. Thank you to my experienced supervisors, principally Dr John Sayer who introduced me to this interesting field, helped me in the transition from clinical to laboratory work and was a continuous source of enthusiasm, ideas and problem solving. Dr Bill Chaudhry helped develop experimental planning and practical skills, including using a hacksaw – which I did not predict during a career in science. Professor Nicholas Simmons was a source of wisdom and objective ideas. Thanks also to Dr Colin Miles and my internal assessors, Professor Timothy Goodship and Professor Hanns Lochmuller, for thoughtful advice.

I am very grateful to Dr Lorraine Eley who taught me many methods, her considerable experience with cilia and confocal microscopy proved invaluable during my search for a "needle in a haystack" – the evasive Kupffer's vesicle. Thanks also to: Ann Marie Hynes, for her cheerful personality, technical skills and willingness to help; Dr Holly Anderson for advice with making "potions" and listening ear amidst challenging times.

The IGM zebrafish group amalgamates various researchers, thanks to: Dr Nicholas Child, Dr Juliane Mueller, Dr Kevin Gillinder, David Burns, Alasdair Wood, Amy-Leigh Johnson for help and good humour during many long days/overnight experiments. I am also immensely grateful to: Lisa Hodgson for help with microscopy, Sue Vecsey and Rebecca McCready for essential aid with formatting my thesis.

From the renal research community, thank you to Dr David Kavanagh, Dr Shabbir Moochhala and Dr Georgina Carr, for their wise, supportive nature and witty informative discussions. Opportunities at meetings enabled exchange of ideas and a fruitful collaboration with Professor Colin Johnson working on *MKS3*. I would like to acknowledge my inspiration for this work, patients and families who are affected by cystic kidney disease related ciliopathies and generous funding awarded from the Mason Medical Research Group, Medical Research Council and Kidney Research UK.

Special thanks to wonderful friends, my gran and Dougall, my lovely fiancé for his understanding, patience and encouragement to persevere. Finally, thank you to my sister, parents, niece and nephew for their unremitting support and love which facilitates me to tackle the challenges of work, to be free to enjoy life with them.

Publications

Simms RJ, Eley L, Sayer JA. 2009. Nephronophthisis. *Eur J Hum Genet.*, 17, 406-16.

Simms RJ, Sayer JA. 2010. Juvenile nephronophthisis on MRI – A potential case of Joubert syndrome? *Pediatr Radiol.*,40, 1581.

Simms RJ, Hynes AM, Eley L, Sayer JA. 2011. Nephronophthisis: a genetically diverse ciliopathy. *Int J Nephrol.*, Epub 2011 May 15.

Simms RJ, Hynes AM, Eley L, Inglis Dm Chaudhry B, Dawe HR, Sayer JA. 2012. Modelling a ciliopathy: *Ahi1* knockdown in model systems reveals an essential role in brain, retinal and renal development. *Cell Mol life Sci.*, 69, 993-1009.

Adams A, Simms RJ, Abdelhamed Z, Dawe HR, Szymanska K, Logan CV, Wheway G, Pitt E, Gull K, Knowles MA, Blair E, Cross SH, Sayer JA, Johnson CA. 2012. A meckelin-filamin A interaction mediates ciliogenesis. *Hum Mol Genet*., 21, 1272-86.

Cheng YZ, Eley L, Hynes AM, Overman LM, Simms RJ, Barker A, Dawe HR, Lindsay S, Sayer JA. Investigating Embryonic Expression Patterns and Evolution of *AHI1* and *CEP290* Genes, Implicated in Joubert Syndrome. *PLoS One*, Epub 2012 Sep 24.

Table of Contents

List of Figures

List of Tables

Abbreviations

ADPKD	Autosomal Dominant Polycystic Kidney Disease
AHI1	Abelson Helper Integration site 1
ARPKD	Autosomal Recessive Polycystic Kidney Disease
ATG	Start Codon - Translation
ATP	Adenosine Triphosphate
BBS	Bardet-Biedl Syndrome
BMP	Bone Morphogenetic Protein
BSA	Bovine Serum Albumin
CAKUT	Congenital Abnormalities of the Kidney and Urinary Tract
CC2D2A	Coiled-coil and C2 domain containing 2A
CEP290	Centrosomal Protein 290
DAPI	4',6-diamidino-2-phenylindole
ddH_2O	double distilled water
DMSO	Dimethyl sulfoxide
DNA	Deoxyribonucleic acid
dpf	days post fertilisation
GFP	Green Fluorescent Protein
GWAS	Genome Wide Association Study
Hh	Hedgehog
HNF1β	Hepatocyte Nuclear Factor 1β
hpf	hours post fertilisation
JBTS	Joubert Syndrome
KV	Kupffer's Vesicle
MABT	Maleic acid buffer with Tween
MCKD	Medullary Cystic Kidney Disease
MKS	Meckel Gruber Syndrome
MO	Morpholino Oligonucleotide
MRI	Magnetic Resonance Imaging
MTS	Molar Tooth Sign
NPHP	Nephronophthisis
PBS	Phosphate Buffered Saline
PBT	Phosphate Buffered Saline with Tween
PCP	Planar Cell Polarity
PCR	Polymerase Chain Reaction
PFA	Paraformaldehyde
PKD	Polycystic Kidney Disease
RCAD	Renal Cysts and Diabetes Syndrome
RNA	Ribonucleic acid
RT-PCR	Reverse Transcriptase Polymerase Chain Reaction
SCC	Sodium Chloride/Sodium Citrate
SEM	Standard Error of the Mean

SH3	Src Homology 3 domain
Shh	Sonic Hedgehog
SLS	Senior-Loken Syndrome
TSC	Tuberous Sclerosis Complex
VHL	von Hippel-Lindau
WT	Wild Type

Chapter 1 Introduction

1.1 Cystic kidney disease – an important area to research

Cystic kidney diseases are an interesting group of distinct conditions characterised by multiple kidney cysts and a varied spectrum in terms of: aetiology; incidence; mode of presentation; association with other organ disease and comorbidities; impact on kidney function and overall prognosis. This variety is what makes cystic kidney disease such an interesting area to research, to try to unveil some of the many areas of uncertainty. Furthermore, cystic kidney disease is an important clinical challenge, in part because it has implications for a significant number of people within the UK, but also because under its umbrella are some 'rare diseases', which the UK government acknowledged a commitment to improving services and developing a strategy for managing patients with 'rare diseases' (Limb, 2011; Mollet et al., 2002). This drive for change followed a report in December 2010 which identified that the needs of patients with 'rare diseases' and their families were not able to be met by the national health service (NHS) (Limb, 2010).

The definition of a 'rare disease' was made by the European Union as one in which the prevalence is less than 1 in 2000 of the general population (Montserrat, 2009, June). Unfortunately, currently in the UK we do not know the exact number of people who are affected by various conditions, however within the field of kidney disease considerable efforts are being made to address this short fall. Collaborative efforts from the Renal Association and the British Association of Paediatric Nephrology have generated informative rare disease websites, www.rarerenal.org, which lists various 'rare diseases'. Some of these conditions already have working groups currently striving to develop web based rare disease registries (RADAR, www.renalradar.org), to enable collection of patient data which is hoped to lead to improved understanding, facilitate research and the delivery of better patient care.

The term 'rare disease' is slightly controversial and on the rare renal disease website, several cystic kidney diseases are listed (incidence/prevalence quoted where known), not all of which would classically be considered as 'rare diseases': autosomal recessive polycystic kidney disease (ARPKD, estimated worldwide prevalence of 1 in 20,000 (Zerres et al., 1998)); renal cysts and diabetes (RCAD, *HNF1β* mutations); medullary

cystic kidney disease (MCKD); nephronophthisis (NPHP, incidence 1 in 50-900,000 (Hildebrandt and Zhou, 2007)); autosomal dominant polycystic kidney disease (ADPKD, estimated worldwide prevalence 1 in 400-1000 (Torres and Harris, 2009)); tuberous sclerosis (incidence of 1 in 6000 (Curatolo et al., 2008)) and von Hippel-Lindau syndrome (incidence of 1 in 36,000 (Joerger et al., 2005)). This classification of a 'rare disease' does not detract from the significance of these disorders. The European Council has suggested that approximately 1 in 17 people will be affected by a 'rare disease' during their life, which equates to 3.5 million people within the UK (Limb, 2011) and acknowledgement by the former chief medical officer for England, Sir Liam Donaldson in 2009, that 'Rare is Common' (Limb, 2011).

Indeed, whether defined as a 'rare disease' or not, the relevance of researching these disorders which often manifest a significant demand on health and social economics, in part because of ineffective collaboration between various specialty services, must continue to be recognised. Within the cystic kidney diseases, certain aspects of the pathogenesis may be shared and collaboration within the research field should continue to be encouraged with the ultimate aim of improving services for patients in the UK.

1.2 Normal renal development

In order to begin to understand the abnormalities which may occur in cystic kidney disease, one must first comprehend normal kidney development. In humans (all vertebrates), kidney development is derived from the intermediate mesoderm with successive differentiation of the initial two pairs of transient kidneys, the pronephros and mesonephros into the final functioning and permanent kidney, the metanephros (Figure 1.1) (Gilbert, 2000; Jennette, 2007). This pattern of development is evolutionarily conserved, with humans, mammals and reptiles developing a metanephric kidney as the final functional kidney (Sukhatme, 2003). This is different in fish as even the initial kidney, the pronephros, is functional and is described in detail below.

In humans, on day 22 of embryological development, the pronephric duct begins to develop from the intermediate mesoderm in front of the somites (Gilbert, 2000). Cells of the pronephric duct move caudally and signal to adjacent nephrogenic mesenchyme to form tubules. Although most of the pronephros regresses, the distal pronephric duct becomes the Wolffian duct, which forms part of the excretory system (Gilbert, 2000). At the end of the fourth week, the non-functional pronephros regresses and

simultaneously, from adjacent mesenchyme, the mesonephric tubules begin to develop (Gilbert, 2000). During mesonephric kidney development, nephrons develop with glomeruli forming from capillaries in each mesonephric segment, which are connected to branches of the aorta (Jennette, 2007). Additionally, the mesonephros is important for development of the male genital tract (Gilbert, 2000). The transient mesonephros begins to degenerate during the sixth week of gestation (Jennette, 2007).

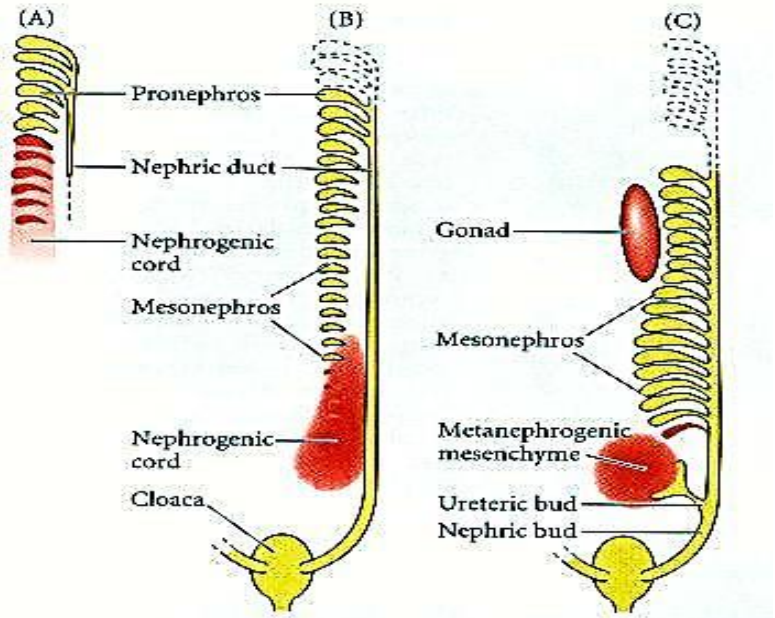

Figure 1.1 Development of the human kidney
The overlapping stages of kidney development begin on day 22 with (A) nephrogenic mesenchyme forming the pronephric duct which migrates caudally developing tubules, constituting the pronephros. (B) As the pronephros degenerates (dashed lines), the mesonephric tubules develop in a caudal direction. The mesonephros eventually regresses as (C) the metanephros, final mammalian kidney, develops from mesenchyme interacting with the ureteric bud, which branches from the nephric duct. Modified from (Gilbert, 2000).

Development of the final kidney, the metanephros, begins in the fifth week and involves interactions between epithelial cells in the ureteric bud (a derivative of the mesonephric duct) and metanephrogenic mesenchyme from the intermediate mesoderm (Gilbert, 2000; Winyard and Chitty, 2008). Coordinated signals between the ureteric bud and metanephrogenic mesenchyme mediates cell proliferation, apoptosis and differentiation leading to serial branching of the ureteric bud which ultimately becomes the collecting ducts and ureter (Winyard and Chitty, 2008). The metanephrogenic mesenchyme, surrounding the tips of the branching ureteric bud, converts to epithelium and forms an epithelial cluster which then differentiates into a nephron (Figure 1.2) (Gilbert, 2000).

Glomeruli begin to form at 8-9 weeks and new nephrons continue to develop until 32-36 weeks (Winyard and Chitty, 2008). The final number of nephrons, the functional units in each human kidney is thought to range between 0.6-1.3 million (Winyard and Chitty, 2008).

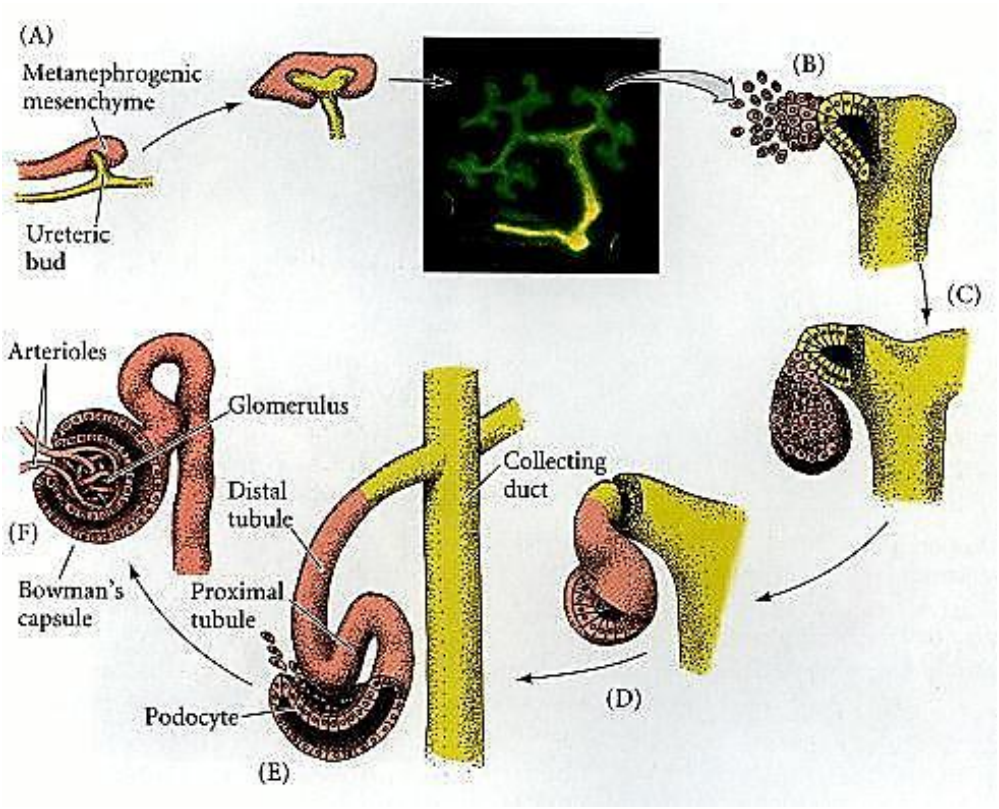

Figure 1.2 Reciprocal interaction between tissues during human kidney development
(A) The ureteric bud enters the metanephrogenic mesenchyme and reciprocal signals induce the ureteric bud to branch with aggregates of mesenchymal cells at the tips of the branches (B). (C) These clusters of mesenchymal cells convert into epithelium and digest the basement membrane of the ureteric bud to connect to the ureteric bud epithelium (D). The epithelialised mesenchyme becomes the nephron (renal tubules and Bowman's capsule, where blood is filtered), the ureteric bud becomes the urine collecting duct (E, F). Modified from (Gilbert, 2000).

1.3 Cystic kidney disease – a heterogeneous group of disorders

The aetiology of cystic kidney diseases includes: hereditary, novel mutations or inherited mutations leading to isolated polycystic kidney disease (PKD) or cystic kidney disease associated with other disorders; developmental aberrations; acquired cysts (Katabathina et al., 2010). Inherited cystic kidney disease is further discussed below (see section 1.4). Developmental abnormalities of the kidneys, 'dysplastic kidneys', may be detected in utero following antenatal ultrasound or at birth, tend to be grouped with other Congenital Abnormalities of the Kidney and Urinary Tract (CAKUT) and are defined as any abnormal development including renal agenesis to cystic kidneys (Winyard and Chitty, 2008). The incidence of a unilateral dysplastic kidney is 1 in 1000 (Winyard and Chitty, 2008) and of a unilateral multicystic dysplastic kidney is 1 in 4300 (Truong et al., 2003). Multicystic dysplastic kidneys are thought to develop because of obstruction of the urinary tract and failure of the ureteric bud to branch (Katabathina et al., 2010; Winyard and Chitty, 2008). If unilateral, a multicystic dysplastic kidney may be associated with vesicoureteral reflux in the contralateral kidney (Katabathina et al., 2010), typically they regress with time and are not functional (Katabathina et al., 2010). Acquired cystic kidney disease is defined as three or more simple cysts which develop in patients with established renal failure not caused by inherited cystic kidney disease (Katabathina et al., 2010). Kidney cysts are observed in 8-13% of people with chronic kidney disease (Katabathina et al., 2010) and this frequency increases in people with established renal failure with longevity of dialysis therapy to 50% following 6 years of dialysis and 100% following 10 years of dialysis (Truong et al., 2003). In this context, cysts are postulated to develop because of destruction of normal kidney parenchyma and compensatory hypertrophy of remaining tubular epithelial tissue (Grantham, 1991). Additionally, simple cysts can develop in the general population, are more common in men and the frequency increases with age, occurring in 11-30% of people over 50 years of age (Ravine et al., 1993). The complications associated with acquired kidney cysts are the same as other cystic kidney diseases and include: bleeding, infection and malignant transformation. In patients with established renal failure, renal tumours occur in 3-7% (Tickoo et al., 2006). Following acceptance of the Bosniak classification system (Israel and Bosniak, 2005) for renal cysts which can be applied to renal ultrasound, computed tomography (CT) or magnetic resonance imaging (MRI), screening criteria have been proposed for selected patient

groups (Floege et al., 2010), to facilitate differentiation between simple cysts and more complex, potentially malignant cysts.

This heterogeneity continues within the group of inherited cystic kidney diseases and is what makes researching cystic kidney disease such an interesting area.

1.4 Inherited cystic kidney disease

Inherited cystic kidney disease is the commonest genetic kidney disease worldwide. This statement is not meant to confuse and should be understood in the context that many of these inherited cystic kidney disease are acknowledged as 'rare diseases' (www.rarerenal.org). The pattern of inheritance can be utilised to categorise cystic kidney disease into autosomal dominant (AD) and autosomal recessive (AR), polycystic kidney disease (PKD).

1.4.1 Autosomal Dominant Polycystic Kidney Disease

Perhaps the most recognised condition, is autosomal dominant polycystic kidney disease (ADPKD), which as noted above has a worldwide prevalence of between 1:400 and 1:1000 (Torres and Harris, 2009). In the UK, ADPKD accounts for 9.6% of all adults requiring renal replacement therapy (dialysis or transplantation) (Byrne et al., 2010). Mutations in two causal genes, *PKD1* (Consort, 1994) on chromosome 16p13.3 and *PKD2* (Hayashi et al., 1997) on chromosome 4q22.1, account for all patients (85% and 15% respectively) with ADPKD. *PKD1* mutations are generally associated with a more severe form of cystic kidney disease and patients may present 20 years earlier than patients with *PKD2* mutations, because of more numerous cysts in the former (Torres, 2009). However in patients with *PKD1* mutations the extent of disease can be highly variable, even within families and does not appear to be associated with the type of mutation. The location of the mutation in the *PKD1* gene has occasionally been linked to the severity of kidney disease and the potential risk for developing cerebral aneurysms (Torres, 2009). In addition to intracranial aneurysms, other extra-renal manifestations of ADPKD are: polycystic liver disease, mitral valve disease (Pirson, 2010), pancreatic cysts, colonic diverticulae (Kumar et al., 2006). The successful identification of the causal genes in ADPKD has enabled researchers to target their studies on understanding mechanisms of the disease and focus on testing novel drug therapies aiming to reduce cell proliferation and fluid secretion (Chang and Ong, 2012).

1.4.2 Autosomal Recessive Polycystic Kidney Disease

ARPKD has an incidence of approximately 1 in 20,000 and is usually identified antenatally or during the neonatal period by enlarged echogenic kidneys (Harris and Torres, 2009). Perinatal mortality rates may be as high as 30%, associated with respiratory insufficiency (Harris and Torres, 2009). Approximately 30% of surviving children with ARPKD will develop kidney failure and require dialysis (Harris and Torres, 2009) or combined liver-kidney transplantation. The pathognomonic features of ARPKD related hepatobiliary disease include: biliary dysgenesis; congenital hepatic fibrosis and intrahepatic bile duct dilatation; cholangitis; portal hypertension and varices (Harris and Torres, 2009). Sometimes the diagnosis of ARPKD may be delayed until adolescence or even adulthood in individuals with hypertension and less severe kidney disease (Harris and Torres, 2009). ARPKD is caused by mutations in *PKHD1* on chromosome 6q21 (Zerres et al., 1994), which encodes the protein fibrocystin. As with other cystic kidney diseases, the presentation and extent of clinical phenotypes of ARPKD are highly variable. It is a rare disease and has been recognised by the RADAR project in the UK. Currently the ARPKD working group are developing a database to record UK patient data and holding family information days, guided and supported by international collaborators.

1.4.3 Other inherited cystic kidney diseases

NPHP (see section 1.5), Joubert Syndrome (JBTS, see section 1.6) and Meckel Gruber Syndrome (MKS, see section 1.7**)** are syndromic PKD and will be described in detail below. Renal cysts and diabetes (RCAD) although first described in 2001 (Kolatsi-Joannou et al., 2001), is probably an under diagnosed syndrome and requires clinical suspicion. The incidence of RCAD is currently uncertain and is caused by mutations in *HNF1β* on chromosome 17q21 (Kolatsi-Joannou et al., 2001), which encodes a widely distributed transcription factor, vital for normal development of the kidney, pancreas, liver and genital tract (Edghill et al., 2006). It is inherited in an autosomal dominant pattern, with new mutations occurring in up to 40% of cases (Heidet et al., 2010). Interestingly, patients with mutations in *HNF1β* do not necessarily have either renal cysts or diabetes, however they have a 50% lifetime risk of developing diabetes (Edghill et al., 2006) and renal disease is the most common phenotype. The renal phenotype is very heterogeneous and includes: glomerulocystic kidneys; multiple renal cysts;

horseshoe kidney and single kidney. Gout and hypomagnesaemia are also recognised features, the latter because HNF1β regulates FXYD2 which is involved in renal tubular handling of magnesium (Adalat et al., 2009).

Tuberous sclerosis complex (TSC) is an autosomal dominant syndrome caused by mutations in tumour suppressor genes which leads to the development of benign hamartomas in various organs including the kidneys, skin, brain, heart, lungs and eyes (Curatolo et al., 2008). Mutations in *TSC1* on chromosome 9q32 (van Slegtenhorst et al., 1997) and *TSC2* on chromosome 16p13 (European Chromosome 16 Tuberous Sclerosis, 1993) encode the proteins hamartin and tuberin respectively, which inhibit the mammalian target of rapamycin pathway to control cell proliferation (Curatolo et al., 2008). The incidence is 1 in 6000 and most patients are diagnosed in infancy (Curatolo et al., 2008). Although seizures, developmental delay and skin lesions are more frequent clinical features, renal involvement has been identified in 70-90% (Lagos and Gomez, 1967) of patients. The pathognomonic renal lesions are multiple angiomyolipomas (abnormal thick walled blood vessels with smooth muscle and adipose tissue), however diffuse cystic kidney disease is well recognised in up to 50% of patients and only rarely, in 2-3% of cases, do malignant renal tumours develop (Curatolo et al., 2008). The cystic kidney disease associated with TSC is usually asymptomatic unless there is an associated contiguous gene deletion of *TSC2* and *PKD1* (both adjacent on chromosome 16) which can lead to severe hypertension, massive cystic kidneys and early onset established renal failure (Curatolo et al., 2008).

Von Hippel-Lindau (VHL) is amongst the differential diagnoses for ADPKD. VHL is a rare, incidence of 1 in 36,000 (Joerger et al., 2005), autosomal dominant, multisystem malignant tumour predisposition syndrome caused by mutations in the tumour suppressor gene *VHL* on chromosome 3p25 (Latif et al., 1993). VHL is associated with haemangioblastomas (retinal, central neural system), renal cell carcinomas, phaeochromocytomas, pancreatic endocrine tumours and renal/pancreatic cysts (Kaelin, 2007). Renal cysts occur in up 60% of patients with VHL, tend to be a few, bilateral, are rarely associated with deteriorating renal function (Kaelin, 2007), however may be pre-malignant (Siroky et al., 2009).

Medullary cystic kidney disease (MCKD) is inherited in an autosomal dominant pattern and is histopathologically identical to NPHP, with normal sized or small kidneys with

corticomedullary cysts, tubular atrophy and interstitial fibrosis. It is caused by mutations in: *MCKD1* on chromosome 1q21 (Christodoulou et al., 1998; Stavrou et al., 2002) with slowly progressive kidney disease leading to established renal failure by 60 years; or *MCKD2* (*UMOD*) on chromosome 16p11.2 (Scolari et al., 1999) which is also associated with gout, hence the alternative name of familial juvenile hyperuricaemic nephropathy (Hart et al., 2002). *MCKD2* is associated with an earlier age of onset with renal impairment beginning from 15 years of age and the development of established renal failure within 10-20 years (Dahan et al., 2001).

Bardet-Biedl Syndrome (BBS) is an autosomal recessive multisystem disorder caused by mutations in up to seventeen genes (*BBS1-12*, *MKS1*, *NPHP6*, *FRITZ/C2ORF86*, *SDCCAG8*, *LZTFL1*) (Cardenas-Rodriguez et al., 2012) which account for approximately 80% of patients (Forsythe and Beales, 2012), thus it is likely that further genes may be discovered. The incidence of BBS is between 1:100-160,000 (Beales et al., 1999) and characteristic features include retinal dystrophy, learning difficulties, obesity, polydactyly, hypogonadism and renal anomalies which occur in up to 40% of patients (O'Dea et al., 1996). The renal manifestations include: the cystic kidney disease NPHP; dysplasia and focal segmental glomerulosclerosis. Similar to some of the above described cystic kidney related disorders, there is intrafamilial variability in the nature and severity of clinical phenotypes in BBS and this is considered to be related to additional genetic mutations (epistasis) which modify the subsequent phenotype (Cardenas-Rodriguez et al., 2012).

From the above descriptions of the inherited cystic kidney diseases (summarised in Table 1.1), a recurring theme within this group appears to be their clinical and genetic heterogeneity. To date, mutations in over 50 different genes (Table 1.2), some of which are allelic, have been identified in patients with cystic kidney disease. These cystic kidney disease related conditions are now referred to as ciliopathies (further discussed see section 1.14) (Hildebrandt et al., 2011), because the protein products encoded by the genes with identified mutations are located in the primary cilium/basal body complex. Although cystic kidney disease can occur in isolation, where the kidney phenotype dominates, often, as suggested above, the cystic kidney disease is part of a multisystem disorder. JBTS (see section 1.6) and MKS (see section 1.7) are cystic kidney disease related multisystem disorders which will be further described below. NPHP is a classic example of both an isolated and an overlapping syndromic cystic kidney disease.

Condition	Inheritance	Clinical features	References
Autosomal dominant polycystic kidney disease	Autosomal Dominant	Enlarged polycystic kidneys, liver cysts, pancreatic cysts, cerebral aneurysms, hypertension, hernias, mitral valve prolapse	(Torres and Harris, 2009)
Autosomal recessive polycystic kidney disease	Autosomal Recessive	Enlarged polycystic kidneys, biliary duct anomalies, hepatic fibrosis, cholangitis, pulmonary hypoplasia	(Sweeney and Avner, 2011)
Nephronophthisis	Autosomal Recessive	Normal sized kidneys with corticomedullary cysts ± retinitis pigmentosa, developmental delay, bronchiectasis, situs inversus	(Hildebrandt and Zhou, 2007)
Renal cysts and diabetes	Autosomal Dominant	Renal dysplasia: glomerulocystic kidneys, multiple renal cysts, horseshoe/single kidney, diabetes mellitus, gout, uterine anomalies	(Edghill et al., 2008)
Tuberous sclerosis	Autosomal Dominant	Seizures, developmental delay, autism, hamartomas, skin lesions, interstitial lung disease, renal angiomyolipomas/cysts	(Roach et al., 1998)
Von Hippel-Lindau	Autosomal Dominant	Haemangioblastomas (retina, cerebellum), phaeochromocytoma, renal cysts/carcinomas	(Kaelin, 2008)
Medullary cystic kidney disease	Autosomal Dominant	Normal sized kidneys with corticomedullary cysts, gout	(Hildebrandt and Otto, 2000)
Meckel Gruber Syndrome	Autosomal Recessive	Enlarged kidneys with renal cystic dysplasia, hepatic developmental anomalies/fibrosis, neurodevelopmental anomalies/occipital encephalocele	(Dawe et al., 2007)
Bardet-Biedl Syndrome	Autosomal Recessive	Retinal dystrophy, obesity, polydactyly, developmental delay, hypogonadism, renal cystic dysplasia	(Forsythe and Beales, 2012)

Table 1.1 Inheritance pattern and clinical features of genetic cystic kidney diseases

Gene Locus	Gene Symbol	Chromosome	Other Gene locus	References
Autosomal Dominant Polycystic Kidney Disease				
PKD1	***PKD1***	16p13.3	-	(Consort, 1994)
PKD2	***PKD2***	4q22.1	-	(Hayashi et al., 1997)
Autosomal Recessive Polycystic Kidney Disease				
FCYT	***PKHD1***	6p21.1-p12.2	-	(Zerres et al., 1994)
Medullary Cystic Kidney Disease				
MCKD1	***MCKD1***	1q21	-	(Christodoulou et al., 1998)
UMOD	***MCKD2***	16p12.3	-	(Scolari et al., 1999)
Nephronophthisis				
NPHP1	***NPHP1***	2q13	JBTS4	(Hildebrandt et al., 1997; Saunier et al., 1997)
NPHP2	***INVS***	9q31	-	(Otto et al., 2003)
NPHP3	***NPHP3***	3q22.1	MKS7	(Olbrich et al., 2003)
NPHP4	***NPHP4***	1p36.22	-	(Mollet et al., 2002)
NPHP5	***IQCB1***	3q21.1	-	(Otto et al., 2005)
NPHP6	***CEP290***	12q21.32	JBTS5, MKS4, BBS14	(Sayer et al., 2006)
NPHP7	***GLIS2***	16p13.3	-	(Attanasio et al., 2007)
NPHP8	***RPGRIP1L***	16q12.2	JBTS7, MKS5	(Wolf et al., 2007)
NPHP9	***NEK8***	17q11.1		(Otto et al., 2008)
NPHP10	***SDCCAG8***	1q44	BBS16	(Otto et al., 2010)
NPHP11	***TMEM67***	8q22.1	JBTS6, MKS3	(Otto et al., 2009)
NPHP12	***TTC21B***	2q24.3	JBTS11	(Davis et al., 2011)
NPHP13	***WDR19***	4p14		(Bredrup et al., 2011)

Gene Locus	Gene Symbol	Chromosome	Other Gene locus	References
	AHI1	6q23.3	JBTS3	(Utsch et al., 2006)
	ATXN10	22q13.31		(Sang et al., 2011)
NPHP14	***ZNF423***	16q12	JBTS?	(Chaki et al., 2012)
	CEP164	11q23.3	JBTS?	(Chaki et al., 2012)
Joubert Syndrome				
JBTS1	***INPP5E***	9q34.3	-	(Bielas et al., 2009)
JBTS2	***TMEM216***	11q13.1	MKS2	(Edvardson et al., 2010; Valente et al., 2010)
JBTS8	***ARL13B***	3q11.2	-	(Cantagrel et al., 2008)
JBTS9	***CC2D2A***	4p15.33	MKS6	(Gorden et al., 2008; Tallila et al., 2008)
JBTS10	***OFD1***	Xp22.2	-	(Coene et al., 2009)
JBTS12	***KIF7***	15q26.1	-	(Dafinger et al., 2011)
JBTS13	***TCTN1***	12q24.11	-	(Garcia-Gonzalo et al., 2011)
JBTS14	***TMEM237***	2q33.2	-	(Huang et al., 2011)
JBTS15	***CEP41***	7q32	-	(Lee et al., 2012a)
JBTS16	***TMEM138***	11q12.2	-	(Lee et al., 2012b)
JBTS17	***C5ORF42***	5p13.2	-	(Srour et al., 2012b)
	TCTN2	12q24.31	MKS8	(Sang et al., 2011)
	TMEM231	16q23.1	-	(Srour et al., 2012a)
Meckel Gruber Syndrome				
MKS1	***MKS1***	17q22	BBS13	(Kyttala et al., 2006)
MKS9	***B9D1***	17p11.2	-	(Hopp et al., 2011)

Gene Locus	Gene Symbol	Chromosome	Other Gene locus	References
Bardet-Biedl Syndrome				
BBS1	***BBS1***	11q13.2	-	(Mykytyn et al., 2002)
BBS2	***BBS2***	16q12.2	-	(Nishimura et al., 2001)
BBS3	***ARL6***	3q11.2	-	(Sheffield et al., 1994)
BBS4	***BBS4***	15q24.1	-	(Mykytyn et al., 2001)
BBS5	***BBS5***	2q31.1	-	(Li et al., 2004)
BBS6	***MKKS***	20p12.2	-	(Katsanis et al., 2000; Slavotinek et al., 2000)
BBS7	***BBS7***	4q27	-	(Badano et al., 2003)
BBS8	***TTC8***	14q31.3	-	(Ansley et al., 2003)
BBS9	***PTHB1***	7p14.3	-	(Nishimura et al., 2005)
BBS10	***BBS10***	12q21.2	-	(Stoetzel et al., 2006)
BBS11	***TRIM32***	9q33.1	-	(Chiang et al., 2006)
BBS12	***BBS12***	4q27	-	(Stoetzel et al., 2007)
BBS15	***C2ORF86***	2p15	-	(Kim et al., 2010)
BBS17	***LZTFL1***	3p21.3	-	(Marion et al., 2012)

Table 1.2 Genes mutated in Cystic Kidney Disease and related syndromes
ADPKD, autosomal dominant polycystic kidney disease; ARPKD autosomal recessive polycystic kidney; BBS, Bardet-Biedl syndrome; JBTS, Joubert syndrome; MCKD, medullary cystic kidney disease; MKKS, McKusick-Kaufman syndrome; MKS, Meckel-Gruber syndrome; NPHP, nephronophthisis; *OFD1* alias *CXORF5*.

1.5 Nephronophthisis

NPHP is an autosomal recessive cystic kidney disease and a leading genetic cause of established renal failure in children and young adults (Hildebrandt et al., 2009a). The incidence varies worldwide from 1 in 50,000 in Canada, to 1 in 61,000 in Finland to 1 in 900,000 in the USA (Hildebrandt and Zhou, 2007). Data from the UK paediatric Renal Registry reports that NPHP accounts for 6.5% of children with established renal failure (Lewis et al., 2007; Lewis et al., 2009), who require renal replacement therapy with transplantation or dialysis in order to sustain life.

NPHP was originally described in an individual patient in 1945 (Smith, 1945) as a medullary cystic kidney disease. In 1951, its description was further defined as a familial NPHP (Fanconi et al., 1951), with progressive chronic tubulointerstitial nephritis leading to established renal failure (Salomon et al., 2009). The term NPHP, describes part of its histology and literally means 'disappearance or disintregration of nephrons' (Wolf and Hildebrandt, 2011), this is because cysts develop by replacing normal tissue, suggesting that apoptosis is a more prominent feature than proliferation (Hildebrandt and Otto, 2005). The other key characteristic histological features of NPHP are: tubular atrophy with tubular basement membrane disruption; interstitial cell infiltrate and fibrosis (Waldherr et al., 1982; Zollinger et al., 1980).

Clinically, children with NPHP typically present with polyuria, nocturia or secondary enuresis (Ala-Mello et al., 1998), caused by an inability to concentrate urine (Krishnan et al., 2008). Children with NPHP may additionally have polydipsia and generalised lethargy, secondary to anaemia (Ala-Mello et al., 1996). NPHP is however clinically heterogeneous and extra-renal manifestations occur in 10-15% of patients (Hildebrandt and Zhou, 2007). The most typical NPHP associated feature is retinal degeneration, however other recognised conditions include: cerebellar vermis hypoplasia (JBTS); occipital encephalocele and hepatic fibrosis (MKS); situs inversus; bronchiectasis; skeletal defects; BBS (Hildebrandt et al., 2009a). When considering the array of possible presentations of a child with NPHP, one must be aware of the genetic heterogeneity; and both the inter and intrafamilial variability. Furthermore many of these causal genes of NPHP are pleiotropic, such as NPHP6, which could therefore lead to a presentation with a JBTS, MKS or even a BBS phenotype (Table 1.1, Table 1.2) (Coppieters et al., 2010).

Since NPHP is a monogenic, recessive condition (Hildebrandt, 2010), by definition affected individuals will have two homozygous or compound heterozygous mutations in a single gene (Wolf and Hildebrandt, 2011). However oligogenicity (see 1.15) has been reported for a number of genes in patients with NPHP (Hoefele et al., 2007). The effect of potential modifier genes are considered to be a factor influencing intrafamilial variation and the severity of disease phenotype (Benzing and Schermer, 2012; Davis et al., 2011; Hoefele et al., 2007).

The list of genes which can cause NPHP continues to grow all the time. Since identification of the first NPHP gene by positional cloning in 1997 (Hildebrandt et al., 1997; Saunier et al., 1997), new genes are regularly being discovered utilising specialised gene hunting techniques combining homozygosity mapping and whole-exome resequencing (Chaki et al., 2012; Otto et al., 2010). The advantages of these techniques are they overcome the difficulty when a small number of affected individuals cluster in a single family and enable detection of candidate genes (Hildebrandt et al., 2009b). Inspite of these considerable achievements, the genetic cause remains undetermined in many patients, as acknowledged following a recent mutation analysis of known NPHP related genes, using DNA pooling and next generation sequencing, failed to identify a mutation in 90 patients, 75% of a cohort with a NPHP related condition (Otto et al., 2011).

Currently, mutations in 17 different genes (Table 1.2) have been identified and together explain the diagnosis in up to 50% of patients with NPHP (Chaki et al., 2012). *NPHP1* was the first gene to be discovered (Hildebrandt et al., 1997; Saunier et al., 1997) and remains the most frequently identified cause of NPHP, accounting for 20-25% of patients (Hildebrandt et al., 2009a). Although the other causal genes have only been identified in small numbers of patients with NPHP, a few key discoveries unveiled a link between these genes, which has facilitated the identification of further candidate NPHP genes. In 2003, mutations in *NPHP2* (*Inversin*) were identified in patients with a younger age of onset, an 'infantile' variant of NPHP, with enlarged cystic kidneys (Otto et al., 2003). The protein products of *NPHP1* and *NPHP2* were found to interact and form a complex with β-tubulin, a key scaffolding protein of primary cilia (Otto et al., 2003). Furthermore at this time, mutations in *NPHP3* (Olbrich et al., 2003) and *NPHP4* (Mollet et al., 2002; Otto et al., 2002), the latter associated with a retinal phenotype, were identified in patients. NPHP1-4 were all found to interact and colocalise on

primary cilia (Mollet et al., 2002; Mollet et al., 2005; Olbrich et al., 2003; Otto et al., 2003). A correlation between the pathogenesis of NPHP and the function of primary cilia was considered (Hildebrandt and Otto, 2005).

Evaluation of the literature of the related cystic kidney disease, PKD, identified that in the *orpk* mouse model of ARPKD, mutations in *Tg737* (encodes the protein polaris, required for intraflagellar transport, cilia assembly and maintenance), resulted in shortened primary cilia in renal epithelial cells (Moyer et al., 1994). This result linking primary cilia to the pathogenesis of ARPKD was confirmed using *IFT*-88, the *Chlamydomonas* orthologue of *Tg737* (Pazour et al., 2000). The association between cilia and ADPKD was identified following work in Caenorhabditis elegans showed that PKD1 and PKD2 homologs, lov-1 and pkd2, are expressed in cilia and work together in the same pathway (Barr et al., 2001). Theories regarding the role of primary cilia in the pathophysiology of ADPKD and consequences of aberrations in their structure or function, were suggested following localisation of the polycystins, the protein products of *PKD1* and *PKD2* to primary cilia of renal epithelial cells (Yoder et al., 2002). The polycystin complex (polycystin 1 is a G protein-coupled receptor whilst polycystin 2 is a cation channel) interact on cilia in kidney tubules to behave as a urinary flow sensor, to mediate calcium influx via the polycystin 2 channel (Gunay-Aygun, 2009; Harris, 2009; Nauli et al., 2003; Zhou, 2009). This localisation of the polycystins on cilia appears to be fundamental for their ability to regulate calcium signalling in response to urinary flow (Gascue et al., 2011).

Furthermore, in 2003, the possibility that abnormalities of primary cilia could lead to protein dysfunction and subsequent disease, even multisystem disease with a significant cystic kidney disease phenotype, was postulated for BBS (Ansley et al., 2003). In 2005, recognition of this data, the fact that the protein products of the genes identified to be mutated in ADPKD and NPHP: *PKD1*, *PKD2*, *NPHP1-5* were all located in the primary cilium/basal body, led to a new hypothesis in humans and animal models (mice, zebrafish): that cystic kidney diseases are ciliopathies (see sections 1.14, 1.16) (Hildebrandt and Otto, 2005). This proposal has helped to guide the direction of subsequent research in the field of NPHP and related conditions, facilitating the identification of cilia related candidate genes and study of primary cilia structure and function.

1.6 Joubert Syndrome

JBTS related disorders are congenital ataxias which were first described in 1968 in 4 siblings in a consanguineous family with hypotonia/ataxia, developmental delay, oculomotor apraxia and an abnormal respiratory pattern (Joubert et al., 1968). The worldwide incidence of JBTS is uncertain, however it is estimated to be between 1:80,000-1:100,000 live births across Europe and America (Kroes et al., 2008; Parisi et al., 2007). Whilst the mode of inheritance in the majority of patients with JBTS is autosomal recessive (Parisi et al., 2007), mutations in *OFD1* have been identified in a few patients, providing an alternative X-linked recessive pattern of inheritance (Coene et al., 2009).

To date, mutations in 19 different genes have been reported in patients with JBTS (Table 1.2). Several of these genes are pleiotropic and can therefore cause isolated NPHP, JBTS and MKS. Mutations in *AHI1* are the leading cause of JBTS and have been identified in 7-11% of patients (Parisi et al., 2006; Valente et al., 2006a), 80% of which have an associated retinal phenotype (Valente et al., 2008). The other frequently reported genetic causes of JBTS are: *CC2D2A* in up to 9% of patients who may develop associated retinal or renal phenotypes (Gorden et al., 2008); *NPHP6* mutations in 7-10% of patients who tend to develop additional oculo-renal features (Sayer et al., 2006; Valente et al., 2008) and *MKS3* in 8% of patients who may develop ocular colobomas (Baala et al., 2007b; Doherty et al., 2010). These four genes are being concentrated on in the work presented herein.

Although genetic heterogeneity is well recognised in JBTS and related disorders, the tendency to develop certain phenotypes or at least clearly associate the predictive nature of mutations in certain genes with development of particular phenotypes has been proposed (Figure 1.3). The purpose of these acknowledgements back in 2008, were to develop a recommended algorithim for the order of genetic testing patients for mutations. This concept is important when performing genetic counselling, particularly in families with known mutations, to help provide prognostic information and direct appropriate screening and ongoing medical management.

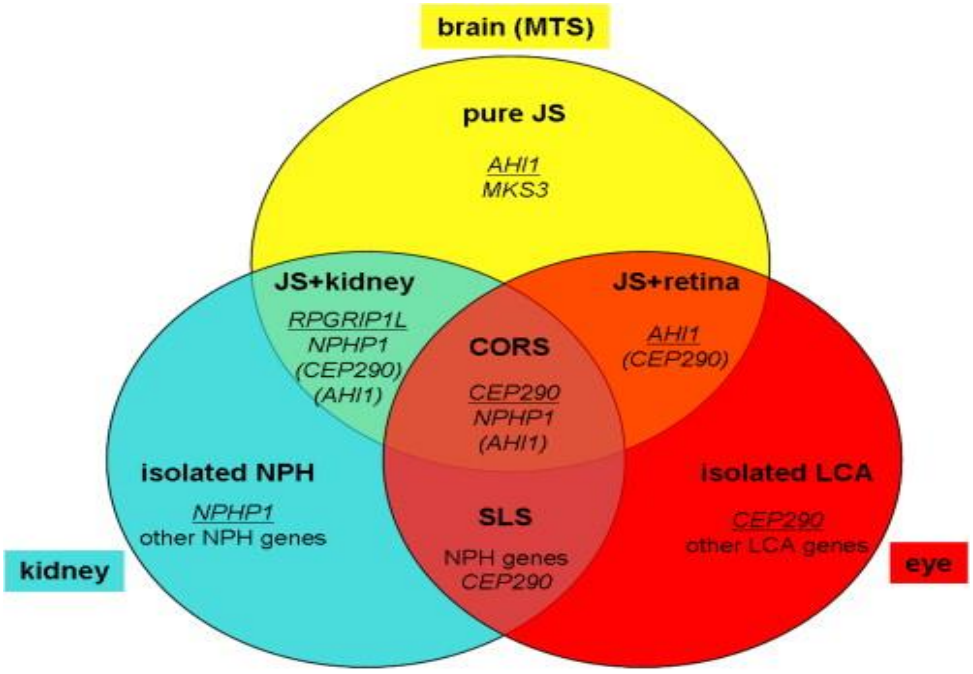

Figure 1.3 Genotype-Phenotype correlations in Joubert Syndrome
This Venn diagram demonstrates both individual and overlapping genotype-phenotype associations identified in mutation screens. Individual phenotypes are represented as: pure JBTS (JS in this figure) (yellow), isolated NPHP (blue) and isolated LCA (red) colours. The overlapping circles represent the syndromic/multiorgan phenotypes associated with certain genes, emphasising their pleiotropy. The relevant genes are listed in each segment, underlined is the main causal gene and bracketed, are rarer causes. CORS, cerebello-oculo-renal syndrome; JBTS, Joubert syndrome; LCA, Leber's congenital amaurosis, retinal dystrophy; NPHP, nephronophthisis; SLS, Senior Loken syndrome, oculo-renal disease. From (Valente et al., 2008).

The pathognomonic radiological feature of JBTS (Parisi et al., 2007; Valente et al., 2008) is a midbrain-hindbrain malformation, which because of its appearance on cerebral MRI, is called ‘molar tooth sign’ (MTS, Figure 1.4) and was described in 1997 (Maria et al., 1997). MTS is characterised by cerebellar vermis hypoplasia, a deep interpeduncular fossa and elongated, thin superior cerebellar peduncles (Parisi, 2009).

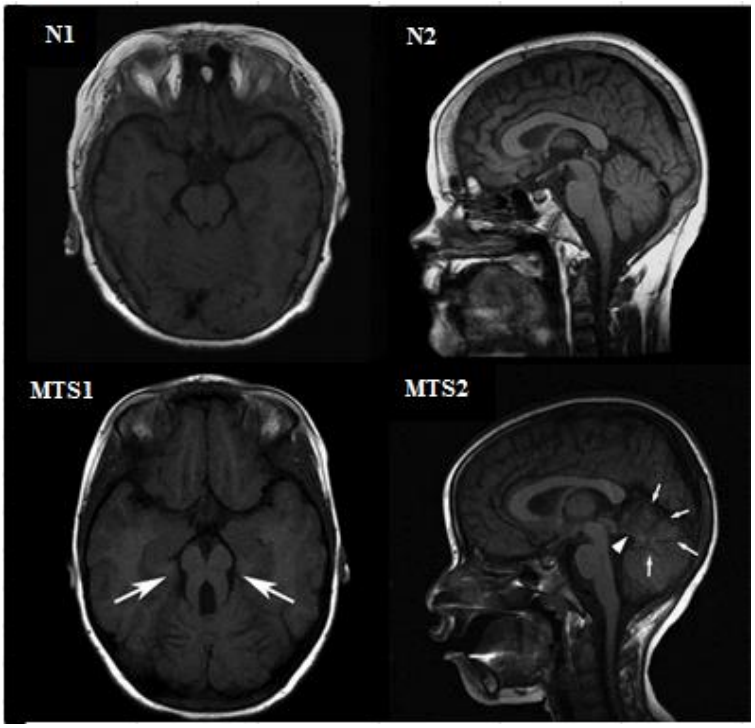

Figure 1.4 Cerebral MRI of a normal cerebellar vermis and Molar Tooth Sign
Magnetic resonance imaging (MRI) of the human brain showing axial (1) and mid-sagittal (2) sections. The molar tooth sign (MTS) is identified in a patient with Joubert Syndrome (MTS1, a deep interpeduncular fossa between white arrows) with an abnormally raised fourth ventricle (white arrowhead, MTS2) and cerebellar vermis hypoplasia (white arrows surround, MTS2). Normal (N1, N2) cerebral images are shown for comparison. Adapted from (Parisi, 2009).

The cardinal clinical features of JBTS are neurological as described above, however multiorgan involvement is recognised, with conditions including: retinal dystrophy, NPHP, hepatic fibrosis and skeletal anomalies (Valente et al., 2008). The variable clinical spectrum of JBTS is still being classified and in part is thought to relate to the heterogeneity of the identified mutated genes. The most recent attempt to create a system to classify JBTS has generated six subgroups based on the principle organ affected and correlating the genotype with phenotype (Table 1.3) (Brancati et al., 2010). The predominant renal condition associated with JBTS is NPHP and occurs in up to 25% of patients (Brancati et al., 2010).

Subgroup	Clinical features	Unaffected organs	Associated genes
Pure JBTS	MTS, cardinal neuro. (hypotonia/ataxia, dev. delay), ± irregular respiration, abnormal eye movements, impaired intellect	kidneys, liver	*CC2D2A*, *TMEM216*, *INPP5E*, *ARL13B*, *OFD1*, *AHI1*, *MKS3*
JBTS-O	Neuro., retinal dystrophy	-	*AHI1*
JBTS-R	Neuro., NPHP	eyes	*NPHP1*, *RPGRIP1L*
JBTS-OR	Neuro., retinal dystrophy, NPHP	-	*NPHP6*
JBTS-H	Neuro., CHF ± colobomas, NPHP	-	*TMEM67*
JBTS-OFD	Neuro., bifid tongue, oral frenulae, polydactyly ± pituitary aplasia	-	*TMEM216*

Table 1.3 Classification of Joubert Syndrome related disorders
CHF, congenital hepatic fibrosis; dev., developmental; JBTS, Joubert syndrome; JBTS-H, JBTS with hepatic defect; JBTS-O, JBTS with ocular defect; JBTS-OFD, JBTS with oro-facio-digital defects; JBTS-OR, JBTS with oculorenal defects; JBTS-R, JBTS with renal defect; MTS, molar tooth sign; neuro., neurological; NPHP, nephronophthisis. From (Brancati et al., 2010).

1.7 Meckel Gruber Syndrome

MKS is an autosomal recessive, embryonically lethal developmental disorder which is considered to be at the severe end of a spectrum of related conditions progressing from isolated retinal dystrophy, to NPHP, to JBTS to MKS (Brancati et al., 2010). The clinical features which define MKS are a triad of large multicystic kidneys, biliary dysgenesis/hepatic fibrosis and neurodevelopmental anomalies, with occipital encephalocele being the most frequent (Logan et al., 2011). Additional clinical features are now recognised, explained by genetic pleiotropy and may include: polydactyly, skeletal dysplasia, cardiac laterality defects and microphthalmia (Salonen and Norio, 1984). MKS is described as a rare condition with previously estimated incidences ranging from 1:9000 in Finland (Salonen and Norio, 1984), 1:13,250 in the USA (Holmes et al., 1976) to 1:140,000 in the UK (Seller, 1978), however more recent (1996-2005) estimates of the incidence in the UK city of Bradford were significantly more at 1:3000 (Logan et al., 2011).

Currently, mutations in nine genes have been identified (Table 1.2) in patients with MKS. These genes account for approximately 75-80% of patients with MKS (Logan et al., 2011). *NPHP6* and *CC2D2A* both account for 20% of patients with MKS, whilst *MKS3* is the third most frequent genetic cause of MKS (Logan et al., 2011). Several of these genes are pleiotropic as can be seen from Table 1.2, however a genotype-phenotype correlation has only been identified for *MKS3* (Otto et al., 2009) and *CC2D2A* (Mougou-Zerelli et al., 2009): missense mutations tend to cause NPHP or JBTS, whilst truncating mutations lead to MKS (Mougou-Zerelli et al., 2009; Otto et al., 2009). Understanding the clinical heterogeneity associated with other genetic causes of MKS remains to be resolved. As identified for JBTS above, the association between certain primary causal genes and modifying genes for NPHP, JBTS, MKS and BBS are shown in Table 1.4.

	Phenotypes			
Gene	**NPHP**	**JBTS**	**BBS**	**MKS**
AHI1	M	Y	-	-
NPHP6	Y, M	Y	Y	Y
CC2D2A	-	Y	-	Y
MKS3	Y	Y	M	Y

Table 1.4 Association between genes and phenotypic spectrum
Gene mutation can either be primary cause of phenotype (Y, yes) or modify (M) leading to the disease phenotype. Phenotypes are listed in increasing order of severity including: NPHP, nephronophthisis; JBTS, Joubert syndrome; BBS, Bardet-Biedl syndrome; MKS, Meckel-Gruber syndrome. Modified from (Davis and Katsanis, 2012).

1.8 Cilia

Cilia were first observed as 'little legs' on protozoa in 1675 (Dobell, 1932), however the term 'cilia', which translates from Latin as 'eyelashes' (Beales, 2012; Müller and Fabricius, 1786), was not thought to be used until 1786. In 1898, realisation that in addition to the previously identified 'motile' cilia, there were another type of cilia was acknowledged, when the latter were reported as a single 'antennae like', sensing structure projecting from the surface of kidney cells (Zimmerman, 1898). The term 'primary cilium' was used to describe these sensory cellular appendages in 1968, because they were noted to develop prior to multiciliated cilia (Sorokin, 1968). Primary cilia are ancient, highly conserved hair-like organelles, with a diameter of approximately 0.25μm (Rodat-Despoix and Delmas, 2009), which extend from the apical surface of most polarised, non-proliferating cells (Satir et al., 2010), the exceptions being myeloid cells, lymphoid cells and intercalated cells of the collecting duct (Latta et al., 1961; Wheatley, 1995). The length of primary cilia varies according to the phenotype and function of the cell it populates, *in vivo* in mammals, it has been reported to extend between 2-5μm long (Pazour and Witman, 2003; Rodat-Despoix and Delmas, 2009).

1.9 Structure of cilia

Cilia develop when the cell cycle becomes arrested and the basal body (BB)/centrosome moves to the apical cell membrane (Pedersen and Rosenbaum, 2008). Here the BB functions as a microtubule organising centre (MTOC) to coordinate access to the cilium and enable the development of the microtubule based 'axoneme' core (Berbari et al., 2009; Davenport and Yoder, 2005; Marshall, 2008) by a process of intraflagellar transport (Pedersen and Rosenbaum, 2008). In all cilia, the central axoneme is composed of nine microtubule doublets, however the presence or absence of an additional central pair of microtubule singlets has been the basis of a classification system for cilia (Berbari et al., 2009; Davenport and Yoder, 2005). Typically, 'motile' '9+2' cilia have an extra central pair of microtubule singlets, which use dynein arms to generate force (Davenport and Yoder, 2005), whereas 'primary' usually 'immotile' '9+0' cilia lack the central pair (Figure 1.5) (Berbari et al., 2009).

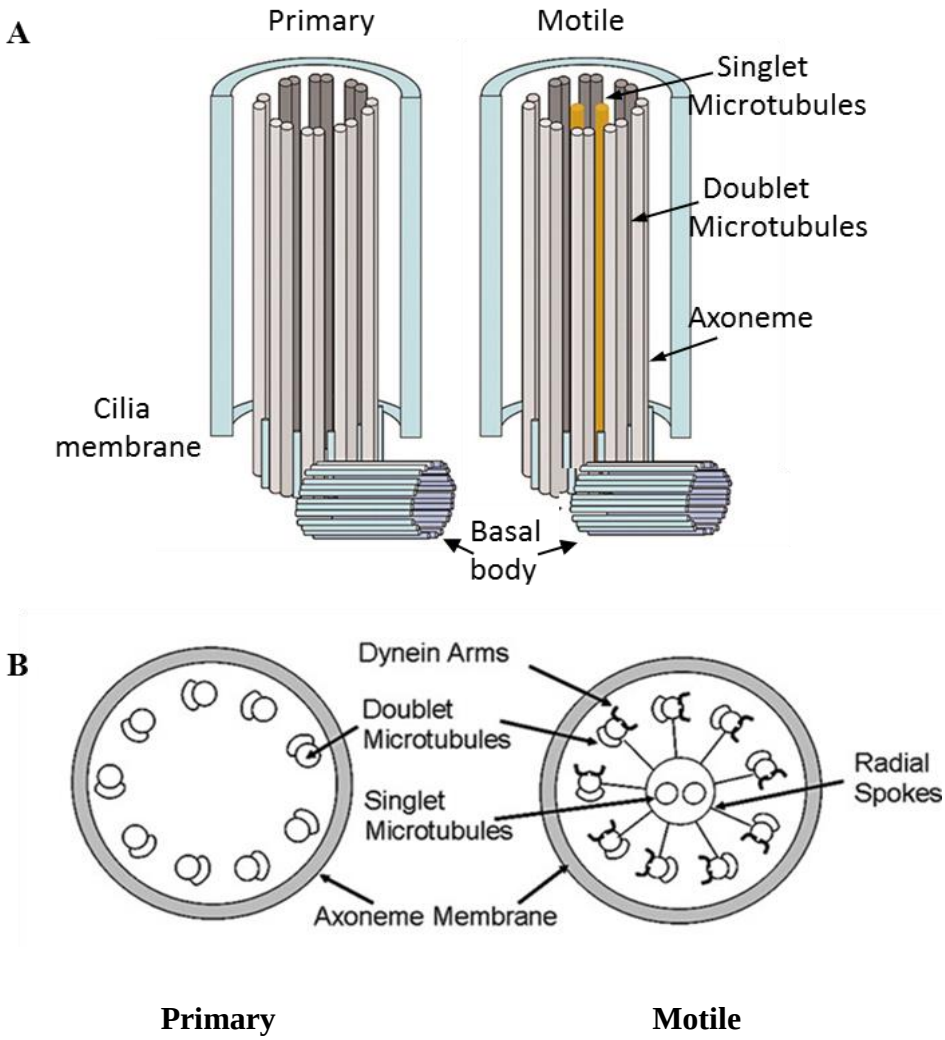

Figure 1.5 Structure of cilia
(**A**) Primary cilia contain nine peripheral microtubule doublets which form the axoneme extending from the basal body, which anchors the cilium and lies perpendicular to the cell membrane. Motile cilia additionally contain a central pair of singlet microtubules. (**B**) Cross section through axoneme of primary '9+0' and motile '9+2' cilia, demonstrating dynein arms and radial spokes in the motile cilia. Adapted from (Davenport and Yoder, 2005).

Although the ultrastructure of cilia as determined by electron microscopy (Figure 1.6) has historically been used to differentiate function, these distinctions are considered inaccurate and too simplistic (Badano et al., 2006b), as there are exceptions, notably at the embryonic node (Berbari et al., 2009): motile primary '9+0' cilia (McGrath et al., 2003); both motile and immotile primary cilia (McGrath et al., 2003); motile '9+2' cilia (Kramer-Zucker et al., 2005; Sarmah et al., 2007) have been identified. Indeed, motile cilia are considered to additionally have a sensory capacity (Bloodgood, 2010). Additionally, uncharacteristically, motile cilia have been detected in renal tubular cells in patients with kidney disease (Ong and Wagner, 2005), although only '9+0' cilia are described (Webber and Lee, 1975). As shown in Figure 1.6A, dynein arms are present in some primary '9+0' cilia and were confirmed to be capable of movement (Kramer-Zucker et al., 2005).

Motility in cilia is mediated by the additional structural components present in '9+2' cilia (see Figure 1.5B): the central microtubules are connected by radial spokes to the outer microtubule doublets which have dynein arms attached and are able to generate movement by ATP dependent reactions (Ibanez-Tallon et al., 2003). The dynein arms are described as the molecular motors of motile cilia (Ibanez-Tallon et al., 2003).

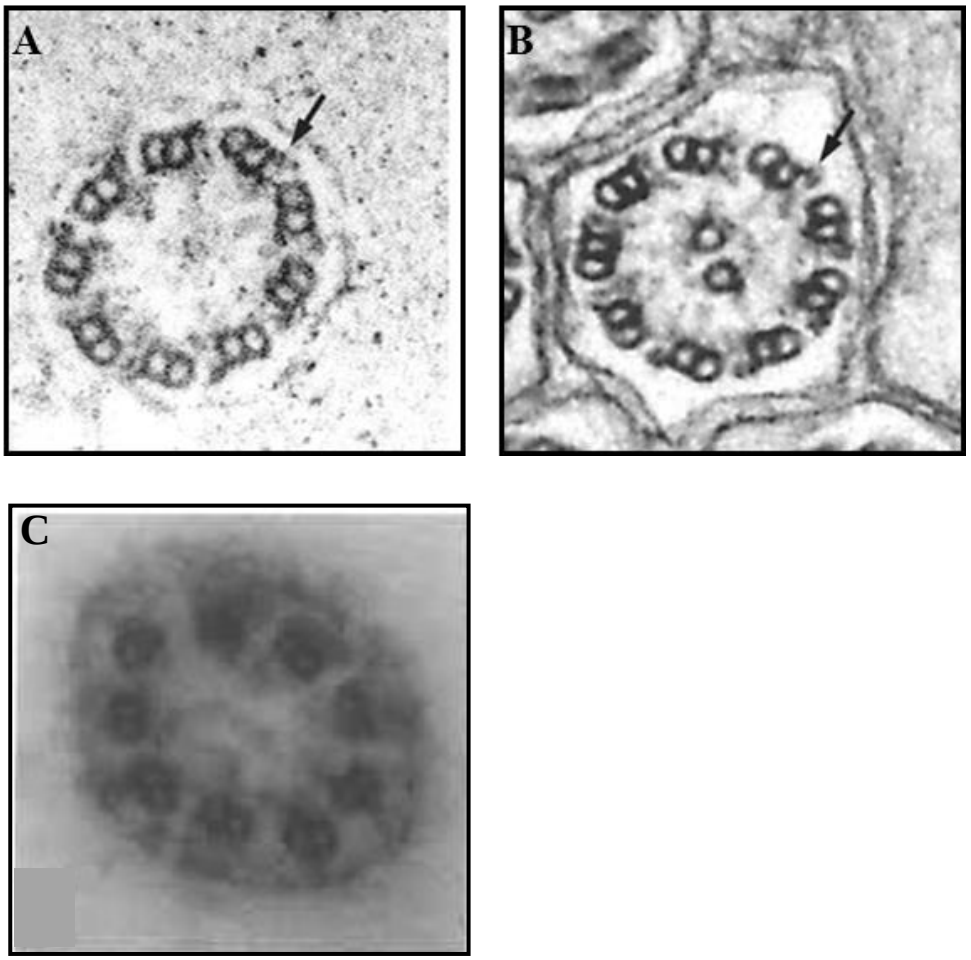

Figure 1.6 Ultrastructure of 'primary' and 'motile' cilia
Transmission electron microscopy showing (**A, C**) the '9+0' microtubule structure of a primary cilium and (**B**) the '9+2' microtubule structure of a typical 'motile' cilium. In both A and B outer dynein arms are arrowed, this supports the fact that primary cilia can be motile (A) or immotile (C). These images have been optimised as far as possible, it is appreciated that the clarity is not ideal. A (ependymal cilia) and B (pronephric cilia) adapted from (Kramer-Zucker et al., 2005) and C (nodal cilia) adapted from (Bellomo et al., 1996).

1.10 Cilia in development

In developing mammals and zebrafish embryos (discussed in section 1.18), the embryonic node or Kupffer's vesicle (KV) respectively, are conserved transient, ciliated structures required for the establishment of normal left-right body patterning (Essner et al., 2005; Essner et al., 2002; Nonaka et al., 1998). In mouse models, although the nodal cilia have a '9+0' structure, two distinct cilia groups have been described, functioning to generate or sense movement (McGrath et al., 2003). In zebrafish, cilia in KV have all been described as motile and only a '9+2' structure has been reported (Kramer-Zucker et al., 2005; Sarmah et al., 2007). There are several studies demonstrating that knockdown of genes whose protein products function in primary cilia or intraflagellar transport leads to aberrant body asymmetry such as: situs inversus (Marszalek et al., 1999; Murcia et al., 2000); altered expression of left-right genes (Kramer-Zucker et al., 2005); reversed cardiac looping (Essner et al., 2005; Schilling et al., 1999; Simms et al., 2012) and is associated with changes in the structure or function of cilia at the node/KV. Although the distinct mechanisms for why cardiac looping is reversed rather than randomised in several zebrafish morphants and mutants remains unclear, hypotheses based on results herein will be discussed in section 3.3.3.

1.11 Function of Primary Cilia

Previously primary cilia were considered innocent bystanders and their role, if any, was certainly, unclear. Even in 1975, following the detection of primary cilia throughout the renal tubules on transmission electron microscopy studies, they were hypothesised to most likely represent vestigial organelles, although the possibility that they may have a sensory role was acknowledged (Webber and Lee, 1975). Revelations in the last 15 years have highlighted the prime importance of cilia in maintaining cellular wellbeing and function, possibly explaining their essential and ubiquitous expression on most cells (Goetz and Anderson, 2010).

The design, location and versatile functional capabilities of primary cilia make them a quintessential organelle for normal development and sustained health. Primary cilia located at the apex of a cell, project directly into the extracellular space and use their extensive surface area to detect environmental cues (Bergmann, 2012). Depending on their location and the activity of the associated tissue, primary cilia can behave as mechanosensors, osmosensors, photosensors or chemosensors, to detect a range of

extracellular stimuli including fluid flow, extracellular fluid composition, shear stress, light, hormones and chemokines (Bergmann, 2012). In response to the detected information, primary cilia mediate activity in appropriate cellular signalling pathways including Wnt non-canonical (planar cell polarity (PCP)), Sonic hedgehog (Shh) and JAK-STAT (Bergmann, 2012) to regulate proliferation, apoptosis, orientated cell development, tissue maintenance and repair (Germino, 2005).

1.12 Cilia in the kidney

In humans and higher vertebrates, the structure of cilia in the kidney is '9+0' (Webber and Lee, 1975). In the pronephros of zebrafish only '9+2' cilia have been identified and are motile (Kramer-Zucker et al., 2005). In the kidney, primary cilia are considered to be behave as mechanosensors and chemosensors, to bend in response to fluid flow (Figure 1.7) (Berbari et al., 2009; Rodat-Despoix and Delmas, 2009). The lateral force generated by fluid flow, mediates an influx of calcium via a polycystin-1/2 complex on the cilia membrane (Nauli et al., 2003), this intracellular calcium is further augmented by calcium release from intracellular stores (Rodat-Despoix and Delmas, 2009; Torres, 2008). The increased calcium inhibits accumulation of cyclic adenosine monophosphate (cAMP), which influences the length of cilia and mediates other downstream pathways (Hoey et al., 2012).

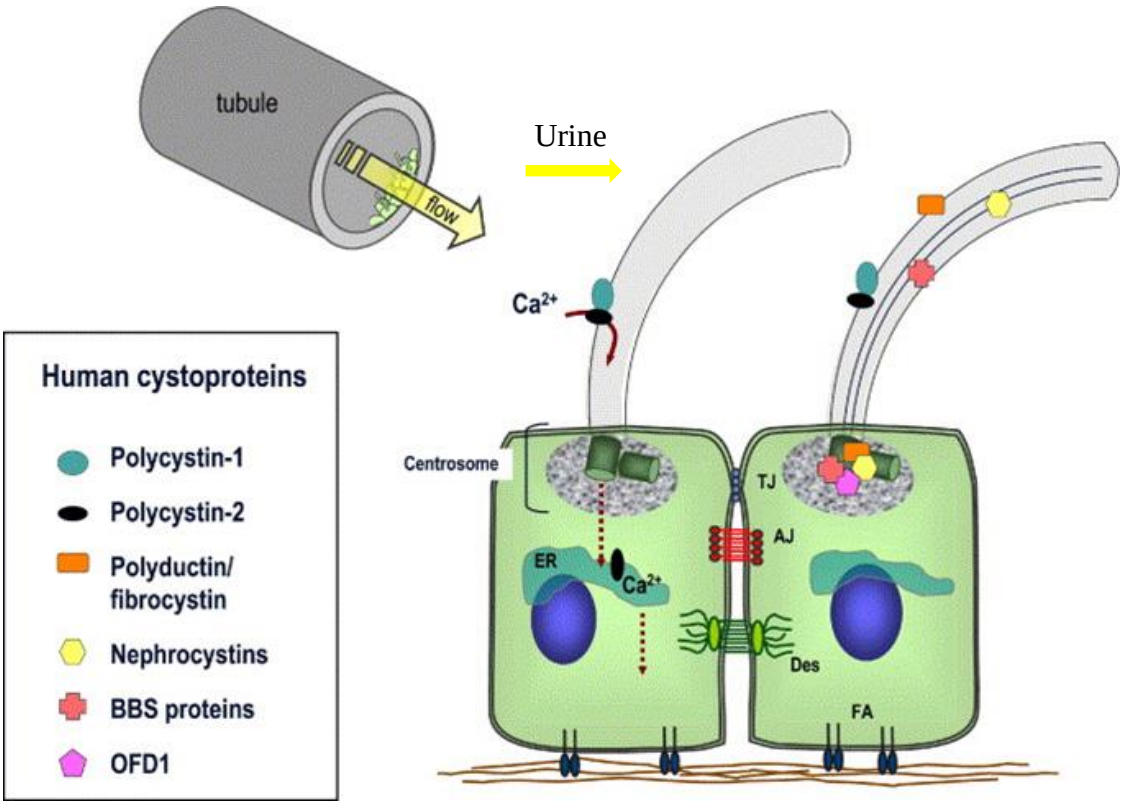

Figure 1.7 Primary cilia function as mechanosensors in the kidney
Urine flowing through a kidney tubule is shown in the top left corner and amplified for the main image to show two kidney cells with primary cilia projecting into the urinary space. In response to urinary flow, primary cilia bend and calcium influx occurs via polycystin receptors localised on the cilium. This initiates intracellular signalling cascades. The presence of the nephrocystins and other cystic kidney disease related proteins are shown to localise on the primary cilia. Adapted from (Siroky and Guay-Woodford, 2006).

1.13 Cilia in Cystic kidney disease

A body of evidence associates primary cilia with cystic kidney disease (Mollet et al., 2002; Olbrich et al., 2003; Otto et al., 2003; Pazour et al., 2000; Yoder et al., 2002) and was discussed in section 1.4. It is recognised that changes in the structure or function of cilia adversely modifies subsequent cellular signalling pathways and leads to aberrant protein interactions, culminating in cystic kidney disease (Berbari et al., 2009; Sang et al., 2011). Although the exact nature of how changes in the ciliary signalling pathways lead to cystic kidney disease remains uncertain, an overview of the current hypotheses follows.

Normal renal tubule morphogenesis requires coordinated cell proliferation, differentiation and spatial orientation of cells along the tubule axis. In order to maintain a constant tubular diameter during lengthening (and prevent circumferential expansion and cyst formation), renal tubules require intrinsic polarisation of mitotic spindles and the ciliary basal body of cells within a tissue plane, known as PCP (Fischer et al., 2006; Hildebrandt et al., 2011). PCP is regulated by the non-canonical Wnt signalling pathway (Berbari et al., 2009). Defective PCP leads to cystic kidney disease (Figure 1.8) and has been shown to precede tubular dilation and cyst formation in the pck rat model of ADPKD (Fischer et al., 2006). Further evidence from mouse and zebrafish studies support the link between ciliary defects, kidney cysts, PCP defects and the non-canonical Wnt signalling pathway (Jones et al., 2008; Oishi et al., 2006; Saburi et al., 2008).

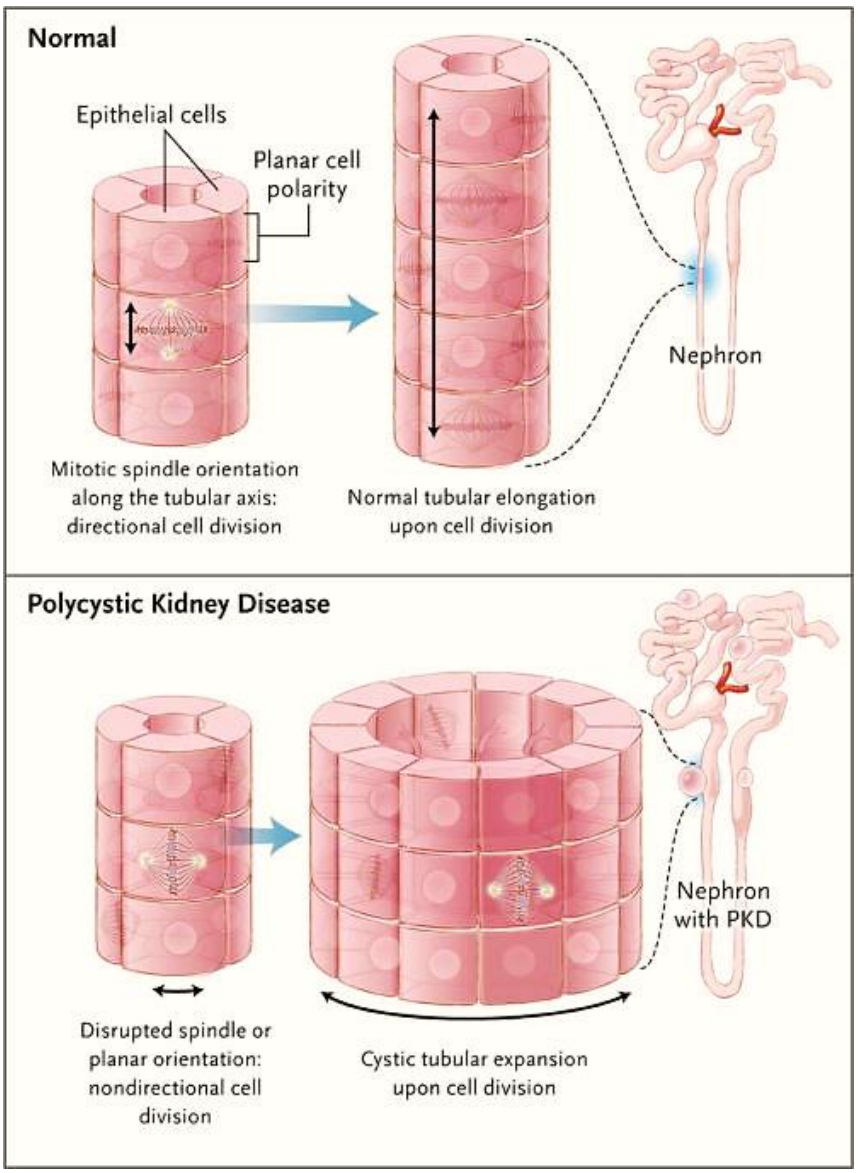

Figure 1.8 Aberrant Planar cell polarity causes cystic kidney disease
During normal renal tubule development (top image), correct mitotic spindle location relative to the renal tubule axis enables orientated cell division to generate a normal longitudinal tubule. If the mitotic spindle becomes disorientated, renal tubular development is disorganised and along a different trajectory and may result in cystic tubular expansion. Taken from (Hildebrandt et al., 2011).

Primary cilia are essential for the normal function of the Shh signalling pathway (Huangfu et al., 2003). The Shh signalling pathway is evolutionarily conserved and plays an essential role in regulating organ development (Figure 1.9) (Goetz and Anderson, 2010; Wilson and Stainier, 2010). Hedgehog (Hh) is a protein which binds to its receptor patched (Ptch) located on the cilia membrane (Rohatgi et al., 2007). Several other effectors of the Hh pathway, the Gli transcription factors, are localised within cilia and upon activation, exit the cilium and travel to the cell nucleus to transcribe Hh target genes (Goetz and Anderson, 2010; Oh and Katsanis, 2012). Impaired Hh signalling is associated with congenital defects, particularly of the nervous system and cancers (Mullor et al., 2002). The Hh pathway has been linked to cystic kidney disease and in particular NPHP, following identification of a cree indian family with mutations in *GLIS2*/*NPHP7* (Attanasio et al., 2007). *GLIS2* encodes the GLIS2 transcription factor which is an effector in the Hh pathway.

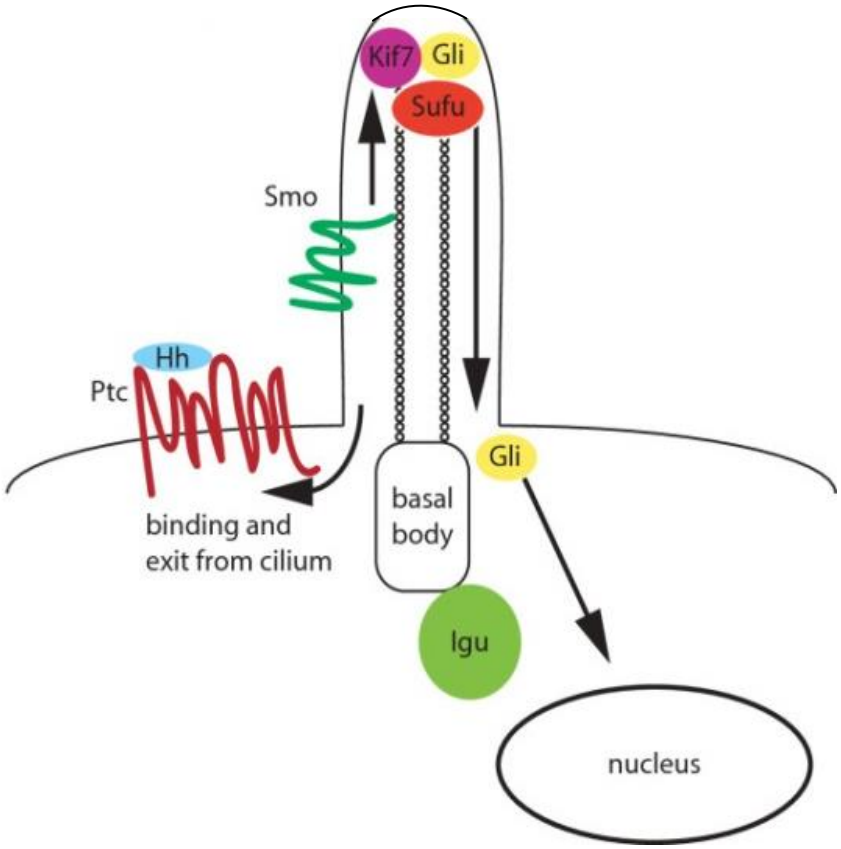

Figure 1.9 Hedgehog signalling and the primary cilium
When Hedgehog (Hh) binds to Patched (Ptc) in the ciliary membrane, the Hh/Ptc complex exits the cilium and Smoothened (Smo) is activated and enters the cilium. Smo utilises the scaffolding protein Kinesin-7(Kif-7) and suppressor of Fused (Sufu) to signal to the Gli proteins, which exit the cilium and travel to nucleus to transcribe Hh target genes. Taken from (Wilson and Stainier, 2010).

Primary cilia also play a key role in regulating cell cycle control and cell division. Disassembly and resorption of the primary cilium are required to enable cell division to occur (Hildebrandt et al., 2011). Specific links between cell cycle control and NPHP were made following the identification of patients with mutations in *NPHP9*/*NEK8* (never in mitosis kinase 8) (Otto et al., 2008). NEK8, the protein product of *NEK8* localises to cilia and centrosomes (Otto et al., 2008) and is a significant player in control of the cell cycle (Hildebrandt et al., 2011). NEK8 also regulates the expression and localisation of polycystin-1 and 2 (Sohara et al., 2008), the ADPKD proteins, which have been independently associated with regulating cell growth (Hildebrandt et al., 2011). The association between cystic kidney disease and cell cycle regulation was further evident following the successful use of roscovitine, a cyclin-dependent kinase inhibitor, to effectively treat mouse models of ARPKD and NPHP (Bukanov et al., 2006).

1.14 Ciliopathies: Cystic kidney disease and beyond

As detailed above, primary cilia play a vital role in controlled cell division, establishing left-right body asymmetry, organogenesis, tissue maintenance and ciliary signalling pathways. Understandably, damage to this fundamental and diverse organelle will lead to a range of adverse 'ciliary' phenotypes (Baker and Beales, 2009). The association between ciliary dysfunction or structural change and cystic kidney disease has been detailed above, with recognition of cystic kidney diseases as ciliopathies (Hildebrandt and Otto, 2005). The ciliopathies are a recently defined heterogeneous group of genetic diseases caused by mutations in a gene, whose defective protein product leads to dysfunctional cellular physiology and a broad range of phenotypes (Baker and Beales, 2009; Hildebrandt et al., 2011; Waters and Beales, 2011). The common phenotypes typically associated with ciliopathies include: cystic kidney disease, retinal degeneration, liver disease, cerebellar hypoplasia/encephalocele, developmental delay, polydactyly, obesity, situs inversus, skeletal dysplasia (Badano et al., 2006b; Waters and Beales, 2011). The presence of several of these ciliary phenotypes overlaps in many clinical syndromes, which have been classified as ciliopathies (Table 1.5) (Badano et al., 2006b). Senior-Loken syndrome is a rare genetic cause of blindness and is characterised by retinal degeneration and cystic renal disease (Adams et al., 2007).

Whilst cystic kidney disease and liver disease are frequently identified in ciliopathies, retinal and neurological disease also recurrently manifest (Waters and Beales, 2011). The group of conditions defined as ciliopathies are predicted to grow, both the London Dysmorphology Database and Online Mendelian Inheritance in Man (OMIM, www.ncbi.nlm.nih.gov/omim) sources have been utilised to review 'ciliopathy' phenotypes and explore combinations of phentoypes (Badano et al., 2006b; Baker and Beales, 2009). Understanding the associated pathophysiology of ciliopathies with their variable and extensive clinical phenotypes, would clearly have a considerable impact on the health and wellbeing of much of society.

Phenotype	SLS	NPHP	JBTS	BBS	MKS
Renal cysts	X	X	X	X	X
Liver disease	X	X	X	X	X
Retinopathy	X	X	X	X	
Cerebellar hypoplasia		X	X	X	
Posterior encephalocele					X
Developmental delay		X	X	X	
Polydactyly			X	X	X
Situs inversus	X	X	X	X	X
Skeletal dysplasia					X
Obesity			X	X	

Table 1.5 Clinical phenotypes associated with several ciliopathies
Clinical features present (X) in conditions which are now defined as ciliopathies. Cystic kidneys (highlighted in blue), liver disease and situs inversus are the most frequent clinical sequelae. BBS, Bardet-Biedl syndrome; JBTS, Joubert syndrome; MKS, Meckel-Gruber syndrome; NPHP, nephronophthisis; SLS, Senior-Loken syndrome. Modified from (Gerdes et al., 2009).

1.15 Ciliopathies: Variable severity and phenotype

The ciliopathy disorders are clearly a heterogeneous group both in terms of clinical presentation and genetic cause (Hildebrandt et al., 2011). Four mechanisms are postulated to contribute to the variability in extent and severity of organ involvement: genetic locus; nature of mutation; presence of triallelism, or additional modifier genes; oligogenicity (Hildebrandt et al., 2011). The term triallelism specifically describes the inheritance pattern when three mutant alleles at two different loci have been identified in an individual with a disease phenotype (Katsanis et al., 2001) and has classically been associated with BBS (Katsanis, 2004). Triallelism is a form of oligogenicity, which is a more general concept and has been defined as heterozygous mutations in at least two different recessive genes which independently do not cause disease, however in combination can (Hildebrandt et al., 2011; Leitch et al., 2008). In some studies the terms, triallelism and oligogenicity have overlapped and been utilised to describe the same phenomenon (Hoefele et al., 2007).

Whilst the nature of the gene locus can influence the occurrence of some ciliopathy phenotypes, such as homozygous *NPHP5* mutations induce retinal degeneration (Otto et al., 2005), generally there is no consistent correlation between genotype and phenotype (Coppieters et al., 2010; Hurd and Hildebrandt, 2011). The nature of the mutation influencing the severity of phenotype, this has been well characterised for the lethal disorder MKS, caused by two truncating mutations (in *MKS1*, *MKS3*, *NPHP3*, *NPHP6*, *NPHP8*), whereas the phenotype is rescued to a milder ciliopathy such a SLS or JBTS, if the mutations are a combination of missense and truncating (Bergmann et al., 2008; Delous et al., 2007; Wolf and Hildebrandt, 2011).

Triallelism and the impact of a modifier gene has been identified in patients with NPHP (Hoefele et al., 2007), JBTS (Tory et al., 2007), BBS (Leitch et al., 2008) and MKS (Hopp et al., 2011). Mutations in *TTC21B* have been identified as an independent cause for NPHP and JBTS, additionally, *TTC21B* has been considered as a modifier gene in ciliopathies, as mutations were detected in up to 5% of a cohort of patients with ciliopathies (Davis et al., 2011). Table 1.6 details the genetic mutations and associated ciliopathies in which triallelism and oligogenicity have been reported. It is expected that this list will continue to grow, as presently only a single heterozygous mutation has

been identified in some patients with NPHP (Chaki et al., 2011), JBTS and MKS (Gorden et al., 2008; Mougou-Zerelli et al., 2009).

Gene	2nd Gene	Ciliopathy	References
NPHP1 (hom)	*NPHP3* (het)	NPHP	(Hoefele et al., 2007)
	NPHP4 (het)	NPHP	(Hoefele et al., 2007)
	NPHP6 (het)	NPHP, SLS	(Tory et al., 2007)
	RPGRIP1L (het)	NPHP, SLS, JBTS	(Hildebrandt et al., 2011)
	AHI1 (het)	NPHP, JBTS	(Tory et al., 2007)
INVS (het)	*NPHP3* (het)	NPHP	(Hoefele et al., 2007)
IQCB1 (hom)	*NEK8* (het)	NPHP	(Otto et al., 2008)
IQCB1 (het)	*RPGRIP1L* (het)	SLS	(Khanna et al., 2009)
NPHP6 (hom)	*NPHP4* (het)	MKS	(Coppieters et al., 2010; Hoefele et al., 2005)
	TMEM67/*MKS3* (het)	BBS	(Leitch et al., 2008)
	AHI1 (het)	NPHP, SLS	(Tory et al., 2007)
	PKHD1 (hom)	MKS	(Baala et al., 2007a)
NPHP6 (het)	*NPHP4* (het)	SLS	(Coppieters et al., 2010)
	RPGRIP1L (het)	JBTS	(Khanna et al., 2009)
	CC2D2A (het)	MKS	(Hopp et al., 2011)
	B9D1 (het)	MKS	(Hopp et al., 2011)
RPGRIP1L (het)	*NPHP6* (het)/*IQCB1* (het)	SLS	(Khanna et al., 2009)
	NPHP3 (comp. het)	SLS	(Khanna et al., 2009)
	MKS1 (het)	BBS	(Khanna et al., 2009)
CC2D2A (hom)	*PKDH1* (het)	MKS	(Hopp et al., 2011)
CC2D2A (het)	*NPHP3* (het)	MKS	(Hopp et al., 2011)
TTC21B (het)	*NPHP4* (het)	NPHP	(Davis et al., 2011)
	C2ORF86 (het)	MKS	(Davis et al., 2011)

Table 1.6 Mutational load reported in patients with ciliopathies
Mutations identified in patients were homozygous (hom) or heterozygous (het). BBS, Bardet-Biedl syndrome; JBTS, Joubert syndrome; MKS, Meckel-Gruber syndrome; NPHP, nephronophthisis; SLS, Senior-Loken syndrome.

1.16 Animal models of cystic kidney disease related ciliopathies

Animal models have been utilised for years to improve understanding of human genetic conditions in terms of identifying causal genes and defining their function. Although genome wide association studies (GWAS) and advanced sequencing technologies in humans have improved the identification of causal genes in human diseases, these techniques do not explain the pathophysiology of the associated disease. Further limitations of simply studying humans to further understand disease pathogenesis, includes ethical barriers and the appropriateness of certain experiments. Whilst human cell lines are available to study biological pathways and improve understanding, cell lines are limited by their locus within the hierarchy of systems and inability to reflect processes at the organ and whole body level. Thus animal models continue to provide an essential tool for understanding the pathogenesis of human diseases. By creating animal models representative of human diseases, the basic biological processes involved in the pathogenesis can be closely studied and manipulated to address specific hypotheses (Aitman et al., 2011).

1.17 Mouse models of cystic kidney disease related ciliopathies

The use of mice and rats, has contributed a wealth of knowledge to the study of human disease, particularly genetic disease (Norris and Grimes, 2012). Accepting the limitations of studying humans, research in mice has generated valuable knowledge regarding the role of cilia in health and disease. Mice are considered an appropriate model because of their genetic, anatomical and physiological similarity to humans (Norris and Grimes, 2012). Both mutant mouse models and embryonic stem cell lines exist for several of the identified ciliopathy genes. Table 1.7 lists the currently characterised mouse models of NPHP, JBTS, MKS and BBS.

Gene locus	Other Gene locus	Mutants	Type	Survival	References
Nphp1	Jbts4	*Nphp1*$^{tm1.1Hung}$	Targeted-null	AV	(Jiang et al., 2008)
		Nphp1^{tm1Jgg}	Targeted-null	AV	(Louie et al., 2010)
Nphp2		*Invs*^{Inv}	Random insertion	AV	(Yokoyama et al., 1993)
Nphp3	Mks7	*Nphp3*^{pcy}	Hypomorphic	AV	(Olbrich et al., 2003)
		Nphp3^{tm1Cbe}	Targeted-null	EL	(Bergmann et al., 2008)
Nphp4		*Nphp4*^{nmf192}	ENU	AV	(Won et al., 2011)
Nphp6	Jbts6, Mks4, Bbs14	*Cep290*^{rd16}	Spontaneous	AV	(Chang et al., 2006)
		Cep290^{tm1jgg}	Targeted-null	AV	(Lancaster et al., 2011)
Nphp7		*Glis2*^{tm1Amj}	Targeted-null	AV	(Kim et al., 2008)
		Glis2^{tm1Tre}	Targeted reporter	AV	(Attanasio et al., 2007)
Nphp8	Jbts7, Mks5	*Rpgrip1l*^{tmUrt}	Targeted-null	Birth	(Vierkotten et al., 2007)
Nphp9	Jbts6	*Nek*^{jck}	Possible hypomorph	AV	(Liu et al., 2002)
Nphp11		*Tmem67*^{tm1Dgen}	Targeted reporter	PNL	(Garcia-Gonzalo et al., 2011)
Nphp12	Jbts11	*Ttc21b*^{aln}	ENU - probably null	EL	(Tran et al., 2008)
Jbts1		*Inpp5e*$^{tm1.15sch}$	Targeted conditional null	EL (global KO)	(Jacoby et al., 2009)
Jbts3		*Ahi1*^{tm1Jgg}	Targeted null	PNL (80%)	(Lancaster et al., 2011; Lancaster et al., 2009)
		Ahi1^{tm1Rujf}	Targeted reporter - null	ND	(Hsiao et al., 2009; Westfall et al., 2010)
Jbts8		*Arl13b*^{hnn}	ENU - null	EL	(Caspary et al., 2007)
Jbts9	Mks6	*Cc2d2a*$^{Gt(AA0274)Wtsi}$	Gene trap - null	EL	(Garcia-Gonzalo et al., 2011)
Jbts10		*Ofd1*$^{tm2.1Bfra}$	Targeted conditional null	Male:EL; female: birth	(Ferrante et al., 2006)
Jbts12		*Kif7*$^{1.2Hui}$	Targeted null	Birth	(Cheung et al., 2009)
		Kif7^{maki}	ENU	El (late)	(Liem et al., 2009)

Gene locus	Other Gene locus	Mutants	Type	Survival	References
Jbts13		*Tctn1*$^{Gt(KST296)8yg}$	Gene trap - null	EL	(Reiter and Skarnes, 2006)
Jbts15		*Tsga14*$^{Gt(AWO157)Wtsi}$	Gene trap - null	EL	(Lee et al., 2012a)
Mks1	Bbs13	*Mks1*$^{del64-323}$	ENU - dominant negative	EL	(Cui et al., 2011)
		Mks1^{1krc}	ENU - probably null	EL	(Weatherbee et al., 2009)
Mks8		*Tctn2*$^{tm1.1Reit}$	Targeted - null	EL	(Garcia-Gonzalo et al., 2011; Sang et al., 2011)
Mks9		*B9d1*$^{tm1a(EUCOMM)Wtsi}$	Gene trap - null	EL	(Dowdle et al., 2011)
Mks10		*B9d2/Tgfb1*^{tm1flv} *(Stumpy)*	Targeted deletion	ND	(Town et al., 2008)
Bbs1		*Bbs1*^{GT1NK}	Gene trap - probably null	EL, AV	(Kulaga et al., 2004)
		Bbs1 $^{tm1Vcs(M390R)}$	Targeted knock-in	AV	(Davis et al., 2007)
Bbs2		*Bbs2*^{tm1Vcs}	Targeted null	AV	(Nishimura et al., 2004)
Bbs3		*Arl6*^{tm1Vcs}	Targeted deletion - transcript specific	AV	(Pretorius et al., 2010)
Bbs4		*Bbs4*^{Gt1Nk}	Gene trap	EL, birth, AV	(Kulaga et al., 2004)
		Bbs4^{tm1Vsc}	Targeted null	EL, birth, AV	(Mykytyn et al., 2004)
Bbs6		*Mkks*$^{Gt(0ST367255)Lex}$	Gene trap	EL, AV	(Ross et al., 2005)
		Mkks^{tm1Vcs}	Targeted null	EL, AV	(Fath et al., 2005)
Bbs7		*Bbs7*^{nulla}	Targeted	ND	(Zhang et al., 2012)
Bbs8		*Tct8*^{tm1Reed}	Targeted reporter - null	AV	(Tadenev et al., 2011)
Bbs11		*Trim32*$^{Gt(BGA355)Byg}$	Gene trap - probably null	AV	(Kudryashova et al., 2009)
		Trim32^{tm1Spc}	Targeted knock-in - hypomorphic	AV	(Kudryashova et al., 2011)

Table 1.7 Mouse mutants of NPHP, JBTS, MKS and BBS ciliopathies

BBS, Bardet-Biedl syndrome; JBTS, Joubert syndrome; MKS, Meckel Gruber syndrome; NPHP, Nephronophthisis. Mutants in: blue boxes are gene traps, targeted alleles; green boxes are spontaneous; orange boxes are chemical mutants. Survival is described as: AV, adult viable; EL, embryonic lethality; ND, not determined; PNL, postnatal lethal. Modified from (Norris and Grimes, 2012).

A few limitations associated with utilising mice to study the more severe ciliopathies including JBTS and MKS is that survival is poor. Often homozygous null mice are embryonically lethal or only a minority survive to adulthood, restricting the ability to study them (Norris and Grimes, 2012). Perhaps reflecting the genetic pleiotropy of NPHP related ciliopathies, not all mouse models display the full array of expected phenotypes, for example, *Nphp1*$^{tm1.1Hung}$ and *Nphph1*^{tm1Jgg} develop retinopathy however do not develop cystic kidneys (Jiang et al., 2008; Louie et al., 2010). Furthermore, the diagnostic molar tooth sign, pathognomonic of JBTS, may be specific to humans and does not appear to be modelled in mice (Norris and Grimes, 2012). Finally, the genetic background of a mouse appears to influence both the survival and expression of certain ciliopathy phenotypes and requires careful control (Norris and Grimes, 2012). These are amongst some of the reasons why additional animal models, such as zebrafish, are required to facilitate further understanding the pathogenesis of the cystic kidney disease related ciliopathies and enable high-throughput drug screening (Norris and Grimes, 2012).

1.18 Zebrafish: a model organism

Zebrafish are recognised as an excellent animal model in which to study development and disease. They were first used by developmental biologists in the 1970s (Hsu et al., 2007) and in 1981, genetic manipulation of zebrafish was first reported, enabling the generation of homozygous lines to study development in a vertebrate model organism (Streisinger et al., 1981). In order to recognise aberrations in development as a consequence of mutations or pathological processes, normal development must first be understood. In 1995, a description of the normal stages of embryonic development in zebrafish was published (Kimmel et al., 1995). From 1996, zebrafish have been utilised to perform large scale mutagenesis screens to identify new genes associated with organogenesis and disease (Driever et al., 1996; Haffter et al., 1996) including kidney development (Drummond et al., 1998). Over the years, the focus of zebrafish in research has expanded from understanding basic science to involve more translational studies modelling several human diseases including: congenital disorders (Fraser syndrome (Carney et al., 2010), Waardenburg syndrome (Dutton et al., 2009)); cancers (melanoma (Patton and Zon, 2005), neuroendocrine carcinoma (Yang et al., 2004), leukaemia (Langenau et al., 2003)); neurodegenerative disorders (Parkinson's disease

(Flinn et al., 2009) and cystic kidney diseases (ADPKD (Mangos et al., 2010), NPHP (Sayer et al., 2006; Schafer et al., 2008; Zhou et al., 2010b)).

In addition to studying development and the pathogenesis of diseases, zebrafish are recognised as a valuable pre-clinical tool for drug screening and therapeutic development (Parng et al., 2002). With the recent development of automated, high-throughput *in vivo* chemical screening, it is feasible that zebrafish may improve the efficacy and cost effectiveness of drug discovery (Letamendia et al., 2012).

In terms of therapeutics, it is exciting to learn that zebrafish are being utilised to understand mechanisms of tissue repair and regeneration of vital organs including the heart (Jopling et al., 2010; Poss et al., 2002), retina (Vihtelic and Hyde, 2000) and kidney (Zhou et al., 2010a). Interestingly, even in adulthood, zebrafish retain the ability to develop new nephrons (Zhou et al., 2010a), suggesting a supply of renal stem cells which would be capable of regenerating kidney function after injury (Reimschuessel, 2001). Transplantation of nephron progenitor cells has been performed and led to successful development of numerous nephrons (Diep and Davidson, 2011). These exciting developments give hope that further research may enable the identification or generation of equivalent human renal progenitor cells (Diep and Davidson, 2011).

Zebrafish are small freshwater tropical fish which measure approximately 3-4cm in length as adults. The qualities of zebrafish which make them attractive models to utilise include their: fecundity (females lay several hundred embryos per spawning), rapid ex-vivo development (major organogenesis is complete by 48hpf), transparency (enabling direct visualisation of organogenesis under light microscopy), conserved genome (75% similar to human) and tractability to study genetics (Hsu et al., 2007).

There are several options for studying genes related to development and disease in zebrafish including: targeted gene 'knockdown' using antisense morpholino oligonucleotides (MO) to assess the effect of temporary loss of gene (Eisen and Smith, 2008); transgenic reporter lines which express a fluorescent signal in a targeted tissue; expression of genes using *in situ* hybridisation and immunohistochemistry (Swanhart et al., 2011). Forward genetic techniques using a chemical mutagenesis screen can be used to identify new causal genes which may lead to certain phenotypes or diseases (Amsterdam and Hopkins, 2006).

Antisense MOs are an accepted, informative, tractable and efficacious technique enabling *in vivo* assessment of gene function in zebrafish. MOs are synthetic DNA analogues composed of: a 6 member 'morpholine' ring; more stable, uncharged phosphorodiamidate backbone of approximately 25 units (Figure 1.10) (Summerton and Weller, 1997). A gene specific MO is designed to bind to mRNA and prevent protein synthesis (Bedell et al., 2011).

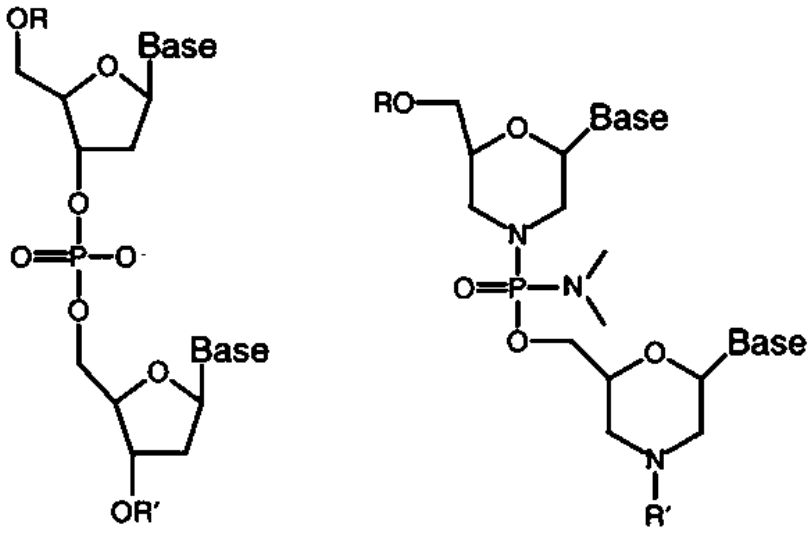

DNA MO

Figure 1.10 Comparative structure of DNA and Morpholino oligonucleotides
Conventional DNA has a 5 member deoxyribose ring and anionic phosphodiester backbone. A morpholino oligonucleotide (MO) has a 6 member morpholine ring and non-ionic phosphorodiamidate backbone. R and R' represent progression of the oligomer chain in the 5' or 3' prime direction respectively. Modified from (Corey and Abrams, 2001).

Since MOs were first shown to effectively knockdown specific gene expression in zebrafish in 2000 (Nasevicius and Ekker, 2000), their widespread use within the research community has resulted in lessons regarding some of their limitations and acknowledgment of the need for essential controls (Bedell et al., 2011). Following microinjection into embryos, MOs are usually very effective for at least 50 hours, although they can lose efficacy as time progresses, they have successfully been used to study later aspects of development (Bedell et al., 2011; Smart et al., 2004). However, a major concern with regards to MOs was that some of the observed 'phenotypes' following MO injection were not related to the targeted sequence, but rather were non-specific, confounding, 'off-target' effects (Eisen and Smith, 2008). Recognised off-target phenotypes include: neural death, with black areas in the usually transparent brain; shortened, bent and 'gnarled' tails, which have an unusual, easily identifiable abnormal appearance (Robu et al., 2007). Although the exact mechanism of 'off-target' effects is not completely understood, they are proposed to be mediated in part by *p53* activation (Robu et al., 2007). It is therefore recommended that co-injection of a p53 MO should be performed at least during initial characterisation of a new MO (Bedell et al., 2011; Eisen and Smith, 2008). Further recommendations for controls in MO experiments are directed at confirming specificity of gene knockdown and validating a phenotype. Suggested methods include: injection of a second, independent MO, such as a splice-site targeting and translation blocking MO; performing RNA rescue by co-injecting the MO sequence with sequence specific mRNA (Bedell et al., 2011).

Although zebrafish have some inherent differences from humans which may be difficult to explain physiologically, they are an outstanding model organism for studying developmental disease (Bedell et al., 2011). In particular, the zebrafish rudimentary kidney has representative features of the human kidney (see section 1.19) and original observations in several species of fish in the 1950s has generated seminal understanding of renal physiology (Smith, 1953).

1.19 Normal development of zebrafish kidney

During embryogenesis in zebrafish, the pronephros is the first kidney to develop and principally functions similarly to the human kidney, to remove waste and balance electrolytes in the blood, to regulate the body composition (Drummond and Davidson, 2010). In comparison, in humans and all mammals, although the pronephros is an important initial stage of kidney development, it does not function (Vize et al., 2003).

In zebrafish, the pronephros is the functional kidney from 2-12dpf (Zhou et al., 2010a), when the mesonephros begins to form around the pronephros and is the final stage of kidney development. The mesonephros functions as the adult zebrafish kidney (Drummond and Davidson, 2010). Contrary to humans, zebrafish kidneys do not have a third stage of development and do not form a metanephros. Since the function of the metanephros involves concentrating urine in mammals (Drummond and Davidson, 2010), this may explain why zebrafish do not develop a metanephric kidney, since they are obligatory water losers, generating large volumes of dilute urine (Westerfield, 1995). Although simple in form, the considerable advantages of the zebrafish pronephros have led to its frequent use in kidney disease research (Drummond, 2000; Drummond, 2005). For these reasons, the zebrafish pronephros was an attractive model to use in this work.

Structurally, the zebrafish pronephros consists of two nephrons (functional units of the kidney) which unite in the midline at a single glomerulus (filtering unit of the kidney) (Drummond, 2000). In comparison, the number of glomeruli per kidney in humans is thought to range between 330,000 to 1,400,000 (Nyengaard and Bendtsen, 1992). From the glomerulus, the pronephric tubules, which are segmentally discrete and representative of the human kidney, extend caudally towards the pronephric ducts, which fuse at the cloaca, the communal exit for urine/faeces in zebrafish (Drummond, 2003; Wingert and Davidson, 2008). The segments of the pronephric tubules in zebrafish are divided into functional segments (similar to humans): proximal convoluted tubule, proximal straight tubule, distal early tubule, corpuscle of stannius (equivalent of human parathyroid gland (Greenwood et al., 2009)), distal late tubule, pronephric ducts, cloaca (Figure 1.11) (Wingert and Davidson, 2008). The suggested function of each tubular segment was identified using *in situ* hybridisation to determine the expression of ion transporters (Drummond and Davidson, 2010) and is detailed in Table 1.8.

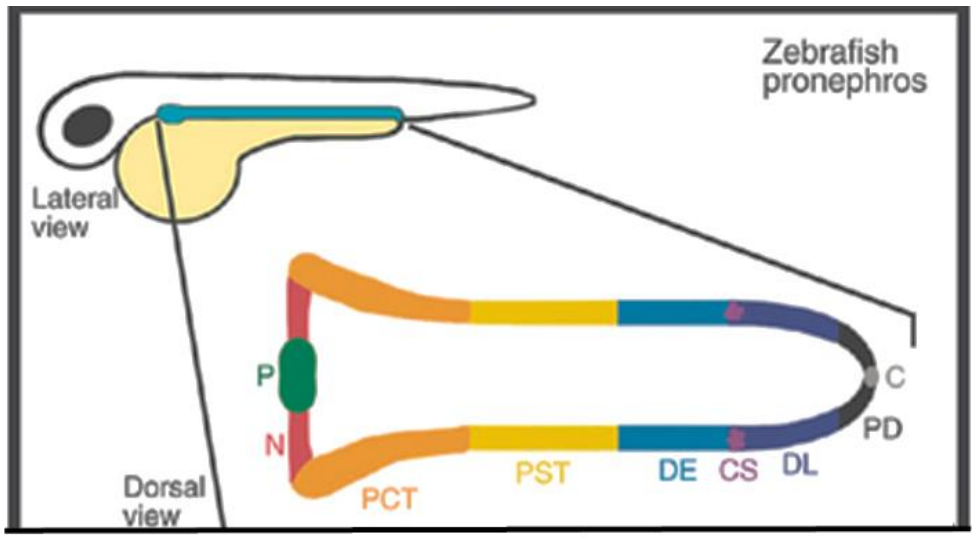

Figure 1.11 Discrete segmentation of zebrafish pronephric tubule
Lateral view of the location of the pronephros (blue) on zebrafish embryo. Dorsal view shows enlargement of the pronephric tubules and pattern of each segment extending from the single glomerulus (P), neck (N), proximal convoluted tubule (PCT), proximal straight tubule (PST), distal early (DE) tubule, corpuscle of stannius (CS, equivalent of human parathyroid gland (Greenwood et al., 2009)), distal late (DL) tubule, pronephric ducts (PD) to the cloaca (C, urethral exit). Modified from (Wingert and Davidson, 2008).

Tubular segment	Constituents/channel	Function	References
PCT	Developed brush border, high columnar epithelial cells	Reabsorption	(Drummond and Davidson, 2010)
	Endocytic receptors: megalin, cubalin	Absorption	(Anzenberger et al., 2006)
	AE2, NBCl, NHE	acid-base homeostasis	(Nichane et al., 2006; Shmukler et al., 2005; Wingert et al., 2007)
PST	*slc13a1*, *trpm7*	Less certain; sulphate and calcium transporters, if mutated result in kidney stones	(Drummond and Davidson, 2010; Elizondo et al., 2005)
DE	*slc12a1*, *Romk2*, *Clck*	Reabsorbs sodium, potassium, chloride, creates dilute urine	(Drummond and Davidson, 2010; Wingert et al., 2007)
DL	*slc12a3*,	Not certain; sodium, chloride absorption, modify dilute urine	(Drummond and Davidson, 2010)

Table 1.8 Structural features and function of pronephric tubule segments

AE2, chloride/bicarbonate anion exchanger; *Clck*, chloride channel; DE, distal early tubule; DL, distal late tubule; NBCl, sodium/bicarbonate cotransporter; NHE, sodium/hydrogen exchanger; PCT, proximal convoluted tubule; PST, proximal straight tubule; Ref., reference; *Romk2*, apical potassium channel; seg., segment; *slc12a1*, sodium-potassium-chloride symporter; *slc12a3*, sodium/chloride cotransporter; *slc13a1*, sodium/sulphate symporter; *trpm7*, calcium cation channel.

The pattern of pronephric development in zebrafish occurs in reverse order, beginning caudally. In terms of time scale, the pronephric ducts are the first to form and this is complete by 24hpf, subsequently between 30-40hpf the pronephric tubules form and finally, following vascularisation, the glomerulus becomes a functional filter by 48hpf (Drummond et al., 1998). Generally, nephrogenesis is divided into four stages (Figure 1.12) which will be detailed below: 1) specification of mesoderm to a nephrogenic determination, 2) epithelialisation and growth of pronephric duct in proximal pattern, 3) differentiation of glomerular and tubular cell types, 4) endothelial cells from the dorsal aorta invade the glomerulus and develop a functional capillary tuft (Drummond, 2003; Drummond, 2000).

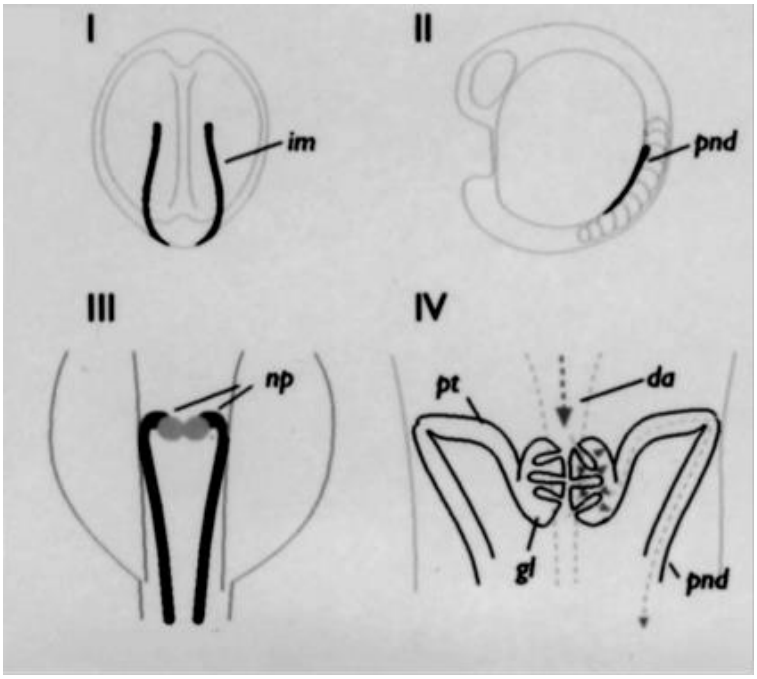

Figure 1.12 Stages of development of the zebrafish pronephros
I In early somitogenesis, the nephrogenic fate of the intermediate mesoderm (im) is visualised using renal transcription factors such as *pax2.1*. **II** Growth and epithelialisation of the pronephric duct (pnd) begins anterior to somite 3 (~11 hpf) and extends caudally, it is defined by expression of transcription factors. **III** Between 24-48hpf differentiation of cells destined to develop into podocytes or tubular cell types occurs, beginning at the pronephric duct (np). **IV** Endothelial cells from the dorsal aorta (da) migrate into the glomerulus (gl) to develop a functional capillary tuft. Modified from (Drummond, 2000).

Early studies of nephrogenesis in zebrafish identified an overlap in the type of cells which were destined to become kidney and blood cells (Kimmel et al., 1990). Both of these cell types are derived from the intermediate mesoderm (IM) and tissue patterning is determined by expression of kidney specific tissue markers (Drummond and Davidson, 2010). From the 3 somite stage (approximately 11hpf (Kimmel et al., 1995)), podocytes, the neck and PCT develop progressively from the IM, anterior to and at pace in concert with sequential somite development (Drummond and Davidson, 2010). Appropriate segmentation of the pronephric tubule requires retinoic acid, which facilitates organisation of the pronephros (Wingert and Davidson, 2008). Organisation of the pronephric tubular epithelium involves mesenchyme to epithelial transition, akin to humans, with establishment of polarised epithelial cells containing ion transporters, enabling osmoregulation (Drummond et al., 1998).

Similar to humans, the zebrafish glomerulus consists of podocytes, which express homologs of nephrin and podocin from 24hpf, which enables development of specialised filters, slit-diaphragms, between podocyte foot processes (Drummond and Davidson, 2010). Between 36-40hpf, podocytes extend foot processes which wrap around the adjacent endothelial cells of the dorsal aorta. Vascularisation is facilitated by podocytes expressing proteins which enable angiogenesis: vascular endothelial growth factor (VEGF) and angiopoietin2. Similarly, nearby endothelial cells destined to be capillary forming, express a VEGF receptor and between 40-48hpf invade the glomerular epithelium, becoming surrounded by podocytes. Although glomerular filtration occurs from 48hpf, the glomerular barrier is not mature in terms of appropriately restricting passage of large molecular weight proteins until approximately 4dpf (Drummond and Davidson, 2010).

The pronephric ducts meet at the cloaca and regulated by bone morphogenetic protein (BMP) signalling forms an opening by 24hpf (Pyati et al., 2006). Since the cloaca is a communal exit for urine and faeces, the proctodeum contributes to its development and surrounds the cloaca during development (Parkin et al., 2009).

1.20 Zebrafish models of cystic kidney disease

Several zebrafish mutants and morphants have been identified with abnormal kidney development and pronephric cysts. An N-ethyl N-nitrosourea (ENU) mutagenesis

screen led to the identification of fifteen different mutants with pronephric cysts, suggesting that at least fifteen genes are required for normal development and function of the pronephros (Drummond et al., 1998). Pronephric cysts were evident by 48hpf and frequently associated with additional phenotypes including: generalised oedema, considered due to loss of osmoregulation; and a ventral body axis curvature (Drummond et al., 1998). Furthermore, the link between cilia and cystic kidney disease was confirmed following an insertional mutagenesis screen identified mutations in ten genes caused pronephric cysts and three of these genes were homologs of intraflagellar transport genes (Sun et al., 2004). The existing zebrafish models of cystic kidney disease and related ciliopathies are listed in Table 1.9.

Human Gene	Zebrafish phenotype	References
PKD1	Pronephic cysts, dorsal axis curvature, hydrocephalus, jaw defects	(Mangos et al., 2010)
PKD2	Pronephric cysts, dorsal axis curvature, pericardial oedema, hydrocephalus, laterality defects	(Obara et al., 2006)
TCF2	Pronephric cysts, underdevelopment of pancreas and liver, small otic vesicles	(Sun and Hopkins, 2001)
INVS	Pronephric cysts, ventral axis curvature, pericardial oedema, laterality defects	(Otto et al., 2003)
NPHP3	Pronephric cysts, ventral axis curvature, pericardial oedema, hydrocephalus, laterality defects, fewer and shorter cilia in KV	(Zhou et al., 2010b)
NPHP4	Pronephric cysts, ventral axis curvature, pericardial oedema, vesicle laterality defects, shorter cilia in KV and PND, vesicle obstructs cloaca formation	(Slanchev et al., 2011)
IQCB1	Pronephric cysts, axis curvature, hydrocephalus	(Schafer et al., 2008)
CEP290	Pronephric cysts, ventral axis curvature, hydrocephalus, loss of retinal tissue	(Sayer et al., 2006)
RPGRIP1L	shortened dorsal axis curvature, thin somites, kinking of the notochord	(Khanna et al., 2009)
NEK8	Pronephric cysts	(Liu et al., 2002)
TMEM67 (MKS3)	Pronephric cysts, axis curvature, pericardial oedema, hydrocephalus, kinking of the notochord, unilateral microphthalmia, altered number of otoliths	(Adams et al., 2012)
TMEM216	Ventral axis curvature, pericardial oedema, hydrocephalus	(Valente et al., 2010)
AHI1	Pronephric cysts, ventral axis curvature, pericardial oedema, hydrocephalus, laterality defects, fewer/loss of cilia in KV, abnormal eye development, altered number of otoliths	(Simms et al., 2012)
ARL13B	Pronephric cysts, ventral axis curvature, laterality defects, fewer cilia in KV and the pronephros	(Duldulao et al., 2009)
CC2D2A	Pronephric cysts, dorsal axis curvature	(Gorden et al., 2008)
OFD1	Axis curvature, pericardial oedema, hydrocephalus, laterality defects, shorter cilia in KV	(Ferrante et al., 2009)

Table 1.9 Zebrafish models of human cystic kidney disease and related ciliopathies
Zebrafish models for: autosomal dominant polycystic kidney disease (ADPKD, blue shading); renal cysts and diabetes (RCAD, orange shading); nephronophthisis (NPHP, green shading); Joubert syndrome (JBTS, pink shading); KV, Kupffer's vesicle. Modified from (Swanhart et al., 2011).

Frequently, cystic kidney disease and aberrant left-right body patterning are co-features, leading to interest in evaluating the ciliated zebrafish organ of laterality, KV. KV arises from dorsal forerunner cells in the tailbud (Essner et al., 2002) and is transiently present between 12-16hpf (8-14 somites), however it regresses with time (Kimmel et al., 1995). Cilia located within KV beat in a counterclockwise pattern to generate leftward fluid and control the left-right development of the brain, heart and gut (as discussed in section 1.10) (Essner et al., 2005).

Understanding the potential mechanisms of cystogenesis can be studied in zebrafish and many cystic mutants have been found to have impaired cell polarity with mislocalisation of $Na^{+}K^{+}$ ATPase channels leading to defective osmoregulation (Drummond et al., 1998).

1.21 Aims of this research

Inherited cystic kidney disease and related ciliopathies encompass a heterogeneous group of monogenic disorders with a curious spectrum of severity. Causal genes continue to be identified and are associated with abnormal structure or signalling mediated by primary cilia. It is evident that many of the ciliopathy proteins interact and even function as protein networks (Sang et al., 2011). However studying the effects of mutations in genes, particularly more than one gene, *in vivo* can be limited by embryonic lethality, the latter can be a problem with mouse models. An advantage of zebrafish as a model organism is the ability to study genetic interactions to evaluate complex disease phenotypes.

We hypothesise that the clinical heterogeneity of cystic kidney disease related ciliopathies is not simply influenced by the gene locus or nature of mutation. Triallelism or oligogenic inheritance will modify the development of particular phenotypes, which will alter prognosis. Since the encoded proteins of the cystic kidney disease related causal genes are located on the primary cilium and basal body complex, changes in primary cilia will be evident.

The frequently associated phenotype of cystic kidney disease links the increasingly severe ciliopathies of NPHP, JBTS and MKS. The aim of this work was to evaluate the influence on phenotype following targeted single and combined knockdown of selected genes. Where possible, this included identifying any association between the development of a phenotype and changes in cilia. Four key causal genes have been chosen to study because of their recognised role in inducing all or two of the ciliopathy spectrum NPHP-JBTS-MKS.

AHI1 was the initial focus of study, Chapter 3, because: it is the leading cause of JBTS, in the middle of the range of severity of ciliopathy conditions; its role has not previously been reported in zebrafish; oligogenicity has been reported in patients with mutations in *AHI1* and *NPHP6*.

In Chapter 4, the aim was to create zebrafish models of three other cystic kidney disease related ciliopathy genes, *CC2D2A*, *NPHP6* and *MKS3*, to individually evaluate the associated phenotypes. To study *CC2D2A*, both a spontaneous zebrafish mutant and morphant were created. Generation of the *NPHP6* zebrafish model was principally to

enable later combined genetic studies with *AHI1* and *CC2D2A*, however an additional aim was to characterise cilia in developing morphants. *MKS3* morphants were created to assess development of the severe end of the ciliopathy spectrum.

Finally, in Chapter 5, the aim was to evaluate oligogenicity in cystic kidney disease related ciliopathies by studying the phenotypes of zebrafish embryos after combined interference with: *nphp6* and *cc2d2a*; *ahi1* and *cc2d2a*; *ahi1* and *nphp6*. When assessing the effect of oligogenicity with *cc2d2a*, both MO knockdown and a *cc2d2a* spontaneous mutant zebrafish model were used.

Chapter 2 Materials and Methods

2.1 Bioinformatics

Various online bioinformatic databases were utilised to identify and compare the human and zebrafish genomes. The Vertebrate Online Annotation database (http://vega.sanger.ac.uk) enabled identification and review of the evidence for nucleotide and amino acid transcipts. The SMART (Simple Modular Architecture Research Tool, http://smart.embl-heidelberg.de) domain was used to provide information regarding the identity and function of components of the proteins. Alignment software was used to evaluate the degree of evolutionary conservation of genes of interest.

2.2 Zebrafish lines and husbandry

Wild type AB[1] or *golden* (homozygous pigmentation mutant useful for developmental studies and in situ hybridisation) (C Nusslein-Volhard, 2002) zebrafish were utilised in most experiments. Additional strains used were:

*claudin-b:*Lyn-GFP: this transgenic line express GFP at epithelial tight junctions (Haas and Gilmour, 2006; Lopez-Schier et al., 2004), with strong expression in the posterior lateral line, telencephalon, otic placode and pronephros. The aim was to facilitate study of the pronephros. This line were a kind gift from Dr S. Burtey.

sentinel: this line have a spontaneous nonsense mutation in *cc2d2a*, the only zebrafish ortholog of *CC2D2A*, a ciliopathy gene known to cause JBTS and related ciliopathies (Gorden et al., 2008). This line were a kind gift from Dan Doherty's laboratory, Washington.

*sentinel:claudin-b:*Lyn-GFP: this transgenic line were created in our laboratory by crossing *sentinel* and *claudin-b:*Lyn-GFP heterozygotes and screening the embryos for GFP expression and *sentinel* phenotype. The purpose of this line was to facilitate study of the pronephros when evaluating combined gene interference to study oligogenicity.

*cmcl2:*GFP: this transgenic line express GFP specifically and intensely in cardiac cells (Huang et al., 2003), highlighting the heart which was useful for assessing left-right

[1] An established wild type line of zebrafish.

patterning and asymmetry during development. This line was kindly loaned by Dr Bill Chaudhry.

2.2.1 Zebrafish maintenance

All zebrafish lines were maintained in our laboratory in standards according to the UK Home Office license regulations. The zebrafish laboratory technician follows guidelines with regards to appropriate breeding to enable maintenace of wild type and mutant stocks which are genotyped for confirmation (C Nusslein-Volhard, 2002). Although as in other vertebrate models such as mice, the genetic background can influence the development of a phenotype, reports of this occurring in zebrafish are rare (Sanders and Whitlock, 2003). This is possibly because of the emphasis on maintaining 'closed, inbred' zebrafish lines and monitoring for the development of lethal mutations which would interfere with analysis of offspring embryos (C Nusslein-Volhard, 2002).

The zebrafish laboratory facilities must be carefully regulated including: water supply, temperature, illumination, cleaning and feeding to maintain the wellbeing and fecundity of the zebrafish (C Nusslein-Volhard, 2002). In our laboratory, the water quality was checked daily in terms of temperature, pH (<6 and >8 is associated with toxicity (C Nusslein-Volhard, 2002)) and conductivity. On a weekly basis, the water was tested for nitrate, nitrites, chlorine and general hardness using Tetra Aquarium 6 in 1 test strips (D Burns, former Zebrafish Technician, personal communication).

2.3 Zebrafish Morpholino Experiments

2.3.1 Overview

All zebrafish MO experiments were performed with the aim of characterising the effect of knockdown of a gene on the subsequent development, focusing on structural and functional changes. Whilst pronephric development was the key focus, extra-renal organs, particularly the brain and eye were evaluated in the context of cystic kidney disease related ciliopathies.

2.3.2 MO Design and preparation

MO were designed with guidance from Gene Tools, www.gene-tools.com, to interfere with mRNA translation or splicing, leading to knockdown of the expression of a specific gene. Usually both splice and translation blocking antisense MOs were

designed to facilitate determining specificity of gene knockdown (discussed in section 1.18). Control MOs were also utilised as recommended (Eisen and Smith, 2008) including a standard control MO (designed by Gene Tools as a negative control, it targets a human beta-globin intron mutation that causes beta-thalessemia and is not known to create any other phenotypes) and a *p53* MO to exclude off-target effects (described in section 1.18). Table 2.1 lists the genes targeted and MO sequences.

Gene	Antisense MO Name	Antisense sequence (5'-…-3')
ahi1	*ahi1*_ie_exon 8 (splice)	CCACACTCTGAAAGGGAAAAACATT
ahi1	*ahi1*_5UTR (translation)	GAGTCATTAGCAGCTTTGTTTTTCC
cc2d2a	*cc2d2a*_ie_exon 14 (splice)	CTTCGTCTGCATAGCCGTACCTGTT
nphp6	*nphp6*_ATG (translation)	AGGCATTCTTCAGGTCAGCTGCAAA
nphp6	*nphp6*_ei_exon 42 (splice)	TGAAAAGTTGCACCTACAGAGGGTC
mks3	*mks3*_ei_exon 4 (splice)	GTAAAAATGACAAGCGCCTACCCAG
	Standard Control	CCTCTTACCTCAGTTACAATTTATA
p53	*p53*	GCGCCATTGCTTTGCAAGAATTG

Table 2.1 Gene targeted and antisense morpholino oligonucleotide sequence

For each MO, in order to determine the optimal MO concentration to create a phenotype without inducing off-target effects or excess mortality, a volume of each stock MO was diluted in varying concentrations of a buffer (danieau solution (58mM NaCl, 0.7mM KCl, 0.4mM $MgSO_4$, 0.6mM $Ca(NO_3)_2$, 5mM HEPES, pH 7.1-7.3) (C Nusslein-Volhard, 2002) and 0.1% phenol red, the latter enables clear visualisation of the solution during injection). This enabled a range of doses of each individual MO to be injected into embryos, to generate a dose concentration curve. These imperative initial experiments were performed at least in triplicate and carefully analysed for phenotypes to enable determination of the optimal MO concentration to utilise in subsequent experiments.

2.3.3 MO injections of zebrafish embryos

Male and female zebrafish adults were placed in breeding tanks separated by a divider, to acclimatise, the evening prior to a planned experiment. The following morning the divider was removed and mating commenced. MO injections were performed in freshly delivered embryos, which were aligned against a microscope slide and injected at the 1-4 cell stage (Figure 2.1).

In advance, needles were pulled from glass capillary tubes using a Micropipette Puller (P-97, Sutter Instruments). Needles were loaded with approximately 4µl of MO containing solution (as described above), to enable numerous injections and direct visualisation of injection delivery. The needle tips were manipulated using precision watchmaker's forceps, to enable injection of a recommended volume of approximately 500-750pL (Rosen, 2009). The approximate volume of injection was assessed by injecting a drop onto a droplet of oil positioned on a micrometer glass slide to confirm the diameter measured 0.1-0.15mm. The volume of injection was determined using the formula: $4/3\pi r^3$, where r is the radius, equivalent to half the diameter.

Following MO injection using an Eppendorf Femtojet microinjector (Eppendorf), embryos were maintained in E2 media (Appendix A) (C Nusslein-Volhard, 2002), with or without 0.003% 1-phenyl-2-thiourea (PTU, Sigma) to suppress pigmentation, this prolongs the transparency of embryos (Westerfield, 1995). The time of delivery of each clutch of embryos was recorded and petri dishes of time-matched uninjected embryos

were also maintained in E2 media, as controls. Thereafter embryos were incubated at 28.5°C and staged by counting somites and hours post fertilisation.

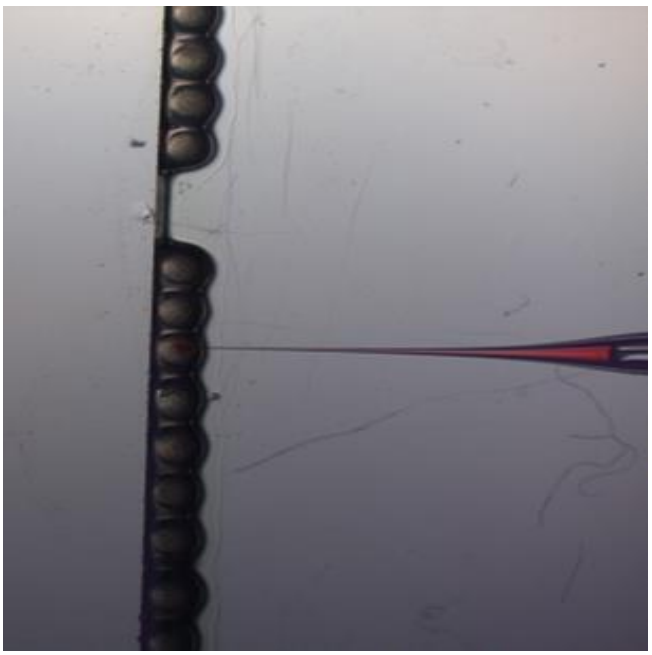

Figure 2.1 Alignment of zebrafish embryos for microinjection
Using a microscope slide, 1-2 cell stage zebrafish embryos were aligned and microinjected. The injected solution contains 0.1% phenol red dye to enable direct visualisation of delivery of morpholino oligonucleotide.

2.3.4 mRNA Rescue

Rescue experiments were performed to further confirm specificity of a MO knockdown by co-injecting 'gene relevant' RNA from a different species (Eisen and Smith, 2008). For example, for *ahi1* morphants, rescue experiments involved co-injecting *ahi1* MO with in vitro transcribed mouse *Ahi1* mRNA (mMessage Machine, Ambion). For *mks3* morphants, phenotypic rescue was performed by co-injecting *mks3* MO with capped human *MKS3* mRNA (a kind gift from Dr John Sayer).

For all rescue experiments, to ascertain an appropriate dose and to ensure there were no overexpression phenotypes a range of doses (50-200pg) of the mouse *Ahi1* or human *MKS3* mRNA were injected into zebrafish embryos.

2.3.5 Mortality assessments

Approximately 4-6 hours post MO injection, all petri dishes of uninjected control and MO injected embryos were reviewed under light microscopy using a stereomicroscope (Leica MZ16 F). All dying or deceased embryos were removed and petri dishes replaced in incubators at 28.5ºC. Petri dishes of embryos were again reviewed at 24, 48 and 72hpf to record mortality and remove any deceased embryos. All mortality data were recorded on data sheets (Appendix B). Where necessary, embryos were transferred to fresh petri dishes or E2 media was replaced.

The maximal duration of any experiment was 5 days, when embryos were euthanised by immersing in a 4mg/ml solution of Tricaine (ethyl-m-aminobenzoate methanesulphonate). The Tricaine solution was prepared by technicians from the zebrafish laboratory, who dissolved 4g of ethyl-m-aminobenzoate methanesulphonate powder in 1L of ddH_2O (double distilled water) and added sodium hydroxide (as required) to achieve a pH of 7.0. The Tricaine solution was stored at 4ºC.

2.3.6 Phenotyping by light microscopy

In order to phenotype zebrafish embryos, they were transferred into a fresh petri dish containing a few drops of 4mg/ml Tricaine, to anaesthetise. To characterise the development of embryos and potential interference by a gene of interest (using MO knockdown), embryos were studied at various time points using a stereomicroscope with a camera (Leica, MZ16F) attached, enabling images to be recorded. Both the

normal developmental phenotype of time matched, uninjected, wild type (WT) control embryos were reviewed in real time and sketches of the normal stages of zebrafish embryonic development were referenced (Kimmel et al., 1995).

Kupffer's vesicle (KV) was reviewed, or fixed for later experiments, at 13-14hpf (8-10 somites, Figure 2.2) because of the optimal size and for consistency of reporting.

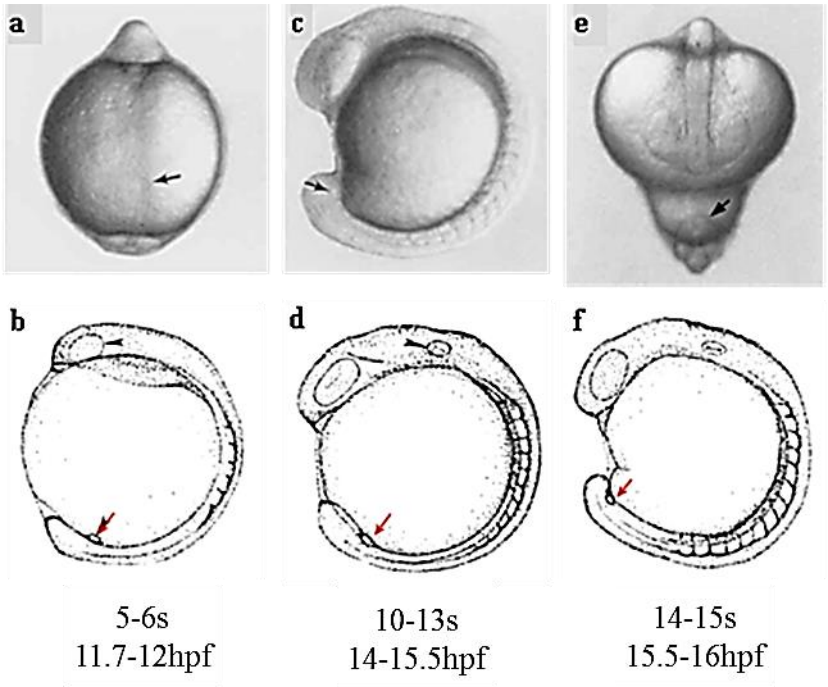

Figure 2.2 Localisation of KV in developing zebrafish embryos
Light microscopy views (**a**, **c**, **e**, arrows) and sketches (**b**, **d**, **f**, lateral view, red arrows) of zebrafish embryos highlighting the localisation of KV in paired dorsal/lateral views (where feasible) significantly facilitated identification of KV in experiments. Modified from Figures 1 and 15 from (Kimmel et al., 1995).

Embryos of or older than 24hpf were dechorionated (using precision foreceps) in order to clearly visualise their features. The other major time points evaluated were: 48 and 72hpf. Often, to carefully follow the development of particular embryos over several days, they were placed in individual wells of 24 multiwell culture plates (Sigma-Aldrich). All observations regarding the appearance of embryos were recorded on a phenotype scoring sheet (Appendix C). Initially, in addition to identifying individual dysmorphic features, embryos were classified as normal, mild, moderate or severe. This grading system was determined by subjectively assessing each dysmorphic feature, with the most marked/severe individual anomaly determining the overall classification, rather than utilising a summative score. The intention was to obtain information regarding the extent of dysmorphology, to identify if this was similar to the variable spectrum of disease seen in patients with NPHP, JBTS and related disorders. However on assessing the reproducibility of this severity classification, by reviewing images of zebrafish, rescoring them and comparing the results to those originally recorded on spreadsheets at the time of the experiment and capture of the image, showed that there was more than acceptable variability in severity scores. This led to the severity score being abandoned in further experiments and not being analysed.

To assess cardiac looping (Appendix D), embryos were reviewed between 48-56hpf (Ahmad et al., 2004) and when *cmcl2:*GFP transgenic embryos were being studied, the fluorescent camera (Leica, MZ16F) was utilised to record images.

The brain phenotype of hydrocephalus was assessed by light microscopy and resin embedding with sectioning as described in section 2.8. Although magnetic resonance histology has been utilised in zebrafish (Ullmann et al., 2010) to create a three dimensional atlas of the zebrafish brain and may have enabled evaluation of an equivalent Molar Tooth Sign, diagnostic of Joubert Syndrome, this was not performed herein. Initially videos were taken to evaluate whether morphant zebrafish embryos could be having seizures, these observations were not particularly frequent and were therefore not further evaluated by performing an electroencephalogram (Pineda et al., 2011).

An assessment of kidney function was attempted to determine whether this may be abnormal and provide an alternative or additional read out from pronephric cysts, incase identification of the latter were being missed. Embryos were anaesthetised in 4mg/ml

Tricaine and aligned, ventral side up, against a microscope slide and perpendicular cover slip in minimal Tricaine/E2 water. Microinjection of a small volume of 10kDa rhodamine labelled dextran (Invitrogen) was performed into the pericardium of wild type embryos at 48 and 72hpf with the intent of optimising a protocol. Embryos were then maintained in E2 water at 28.5°C to be reviewed at 24 and 48 hours post injection and photographed using a fluorescent microscope (Leica, MZ16F). Although mortality rates as a consequence of the pericardial injection were acceptable, no reliable fluorescent signal was detected in the embryos. These preliminary experiments were performed at an early stage of working with zebrafish and fluorescent microscopy skills were likely inadequate, in particular the ability to attempt to quantify the intensity of detected fluorescence. Clearly following publication of methods by others who had successfully performed this assay of kidney function (Tobin and Beales, 2008), it would have been important to review embryos a few hours following injection. This interesting area was not further pursued because of the generation of more fruitful results in various other experimental pathways at that time.

2.3.7 Mounting and imaging zebrafish embryos

For imaging KV following immunofluorescence, embryos were placed on either: a single well concavity slide (VWR) which was subsequently inverted and imaged through the coverslip (VWR); or placed in a glass based six well tissue culture plates (Iwaki, www.well.ox.ac.uk/cytogenetics/downloads/Iwaki.pdfref) which could be imaged through directly. Embryos were placed in Vectashield hardset mounting medium with DAPI (4',6-diamidino-2-phenylindole, which stains nuclei, Vector Labs) and positioned to enable imaging through the dorsal side. If the concavity slides were used, a coverslip was applied and nail varnish utilised to maintain adherence. The ability to image KV herein was similar regardless of whether imaging whole mount embryos or following dissection and removal of the yolk sac. All embryos were stored in the dark at 4ºC until imaged. Whole mount imaging of 48-72hpf embryos following immunofluorescence was performed as above.

For light microscopy imaging of live or fixed embryos of 24-72hpf, embryos were placed in a petri dish in a small volume of E2 water (± Tricaine for anaesthetic effect) or 3% methylcellulose, the latter particularly if they had a curly tail or imaging of cardiac looping was being performed. 3% methylcellulose was made by dissolving 3g

methylcellulose (M0387, Sigma) in 100ml ddH_2O, dispensed into eppendorfs and stored at -20ºC until used. When mounting embryos, the 3% methylcellulose was defrosted and maintained on ice on the bench or at 4ºC. After considerable trial and error of various different methods of imaging and mounting embryos during this research, a methodology paper was subsequently published which proved insightful (Jaffe et al., 2010).

2.4 Zebrafish RNA isolation and RT-PCR

2.4.1 Overview

Uninjected WT 'control' embryos or embryos following MO injection were reviewed using light microscopy, dechorionated using precision watchmaker's forceps and fixed prior to RNA isolation. This procedure was performed for embryos individually and in groups of 20-30. RNA isolation using a standard Trizol protocol was repeated at various time points including 12, 24 and 72 hpf. RNA concentrations were determined using a Nanodrop Spectrophotometer (ND-800, Labtech) and equal concentrations of RNA were incorporated into RT-PCR reactions. Agarose gel electrophoresis (see section 2.4.7) was performed and gels visualised under ultraviolet (UV) light using a Geldoc camera to determine the size of bands.

2.4.2 Fixation for RNA isolation from zebrafish embryos

Selected individual embryos were placed in a petri dish containing phosphate-buffered saline (PBS) and a few drops of 4mg/ml Tricaine for 1min to euthanise. Embryos were then washed in PBS, transferred to individual universal containers in minimal PBS and transported to the main laboratory on ice. Embryos were either stored at -20ºC or RNA was isolated from them (see sections 2.4.3, 2.4.4). It is important to avoid 4% paraformaldehyde (PFA) when fixing zebrafish specimens for RNA isolation as this prevents Trizol from being able to penetrate and separate samples.

2.4.3 Tissue homogenisation

In a fumehood, 1ml of Trizol (Invitrogen) was added to a universal container containing a single, fixed zebrafish embryo. A TissueRuptor (Qiagen) was then used to homogenise tissue. The 1ml sample was transferred into a screw top eppendorf to proceed with RNA isolation.

2.4.4 RNA Isolation

The 1ml Trizol/homogenised zebrafish solution was centrifuged at 12,000G for 10mins at 2-8ºC in a microcentrifuge (Eppendorf 5415D**)**. This separates the insoluble material from the supernatant, which contains RNA and can be aspirated into a fresh screw top eppendorf, to incubate for 5mins at room temperature. 0.2ml of chloroform was then added to the supernatant, the screw tap tightly applied and the eppendorf shaken manually for 15s then incubated at room temperature for 2.5mins. The chloroform-supernatant solution was further centrifuged at 12,000G for 15mins at 2-8ºC, this resulted in separation of the mixture into three phases. Theoretically, RNA is present in the colourless upper aqueous phase and should have a volume of two thirds of the chloroform-supernatant solution. Therefore approximately 600µl of supernatant (which should contain RNA) was carefully aspirated into a fresh eppendorf. The RNA was precipitated by adding 0.5ml isopropyl alcohol and incubated at room temperature for 10mins, then centrifuged at 12,000G for 10mins at 2-8ºC. This resulted in a pellet of RNA forming at the bottom edge of the eppendorf, bathed in supernatant, which was aspirated and discarded. The RNA pellet was washed and vortexed in 1ml of 75% ethanol, then centrifuged at 7,500G for 5mins at 2-8ºC. The remaining ethanol was removed and the RNA pellet air dried at room temperature for 5-10mins. The RNA pellet was resuspended in 10µl of RNAse free water and incubated at 57.5ºC for 10mins to dissolve.

2.4.5 Determining RNA concentration

After appropriately calibrating the Nanodrop Spectrophotometer (ND-800, Labtech), the concentration (ng/µl) of RNA isolated was quantified using 1µl of RNA. RNA stocks were then stored in individual eppendorfs at -20ºC.

2.4.6 RT-PCR protocol

All reactions were performed in PCR multiwell plates (Sigma) and prepared on ice. Equal concentrations of RNA were used in each experimental group for RT-PCR reactions by diluting with RNAse free water where necessary. For the reverse transcription reaction, a Superscript VILO cDNA synthesis kit (Invitrogen) was used, with a 10µl reaction volume: 2µl chosen RNA, 2µl VILOx5 mix (random primers, magnesium chloride ($MgCl_2$), and deoxyribonucleotide triphosphates (dNTPs, which

are essential for building cDNA)), 1µl 10xSuperScript (reverse transcriptase) enzyme mix and 5µl RNAse free H_2O. A ddH_2O sample was also run as a control and in parallel, a further control reaction was run in which no 10xSuperScript (reverse transcriptase) enzyme mix was included. The following conditions were set: 25°C for 10mins, 42°C for 60mins, 85°C for 5mins. Samples were then stored at 4°C or on ice whilst the PCR reaction was being prepared, or alternatively at -20°C if PCR was deferred to the following day.

For PCR reactions, a Taq PCR Master Mix kit (Qiagen) and Peltier Thermal Cycler were used. A 20 µl reaction volume included: 2µl cDNA (from reverse transcription reaction above), 1µl 10µM forward primer, 1µl 10µM reverse primer, 10µl Taq PCR Master Mix (DNA Polymerase enzyme, $MgCl_2$, PCR Buffer and dNTPs), 6µl RNAse free H_2O. An online program, Primer3 (www.ncbi.nlm.nih.gov/tools/primer-blast/) was used to facilitate design of specific primers and provided relevant primer melting temperatures and the predicted PCR product size. For each gene, specific primer pairs, annealing temperatures and PCR cycles were used as shown in Table 2.2. Samples were then stored at 4°C, on ice, or alternatively at -20°C until an agarose gel electrophoresis was performed (see section 2.4.7).

Gene	Primer sequence (5'-…-3')	Annealing Temp.	PCR cycles
ahi1	F: GAGGTCAGATGGGCTGTTTT	55°C	35
ahi1	R: AGACCCAGGCATAACTTCG		
cc2d2a	F: CCCGTCTCGCTCAACTGTAT	56°C	35
cc2d2a	R: GTTGGGCTTCTCTGGTTCCT		
nphp6	F: TGGAGCAGGAGAAGGTGAGT	55°C	30
nphp6	R: GGGATGGGGTATCAGAACCT		
mks3	F: GAGCCTGTCTTGCGTGAAAT	54°C	30
mks3	R: CCGCAAACACAAGACTGAGA		

Table 2.2 Zebrafish gene specific primer pairs and PCR information
Forward and reverse primer pair sequences for the zebrafish genes. Oligonucleotide primers were ordered from Integrated DNA Technologies (http://eu.idtdna.com/site). The annealing temperature and number of PCR cycles used are shown for each primer pair.

2.4.7 Agarose gel electrophoresis

RT-PCR products were run on 1 to 2% agarose gels (depending on the predicted size of products), prepared by dissolving 1-2g of agarose (Sigma) in approximately 100ml of 1 x TAE buffer (Appendix E) in a conical flask, heated in a microwave on full power for 2-3mins. Meanwhile, an appropriately sized gel tray and comb were prepared. The conical flask containing hot agarose solution was placed in cool water for approximately 10s prior to adding 100µl GelRed (Biotium) and mixing, this enables PCR samples to fluoresce. The agarose gel was then poured into a gel tray with a comb in situ and allowed to set at room temperature for 15-30mins.

When solid, the comb was removed and agarose gel immersed in a tank of 1xTAE buffer. Samples to be run on the gel were prepared in a multiwell plate and consisted of 3µl of 6 x loading dye added to 5µl of each RT-PCR product. A standard 100bp DNA ladder (Biolabs) was used to size products and gels run at 100-120 volts. Images of gels were captured using a Geldoc Camera (http://uvp.com/geldocit.html）.

2.4.8 Excision of RT-PCR bands and PCR clean-up

To extract a band of interest from an agarose gel, the gel was positioned on top of a UV transilluminator. A scalpel was used to cut around the edges of the band, with as minimal excess gel as possible. Safety eye wear and a face shield must be worn when using the UV transilluminator. The band was placed in an eppendorf of known weight and subsequently weighed, to enable calculation of the weight of the gel containing the band. A gel volume of 100mg is equivalent to 100µl, this theory is important and enables determination of the appropriate volumes of solutions to be used during subsequent gel extraction and purification. A Gel extraction and purification kit (Qiagen) and protocol were used (page 25 (Qiagen, 2008)) to extract cDNA from the gel band. Three volumes of QG buffer (which contains a pH indicator, if yellow indicates the pH < 7.5) were added to the gel volume and incubated at 50°C for up to 10mins, until the gel had dissolved. The dissolved gel mixture should be a yellow colour, which suggests the pH is appropriately <7.5, otherwise it must be acidified by adding 3M sodium acetate (included in Qiagen kit). To increase the DNA yield of smaller DNA fragments (<500bp), the Qiagen protocol recommended adding 1 gel volume of isopropanol to the gel mixture (Qiagen, 2008). A QIAquick spin column was

placed in a collection tube and then filled with the gel mixture, prior to being centrifuged at room temperature for 1min using a microcentrofuge (Eppendorf 5415D). The liquid which filtered through and gathered in the collection tube was disposed of then another 0.5ml buffer QG was added to the spin column and centrifuged for a further 1min. To wash the sample, 0.75ml buffer PE was added to the spin column and incubated at room temperature for 2-5mins, prior to a 1min centrifuge. The fluid which filtered through was again discarded and a further 1min centrifuge performed. The QIAquick spin column was transferred into a fresh microcentrifuge tube, 30µl RNAse free water was added and the sample incubated for 2mins before a final 1 min centrifuge. The cDNA sample should be stored at -20°C.

For direct sequencing (MWG Eurofins), in separate microcentrifuge tubes: 10µl of cDNA sample was premixed with 1µl of 10pmol/ml of relevant forward oligonucleotide primer; a further 10µl of cDNA sample was premixed with 1µl of 10pmol/ml of relevant reverse oligonucleotide primer. The quality of the sequenced data was reviewed by assessing the relevant chromatogram. Subsequently, the sequenced data was identified by pasting it into a programme called BLAT (http://genome.ucsc.edu/cgi-bin/hgBlat?command=start), which mapped the sequence within the genome.

2.5 *Sentinel* Genotyping, Sequencing and Rapamycin therapy

2.5.1 Overview

Sequencing of the *sentinel* mutant zebrafish genomic DNA identified a spontaneous nonsense mutation (G>A) in exon 14 of *cc2d2a*, resulting in a premature stop codon rather than a tryptophan at amino acid position 491 (Owens et al., 2008). In order to confirm the genotype of *sentinel* embryos, PCR using specific dCAP (derived Cleaved Amplified Polymorphic Sequence) primers was required. This technique introduces a restriction enzyme site into WT embryos and following a restriction enzyme digest it was evident that WT embryos have a smaller product (128bp), compared with *sentinel* embryos (156bp), in which the DNA was not cut (Gorden et al., 2008). Appropriate controls must be used with each experiment including WT embryos with and without the addition of the restriction enzyme. Since the *sentinel* mutant zebrafish were predicted to develop pronephric cysts in up to 33% (Gorden et al., 2008), treatment of embryos with Rapamycin (Sigma) was attempted.

2.5.2 *Sentinel* Genotyping

At 72hpf, suspected *sentinel* morphants (10-20 embryos) identified by their characteristic sine wave shaped tail were euthanised in 4mg/ml Tricaine for a few minutes. The Tricaine was removed and they were bathed in PBS and transported to the main laboratory on ice. Embryos were transferred into a cone shaped eppendorf and 60µl of sodium hydroxide (25mM)/ethylenediaminetetraacetic acid (EDTA, 0.2mM) was added. Embryos were placed in a thermomixer at 95°C for 45mins. Subsequently 60µl of 40mM Tris/HCl was added to the embryo mixture and vortexed for 60s. The DNA must be stored at -20°C unless progressing immediately onto PCR with dCAP primers.

The 20µl PCR reaction included: 2µl DNA, 10µl Taq PCR Master Mix (Qiagen, DNA Polymerase enzyme, $MgCl_2$, PCR Buffer and dNTPs), 1µl forward (5'-TAGCCGTACCTGTTTTCTTTTCCAGGATAT-3') oligonucleotide primer, 1µl reverse (5'-GAGAGACTGCAGGACGAGCAGGA-3') oligonucleotide primer and 6µl RNAse free water. PCR conditions included an annealing temperature of 61°C and 30 cycles. To confirm adequate extraction of DNA and of the expected size (156bp), gel electrophoresis and imaging (as in section 2.3.7) was performed.

The 20µl restriction enzyme digest reaction included: 5µl PCR DNA, 0.2µl restriction enzyme (EcoRV), 2µl restriction enzyme buffer 3, 0.2µl bovine serum albumin (1mg/ml BSA) and 12.6µl RNAse free water. The restriction enzyme/PCR DNA mix was incubated at 37°C for a minimum of 4 hrs. Subsequently, the products were run on a 2% agarose gel (prepared as in section 2.4.7), *sentinel* embryos were confirmed as those measuring 156bp, in which the restriction enzyme did not cut the DNA.

2.5.3 Rapamycin treatment

Rapamycin (Sigma) powder was dissolved in 1% DMSO (dimethyl sulfoxide) and diluted in E2 media, to prepare treatment solutions of 0.1µM and 0.05µM. Embryos from 3 pairs of *golden* zebrafish were collected to form a control group and 3 pairs of *sentinel* zebrafish. There were four treatment arms based on the different media which embryos were bathed in: E2 (standard incubation media), 0.05% DMSO/E2 (drug vehicle), 0.05µM Rapamycin/0.05% DMSO (Rapa B) or 0.1µM Rapamycin/0.05% DMSO (Rapa A). 40-100 *golden* and *sentinel* embryos from 2 different pairs were

bathed in each of the above solutions and incubated at 28.5ºC. Both *golden* and *sentinel* embryos from the 3rd mating pairs were maintained in E2 media for the first 24hpf, then separated into groups to be bathed in the drug vehicle or Rapamycin treatments from 24-48hpf, to assess the effect of delaying the onset of exposure to treatment. The experiment protocol is shown as a flow chart in Figure 2.3. Each media was removed and replaced every 24 hours to maintain continuous exposure. Mortality assessments and determination of phenotypes/side effects were performed as above (see sections 2.3.5-2.3.6).

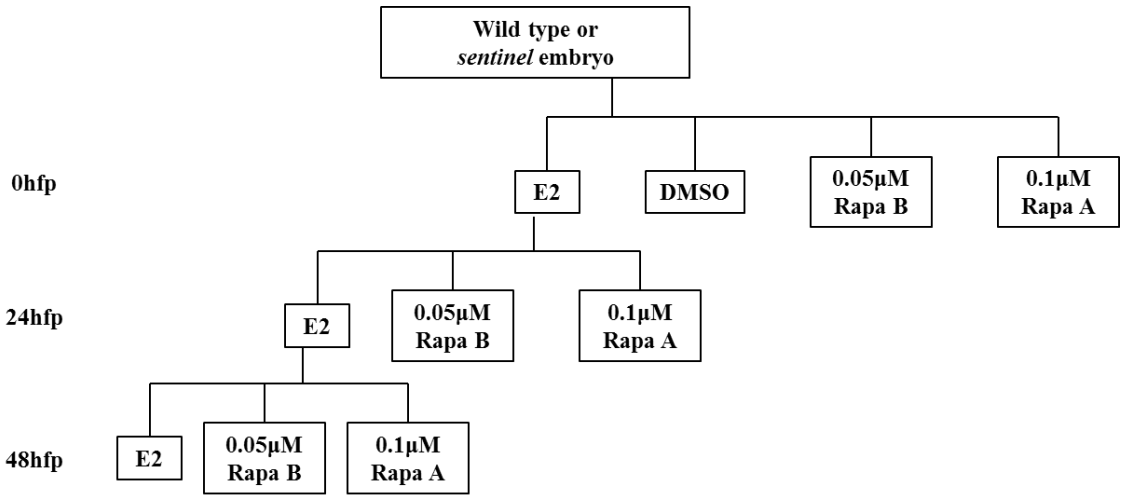

Figure 2.3 Protocol for Rapamycin treatment trial in zebrafish embryos
Following birth wild type and *sentinel* embryos were divided into 4 different treatment groups: E2 (standard incubation media), 0.05% DMSO (dimethyl sulfoxide, the drug vehicle), 0.05µM Rapamycin/0.05% DMSO (Rapa B), 0.1µM Rapamycin/0.05% DMSO (Rapa A). The treatment solutions were replaced with fresh solution every 24hrs. To assess the effect of exposure to treatment at different stages of development, additional embryos which had been maintained in E2 media from birth were exposed to the Rapamycin therapies from 24 and 48hpf. Mortality and phenotypes were assessed using standard methods. hrs, hours; Rapa, Rapamycin.

2.6 *In situ* hybridisation

2.6.1 Overview

In order to define the expression of *ahi1* during zebrafish development, clusters of uninjected WT *golden* embryos were fixed at various time points and a typical *in situ* hybridisation protocol (Thisse and Thisse, 2008) performed. Additionally, to facilitate localisation of KV in WT and following *ahi1* MO injection, a *charon* riboprobe (a kind gift from Dr Hibi) was used. Embryos were mounted in 3% methylcellulose or PBS media and images captured using a stereomicroscope (Leica, MZ16F) or axioplan microscope (Axiocam HRC, Zeiss). Embryos were stored in PBT (phosphate buffered saline/0.1% Tween-20) in the dark at 4°C.

2.6.2 Embryo fixation and preparation for *in situ* hybridisation

Only *golden* embryos were used for *in situ* hybridisation as these have minimal pigment and avoid the need to bleach embryos. Embryos of greater or equal to 24hpf must be dechorionated prior to fixation. Embryos of 8-10 somites (for KV), can be dechorionated following fixation. After selection of embryos, they were incubated in 4% PFA at 4°C overnight. Subsequently, in a fumehood, PFA was removed and embryos were washed in PBS for 5 mins (twice). A dehydration series was then performed, involving 5min washes in 25%, 50%, 75% methanol in ddH_2O, up to 100% methanol (for at least 2 hours). Embryos were stored at -20°C or progressed onto the *in situ* hybridisation protocol.

2.6.3 Preparation of *in situ* hybridisation probes

To generate an *ahi1* template to make riboprobes, PCR (35 cycles, annealing temperature 55°C) was performed using genomic zebrafish DNA and *ahi1* specific oligonucleotide primer pairs: forward (5'-TCATTCGTGTACTGTGCCAAG-3') and reverse (5'-CAACCTGGTCACCTGTCTCA-3'). This generated a 544bp *ahi1* PCR fragment which was cloned into a pGEM-T Easy vector (Promega), with T7 and SP6 promoters on either side, which facilitated production of sense and antisense transcripts respectively. To linearize the vector containing the *ahi1* template, a restriction enzyme digest using EcoRV was performed at 37°C for 2 hours. A Digoxigenin (DIG)-labelled UTP (Roche Diagnostics) is incorporated into the following reaction to label the probe:

1µg cDNA template (use the concentration determined using a Nanodrop Spectrophotometer to calculate the volume), xµl (13µl total volume when combined with cDNA template) RNAse free water, 2µl 10xNTP labelling mix, 2µl transcription buffer, 1µl RNAse inhibitor and 2µl RNA polymerase (a SP6 RNA polymerase is used for the antisense probe and a T7 RNA polymerase to generate the sense (control) probe). The reaction was incubated at 37°C for 2 hours. The DIG labelling reaction was terminated by adding 2µl 0.2M EDTA (pH8).

For extraction of the probe 80µl DEPC treated (diethylpyrocarbonate, RNAse free) Tris EDTA, 10µl 4M lithium chloride (LiCl) and 250µl 100% ice cold ethanol were added and incubated at -80°C for 2 hours. Subsequently the probe mixture was centrifuged at 4°C for 30mins, the probe should be visible as a pellet, the supernatant was removed and discarded. The probe pellet was then air dried at room temperature for 5-10 mins. Finally, 100µl of DEPC treated Tris EDTA and 2µl RNAse inhibitor were added. The quality of the probe was checked by running it on a 1% agarose gel, where two distinct bands representing RNA should be seen. Unfortunately there were no bands visible on the gel in which I had attempted to prepare the *ahi1* probe and since Dr John Sayer had performed the experiment in parallel, he kindly donated his *ahi1* probe.

The antisense *Shh* and *cardiac myosin light chain 2* (*cmcl2*) probes were gratefully received from Dr Nic Child. Sense probes and no probe were used as negative controls.

2.6.4 *In situ* hybridisation protocol

Day 1

All media contained 0.1% DEPC and Tween-20. Embryos must be in 100% methanol to begin and were transferred into flat base eppendorfs, approximately 20 embryos from each group per eppendorf. They were rehydrated by 5min washes at room temperature in: 75% methanol in PBT, 50% methanol in PBT, 25% methanol in PBT and four washes in PBT. Embryos were permeabilised by incubating in Proteinase K (10µg/ml, Roche, a protease which digests and removes unwanted, contaminated proteins during extraction of DNA) in PBT at room temperature. The duration of incubation depends on the age of embryos:

8-10 somites (KV) - 3mins; 24hpf - 15mins; 48hpf - 30mins; 72hpf - 40mins.

The Proteinase K solution was removed and embryos were briefly washed in PBT (3mins) and the permeabilisation reaction ceased by refixing in 4% PFA at room temperature for 20mins.

The PFA was removed and embryos were profusely washed (5 times) for 5mins each, at room temperature. Prehybridisation was performed by incubating embryos in the pre-hyb mix for 2-3 hours at 65°C in a water bath. The pre-hyb mix contains: 50% Formamide, 5 x SCC (3M sodium chloride/0.3M sodium citrate, pH6), 0.1% Tween-20 in DEPC H_20, tRNA (500µg/ml Baker's yeast as a block) and heparin (50µg/ml). In practice it was useful to prepare a stock of prehyb without tRNA and heparin as washes on day 2 do not contain these constituents.

The pre-hyb solution was removed and to perform hybridisation, 5µl of chosen RNA probe (antisense or sense) was added to 300µl of fresh 'prehyb' including tRNA and heparin, and incubated at 65°C in a water bath overnight. As a negative control, no probe was added to 300µl of fresh 'prehyb' including tRNA and heparin, to eppendorfs of appropriately age matched embryos which were also incubated at 65°C in a water bath overnight.

Day 2

A thermomixer set at 65°C was required to maintain a constant temperature during exchange of washes, otherwise embryos were maintained in the water bath at 65°C. No tRNA or heparin was included in the stock prehyb solution which was prepared on day 1.

The hybridisation solution was removed and the following 15min washes at 65°C performed: 75% prehyb/2 x SCC, 50% prehyb/2 x SCC, 25% prehyb/2 x SCC, 2 x SCC; then two 30min washes in 0.2 x SCC.

Further 10min washes at room temperature included: 75% 0.2 x SCC/PBT, 50% 0.2 x SCC/PBT, 25% 0.2 x SCC/PBT and PBT. During the final wash, embryos were transferred to glass beakers (2ml solution per beaker), using separate pipettes to avoid inadvertent mix up of embryos.

Embryos were then incubated in a 1% blocking solution (Roche) in MABT (maleic acid buffer/tween, pH7.5) on a rocker at room temperature for 2-5 hours. Meanwhile, the anti-DIG-AP (alkaline phosphatase) antibody (1:5000, Roche) was dissolved in 1% blocking solution/MABT at 4°C for 1 hour. The blocking solution was removed from the embryos and they were incubated in the prepared anti-DIG antibody/blocking solution on a gentle rocker at 4°C overnight.

Day 3

The antibody/blocking solution was removed and embryos were washed in PBT at room temperature for 15mins, 8 times. Embryos were then stored in PBT at 4°C for 2 days prior to staining.

Day 4

PBT was removed and embryos were washed in NTMT (100mM tri HCl pH9.5, 50mM $MgCl_2$, 100mM NaCl, 0.1% Tween-20) at room temperature for 5mins, 3 times. Embryos were then incubated in staining solution (18µl BCIP/NBT (Roche)/ml NTMT) in the dark and carefully checked at 15min intervals (earlier if the first time a probe was used) using a stereomicroscope. When satisfied with the level of staining, which typically varied depending on the age of embryos, the staining solution was removed and embryos were washed in PBT for 5min, 3 times. Thereafter embryos must be maintained in the dark and preferably at 4°C.

For optimal imaging of embryos, depending on their age, they were mounted in 3% methylcellulose, or small volumes of PBT, in 30mm petri dishes and images were captured using a stereomicroscope (Leica, MZ16F) or axioplan microscope (Axiocam HRC, Zeiss). To further concentrate and enhance the signal, embryos were dehydrated in graduated washes up to 100% methanol, then rehydrated back to PBT and re-imaged. To attempt to tackle the problem of a pigmented yolk sac (a consequence of exposure to light), embryos were washed in BABB (benzyl alcohol, benzyl benzoate 1:2), which increases the overall transparency of embryos, however in practice, this solution was difficult to work with effectively. The staining protocol could be repeated if imaging was suboptimal, by washing embryos back to NTMT, providing they had not already been refixed in 4% PFA.

2.7 Wholemount Immunohistochemistry

2.7.1 Overview

In order to evaluate cilia at various stages of development, embryos (both uninjected WT controls and following MO injection) were fixed at various time points. In particular, cilia were studied in the developmental organ of laterality, KV and in the pronephros. A standard immunofluorescence protocol was performed using antibodies to detect cilia, centrosomes or the apical epithelium of KV. Embryos were mounted and imaged using confocal microscopy (LSM 510Meta, Zeiss and A1R Confocal, Nikon).

2.7.2 Selection of embryos and fixation for Immunofluorescence

*Claudin-b:*Lyn-GFP transgenic zebrafish embryos were predominantly used in experiments for immunofluorescence, as the *claudin-b* is expressed at epithelial cell junctions of KV and the pronephros. When double antibody staining was performed, golden zebrafish embryos were used, to avoid confusion of GFP signal. Embryos were selected at 8-10 somites (for KV) and 72hpf (to study the cloaca of the pronephros) and manually dechorionated. Embryos were fixed in 4% PFA at 4°C: for 1-2 hours (minimum of 1hr, max 1-5hrs for 8-10 somite stage) or overnight at 4°C for 72hpf embryos. Subsequently, PFA was removed and embryos were washed in PBT for 5mins. Embryos were either dehydrated in 5min washes up to 100% methanol and stored at 4°C or -20°C (for longer periods) until use, or immediately processed into the immunofluorescence protocol.

2.7.3 Wholemount Immunofluorescence protocol and antibodies

Approximately 20 embryos from each group were transferred into screw top eppendorfs and all washes/incubations were performed on a rocker at room temperature, unless otherwise stated. To permeabilise embryos, they were washed in ddH2O for 5mins, then pre-chilled (-20°C) acetone at -20°C for 7mins. Embryos were washed in ddH_2O for 5mins and transferred to a fresh eppendorf before addition of block (5% BSA/PBS and 1% DMSO and 0.1% Tween) for 2 hours. The block was removed and the primary antibody (Table 2.3) added to 5% BSA/PBS, to incubate at 4°C overnight. The following day, the primary antibody was removed and embryos washed in PBS for 5mins, 3 times. Embryos were then transferred into a fresh eppendorf, wrapped in tin foil (to maintain in the dark) and the secondary antibody (Table 2.3) in 5% BSA/PBS

applied, overnight at 4°C. The following day, the secondary antibody was removed, embryos were maintained in the dark and washed in PBS for 5mins, 4 times, prior to storing in the dark at 4°C until imaging.

The dilution of primary and secondary antibodies (Table 2.3) was determined following a series of experiments testing different dilutions to identify the optimal signal with the minimal background. The initial choice of antibody dilutions tested were as a result of previous experience in the laboratory performing immunofluorescence on cells or published methods (Kramer-Zucker et al., 2005).

When double antibody staining was performed, the primary antibodies were put on together, however the secondary antibodies were put on sequentially because that is custom in our laboratory, although it was acknowledged that there would be little risk of the secondary antibodies cross reacting if put on together.

Primary Antibody	Dilution	Secondary Antibody	Dilution
Mouse Acetylated tubulin, Sigma, T6793	1:500	Donkey Alexa Fluoro (red) 594, Invitrogen	1:200
Rabbit Pericentrin, Abcam, AB4448	1:200	Goat FITC (green) 488, Invitrogen	1:200
Rabbit Atypical protein kinase C, Santa Cruz, SC216	1:500	Goat FITC (green) 488, Invitrogen	1:200

Table 2.3 Antibodies and dilutions used in immunofluorescence
Species and dilution of primary and secondary antibodies used for immunofluorescence.

2.7.4 Preparation for imaging

After trialling several methods of mounting 8-10 somite stage embryos, the following technique was chosen as optimal (similar to section 2.3.7). Embryos were placed on Vectashield hardset mounting media with DAPI, on ultra thin (0.175 ± 0.02µm) glass culture plates (Iwaki), or occasionally if 72hpf, on inverted concavity microscope slides and imaged through coverslips. Following the immunofluorescence protocol and mounting, embryos were stored in the dark at 4ºC, prior to imaging with confocal microscopy (LSM 510Meta, Zeiss and A1R Confocal, Nikon). Images and z-stacks were captured using a 20x lens and 3x optical zoom.

2.7.5 Measuring cilia length on confocal images

To measure the length of cilia in KV, the following method was recommended by Dr Aoife Waters from Professor Phil Beales zebrafish laboratory in London. Z-stack images of KV captured during confocal microscopy were opened in the simple neurite tracer programme (Fiji). After selecting the z-stack image of KV of maximal diameter, with most cilia in view, the length of each cilium (in µm, 9-29 cilia per embryo) was measured and the average length of cilium per embryo was calculated.

2.8 Zebrafish Histology

2.8.1 Overview

To evaluate the histology of eye, brain and kidney development associated with NPHP related ciliopathies, histological examination was performed following MO knockdown in zebrafish embryos. Uninjected WT controls and embryos following MO injection were fixed at 72-120hpf. Embryos were embedded in resin, sectioned on a microtome, mounted on slides, stained and imaged.

2.8.2 Fixation for histological studies

Groups of both WT controls and morphant embryos between 72-120hpf were selected, dechorionated and euthanised in 4mg/ml Tricaine for 1min. Embryos were washed in PBS at room temperature for 5mins and then fixed in 4% PFA at 4°C overnight. The following day, embryos were washed in PBS for 5mins twice and dehydrated by washing in an ascending ethanol series as follows: 25% ethanol/ddH2O for 5mins, 50%

ethanol/ddH_2O for 5mins, 75% ethanol/ddH_2O for 5mins, 100% ethanol. Embryos were then stored in 100% ethanol at 4°C until ready for resin embedding.

2.8.3 Resin embedding protocol

The evening prior to resin embedding, silica crystals (Sigma**)** were dehydrated by inserting them in an open glass jar into a 60°C oven overnight. Embryos stored in 100% ethanol were divided into groups of up to 20 embryos per eppendorf. A further two 30min washes in 100% ethanol were performed at room temperature. A fresh eppendorf containing hardener 1 (benzoyl peroxide) media (Technovit 8100, Heraeus Kulzer GmbH) was prepared and approximately 5 embryos transferred (in minimal 100% ETOH) to the eppendorf. Embryos were allowed to sink to the bottom of the eppendorf, which can take up to 10 mins. Hardener 1 was removed using a pipette and fresh hardener 1 added to the eppendorf, which was incubated at room temperature for 1 hour, with a further replacement of hardener 1 during this time, to maximally dehydrate.

An airtight container was prepared containing dehydrated silica crystals (blue in colour) and a rack for holding up to 6 moulds. A solution of hardener 1 and hardener 2 (N,N,3,5-tetramethylaniline, very viscous) was prepared (30:1, 1.7ml hardener 1, 57µl hardener 2 per mould) and poured into a mould. Up to 5 embryos were transferred in minimal hardener 1 to the mould and carefully orientated (the heads were closely aligned to an edge), to facilitate sectioning. A plastic plug was carefully position on top of the mould and the airtight container carefully incubated at 4°C for 24-72 hours to harden into a resin.

2.8.4 Preparing resin block for sectioning

The resin blocks were removed from the mould and dried. The embryos should be clearly visible in the resin block and were reviewed with a stereomicroscope to plan removal as a wedge from the resin block. A bench top vice was used to hold the mould and a hacksaw, to cut out the block of embryos with a small volume of surrounding resin. The resin edges were filed, to ensure smooth and the base of the zebrafish resin block was glued (Super Glue, Loctite) at 90° onto the remaining resin block and allowed to set for 24 hours. The following day, to maintain continuous orientation of sections, the top right corner of the resin block was cut off using a scalpel.

2.8.5 Microtome sectioning

The prepared resin block was sectioned at 5µm. Sections were positioned on a microscope slide using 15% ethanol/ddH_2O as an adherent and air dried overnight.

2.8.6 Staining histology sections

A standard methylene blue-basic fuschin staining protocol was used (Bennett et al., 1976). The necessary solutions were prepared and decanted into 50ml falcon tubes in which microscope slides could be dipped. To make 50ml of the methylene blue-basic fuschin stain the following were mixed: 10ml methylene blue (0.5g methylene blue in 400ml ddH_2O), 10ml basic fuschin (0.5g basic fuschin in 400ml ddH_2O), 17.5ml phosphate buffer pH6.8 ((49ml 0.2M sodium phosphate dibasic anhydrous (28.4g $Na_2H_2PO_4$ in 1L ddH_2O)); 51ml 0.2M sodium phosphate monobasic monohydrate (27.8g $NaH_2PO_4H_2O$ in 1L ddH_2O); 100ml ddH_2O) and 12.5ml 95% ethanol.

The protocol which appeared optimal for staining slides was: 20 dips in methylene blue-basic fuschin stain, 15 dips in ddH_2O, 10 dips in 95% ethanol and 15 dips in water. Slides were left to dry in a fumehood overnight. The following day, coverslips were applied using DPX (Distrene, Plasticiser, Xylene) mountant (Sigma). Images were obtained using 20-40x objectives on an axioplan microscope (Axiocam HRC, Zeiss).

2.9 Electron Microscopy

2.9.1 Overview

To evaluate changes to cilia within KV, wholemount scanning electron microscopy (SEM) was performed in uninjected WT controls and following MO knockdown in zebrafish embryos.

2.9.2 Fixation and processing for Electron microscopy

Embryos were fixed at the 8-10 somite stage in 2% glutaraldehyde in Sorenson's phosphate buffer for 24 hours at 4°C. Further preparation including dehydration and processing of embryos was performed by Dr Kath White and Ms Tracey Davey at the Electron Microscopy Research Services (EMRS), Newcastle University.

2.9.3 Mounting and imaging

Embryos were mounted onto SEM aluminium stubs using self adhesive tape. Images were captured with help from the EMRS using a Cambridge Stereoscan 240 SEM. KV could not be identified in any embryos (n=40) and therefore no comments regarding the structure of cilia within KV can be made. Possible reasons for the failure to identify KV could be because of: damage during fixation; distortion of the embryo surface during mounting; malorientation of embryos during mounting leading to KV effectively being hidden from the SEM.

2.10 Statistical analyses

A minimum of 3 different spawning pairs of zebrafish were utilised to generate embryos for experiments. Additionally several experiments were repeated to assess reproducibility and consistency of results. Data was recorded in GraphPad Prism software, which was used to calculate means and standard error of the means (SEM). Where appropriate, contingency tables were generated to compare phenotypes. When comparing two different groups, Fisher's exact test was used and a Chi-squared test to compare greater than two groups. Graphs were created using the GraphPad Prism software.

Chapter 3 Characterisation of a novel zebrafish model of the ciliopathy Joubert Syndrome using *ahi1* knockdown

3.1 Introduction

Mutations in *Abelson-helper integration site-1* (*AHI1*) are the most common genetic cause of JBTS, accounting for approximately 12% of affected individuals (Parisi et al., 2006). A range of different pathogenic mutations (including nonsense, missense, splice site, insertion and frameshift) have been identified in patients, with no single founder mutation, even in consanguineous families. In addition to the pathognomonic, neurodevelopmental anomaly of 'molar tooth sign' (MTS) on cerebral MRI (Maria et al., 1999), patients with *AHI1* mutations have been found to have: the cystic kidney disease, NPHP (Utsch et al., 2006) and retinopathy, such as Leber's congenital amaurosis (Valente et al., 2006a) in up to 20% of cases.

3.1.1 Human *AHI1* Genomic and Proteomic Information

Human *AHI1* has been mapped to chromosome 6q23.2-23.3 (Ferland et al., 2004). There are 18 transcripts for this gene, 10 of which are protein coding, for the Ahi1 protein, Jouberin. Using the online Vertebrate Genome Annotation database (http://vega.sanger.ac.uk), a transcript with 5921bp (*AHI1_008* OTTHUMT00000391948) has the best supporting evidence, consensus coding sequence data and encodes an 1196 amino acid protein called Jouberin. Using SMART (Simple Modular Architecture Research Tool, http://smart.embl-heidelberg.de) domain analysis, Jouberin is predicted to have an N-terminal coiled-coil domain, 6 WD40 repeats and a Src homology domain (SH3) (Figure 3.1). The functional implications of Jouberin can be hypothesised from this structural information. Coiled-coil domains have been described as structural motifs (Mason and Arndt, 2004), this suggests that Jouberin could be an important scaffolding protein and plays a role in maintaining tissue structure (Hsiao et al., 2009). Whilst, SH3 domains are recognised as important in protein to protein interactions (Mayer, 2001), Jouberin has been shown to interact with nephrocystin-1 (Eley et al., 2008), mks-1 (Sang et al., 2011) and inversin (nphp2) (Sang et al., 2011). *Ahi1* mRNA is expressed in human fetal kidney tissue (Ferland et al., 2004). Jouberin is known to be expressed in human fetal and adult cerebellum and the

medulla of the brainstem (Ferland et al., 2004); also in renal epithelial collecting duct cells at cell-cell junctions and at the basal body of primary cilia (Eley et al., 2008).

Figure 3.1 *AHI1* gene transcript and partial protein product (Jouberin) structure in humans and zebrafish
(**A**) *AHI1* transcript in humans (OTTHUMT00000391948) and schematic representation of encoded protein product, Jouberin (**B**). (**C**) *ahi1* transcript in zebrafish (OTTDART00000049821) and schematic representation of encoded protein product, Jouberin (**D**). aa, amino acids; CC, coiled coil; Ch., chromosome; WD40 repeats; SH3, Src homology domain.

3.1.2 *AHI1* evolutionary conservation

AHI1 is highly conserved throughout evolution and has been shown to be particularly conserved between humans and a hierarchy of mammals including mice, rats, hamsters, cats and cows (Jiang et al., 2002). To date, orthologues of *AHI1* have been identified (http://ensembl.org) in 54 species, all vertebrates including zebrafish and a range of invertebrate model organisms such as *Drosophilia melanogaster*, *Caenorhabditis elegans* and in the ciliated protozoa *Tetrahymena thermophilia* (Simms et al., 2012). Previously, expression of *ahi1* mRNA has been shown in the brain, retina and inner ear of zebrafish between 2.5-5.2 days post fertilisation (dpf) (Doering et al., 2008). Figure 3.2 shows the evolutionary conservation of Jouberin between humans, mice and zebrafish.

Figure 3.2 Evolutionary conservation of Ahi1 (Jouberin) in humans, mice and zebrafish

Jouberin peptide sequence alignment in humans (OTTHUMP00000234456), mice (ENSMUSP00000101164) and zebrafish OTTDARP00000039088). Conservation of amino acid alignment (red font).

3.1.3 Aims of this chapter

The main aim of this chapter was to utilise zebrafish as a model organism to elucidate the role of *ahi1* in the development of the kidney, brain and retina. To evaluate this, temporal expression of *ahi1* during zebrafish embryonic development was investigated. To study the effect of interference with *ahi1* expression on the development of JBTS, *ahi1* knockdown was performed in zebrafish embryos and a cerebello-oculo-renal phenotype was hypothesised. The pathogenesis of this ciliopathy was evaluated by studying cilia in Kupffer's Vesicle (KV), the zebrafish organ of laterality, and the effect on: cardiac left-right development; rudimentary renal (pronephric duct) development and cystogenesis.

3.2 Results

3.2.1 Expression of *ahi1* during zebrafish embryogenesis

In order to ascertain the spatial and temporal expression of *ahi1* in zebrafish during development, *in situ* hybridisation was performed, using an *ahi1* antisense riboprobe, in whole mount WT embryos at key time points (Figure 3.3). At the 8 somite (8s) stage, *ahi1* is expressed in the eye, notochord and KV (Figure 3.3A-B). At 24hpf, *ahi1* is expressed in the retina, midbrain and hindbrain (Figure 3.3C-D). By 48hpf, *ahi1* continues to be expressed in the retina and is also seen in the hypothalamus and inner ear (Figure 3.3E-F). At 72hpf, expression of *ahi1* continues in the inner ear, specifically the ganglion cell and pigmented epithelial retinal cell layers and is also seen in the olfactory bulbs (Figure 3.3G-H). The pattern of expression of *ahi1* was similar using two additional riboprobes which targeted different regions of the *ahi1* transcript. The *in situ* hybridisation was repeated using these two additional *ahi1* probes as the expression was fairly ubiquitous, to determine if other riboprobes may generate a more specific focused signal, this did not occur. The riboprobe used in Figure 3.3 was chosen because it generated the most intense and specific staining in the most timely manner. Expression of *ahi1* in the developing pronephros of zebrafish at 48hpf was identified on tissue sections by performing resin embedding and tissue sectioning at 5μm following whole mount *in situ* hybridisation (Figure 3.4).

Overall the expression of *ahi1* appears ubiquitous particularly during the first 24hpf confirmed by utilising three different riboprobes. Since the *ahi1* riboprobe *in situ* experiments followed several learning attempts in which riboprobes with published expression patterns (*shh* (Wang et al., 2007); *cmcl2* (Ott et al., 2008)) were recapitulated as shown in Figure 3.6, this likely reflects the nature of the *ahi1* riboprobes used herein. Of note, the same images were used to demonstrate the expression of *ahi1* during embryogenesis in these figures as used in the peer reviewed and accepted publication (Simms et al., 2012) of this data as shown in Figure 2 of Appendix F.

Figure 3.3 Expression of *ahi1* during zebrafish embryogenesis
Lateral (A, C, E, G) and dorsal (B, D, F, H) images of whole-mount *in situ* hybridisation using an *ahi1* antisense riboprobe on golden, wild type embryos at 8 somites (8s) (A, B), 24hpf (C, D), 48hpf (E, F) and 72hpf (G, H). *ahi1* is expressed as follows: at 8s in the eye (black arrowhead, A), diffusely in the notochord and in Kupffer's vesicle (white arrow, A, B); at 24hpf in the midbrain, hindbrain (arrows, C, D) and retina (arrowhead, C); at 48hpf in the retina, hypothalamus (arrow, E, F) and inner ear; at 72hpf in the inner ear (arrowhead, G), olfactory bulbs (arrowheads, H), and specific retinal layers (GCL and RPE, H). GCL=ganglion cell layer, hpf=hours post fertilisation, RPE=retinal pigmented epithelium.

Figure 3.4 Expression of *ahi1* in zebrafish pronephros.
Transverse section at the level of the medial tubules of the pronephros following whole-mount *in situ* hybridisation using an *ahi1* antisense riboprobe on golden, wild type embryos at 48 hpf. In both images, the arrows demonstrate *ahi1* expression in the pronephros. Images were taken with a 20x (**A**) and 40x (**B**) objective lens. Scale bars are 20µm. n=notochord, s=somites.

3.2.2 Expression of control *in situ* hybridisation probes during zebrafish embryogenesis

To exclude nonspecific background staining, whole mount *in situ* hybridisation was performed using an *ahi1* sense riboprobe and a 'no probe' control during temporal zebrafish development (Figure 3.5). There was no specific staining of embryos using the *ahi1* sense riboprobe and no background staining when no riboprobe was used. In parallel with *ahi1* riboprobe experiments, positive controls for the *in situ* hybridisation technique were performed and generated similar results to those published, using *shh* antisense (Concordet et al., 1996; Wang et al., 2007) and *cardiac myosin light chain 2* (*cmcl2*) antisense (Ott et al., 2008; Wythe et al., 2011) riboprobes in WT zebrafish embryos (Figure 3.6). *shh* is expressed in the notochord at the 8s stage (Figure 3.6A), in the eye and floor plate at 24hpf (Figure 3.6C) and additionally in the telencephalon, diencephalon, hypothalamus and pharyngeal arches by 48hpf (Figure 3.6E). *cmcl2* expression is not present at the 8s stage (Figure 3.6B), however it is seen clearly and specifically in the single zebrafish ventricle at both 24 and 48hpf (Figure 3.6, F).

Figure 3.5 *In situ* hybridisation controls for *ahi1* antisense riboprobe during zebrafish embryogenesis
Lateral views of whole-mount *in situ* hybridisation using *ahi1* sense riboprobe (A, C, E, G) and no probe (B, D, F, H) on golden, wild type embryos at 8 somites (8s) (A, B), 24hpf (C, D), 48hpf (E, F) and 72hpf (G, H). hpf, hours post fertilisation.

Figure 3.6 *In situ* hybridisation positive controls for *ahi1* antisense riboprobe during zebrafish embryogenesis
Lateral views of whole-mount *in situ* hybridisation using s*hh* antisense (**A**, **C**, **E**, **G**) and *cmcl2* antisense (**B**, **D**, **F**, **H**) riboprobes on golden, wild type embryos at 8 somites (8s) (**A**, **B**), 24hpf (**C**, **D**), 48hpf (**E**, **F**) and 72hpf (**G**). s*hh* is expressed in the notochord (**A**) at the 8s stage; in the eye and floorplate at 24hpf (**C**); additionally in the telencephalon, diencephalon, hypothalamus and pharyngeal arches at 48hpf (**E**) and 72hpf (**G**). *cmcl2* expression is not detectable at the 8s stage (**B**), however at 24hpf (**D**) and 48hpf (**F**) it is evident specifically in the single ventricle. *cmcl2*, *cardiac myosin light chain 2*; hpf, hours post fertilisation; *shh*, *sonic hedgehog*.

3.2.3 Design and effect of *ahi1* morpholino oligonucleotides

In order to study the effects of gene knockdown in zebrafish models of human disease, MOs were created to interfere with *ahi1* expression.

Figure 3.7 shows the target sites for both the *ahi1* translation and splice blocking MOs on the zebrafish *ahi1* exon sequence. The splice blocking MO leads to an inframe deletion in exon 8 and a predicted loss of 3 WD40 repeats from the encoded protein, Jouberin.

The injection of MOs is performed promptly after fertilisation, at the 1-4 cell stage, and any increased mortality associated with MO delivery was evaluated at 24hpf. Figure 3.8 depicts the mortality at 24hpf as mean percentage and standard error of the mean for a range of doses of *ahi1* splice and translation blocking MOs. 24hpf mortality data is also shown for uninjected WT control embryos from the same parental pairs and for embryos injected with a standard negative control MO. It must be acknowledged that 24hpf mortality rates for controls, both standard negative control MO injected and uninjected WT embryos, were at times as high as 50% (Figure 3.8C). Most users of our zebrafish facility have experienced this problem periodically and there has been no consensus as to why this can occur. As discussed in section 2.2.1, the facilities within the zebrafish laboratory are carefully monitored. A collective decision amongst zebrafish researchers in our laboratory has therefore been to keep careful records to monitor mortality rates and providing the mortality rates in the MO injected embryos were not significantly different from matched control experiments, not to exclude such work as on occasions this may restrict the ability to generate data. An alternative method to consider in future when evaluating data would be to subtract the percentage mortality in controls from the percentage mortality in MO injected embryos.

With *ahi1* splice blocking MO, there is a dose dependent association between MO dose and 24hpf mortality (Figure 3.8A). There was no significant difference in mortality rates at 24hpf between MO injected and uninjected embryos.

Figure 3.7 *ahi1* morpholino oligonucleotide design
(A) Schematic representation of zebrafish *ahi1*showing target sites of translation (ATG) and splice (*ahi1*iex8) blocking morpholino oligonucleotides (MO). (B) Schematic representation of the effect of the splice blocking MO designed to target exon 8, leading to an inframe deletion and loss of 3 WD40 repeats from the protein product, Jouberin (C).

Figure 3.8 Mortality at 24hpf following MO injection
Mortality at 24 hours post fertilisation (hpf) is shown as mean percentage (%) and standard error of the mean (where appropriate) in zebrafish embryos injected with morpholino oligonucleotide (MO) compared to matched uninjected wild type (WT) controls. (A) *ahi1* splice (Sp) MO induces a dose dependent effect on mortality. (B) *ahi1* translation (ATG) blocking MO has a more variable effect on mortality. (C) Injection of a standard control (Std Con) MO induced no significant difference ($p=0.92$, unpaired t-test) in mortality at 24hpf compared to uninjected WT controls
.

3.2.4 Phenotypes of zebrafish morphants created by *ahi1* MO knockdown

Zebrafish embryos were phenotyped by light microscopy at 72hpf. Uninjected WT embryos and those injected with a standard negative control (Std Con, defined in section 2.3.2) MO were phenotypically normal (Figure 3.9A, B). However, both *ahi1* splice (*ahi1* Sp) and *ahi1* translation (*ahi1* ATG) targeting MOs caused abnormal development including a curved body axis, hydrocephalus, cardiac oedema and altered number of otoliths (Figure 3.9). Additionally *ahi1* morphants develop cysts throughout the pronephros (Figure 3.10) and cystic dilatation of the distal pronephros at the cloaca (Figure 3.11).

Figure 3.10 shows light and fluorescent microscopy images of uninjected *claudin-b:*Lyn-GFP transgenic WT and *ahi1* splice MO injected zebrafish embryos, highlighting the cysts throughout the pronephros in the *ahi1* morphants (Figure 3.10C-F).

In addition to light microscopy of cloacal dilatation, Figure 3.11 shows: resin histology cross sections of dilated pronephric tissue at the level of the posterior tubules (Figure 3.11D) and cloaca (Figure 3.11F) in *ahi1* morphants; fluorescent microscopy of cystic dilatation of the cloaca in *claudin-b:*Lyn-GFP transgenic *ahi1* morphants (Figure 3.11H), compared to uninjected WT controls.

Figure 3.9 Phenotype following *ahi1* MO knockdown at 72 hpf
Lateral views show wild type uninjected (A) zebrafish embryos and those following injection with a standard negative control MO (Std Con MO, B) were morphologically normal. Injection of *ahi1* splice (Sp, C, D) and translation (ATG, E, F) blocking MOs leads to curved body axis, hydrocephalus (arrows), cardiac oedema (*), pronephric cysts and altered number of otoliths (single in F (arrowhead). hpf, hours post fertilisation; MO, morpholino oligonucleotide.

Pg2 Fig 3.9

Figure 3.10 *ahi1* knockdown induces pronephric cysts in zebrafish embryos
Light and fluorescent microscopy images of pronephric cysts in golden (A, C-E) and *claudin-b*:Lyn-GFP transgenic (B, F) zebrafish embryos at 72hpf. Lateral views of wild type, uninjected embryos were normal (A, B). 1-4ng of *ahi1* splice blocking MO induces proximal (lateral and dorsal views, arrowed, C, D) and distal (at the cloaca, arrowed E, F) pronephric cysts. MO, morpholino oligonucleotide; hpf, hours post fertilisation.

Figure 3.11 *ahi1* knockdown induces cystic dilatation, cloacal dilatation and obstruction in zebrafish embryos

Light microscopy images of distal pronephric cysts (arrows) leading to cloacal obstruction in golden *ahi1* morphant (*ahi1* Sp MO) embryo at 72hpf (B), compared to uninjected wild type (WT) control (A). Resin histology 5μm sections through the pronephros (arrows) in embryos at 72hpf, stained with methylene blue-basic fuchsin stain. Images taken with a 40x objective lens at the level of the posterior pronephric tubules (arrows, C-D) and the cloaca (E-F). In *ahi1* morphants, the posterior tubules are modestly dilated (D, diameter 5μm), compared to WT controls (C, diameter 3μm). This pronephric dilatation becomes more pronounced in *ahi1* morphants at the level of the cloaca (F, diameter 10μm), compared to WT controls (E, diameter 2μm). Scale bar = 10μm. Fluorescent images of the cloaca (G,H) using the *claudinb:*Lyn-GFP transgenic line, taken with a 20x objective. *ahi1* morphants have cystic dilatation of the cloaca (H, arrow), compared to WT controls (G). Scale bar = 50μm.

At 48 and 72hpf, *ahi1* morphant embryos may also have abnormal eye development including coloboma formation seen on light microscopy; and retinal dystrophy is identified on resin histology cross sections of the eyes (Figure 3.12). There is loss of formation of the normal discrete retinal layers (Liu et al., 2011) in *ahi1* morphants (Figure 3.12F, H) compared to uninjected WT controls (Figure 3.12E, G).

To further characterise the apparent hydrocephalus and disruption to the development of the brain induced by *ahi1* knockdown in zebrafish morphants, resin histology cross sections through the brain at the level of the otic vesicle reveals both hydrocephalus and expansion of the notochord (Figure 3.13), compared to uninjected WT controls.

Development of the rudimentary ear is altered in *ahi1* morphants as shown by lateral and dorsal light microscopy images of their heads (Figure 3.14). *ahi1* morphants may develop an empty otic vesicle, or an abnormal number of otoliths (one or three), compared to uninjected WT controls, which usually develop two otoliths.

Figure 3.12 *ahi1* knockdown induces coloboma formation and retinal dystrophy in zebrafish embryos

Light microscopy images comparing the eyes of uninjected wild type (WT) embryos (A, B) and *ahi1* morphants (C, D) at 48hpf and 72hpf. In *ahi1* morphants there is abnormal eye development with coloboma formation (arrowed, C, D). Resin histology of eyes at 72hpf, sectioned at 5-7μm and stained with methylene blue-basic fuchsin stain. Images taken with a 20x (E, F) and 40x (G, H) objective lens, scale bars = 20μm. In WT control embryos (E, G), there is normal retinal lamination (arrowed, E) including formation of the ganglion cell layer (GCL), inner nuclear layer (INL) and outer nuclear layer (ONL). In *ahi1* morphants (F, H) there is severe disruption to normal retinal development, with failure of discrete retinal layer formation, however, the outer retinal pigmented epithelium (RPE, arrowed in F) remains present. hpf, hours post fertilisation.

Figure 3.13 *ahi1* knockdown induces hydrocephalus and abnormal brain development in zebrafish embryos

Light microscopy images demonstrating hydrocephalus (arrowed, B, C) and abnormal hindbrain development in *ahi1* morphant zebrafish embryos, compared to normal brain development in uninjected wild type (WT) control embryos (A) at 72hpf. Resin histology cross sections (5-7μm) through the brain at the level of the otoliths in WT controls (D) and *ahi1* morphants (E, F) at 72hpf. In *ahi1* morphants there is hydrocephalus (asterisk, E, F) and expanded notochord (midline diameter 52μm in *ahi1* morphants, compared to 34μm in WT controls. Scale bar = 50μm. hpf, hours post fertilisation; N, notochord.

Figure 3.14 *ahi1* knockdown induces abnormal ear development with altered number of otoliths in the otic vesicle of zebrafish embryos
Light microscopy lateral (A, C, E, G) and dorsal (B, D, F, H) images of the head of zebrafish embryos focusing on the otic vesicles (developmental ear) at 72hpf. Uninjected wild type (WT) control embryos have 2 otoliths in each otic vesicle (A, B), whilst *ahi1* morphants have either no otoliths and an empty otic vesicle (C, D), a single otolith (E, F), or three otoliths (left otic vesicle G, H). hpf, hours post fertilisation.

The mean frequencies of the development of each abnormal phenotype at 72hpf following injection of *ahi1* splice (*ahi1* Sp) or translation (*ahi1* ATG) blocking MO are shown in Figure 3.15. The frequency of development of abnormal phenotype is predominantly dose dependent, with generally lower doses of splice (Figure 3.15A-C**)** blocking MO required to induce a phenotype (mean percentage (±SEM)). Injection of 1-2ng of *ahi1* Sp MO induced the following frequency of phenotypes: pronephric cysts in 7% (±3.1%) to 10.9% (±2.7%); curved body axis in 36.2% (±7.6%) to 39.9% (±7.6%); cardiac oedema in 34.5% (±6.9%) to 35.1% (±6.9%); hydrocephalus in 20.4% (±4.6%) to 29.3% (±5.4%); otic defects in 2% (±0.7%) to 3.7% (±1.2%) and colobomas in 0.5% (±0.4%) to 0.9% (±0.5%). With injection of 4-6ng of *ahi1* ATG MO, the following frequency of phenotypes occurred: pronephric cysts in 3.8% (±3.1) to 7.5% (±3.6%); curved body axis in 11.8% (±4.9%) to 27% (±7.8%); cardiac oedema in 13% (±6.4%) to 25.5% (±6.5%); hydrocephalus in 3% (±0.7%) to 12.5% (±4.3%); otic defects in 0.8% (±0.8%) to 3% (±3%) and colobomas (at 4ng only) in 0.5% (±0.5%). This array of abnormal phenotypes identified in the *ahi1* morphant zebrafish, including curved body axis, cardiac oedema, hydrocephalus, pronephric cysts, otic defect and retinal anomalies are characteristic of a zebrafish ciliopathy model (Ferrante et al., 2009; Obara et al., 2006).

3.2.5 Specificity of *ahi1* MO knockdown in *ahi1* zebrafish morphants

To ensure the described phenotype of *ahi1* morphants was not an off-target or non-specific effect, appropriate control experiments were performed in parallel and embryos evaluated at 72hpf. Zebrafish embryos injected with either a standard negative control (Std Con) MO (Figure 3.9B) or *p53* MO (Figure 3.16B) alone were phenotypically normal. Following the combined injection of *ahi1* splice and *p53* MO or *ahi1* translation blocking and *p53* MO images show that embryos continue to develop a morphant phenotype (Figure 3.16C-D), excluding off-target effects.

The complete rescue of the *ahi1* morphant phenotype to a normal appearance, following coinjection of mouse *Ahi1* mRNA with *ahi1* MO, confirms specificity of the *ahi1* MO sequence used for knockdown (Figure 3.16F). All embryos injected with mouse *Ahi1* mRNA alone (100%, n=117), and 99% of uninjected embryos (n=2699) or those injected with standard control MO (n=197) were phenotypically normal (Figure 3.17). There was a statistically significant fall in the percentage of *ahi1* morphants and rescue

to a normal phenotype, following co-injection of 100pg mouse *Ahi1* mRNA with 2-4ng of *ahi1* MO, compared to embryos injected with 2-4ng *ahi1* MO alone ($p < 0.0001$, chi-squared test). Figure 3.17B shows quantification of the raw numbers of embryos by normal WT or abnormal morphant phenotype when classified by treatment with injection of 2-4ng *ahi1* MO alone (n=517) or co-injection of 100pg mouse *Ahi1* mRNA with 2-4ng of *ahi1* MO (n=88). The degree of overall rescue from *ahi1* morphant to WT appearance and reduced frequency of the majority of abnormal phenotypes (curly tail, cardiac oedema, hydrocephalus and pronephric cysts) following co-injection of *ahi1* MO and mouse *Ahi1* mRNA were statistically significant ($p < 0.0001$, chi-squared test).

Figure 3.15 Quantification of abnormal phenotypes at 72hpf following injection with *ahi1* splice or translation blocking MO

Data are displayed as mean ± SEM. The percentage frequency of each abnormal phenotype was higher following injection of a lower dose of *ahi1* splice (Sp) MO (A-C), compared to following injection of an equivalent dose of *ahi1* translation (ATG) MO (D-F). With *ahi1* Sp MO knockdown, there was a dose dependent effect on the frequency of curly tail, cardiac oedema, hydrocephalus and coloboma (B, C). Following *ahi1* ATG MO knockdown, there was a dose dependent effect on the frequency of pronephric cysts, curly tail, cardiac odema and otic defects (D-F). The total number of zebrafish embryos phenotyped at 72hpf following *ahi1* Sp MO were 1498 and following *ahi1* ATG MO were 458. hpf, hours post fertilisation; MO, morpholino oligonucleotide.

Figure 3.16 Exclusion of off-target effects and confirmation of specificity of phenotype with *ahi1* MO knockdown

Lateral views of zebrafish embryos 72 hours post fertilisation. Wild type (WT) uninjected (A), embryos injected with *p53* MO alone (B) and embryos injected with mouse *Ahi1* mRNA alone (E), were morphologically normal. Embryos co-injected with *p53* MO and *ahi1* splice (C) or translation blocking (D) MOs continued to develop a morphant phenotype including hydrocephalus (C, (*)), pronephric cysts (D, arrowhead) and altered number of otoliths (C, arrow), and excludes the possibility of off-target effects. Co-injecting mouse *ahi1* mRNA with *ahi1* splice blocking MO rescued embryos to a normal phenotype (F), confirming the specificity of targeted *ahi1* MO knockdown. MO, morpholino oligonucleotide.

Figure 3.17 Rescue of *ahi1* morphant phenotype following co-injection with mouse Ahi1 mRNA

(A) Percentage of normal wild type (WT) and abnormal morphant phenotype of embryos: uninjected (n=2699); 2ng standard control MO (n=197); 100pg mouse *Ahi1* mRNA (n=117); 2-4ng *ahi1* MO (n=517); coinjection of mouse *Ahi1* mRNA and 2-4ng *ahi1* MO (n=88). Rescue to WT phenotype by coinjection with 100pg mouse *Ahi1* mRNA was statistically significant (*, $p < 0.0001$, chi-squared test). (B) Raw quantification of overall rescue from *ahi1* morphant to WT phenotype after co-injection with 100pg mouse *Ahi1* mRNA was statistically significant (*, $p < 0.0001$, chi-squared test). (C) There was a statistically significant rescue of *ahi1* morphants to the WT phenotype, and reduced frequency of anomalies (curly tail, cardiac oedema, hydrocephalus, pronephric cysts) after co-injection with mouse *Ahi1* mRNA (*, $p < 0.0001$, chi-squared test). Data are % mean ± SEM. MO, morpholino oligonucleotide.

3.2.6 Specificity of *ahi1* splice MO knockdown and direct sequencing

RT-PCR of (equal concentrations of isolated RNA from) individual uninjected WT zebrafish embryos at 24-72hpf revealed the expected product size of 807bp. However, in *ahi1* splice MO injected zebrafish embryos there was abnormal splicing suggested by an additional smaller RT-PCR product (faint band at 453bp) at 24 and 72hpf (Figure 3.18A). Additionally there is almost complete loss of expression of *ahi1* (faint 807bp band) at 48hpf with recovery by 72hpf due to the waning effect of MO knockdown (Figure 3.18A).

The smaller PCR fragment was isolated from the gel, purified and sent for sequencing, which identified a 453bp product created by an inframe deletion of exon 8 and introduction of a premature stop codon (Figure 3.18B). The chromatogram showing the quality of the sequenced smaller *ahi1* product is also shown (Figure 3.18C).

Figure 3.18 Evidence of *ahi1* splice MO knockdown by RT-PCR and direct sequencing
(A) RT-PCR of single embryos at 24, 48 and 72hpf following *ahi1* splice MO knockdown reveals a smaller RT-PCR product (white arrowhead) compared to uninjected wild type (WT) control embryos. The normal RT-PCR product of 807bp is maximally reduced in *ahi1* morphants at 48hpf, with recovery at 72hpf. (B) Direct sequencing of the smaller product (453bp) in *ahi1* morphants identifies direct skipping of exon 8 and introduction of a premature stop codon. bp, base pairs; hpf, hours post fertilisation; MO, morpholino oligonucleotide.

Figure 3.18 (C) Evidence of *ahi1* splice MO knockdown by direct sequencing
Chromatogram showing good quality of sequencing of smaller *ahi1* product at 72hpf. hpf, hours post fertilisation.
NB this is 2nd page of Figure 3.18

3.2.7 Gross morphology of Kupffer's vesicle in *ahi1* MO injected embryos

KV was evaluated to determine whether this ciliated structure may offer an explanation for the ciliopathy phenotype which *ahi1* morphants develop (Figure 3.9, Figure 3.10, Figure 3.11, Figure 3.12, Figure 3.13, Figure 3.14). Figure 3.19 contains light microscopy images and shows KV, seen as a spherical concave sac at the tailbud, is evident in time-matched WT and *ahi1* MO injected embryos at 8-10 somites. There are no obvious differences in the gross morphology of KV between uninjected WT control and *ahi1* MO injected zebrafish embryos.

In situ hybridisation was also performed using a *charon* riboprobe, which is specifically expressed around KV (Hashimoto et al., 2004), and confirmed no overt change in the pattern of expression following *ahi1* MO injection (Figure 3.19C, F).

3.2.8 Loss of cilia from Kupffer's vesicle following *ahi1* MO injection

Fluid flow generated by cilia within KV is essential for determining patterning of left-right asymmetry (Essner et al., 2005). Immunostaining of cilia using an antibody to acetylated tubulin showed loss of cilia in *ahi1* MO injected embryos (Figure 3.20). The zebrafish embryos utilised for immunostaining express *claudin-b* at cell to cell junctions (tight junctions) of KV epithelial cells and this expression is also abnormal and disrupted in *ahi1* MO injected embryos compared to WT embryos.

To further evaluate KV and cilia, immunostaining was performed using two antibodies, anti-acetylated tubulin to highlight cilia and pericentrin to identify centrosomes. This was an attempt to determine more about the extent of disruption to ciliogenesis following *ahi1* MO injection, for example, whether centrosomes were able to form. This experiment was additionally performed in embryos injected with the standard mismatched control (Std Con) MO to identify whether there were any anomalies noted regarding cilia as a consequence of MO injection. Figure 3.21 shows that in uninjected WT, Std Con MO injected and *ahi1* MO injected embryos there was no discrete centrosomal staining, demonstrating failure of the pericentrin antibody to work. Further evidence of failure of the pericentrin antibody to work was the presence of cilia in the uninjected WT, Std Con MO injected and in some *ahi1* MO injected embryos, implying that centrosomes were present however not identified by the pericentrin antibody. This failure of the pericentrin antibody to work occurred despite attempting to optimise

conditions including dilutions of antibody used and duration of incubation. Subsequently following further evaluation, it is possible that the pericentrin antibody utilised herein does not react with zebrafish and an alternative antibody such as γ-tubulin could have utilised as a centrosomal marker (Lessman, 2012). In future work, this could be performed as it would be interesting to further clarify the apparent loss of cilia identified in some *ahi1* morphants.

Figure 3.19 The gross morphology of Kupffer's vesicle is preserved in *ahi1* MO injected embryos

Images of uninjected wild type (WT) control (A-C) and *ahi1* MO injected (D-F) golden zebrafish embryos at the 8-10 somite stage to illustrate Kupffer's vesicle (KV, arrowed). Both lateral (A, D) and dorsal (B, E) light microscopy images of live embryos at the 8-10 somite stage confirm the presence of KV in both WT (A, B) and *ahi1* MO injected (D, E) embryos. A *charon in situ* hybridisation probe is expressed in the region around KV, confirming its presence in both WT controls (C) and *ahi1* MO injected embryos (F).

Figure 3.20 Loss of cilia from Kupffer's vesicle in *ahi1* MO injected embryos
Confocal microscopy images of *cldnb*:Lyn-GFP zebrafish embryos following fixation at the 8-10 somite stage and fluorescent immunostaining using anti-acetylated tubulin (AT, red) to study cilia in Kupffer's vesicle (KV). Overlay images using 20x objective (KV arrowed, A, E, scale bar = 50µm) and higher magnification (zoom of 3) showing individual (B, C, F, G, scale bars = 20µm) and overlay (D, H, scale bars = 20µm) images. Uninjected wild type (WT, A-D) control embryos show *cldnb*:Lyn-GFP expression in an organised pattern at epithelial cell-cell junctions within KV (B) and apical cilia (red, C) extending from cells lining KV. *ahi1* MO injected embryos (E-H) have disorganised expression of *cldnb*:Lyn-GFP (F) and loss of cilia (G) from KV. MO, morpholino oligonucleotide.

Figure 3.21 Cilia remain present in Kupffer's vesicle in Standard Control MO injected embryos and some *ahi1* MO injected embryos
Confocal microscopy images of *cldnb*:Lyn-GFP zebrafish embryos following fixation at the 8-10 somite stage and double fluorescent immunostaining using anti-acetylated tubulin (AT, red) and pericentrin (PC, green) to study cilia and centrosomes respectively in Kupffer's vesicle (KV). Images are standard control MO injected (Std Con, A-C), *ahi1* MO injected (D-F) and uninjected wild type (WT, G, H) for comparison. Individual green channel images (A, D) fail to show discrete centrosome staining, KV is represented as a dark lumen. Individual red channel images (B, E, G) show staining of cilia at KV in Std Con (B), some *ahi1* (E) MO injected embryos and WT (G). Overlay fluorescent images (C, F, H) are shown. All images were taken using a 20x objective and zoom of 3, scale bars = 20µm. GFP, green fluorescent protein; MO, morpholino oligonucleotide.

Since the experiments performed thus far suggest that the presence of cilia in KV following *ahi1* MO injection is variable, a further attempt to evaluate this involved double antibody staining using atypical protein kinase C (aPKC, to study the apical epithelial membrane of KV) (Amack et al., 2007) and anti-acetylated tubulin to stain for cilia. This experiment was performed in golden embryos fixed at 8-10 somites. Figure 3.22 shows further evidence of the variable appearance of KV following *ahi1* MO injection. The development of KV appears organised and normal in some *ahi1* MO injected embryos (Figure 3.22A-C), however the apical epithelial membrane (green, Figure 3.22A, C) whilst apparent in these images is not clearly distinct from the rest of embryo and likely reflects background staining and failure of the aPKC antibody to work. In other *ahi1* MO injected embryos with more marked disruption of KV (white arrow, Figure 3.22D-F), it is impossible to ascertain anything meaningful regarding the appearance of the apical epithelial membrane (Figure 3.22D) and only a reduction in the number of cilia (Figure 3.22) can be identified.

Analysis of the presence or absence of cilia in KV in uninjected WT, *ahi1* MO injected and Std Con MO injected embryos is shown in Figure 3.23. The raw number of embryos for each treatment group is graphed in Figure 3.23A and shows that only 3 of 32 embryos injected with *ahi1* MO had a ciliated KV, compared to 30 of 35 uninjected WT embryos. This was a statistically significant difference, $p < 0.0001$, using a chi-squared test. A stacked bar chart (Figure 3.23B) shows the same data as percentages and highlights that the majority of Std Con MO injected embryos also had a ciliated KV. This excludes the possibility than abnormality in KV is induced by injection of a MO alone.

Although *ahi1* MO injected embryos generally had no cilia in KV, when they were present, the cilia appeared shorter and stubbier than in uninjected wild type embryos. A simple neurite tracer application from Fiji software package was used to formally measure the length of all cilia using z-stack images of KV, at the level of the maximal diameter of KV. Figure 3.23C graphs the mean and standard error of the mean length of cilia in KV in *ahi1* MO injected embryos (3.5±0.5μm) compared to uninjected WT embryos (5.7±0.3μm) and shows that cilia in KV were significantly ($p=0.0057$, unpaired t-test) shorter in *ahi1* MO injected embryos.

Figure 3.22 Variable spectrum of disruption to the development of Kupffer's Vesicle in *ahi1* MO injected zebrafish

Confocal microscopy images of golden zebrafish embryos injected with *ahi1* MO following fixation at the 8-10 somite stage and double fluorescent immunostaining using atypical protein kinase C (aPKC, green, A, D) antibody to label the apical membrane of KV cells and anti-acetylated tubulin (AT,red, B, E) antibody to label cilia. Whilst the development of KV appears normal in some *ahi1* MO-injected embryos (A-C), in others there is marked disruption of the KV apical membrane (D), with reduction in the number of cilia (E). Images were taken with a 20x objective and zoom of 3. Scale bars = 20 µm. MO, morpholino oligonucleotide.

Figure 3.23 Analysis of cilia in Kupffer's vesicle of *ahi1* MO injected embryos
(A) Quantification of KV phenotype, whether ciliated or not, as determined by confocal microscopy of embryos fixed at 8-10 somite stage and labelled with anti-acetylated tubulin antibody to detect cilia. *ahi1* MO injected embryos (n=32) had a statistically significant reduction in the number of embryos with cilia in KV (*, $p < 0.0001$ chi-squared test), compared to uninjected wild type (WT) control embryos (n=35) and embryos injected with a standard control (Std Con) MO (n=5). (B) Stacked bar chart showing the percentage reduction in KV with cilia in *ahi1* morphants, compared to uninjected and Std Con MO injected embryos. (C) Data are shown as mean ± SEM of length of cilia in in KV. Cilia in KV were significantly shorter, when present, in *ahi1* MO injected embryos (n=2, 3.50± 0.50µm), compared to uninjected WT controls (n=6, 5.68± 0.25µm) (*, p=0.0057, unpaired t-test). Simple neurite tracer (Fiji software) was used to measure the length of cilia from confocal z-stack images of embryos labelled with anti-acetylated tubulin antibody. Approximately 20 cilia in KV were measured per embryo. MO, morpholino oligonucleotide.

3.2.9 Left-right asymmetry defects following *ahi1* MO injection

Leftward fluid flow, generated by cilia beating in KV, is essential for left-right body patterning and determining the laterality of organogenesis (Amack et al., 2007; Essner et al., 2005). Cardiac left-right asymmetry begins from around 24hpf, when the initially straight cardiac tube 'jogs' to the left and subsequently from 36hpf the heart tube 'loops' to the right, leading to the final positioning of the single ventricle to the right of the single atrium by approximately 48hpf (Ahmad et al., 2004). This two stage development of cardiac asymmetry is considered predictable from the initial position of the heart tube (jogging) to the final direction of the heart (looping) and was suggested to be coupled by the same genetic signalling mechanism and predicted by the initial heart tube position in embryos with a normal notochord (Chen et al., 1997; Chin et al., 2000). However in zebrafish embryos with an abnormal notochord, which mediates a 'midline barrier' to genetic molecular signals, the initial heart tube position and subsequent direction of heart looping were found to be uncoupled or randomised (Chin et al., 2000). Further midline barriers mediated by Bmp signalling and *lefty2* expression regulate left-right patterning and understanding of these conserved important pathways continues to be established (Lenhart et al., 2011).

The normal pattern of cardiac looping in zebrafish embryos is rightward or D-looping. Alterations in cardiac looping and ultimate cardiac laterality can be a consequence of abnormal fluid flow in KV and a read out of cilial defects. Indeed, an absence of normal cilia in KV of zebrafish morphants has been shown to be associated with loss of fluid movement in KV (Kramer-Zucker et al., 2005). Although one might expect this to lead to randomisation of left-right patterning (Amack and Yost, 2004), loss of cilia in KV has been shown to lead to aberrant (predominantly right-sided) expression of left-right genes such as *southpaw* (*spaw*) (Kramer-Zucker et al., 2005). *spaw* is a zebrafish nodal related gene and has been identified as the earliest marker of left-right asymmetry showing strong left-sided expression at the 10-12 somite stage (Long et al., 2003). MO knockdown of *spaw* leads to loss of downstream asymmetrical molecular markers (Essner et al., 2005), thus clearly it plays a fundamental role.

Cardiac looping can be evaluated by light microscopy, however the use of transgenic zebrafish which express GFP under a *cardiac myosin light chain* (*cmcl2*) promoter highlights the heart (Huang et al., 2003), making scoring more obvious and enabling the

acquisition of clearer images. Figure 3.24 shows paired light and fluorescent microscopy ventral images of the three different patterns of cardiac looping used to score the embryos. An uninjected WT control embryo displays the normal rightward looping (D-looping), whereas *ahi1* morphants showed either no looping, with a straight heart tube (this midline heart position is also referred to as randomised) (Chin et al., 2000), or reversed leftward looping (L-looping) (Figure 3.24). Quantification of the cardiac looping phenotype revealed that all uninjected WT control embryos had normal, D-looping (n=145), whereas in *ahi1* morphants only 58 of 221 (26%) developed D-looping. In the remaining *ahi1* morphants: 13 (6%) failed to develop a cardiac loop and had a straight heart tube; whilst 150 (68%) had a reversed appearance with a L-loop. This difference in normal D-looping between uninjected WT control embryos and *ahi1* morphants was statistically significant ($p < 0.0001$, chi-squared test) (Figure 3.25A). To ascertain whether altered cardiac left-right asymmetry was a consequence of MO injection alone, a standard negative control MO was injected. Only 1 of 39 embryos injected with the Std Con MO developed the reversed cardiac L-loop, the rest of the embryos developed normal D-looping. Figure 3.25B is a stacked bar chart displaying the percentage cardiac looping phenotype of each experimental group.

Figure 3.24 Defects in heart laterality after *ahi1* knockdown in *cmcl2*-GFP zebrafish embryos

Paired light and fluorescent microscopy ventral images of *cardiac myosin light chain 2* (*cmcl2*-GFP) zebrafish embryos at 56 hours post fertilisation (hpf) to assess cardiac looping. The normal rightward looping (D-looping) of the zebrafish heart tube leads to positioning of the single ventricle (V) to the right of the single atrium (A) as seen in uninjected wild type (WT) control embryos (A, B). In contrast, in *ahi1* morphant embryos there is either no looping of the heart tube (C, D) or a reversal of the normal pattern with leftward looping (L-looping, E , F).

Figure 3.25 Analysis of cardiac looping reveals laterality defects in *ahi1* MO injected embryos

(A) Quantification of orientation of cardiac looping at 56hpf in cardiac myosin light chain 2 (*cmcl2*-GFP) embryos. Normal looping is to the right (D-looping), alternatives are no looping or looping to the left. There is a significant reduction in frequency of normal cardiac D-looping in *ahi1* MO injected embryos (n=221) (*, $p < 0.0001$, chi squared test), compared to uninjected wild type (WT) controls (n=145) and embryos injected with a standard control (Std Con) MO (n=39). (B) Stacked bar chart showing the percentage frequency of each cardiac looping orientation in each experimental group (D-loop, white; no loop, checked; L-loop, black). hpf, hours post fertilisation; MO, morpholino oligonucleotide.

3.2.10 *ahi1* morphants develop dilated cloacae and variable loss of pronephric cilia

Given the previous identification of cystic dilatation of the distal pronephros and cloaca of *ahi1* morphants using both light and fluorescent microscopy, which was confirmed on histology sections (Figure 3.11), it was important to evaluate whether this cyst formation and dilatation of the cloaca in *ahi1* morphants was associated with differences in pronephric cilia. At 72hpf, *claudin-b:*Lyn-GFP transgenic WT and *ahi1* morphant embryos were fixed in 4% PFA and immunostaining performed using anti-acetylated tubulin antibody to detect cilia. Confocal microscopy images of uninjected WT control embryos show that the pronephric ducts are lined by cilia and meet in apposition at the cloaca (Figure 3.26A, B). In *ahi1* morphants, there is dilatation of the cloaca (Figure 3.26D, F) and a variable appearance of pronephric cilia. Compared to 100% (n=48) of uninjected WT control embryos which had an undilated cloaca and pronephric ducts closely apposed, 75% (n=30) of *ahi1* morphants had a dilated cloaca (Figure 3.27A, B). This difference in cloacal appearance was statistically significant, $p < 0.0001$, chi-squared test.

In a minority of *ahi1* morphants, cilia remain present lining the dilated cloaca (Figure 3.26C, D). Whilst the pronephric cilia appeared shorter in length when present in *ahi1* morphants compared to uninjected WT controls, it was not possible to quantify the length of individual cilia (Figure 3.26C). In most other *ahi1* morphants, there was complete absence of cilia from the pronephros (Figure 3.26E). All uninjected WT control embryos (n=9) had cilia lining the distal pronephric ducts compared to only 1 of 8 *ahi1* morphants (Figure 3.27C), this loss of pronephric cilia from *ahi1* morphants was statistically significant ($p < 0.0003$, chi-squared test).

Figure 3.26 Variable spectrum of disruption to cilia at the cloaca in *ahi1* morphant zebrafish embryos

Confocal microscopy images of *claudinb:*Lyn-GFP zebrafish embryos fixed at 72hpf and immunostained with anti-acetylated tubulin antibody (AT, red, A-C) to identify cilia. Uninjected wild type controls (WT, A, B) have cilia (arrows, A) lining the pronephros which meets at the cloaca (B). In *ahi1* morphants, the pronephric ducts are dilated at the cloaca (star, D, F), with variable preservation of cilia (enlarged image, arrows, C) or complete absence of cilia (E). Images were taken with a 20x objective and zoom of 3. Scale bars = 50 μm.

Figure 3.27 Analysis of cloaca for dilatation and cilia in *ahi1* MO injected zebrafish embryos

(**A**) Quantification of cloaca phenotype in *claudinb*:Lyn GFP zebrafish embryos at 72 hours post fertilisation (hpf) reveals that there was a statistically significant difference between *ahi1* morphants, which mostly have a dilated cloaca (n=30), compared to the normal apposed appearance of the cloaca in uninjected wild type (WT) controls (n=48, *, $p < 0.0001$ chi-squared test). (**B**) Stacked bar chart showing the percentage difference in the cloaca phenotype between *ahi1* morphants and WT zebrafish embryos. (**C**) Cilia were mainly absent from the cloaca in *ahi1* morphant (n=7) zebrafish embryos compared to WT controls (n=9, *, $p < 0.0003$ chi-squared test).

3.3 Discussion

3.3.1 Creating a zebrafish model to study *AHI1*

In order to study the role of *AHI1* in development, the presence of a representative *ahi1* gene transcript and conservation of its encoded protein, Jouberin, was first confirmed in the zebrafish veterbrate model organism. The temporal expression of *ahi1* during development, was identified including in the: fundamental ciliated organising centre, KV; eye; brain; inner ear; olfactory bulbs and pronephros. To ascertain a functional role for *ahi1* in organogenesis, MOs were used to knockdown *ahi1* and a detrimental effect on normal development was detected. Abnormal phenotypes identified in *ahi1* morphants included abnormal body curvature, hydrocephalus, cardiac anomalies, pronephric cysts, eye and ear defects. This range of anomalies is well recognised in zebrafish models of ciliopathy disorders (NPHP, JBTS, MKS) and cystic kidney disease following silencing of ciliary genes (Ferrante et al., 2009; Kramer-Zucker et al., 2005; Obara et al., 2006; Sullivan-Brown et al., 2008).

Specificity of the *ahi1* morphant zebrafish model was confirmed by co-injecting embryos with mouse *Ahi1* mRNA, which rescued the ciliopathy phenotypes back to a normal pattern of development in the majority of embryos.

3.3.2 Abnormalities of Kupffer's vesicle in *ahi1* morpholino injected zebrafish embryos

Following *ahi1* MO knockdown, disruption of the apical membrane of cells lining the zebrafish organising centre, KV and a dramatic loss of cilia in the majority of embryos were observed. Interestingly, disruption to apical tissue organisation and cytoskeleton networks has previously been identified in murine IMCD3 kidney cell culture model systems of *Ahi1* knockdown (Hsiao et al., 2009; Sang et al., 2011; Simms et al., 2012). siRNA mediated knockdown of *Ahi1* in murine renal collecting duct cells was associated with a significant reduction in the formation of cilia, from 74% in negative control transfected cells to only 24% in *Ahi1* siRNA treated cells (see Figure 7a,b of Appendix F) (Simms et al., 2012). The efficacy of the described siRNA knockdown experiments was confirmed by western blotting and all siRNA experiments and cell culture work was performed by Dr Helen Dawe, University of Exeter.

In the few *ahi1* MO injected zebrafish embryos with detectable cilia in KV, the length of cilia was found to be significantly shorter than the length of cilia in KV of WT embryos. This work provides more detailed evidence of the nature of 'KV defects' in zebrafish embryos following *ahi1* MO knockdown. Previously, nonspecific abnormalities in KV were reported in approximately 45% of zebrafish embryos in which *ahi1* was knocked down (Sang et al., 2011).

Further nonspecific abnormalities in KV have been reported following MO knockdown of other genes which are known to cause ciliopathy disorders (NPHP, JBTS, MKS) including *nphp1*, *nphp4*, *nphp5* and *nphp8* in zebrafish embryos (Sang et al., 2011).

Similarly, in a zebrafish model of NPHP and MKS created by *nphp3* MO knockdown, fewer and shorter cilia were detected in KV, suggesting that *nphp3* must play a role in ciliary function (Zhou et al., 2010b).

In the ciliopathy, BBS, knockdown of 6 *BBS* genes (*bbs2* and *bbs4-bbs8*) in zebrafish also resulted in a range of abnormalities within KV including: a reduction in KV diameter; complete absence of KV; progressive loss of cilia; shorter cilia and ultimately complete absence of cilia (Yen et al., 2006). The authors (Yen et al., 2006) suggested that the progressive loss of cilia from KV inferred that BBS proteins were required for the maintenance of cilia.

In order to try to understand the functional implications on development of abnormalities within KV, including short or absent cilia, live imaging to study cilia motility within KV has been performed. Knockdown of *cordon-bleu*, a gene involved in neural tube formation, therefore important in body patterning and morphogenesis, resulted in shorter cilia within KV (Ravanelli and Klingensmith, 2011). Live imaging of *cordon-bleu* zebrafish morphants revealed disturbed fluid flow within KV (Ravanelli and Klingensmith, 2011). Sufficient, effective fluid flow within KV is essential to enable the establishment of asymmetrical left-right body patterning and has been reported as a requirement for normal organogenesis of the kidney and brain (Kramer-Zucker et al., 2005). Unfortunately live imaging to assess KV in the zebrafish embryos herein was not feasible and therefore cilia motility or fluid flow in the *ahi1* MO injected embryos cannot be commented on.

3.3.3 Abnormalities of cilia in Kupffer's vesicle mediates aberrant left-right body patterning in *ahi1* morpholino injected zebrafish embryos

Leftward fluid flow induced by cilia beating in KV, is responsible for determining left-right body asymmetry (Kramer-Zucker et al., 2005). This fact is widely accepted however is established via a complex series of genetic signalling interactions. At least five pathways are proposed to play a role in the development of KV and establishment of left-right asymmetry: dorsal forerunner cells must develop and form KV; nodal signalling pathways control expression of a ciliary motor protein (left-right dynein) which directs fluid flow; cilia must develop in cells lining the lumen of KV and become motile (Essner et al., 2005). It has been suggested by examining left-right mutants and morphants that subtle interference in any of the steps in KV development and the establishment of left-right asymmetry pathway leads to a uniform endpoint of aberrant left-right asymmetry, however this may be mediated by altered expression of various downstream left-right genes (Essner et al., 2005). Whilst changes within KV and cilia are most likely to account for the altered left-right patterning, two further caveats are notable: cilia are also found in other midline structures such as the notochord which is considered to play a role in left-right development (Danos and Yost, 1996); additionally the proteins of many of the studied genes are expressed in other non-ciliary locations which may have an influence (Essner et al., 2005)

Herein it was interesting to identify that heart laterality as assessed by cardiac looping, was defective, with development of a L-loop in the majority of *ahi1* morphant embryos. This predominantly reversed cardiac looping in *ahi1* morphants was slightly surprising, since loss of cilia from KV was the prevalent finding, one might have expected an equal split or randomisation (Oteiza et al., 2010; Schneider et al., 2010) between L-looping and no looping of the cardiac tube. Our results would suggest that *ahi1* is essential for the development of cilia in KV and that *ahi1* interferes with expression of left-right nodal genes such as *spaw*. In future work, this could be further established by performing *in situ* experiments utilising a *spaw* probe. An alternative hypothesis for the reversed cardiac looping identified herein in *ahi1* morphants may be that left-right developmental signalling is arrested following the initial jogging of the heart to the left and there is a failure of subsequent looping to right. This latter hypothesis could be addressed by assessing both cardiac jogging and looping phenotypes and ascertaining whether these were coupled or not.

Cilia length (Lopes et al., 2010) is recognised to play an important influence on the speed and direction of fluid flow within KV and mediate asymmetrical expression of molecular markers. Unfortunately assessment of cilia motility and fluid flow in the *ahi1* MO injected embryos was not feasible as real time imaging of cilia within KV was not feasible, all of the embryos in the experiments herein were fixed, furthermore cilia were undetected in the majority.

Assumedly, fluid flow within KV of *ahi1* morphants with short or absent cilia, would not be coordinated and either too slow, not leftward, or randomised, therefore limit the correct expression of asymmetric genes essential for establishing normal left-right asymmetry and organogenesis (Essner et al., 2005).

Loss of cilia (Schneider et al., 2010) and shorter cilia (Lopes et al., 2010) in KV leading to defective left-right asymmetry has been reported in other zebrafish models of NPHP (Slanchev et al., 2011; Zhou et al., 2010b) and in studies of ciliary genes (Duldulao et al., 2009; Ferrante et al., 2009; Oteiza et al., 2010). In the ciliopathy, BBS, knockdown of *bbs4-bbs8* resulted in altered cardiac looping in 5-30% of zebrafish embryos and as noted above was associated with a range of abnormalities within KV (Yen et al., 2006). Shorter cilia were detected in KV following MO knockdown of PCP genes *wnt11* and *prickle1a* (Oteiza et al., 2010). This was associated with 'randomised' heart laterality, which following closer review was predominantly leftward cardiac looping (Oteiza et al., 2010). Interestingly, other groups investigating ciliopathy genes such as *nphp4* have reported 'randomised' heart looping in zebrafish morphants, however after examining their work, leftward looping also appears to be more prevalent than middle or no loop (Slanchev et al., 2011). These findings of predominantly leftward cardiac looping rather than truly randomised organ laterality were evident in our *ahi1* morphants and hypotheses for why this may be are suggested above.

3.3.4 Alterations in cilia in *ahi1* morphant zebrafish embryos are associated with pronephric cysts and dilatation of the cloaca

The development of cysts within the pronephros of *ahi1* morphants were identified by light and fluorescent (using *claudinb:*Lyn-GFP transgenic embryos) microscopy, which was confirmed on resin histology sections. Of particular interest, dilatation of the distal pronephros at the cloaca and a variable pattern of cilia expression including complete absence of cilia from some *ahi1* morphants were observed.

Previously, cystic dilation and obstruction of the cloaca has been reported in zebrafish models of a related ciliopathy gene, *nphp4* (Burckle et al., 2011; Slanchev et al., 2011). These groups report no reduction in the number of cilia on cells in the pronephric duct, however cilia are described as shorter (Burckle et al., 2011), curly, disorientated (Slanchev et al., 2011) and less motile (Burckle et al., 2011). Inspite of this, they concluded that cloacal abnormalities were likely independent of ciliogenesis but rather structural, related to defective migration of distal pronephric duct cells which they observed during live imaging (Slanchev et al., 2011).

It would have been interesting to assess the motility of cilia, when present, in the distal pronephros/cloaca in the *ahi1* morphant embryos herein, to determine whether the cystic dilation is mediated by dysfunctional cilia motility. Unfortunately embryos were fixed prior to performing antibody staining to detect cilia. Additionally it would have been interesting to assess whether the *ahi1* morphants with a dilated cloaca were in fact obstructed, by injecting the pericardium with a rhodamine labelled dextran and evaluating clearance from the pericardium and/or via the cloaca (Hentschel et al., 2005). Despite attempts and practice, the performance of pericardial injections in *ahi1* morphants with a dilated cloaca was not reproducible, perhaps because embryos frequently had a curved body axis, which caused difficulties with manipulating them into an appropriate position.

3.3.5 *ahi1* knockdown in zebrafish is associated with defective ciliogenesis

Mechanisms for how *ahi1* knockdown may influence the length of cilia could be because Jouberin contains coiled coil domains important for maintaining the structure of cellular scaffolding (Hsiao et al., 2009), or because Jouberin interacts with Rab8a (a protein involved in membrane trafficking) thus the proteins together regulate cilium formation (Hsiao et al., 2009). Furthermore, the presence of SH3 domains within Jouberin emphasises its role as an interacting protein. This is supported by the proposition that Jouberin behaves as a bridging protein to link three protein modules which function to mediate apical organisation, Hh signalling and maintaining cilia integrity. Together these protein modules make up the recently identified NPHP-Joubert-Meckel-Gruber protein network (Sang et al., 2011). Ideally it would have been interesting to assess the motility of cilia (when present) by performing live imaging of *ahi1* MO injected embryos. Also, particularly when cilia were not detected, it would

have been interesting to further evaluate the extent of this structural aberration using other basal body/centrosomal antibodies. The use of three dimensional cell culture models would have complimented further evaluation of the role of *ahi1* in ciliogenesis and tissue PCP.

Chapter 4 Zebrafish models demonstrating the phenotypic spectrum of Joubert Syndrome related ciliopathies caused by *cc2d2a, nphp6* and *mks3* knockdown

4.1 Introduction

The ciliopathy JBTS is an autosomal recessive genetically heterogeneous disorder, with up to 19 causal genes presently identified, which together account for 50% of patients (refer to Table 1.2). The phenotype of affected individuals is very variable, even within the same family and genetic pleiotropy is evident (Coppieters et al., 2010). For example, *NPHP6* mutations can cause isolated blindness or NPHP, as well as JBTS and BBS, with additional features of obesity and hypogonadism (Forsythe and Beales, 2012; Leitch et al., 2008), however there is a poor genotype-phenotype correlation (Coppieters et al., 2010). Interestingly, at least 3 genes, *CC2D2A*, *NPHP6* and *MKS3/TMEM67*, can cause both JBTS and the more severe, often lethal, related ciliopathy, MKS (Bachmann-Gagescu et al., 2012). Both *CC2D2A* and *NPHP6* each account for approximately 20% of patients diagnosed with MKS. *MKS3* is the third most frequently identified cause of MKS and accounts for approximately 10% of patients (CA. Johnson, personal communication).

Understanding of the clinical heterogeneity remains primitive, however, oligogenicity, whereby a third mutation in a different gene, in combination with a pathogenic compound heterozygous or homozygous mutation, has been hypothesised as a mechanism for modifying the severity of a clinical phenotype (Hoefele et al., 2007). Oligogenicity has been identified in patients with ciliopathy syndromes including NPHP (Hoefele et al., 2007), JBTS (Tory et al., 2007) and BBS (Katsanis et al., 2001).

4.1.1 Zebrafish models of JBTS related ciliopathies

In 2008, a zebrafish mutant, *sentinel*, with a spontaneous nonsense mutation in *cc2d2a*, was reported to develop a sine wave shaped tail and pronephric cysts (Gorden et al., 2008), however further details characterising the phenotype were sparse and not published. The *sentinel* zebrafish did however appear to be a useful model for evaluating oligogenicity, as when *nphp6* (which colocalises with *cc2d2a* at the basal body of cilia) was knocked down in *sentinel* embryos, there was a synergistic increase in the development of pronephric cysts (Gorden et al., 2008). However, no

oligogenicity was identified in a cohort of patients with JBTS including consanguineous families (Gorden et al., 2008). Interestingly however in patients with the more severe MKS ciliopathy, missense changes in both *NPHP6* and *CC2D2A* have been identified (Hopp et al., 2011).

In 2006, MO knockdown of *nphp6* was used to create a zebrafish model of JBTS, with pronephric cysts and developmental defects in the retina, cerebellum and otic cavity (Sayer et al., 2006). No difference in the length or motility of cilia were detected in the pronephros of zebrafish cystic *nphp6* morphants (Sayer et al., 2006), however cilia in KV were not assessed/reported.

There are no zebrafish models of MKS caused by *mks3* knockdown and although there was a mouse model with cystic kidney disease (Cook et al., 2009), it lacked the associated features of MKS including cerebellar anomalies/occipital encephalocele, liver cysts. Furthermore in the mouse model challenges of infertility and mortality within 3 weeks, limited their ability to study the pathogenesis of MKS (Cook et al., 2009).

4.1.2 Aims of this chapter

In order to study a spectrum of JBTS related ciliopathies (NPHP, MKS), the aim was to create zebrafish models of these human disorders, in particular to characterise the phenotypes associated with each of the following ciliary genes: *CC2D2A*, *NPHP6* and *MKS3*.

To study *CC2D2A*, further definition of the *sentinel* zebrafish mutant phenotype during development was sought, including evaluating the retina and cilia within KV. Furthermore, since homozygous *sentinel* embryos have been reported to develop pronephric cysts in up to 33% (Gorden et al., 2008), the response to Rapamycin (an antiproliferative therapy proven to be effective in mouse (Shillingford et al., 2006) and zebrafish (Tobin and Beales, 2008) models of cystic kidney diseases, and being evaluated in human patients with ADPKD (Serra et al., 2007)) was assessed. Additionally, an aim was to create and characterise an alternative zebrafish model of *CC2D2A* related ciliopathies, by MO knockdown of *cc2d2a*. The *cc2d2a* morphants would enable a study of the effect of gene dose, which would be informative for later

work, Chapter 5, evaluating oligogenicity. Secondly, the *cc2d2a* morphants were generated to increase the data regarding *cc2d2a* in development and ciliopathy diseases.

Using *nphp6* MO knockdown, an aim herein was to recapitulate the published ciliopathy phenotype (Sayer et al., 2006) to demonstrate the genetic pleiotropy and by studying cilia within KV, to evaluate any subsequent effect on cardiac left-right asymmetry.

Finally, to study the severe end of the ciliopathy spectrum, an aim was to create a zebrafish model of MKS by *mks3* knockdown, to characterise the phenotype and study the effect of interference with *mks3* on development.

4.2 Results

4.2.1 *CC2D2A* genomic and proteomic information in humans and zebrafish

Human *CC2D2A* was mapped to chromosome 4p15.33 (Noor et al., 2008) and confirmed as a pathogenic ciliopathy gene by homozygosity mapping of consanguineous families with JBTS (Gorden et al., 2008) and MKS (Tallila et al., 2008). Interestingly, a correlation between *CC2D2A* genotype and ciliopathy phenotype was suggested following identification of missense mutations leading to JBTS and null mutations causing MKS (Mougou-Zerelli et al., 2009). *CC2D2A* in both humans (Tallila et al., 2008) and zebrafish (Gorden et al., 2008) contains 38 exons.

Using the online Vertebrate Genome Annotation database (http://vega.sanger.ac.uk), 17 human *CC2D2A* transcripts, 7 of which were protein coding were identified. The best evidence supports a transcript (*CC2D2A_002* OTTHUMT00000359906) with 5175bp and encodes the associated 1620 amino acid protein, CC2D2A (OTTHUMP00000217873) (Figure 4.1A,B). CC2D2A contains 3 coiled-coil domains and a C2 domain. As previously noted, coiled-coil domains are structurally important (Mason and Arndt, 2004), whilst C2 domains involve calcium-dependent binding and mediate signal transduction (Tallila et al., 2008). CC2D2A is strongly expressed in fetal: brain and kidney tissue; adult: retina, kidney, heart and lung tissue (Gorden et al., 2008).

No zebrafish orthologues for *CC2D2A* were apparent using the 'vega.sanger' database, however using the ensembl browser (www.ensembl.org/Danio_rerio) a single, representative transcript (ENDSDART00000126768) on chromosome 23.2 was identified, which consisted of 5001bp and encoded a cc2d2a protein product (ENDSDARP00000107405) of 1666 amino acids. The zebrafish cc2d2a protein consisted of 5 coiled-coil domains (Burkhard et al., 2001) and a C2 domain (involved in signal transduction and vesicular trafficking (Sutton and Sprang, 1998)) (Figure 4.1C,D). Figure 4.1E shows the effect of the nonsense mutation in *sentinel* zebrafish, which leads to a stop codon, instead of a tryptophan, in exon 14 of *cc2d2a* (Owens et al., 2008). The *sentinel* mutation is associated with loss of 68% of the cc2d2a protein and therefore is considered likely to be physiologically relevant (Owens et al., 2008). The *sentinel* zebrafish was initially identified as a protective mutant from

aminoglycoside induced hair cell death (Owens et al., 2008), which led to early hypotheses that *cc2d2a* may play a role in regulating cilia.

Figure 4.1 CC2D2A gene transcript and partial protein product structure in humans and zebrafish

(A) *CC2D2A* gene transcript in humans (OTTHUMT00000359906) and schematic representation of encoded protein product, coiled coil domain containing protein 2A (CC2D2A), with 3 coiled-coil domains and 1 C2 domain, consisting of 1620 amino acids (OTTHUMP00000217873) (B). (C) *cc2d2a* transcript in zebrafish (ENDSDART00000126768) and schematic representation of encoded protein product, cc2d2a (ENDSDARP00000107405) (D). (E) Schematic representation of zebrafish *cc2d2a* showing the nonsense mutation, a stop codon present in exon 14. aa, amino acids; CC, coiled coil; Ch., chromosome; C2 domain

4.2.2 *CC2D2A* evolutionary conservation

CC2D2A is highly conserved with orthologues in a diverse range of species from humans to sea anemones, mice, chicken, cattle and monkeys (Gorden et al., 2008). Using multalin, the evolutionary conservation between humans, mice and zebrafish is shown (Figure 4.2). Zebrafish *cc2d2a* is 56% identical and 73% similar to human *CC2D2A* (Owens et al., 2008).

Figure 4.2 Evolutionary conservation of Cc2d2a in humans, mice and zebrafish
Cc2d2a peptide sequence alignment in humans (homo sapiens, OTTHUMP000000217873), mice (mus musculus, ENSMUSP00000048320), zebrafish (danio rerio, ENSDASP00000107405) and consensus sequence is shown (Multalin). Conservation of amino acid alignment (red font).

4.2.3 Establishment of *sentinel* and transgenic *sentinel:claudin-b:*Lyn-GFP zebrafish

A *sentinel* zebrafish line was established in our laboratory following the kind gift of a batch of embryos from Dan Doherty's laboratory in Washington. Once mature, in order to facilitate utilising the *sentinel* zebrafish line particularly to study the pronephros, adult *sentinel* zebrafish heterozygotes were crossed with transgenic *claudin-b:*Lyn-GFP line, which are recognised for their prominent GFP expression within the pronephros (Haas and Gilmour, 2006). The F2 offspring were phenotyped at 72hpf and the parents of embryos with both a sinusoidal shaped tail and an appropriate GFP signal were maintained as a heterozygote *sentinel:claudin-b:*Lyn-GFP strain.

Figure 4.3 shows light and fluorescent microscopy images of the temporal development of *sentinel:claudin-b:*Lyn-GFP zebrafish embryos at 24-72hpf. By 72hpf, both hydrocephalus and the characteristic sine wave shaped tail were evident in *sentinel* homozygous embryos. Claudin-b was also prominently expressed in the telencephalon, otic placode and the posterior lateral line (Lopez-Schier et al., 2004).

4.2.4 Confirmation of *sentinel* genotyping and sequencing

To confirm the association between phenotype and genotype, a single embryo with a sine wave shaped tail (presumed *sentinel*) and a linear (presumed WT) tail were fixed and DNA was isolated. PCR using dCAP primers which introduce a restriction enzyme site into the WT embryos was performed and an agarose gel run to confirm adequate DNA from each sample, both measured the expected 156bp (Figure 4.4C). Subsequently a restriction enzyme digest was performed which resulted in a smaller product in WT embryos (128bp, as the enzyme cuts the DNA) compared to *sentinel* homozygotes (156bp, Figure 4.4D). The *sentinel* and WT products visualised in the agarose gel were cut out, purified and sent for direct sequencing to identify the molecular difference. The chromatograms are shown in Figure 4.5. The cDNA sequences show the relevant difference in the WT, which encodes a tryptophan amino acid, whilst in the *sentinel* mutants, a nonsense mutation (G>A) in exon 14 resulted in a stop codon and truncation of the protein at 491 amino acids (Figure 4.5B). This work confirms the published mechanism of the *sentinel* mutation, which was considered

significant and to cause loss of the *cc2d2a* gene and protein function (Owens et al., 2008).

Figure 4.3 Development of *sentinel* and transgenic *sentinel:claudin-b:*Lyn-GFP zebrafish embryos
Lateral views of *sentinel* (s*nl*) (A,C,E) and *snl:cldn-b:*Lyn-GFP (B,D,F) zebrafish embryos at 24, 48 and 72 hours post fertilisation (hpf). The characteristic sine wave shaped tail (*, E-F) of *snl* homozygous zebrafish embryos is evident at 72hpf.

Figure 4.4 Genotyping of *sentinel* zebrafish embryos
Lateral views of presumed homozygote *sentinel* (*snl/snl*) with sine wave shaped tail (A) and golden uninjected wild type control (+/+ WT) (B) zebrafish embryos at 72hpf. DNA was isolated from each single embryo and PCR performed with dCAP primers, which introduce a restriciton enzyme recognition site into WT embryos. The agarose gel (C) confirms sufficient DNA for each sample (156 bp). Following a restriction enzyme digest, the gel (D) shows the *snl* homozygotes have a product of 156bp, whereas WT embryos are cut and have a smaller product of 128bp. This confirms the phenotype. bp, base pairs; hpf, hours post fertilisation.

Figure 4.5 Sequencing of *sentinel* (*snl*) and uninjected wild type (WT) zebrafish embryos at 72hpf

(A) Chromatogram of PCR product across predicted point mutation in *snl* mutant obtained by RT-PCR of RNA at 72 hpf. Zoomed view of WT and *snl* mutant cDNA sequencing (B) shows there was a nonsense mutation (G>A), (circled in red in each sequence), in the *snl* homozygous embryos resulting in a trytophan changing to a premature stop codon and truncation at 498 amino acids, compared to the WT controls. hpf, hours post fertilisation; Lys, lysine; Ser, serine; STOP, stop codon; Trp, tryptophan.

4.2.5 Phenotypes of *sentinel* mutants includes hydrocephalus, cardiac anomalies, pronephric cysts and ocular defects

Embryos born from *sentinel* heterozygous matings were phenotyped by light and fluorescent microscopy at 72hpf. A sine wave shaped tail, defining a *sentinel* homozygote was identified in only 12% (n=153) of embryos, rather than in 25% as would be expected from Mendelian genetics. The frequency of aberrant ciliopathy type phenotypes detected in the *sentinel* mutants is shown in Figure 4.6A. The mean mortality rate in *sentinel* embryos was 12% and 3% at 24 and 72hpf respectively (Figure 4.6B).

A variable severity of cardiac oedema (Figure 4.7B-D) occurs in up to 3% (n=36), hydrocephalus (Figure 4.7D) in 1% (n=12), proximal pronephric cysts (Figure 4.8C-H) in 0.5% (n=6) and ocular anomlies (Figure 4.9) in 0.2% (n=2) of homozygous *sentinel* mutants. Ocular anomalies include either unilateral microphthalmia or a coloboma. To further assess the eyes of *sentinel* mutants, embryos were fixed at 5 days post fertilisation (dpf), embedded in resin and sectioned to obtain 5μm cross sections of the eyes. Although the outer retinal pigmented epithelial layer is grossly preserved in *sentinel* mutants, there is indistinct definition of the other retinal layers, compared to uninjected WT embryos (Figure 4.10). No abnormalties of development of the otic placode or vesicles were detected in *sentinel* mutants.

Unfortunately a much lower frequency of aberrant phenotypes were detected in the offspring of *sentinel* heterozygous matings herein than in the previously published work using *sentinel* mutant zebrafish, even allowing for a degree of incomplete penetrance of phenotypes (Gorden et al., 2008). It is difficult to determine how this significant caveat could be modified for future work utilising *sentinel* mutants, since breeding of homozygous zebrafish mutants who may develop a severe phenotype is not encouraged and is usually associated with failure to survive.

Figure 4.6 Phenotypes & Mortality rates of *sentinel* zebrafish embryos
(A) Quantification of the percentage (%) frequency of abnormal phenotypes at 72hpf in embryos born from two *sentinel* (*snl*) heterozygous (het) parents (n=1254). A sine wave tail phenotypically defines a *snl* embryo, however only 12% (n=153) of clutches of embryos were identified with this appearance. The low percentage of *snl* homozygotes may account for the overall low percentage of abnormal phenotypes. 2% (n=24) had a non-sine wave curly tail, 3% (n=32) had cardiac oedema, 1% (n=12) had hydrocephalus, 0.5% (n=6) had pronephric cysts and 0.2% had an abnormal eye (either coloboma or unilateral micropthalmia, n=2). A cyclops appearance was not identified in any embryos. (B) The percentage mortality rates at 24 (n=178) and 48 (n=35) hpf are shown as mean and standard error of the mean in embryos born from *snl* het parents. hpf, hours post fertilisation.

Figure 4.7 Phenotypes (Tail, Cardiac, Brain) in *sentinel* zebrafish embryos at 72hpf

The characteristic sine wave shaped tail of *sentinel* (*snl*) mutant zebrafish is shown in (B), compared to the normal appearance of uninjected wild type (WT) controls (A). The variable spectrum of severity of cardiac anomalies and oedema are highlighted (*) in B-D. Hydrocephalus is arrowed in D.

Figure 4.8 Pronephric cysts in *sentinel* and *sentinel:claudin-b:*Lyn-GFP zebrafish embryos at 72hpf

Light and fluorescent microscopy images of the normal appearance of uninjected wild type (WT) *claudin-b:*Lyn-GFP (*cldn-b:*GFP) controls (A, B), compared to *sentinel* (*snl)* and *sentinel:claudin-b:*Lyn-GFP (*snl:cldn-b:*GFP) zebrafish mutant embryos. Some *snl* mutants display proximal pronephric cysts (arrowed, lateral view (C, D), dorsal view (E); large cysts at the level of the proximal convuluted/straight tubule (red dotted line, F); distal pronephros (arrowed, G, H). The variable severity of developmental deformities in the *snl* mutants is evident.

Figure 4.9 Abnormal eye development in *sentinel* zebrafish embryos at 72hpf
Light microscopy, lateral and dorsal, images focusing on the eyes of an uninjected wild type (WT, A-C) and a *sentinel* (*snl*, D-G) mutant zebrafish embryo. In the *snl* mutant embryo, there is abnormal eye development with both unilateral microphthalmia (black arrows, D-G) and a coloboma (red arrow, E).

Figure 4.10 Abnormal retinal histology in *sentinel* zebrafish embryos
Resin histology 5µm sections of the eyes of uninjected wild type (WT, A, B) and *sentinel* (*snl*, C, D) mutant zebrafish embryos, stained with methylene blue-basic fuchsin stain. A shows overview of the normal retina, with formation of discrete retinal layers from 72 hours post fertilisation. B-D show that at 5 days post fertilisation, whilst the retinal pigmented epithelial layer is preserved in *snl* mutants (C, D), there is disorganisation of retinal development, with loss of definition of retinal layers. Images are taken with 20x objective (A-C) and 40x objective (D). Scale bars = 20µm

4.2.6 Gross reduction in number of cilia in Kupffer's vesicle of *sentinel* mutants

Since cc2d2a is known to be expressed at the basal body of cilia and *sentinel* mutants develop a ciliopathy phenotype, KV was grossly assessed. Immunostaining of cilia using an antibody to acetylated tubulin showed a reduction in the number of cilia in an 8-10 somite stage embryo born from heterozygous *sentinel:claudin-b:*Lyn-GFP zebrafish pairs (Figure 4.11). In addition to an overall reduction in the number of cilia, there was no apparent expression of claudin-b at epithelial cell junctions of KV. Therefore, although KV in *sentinel* embryos appears to continue to develop as a cavity with some cilia, the organisation and polarity of its epithelium could not be further evaluated and may be abnormal. Several *sentinel* embryos were damaged during processing for KV imaging and the numbers actually assessed were very small. Samples were fixed, therefore cilia motility and fluid flow within KV could not be assessed, however would be interesting to perform in future work.

Figure 4.11 Reduction in number of cilia in Kupffer's vesicle in embryo from heterozygous *snl* zebrafish parents

Confocal microscopy images of *cldnb*:Lyn-GFP wild type (WT, A-C) and those born to heterozygous *sentinel:cldnb:*Lyn-GFP (*snl*, D-F) parents, following fixation at the 8-10 somite stage and fluorescent immunostaining using anti-acetylated tubulin (red) to study cilia in Kupffer's vesicle (KV). Overlay images of KV (arrowed, scale bar = 50µm, 20x objective) in WT (A) and *snl* (D) embryos. Higher magnification images B, C, E, F (zoom of 3, scale bar = 20µm). Red laser shows a normally ciliated (arrowed) KV in WT (B), whilst a sparse number of cilia are apparent in *snl* (E) embryos. In WT (C) expression of *cldnb*:Lyn-GFP at epithelial cell-cell junctions within KV is organised (C). In this *snl* (F) there is no distinct delineation of KV epithelium (*cldnb*:Lyn-GFP), cilia are sparse (arrow).

4.2.7 No reduction in aberrant phenotypes in *sentinel* mutants following Rapamycin therapy

Rapamycin was dissolved in 0.05% DMSO (drug solvent vehicle) and added to E2 zebrafish water to make concentrations of 0.1μM (Rapa A) and 0.05μM (Rapa B). These concentrations of Rapamycin therapy were chosen because previous zebrafish models of ciliopathies have shown efficacy in reducing pronephric cysts with Rapamycin concentrations between 0.002-0.1μM (Tobin and Beales, 2008). To ensure any effects were genuine and not secondary to the drug vehicle, DMSO or E2 media alone, these solutions were evaluated in parallel, therefore there were four arms being assessed in total. Where relevant, each solution of Rapamycin was replaced every 24 hours, to ensure continued exposure, as has been performed in previous zebrafish studies using Rapamycin (Makky et al., 2007).

The toxicity of Rapamycin therapy was investigated by evaluating mortality in uninjected WT and *sentinel* mutants at 24 and 72 hours following exposure to the drug. There was no significant difference in 24 hour mortality rates (24-44%) between any of the four solutions in either WT or *sentinel* embryos (Figure 4.12A). Longer term toxicity was low, less than 4% in any treated group, and was evaluated by calculating mortality between 24-72 hours following exposure to each media (Figure 4.12B). Delaying the onset of exposure to either concentration of Rapamycin therapy did not alter mortality rates at 72 hours, which remained less than 4% (Figure 4.12C).

The side effect profile following exposure to Rapamycin therapy from 0hpf was investigated by evaluating the phenotype of WT embryos at 72hpf. There was no significant difference in the frequency of abnormal phenotypes in WT embryos exposed to each media (Figure 4.12D).

Figure 4.12 Safety and Efficacy of Rapamycin therapy for use in zebrafish embryos

Wild type (WT) and *sentinel* (*snl*, born to heterozygous *snl* parents) embryos were selected from the same parental pairs and exposed to four different media: E2, 0.05% DMSO (a solvent vehicle for Rapamycin), Rapa A (0.1µM), Rapa B (0.05µM). There was no significant difference (chi-squared test) in the mortality rates of WT and *snl* embryos at 24 (A) and 72 (B) hpf/following 24 or 72 hours exposure to the four different media. (continued next page)

NB 2 pages

Pg2 of Fig The delayed introduction of Rapamycin therapy to later stages of 24 and 48hpf (C) did not alter mortality rates. The side effect profile of eachmedia was evaluated at 72hpf in WT embryos exposed from 0hpf (D). All embryos exposed to standard E2 media were phenotypically normal. There was no significant difference in the frequency of abnormal phenotypes in WT embryos exposed to different media, however some developmental anomalies occurred in embryos exposed to 0.05% DMSO and increasing concentrations of Rapamycin therapy (dose-dependent). All WT embryos exposed to Rapa A or B from 24hpf and 48hpf were phenotypically normal, suggesting any toxicity is associated with early exposure (prior to 24hpf). No WT embryos developed an abnormal eye phenotype or pronephric cysts. The efficacy of two doses of Rapamycin therapy was evaluated in *snl* embryos exposed from fertilisation (0hpf, E). The timing of initiation of Rapamycin was also evaluated, in *snl* embryos exposed from 24hpf and 48hpf (F). There was no significant difference in the percentage frequency of abnormal phenotypes of *snl* embryos treated with different doses of Rapamycin therapy and no difference introduced by varying the timing of initiation of therapy. DMSO, dimethyl sulfoxide; E2, standard zebrafish embryo media; hpf, hours post fertilisation; Rapa, Rapamycin.

However, it is likely that the DMSO drug vehicle and increasing concentrations of Rapamycin exert a toxic effect, since: 100% of WT embryos exposed to the standard E2 zebrafish media were normal; 6% of WT embryos exposed to DMSO were abnormal and up to 9% of WT embryos were abnormal following exposure to Rapamycin in a dose-dependent manner (Table 4.1, Figure 4.13). No WT embryos developed pronephric cysts or an abnormal eye phenotype following exposure to Rapamycin. Of note, all WT embryos with delayed exposure to Rapa A (0.1μM) or B (0.05μM) from 24hpf and 48hpf were phenotypically normal (Figure 4.13D), suggesting any toxicity is associated with early exposure (prior to 24hpf) to Rapamycin.

	Phenotype					
Media	**Normal %**	**Other Curly tail %**	**Cardiac oedema %**	**Hydrocephalus %**	**Otic defect %**	**Total n**
E2	100	0	0	0	0	96
0.05% DMSO	94	6	6	0	0	54
Rapa B (0.05μM)	95	3	5	0	0	68
Rapa A (0.1μM)	91	9	6	1	1	64

Table 4.1 Effect of Rapamycin therapy and drug vehicle media on wild type zebrafish embryos
Percentage (%) frequency of phenotypes at 72hpf of wild type zebrafish embryos exposed to various media from 0hpf. 'Other curly tail' describes a non-sine wave curly tail, to distinguish from *sentinel* embryos (sine wave shaped curly tail). 100% of embryos kept in standard E2 media were normal. 6% (n=3) of embryos exposed to the drug vehicle 0.05% DMSO had an abnormal curly tail and cardiac oedema. In embryos exposed to Rapamycin therapy, the frequency of anomalies increased in a dose dependent manner. This suggests there is some toxicity associated with 0.05% DMSO and increasing concentrations of Rapamycin therapy. Of note, all embryos exposed to Rapa A or B from 24hpf and 48hpf were phenotypically normal, suggesting any toxicity is associated with early exposure (prior to 24hpf). No embryos developed an abnormal eye phenotype or pronephric cysts. Data are reported as percentages, except the column entitled 'Total n', which is the total raw data numbers. DMSO, dimethyl sulfoxide; Rapa A, 0.1μM Rapamycin; Rapa B, 0 05μM Rapamycin.

Figure 4.13 Phenotypes of wild type zebrafish embryos exposed to Rapamycin: toxicity associated with dose and timing of onset of exposure

Light microscopy images of wild type (WT) zebrafish embryos at 72hpf. (A) shows a normal WT embryo maintained in the standard embryo media (E2) from 0hpf. (B, C) show WT embryos maintained in two different doses of Rapamycin (Rapa B= 0.05µM, Rapa A=0.1µM) from 0hpf, the media was replaced every 24hpf. B has developed gross cardiac odema (*), whilst exposure to a higher dose of Rapamycin (0.1µM) from 0hpf can lead to more severe developmental anomalies (C) including growth arrest (short tail) and a single otolith (arrow, C). D is a WT embryo maintained in E2 for the first 24hpf prior to exposure to high dose Rapamycin (Rapa A, 0.1µM) from 24hpf. D has a normal appearance (n=85), suggesting any toxicity associated with Rapamycin occurs during early exposure, in the inital 24hrs of development.

The efficacy of the two doses of Rapamycin therapy (0.1μm and 0.05μm) following exposure from fertilisation (0hpf) was evaluated in *sentinel* embryos by phenotyping at 72hpf (Figure 4.12E). There were fewer normal embryos (66%) after being maintained in the standard E2 media, compared to 75% and 80% of embryos appearing normal after being maintained in 0.1μM and 0.05μM Rapamycin respectively, however this difference was not statistically significant. There were similar numbers of homozygous *sentinel* embryos exposed to each of the media/Rapamycin treatments (n=5-8). Figure 4.14 shows light microscopy images of the aberrant phenotypes of *sentinel* embryos maintained in each of the different media/Rapamycin therapy. A *sentinel* embryo maintained in the drug vehicle 0.05% DMSO developed a dorsal curly tail, pronephric cyst, single otolith and unilateral microphthalmia (Figure 4.14D). There was no significant difference in the frequency of abnormal phenotypes in *sentinel* embryos, particularly no reduction in hydrocephalus or pronephric cysts following treatment with Rapamycin 0.05-0.1μM therapy (Figure 4.12E). Whilst delaying the initiation of exposure to Rapamycin therapy from 0hpf (n=225) to 24hpf (n=152) resulted in a dose dependent reduction in the frequency of cardiac oedema from 9-23% to 3%, this difference was not statistically significant (Figure 4.12F). Overall, there was no significant difference in the percentage frequency of abnormal phenotypes in *sentinel* embryos as a consequence of varying the timing of initiation of Rapamycin therapy (Figure 4.12F). Up to 48 hours of a dose range of 0.05-0.1 μM of Rapamycin therapy is not efficacious in preventing aberrant development in *sentinel* mutants.

Figure 4.14 Phenotypes of *sentinel* zebrafish embryos exposed to Rapamycin from 0hpf

Light microscopy images of *sentinel* zebrafish embryos at 72hpf. (A, B) shows a *sentinel* (*Snl*) embryo maintained in the standard embryo media (E2). The characteristic sine wave tail is evident and a pronephric cyst is arrowed (A, B). C, D show *snl* embryos maintained in 0.05% DMSO (the solvent vehicle for Rapamycin). D shows a *snl* which has developed cardiac oedema (*), a pronephric cyst (black arrow), a single otolith (black arrowhead) and unilateral microphthalmia (white arrow). E,F show *snl* embryos which have been maintained in two different doses of Rapamycin (E, Rapa B= 0.05µM) and (F, Rapa A=0.1µM) from 0hpf, the media was replaced every 24hpf. In addition to the characteristic sine wave shaped tail, F has developed cardiac odema (*). DMSO, dimethyl sulfoxide; Rapa, Rapamycin.

4.2.8 Design of *cc2d2a* morpholino oligonucleotide to mimic *sentinel* mutants

Since the number of *sentinel* homozygous offspring from *sentinel* heterozygous crossings was lower than anticipated and because studying oligogenicity would be important to try to understand the variable clinical phenotype even within families, we sought to create an alternative zebrafish model of *cc2d2a* related ciliopathies. In order to study the effects of *cc2d2a* gene knockdown, a MO was designed. Figure 4.15 shows the exon map of *cc2d2a* in zebrafish, the spontaneous mutation in exon 14 responsible for *sentinel* mutants (Figure 4.15A) and how the *cc2d2a* MO (Figure 4.15B) was designed to target exon 14 and therefore mimic the *sentinel* mutation.

4.2.9 Evidence of *cc2d2a* morpholino oligonucleotide knockdown

RT-PCR of equal concentrations of isolated RNA from individual uninjected WT and *cc2d2a* splice blocking MO injected zebrafish embryos was performed at 24-72hpf. In the WT embryos, the expected *cc2d2a* product size of approximately 692bp was evident. In both WT and *cc2d2a* splice blocking MO injected embryos there was an additional larger band of approximately 800bp, likely the result of mispriming and does not appear to be functionally relevant. However sequencing of this additional 800bp band would be required to determine its exact identity. Importantly, in *cc2d2a* splice blocking MO injected embryos there was a maximal reduction in the normal RT-PCR product at 24hpf and an additional smaller product measuring approximately 500bp (Figure 4.15C). Although this smaller RT-PCR product at 24hpf was not cut out and sent for direct sequencing because of time constraints, we postulate that it represents splicing of exon 14 (which would result in loss of 157bp) and therefore an expected product of 535bp in *cc2d2a* morphants. Formal direct sequencing of the smaller approximately 500bp product would have to be performed in order to confirm or refute this hypothesis. Of note, although a maximal knockdown or reduction of the normal *cc2d2a* product is evident at 24hpf, a modestly sized normal product band persists, this acknowledges a limitation of MO experiments, the fact that MO knockdown is incomplete (Bill et al., 2009). The increased intensity of the normal *cc2d2a* product of approximately 692bp at 48 and 72hpf in *cc2d2a* MO injected embryos would be in keeping with the reported temporary effect of some MO (Eisen and Smith, 2008).

Figure 4.15 *cc2d2a* morpholino design
(A) Schematic representation of zebrafish *cc2d2a* showing the spontaneous nonsense mutation, a stop codon, present in exon 14 of *sentinel* mutants. (B) Schematic representation of the splice blocking (*cc2d2a* ie14) morpholino oligonucleotide (MO) designed to mimic the spontaneous mutation in *sentinels*, by targeting the same exon (14). All MO sequences are in the Methods/Appendix. (C) RT-PCR of single embryos at 24-72hpf following *cc2d2a* splice MO knockdown reveals maximal reduction of the normal 692bp product at 24hpf and an additional smaller product in *cc2d2a* morphants measuring approximately 500bp (white arrow). The larger band at 800bp in all 24-48hpf embryos does not appear relevant. hpf, hours post fertilisation; MO, morpholino oligonucleotide; WT, wild type.

4.2.10 Phenotypes of zebrafish morphants created by *cc2d2a* MO knockdown

Zebrafish embryos were phenotyped by light microscopy at 72hpf. Uninjected WT embryos were phenotypically normal (Figure 4.16A). Embryos were injected with a dose range of 4-8ng of *cc2d2a* splice blocking MO (*cc2d2a* MO) which led to abnormal development including a dorsally curved body axis, hydrocephalus, cardiac oedema, pronephric cysts, a wavy notochord, altered number of otoliths (Figure 4.16) and abnormal eye development (Figure 4.17). A 6ng dose of *cc2d2a* MO resulted in the most prevalent frequency of abnormal phenotypes (Figure 4.18B) without resulting in an excess mortality rate at 24 hours (Figure 4.18A). Although the overall 24 hpf mortality rate in embryos injected with 6ng *cc2d2a* MO was 15% compared to 24% in embryos injected with 4ng *cc2d2a* MO, the relative 24 hpf mortality rate (to appropriately matched uninjected embryos) was higher (5:1) with the increased (6ng) dose of *cc2d2a* MO, confirming the expected dose dependent effect of MO.

If *cc2d2a* morphants injected with 6ng MO developed a curly tail (14%, n=21), it was always a dorsal curly tail (Figure 4.16B, C), possibly mimicking the sine wave pattern of *sentinel* mutants. Proximal pronephric cysts were detected in 7% (n=10, Figure 4.16B, D) of 6ng *cc2d2a* morphants. In only 1% of 6ng injected *cc2d2a* morphants, an abnormal number of otoliths (Figure 4.16C) or a wavy notochord (Figure 4.16D, Figure 4.18B) were detected. Abnormalities of rudimentary ear and notochord development were not apparent in homozygous *sentinel* mutants.

Abnormal eye development occurred in 2% (n=3) of 6ng injected *cc2d2a* morphants and included microphthalmia and coloboma formation (Figure 4.17). This low frequency of aberrant ocular phenotypes was similar in homozygous *sentinel* embryos.

Figure 4.16 Phenotype with *cc2d2a* MO knockdown
Lateral views of zebrafish embryos 72 hours post fertilisation. A is an uninjected wild type control (WT) and is phenotypically normal. Embryos injected with 6ng of *cc2d2a* splice MO develop a range of anomalies including: cardiac oedema (*); hydrocephalus (white arrows, B, C); pronephric cysts (B, D), altered number of otoliths (single in C, white arrowhead) and a wavy notochord (red arrow, D). MO, morpholino oligonucleotide.

Figure 4.17 Abnormal eye development in zebrafish embryos injected with *cc2d2a* MO

Lateral views of the head of zebrafish embryos 72 hours post fertilisation. A is an uninjected wild type control (WT) and is phenotypically normal. Embryos injected with *cc2d2a* splice MO (arrows, B-D) have abnormal eye development including microphthalmia or coloboma formation. MO, morpholino oligonucleotide.

Figure 4.18 Mortality at 24hpf and phenotypes at 72hpf of zebrafish embryos following *cc2d2a* MO injection

Mortality at 24hpf (A) is not significantly higher in embryos injected with *cc2d2a* MO (n=234), compared to uninjected wild type controls (n=85, p=0.31, chi-squared test). The percentage mortality rises in both *cc2d2a* MO injected embryos from 15% (6ng, n=151) to 24% (4ng, n=83) and from 3% to 10% in matched WT embryos, however the mortality ratio of *cc2d2a* MO injected embryos relative to WT embryos falls from 5:1 (6ng) to 2.4:1 (4ng), confirming the dose dependent effect of increasing MO dose on mortality. Graph B shows the percentage frequency of abnormal phenotypes at 72hpf in embryos injected with 6ng (n=150) of *cc2d2a* MO. 7% of embryos developed pronephric cysts following 6ng of *cc2d2a* MO. hpf, hours post fertilisation; MO, morpholino oligonucleotide.

4.2.11 *NPHP6* Genomic and Proteomic Information in humans and zebrafish

Human *NPHP6* was identified by positional cloning on chromosome 12q21.32 in 2006 (Sayer et al., 2006). Using the online Vertebrate Genome Annotation database (http://vega.sanger.ac.uk), *NPHP6* is shown to consist of 54 exons (Figure 4.19A) and has 7 transcripts, 4 of which are protein coding. The transcript (OTTHUMT00000406344) has 7948bp, the best supporting evidence and encodes the protein, nephrocystin-6 (OTTHUMP00000242341) which consists of 2479 amino acids and 13 coiled-coil domains (Figure 4.19B). Nephrocystin-6 expression is evident to varying degrees in an extensive array of human tissues. Real-time PCR analysis of human tissues identified highest expression in the neural retina, nasal epithelium, spinal cord, thyroid gland, testis, heart, lung, bone marrow, cerebellum and uterus. Weaker expression was also identified in the fetal brain, kidney and to a lesser extent in the trachea, thymus, muscle, salivary gland, liver, and placenta (Papon et al., 2010).

In zebrafish a *nphp6* orthologue has been identified on chromosome 25, consists of 53 exons (Figure 4.19C) and has a single transcript (OTTDART00000051136) of 7706bp. This *nphp6* transcript encodes a protein (OTTDARP00000040195) of 2439 amino acids, consisting of 19 coiled-coil domains (Figure 4.19D).

4.2.12 *NPHP6* is conserved throughout evolution

NPHP6 is highly conserved throughout evolution, with 49 orthologues currently identified (http://ensembl.org) in mammals (Chang et al., 2006), birds, amphibians, zebrafish (http://www.ncbi.nlm.nih.gov/gene) and a range of invertebrate model organisms including the honeybee *Apis mellifera*, the sea squirt *Ciona intestinalis* (Sayer et al., 2006) and in the ciliated protozoa *Tetrahymena thermophilia*. Figure 4.20 shows the evolutionary conservation of Nphp6 (nephrocystin-6) or centrosomal protein 290 (cep290) between humans, mice and zebrafish. The conserved amino acid regions are shown in red.

Figure 4.19 *NPHP6* gene transcript and partial protein product structure in humans and zebrafish
(A) *NPHP6* gene transcript in humans (OTTHUMT00000406344) and schematic representation of encoded protein product, centrosomal protein of 290kDa (CEP290) which includes 13 coiled-coil domains (CC) and has 2479 amino acids (OTTHUMP00000242341) (B). (C) *nphp6* gene transcript in zebrafish (OTTDART00000051136) and schematic representation of encoded protein product, cep290 (OTTDARP00000040195), which includes 19 CC domains and has 2439 amino acids (D). aa, amino acids; Ch., chromosome.

Figure 4.20 Evolutionary conservation of Nphp6 (CEP290) in humans, mice and zebrafish

Nphp6 (CEP290) peptide sequence alignment in humans (OTTHUMP00000242341), mouse (ENSMUSP00000130899) and zebrafish (OTTDARP00000040195). Conservation of amino acid alignment (red font).

4.2.13 Design and effect of *nphp6* morpholino oligonucleotides

Both translation (ATG) and splice (ie42) blocking MO were created to interfere with *nphp6*. Figure 4.21A shows the 53 exons in zebrafish *nphp6* and the target sites for both *nphp6* MO on the predicted zebrafish *nphp6* exon sequence. The splice blocking MO targets exon 42 and leads to abnormal splicing with inclusion of a 1227bp intron after exon 43 (Figure 4.21B). At the protein level, the intron is included after 2029 amino acids and results in loss of 2 coiled coil domains from the nephrocystin-6 protein (Figure 4.21C).

Following the injection of *nphp6* MO at the 1-4 cell stage and again at 24hpf, mortality rates were assessed. Figure 4.22 depicts the mortality at 24hpf as mean percentage and standard error of the mean for a range of doses of *nphp6* splice and translation blocking MO. Comparative 24hpf mortality data is also shown for uninjected WT control embryos from the same parental pairs. Both *nphp6* splice (Figure 4.22A) and *nphp6* translation (Figure 4.22B) blocking MO induced a dose dependent effect on 24hpf mortality rates. However there was no significant difference in mortality rates at 24hpf between MO injected and uninjected embryos, as shown in Figure 4.22.

Figure 4.21 Design of *nphp6* MO and the effect of the splice blocking MO at the protein level
(A) Schematic representation of zebrafish *nphp6* showing target sites of translation (ATG) and splice (*nphp6*iex42) blocking morpholino oligonucleotides (MO). (B) The splice blocking MO, *nphp6*iex42, designed to target exon 42, leads to abnormal splicing with inclusion of a 1227bp intron (red) after exon 43. At the protein level, the intron is included after 2029 amino acids and results in loss of 2 coiled coil domains (C).

Figure 4.22 Mortality at 24hpf following *nphp6* MO injection
Mortality at 24 hours post fertilisation (hpf) is shown as mean percentage (%) and standard error of the mean (where appropriate) in zebrafish embryos injected with a range of morpholino oligonucleotide (MO) doses. Matched uninjected wild type (WT) controls are shown. Both *nphp6* splice (A) and *nphp6* translation blocking (B) MO induce a dose dependent effect on mortality. For the splice blocking MO (A), total numbers of embryos at 24hpf were 547 from 7 pairs (6ng), 342 from 3 pairs (4ng) and 73 from 1 pair (2ng). For the translation blocking MO (B), total numbers of embryos at 24hpf were 430 from 4 pairs (2ng) and 303 from 2 pairs (1ng).

4.2.14 Phenotypes of zebrafish morphants created by *nphp6* MO knockdown

Zebrafish embryos were phenotyped by light microscopy at 72hpf. Uninjected WT embryos were phenotypically normal (Figure 4.23A). Embryos injected with either *nphp6* splice (*nphp6* Sp) or *nphp6* translation (*nphp6* ATG) targeting MO had abnormal development including: convergent extension defects leading to shortened or curved body axis; hydrocephalus, cardiac oedema and altered number of otoliths (Figure 4.23B-E). Additionally *nphp6* morphants develop cysts of varying sizes throughout the pronephros (Figure 4.24) and cystic dilatation of the distal pronephros at the cloaca in some embryos (Figure 4.24E).

Figure 4.23 Phenotype with *nphp6* MO knockdown
Lateral views of zebrafish embryos 72 hours post fertilisation. Wild type (WT) uninjected control embryos are phenotypically normal (A). Embryos injected with *nphp6* translation (B, C) and splice (D, E) blocking MO develop hydrocephalus (black arrows), cardiac oedema (*), curved body axis (C-E) and altered number of otoliths (none, black arrowhead, E). MO, morpholino oligonucleotide.

Figure 4.24 *nphp6* MO knockdown induces pronephric cysts in zebrafish embryos
Lateral views of pronephric cysts (black arrowheads) in *nphp6* morphants at 72 hours post fertilisation (B-E). (A) is a phenotypically normal uninjected wild type (WT) control embryo. *nphp6* morphants develop proximal (B-C), distal (D) and cloacal (E) pronephric cysts. The cloaca in E is very dilated and distorted, this embryo also has hydrocephalus and a single otolith.

The abnormal eye and ear development found in *nphp6* morphants was further characterised by light microscopy images of their heads at 72hpf. Abnormal rudimentary ear development was identified as an empty otic vesicle or a single otolith (Figure 4.25B-D). Anomalies of eye development included unilateral microphthalmia and coloboma formation (Figure 4.25E-H).

The mean frequency of the development of each abnormal phenotype at 72hpf following injection of a dose range of *nphp6* translation (*nphp6* ATG) or splice (*nphp6* Sp) blocking MO is shown in Figure 4.26. The frequency of development of abnormal phenotypes was dose dependent, with higher doses of splice (Figure 4.26B) blocking MO required to induce a phenotype (mean percentage (±SEM)) compared to translation blocking MO (Figure 4.26A). Injection of 1-2ng of *nphp6* ATG MO induced the following frequency of phenotypes: curved body axis in 11.3% (±7.5%) to 13.5% (±6.9%); cardiac oedema in 13.3% (±8.4%) to 15.7% (±7.8%); pronephric cysts in 5.7% (±3.8) to 6% (±3.5%); hydrocephalus in 3.7% (±0.3%); otic defects in 0.7% (±0.7%) to 1.3% (±0.3%) and colobomas in 0.7% (±0.7%) to 1.3% (±0.3%). Injection of 4-8ng of *nphp6* Sp MO induced the following frequency of phenotypes: curved body axis in 16% (±14%) to 56.7% (±17%); cardiac oedema in 13% (±10%) to 56.7% (±17%); hydrocephalus in 2.5% (±0.5%) to 42.7% (±22.6%); pronephric cysts in 1.5% (±1.5) to 19.3% (±8.3%); otic defects in 2% (±1%) to 16.3% (±13%) and colobomas in 1.5% (±1.5%) to 6.3% (±6.3%). These abnormal developmental phenotypes identified in the *nphp6* zebrafish morphants are characteristic of a zebrafish ciliopathy.

Figure 4.25 Abnormal eye and ear development following *nphp6* MO knockdown
Views of the head of zebrafish embryos at 72 hours post fertilisation, focusing on the otic vesicles (A-D) and eyes (A, E-H). Wild type (WT) uninjected control embryos have normal eyes of equal size and two otoliths in each otic vesicle (green arrows, A). Lateral views of embryos injected with *nphp6* MO show abnormal ear development with either an empty otic vesicle (black arrow, B-C) or a single otolith (red arrow, D). Abnormal eye development includes unilateral microphthalmia (black arrowheads, lateral (E) and dorsal (F) views) and coloboma formation (red arrowheads, lateral (G) and ventral (H) views) in *nphp6* morphants. MO, morpholino oligonucleotide.

Figure 4.26 Quantification of abnormal phenotypes at 72hpf following injection with *nphp6* splice or translation blocking MO

Data are displayed as mean ± SEM. The percentage frequency of each abnormal phenotype was higher following *nphp6* splice (Sp) MO (B) knockdown, compared to following *nphp6* translation (ATG) MO (A) knockdown. There was a dose dependent effect on the frequency of each abnormal phenotype. The total number of zebrafish embryos phenotyped at 72hpf following each dose of *nphp6* ATG MO was 236 (2ng) and 158 (1ng) (A). The total number of zebrafish embryos phenotyped at 72hpf following each dose of *nphp6* Sp MO were 84 (8ng), 216 (6ng) and 261 (4ng). MO, morpholino oligonucleotide.

4.2.15 Specificity of *nphp6* splice MO knockdown and direct sequencing

RT-PCR of (equal concentrations of isolated RNA from) individual uninjected WT zebrafish embryos at 24hpf revealed the expected product size of 309bp. RT-PCR of single *nphp6* splice MO injected zebrafish embryos at 24hpf suggested abnormal splicing by the presence of an additional larger RT-PCR product (band greater than 1000bp, Figure 4.27A). The larger RT-PCR fragment identified in *nphp6* MO injected embryos was isolated from the gel, purified and sent for sequencing, which identified a 1536bp product created by inclusion of the intron (1227bp) situated after exon 43 (Figure 4.27B).

Figure 4.27 Evidence of *nphp6* splice MO knockdown by RT-PCR and direct sequencing
(A) RT-PCR of single embryos at 24hpf following *nphp6* splice MO knockdown reveals an additional larger RT-PCR product (circled in white), compared to uninjected wild type (WT) control embryos, which only have the normal RT-PCR product of 309bp. (B) Direct sequencing (data not shown) confirmed the identity of the larger product in *nphp6* morphants which included intronic sequence after exon 43, confirming abnormal splicing. hpf, hours post fertilisation.

4.2.16 Shorter cilia in Kupffer's vesicle of *nphp6* MO injected embryos

KV was evaluated to determine whether there were any overt differences in cilia which may facilitate explanation of the ciliopathy phenotype in *nphp6* morphants (Figure 4.23, Figure 4.24, Figure 4.25). Immunostaining of cilia using an antibody to acetylated tubulin showed fewer and shorter cilia in *nphp6* MO injected embryos (n=8) compared to uninjected WT (Figure 4.28). The zebrafish embryos utilised for immunostaining express *claudin-b* at cell to cell junctions (tight junctions) of KV epithelial cells and this expression is also abnormal and less distinct in *nphp6* MO injected embryos.

Figure 4.28 Shorter cilia in Kupffer's Vesicle of *nphp6* MO injected zebrafish embryos

Confocal microscopy images of *cldb*:Lyn-GFP wild type (WT, A-C) and *nphp6* MO injected (D-F) zebrafish embryos following fixation at the 8-10 somite stage and fluorescent immunostaining using anti-acetylated tubulin (AT, red, B, E) antibody to label cilia. Cilia appear shorter and of a reduced number in KV of *nphp6* MO injected embryos (E-F), compared to uninjected WT (B-C). Images were taken with a 20x objective, zoom of 3. Scale bars = 20 μm. KV, Kupffer's vesicle; MO, morpholino oligonucleotide.

4.2.17 Dose dependent left-right cardiac asymmetry defects following *nphp6* MO injection

To evaluate whether the shortened cilia within KV of *nphp6* MO injected embryos would impede generation of sufficient fluid flow to establish normal left-right body patterning, cardiac looping was evaluated at 56hpf (Essner et al., 2005). Cardiac looping was evaluated by light microscopy, as the *cardiac myosin light chain* (*cmcl2*-GFP) transgenic zebrafish were not available for injection. Images were not acquired as the heart does not project as overtly using light microscopy, however scoring was as described in section 3.2.9. Figure 4.29A shows quantification of the raw numbers of cardiac looping phenotype in uninjected WT control embryos (n=80) and *nphp6* morphants (n=74) at 56hpf. There was a significant reduction in the normal, D-looping (n=11) asymmetry in *nphp6* morphants compared to uninjected WT control embryos (n=79, $p < 0.0001$, chi-squared test). Figure 4.29B shows the percentage frequency of cardiac looping following 6-8ng of *nphp6* MO, 15% develop normal D-looping whilst 80% develop L-looping.

The effect on cardiac looping appears to be dose dependent. In morphants injected with 6ng *nphp6* MO, 7 (24%) develop D-looping, 21 (72%) develop L-looping and only 1 (4%) develop no loop. Expressed as a ratio of left:right cardiac looping, 6ng *nphp6* MO leads to 3:1 developing L-looping relative to normal D-looping. Following a higher dose of *nphp6* MO (8ng), 4 (9.3%) develop D-looping, 36 (83.7%) develop L-looping and 3 (7%) develop no loop. The 8ng dose of *nphp6* MO leads to 9:1 developing L-looping relative to normal D-looping.

Figure 4.29 Analysis of cardiac looping reveals laterality defects in *nphp6* morphants at 56hpf

Quantification of orientation of cardiac looping at 56hpf in zebrafish embryos (A) reveals there is a significant reduction in the normal rightward cardiac looping (D-looping) in *nphp6* morphants (n=11, *, $p < 0.0001$, chi squared test), compared to uninjected wild type (WT) controls (n=79). (B) Stacked bar chart showing the percentage frequency of cardiac looping orientation in each experimental group. In the WT embryos, 99% (n=79) have D-looping and 1% (n=1) L-looping, compared to *nphp6* morphants in which 15% (n=11) have D-looping, 5% (n=4) have No looping and 80% (n=59) have L-looping. hpf, hours post fertilisation.

4.2.18 Cilia are present in the distal pronephros however appear reduced in number and shorter in the cloaca of *nphp6* morphants

At 72hpf, *claudin-b:*Lyn-GFP transgenic *nphp6* morphant embryos were fixed in 4% PFA and immunostaining performed using anti-acetylated tubulin antibody to detect cilia. Using confocal microscopy the distal pronephric ducts and cloaca were studied (Figure 4.30) and the presence of cilia confirmed in the pronephros more proximal to the cloaca (Figure 4.30E,F) in all *nphp6* morphants (n=6). However in some *nphp6* morphants, the number of cilia appeared to reduce and even be absent (Figure 4.30E, F) or very short at the cloaca (Figure 4.30H, I). Unfortunately it was not possible to formally quantify the length of individual cilia to detect any differences from cilia in uninjected WT control embryos.

Figure 4.30 Cilia in the distal pronephros and cloaca of *nphp6* morphant zebrafish embryos

Confocal microscopy images of *claudinb:*Lyn-GFP zebrafish embryos following fixation at 72hpf and immunostaining with anti-acetylated tubulin antibody (AT, red) to identify cilia. Uninjected wild type control (WT, A-C) embryos have cilia (white arrows, B) lining the pronephros which meet in apposition at the cloaca (A, C). In *nphp6* morphants, cilia are present in the distal pronephros, however reduce in number/disappear as the cloaca is approached (white circle, E, F). G-I show a cross sectional view of a dilated cloaca in an *nphp6* morphant with what appears to be short cilia. Images were taken with a 20x objective and zoom of 3. Scale bars = 20 µm.

4.2.19 *MKS3* Genomic and Proteomic Information in humans and zebrafish

Human *MKS3* was identified on chromosome 8q22.1 in 2006 (Smith et al., 2006). Using the online Vertebrate Genome Annotation database (http://vega.sanger.ac.uk), human *MKS3* is shown to consist of 28 exons (Figure 4.31A) and has 22 transcripts, 8 of which are protein coding. The transcript with the best evidence is OTTHUMT00000329641, has 4651bp and encodes the protein, meckelin (OTTHUMP00000203157) which consists of 995 amino acids and has 4 transmembrane domains (Figure 4.31B). Of note, *Smith et al*. reported that meckelin consists of 3-7 transmembrane domains (Smith et al., 2006). Meckelin is expressed in the human embryonic kidney (proximal renal tubule epithelial cells), liver, retina and hindbrain (Dawe et al., 2007) and localises at the ciliary transition zone of the primary cilium (Williams et al., 2011).

Using the http://vega.sanger.ac.uk database, 1 zebrafish orthologue of *MKS3* was identified on chromosome 16, consisting of 28 exons. There were 2 *mks3* transcripts, 1 of which was protein coding (OTTDART00000042166) with 3193bp (Figure 4.31C). This *mks3* transcript encodes a protein, meckelin (OTTDARP00000033569) of 982 amino acids, consisting of 5 transmembrane domains (Figure 4.31D).

4.2.20 *MKS3* is conserved throughout evolution

MKS3 is highly conserved throughout evolution, with orthologues in 52 vertebrate species (http://ensembl.org), including zebrafish and a range of invertebrate model organisms: *Drosophilia melanogaster*, *Caenorhabditis elegans*; *Chlamydomonas reinhardtii* plant (Hodges et al., 2010) and the unicellular organism *Trypanosoma cruzi* (Smith et al., 2006). Figure 4.32 shows the evolutionary conservation of meckelin between humans, mice and zebrafish. The conserved amino acid regions are shown in red.

Figure 4.31 *MKS3* gene transcript and partial protein product structure in humans and zebrafish
(A) *MKS3* gene transcript in humans (OTTHUMT00000329641) has 28 exons and schematic representation of encoded protein product, Meckelin which includes 4 transmembrane domains (TM) and has 995 amino acids (OTTHUMP00000203157) (B). (C) *mks3* gene transcript in zebrafish (OTTDART00000042166) has 28 exons and schematic representation of encoded protein product, meckelin (OTTDARP00000033569), which has 5 TM domains and 982 amino acids (D). aa, amino acids; Ch., chromosome.

Figure 4.32 Evolutionary conservation of Mks3 protein, Meckelin, in humans, mice and zebrafish

Meckelin peptide sequence alignment in humans (homo sapiens, ENSP00000389998), mice (mus musculus, ENSMUSP00000103928) and zebrafish (danio rerio, ENSDARP00000116688). Conservation of amino acid alignment (red font).

4.2.21 Design and effect of *mks3* morpholino oligonucleotide

A splice (*mks3*ei4) blocking MO was designed to interfere with *mks3* expression. Figure 4.33A shows the MO target site on the predicted zebrafish *mks3* exon sequence. The *mks3* ei4 MO induces abnormal splicing and a predicted inclusion of a 165bp intron after exon 3 (Figure 4.33B, Figure 4.34) resulting in a premature stop codon after 144 amino acids and loss of 4 transmembrane domains from meckelin (Figure 4.33C).

There was a dose dependent increased mortality rate at 24hpf in embryos injected with *mks3* MO compared to uninjected WT controls (Figure 4.35). The 24hpf mortality rate associated with *mks3* MO was 52.4% (±6.8%) for 2ng and 67.2% (±5.7%) for 4ng.

4.2.22 Specificity of *mks3* splice MO knockdown and direct sequencing

RT-PCR of (equal concentrations of isolated RNA from) individual uninjected WT zebrafish embryos at 24hpf revealed the expected product size of 390bp. However, in *mks3* splice MO injected zebrafish embryos there was abnormal splicing suggested by an additional larger RT-PCR product over 500bp (circled in white, Figure 4.34A). This larger PCR fragment was isolated from the gel, purified and sent for sequencing (Figure 4.34B), which identified a 555bp product created by inclusion of the intron (165bp) situated after exon 3. This splicing defect led to an alternative reading frame after amino acid 125, a premature stop codon after amino acid 144, predicting a truncated protein.

Figure 4.33 Design of *mks3* splice blocking MO and the effect at the protein level
(A) Schematic representation of zebrafish *mks3* showing the target site of the splice blocking MO is exon 4 (*mks3*ei4). Knockdown with *mks3* MO leads to abnormal splicing with inclusion of a 165bp intron (red) after exon 3 (B). At the protein level, this leads to an alternative reading frame after 125 amino acids and a premature stop codon after 144 amino acids, resulting in a truncated protein with loss of 4 transmembrane domains (C). MO, morpholino oligonucleotide.

Figure 4.34 Evidence of mks3 splice MO knockdown by RT-PCR and direct sequencing
(A) RT-PCR of single zebrafish embryos at 24hpf following *mks3*splice MO knockdown reveals an additional larger RT-PCR product (circled in white), compared to uninjected wild type (WT) control embryos, which only have the normal RT-PCR product of 390bp. (B) Direct sequencing of the larger product (555bp) in *mks3* morphants identifies that it includes the intron (165bp) situated after exon 3, as a result of abnormal splicing. bp, base pairs; hpf, hours post fertilisation; *mks3*cDNA, reference *mks3* cDNA sequence.

Figure 4.35 Mortality at 24hpf following *mks3* MO injection
Mortality at 24 hours post fertilisation (hpf) is shown as mean percentage (%) and standard error of the mean in zebrafish embryos injected with two different doses of morpholino oligonucleotide (MO). Matched uninjected wild type (WT) controls are shown. There is a dose dependent effect on mortality associated with *mks3* MO injection. The total numbers of embryos at 24hpf were 837 from 12 pairs (4ng) and 968 from 16 pairs (2ng).

4.2.23 Phenotypes of zebrafish morphants created by *mks3* knockdown

Zebrafish embryos were phenotyped by light microscopy at 72hpf. *mks3* morphants develop abnormally with: a curved body axis; tail and notochord anomalies; hydrocephalus; pronephric cysts; cardiac oedema; altered number of otoliths and unilateral microphthalmia. Pronephric cysts are evident both proximally (Figure 4.36B-D) and distally at the cloaca (Figure 4.36E-F), which in some embryos led to an obstructive picture with cystic dilatation extending proximally and the development of gross generalised oedema (Figure 4.36F). The pronephros was examined histologically by sectioning resin embedded embryos at 5dpf. Figure 4.36G-H shows the pronephros of *mks3* morphants was dilated to a diameter of 29.2-29.7μm compared to a pronephros diameter of 9.7-13.6μm in uninjected WT controls.

Figure 4.36 *mks3* knockdown induces pronephric and cloacal cysts, leading to obstruction of the cloaca

Lateral views of zebrafish embryos at 72 hours post fertilisation (A-F). Wild type (WT) uninjected control embryos are normal (A). Embryos injected with *mks3* MO develop pronephric cysts both proximally (arrow, B-D) and distally at the cloaca (arrow E, arrowhead F). The cloacal cyst (E) appears to cause outflow obstruction as there is marked associated cardiac oedema (*). The large cloacal cyst (arrowhead F) leads to proximal cystic dilatation of the pronephros (arrows). Resin histology 5µm sections through the pronephros (arrows) at 5 days (G-H) reveals dilatation in *mks3* morphants (diameter 29.2-29.7µm, H), compared to WT controls (diameter 9.7-13.6µm, G). Scale bars = 20µm. Stained with methylene blue-basic fuchsin stain.

In addition to abnormalities of the pronephros, *mks3* morphants develop variable severities of hydrocephalus by 72hpf. Anomalies of brain development including encephalocele formation are evident on resin histology sections by 5dpf (Figure 4.37). *mks3* morphants develop convergent extension defects, which are common to many ciliopathy genes, however interestingly they also develop abnormal notochords and tails. Compared to uninjected WT control embryos, *mks3* morphants frequently develop wavy notochords (Figure 4.38B-E), which in severe cases can extend dorsally through the floorplate, neural tube, myotomes and dorsal fin layers to the surface (Figure 4.38C). In *mks3* morphants without convergent extension defects, abnormalities which appeared like vacuoles were observed within the dorsal fin of the tail (Figure 4.38F-I). Figure 4.39 shows images of the heads of *mks3* morphants at 72hpf, focusing on eye and ear abnormalities. Eye development is disturbed with unilateral microphthalmia (Figure 4.39G-H) and rudimentary ear development is altered in *mks3* morphants with either an empty otic vesicle, a single otolith or 3 otoliths (Figure 4.39C-H).

Figure 4.37 *mks3* knockdown induces hydrocephalus and abnormal brain development in zebrafish embryos
Lateral views of zebrafish embryos at 72hpf (A-F). Wild type (WT) uninjected control embryos are normal (A). Embryos injected with *mks3* MO develop hydrocephalus (arrows, B-F). Resin histology 5µm sections through the brain at 5dpf (G-H) reveals an encephalocele in *mks3* morphants (arrow, H) compared to WT controls (G). Scale bars = 20µm. Stained with methylene blue-basic fuchsin stain. dpf, days post fertilisation; hpf, hours post fertilisation; MO, morpholino oligonucleotide.

Figure 4.38 *mks3* knockdown induces notochord defects and abnormal tail development in zebrafish embryos
Lateral views of zebrafish embryos 72hpf (A-F). Wild type (WT) uninjected control embryos are normal (A). Embryos injected with *mks3* MO (B-I) develop abnormal, wavy notochords (B-E), in severe cases the notochord projects dorsally to the skin surface (B). *mks3* morphants also have abnormal tail development (F-I), with disruption of myotome and fin layers (arrows), representative of human meningoceles. hpf, hours post fertilisation; MO, morpholino oligonucleotide.

Figure 4.39 Abnormal ear and eye development following *mks3* MO knockdown
Views of the head of zebrafish embryos at 72 hours post fertilisation, focusing on the otic vesicles (A-F) and eyes (A, B, G, H). Wild type (WT) uninjected control embryos have normal eyes of equal size and two otoliths in each otic vesicle (black arrows, A, B). *mks3* morphants show abnormal ear development with either a single otolith (black arrow, lateral and dorsal views, C-D), unilateral empty otic vesicle (black arrow, E, H) or 3 otoliths in an otic vesicle (black arrows, F). Abnormal eye development with unilateral microphthalmia (red arrows, G-H) is also seen in *mks3* morphants. MO, morpholino oligonucleotide.

The mean percentage (±SEM) frequency of the development of each abnormal phenotype at 72hpf following injection of 2-4ng of *mks3* splice blocking MO increased in a dose dependent manner. Figure 4.40 shows a graph of the frequency of each phenotype following injection of 2-4ng of *mks3* MO: convergent extension defect with curly tail in 22.1% (±4.3%) to 25.5% (±4.6%); cardiac oedema in 20.7% (±4.9%) to 28.3% (±3.7%); hydrocephalus in 13.3% (±3.5%) to 13.8% (±2.7%); pronephric cysts in 9.3% (±2.4%) to 11.2% (±1.5%); otic defects in 3.9% (±1.8%) to 7.2% (±2.4%); meningocele/vacuolated dorsal fin 2.3% (±1.2%) to 4.3% (±3.8%); wavy notochord in 1.7% (±0.9%) to 4.7% (±1.3%) and abnormal eye development in 1% (±1%) to 2.6% (±1.6%).

Figure 4.40 Quantification of abnormal phenotypes at 72hpf following injection with *mks3* splice blocking MO

Data are displayed as mean ± SEM. Following injection with 2-4ng of *mks3* splice blocking MO, there was a dose dependent effect on the percentage frequency of each abnormal phentoype (A). The total number of zebrafish embryos phenotyped at 72hpf following *mks3* MO injection of: 2ng was 325 and 4ng was 233. hpf, hours post fertilisation; MO, morpholino oligonucleotide.

4.2.24 Specificity of *mks3* MO knockdown in *mks3* zebrafish morphants

To evaluate the specificity of morphant phenotypes induced by *mks3* MO knockdown, embryos were coinjected with human *MKS3* mRNA to see if this rescued the morphant phenotype. Embryos were injected with 50-100pg of human *MKS3* mRNA alone and phenotyped by light microscopy at 72hpf confirmed normal morphology in 96% of embryos (n=197, Figure 4.41B). Subsequently, coinjection of 50-100pg of *MKS3* mRNA and 2-4ng of *mks3* MO resulted in partial (n=69, Figure 4.41C) and complete (n=249, Figure 4.41D) rescue from the *mks3* morphant phenotype in 22% and 78% respectively (n=318). Quantification of the raw numbers of embryos with a normal WT appearance or morphant phenotype are classified by treatment group following 2-4ng of *mks3* MO alone (n=691) or co-injection with 50-100pg of human *MKS3* mRNA (n=318, Figure 4.42A). The raw overall rescue from a morphant phenotype to a normal WT appearance in embryos co-injected with 50-100pg of human MKS3 mRNA and 2-4ng of mks3 MO was just significant (*, p=0.052, chi-squared test). When comparing the frequency of individual morphant phenotypes (curly tail, cardiac oedema, hydrocephalus, meningocele, pronephric cyst, wavy notochord, abnormal eye, otic defect) of embryos injected with *mks3* MO alone and those rescued with human *MKS3* mRNA, there was a significant decrease in the raw numbers ($p < 0.0001$, chi-squared test) and percentage frequency (p=0.0058, chi-squared test) of abnormal phenotypes in embryos co-injected with human *MKS3* mRNA (Figure 4.42B). A normal morphological appearance was recovered in a mean of 83.8% (±4.7%, ±SEM) of embryos coinjected with *mks3* MO and human *MKS3* mRNA. The human mRNA is not predicted to be affected by the zebrafish MO as it does not share any target sequence.

Figure 4.41 Rescue of *mks3* morphant phenotype by co-injection of *mks3* MO with human *MKS3* mRNA

Lateral views of zebrafish embryos 72 hours post fertilisation. Wild type uninjected (A) and embryos injected with 50-100pg of human *MKS3* mRNA alone (B) were morphologically normal. Partial (C) and complete (D) rescue of embryos co-injected with *mks3* MO and 50-100pg of human *MKS3* mRNA. A small notochord defect is arrowed in C. MO, morpholino oligonucleotide.

Figure 4.42 Quantification of Rescue of *mks3* morphant phenotype
Raw quantification of overall rescue from a morphant phenotype to a normal, wild type appearance in embryos co-injected with 50-100pg of human *MKS3* mRNA and 2-4ng of *mks3* MO (n=318). The degree of rescue to the normal wild type phenotype was just significant (*, p=0.052, chi-squared test). The total number of embryos injected with 2-4ng of *mks3* MO alone was 691. (B) Percentage of each phenotype shown as mean ± SEM, in embryos injected with 2-4ng of *mks3* MO alone, compared to those co-injected with 50-100pg human *MKS3* mRNA. There was a significant degree of rescue to the wild type phenotype and reduction of each abnormal phenotype following co-injection with *MKS3* mRNA (*, p=0.0058, chi-squared test). MO, morpholino oligonucleotide.

4.3 Discussion

In order to study a spectrum of severity of cystic kidney disease related ciliopathies and to enable later evaluation of the potential role of oligogenicity which may influence the clinical heterogeneity, it was important to develop robust models of individual gene morphants. Zebrafish models were created and the phenotypes were evaluated in detail to determine the role of *CC2D2A*, *NPHP6* and *MKS3* during development.

4.3.1 Zebrafish models to study CC2D2A - the *sentinel* mutant zebrafish

Embryos born from *sentinel* heterozygous zebrafish were phenotyped at 72hpf. In homozygotes with a pathognomonic sine wave shaped tail, the nonsense mutation in *cc2d2a* was confirmed by genotyping and sequencing, consistent with previously published work (Gorden et al., 2008). In all of the experiments, it was disappointing to find that only 12% of embryos were *sentinel* homozygotes rather than nearer 25% which is what would have been expected from Mendelian genetics. Increased mortality in *sentinel* homozygotes may be a reason for this reduction in numbers as mortality at 24hpf was 12% in *sentinel* embryos. However confirmation of this potential explanation was not possible as genotyping deceased (necrotic) embryos is not feasible.

The low numbers of *sentinel* homozygotes corresponded to an overall low frequency of aberrant ciliopathy phenotypes. In particular pronephric cysts were only detected in 0.5% of all *sentinel* offspring, equivalent to 4.2% of *sentinel* homozygotes. The pronephric cyst phenotype has been described as incompletely penetrant yet reported to occur in 33-50% of *sentinel* homozygotes (Bachmann-Gagescu et al., 2011; Gorden et al., 2008) at 6dpf. However disappointingly, in the experiments herein, the pronephric cyst phenotype was considerably less penetrant. Working within our Home Office animal licence only enabled work with zebrafish embryos to be performed up to 5dpf when they become capable of independent feeding and must be euthanised. It is therefore possible that by studying the pronephros within this limited time, the development of pronephric cysts which may become apparent beyond 5dpf were missed.

Interestingly, although low in frequency, the phenotypes of cardiac oedema, hydrocephalus and pronephric cysts detected in the *sentinel* homozygous mutants herein were of varying severity, consistent with the genetic pleiotropy apparent in patients with

CC2D2A mutations. A genotype-phenotype correlation has been suggested in patients following the identification of missense *CC2D2A* mutations being associated with JBTS, whilst truncating *CC2D2A* mutations have resulted in the more severe *MKS* disorder (Mougou-Zerelli et al., 2009; Tallila et al., 2008).

Developmental anomalies of the rudimentary ear, the otic placode, were not detected in any *sentinel* homozygous mutants in this work, although can be a recognised feature of other ciliopathy models (Lee et al., 2012a; Simms et al., 2012). This protection of normal development of the ear in *sentinel* mutants may relate to how the *sentinel* zebrafish were first discovered, as a protective mutant from aminoglycoside-antibiotic-induced mechanosensory hair cell death (Owens et al., 2008).

Ocular anomalies including oculomotor apraxia, colobomas and retinal defects are reported in patients with *CC2D2A* mutations and JBTS or MKS (Mougou-Zerelli et al., 2009). Detection of these ocular anomalies including colobomas and unilateral microphthalmia were confirmed herein in a low proportion of *sentinel* homozygous zebrafish embryos. On retinal histology sections of 5dpf *sentinel* homozygotes, the outer retinal pigmented epithelial layer was preserved, however there was indistinct definition of the other retinal layers. These findings are in contrast to those subsequently reported by *Bachmann-Gagescu et al.*, who identified an overall normal eye size and retinal lamination, however a thinner photoreceptor cell layer in *sentinel* homozygous mutants at 5dpf (Bachmann-Gagescu et al., 2011). Reasons for these differing results may be the phenotypic heterogeneity associated with *CC2D2A* mutations and other ciliopathy genes.

Since cc2d2a is known to be expressed at the basal body of cilia (Bachmann-Gagescu et al., 2011; Gorden et al., 2008) and *sentinel* mutants develop a ciliopathy phenotype, it is possible that *CC2D2A* plays a role in the regulation of cilia (Owens et al., 2008). In this work, cilia were evaluated in the developmental zebrafish organising centre, KV and a reduction in the number of cilia in embryos born from heterozygous *sentinel:claudin-b:*Lyn-GFP zebrafish pairs was detected. To my knowledge, this is the first report following evaluation of KV in *sentinel* embryos. Unfortunately further assessment of cilia within KV in terms of motility and fluid flow was not possible. However, of notable interest was the apparent disruption or lack of clearly organised epithelial cell to cell junctions of KV. This combination of abnormal features within KV in *sentinel*

embryos may lead to defective left-right body patterning and ciliopathy phenotypes, ideally future work would address this by evaluating subsequent left-right body asymmetry.

Cilia within the pronephros of *sentinel* homozygous mutants have previously been grossly studied at 48hpf and no obvious differences in the number or structure of cilia were noted (Gorden et al., 2008).

The transgenic *sentinel:claudin-b:*Lyn-GFP zebrafish line were developed to facilitate studying the pronephros for cysts with the particular intention of testing the influence of drug therapies on cyst development. This work was performed in December 2009 when there was considerable interest in the mTOR (mammalian target of rapamycin) inhibitors as a potential treatment for the related cystic kidney disease, ADPKD. There was evidence of a reduction in cyst volume with preserved kidney function in a rat model of ADPKD (Tao et al., 2005) and two mouse models of polycystic kidney disease (Shillingford et al., 2006) after treatment with Rapamycin. Furthermore, zebrafish models of the ciliopathies NPHP and BBS, specifically *nphp2*, *nphp6*, *bbs6* and *bbs8* morphants treated with 0.002-0.1μM of Rapamycin effectively had a reduction in the development of pronephric cysts (Tobin and Beales, 2008).

A significant difference in the efficacy of Rapamycin therapy in reducing any of the aberrant *sentinel* phenotypes particularly no reduction in hydrocephalus or pronephric cysts was detected herein. Embryos were treated with 0.05-0.1μM of Rapamycin and it could be that a higher dose may have been more effective, as whilst a dose range of 0.002-0.1μM Rapamycin was reported to be effective, the images in the published work related to a treatment dose of 10μM (Tobin and Beales, 2008). However, perhaps more importantly, the overall low numbers of *sentinel* homozygotes and therefore low frequency of aberrant phenotypes made it difficult to detect a significant difference between treatment groups.

In the Rapamycin therapy experiments, embryos were not dechorionated and permeability of the chorion to Rapamycin was assumed because previous groups using Rapamycin have not dechorionated embryos and generated successful results (Makky et al., 2007; Tobin and Beales, 2008). Although there is no data available regarding the pharmacokinetics or in particular the half life of Rapamycin therapy in zebrafish, in the Rapamycin trial performed herein, the treatment solutions were replaced every 24 hours

to try to control for the potential of any therapeutic effect waning after 24 hours. It would however have been useful to be able to determine the half life of Rapamycin in zebrafish to ensure that the dose was appropriate.

Although there was an increased frequency of cardiac oedema in WT embryos exposed to Rapamycin therapy, this was not statistically significant and was only associated with early exposure, from zero hours post fertilisation. There was no significant difference in mortality rates in any of the treatment groups.

Treatment trials with Rapamycin therapy were prematurely ceased because of the publication of negative results regarding the efficacy of mTOR inhibitors in patients with ADPKD, no reduction in cystic kidney volume (Serra et al., 2010) or change in kidney function (Serra et al., 2010; Walz et al., 2010).

4.3.2 Creating zebrafish models to study *CC2D2A* - MO knockdown

MO knockdown of *cc2d2a* confirmed the abnormal phenotypes detected in *sentinel* homozygotes, implicating that *cc2d2a* has a role to play in normal organogenesis of the brain, kidney and eye. To my knowledge, this is the first work to use MO knockdown to study *cc2d2a* in combination with studies in *cc2d2a* mutant zebrafish.

Interestingly if a *cc2d2a* morphant developed a curly tail, this was always a dorsal body curvature, akin to the sine wave shape of *sentinel* homozygotes. There are few other ciliopathy morphants which consistently develop a dorsal body curvature, however *pkd2* morphants mimicking ADPKD are one such example (Sun et al., 2004). The significance of whether dorsal or ventral body curvature develops in zebrafish mutants and morphants is not known, however the mechanisms of abnormal convergent extension and disrupted PCP signalling are of considerable interest (Torban et al., 2004) and being evaluated in other ciliopathy disorders (Ferrante et al., 2009).

An abnormal ocular phenotype was again observed in *cc2d2a* morphants including colobomas and microphthalmia, consistent with the developmental anomalies apparent in *sentinel* homozygotes. An abnormal developmental ear phenotype with a reduced number of otoliths was evident in a small percentage of *cc2d2a* morphants, this phenotype does occur in other ciliopathy morphants (Ferrante et al., 2009; May-Simera et al., 2010; Simms et al., 2012), however did not occur in *sentinel* homozygotes

suggesting that the potential protective effect of *cc2d2a* (Owens et al., 2008) on the normal development of the rudimentary ear was interfered with by our *cc2d2a* targeting MO.

The identification of an abnormal, wavy notochord in some *cc2d2a* morphants was of particular interest as this phenotype had not previously been observed in any MO experiments herein. Normally, the notochord functions transiently as an essential rod-like structure which acts like a skeletal tissue for developing embryos enabling them to generate movement (Anderson et al., 2007). Additionally the notochord produces growth factors which facilitate differentiation of the surrounding tissues which is important in the development of the central nervous system (CNS) and left-right body asymmetry (Stemple, 2005). Therefore defects in the appearance of the notochord in *cc2d2a* morphants may be associated with impaired motility of embryos and abnormal CNS development, which can be pathognomonic of JBTS and MKS in patients.

4.3.3 Zebrafish models to study *NPHP6*

Since mutations in *NPHP6* are a recognised cause of NPHP, JBTS and MKS, the role of *nphp6* in the normal development of the kidney, brain and eye has been investigated. The temporal expression of *nphp6* in the retina and cerebellum of zebrafish embryos at 24-48hpf has been confirmed by *in situ* hybridisation (Sayer et al., 2006). A functional role for *nphp6* in normal organogenesis was suggested when targeted splice and translation blocking MO led to aberrant kidney, brain, eye and ear development in zebrafish morphants (Sayer et al., 2006). In this work, similar splice and translation blocking *nphp6* MO were utilised to recapitulate the developmental ciliopathy phenotypes in zebrafish embryos, however there were some interesting differences identified in our results.

Similar to *Sayer et al.* (2006), a difference in the penetrance of ciliopathy phenotypes was apparent depending on whether the splice or translation blocking *nphp6* MO was used. There was an increased frequency of developmental defects following *nphp6* splice blocking MO injections, this was in contrast to *Sayer et al.* (2006).

In the experiments reported herein, the occurrence of pronephric cysts diffusely throughout the pronephros and cloaca reproduced the published (Sayer et al., 2006) *nphp6* morphant models of JBTS. Obstructive cloacal cysts and defective cloaca

formation have also been described in *nphp4* (Slanchev et al., 2011) and *ahi1* (Simms et al., 2012) zebrafish models of NPHP related ciliopathies. Confocal microscopy and immunofluorescence were used to confirm that whilst cilia remain present in the pronephros of *nphp6* morphants at 72hpf, in some morphants they appeared reduced in number and even to disappear towards the cloaca. Unfortunately further characterisation of these cilia in terms of motility or length was not possible. There have however been reports of no difference in the length (Sayer et al., 2006; Tse, 2012) or motility (Sayer et al., 2006) of cilia in the pronephros of *nphp6* zebrafish morphants.

The abnormal eye and ear phenotypes associated with *nphp6* morphants herein included retinal coloboma formation, unilateral microphthalmia and defective ear development with reduction or complete absence of otoliths. The eye and ear phenotypes reported in the *nphp6* morphant zebrafish embryos created in this work are entirely consistent with published developmental defects (Sayer et al., 2006). Ideally, further assessment of the eye phenotypes by performing retinal histology would have been informative. Nephrocystin-6 is known to be expressed in connecting cilium of mouse photoreceptor cells (Sayer et al., 2006) and interesting sensory cilia in the photoreceptors of *nphp6* morphants have recently been described as shortened (Tse, 2012).

Since *NPHP6* related disorders are developmental ciliopathies, evaluation of cilia within the zebrafish organising centre, KV was performed. Using confocal micropscopy and immunostaining of cilia in fixed *nphp6* MO injected embryos, fewer and shorter cilia in KV compared to uninjected WT embryos were identified. These results have been confirmed in a recent publication evaluating cilia in *nphp6* zebrafish morphants (Tse, 2012).

The shortened cilia within KV of *nphp6* MO injected embryos appear to be functionally unable to generate sufficient fluid flow to establish normal left-right body patterning. Cardiac looping at 56hpf was evaluated by light microscopy and a significant reduction in the normal, D-looping cardiac asymmetry was detected in *nphp6* morphants compared to uninjected WT control embryos. To my knowledge, this is the first report of aberrant left-right cardiac development in *nhph6* morphants. Situs inversus can occur in patients with *NPHP6* mutations, however is a rare finding (Baala et al., 2007a). Hypotheses and potential mechanisms for the reversal of cardiac looping detected in

nphp6 morphants herein are considered during discussion of the reversed cardiac looping apparent in *ahi1* morphants in section 3.3.3.

4.3.4 Creating a zebrafish model to study *MKS3*

Mutations in *MKS3* cause disorders at the severe end of the ciliopathy spectrum, JBTS and the lethal condition MKS characterised by a triad of cystic kidneys, liver fibrosis and neurodevelopmental defects including occipital encephalocele (Dawe et al., 2007). Expression of meckelin, the protein product of *MKS3* has been confirmed in human embryonic kidney, liver, retina and hindbrain (Dawe et al., 2007), however animal models to further evaluate the function of meckelin are limited. In 2009, a mouse model of *MKS3* (Cook et al., 2009) was identified caused by a spontaneous deletion in *MKS3* resulting in bilateral polycystic kidneys; hydrocephalus and retinal degeneration in some embryos. However these *Mks3* mutant mice do not develop some of the other typical MKS phenotypes described in patients including hepatic duct dysplasia/cysts, occipital encephalocele and polydactyly. They are further limited as an *MKS* model by infertility and death within 3 weeks of birth (Cook et al., 2009). In order to overcome some of these limitations and further evaluate the role of *MKS3* in organogenesis, MOs were used to knockdown *mks3* in zebrafish embryos and an abnormal effect on development was identified.

Aberrant phenotypes detected in *mks3* morphants were typical of other zebrafish ciliopathy models (Ferrante et al., 2009; Sayer et al., 2006; Slanchev et al., 2011; Zhou et al., 2010b) and beginning with the highest frequency included abnormal body curvature, cardiac oedema, hydrocephalus, pronephric cysts, ear defects, 'meningoceles', wavy notochords and eye defects. In order to attempt to increase the frequency of abnormal features, particularly of pronephric cysts, the MO dose was uptitrated, however unfortunately, as predicted this led to an increased 24 hour mortality rate and experiments were not practically feasible (in terms of yield) beyond 4ng *mks3* MO.

To confirm specificity of our *mks3* morphant zebrafish model, embryos were co-injected with human *MKS3* mRNA, which rescued the ciliopathy phenotypes back to a normal WT pattern of development in 78% of embryos.

Interestingly, in the *mks3* morphants, pronephric cysts of variable size developed diffusely throughout the pronephros and cloaca, similar to the kidney phenotypes described with other ciliopathy genes: *nphp4* (Slanchev et al., 2011), *nphp6* (Sayer et al., 2006) and *ahi1* (Simms et al., 2012). Although evaluation of cilia in KV or the pronephros of the *mks3* zebrafish model would have been interesting, this was not performed because the *mks3* MO work was undertaken as a consequence of a collaboration with Professor Colin Johnson. The focus of this *mks3* related collaboration was to create zebrafish models to evaluate whether *mks3* may interact with *filamin A* (an actin-binding protein). The theory was that *mks3-filamin A*: interact, mediate ciliogenesis and adversely influence Wnt signalling which may be important in the pathogenesis of MKS. The personally performed zebrafish work was united with data from Professor Colin Johnson's laboratory and published (Appendix G (Adams et al., 2012)). The *filamin A* zebrafish work was not presented in this thesis as although an interesting interacting partner and relevant methodically to the combination MO experiments performed in Chapter 5, *filamin A* did not originally relate clearly to the cystic kidney disease ciliopathy story. The specific *mks3* and *filamin A* zebrafish data are shown in Figure 5 and Supplementary Figures 5-6 of Appendix G).

To date, in the other ciliary genes (*AHI1*, *CC2D2A* and *NPHP6*) in which cilia were evaluated in KV/the pronephros herein, the general finding has been of defective ciliogenesis with a shortening of cilia and/or reduction in number of cilia. Consistent with this pattern of defective ciliogenesis, in human and mouse kidney cell lines following *MKS3* siRNA there is loss of cilia (Adams et al., 2012). However in contrast, in the *Mks3* mouse model, cilia were reported as longer in mutants (Cook et al., 2009). Therefore it would be interesting in future experiments to explore cilia in the zebrafish *mks3* morphant.

As previously observed in some *cc2d2a* morphants, a 'wavy' notochord was identified in up to 5% of *mks3* morphant zebrafish embryos. A similar pattern of abnormal 'wavy' notochord development has been reported in *sneezy* mutants (Stemple, 2005), which have a mutation in the α subunit of the coatomer vesiclular complex (Coutinho et al., 2004). *Sneezy* mutants, like other coatomer mutants, with this 'wavy' notochord appearance, fail to develop the normal perinotochordal basement membrane and the essential secretion of signalling proteins is blocked (Coutinho et al., 2004). Corresponding the implications surrounding this destruction to the normal development

of the notochord in *sneezy* mutants to *mks3* morphants and recognising the critical role of the notochord during development, provides compelling evidence to suggest that *mks3* is required for normal organogenesis and tissue differentiation (Stemple, 2005).

The identification of dorsal extension of the notochord to breach the dorsal fin layers, reaching the surface in some *mks3* morphants, suggests more severe developmental defects than those seen in *cc2d2a* morphants, however the overall numbers were low. In patients with *CC2D2A* mutations a genotype-phenotype association has been indicated since those with misense mutations tend to develop JBTS, whilst those with null *CC2D2A* mutations develop the more severe MKS (Mougou-Zerelli et al., 2009).

The abnormal eye and ear development observed in the *mks3* morphants was not evaluated beyond light microscopy since it is not a prominent clinical feature in affected patients. As previously discussed aberrant eye and ear development can be a typical feature of ciliary genes in zebrafish models of ciliopathy related disorders.

Chapter 5 Using zebrafish models to explore the genetics of nephronophthisis related ciliopathies focusing on *nphp6*, *cc2d2a* and *ahi1*

5.1 Introduction

NPHP and the associated ciliopathies: JBTS and MKS, are autosomal recessive conditions with considerable genetic heterogeneity. Over forty causal genes have been identified in patients with ciliopathies (Waters and Beales, 2011) (Table 1.2). Table 5.1 lists the currently identified mutated genes in patients with NPHP, JBTS and MKS. The capability of mutations in several genes particularly *NPHP6* (Coppieters et al., 2010), *CC2D2A* (Mougou-Zerelli et al., 2009), *AHI1* (Dixon-Salazar et al., 2004; Louie et al., 2010), *MKS3* (Baala et al., 2007b; Doherty et al., 2010; Smith et al., 2006), *RPGRIP1L* (Arts et al., 2007; Delous et al., 2007; Doherty et al., 2010), and *NPHP3* (Olbrich et al., 2003; Omran et al., 2002) to cause a variable range and spectrum of clinical phenotypes is highlighted in Table 5.1 and emphasises the genetic pleiotropy. Although mutations in certain genes, may be more likely to be associated with a specific phenotype, such as homozygous *NPHP5* mutations leading to retinal degeneration (Otto et al., 2005), for most genes there has been difficulty in determining a genotype-phenotype association (Coppieters et al., 2010). This is clinically important as when a mutation is known, it would enable the appropriate screening of selected potentially affected organs, facilitate the delivery of prognostic information to patients and guide genetic counselling. However in practice, even when the mutation is known, there can be considerable variation in the severity of phenotypes within families (Caridi et al., 2006; Hoefele et al., 2007).

In the related ciliopathy, BBS, mutations in more than one gene have been identified (Katsanis et al., 2001), suggesting oligogenicity, where an abnormality in a third allele may modify the severity or nature of presentation and prognosis. In 2007, this theory was applied to patients with NPHP and led to the screening of four genes (*NPHP1-NPHP4*), which were known to interact at the protein level, for mutations (Hoefele et al., 2007). This resulted in several novel findings underlying the genetic basis of NPHP. Triallelism (two homozygous mutations in one gene and an additional heterozygous mutation in another gene); digenic disease (heterozygous mutations in two

different genes) and a single heterozygous mutation, with no second mutation were identified in patients known to have NPHP (Hoefele et al., 2007).

Nephronophthisis			Joubert Syndrome			Meckel Gruber Syndrome		
Gene locus	**Gene symbol**	**Chromosome**	**Gene locus**	**Gene symbol**	**Chromosome**	**Gene locus**	**Gene symbol**	**Chromosome**
NPHP1	**NPHP1***	2q13	JBTS1	**INPP5E**	9q34.3	MKS1	**MKS1**	17q22
NPHP2	**INVS**	9q31	JBTS2	**TMEM216**	11q13.1	MKS2	**MKS2**	11q13
NPHP3	**NPHP3***	3q22.1	JBTS3	**AHI1***	6q23.3	MKS3	**TMEM67***	8q22.1
NPHP4	**NPHP4**	1p36.22	JBTS4	**NPHP1***	2q13	MKS4	**CEP290***	12q21.32
NPHP5	**IQCB1**	3q21.1	JBTS5	**CEP290***	12q21.32	MKS5	**RPGRIP1L***	16q12.2
NPHP6	**CEP290***	12q21.32	JBTS6	**TMEM67***	8q21.1-q22.1	MKS6	**CC2D2A***	4p15.33
NPHP7	**GLIS2**	16p13.3	JBTS7	**RPGRIP1L***	16q12.2	MKS7	**NPHP3***	3q22.1
NPHP8	**RPGRIP1L***	16q12.2	JBTS8	**ARL13B**	3q11.2	MKS8	**TCTN2***	12q24.31
NPHP9	**NEK8**	17q11.1	JBTS9	**CC2D2A***	4p15.33	MKS9	**B9D1**	17p11.2
NPHP10	**SDCCAG8**	1q44	JBTS10	**OFD1**	Xp22.2			
NPHP11	**TMEM67***	8q22.1	JBTS11	**TTC21B**	2q24.3			
NPHP12	**TTC21B**	2q24.3	JBTS12	**KIF7**	15q26.1			
NPHP13	**WDR19**	4p14	JBTS13	**TCTN1**	12q24.11			
	AHI1*	6q23.3	JBTS14	**TMEM237**				
	ATXN10	22q13.31	JBTS15	**CEP41**	7q32			
NPHP14	**ZNF423**	16q12	JBTS16	**TMEM138**	11q12.2			
	CEP164	11q23.3	JBTS17	**C5ORF42**	5p13.2			
				TCTN2*	12q24.31			
				TMEM231	16q23.1			

Table 5.1 Molecular genetics of Nephronophthisis, Joubert Syndrome and Meckel Gruber Syndrome
*Highlights genetic pleiotropy, ability of gene to induce variable spectrum of phenotypes.

Triallelism has been reported in patients with NPHP, JBTS and MKS caused by: homozygous *NPHP1* and heterozygous *NPHP3* (Hoefele et al., 2007) or *NPHP4* (Hoefele et al., 2007) or *NPHP6* (Tory et al., 2007) or *AHI1* (Tory et al., 2007) mutations (Hoefele et al., 2007; Tory et al., 2007); homozygous *NPHP6* and heterozygous *NPHP4* (Hoefele et al., 2005) or *AHI1* (Tory et al., 2007) or *MKS3* (Leitch et al., 2008) mutations (Table 1.6). Digenic inheritance of MKS has been described as a consequence of heterozygous mutations in *NPHP6* and *CC2D2A* (Table 1.6) (Hopp et al., 2011).

Failure to identify a second mutation in autosomal recessive disorders emphasises that several NPHP related causal genes are as yet undiscovered. This concept has recently been confirmed following analysis of 18 NPHP associated ciliopathy genes by DNA pooling and next generation sequencing failed to identify a causal gene in 90 of 120 affected patients (Otto et al., 2011). Furthermore, only a single heterozygous mutation was identified in 21 patients with NPHP, JBTS or MKS. Interestingly, this study did not identify any evidence of oligogenicity, however investigators admitted that the methods used may have been insufficiently sensitive (Otto et al., 2011).

In 2011, in order to further evaluate potential relationships between genotype and phenotype, clinical data were reviewed in a worldwide cohort of patients with NPHP related ciliopathies and known mutations (Chaki et al., 2011). It was hypothesised that genotype-phenotype associations were influenced by gene locus heterogeneity, allelism and the effect of additional modifier genes. Investigators concluded that gene locus heterogeneity was the most important influence on subsequent phenotype, however as mutation screening was not performed in all NPHP genes in the study, the impact of oligogenicity could not be evaluated (Chaki et al., 2011).

5.1.1 Aims of this chapter

The possibility of known or unidentified genes epistatically modifying the clinical phenotype in the NPHP related ciliopathies is an interesting mechanism to further study. Several of the NPHP, JBTS and MKS protein products interact and have been shown to function in pathways (Sang et al., 2011), suggesting that many of these genes may closely interact.

Zebrafish models have previously been utilised when evaluating NPHP related phenotypes and to determine the physiological relevance of potential genetic interactions. Combined MO knockdown of *nphp5* and *nphp6* demonstrated synergy of morphant phenotypes including pronephric cysts and hydrocephalus, underlining a genetic interaction between *NPHP5* and *NPHP6* (Schafer et al., 2008). Following recognition of interaction between CC2D2A and NPHP6 at the protein level, MO knockdown of *nphp6* in *sentinel* (*cc2d2a* mutant) zebrafish resulted in a synergistic increase in pronephric cysts, again proving a physiologically relevant genetic interaction between these two NPHP related ciliopathy genes (Gorden et al., 2008). The concept 'genetic interaction' when discussed herein is considered to relate to an inferred functional relationship between genes or signalling pathways or even the encoded proteins, suggested by a synergistic increase in the frequency or severity of phenotype induced following mutation or knockdown of two genes (Mani et al., 2008). An acceptable alternative term may be 'molecular interaction'.

The aim of this chapter was to evaluate oligogenicity in NPHP related ciliopathies. Since oligogenicity has previously been described in patients with NPHP/JBTS/MKS caused by mutations in *NPHP6* and *AHI1* (Tory et al., 2007) or *CC2D2A* and *NPHP6* (Hopp et al., 2011), the aim was to focus on these genes. In addition to using MO knockdown of combinations of *ahi1*, *nphp6* and *cc2d2a* in zebrafish to evaluate the effect on organogenesis and create models of NPHP related ciliopathies, the effect of MO knockdown of *nphp6* or *ahi1* in *sentinel* (*cc2d2a* mutant) embryos, which have been proposed as a useful model for evaluating oligogenicity (Gorden et al., 2008), were studied.

Initially, using *nphp6* MO knockdown in *sentinel* embryos, the aim was to recapitulate the published ciliopathy phenotype (Gorden et al., 2008). Subsequently, evaluation of the potential interaction between *AHI1* and *CC2D2A* by two different methods: performing *ahi1* MO knockdown in *sentinel* embryos and combined *ahi1* and *cc2d2a* MO knockdown was performed. Finally, *ahi1* and *nphp6* MO knockdown in zebrafish embryos was completed to further evaluate the digenic inheritance of NPHP related ciliopathies, which has been described in patients (Tory et al., 2007) (Table 1.6).

5.2 Results

5.2.1 Phenotypes following *nphp6* MO knockdown in *sentinel* (*cc2d2a* mutant) embryos

Embryos were phenotyped by light microscopy at 72hpf. A reminder of the typical phenotypes associated with *sentinel* embryos and *nphp6* morphants in isolation are shown (Figure 5.1). Uninjected *sentinel* homozygous embryos alone develop a characteristic dorsal sine wave shaped tail (Figure 5.1A). WT embryos injected with *nphp6* splice blocking MO develop a ventral curly tail, hydrocephalus, cardiac oedema and empty otic vesicle (Figure 5.1B).

Embryos born from *sentinel* heterozygous matings were injected with 4-6ng of splice blocking *nphp6* MO and develop a range of abnormal phenotypes including ventral/dorsal curly tail, cardiac oedema, hydrocephalus, wavy notochord (Figure 5.1C-D), pronephric cysts, aberrant rudimentary eye and ear development including absent otoliths in the otic vesicle (Figure 5.2D-I). In order to exclude non-specific off-target effects, *nphp6* MO was co-injected with *p53* MO into *sentinel* embryos. Figure 5.1E shows that *sentinel* embryos injected with *nphp6* and *p53* MOs continue to develop an aberrant phenotype with disrupted organogenesis including dorsal curly tail, cardiac oedema, hydrocephalus and unilateral microphthalmia.

Figure 5.1 Phenotypes following combination of *nphp6* MO knockdown in *sentinel* (*snl*) zebrafish embryos

Lateral views of zebrafish embryos at 72 hours post fertilisation. Uninjected *sentinel* (*snl*, A) zebrafish embryos have a characteristic sine wave shaped tail. B is a wild type (not *snl*) embryo injected with *nphp6* MO which has a ventrally curved tail, hydrocephalus, cardiac oedema and empty otic vesicle (black arrowhead). Combination of *nphp6* MO knockdown in *snl* embryos (C, D) induces a range of abnormal phenotypes including wavy notochord (C), cardiac oedema, hydrocephalus, dorsal curly tail (D) and delayed development of otoliths in the otic vesicle (black arrowhead, D). *Snl* embryos additionally co-injected with *nphp6* and *p53* MOs (E) continue to develop an aberrant phenotype with dorsal curly tail, cardiac oedema, hydrocephalus and unilateral microphthalmia (red arrow), excluding the possibility of the combination resulting from an off-target effect. MO, morpholino oligonucleotide.

Focusing on the development of pronephric cysts, cropped images of an uninjected *sentinel* zebrafish embryo with no cyst (Figure 5.2A) can be compared with the variable size of proximal pronephric cysts which developed in *sentinel* embryos injected with *nphp6* MO by 72hpf (Figure 5.2D, G).

No abnormal eye or ear development was apparent by light microscopy in this cohort of *sentinel* embryos alone (Figure 5.2B-C), however following injection of *sentinels* with 4-6ng of *nphp6* MO colobomas (Figure 5.2E, H) and fewer or absent otoliths were identified in the otic vesicles (Figure 5.2 E-F, I).

Figure 5.2 Pronephric cysts and abnormal eye and ear development following combination of *nphp6* MO knockdown in *sentinel* (*snl*) zebrafish embryos
Cropped views of *snl* zebrafish embryos at 72 hours post fertilisation, focusing on the proximal pronephros (A, D, G), eyes (B, E, H) and otic vesicles (C, F, I). Compared to uninjected *snl embryos* (A-C), *snl* embryos injected with *nphp6* MO develop pronephric cysts (red arrows, D, G), colobomas (black arrows, E, H) and fewer otoliths in the otic vesicle (single, black arrowhead, F, I(dorsal view)). MO, morpholino oligonucleotide.

5.2.2 Mortality and frequency of abnormal phenotypes following *nphp6* MO knockdown in *sentinel* (*cc2d2a* mutant) embryos

Mortality at 24hpf was evaluated to ascertain whether *nphp6* and *cc2d2a* gene combinations where functionally associated with lethality. The mean percentage (%) and standard error of the mean (±SEM) mortality at 24hpf was calculated for: *sentinel* embryos alone (n=208); WT embryos injected with 4ng (n=342) and 6ng (n=547) of *nphp6* MO; *sentinel* embryos injected with 4ng *nphp6* MO (n=273) and *sentinel* embryos injected with 6ng *nphp6* MO (n=145). Figure 5.3 shows the mean 24hpf mortality was similar in *sentinel* zebrafish embryos alone (24%), WT embryos injected with 4ng *nphp6* MO alone (22%) and *sentinel* embryos injected with 4ng *nphp6* MO (23%). Injection of 6ng of *nphp6* MO alone was associated with an increased 24hpf mortality of 49% and when this dose of *nphp6* MO was injected into *sentinel* embryos, mortality rose dramatically up to 70%.

The total numbers of embryos surviving to 72hpf to be assessed for phenotypes in each group were: 321 *sentinel* embryos; 261 WT embryos injected with 4ng *nphp6* MO; 216 WT embryos injected with 6ng *nphp6* MO; 144 *sentinel* embryos injected with 4ng *nphp6* MO and 43 *sentinel* embryos injected with 6ng nphp6 MO.

Figure 5.3 Mortality at 24hpf following combination of *nphp6* MO knockdown in *sentinel* (*snl*) zebrafish embryos

Mortality at 24hpf is shown as mean percentage (%) and standard error of the mean in *snl* zebrafish embryos alone, wild type zebrafish embryos injected with 4-6ng *nphp6* MO alone and *snl* embryos injected with 4-6ng *nphp6* MO (A). The mean 24hpf mortality is similar in *snl* zebrafish embryos alone (24%), wild type embryos injected with 4ng *nphp6* MO alone (22%) and *snl* embryos injected with 4ng *nphp6* MO (23%). Injection of 6ng of *nphp6* MO alone is associated with a much higher 24hpf mortality of 49% and in *snl* embryos this rises to 70%. hpf, hours post fertilisation. MO, morpholino oligonucleotide.

The mean and standard error of the mean (where applicable) frequency of the development of each abnormal phenotype by 72hpf including curly tail, cardiac oedema, hydrocephalus and pronephric cysts were graphed in Figure 5.4. Both graphs show the same data, however Figure 5.4A emphasises the frequency of each phenotype across the range of interference in *cc2d2a* and *nphp6*.

Focusing on the frequency of pronephric cyst development, only 1.5% (±1.5%) of uninjected *sentinel* embryos and WT embryos injected with 4ng *nphp6* MO developed pronephric cysts detected by light microscopy at 72hpf. The dose dependent effect of *nphp6* MO was clearly demonstrated, as a 6ng dose of *nphp6* MO alone (injected into WT embryos) was associated with pronephric cysts in up to 17% (±9.9%) of morphants at 72hpf. A dose dependent functional interaction between *cc2d2a* and *nphp6* was implied by the propagation in the development of pronephric cysts in 9% of *sentinel* embryos injected with 4ng *nphp6* MO and 33.5% (±16.5%) of *sentinel* embryos injected with 6ng of *nphp6* MO (Figure 5.4A). The frequency of pronephric cysts in *sentinels* injected with each dose of *nphp6* MO was more than the sum of combining the individual frequencies of pronephric cysts. This synergistic increase in the development of pronephric cysts implied a functionally relevant genetic interaction between *cc2d2a* and *nphp6*.

Similarly, there was a dose dependent synergistic increase in the frequency of development of curly tail and cardiac oedema from 10.5% (±9.5%) and 2.5% (±0.5%) respectively in uninjected *sentinels*, to 74.5% (±25.5%) and 81.5% (±18.5%) respectively in *sentinels* injected with 6ng *nphp6* MO.

The frequency of development of hydrocephalus in *sentinels* alone was only 0.5% (±0.5%) and was confirmed as dose dependent with *nphp6* MO. Injection of 4-6ng of *nphp6* MO in WT embryos induced hydrocephalus increasing from 9.5% (±7.5%) to 30.8% (±10.6%) of morphants. The injection of 4ng *nphp6* MO into *sentinel* embryos led to a synergistic increase in the frequency of hydrocephalus to 36%, however this synergy was not sustained when the higher dose of 6ng *nphp6* MO was injected into sentinels, as this resulted in hydrocephalus in only 22% (±22%). It may be that the marked increase in mortality that occurred when 6ng *nphp6* MO was injected into *sentinels* accounted for the reduction in frequency of hydrocephalus, as embryos were dying rather than surviving to develop hydrocephalus.

Figure 5.4 Percentage frequency of abnormal phenotypes at 72hpf following combination of *nphp6* MO knockdown in *sentinel* (*snl*) zebrafish embryos
Data are displayed as mean ± SEM. A emphasises the range of phenotypes in each group of zebrafish embryos. B highlights the effect of the individual genes (*cc2d2a* in *snl*; *nphp6* MO) and gene combinations on the frequency of abnormal phenotypes. The percentage frequency of each abnormal phenotype increases in a dose dependent manner following 4-6ng of *nphp6* MO knockdown alone (2-42%) and is generally low (1-11%) in *snl* embryos alone (A). The frequency of abnormal phenotypes following 6ng of *nphp6* MO alone is similar to the cumulative effect of 4ng of *nphp6* MO in *snl* embryos (B). The cumulative effect of 4 or 6ng of *nphp6* MO in *snl* zebrafish embryos has a synergistic effect on each abnormal phenotype except for hydrocephalus in *snl* embryos injected with 6ng of *nphp6* MO (B). The total numbers of embryos were 321 (*snl* zf), 261 (4ng *nphp6* MO), 216 (6ng *nphp6* MO), 144 (*snl* zf+4ng *nphp6* MO) 43 (*snl* zf+6ng *nphp6* MO). hpf, hours post fertilisation; SEM, standard error of the mean; zf, zebrafish. MO, morpholino oligonucleotide.

The abnormal development of the eye and ear associated with *sentinels* and *nphp6* MO were not plotted on the graphs in Figure 5.4, this was because by light microscopy no abnormal phenotypes were identified in this cohort of *sentinel* embryos alone and more importantly, there was not a synergistic increase in frequency of abnormal eye development. Ocular anomlies were detected in 0.2% (n=2) of homozygous *sentinel* mutants in the earlier cohort of embryos used in experiments in 4.2.5 (Figure 4.9, Figure 4.10). Abnormal eye development was detected in 1.5% (±1.5%) and 3% (±3%) following 4 and 6ng *nphp6* MO alone. When the same doses of 4 and 6ng *nphp6* MO were injected into *sentinel* embryos, this low frequency of abnormal eye development was maintained at only 1% and 3.5%, most likely reflecting the effect of *nphp6* MO alone.

Although no abnormal rudimentary ear development was observed in *sentinel* mutants alone, when embryos were injected with 4ng *nphp6* MO the occurrence of abnormal ear development rose to a frequency of 9%, compared to only 2% (±1%) in WT embryos injected with 4ng *nphp6* MO alone. This apparent synergistic increase in the frequency of abnormal ear development was dose dependent and occurred in 7.3% (±5.7%) of WT embryos injected with 6ng *nphp6* MO alone which dramatically increased to 36% (±14%) when *sentinel* embryos were injected with 6ng *nphp6* MO. This suggests that *cc2d2a* may be modifying the aberrant effect of *nphp6* on ear development.

Although reporting results of the same data, the layout of the graph in Figure 5.4B focuses on comparing the effects of the individual (*cc2d2a* in *sentinel*; *nphp6* MO) genes with the gene combinations, on the frequency of development of abnormal phenotypes. It was clearly evident that in *sentinel* embryos alone and WT embryos injected with 4ng *nphp6* MO, the frequency of each abnormal phenotype was much lower than in any of the combinations (4-6ng *nphp6* MO in *sentinels*). However, the frequency of developmental anomalies were similar between embryos injected with 6ng of *nphp6* MO alone and the combined effect of *sentinel* embryos injected with 4ng *nphp6* MO (Figure 5.4B). As described above, the cumulative effect of 4 or 6ng of *nphp6* MO in *sentinel* zebrafish embryos had a synergistic effect on each abnormal phenotype except for hydrocephalus in *sentinel* embryos injected with 6ng of *nphp6* MO.

5.2.3 Phenotypes following *ahi1* MO knockdown in *sentinel* (*cc2d2a* mutant) embryos

The abnormal phenotypes previously identified in WT embryos injected with *ahi1* splice blocking MO include: curved body axis, cardiac oedema, hydrocephalus, pronephric cysts, otic defects and retinal anomalies and were extensively imaged in Figure 3.9, Figure 3.10, Figure 3.11, Figure 3.12, Figure 3.13 and Figure 3.14.

Embryos born from *sentinel* heterozygous matings were injected with 0.5-2ng of splice blocking *ahi1* MO and phenotyped by light microscopy at 72hpf. Figure 5.1A shows an uninjected *sentinel* homozygous embryo with cardiac oedema and the characteristic dorsal sine wave shaped tail. *Sentinel* embryos injected with 0.5-2ng *ahi1* MO developed a typical range of ciliopathy phenotypes including curly tail, cardiac oedema, hydrocephalus, pronephric cysts, abnormal ear and eye development. Predominantly proximal pronephric cysts of varying size were clearly evidence in *sentinel* embryos injected with *ahi1* MO (Figure 5.5B, D-I). Hydrocephalus of varying severity was present in many *sentinel ahi1* morphants (*sentinel* embryos injected with *ahi1* MO, Figure 5.5C-E, G**,** Figure 5.6E) and a curly tail, with a pronounced sine wave appearance was also evident in some morphants (Figure 5.5B-D).

In these experiments, uninjected *sentinel* embryos rarely (0.3%, n=2 of 933) developed abnormal eyes as determined by light microscopy, such as colobomas (Figure 5.6B-D) or unilateral microphthalmia (Figure 5.6E-F). Low dose (0.5ng) *ahi1* MO alone in WT embryos failed to induce any abnormal eye development (n=58) as detected by light microscopy. However when combined, 0.5ng *ahi1* MO injected into *sentinel* embryos there was a modest increased frequency of abnormal eye development (0.4%, n=1 of 243, Figure 5.8). This synergy was more convincing following injection of higher doses (1-2ng) of *ahi1* MO into *sentinel* embryos, leading to abnormal eye development in 6.5% ± 2.9% (n=18 of 291) and 15.3% ± 2.3% (n=16 of 105) embryos respectively.

In uninjected *sentinel* embryos and WT embryos injected with 0.5ng *ahi1* MO the rudimentary ear development appeared grossly normal by light microscopy, with all embryos developing 2 otoliths in each otic vesicle (Figure 5.6A). However when combined (0.5ng *ahi1* MO injected into *sentinel* embryos) up to 2% ± 2% of morphants developed an abnormal number of otoliths (none or single) in the otic vesicle (Figure 5.6B-C). A synergistic relationship was again apparent with increasing doses of *ahi1*

MO injected into *sentinel* embryos, increasing the frequency of abnormal ear development from 2% (1ng *ahi1* MO alone) to 9.3% in 1ng *ahi1 sentinel* morphants and 3.7% (2ng *ahi1* MO alone) to 8.7% in 2ng *ahi1 sentinel* morphants.

Figure 5.5 Hydrocephalus and pronephric cysts following combination of *ahi1* MO knockdown in *sentinel* (*snl*) zebrafish embryos

Lateral views of zebrafish embryos at 72 hours post fertilisation. Uninjected *sentinel* (*snl*, A) zebrafish embryo with cardiac oedema (*) and characteristic sine wave shaped tail. B-I are *snl* embryos injected with *ahi1* MO and display a range of abnormal phenotypes including hydrocephalus (black arrowhead C-E, G) and pronephric cysts (red arrow B, D-I). A pronounced dorsal sine wave shaped tail is seen in D. MO, morpholino oligonucleotide.

Figure 5.6 Abnormal eye and ear development following combination of *ahi1* MO knockdown in *sentinel* (*snl*) zebrafish embryos

Cropped views of *snl* zebrafish embryos at 72 hours post fertilisation, focusing on the eyes and otic vesicles. Compared to uninjected *snl* embryos which predominantly have normal eyes and 2 otoliths in each otic vesicle (A), *snl* embryos injected with *ahi1* MO have abnormal development of the eyes (black arrowheads) and rudimentary ear (red arrow) (B-F). (B) A coloboma and empty otic vesicle, (C) coloboma and single otolith, (D) coloboma. E and F are lateral and dorsal views of an embryo with unilateral microphthalmia of the right eye (black arrowhead, F). MO, morpholino oligonucleotide.

5.2.4 Mortality following *ahi1* MO knockdown in *sentinel* (*cc2d2a* mutant) embryos

Previously, a dose dependent association between *ahi1* splice blocking MO dose and 24hpf mortality was demonstrated (Figure 3.8). Mortality at 24hpf was evaluated to ascertain whether *ahi1* and *cc2d2a* gene combinations were functionally associated with lethality. The mean percentage (%) and standard error of the mean mortality at 24hpf was calculated for: *sentinel* embryos alone (n=999); *sentinel* embryos injected with 0.5ng *ahi1* MO (n=340); *sentinel* embryos injected with 1ng *ahi1* MO (n=438) and *sentinel* embryos injected with 2ng *ahi1* MO (n=303). Figure 5.7 shows that the mean 24hpf mortality rose in a predominantly dose dependent manner when *sentinel* zebrafish were injected with *ahi1* MO. Mean and standard error of the mean 24hpf mortality rates were only 4.8% ± 1.4% in uninjected *sentinel* embryos, however when injected with 0.5-1ng of *ahi1* MO this rose to between 27% ± 4.9% and 26.3% ± 7.4%. The increased lethality associated with injecting 2ng of *ahi1* MO in *sentinel* embryos was 49.3% ± 4.8% (Figure 5.7).

Figure 5.7 Mortality at 24hpf following combination of *ahi1* MO knockdown in *sentinel* (*snl*) zebrafish embryos

Mortality at 24hpf is shown as mean percentage (%) and standard error of the mean (SEM) in *snl* zebrafish embryos alone and *snl* embryos injected with 0.5-2ng of *ahi1* MO (A). The mean 24hpf mortality is only 4.8% ± 1.4% in *snl* zebrafish embryos alone and rises in a predominantly dose dependent manner when *snl* embryos are injected with: 0.5ng *ahi1* MO (27% ± 4.9%), 1ng *ahi1* MO (26.3% ± 7.4%) and 2ng *ahi1* MO (49.3% ± 4.8%). MO, morpholino oligonucleotide.

5.2.5 Frequency of abnormal phenotypes following *ahi1* MO knockdown in *sentinel* (*cc2d2a* mutant) embryos

The total numbers of *sentinel* and *ahi1* MO injected embryos surviving to 72hpf to be assessed for phenotypes in each group were: 933 uninjected *sentinel* embryos; 58 WT embryos injected with 0.5ng *ahi1* MO injected; 793 WT embryos injected with 1ng *ahi1* MO; 517 WT embryos injected with 2ng *ahi1* MO; 246 *sentinel* embryos injected with 0.5ng *ahi1* MO; 291 *sentinel* embryos injected with 1ng *ahi1* MO and 105 *sentinel* embryos injected with 2ng *ahi1* MO.

The mean and standard error of the mean (where applicable) frequency of the development of each abnormal phenotype following *ahi1* MO knockdown in *sentinel* embryos by 72hpf was graphed in Figure 5.8. The phenotypes which developed, from most to least frequent, included: curly tail, cardiac oedema, hydrocephalus, pronephric cysts. Abnormal rudimentary ear development was more frequent than abnormal eye development until a 2ng dose of *ahi1* MO was injected into *sentinel* embryos.

In the cohort of uninjected *sentinel* embryos (born from the same pairs of *sentinels* as those injected with doses of *ahi1* MO), the frequency of abnormal phenotypes, apart from curly tail (13.9% ± 3.7%) was low (0-3%). Similarly with 0.5ng *ahi1* MO knockdown alone (in WT) the frequency of aberrant phenotypes was also low (0-5%). However, when 0.5ng of *ahi1* MO was injected into *sentinel* embryos there was a more than additive increase in the frequency of abnormal phenotypes detected by light microscopy (Figure 5.8). This synergistic effect on phenotype can be clearly seen in Table 5.2 by summing the columns. Most importantly the frequency of pronephric cysts rose to 15% ± 9.7% and rates of hydrocephalus increased to 18.7% ± 3.7% with 0.5ng *ahi1* MO knockdown in *sentinel* embryos.

The synergistic increase in the frequency of each abnormal phenotype occurred for each dose combination of *ahi1* with *sentinel* embryos, suggesting a genetic interaction. Again focusing on the NPHP related ciliopathy phenotypes of pronephric cysts and hydrocephalus, increased doses of *ahi1* MO knockdown in *sentinel* embryos led to pronephric cysts in 41.8% (± 9.6%) to 45.7% (± 7.3%) of embryos (Figure 5.8). Similarly increased doses of *ahi1* MO in *sentinel* embryos leads to a frequency of hydrocephalus between 47.3% (± 13.8%) and 55% (± 1.5%) (Table 5.2).

Figure 5.8 Percentage frequency of abnormal phenotypes following combination of *ahi1* MO knockdown in *sentinel* (*snl*) zebrafish embryos

The mean and SEM frequency of abnormal phenotypes for *snl* zebrafish embryos alone (white bars, n=933), wild type (WT) embryos injected with 0.5ng *ahi1* MO alone (green striped bars, n=58), 1ng *ahi1* MO alone (black striped bars, n=793), 2ng *ahi1* MO alone (red striped bars, n=517) and the combination of *snl* embryos injected with 0.5ng *ahi1* MO (green bars, n=246), 1ng *ahi1* MO (black bars, n=291) and 2ng *ahi1* MO (red bars, n=105) are shown. The mean frequency of abnormal phenotypes is low (0-14%) in *snl* embryos alone (white bars) and WT embryos injected with 0.5ng *ahi1* MO alone (green striped bars). There is a synergistic and dose dependent increase in abnormal phenotypes when 0.5-2ng of *ahi1* MO is injected into *snl* embryos. MO, morpholino oligonucleotide.

	Curly tail (%)	Cardiac oedema (%)	Hydrocephalus (%)	Pronephric cysts (%)	Abnormal eye (%)	Otic defect (%)
***snl* zebrafish alone**	13.9 ± 3.7	3.0 ± 0.7	1.0 ± 0.8	1.0 ± 0.8	0.3 ± 0.3	0.0 ± 0.0
0.5ng *ahi1* MO alone	3.0 ± 0.0	5.0 ± 0.0	2.0 ± 0.0	0.0 ± 0.0	0.0 ± 0.0	0.0 ± 0.0
***snl* + 0.5ng *ahi1* MO**	35.3 ± 5.0	30.7 ± 8.1	18.7 ± 3.1	15.0 ± 9.7	0.4 ± 0.4	2.0 ± 2.0
1ng *ahi1* MO alone	36.2 ± 7.6	34.5 ± 6.9	20.4 ± 4.6	7.0 ± 3.1	0.5 ± 0.4	2.0 ± 0.7
***snl* + 1ng *ahi1* MO**	69.8 ± 10.9	78.3 ± 9.5	47.0 ± 13.8	41.8 ± 9.6	6.5 ± 2.9	9.3 ± 2.8
2ng *ahi1* MO alone	39.9 ± 7.6	35.1 ± 6.9	29.3 ± 5.4	10.9 ± 2.7	0.9 ± 0.5	3.7 ± 1.2
***snl* + 2ng *ahi1* MO**	84.0 ± 7.0	89.3 ± 4.5	55.0 ± 1.5	45.7 ± 7.3	15.3 ± 2.3	8.7 ± 2.2

Table 5.2 Frequency of abnormal phenotypes in *sentinel* and 0.5-2ng *ahi1* MO injected embryos
Percentage (%) frequency of abnormal phenotypes at 72hpf in *sentinel* (*snl*) zebrafish embryos alone, wild type embryos injected with 0.5ng or 1ng or 2ng *ahi1* MO alone and the combination of *snl* embryos injected with 0.5ng or 1ng or 2ng of *ahi1* MO. MO, morpholino oligonucleotide.

5.2.6 Alternative assessment of *ahi1* and *cc2d2a* genetic interaction: Phenotypes and mortality following combined *ahi1* MO and *cc2d2a* MO knockdown in wild type zebrafish embryos

Although a genetic interaction between *AHI1* and *CC2D2A* was suggested above by the synergistic increase in several ciliopathy phenotypes including pronephric cysts and hydrocephalus, there were limitations of relying on the *sentinel* (*cc2d2a* mutant) zebrafish to study the effect of interference with *CC2D2A*. In order to overcome this, a *cc2d2a* zebrafish morphant was created and characterised in section 4.2.10, Figure 4.16, Figure 4.17 and Figure 4.18. Below, the phenotypes generated by combining *ahi1* and *cc2d2a* splice blocking MO, which alone caused minimal developmental anomalies, are described.

WT embryos generated from matched zebrafish were injected with: 0.5ng *ahi1* MO alone; 4ng *cc2d2a* MO alone; or a combined solution of 0.5ng *ahi1* MO and 4ng *cc2d2a* MO. Phenotyping by light microscopy was performed at 72hpf. The frequency of abnormal phenotypes generated by 0.5ng *ahi1* MO alone (n=58) were low and included curly tail (3%, n=2), cardiac oedema (5%, n=3) and hydrocephalus (2%, n=1) (Figure 5.9A). The frequency of abnormal phenotypes (mean ± standard error of the mean) generated by 4ng *cc2d2a* MO alone (n=96, Figure 5.9B) were low and included curly tail (0.7% ± 0.7%, n=1), cardiac oedema (1.7% ± 1.7%, n=3) and pronephric cysts (2.7% ± 2.7%, n=1). When these doses of MO were combined (0.5ng *ahi1* and 4ng *cc2d2a*, n=10), there was a marked increase in the frequency of all phenotypes with hydrocephalus in 50% and pronephric cysts in 10%. Additionally combined *ahi1* and *cc2d2a* MO knockdown at these doses led to abnormal eye (30%) and ear (40%) development (Figure 5.10A). However the number of embryos surviving to be phenotyped at 72hpf following combined *ahi1* and *cc2d2a* MO injection were low (n=10) because of increased mortality rates at 24hpf (Figure 5.10B). Compared to paired uninjected WT embryos whose 24hpf mortality rate was 26%, the mortality rate in embryos injected with combined 0.5ng *ahi1* and 4ng *cc2d2a* MOs was 88%, a relative 24hpf mortality rate 3.4 times that of WT.

Figure 5.9 Phenotypes following combination of low dose *ahi1* and *cc2d2a* MO knockdown in zebrafish embryos

Lateral views of zebrafish embryos at 72 hours post fertilisation. Wild type (WT) zebrafish embryos injected with a low dose of *ahi1* MO (0.5ng, A) and *cc2d2a* MO (4ng, B) alone showed minimal cardiac oedema (*, A) or were phenotypically normal. WT zebrafish embryos co-injected with low dose *ahi1* (0.5ng) and *cc2d2a* (2ng) MOs develop abnormal phenotypes, which persist when also co-injected with *p53* MO (to exclude off-target effects, C-F). The range of abnormal phenotypes following co-injection of low dose *ahi1* and *cc2d2a* MOs includes: cardiac oedema (*, D, E); hydrocephalus (black arrowhead, C-F); curved body axis (D, E); pronephric cysts (red arrow E); coloboma (black arrow, G); single otolith (green arrow, F, G). MO, morpholino oligonucleotide.

Figure 5.10 Percentage frequency of abnormal phenotypes following combined MO knockdown using 0.5ng *ahi1* and 4ng *cc2d2a* in zebrafish embryos and associated mortality at 24hpf

Low dose (0.5ng) *ahi1* MO alone (black bars, n=58) and 4ng *cc2d2a* MO alone (green bars, n=96) induce a low frequency (≤5%) of abnormal phenotypes (B). The combined MO knockdown of 0.5ng *ahi1* and 4ng *cc2d2a* (red bars, n=10) leads to a synergistic increase in the frequency of development of each abnormal phenotype (B). Mortality at 24hpf (A) is shown as mean percentage (%) and standard error of the mean (where possible) in zebrafish embryos following: 0.5ng of *ahi1* MO alone, 4ng *cc2d2a* MO alone and co-injection of 0.5ng *ahi1* MO + 4ng *cc2d2a* MO. hpf, hours post fertilisation; MO, morpholino oligonucleotide.

To attempt to circumvent the high toxicity associated with combined 0.5ng *ahi1* and 4ng *cc2d2a* MO injection, a lower dose of *cc2d2a* MO (2ng) was used in future combination injections. Additionally, in case the combination of MOs were inducing death via programmed cell death or *p53* mediated off-target effects (Robu et al., 2007), *p53* MO was co-injected with future combination injections to knockdown p53 and ameliorate this effect.

5.2.7 Assessing *ahi1* and *cc2d2a* genetic interaction: Mortality rates and phenotypes following combined *ahi1* MO, low dose *cc2d2a* MO and *p53* MO knockdown in wild type zebrafish embryos

WT embryos were injected with a combination of 0.5ng *ahi1* MO, 2ng *cc2d2a* MO and 2ng *p53* MO. The lower dose combination of *ahi1* and *cc2d2a* MO and addition of *p53* MO resulted in a reduced mean (± standard error of the mean) 24hr mortality rate of 49% (± 4%). These results were plotted with the mean 24hr mortality rates of embryos following injection of 0.5ng *ahi1* MO alone, 4ng *cc2d2a* MO alone and uninjected WT matched embryos for each group (Figure 5.11A). As would be expected, the 24hpf mortality rates were higher following a MO injection, however even with combined MO injection, the relative 24hpf mortality rates were now between 1.2 and 1.4 times that of matched uninjected WT embryos (Figure 5.11A).

Figure 5.11 Mortality at 24hpf and percentage frequency of abnormal phenotypes following combined *ahi1, cc2d2a* and *p53* MO knockdown in zebrafish embryos
(A) Mortality at 24hpf is shown as mean percentage (%) and standard error of the mean (where possible) in zebrafish embryos following: 0.5ng of *ahi1* MO alone, 4ng *cc2d2a* MO alone and co-injection of 0.5ng *ahi1* MO, 2ng *cc2d2a* MO and 2ng *p53* MO. Mortality in uninjected WT matched for each MO experiment are shown (white bars). Low dose (0.5ng) *ahi1* MO alone (black bars, n=58) and 4ng *cc2d2a* MO alone (green bars, n=96) induce a low frequency (<5%) of abnormal phenotypes (B). The combined MO knockdown of 0.5ng *ahi1*, 2ng *cc2d2a* and 2ng *p53* MO leads to a synergistic increase in the frequency of each abnormal phenotype (B, red bars, n=53). hpf, hours post fertilisation; MO, morpholino oligonucleotide; WT, wild type.

Phenotyping by light microscopy was performed at 72hpf. The number of embryos injected with 0.5ng *ahi1* MO, 2ng *cc2d2a* MO and 2ng *p53* MO which survived to be phenotyped at 72hpf were 53. The range of abnormal phenotypes which developed included a curly tail (Figure 5.9D-E); cardiac oedema and abnormal cardiac development (Figure 5.9D-G); hydrocephalus (Figure 5.9C-G); pronephric cysts (Figure 5.9E) and single otolith in otic vesicles (Figure 5.9C, F-G). No abnormal eye development was detected by light microscopy following 0.5ng *ahi1* MO alone; 4ng *cc2d2a* MO alone; or combined 0.5ng *ahi1* MO, 2ng *cc2d2a* MO and 2ng *p53* MO. Figure 5.11B shows the frequency of abnormal phenotypes generated by 0.5ng *ahi1* MO alone, 4ng *cc2d2a* MO alone and lower dose combination MO (0.5ng *ahi1*, 2ng *cc2d2a* and 2ng *p53*). Despite using a lower dose of *cc2d2a* MO (2ng) in the combination injection (with 0.5ng *ahi1* and 2ng *p53* MO), there was a synergistic increase in the frequency of all phenotypes and abnormal ear development with altered otolith numbers were identified (Figure 5.11B, Table 5.3).

	Curly tail (%)	Cardiac oedema (%)	Hydrocephalus (%)	Pronephric cysts (%)	Otic defect (%)
0.5ng *ahi1* MO alone	3.0 ± 0.0	5.0 ± 0.0	2.0 ± 0.0	0.0 ± 0.0	0.0 ± 0.0
4ng *cc2d2a* MO alone	0.7 ± 0.7	1.7 ± 1.7	0.0 ± 0.0	2.7 ± 2.7	0.0 ± 0.0
0.5ng *ahi1* + 2ng *cc2d2a* + 2ng *p53* MO	38.0 ± 27.0	53.0 ± 9.0	17.0 ± 6.0	9.5 ± 5.5	2.0 ± 2.0

Table 5.3 Frequency of abnormal phenotypes in *ahi1* and *cc2d2a* MO injected embryos

Percentage (%) frequency of abnormal phenotypes at 72hpf in WT embryos injected with 0.5ng *ahi1* MO alone, 4ng *cc2d2a* MO alone or combination of: 0.5ng *ahi1* MO, 2ng *cc2d2a* MO and 2ng *p53* MO. Data are shown as mean ± standard error of the mean where possible. No abnormal eye development was apparent by light microscopy. MO, morpholino oligonucleotide.

The similarities in the synergistic increase in frequency of aberrant phenotypes following injection of 0.5ng *ahi1* MO into *sentinel* embryos can be compared with the effect of combination MO knockdown of 0.5ng *ahi1* and 2ng *cc2d2a* MO (and 2ng *p53* MO) by studying Table 5.2 and Table 5.3 *ahi1* MO knockdown in *sentinel* embryos compared to combined MO knockdown in WT embryos led to: a curly tail in 35.3% and 38% respectively; hydrocephalus in 18.7% and 17% respectively and pronephric cysts in 15% and 9.5% respectively. Both experiments support a genetic interaction between *ahi1* and *cc2d2a* and suggest that the combination MO injections closely mimic the perhaps more physiological MO knockdown in the spontaneous zebrafish mutant, *sentinel*.

5.2.8 Evaluating the role of gene dosage in *ahi1* and *cc2d2a* genetic interactions

Although when higher doses of MOs were used in combination injections they could be associated with increased early mortality, the above experiments enabled some hypotheses to be made regarding the effect of gene dosage on certain phenotypes. Figure 5.12 shows the percentage frequency of abnormal phenotypes following 0.5ng *ahi1* MO alone; 4ng *cc2d2a* MO alone; combined 0.5ng *ahi1* MO, 2ng *cc2d2a* MO and 2ng *p53* MO; combined 0.5ng *ahi1* MO and 4ng *cc2d2a* MO. Unfortunately the 2ng *cc2d2a* MO dose alone or the combination of 0.5ng *ahi1* MO and 2ng *cc2d2a* MO without *p53* MO were not injected and for completeness should have been performed.

The more than double increase in frequency of curly tail (38% to 80%) and hydrocephalus (17% to 50%, Figure 5.12) phenotypes when an additional 2ng of *cc2d2a* MO was combined with 0.5ng *ahi1* MO/2ng *cc2d2a* MO was of curious interest and cannot be logically explained, particularly when 4ng *cc2d2a* MO alone only induced these phenotypes in very low frequency. This observation may reflect the complex interplay and unpredictable synergy on phenotype between interacting genes.

Low dose (0.5ng) *ahi1* MO alone did not induce any pronephric cysts in these experiments, however appeared to play an influential role when it was combined with 4ng *cc2d2a* as there was a synergistic increase in phenotype which led to pronephric cysts in 10% of embryos. However, the fact that the frequency of pronephric cysts was similar (9.5%) when 0.5ng *ahi1* MO was combined with only 2ng *cc2d2a* MO may

suggest that there will be a maximal effect of a gene interaction and it will not all be explained by ‘gene dosage’.

Figure 5.12 Effect of gene dosage on the frequency of abnormal phenotypes following combined *ahi1* and *cc2d2a* MO knockdown in wild type zebrafish embryos

Low dose (0.5ng) *ahi1* MO alone (black bars, n=58) and 4ng *cc2d2a* MO alone (green bars, n=96) induce a low frequency (≤5%) of abnormal phenotypes. Combination of 0.5ng *ahi1*, with a lower dose (2ng) *cc2d2a* and 2ng *p53* MO leads to a synergistic increase in the frequency of abnormal phenotypes (red checked bars, n=53). Combination injection with an additional 2ng *cc2d2a* MO and without *p53* MO further increases the frequency of aberrant phenotypes (red bars, n=10). MO, morpholino oligonucleotide.

The abnormal eye phenotype which was not apparent with low dose individual knockdown of *ahi1* or *cc2d2a*, however was detected in up to 30% of embryos following combination knockdown suggested a powerful interplay between these two genes regarding eye development or subsequent degeneration. In Figure 3.3 expression of *ahi1* was shown in the retina of zebrafish from the 8 somite stage to at least 72hpf. Elsewhere it has been reported that cc2d2a localises to the connecting cilium in photoreceptors of zebrafish (Bachmann-Gagescu et al., 2011).

5.2.9 Phenotypes and mortality rates following combined *ahi1* MO and *nphp6* MO knockdown in wild type zebrafish embryos

To attempt to further understand the oligogenicity and digenic inheritance identified in patients with NPHP/JBTS/MKS caused by mutations in *NPHP6* and *AHI1* (Tory et al., 2007), WT embryos were injected with a combination of *nphp6* and *ahi1* splice blocking MO. Above, injection of 0.5ng *ahi1* MO alone (n=58) was shown to be associated with a low frequency of abnormal phenotypes (≤5%, Table 5.2, Figure 5.9A, Figure 5.10A), this dose was therefore chosen for combination injections with *nphp6* MO.

In section 4.2.14, following injection of 4-6ng of *nphp6* splice blocking MO, the development of aberrant phenotypes including: curly tail, cardiac oedema, hydrocephalus, pronephric cysts (proximal, distal and cloacal), abnormal eye and ear development (Figure 4.23, Figure 4.24, Figure 4.25 and Figure 4.26B) was confirmed. Even with an *nphp6* splice blocking MO dose of 4ng the frequency of abnormal phenotypes such as curly tail, was up to 16% (Figure 4.26B). However injection of 2ng *nphp6* splice blocking MO alone was not associated with any abnormal phenotypes (Figure 5.13B, n=64), therefore a 2ng dose of *nphp6* MO was selected for combination injections with *ahi1* MO.

WT embryos were injected with a combination of 0.5ng *ahi1* MO and 2ng *nphp6* MO and phenotyped by light microscopy at 72hpf (n=19). The range of abnormal phenotypes seen following co-injection of *ahi1* and *nphp6* MOs included: curved body axis, more often dorsal (Figure 5.13C, F); cardiac oedema (Figure 5.13C, D, F, G); hydrocephalus (Figure 5.13C, F, G); pronephric cysts (Figure 5.13D, G); coloboma (Figure 5.13C); unilateral microphthalmia (Figure 5.13G); empty otic vesicle (Figure

5.13F, G) and single otolith in the otic vesicle (Figure 5.13D). The frequency of these phenotypes were shown in Figure 5.14A, with a curly tail in 53%, hydrocephalus in 47%, pronephric cysts in 11% and developmental eye and ear anomalies in 26-31%. The mean 24hpf mortality rate following combined MO injection was 72.5% (± 5.5%), this was 1.7 times higher than matched uninjected WT embryos (41.5% ± 15.5%).

To assess and again control for the effect of toxicity potentially mediated by off-target effects (Robu et al., 2007), when combined MO injections were performed, the 0.5ng *ahi1* and 2ng *nphp6* MO combination were also injected with 2ng *p53* MO (n=26). This confirmed that the development of abnormal phenotypes continued when also co-injected with *p53* MO (Figure 5.13E). A synergistic increase in the frequency of abnormal phenotypes following co-injection of *ahi1*, *nphp6* and *p53* MOs were again apparent (Figure 5.14B). No pronephric cysts were detected by light microscopy and the frequency of abnormal eye and ear development was only 4%, this may be because the overall number of embryos phenotyped was low, or as previously discussed, because embryos were phenotyped at 72hpf.

Figure 5.13 Phenotypes following combination of low dose *ahi1* and *nphp6* MO knockdown in zebrafish embryos

Lateral views of zebrafish embryos at 72 hours post fertilisation. Golden zebrafish embryos injected with a low dose of *ahi1* MO (0.5ng, A) and *nphp6* MO (2ng, B) alone were phenotypically normal. Golden zebrafish embryos co-injected with low dose *ahi1* and *nphp6* MOs (C, D, F, G) develop abnormal phenotypes, which persist when also co-injected with *p53* MO (to exclude off-target effects, E). The range of abnormal phenotypes seen following co-injection of *ahi1* and *nphp6* MOs includes: hydrocephalus (black arrowhead C, E, F, G); curved body axis (C, E, F); cardiac oedema (C-G); pronephric cysts (red arrowhead D, G); coloboma (black arrow C); unilateral microphthalmia (green arrow G); empty otic vesicle (red arrow F, G) and single otolith (red arrow D). MO, morpholino oligonucleotide.

Figure 5.14 Percentage frequency of abnormal phenotypes following individual and combined *ahi1* and *nphp6* (±*p53*) MO knockdown in zebrafish embryos
0.5ng *ahi1* MO alone induces a low frequency of abnormal phenotypes and no pronephric cysts, developmental eye or ear abnormalties (black bars, A-B, n=58). 2ng of *nphp6* MO alone does not induce any developmental anomalies (green bars, A-B, n=64). Combined MO knockdown using 0.5ng *ahi1* and 2ng *nphp6* leads to a synergistic increase in the frequency of each abnormal phenotype (red bars, A, n=19). B shows the synergistic increase in the frequency of abnormal phenotypes when 2ng *p53* MO is combined with 0.5ng *ahi1* and 2ng *nphp6* MOs (red/white checked bars, n=26). MO, morpholino oligonucleotide.

Figure 5.15 shows the comparison in the mortality rates at 24hpf in matched uninjected WT embryos to mortality following *ahi1*, *nphp6* MO combination with or without *p53* MO knockdown. As would be expected, 24hpf mortality rates were higher following a MO injection. The addition of *p53* MO to a combination injection reduced relative mortality rates from 1.7 times to 1.1 times that of matched uninjected WT embryos (Figure 5.15).

Figure 5.15 Mortality rates at 24hpf following combined *ahi1* and *nphp6* ± *p53* MO knockdown compared to matched uninjected zebrafish embryos

Data are shown as mean percentage (%) and standard error of the mean. Mortality rates are increased following combined MO injections. Mortality at 24hpf following injection of 0.5ng *ahi1* and 2ng *nphp6* MO (black bar) is 72.5% (1.7 times) compared to 41.5% in matched uninjected WT embryos (white bar). Mortality at 24hpf following injection of 2ng *p53* MO in combination with 0.5ng *ahi1* and 2ng *nphp6* MO (black/white checked bar) is 68% (1.1 times) compared to 59.5% in matched uninjected WT embryos (white spotted bar). comb, 0.5ng *ahi1*+2ng *nphp6*; MO, morpholino oligonucleotide; WT, wild type.

To increase the number of embryos studied in the *ahi1* and *nphp6* MO combination experiments, because the ciliopathy phenotypes continued to develop with the addition of *p53* MO, this data was pooled for subsequent phenotypical analysis. Although injection of 2ng *nphp6* MO alone (n=64) was not associated with the development of any abnormal phenotypes and injection of 0.5ng *ahi1* MO alone (n=58) led to a curly tail, cardiac oedema or hydrocephalus in less than five percent of embryos, when embryos were injected with a combination of 0.5ng *ahi1* MO and 2ng *nphp6* MO, with or without 2ng *p53* MO (n=45), there was a dramatic increase in the frequency of ciliopathy phenotypes. Figure 5.16A shows the synergistic increase in the frequency of curly tail (51.5% ± 1.5%), cardiac oedema (70% ± 7%), hydrocephalus (41% ± 6%), pronephric cysts (5.5% ± 5.5%), abnormal eye (15% ± 11%) and aberrant ear (17.5% ± 13.5%) development. This data strongly suggested a genetic interaction between *ahi1* and *nphp6*. Although the graphs in Figure 5.14A,B and Figure 5.16A appear very similar, the subtle difference is that Figure 5.16 is a pool of the results shown in Figure 5.14A,B to increase the data numbers.

The mean mortality rates at 24hpf were compared between individual *ahi1* or *nphp6* MO injections and combination *ahi1* and *nphp6* MO injections relative to matched uninjected embryos (Figure 5.16B). The increase in 24hpf mortality rates relative to uninjected embryos following 0.5ng *ahi1* MO was 1.2 times, following 2ng *nphp6* MO was 1.1 times and following combination of *ahi1* and *nphp6* was 1.4 times.

Figure 5.16 Percentage frequency of abnormal phenotypes and mortality at 24hpf following combined *ahi1* and *nphp6* MO knockdown in zebrafish embryos
Injection of 0.5ng *ahi1* MO alone induces a low frequency of abnormal phenotypes and no pronephric cysts, developmental eye or ear abnormalties (black bars, A, n=58). 2ng of *nphp6* MO alone does not induce any developmental anomalies (green bars, A, n=64). Combined MO knockdown using 0.5ng *ahi1* and 2ng *nphp6* ±2ng *p53* MO (red bars, A, n=45) leads to a synergistic increase in the frequency of each abnormal phenotype. Mortality at 24hpf is shown (B) as mean percentage (%) and standard error of the mean in zebrafish embryos following: 0.5ng of *ahi1* MO alone, 2ng *nphp6* MO alone and co-injection of 0.5ng *ahi1* MO + 2ng *nphp6* MO ± 2ng *p53* MO (B). Mortality rates in uninjected WT embryos matched for each group (white bars). MO injections are associated with a relative increase in 24hpf mortality rates. hpf, hours post fertilisation; MO, morpholino oligonucleotide; WT, wild type.

5.3 Discussion

The NPHP related ciliopathies are well recognised for their genetic heterogeneity, however the mechanisms which lead to the associated clinical heterogeneity remain incompletely understood. In this chapter by utilising zebrafish models, the role of oligogenicity was explored and the effect on subsequent phenotype was evaluated.

Previously, oligogenicity has been evaluated when studying normal kidney development, disease pathophysiology and the effect on the severity of phenotype, in zebrafish models. In podocyte development, combination knockdown of *wt1* and *foxc1a* resulted in complete failure of podocytes to form (O'Brien et al., 2011). The genetic interaction between *WT1* and *FOXC1A* was confirmed by co-immunoprecipitation and protein studies which demonstrated a physical interaction (O'Brien et al., 2011).

The pathophysiology of ADPKD has been further evaluated in zebrafish by combined MO knockdown of *pkd2* and *sec10* (part of the 'exocyst', a protein membrane trafficking complex), which led to a synergistic increase in the frequency of cilia phenotypes including pronephric cysts (Fogelgren et al., 2011). This genetic interaction was supported by co-localisation data and biochemical interaction of proteins (Fogelgren et al., 2011).

In NPHP, the functional role of *NPHP2* and *NPHP9* on pronephros development and left-right patterning was studied in zebrafish (Fukui et al., 2012). Combined *nphp2* and *nphp9* MO knockdown led to a synergistic increase in pronephric cysts and abnormal left-right cardiac development. Since nphp9 mRNA rescued *nphp2* morphants, however the converse was not true, it was postulated that nphp9 must function downstream of nphp2 (Fukui et al., 2012).

Although the extra-renal manifestations of NPHP are variable, *NPHP5* and *NPHP6* mutations are usually associated with retinal degeneration (Schafer et al., 2008). To evaluate a functionally relevant, potential genetic interaction, combined MO knockdown of *nphp5* and *nphp6* in zebrafish was performed and led to a synergistic increase in the frequency of morphant phenotypes including pronephric cysts and hydrocephalus. This genetic interaction was confirmed by identifying the protein

binding sites where the physical interaction occurs between nephrocystins 5 and 6 (Schafer et al., 2008).

In BBS, a NPHP related oligogenic ciliopathy, combined MO knockdown of *mgc1203* (which encodes a pericentriolar protein and co-localises with BBS proteins, however cannot cause BBS alone) with *bbs4* or *bbs6* or *bbs1* led to an increased frequency and severity of BBS phenotypes (Badano et al., 2006a). It was concluded that combined MO knockdown in zebrafish was a useful method for evaluating the effect of epistatic mutations (for example in *mgc1203*) and trying to improve understanding of the subsequently variable clinical phenotype.

In order to study potential genetic interactions, it was important to initially define the range and frequency of aberrant developmental phenotypes induced by interfering with the expression of a single gene. In Chapter 3, Figure 3.9, the effect of *ahi1* on development following a range of doses of MO knockdown was characterised. In Chapter 4 the effect of *cc2d2a* using the *sentinel* mutant and a range of doses of MOs to knockdown *cc2d2a* and *nphp6* were individually characterised. This prior work enabled the study of the effects of combinations of gene interference: *cc2d2a* and *nphp6*; *cc2d2a* and *ahi1*; *ahi1* and *nphp6* to be reported herein.

5.3.1 Recapitulation of genetic interaction between *CC2D2A* and *NPHP6* using *sentinel* (*cc2d2a* mutant) embryos

Patients with MKS caused by mutations in *CC2D2A* and *NPHP6* have been identified (Hopp et al., 2011), suggesting this gene combination may lead to austere developmental anomalies and account for ciliopathies at the severe end of the spectrum. Embryos born from *sentinel* heterozygous matings injected with 4 or 6ng of splice blocking *nphp6* MO developed pronephric cysts in 9% and 36% respectively. This was a synergistic increase in the frequency of pronephric cysts identified compared to those identified in *sentinel* embryos alone (1.5%), embryos injected with 4ng *nphp6* (1.5%) or 6ng *nphp6* (17%) MO alone. A limitation of this work when studying embryos born to *sentinel* heterozygous parents, was a failure to genotype every embryo, this may account for the low frequency of phenotypes/pronephric cysts identified in this group, as some may have been heterozygous. Ideally in future to avoid this potential ambiguity, gentopying would be performed in all embryos.

It is important to note the marked increase in frequency in pronephric cysts associated with a 6ng dose of *nphp6* MO alone, this dose appeared to clearly be associated with a cystic phenotype and was similar to the published percentage of cysts detected in WT embryos injected with 5ng *nphp6* (20%) splice blocking MO (Gorden et al., 2008). Although a synergistic increase in the frequency of pronephric cysts (36%) with injection of 6ng *nphp6* MO into embryos born from *sentinel* heterozygous parents was detected, this was much lower than the 89% of pronephric cysts reported in the original *nphp6* and *sentinel* paper (Gorden et al., 2008). Whilst methods for detecting pronephric cysts were not described in the publication, the only supporting evidence they showed for pronephric cysts were light microscopy images (Gorden et al., 2008) and there was no description of experiments involving histology. *Gorden et al.* (2008) did however report a much higher percentage of pronephric cysts (33%) in *sentinel* embryos alone and they phenotyped for up to 6dpf. This extended period of study was not feasible with our animal license and therefore the possibility of later development of perhaps more overt pronephric cysts, beyond 72hpf when they were phenotyped cannot be excluded.

In addition to inducing a synergistic increase in the development of pronephric cysts, markedly more curly tails in up to 74.5% were identified when embryos born to *sentinel* heterozygous parents were injected with 6ng *nphp6* MO. This may suggest that interaction between *cc2d2a* and *nphp6* subsequently mediates changes in PCP pathways. To date reports of CC2D2A and NPHP6 interacting have focused on the basal body (Gorden et al., 2008), however it would be interesting to explore further downstream signalling pathways. Future experiments to assess for potential changes in PCP pathways could involve performing *in situ* hybridisation of PCP genes before and after MO knockdown of *cc2d2a* or *nphp6*.

Previously, the use of proteomic studies to assess the NPHP related ciliopathies resulted in a model which groups the various genes into pathways and relevant associated proteins into functional networks (Sang et al., 2011). Cc2d2a has been suggested to function in Hh signalling and Nphp6 in maintaining cilia architecture (Sang et al., 2011). In future work it would therefore be interesting to evaluate for any changes in Hh signalling following *cc2d2a* MO knockdown. This could be evaluated by performing *in situ* hybridisation using a *shh* riboprobe following MO knockdown of *cc2d2a* in zebrafish embryos.

The original *sentinel nphp6* paper (Gorden et al., 2008) did not identify any additional developmental defects such as brain malformation or cardiac laterality defects, however a synergistic increase in the frequency of developmental anomalies in several other organs was observed herein. There was a synergistic increase in the frequency of cardiac oedema from 2.5% in embryos born to *sentinel* heterozygous parents, 39% when WT were injected with 6ng *nphp6* MO and 81.5% when *sentinel* were injected with 6ng *nphp6* MO. The gross readout of cardiac oedema may reflect primary developmental anomalies of the heart linked to disordered left-right patterning (previously shown in *nphp6* morphants in section 4.2.17) or secondary to structural or functional anomalies of the pronephros.

Hydrocephalus was a frequent phenotype seen in WT embryos injected with 4-6ng *nphp6* MO alone (9.5-30.8%) and of low frequency in embryos born to *sentinel* heterozygous parents (0.5%). When 4ng *nphp6* MO was injected into *sentinel* embryos there was a synergistic increase in hydrocephalus in up to 36% of embryos, however this was not sustained when 6ng *nphp6* MO was injected (22%), possibly because more of the embryos which would mature to develop hydrocephalus were dying within the first 24hpf. Certainly increased rates of mortality at 24hpf were evident following injection of 6ng *nphp6* MO into WT (49%) or *sentinel* (70%) embryos. If projecting this data from zebrafish models to humans, this combination of *nphp6* and *sentinel* (*cc2d2a*) may represent the MKS end of the ciliopathy spectrum, associated with high perinatal mortality (Alexiev et al., 2006).

By light microscopy, the frequency of abnormal eye development was not altered by combining *nphp6* MO knockdown in embryos born from *sentinel* heterozygotes and remained low, between 1-3.5%, similar to rates following *nphp6* MO knockdown alone. In matched experiments no abnormal eye development was detected in embryos born to *sentinel* heterozygous parents, this would be in keeping with the absence of detection of phenotypes other than pronephric cysts previously reported (Gorden et al., 2008). However these latter results are in contrast with the very low frequency, although definitely abnormal eye development reported albeit in a different clutch of *sentinel* embryos in Chapter 4, Figure 4.9. Interestingly, the abnormal retinal phenotype and altered visual function of *sentinels* (Bachmann-Gagescu et al., 2011) has subsequently been reported in detail and confirmed by *Gorden et al.* (2008) who initially evaluated *nphp6* in *sentinels* (Gorden et al., 2008). Unfortunately they did not explore the impact

of additional *nphp6* knockdown, which would have been interesting, particularly since it is known that *NPHP6* mutations are the leading cause of isolated congenital retinal degeneration (den Hollander et al., 2006).

Although to date, there are no publications relating to abnormal ear development or hearing impairment in the NPHP related ciliopathies, a synergistic increase in the frequency of abnormal development of the rudimentary ear in zebrafish models of *CC2D2A* and *NPHP6* mutations were observed in this work. This was perhaps surprising, as *CC2D2A* may have been hypothesised to play a protective role in ear development, since the *sentinel* zebrafish were initially discovered as a protective mutant during a screen for genes influencing aminoglycoside induced hair cell death (Owens et al., 2008).

Previously, *in situ* hybridisation in developing zebrafish embryos of *nphp6* alone has identified expression predominantly in the tail, cerebellum and retina (Sayer et al., 2006), whilst *cc2d2a* alone was expressed ubiquitously at 64 hpf (Owens et al., 2008). In future experiments it would be informative to further define the expression of *cc2d2a* during development. Subsequently, another method of further evaluating the apparent genetic interaction between *CC2D2A* and *NPHP6* would be to perform double *in situ* hybridisation using *cc2d2a* and *nphp6* riboprobes to assess for co-expression.

5.3.2 Genetic interaction between *CC2D2A* and *AHI1* using *ahi1* knockdown in *sentinel* (*cc2d2a* mutant) embryos

Whilst oligogenic inheritance has been described in patients with JBTS caused by a heterozygous mutation in *AHI1* and a homozygous mutation in *NPHP6* or *NPHP1* (Tory et al., 2007), digenic inheritance has not yet been described for *AHI1* and *CC2D2A*. However, it may be that mutations are present in affected individuals, however not yet identified, as screening or mutation analysis of the various NPHP associated ciliopathy genes does not occur routinely because of the limitation of resources. Furthermore, previously patients with JBTS have been reported even when only a single heterozygous change in *AHI1* (Otto et al., 2011; Parisi et al., 2006) was identified, meaning the second disease causing mutation remains unidentified.

Both CC2D2A (Gorden et al., 2008) and Jouberin (Eley et al., 2008; Hsiao et al., 2009) colocalise at the basal body of primary cilia, however information regarding protein

interaction is currently sparse. Such an interaction may be postulated if we recognise that Jouberin is suggested to behave as a bridging protein to link the 'Hh signalling' module, including CC2D2A, to other functioning networks in the NPHP, JBTS, MKS ciliopathy disorders (Sang et al., 2011).

Embryos born from *sentinel* heterozygous matings injected with 0.5-2ng of *ahi1* splice blocking MO developed pronephric cysts in 15% to 45.7% in a dose dependent manner. This was a synergistic increase from the frequency of pronephric cysts of 1-10.9% detected by interruption of *CC2D2A* or *AHI1* alone. These genes are frequently associated with causing JBTS and MKS, therefore it was perhaps not suprising that there was also a synergistic increase in the frequency of hydrocephalus. Most strikingly, the frequency of hydrocephalus increased from 1-2% in embryos born to *sentinel* heterozygotes or WT injected with 0.5ng *ahi1* MO alone, to 18.7% when combined.

Similar to the synergistic increase in frequency of curly tail, cardiac oedema and abnormal ear development detected in embryos born to *sentinel* heterozygotes injected with *nphp6* MO, this occurred when *sentinels* were injected with *ahi1* MO. The strong synergistic influence on altering body curvature associated with *AHI1* and *CC2D2A* interacting, ranging between 35.3-84%, may in part relate to the fact that *sentinel* mutants have a characteristic dorsal body curvature and again may implicate a role for disordered PCP.

In 3.2.9 altered cardiac looping and left-right body patterning was detected in *ahi1* morphants. This propensity to aberrant cardiac development may facilitate explanation of the synergistic increase in cardiac oedema detected when embryos born to *sentinel* heterozygotes were injected with *ahi1* MO. Compared to a frequency of cardiac oedema of 3-35.1% following interference with *CC2D2A* or *AHI1* alone, this increased to 30.7-89.3% with combination experiments. Again, the cardiac oedema may reflect defective pronephric function, failing to sufficiently filter body fluid.

Although mutations in *AHI1* or *CC2D2A* are not known to cause isolated blindness in humans, up to 20% of patients with associated cerebral-renal disorders are blind (Gorden et al., 2008; Parisi et al., 2006; Valente et al., 2006a). It was therefore interesting to identify a synergistic increase in the frequency of abnormal eye development on light microscopy when *ahi1* MO was injected into embryos born to

sentinel heterozygotes. Isolated interference with *cc2d2a* or *ahi1* led to aberrant eye development in a maximum of 0.9% of embryos, compared to up to 15.3% when 2ng *ahi1* was injected into embryos born to *sentinel* heterozygotes. A mechanism of this interaction may be the fact that in photoreceptors both *AHI1* (Hsiao et al., 2009) and *CC2D2A* (Bachmann-Gagescu et al., 2011) have been shown to independently regulate vesicular trafficking via their relationships with Rab8 (Rab8a). Following knockdown of *AHI1* or *CC2D2A* in cell models, Rab8 was mislocalised which led to aberrant trafficking in photoreceptors (Bachmann-Gagescu et al., 2011; Hsiao et al., 2009).

The synergy in all ciliopathy phenotypes detected when embryos born to *sentinel* heterozygotes were injected with *ahi1* MO provides compelling evidence for a genetic interaction between *CC2D2A* and *AHI1*. However a regretable limitation of this work was the uncertainty of the genotype of embryos born to *sentinel* heterozygotes, to try to overcome this, the alternative zebrafish MO mediated model of *cc2d2a* related ciliopathies (created in section 4.2.10) was used and combination MO injections were performed to knockdown *cc2d2a* and *ahi1*.

5.3.3 Recapitulation of the genetic interaction between *CC2D2A* and *AHI1* using MO knockdown in wild type embryos

Whilst *sentinel* zebrafish have been postulated to be a useful zebrafish line to study oligogenicity (Gorden et al., 2008), there were limitations associated with their use as a tractable model to study the effect of interference with *cc2d2a*; possibly because of incomplete penetrance of important phenotypes such as pronephric cysts (Gorden et al., 2008) and potentially increased early mortality in *sentinel* homozygotes.

Although the frequency of aberrant ciliopathy developmental phenotypes was less than 5% when performing 0.5ng *ahi1* or 4ng *cc2d2a* MO injections individually, with 24hpf mortality rates 1.2 to 1.4 times relative to matched WT embryos, when injected in combination although a synergistic increase in abnormal phenotypes was induced, this dose combination was associated with excess lethality. Injection of 0.5ng *ahi1* and 4ng *cc2d2a* MO led to the 24hpf mortality rate rising to 88%, 3.4 times the matched WT 24hpf mortality rate. In order to enable more embryos to survive to be phenotyped at 72hpf following combined *ahi1* and *cc2d2a* MO injection, the dose of *cc2d2a* MO was reduced to 2ng for future experiments. Unfortunately the 2ng dose of *cc2d2a* MO was not injected into WT embryos alone, however since MO injections tend to have a dose

dependent effect on the development of abnormal phenotypes, it would be expected that any aberrancies associated with a 2ng dose of *cc2d2a* MO would be less than the 2.7% frequency which was induced by a 4ng dose of *cc2d2a* MO.

There was a synergistic increase in the frequency of pronephric cysts, hydrocephalus, curly tail and cardiac oedema when WT embryos were injected with a combination of 0.5ng *ahi1* and 2ng *cc2d2a* MOs. This dose combination enabled increased survival of embryos to be phenotyped at 72hpf. With combination knockdown of *cc2d2a* and *ahi1*, the frequency of pronephric cysts increased to 9.5% and hydrocephalus to 17%. Although there was a synergistic increase in the frequency of pronephric cysts, this was still only up to 9.5% and if embryos had been phenotyped at a later date, such as 5dpf, this frequency may have further increased. If these experiments were to be repeated, it would definitely be wise to consider reviewing embryos at 72hpf and 5dpf as this may allow for maximal capture of data, ideally without any excess death of embryos between 72hpf and 5dpf.

The synergistic increase in the frequency of cardiac oedema to 53% may again relate to a combination of: aberrant cardiac looping/development. It was evident herein (3.2.9) that *ahi1* knockdown alone adversely interfered with cardiac development; with oedema presumed secondary to impaired pronephric clearance of fluid. Cardiac looping was not formally assessed in the combination morphants, however would have been interesting to evaluate. Again, although not formally assessed or documented, a reduced frequency of heart beat was noted when phenotyping morphants at 72hpf, compared to that of WT embryos. This may have preceded subsequent mortality and from observations whilst performing experiments, it would be surprising if all morphants which were phenotyped at 72hpf would survive to be phenotyped at 5dpf.

Although of low frequency, the combination of 0.5ng *ahi1* and 2ng *cc2d2a* MOs led to abnormal ear development with altered numbers of otoliths, whilst knockdown of either MO alone at this dose did not. When the *cc2d2a* MO dose was reduced from 4ng to 2ng in combination injections, abnormal eye development no longer occurred. This may suggest a gene dosage effect was required to induce abnormal eye development, or in the context of eye development that *cc2d2a* plays more of an influence than *ahi1*.

The synergistic increase in the frequency of aberrant phenotypes continued when *p53* MO was added to the *ahi1* and *cc2d2a* MO combination, excluding the induction of off-

target effects (Robu et al., 2007) and confirmed a genetic interaction between *AHI1* and *CC2D2A* as originally identified with the injection of *ahi1* MO into *sentinel* (*cc2d2a* mutant) embryos. The use of combination MO knockdown generated similar results to the perhaps more physiological evaluation of a genetic interaction between *AHI1* and *CC2D2A* using *ahi1* knockdown in *sentinel* mutants, however proved to be a robust and efficacious model for evaluating genetic interactions. It would be useful for this apparent genetic interaction between *AHI1* and *CC2D2A* to be assessed at the protein level and an interesting expansion of the work evaluating interacting protein networks (Sang et al., 2011) in the NPHP, JBTS and MKS ciliopathy disorders. The current absence of the identification of patients with NPHP related ciliopathies caused by digenic mutations in *AHI1* and *CC2D2A* may relate to the fact that the cost implications restrict the widespread assessment of several other genes and screening is therefore currently not routinely available. It is however noteworthy that in a recent attempt to further characterise and understand the phenotypic variation in NPHP associated ciliopathies, mutation analysis of eighteen ciliopathy genes including *AHI1* and *CC2D2A* was undertaken and failed to identify any oligogenicity (Otto et al., 2011). Furthermore a causal mutation was not identified in any of the eighteen ciliopathy genes in 75% (n=90) of patients in the cohort with NPHP related ciliopathies, suggesting that several causal genes remain currently unidentified.

In future experiments, to further evaluate the potential impact of an interaction between *CC2D2A* and *AHI1* it would be interesting to evaluate differences in *ahi1* expression by *in situ* hybridisation following MO knockdown of *cc2d2a*.

5.3.4 Genetic interaction between *AHI1* and *NPHP6* using combined *ahi1* and *nphp6* knockdown in wild type embryos

Patients with JBTS caused by heterozygous mutations in both *AHI1* and *NPHP6* have been identified (Hopp et al., 2011), however since the numbers were low, it was not clear whether this influenced the subsequent phenotype. Both Jouberin (Eley et al., 2008; Hsiao et al., 2009) and nephrocystin-6 (Valente et al., 2006b) colocalise at the basal body of primary cilia, however to date there is no information regarding if a direct interaction exists between the proteins. A functional interaction is plausible from the proposed model of NPHP-JBTS-MKS protein network, which suggests that Jouberin

acts as a bridging protein to the 'cilia integrity' complex which consists of NPHP6, NPHP5 and Ataxin10 (Sang et al., 2011).

WT embryos injected with a combination of low doses of *ahi1*(0.5ng) and *nphp6*(2ng) MO which when injected in isolation did not, or only minimally (less than 5%) induced abnormal cardiac, brain and renal development, led to a synergistic increase in the frequency of abnormal organogenesis. The frequency of pronephric cysts detected at 72hpf increased from occurring in no embryos injected with low dose of either *ahi1* or *nphp6* MO alone, to 11% in combination morphants. The frequency of pronephric cysts with this combination of gene interference could more than likely have been further increased by uptitrating the MO doses, however initially it seemed important to evaluate if there was an effect by combining subeffective individual doses. Hydrocephalus occurred in 47% of embryos following combination of *ahi1* and *nphp6* compared to only 2% of embryos with knockdown of either gene alone, using the same MO doses. Since both *AHI1* and *NPHP6* are important causes of JBTS which is characterised by abnormal brain development and in particular cerebellar vermis hypoplasia(Parisi et al., 2007), it is not surprising that this was a prevalent phenotype.

A synergistic increase in the frequency of abnormal eye and ear development were also evident. Eye anomalies were only studied by light microscopy and occurred in up to 26% of combination morphants, compared to none of the embryos injected with either low dose of *ahi1* or *nphp6* MO alone. We may assume this phenotype is caused by the effect of *NPHP6* predominantly as we know it is the leading cause of isolated congenital retinal degeneration (den Hollander et al., 2006) and when low dose *ahi1* (0.5ng) was combined with a low/subeffective dose of *nphp6* (2ng) no abnormal eye development occurred.

Curiously, abnormal ear development, with altered numbers of otoliths occurred with a frequency of up to 31% in *ahi1* and *nphp6* combination morphants. This phenotype is not described in patients, however may represent a general marker of abnormal ciliopathy phenotypes in the zebrafish model organism (Colantonio et al., 2009).

The combination of *ahi1* and *nphp6* MOs led to a 24hpf mortality rate 1.7 times that of matched WT embryos, therefore to try to minimise any increased mortality associated with programmed cell death or off-target effects, *p53* MO was added to the combination of individual MO doses. This successfully reduced the relative 24hpf mortality rate to a

comparable 1.1 times that of matched WT embryos. The lethality associated with a combination of *AHI1* and *NPHP6* interference may have been predicted and disease severity has recently been recognised in patients with NPHP related ciliopathies, where the disease phenotypes were most severe when two null allelles occurred in *NPHP6* and *AHI1* (Chaki et al., 2011).

Understandably the identification of high 24hr mortality rates following individual or combined MO experiments may lead to concerns regarding the risk of off-target effects leading to confounding, however the experiments performed above were controlled for this by repeating with co-injection of a *p53* MO. Additionally, as discussed in section 3.2.3 the consensus amongst fellow zebrafish workers was that it was acceptable to include these experiments in data analysis providing there was consistent and careful comparison with matched control embryos. Furthermore there is patient data to support recognition of the severest phenotypes associated with mutations in *NPHP6* and *AHI1* (Chaki et al., 2011).

A synergistic increase in abnormal phenotypes, particularly hydrocephalus still occurred, when *ahi1*, *nphp6* and *p53* MOs were combined, however there was no synergistic increase in the frequency of pronephric cysts. There is no logical explanation for this, however may be explained by the overall low number of embryos included in the experiment. Ideally, to exclude any ambiguity, this experiment would be repeated aiming to generate larger numbers of morphants at least surviving to be phenotyped at 72hpf to 5dpf, to potentially enable the later detection of pronephric cysts. Overall, the combined knockdown of *ahi1* and *nphp6* was associated with a synergistic increase in the spectrum of ciliopathy phenotypes suggesting a genetic interaction. In future work, this apparent genetic interaction could be further explored by injecting different combinations of MO dose, to attempt to determine if there was an influence on subsequent phenotypes, trying to advance understanding of epistasis and genotype-phenotype correlations. In the recent evaluation of genotype and phenotype in 440 patients with NPHP related ciliopathies, they concluded that the gene locus was the key determinant of subsequent clinical characteristics (Chaki et al., 2011). Although they carefully studied the phenotypes associated with the known/identified causal gene, they did not perform screening for additional mutations, thus the influence of oligogenicity, which is likely to occur in at least some of these patients, cannot be considered.

To further evaluate the effect of an interaction between *AHI1* and *NPHP6*, in future work *nphp6* MO knockdown could be performed followed by comparing the effect on *ahi1* expression using *in situ* hybridisation. Alternatively further evaluation of protein to protein interactions between Jouberin and nephrocystin-6 could be performed to identify potential physical and functional interactions, as modelled in the recent ciliopathy protein network and NPHP related gene pathway paper (Sang et al., 2011).

The experiments reported herein support the hypotheses that there are genetic interactions between many of the ciliopathy genes. This work confirms a genetic interaction between *NPHP6* and *CC2D2A* and reports novel data proving an interaction between both: *AHI1* and *CC2D2A*; *AHI1* and *NPHP6*.

Chapter 6 Concluding Discussion

6.1 Summary of findings

This work focused on studying the developmental phenotypes induced by knockdown of certain genes known to cause cystic kidney disease and related ciliopathies. At times this involved assessing if the phenotypes were associated with a change in cilia, since increasingly these organelles are considered to play an important role in the pathogenesis of cystic kidney disease. A principal aspiration of this work was to try to further understanding of the clinical heterogeneity of cystic kidney disease related ciliopathies by studying oligogenicity and to ascertain if any reliable genotype-phenotype predictions could be determined. Zebrafish embryos were a tractable and useful model organism for this work. The key findings are outlined below and will subsequently be further discussed.

1) *ahi1* is normally expressed in developing zebrafish embryos in KV (the organ of laterality), the retina, brain and pronephros. *ahi1* knockdown in zebrafish embryos caused abnormal development with a curved body axis, hydrocephalus, pericardial oedema, pronephric cysts and retinal anomalies, creating a novel zebrafish model of the cystic kidney disease related ciliopathy, JBTS.

2) *ahi1* knockdown in zebrafish was associated with disruption to cilia in both KV and the distal pronephros, at the cloaca. Following *ahi1* knockdown, cilia were mostly absent from KV, or if present, they appeared shorter. Similarly, in the cloaca which was dilated, cilia were predominantly absent or shorter in *ahi1* morphants. As a consequence of loss of cilia from KV and presumed associated impaired nodal flow, establishment of left-right patterning was altered, which led to reversed cardiac asymmetry.

3) In *sentinel* zebrafish mutants (spontaneous mutation in *cc2d2a*) a low frequency of ciliopathy phenotypes were identified, however novel findings included: hydrocephalus; coloboma; unilateral microphthalmia and aberrant retinal development. Rapamycin had no effect on reversing or reducing the low frequency of phenotypes in *sentinel* mutants.

4) An alternative model of *CC2D2A* related ciliopathies was created by performing *cc2d2a* knockdown in zebrafish and generated an increased frequency of phenotypes

(compared to *sentinel* mutants) which included: dorsal curved axis, pericardial oedema, hydrocephalus, pronephric cysts, wavy notochord, coloboma and unilateral microphthalmia.

5) A zebrafish *nphp6* morphant was created and in addition to developing the typical ciliopathy phenotypes of: curved body axis; cardiac oedema, hydrocephalus, eye and ear anomalies; cysts were identified throughout the pronephros with cystic dilatation at the cloaca. Evaluation of cilia at KV revealed fewer and shorter cilia following *nphp6* knockdown which was associated with aberrant left-right body patterning and reversed cardiac asymmetry.

6) The severe end of the cystic kidney disease related ciliopathy spectrum was modelled by performing *mks3* knockdown in zebrafish embryos. In addition to typical ciliopathy phenotypes, cysts were apparent throughout the pronephros leading to dilatation at the cloaca and associated with gross generalised oedema. Interestingly, development of the notochord and tail were markedly abnormal in some *mks3* morphants: with a wavy notochord extending dorsally through the floorplate and myotomes to the surface; or the appearance of vacuoles within the dorsal fin. These developmental anomalies likely represent the severe end of the spectrum of ciliopathies.

7) A genetic interaction between *NPHP6* and *CC2D2A* was demonstrated in zebrafish by creating a synergistic increase in the frequency of ciliopathy phenotypes following *nphp6* knockdown in *sentinel* mutants. A similar genetic interaction was suggested between *AHI1* and *CC2D2A* when *ahi1* knockdown in *sentinel* mutants led to a synergistic increase in ciliopathy phenotypes.

8) A genetic interaction between *AHI1* and *CC2D2A* was further evaluated by creating an alternative model using combined MO knockdown of *ahi1* and *cc2d2a* in zebrafish embryos. A synergistic increase in ciliopathy phenotypes confirmed a likely genetic interaction and even a potential for oligogenic inheritance.

9) The genetic association between *AHI1* and *NPHP6* was modelled in zebrafish embryos by performing combined MO knockdown of *ahi1* and *nphp6* and yielded a synergistic increase in ciliopathy phenotypes.

6.2 *ahi1* knockdown in zebrafish is associated with loss of cilia and models Joubert Syndrome

Although the frequency of developmental anomalies following *ahi1* knockdown in zebrafish was dose dependent, interestingly, on subjective observation there was a variable spectrum of severity, very much reflecting the clinical heterogeneity which is apparent in patients. The mechanisms of this variability in the context of monogenic JBTS related disease, following only *ahi1* knockdown, unfortunately remains a puzzle.

The higher prevalence of brain anomalies and hydrocephalus, than pronephric cysts or retinal disease in the *ahi1* zebrafish morphants reported herein is also in keeping with the pattern of *ahi1* related JBTS in humans. The most frequent clinical findings associated with *AHI1* mutations in patients are molar tooth sign (on cerebral MRI) with retinal disease or additional cystic kidney disease (Valente et al., 2008).

Following examination of KV in many embryos, it was apparent that injection of *ahi1* MO resulted in complete loss of cilia or development of shorter cilia. Several different antibodies were utilised to further attempt to identify cilia, associated centrosomes or the apical epithelium of KV where cilia should sprout from, however these confirmed absence of cilia or occasionally the presence of shorter cilia. These findings may be explained physiologically by recall that Jouberin, the protein product of *AHI1* is expressed at the basal body and is now recognised to function as part of the ciliary transition zone which regulates ciliogenesis (Davis and Katsanis, 2012). This work mimics the identification of shortening and loss of cilia in KV of *nphp3* zebrafish models of the related ciliopathies NPHP and MKS, which led authors to hypothesise that the encoded protein was involved in the development of cilia (Zhou et al., 2010b).

In *ahi1* morphants, as a consequence of loss or shortening of cilia, reversal of left-right cardiac asymmetry was evident. This association between aberrations in left-right body patterning as a consequence of changes in cilia in KV has been reported in other zebrafish ciliopathy models (Slanchev et al., 2011; Zhou et al., 2010b) and is understandable because fluid flow generated by cilia in KV is responsible for determining body asymmetry (Kramer-Zucker et al., 2005). Although mutations in *AHI1* have not yet been linked with situs inversus in humans, other developmental cardiac defects, such as an atrial septal defect have been identified (Dixon-Salazar et al., 2004).

Cystic dilatation of the cloaca and the absence or existence of shorter cilia was an interesting finding in *ahi1* morphants. This pattern of abnormal cloacal development and ciliary changes has been reported in other zebrafish models of cystic kidney disease including *nphp6* (Sayer et al., 2006) and *nphp4* (Slanchev et al., 2011). The protein products of *AHI1, NPHP6* and *NPHP4* are all expressed in the basal body of cilia (Eley et al., 2008; Sayer et al., 2006; Slanchev et al., 2011) and it has been suggested that the basal body regulates the Wnt PCP signalling pathway (Burckle et al., 2011), which coordinates orientated cell growth (Borovina et al., 2010). Recently, knockdown of *wtip*, a gene whose protein product is expressed in the basal body, led to pronephric cysts with malformation of the cloaca and was associated with: fewer ciliated cells and reduced motility of cilia (Bubenshchikova E., 2012). The resulting ciliopathy phenotypes observed in *wtip* morphants were similar to *vangl2* morphants, suggesting an association between the development of cloacal abnormalities and PCP (Borovina et al., 2010; Bubenshchikova E., 2012; Burckle et al., 2011). The reported aberrant cloaca and ciliary findings are similar to those detected in this work in *ahi1* morphants.

6.3 Future work involving *AHI1*

This work on the role of *AHI1* in cystic kidney disease and related ciliopathies has led to several further questions which could be investigated. Live imaging could be used to assess whether when present, cilia in *ahi1* morphants are motile or not. Injection of fluorescent dextran into the pericardium followed by assessment of the intensity of fluorescence remaining 24 hours later could be performed to assess kidney function and whether dilatation of the cloaca was associated with obstruction.

To further understand the generalised oedema which many *ahi1* morphants developed, immunofluorescence using an antibody to alpha6F Na^+/K^+ ATPase could be performed to assess cell polarity and determine whether the membrane transporter is not located at its expected site of the basolateral membrane. Several zebrafish mutants with pronephric cysts have been found to mislocalise Na^+/K^+ ATPase (Drummond et al., 1998) within cells leading to aberrant osmoregulation.

Since several mechanisms are likely to be involved in the pathogenesis of *AHI1* related ciliopathies and given the cloacal phenotype, it would be interesting to knockdown *ahi1* in zebrafish *trilobite* embryos, which have a mutation in the central PCP gene, *vangl2*. Previously, this type of experiment has identified a synergistic increase in pronephric

cysts following *nphp4* knockdown in *trilobites* (Burckle et al., 2011). Similarly, it would be interesting to evaluate whether there were changes in the expression of *Shh* following *ahi1* knockdown by performing *in situ* hybridisation to evaluate the expression of *Shh* on *ahi1* morphants.

6.4 Models of *CC2D2A* related ciliopathies and further work

Characterisation of *sentinel* embryos, with a spontaneous mutation in *CC2D2A* led to the novel identification of additional ciliopathy phenotypes including hydrocephalus, cardiac oedema and ocular anomalies, which were confirmed on histology. Interestingly, the ocular phenotype of *sentinel* embryos has subsequently been further characterised and although different anomalies were reported (Bachmann-Gagescu et al., 2011), this may be explained by genetic heterogeneity. However, a limitation of this work using *sentinel* embryos was that genotyping was not always performed and therefore embryos which were not genotyped were presumed to be *sentinels* until 72hpf when a sine wave tail became apparent as a distinguishing feature. If future work were performed using *sentinel* embryos, genotyping should be routine. The idea of working with *sentinel* embryos was to facilitate studying oligogenicity and therefore clear characterisation of respective mutants and morphants was required prior to evaluating double gene knockdown.

A reduction in the number of cilia in KV in *sentinel* mutants detected herein may be explained physiologically by the recent identification of CC2D2A as a transition zone complex protein involved in regulating ciliogenesis (Davis and Katsanis, 2012). It would have been interesting to assess if this impacted on left-right asymmetry by analysing cardiac looping in *sentinel* embryos, this could be performed in future work.

Generation of *cc2d2a* morphants using a MO designed to knockdown the same exon which is mutated in *sentinel* embryos resulted in an increased frequency of phenotypes including pronephric cysts, hydrocephalus and ocular anomalies. Interesting if a convergent extension defect developed in *cc2d2a* morphants, it was always a dorsal body curvature, like the sine wave shaped tail of *sentinel* mutants, the significance of this is unclear, however the *cc2d2a* morphants were certainly representative. The *cc2d2a* morphants were a useful model to characterise because the frequency of anomalies in *sentinel* embryos was lower than expected.

Following publication of a proposed model of CC2D2A functioning in a network with MKS1 and TCTN2 to regulate Hh signalling (Sang et al., 2011), in future work it would be interesting to assess the expression of *Shh* in *sentinel* mutants and *cc2d2a* morphants using *in situ* hybridisation. This may be particularly informative in *cc2d2a* morphants with a wavy notochord, since Hh signalling is required for normal development of the notochord (Choi and Harfe, 2011).

It was disappointing that treatment with Rapamycin had no significant impact on reducing the ciliopathy phenotypes in *sentinel* mutants. This may be because the overall frequency of aberrant phenotypes was low in *sentinel* mutants and it may have been worthwhile repeating the Rapamycin therapy experiment in *cc2d2a* morphants. Or perhaps as a positive control, *nphp6* morphants should also have been treated, since Rapamycin has been reported to effectively reduce the development of pronephric cysts in *nphp6* morphants (Tobin and Beales, 2008). However at the time of these experiments, results of clinical trials in human patients with cystic kidney disease failed to show any beneficial reduction in the volume of cysts (mTOR inhibitors) (Serra et al., 2010; Walz et al., 2010), thus it seemed appropriate to terminate this avenue of enquiry.

6.5 Characterisation of *nphp6* and *mks3* morphants models the severe end of the nephronophthisis related ciliopathy spectrum

To enable future combined gene knockdown studies, *nphp6* knockdown was performed to characterise a representative model (Sayer et al., 2006). The development of cysts throughout the pronephros and in particular at the cloaca, which was dilated, was interesting. Evaluating any changes in the expression of *Shh* in *nphp6* morphants and performing *nphp6* knockdown in *trilobites* would again be informative to evaluate signalling pathways. The observation of a gross reduction in the number of cilia at the cloaca in *nphp6* morphants with a dilated cloaca reported herein was in contrast to a report of no difference in the length nor motility of cilia in the pronephros (Tse, 2012), the contrasting findings may relate to genetic pleiotropy.

Fewer and shorter cilia at KV were identified following *nphp6* knockdown herein and these results have recently been confirmed (Tse, 2012). The apparent shortening of cilia in KV was functionally relevant as this work shows it was associated with aberrant left-right body patterning and in particular reversal of cardiac asymmetry. These findings

confirm the rare although real occurrence of cardiac defects particularly situs inversus which is seen in some patients with *NPHP6* mutations (Baala et al., 2007a).

The identification of cysts throughout the pronephros and dilatation of the cloaca in *mks3* morphants was again an interesting observation. In this work, knockdown of *ahi1*, *nphp6* and *mks3* have independently been shown to lead to dilatation of the cloaca in some embryos. Although cilia were not studied in the *mks3* morphants, in both *ahi1* and *nphp6* morphants cilia were shorter or absent. In future work, studying potential aberrant mechanisms of PCP/cloacal development as performed in the *nphp4* model (Slanchev et al., 2011) may facilitate understanding of the pathogenesis.

In *mks3* morphants in addition to dilatation of the cloaca, gross generalised oedema developed in some embryos and in future work utilising this model, it may be prudent to assess whether the cloaca was obstructed. The abnormal development of the notochord and tail in *mks3* morphants may again reflect changes in *Shh* activity and could similarly be assessed in future experiments.

6.6 Assessing the interplay between: *NPHP6* and *CC2D2A*; *AHI1* and *CC2D2A*; *NPHP6* and *AHI1*.

A growing body of evidence supports the physical and functional interaction between numerous ciliary proteins (Davis and Katsanis, 2012; Sang et al., 2011), which when disturbed lead to a variety of cystic kidney disease related ciliopathies. Whilst mutations in *NPHP6* (Baala et al., 2007a; Leitch et al., 2008; Sayer et al., 2006) and *AHI1* (Utsch et al., 2006) are independently capable of causing disease, they are also acknowledged as genetic modifiers (Louie et al., 2010; Tory et al., 2007). The extent to which assessing the mutation load in patients with ciliopathies is evaluated is variable and may be limited by both the cost and success of screening for mutations. Recently, an attempt to tackle this by ascertaining causal mutations in a large cohort of patients with NPHP related ciliopathies using DNA pooling and next generation sequencing failed to identify any mutations (in 18 known genes) in 75% of patients (Otto et al., 2011). This suggests that many unidentified genes are yet to be discovered or the screening technique was not sufficiently sensitive to detect mutations.

A key interest for many scientists and clinicians is to try to explain the variable clinical phenotype to help counsel patients and direct investigations appropriately. In this work, two methods of assessing a potential association between genes were performed. The

first involved recapitulating the knockdown of *nphp6* in *sentinel* mutants which led to a synergistic increase in the frequency of all phenotypes, suggesting an interaction between the genes *NPHP6* and *CC2D2A*. The protein products of these genes are expressed in the basal body and it has been proposed that they play a role in maintaining the cilium and downstream Hh signalling respectively (Sang et al., 2011). More recently, oligogenicity has been described in patients with MKS as a consequence of heterozygous missense changes in *CC2D2A* and *NPHP6* (Hopp et al., 2011).

Although to date, no triallelism or oligogenic inheritance has been described for *AHI1* and *CC2D2A* in patients, both Jouberin (Eley et al., 2008) and CC2D2A (Gorden et al., 2008) are expressed in the basal body, therefore it seemed a reasonable hypothesis that they may interact. Additionally, Jouberin has been described as a bridging protein, linking CC2D2A with other proteins in the 'NPHP-JBTS-MKS' protein network (Sang et al., 2011). Following *ahi1* knockdown in *sentinel* mutants a synergistic increase in several phenotypes was observed including pronephric cysts, hydrocephalus and abnormal eye development. The abnormal eye development was interesting since to date, mutations in neither *AHI1* nor *CC2D2A* have been identified as causes of blindness, however mutations in either gene seem to upregulate retinal degeneration (Louie et al., 2010), perhaps because of an interaction with Rab8a (Bachmann-Gagescu et al., 2011; Hsiao et al., 2009). The apparent genetic interaction between *AHI1* and *CC2D2A* reported herein was also demonstrated using combined MO knockdown in WT zebrafish and following co-injection of *p53* to exclude non-specific, 'off-target' effects. The fact that *AHI1* and *CC2D2A* mutations have not yet been reported in patients more likely reflects a failure to identify the mutations rather than their lack of co-existence, this argument is supported by recall of occasions when only a single heterozygous mutation has been identified in a patient with NPHP, JBTS or MKS recessive ciliopathies (Otto et al., 2011).

Compound heterozygous *NPHP6* and heterozygous *AHI1* mutations have on rare occasions been reported in patients with JBTS (Tory et al., 2007). Furthermore both NPHP6 and Jouberin have been found to have similar, however independent expression patterns in the human kidney, brain and retina (Cheng et al., 2012). Since *NPHP6* and *AHI1* are frequent causes of particularly developmental brain and retinal anomalies in patients, oligogenicity was evaluated by performing combined MO knockdown in zebrafish embryos. This work demonstrated a synergistic increase in the frequency of

ciliopathy phenotypes including pronephric cysts, hydrocephalus and abnormal eye development, confirming a genetic interaction.

Unfortunately despite the synergy identified, the combined gene interference data presented herein does not identify a clear association between the increase in a specific phenotype and a particular combination of genotypes. Understanding this clinical heterogeneity remains a challenge, however advances in the knowledge of the function and interactions of proteins in the ciliary network is likely to help resolve this clinically important issue. With regards to *AHI1* and *NPHP6*, future work to study interactions could include evaluating alterations in expression of *ahi1* by *in situ* hybridisation following knockdown of *nphp6*. Additionally to evaluate downstream signalling pathways such as Hh signalling and PCP, *in situ* hybridisation using *Shh* and *vangl2* probes could be used to assess expression in morphants following combined knockdown of *ahi1* and *nphp6*.

6.7 Cystic kidney disease related ciliopathies beyond 2012

Although the nature of genetic mutations often suggest a clue to the clinical phenotypes which patients with NPHP, JBTS and MKS related ciliopathies may develop, this involves a huge leap within the hierarchy of systems. The widespread availability of detailed genetic knowledge will inevitably be limited by cost and methods to perform reliable targeted genomic sequencing. Further understanding the various steps involved from molecular communication within signalling pathways, which appears to be instigated around cellular organelles such as the cilium, to the interplay between proteins which leads to the development of renal, cerebral and retinal disease of varying severity in patients, will require ongoing collaboration between researchers from different disciplines across the field. Whilst the cilium on the apical cell surface is currently and for understandable reasons, receiving much attention, it is worth considering it analogous to an iceberg, with a significant proportion of its functionbelow the surface. Perhaps maintaining a degree of focus on the intracellular activity and basolateral cell surface is prudent, as these are almost certainly significantly involved.

In this work, the field of cystic kidney disease related ciliopathies has been thoughtfully and carefully studied. In line with the advancing developments of science generated throughout the genomic era, there has been the discovery of several causal genes including detailed characterisation by whole exome sequencing (Hong and Oh, 2010).

Whilst one acknowledges that information can be very powerful, an essential component or tool of this weaponry is to understand the meaning and relevance of this information. Working through this large volume of information is a current challenge for the scientific community and to facilitate this computerised tools are being developed (Hong and Oh, 2010). Indeed, it would be anticipated that with the increasing availability of genetic information and the evolving field of personalised medicine, that explanations and appropriate interventions will continue to be sought (Hong and Oh, 2010). There is little doubt that improved understanding of the variable pathophysiology and identification of treatments, likely combination therapies, will involve further understanding of proteomics.

In terms of the future study of cystic kidney disease related ciliopathies, it would seem prudent to build on the acquired genetic knowledge, however accept it is a variant which will in part influence the multifaceted pathophysiology of these clinically heterogeneous conditions. It will be exciting to continue to be involved in the evolution of this field and hopefully through teamwork contribute to improvements in patient centred health care.

6.8 If researching the topic of Zebrafish models of cystic kidney disease related ciliopathies now…

If this research were to be conducted now, the aim would be to focus more on the cystic kidney phenotype and understanding the pathogenesis. During the discussion of each chapter throughout this thesis further relevant experiments that ideally would be performed have been suggested in relation to the results presented.

In terms of methods, the zebrafish would continue to be utilised as a model, however three additional experiments would be performed when assessing each gene. The first would involve live microscopy imaging of KV following MO injection to assess cilia motility when present and the effect on fluid flow. Secondly, an assessment of kidney function would be performed on embryos at three days following MO knockdown by injecting a rhodamine labelled dextran into the pericardium and assessing for changes in the intensity of fluorescence, as a marker of renal clearance. Finally, further *in situ* hybridisation experiments would be performed to evaluate: alterations in the expression of a gene following MO knockdown of another gene for example *in situ* using an *ahi1* riboprobe following *nphp6* MO knockdown; double *in situ* using an *ahi1* and a *nphp6*

riboprobe to look for coexpression which may provide further evidence of a genetic interaction. For all of these experiments, essential controls would include uninjected embryos and embryos injected with a standard negative control MO.

In addition to zebrafish experiments, it would be interesting to perform cell culture work to further assess genetic interactions and evaluate changes to cilia. This would include co-immunoprecipitation experiments to assess for an interaction between: cc2d2a and nephrocystin-6; cc2d2a and jouberin; jouberin and nephrocystin-6. Finally siRNA knockdown of individual genes and gene combinations could be performed followed by immunofluorescence to study the effects on cell structure (tight junctions, adherens junctions) and ciliogenesis.

Appendices

Appendix A: E2 Media modified from (C Nusslein-Volhard, 2002).

To make a 1L solution: 5ml of E2A media, 1ml E2B media, 1ml E2C media added to double distilled water (ddH_20). Ensure pH is approximately 7.25 (7.0-7.5). Store at room temperature.

E2A media – To make a 1L solution, dissolve the following reagants in ddH_20.

87.5g NaCl, 3.75g KCl, 12g $MgSO_4$, 2.06g KH_2PO_4, 0.69g Na_2HPO_4

Autoclave, then store at 4°C.

E2B media – Dissolve 5.5g $CaCl_2$ in 100ml ddH_20.

Autoclave, then aliquot into 1ml screw top eppendorfs, store at -20°C.

E2C media – Dissolve 3g $NaHCO_3$ in 100ml ddH_20.

Autoclave, then aliquot into 1ml screw top eppendorfs, store at -20°C.

Appendix B: Zebrafish experiment mortality data sheet

NPHP ZF Mortality Record - RS - IHG_1_2009						
Experiment: No.	Description					
Date:						
Arm	**Wild Type**					
Time						
No. embryos (baseline)						
24hpf (A/D)						
24hpf (%D)						
48hpf (A/D)						
48hpf (%D)						
72hpf (A/D)						
72hpf (%D)						
Experiment: No. Date	Description					
Arm	**Wild Type**					
Time						
No. embryos (baseline)						
24hpf (A/D)						
24hpf (%D)						
48hpf (A/D)						
48hpf (%D)						
72hpf (A/D)						
72hpf (%D)						
Experiment: No. Date	Description					
Arm	**Wild Type**					
Time						
No. embryos (baseline)						
24hpf (A/D)						
24hpf (%D)						
48hpf (A/D)						
48hpf (%D)						
72hpf (A/D)						
72hpf (%D)						

Appendix C: Zebrafish experiment phenotype data sheet

NPHP Zebrafish Phenotypes_RS_IHG_2009								*Mild, moderate, severe. **Photo	
Experiment									
Arm				**Date**		Time of Phenotype			
Fish No.**	Severity*	Curly tail	Body curve	Cardiac oedema	Renal cyst	Hydrocephalus	Other brain/notochord	Coloboma/other eye	Otic placode
1									
2									
3									
4									
5									
6									
7									
8									
9									
10									
11									
12									
13									
14									
15									
16									
17									
18									
19									
20									
21									
22									
23									

Appendix D: Zebrafish cardiac looping data sheet

Zebrafish Cardiac Looping Record_RS_IGM_2011 **Image		
Exp +Date:		Arm:
RECORD as if ZF are VENTRALLY ie face up, looking at you		
Cardiac	Jogging t (26-30hpf)	Looping t (30-60hrs) aim 48hpf
Fish No.**	Atrium Left / Mid (NO) / Right	Ventricle Right(D)/Mid(NO)/Left(L)
1		
2		
3		
4		
5		
6		
7		
8		
9		
10		
11		
12		
13		
14		
15		
16		
17		
18		
19		
20		
21		
22		
23		
24		
25		
26		
27		
28		
29		
30		
31		
32		
33		
34		
35		
36		
37		
38		
39		
40		

Appendix E: Preparing 1xTAE buffer for agarose gel electrophoresis

To make a 1L solution of 1xTAE buffer add 20ml of 50xTAE stock to 980ml of ddH_20.

Make 50x TAE:

To make a 1L solution, dissolve 242g Trizma Base (T1503, Sigma) in 57.1ml glacial acetic acid (A/0360/PB117, Fisher Scientific), add 100ml 0.5M EDTA (pH 8.0, BPE118-500, Fisher Scientific). Add ddH_2O to make a total volume of 1 litre.

Make a 0.5M EDTA solution:

Dissolve 186.1g EDTA in 800ml ddH_2O, adjust pH to 8.0 with NaOH. Add ddH_2O to make a total volume of 1 litre.

Appendix F: ***Simms RJ., A.M. Hynes, L Eley, D Inglis, B Chaudhry, H.R. Dawe, J.A. Sayer. 2012. Modelling a ciliopathy: Ahi1 knockdown in model systems reveals an essential role in brain, retinal and renal development. Cell Mol Life Sci., 69, 993-1009.***

Appendix G: Adams M, R.J, Simms, Z Abdelhamed, H.R. Dawe, K Szymanska, C.V Logan, G Wheway, E Pitt, K Gull, M.A. Knowles, E Blair, S.H. Cross, J.A Sayer, C.A. Johnson. 22012. A meckelin-filamin A interaction mediates ciliogenesis. *Hum Mol Genet*., 21, 1272-86.

Supporting Information: figure legends

Figure S1: Meckelin protein sequence and nucleotide sequence of the *FLNA* encoding the meckelin-interacting region

A. Meckelin amino acid sequence predicted from transcript NM_153704.5 showing the indicated domains, two epitopes for rabbit polyclonal antibodies ('Nt Ab' and 'Ct Ab', see Figure 1A), and the location of the MKS pathogenic mutation p.919delF (red). The C-terminal intracellular domain, including the coiled-coil domain (underlined) is shown in grey shading.

B. Filamin A (*FLNA*) amino acid sequence for the meckelin interacting domain (6531-7017 nt) from transcript NM_001456.3, encoding amino acids 2171-2339 between the hinge and dimerisation domain of filamin A encompassing *FLNA* repeats 20 to 22 (see Figure 1D).

Figure S2: Characterization of anti-meckelin antibodies, HA-vectors and non-ciliary effects of meckelin knockdown

A. Characterization of anti-meckelin antibodies against either the N-terminus (α-meckelin Nt, left panel) or the C-terminus (α-meckelin Ct, right panel) using immunoblotting (IB) of endogenous protein isoforms. The full-length of meckelin is 110 kDa, with the sizes of shorter protein species indicated.

B. Transfection and expression of full-length wild-type HA-meckelin (size 110 kDa) followed by immunoblotting (IB) with antibodies against either HA (left panel) or meckelin Ct (right panel).

C. Immunostaining and confocal microscopy of ciliated IMCD3 cells for meckelin (green; Ct Ab) and filamin A (red). A 2μm baso-lateral projection is shown in the upper panels demonstrating a vesicular-like meckelin distribution (arrowhead)

colocalisation with baso-lateral filamin A. Lower panels show immunostaining for meckelin (green) and actin (red). A 2μm basal projection shows meckelin 'cables' (arrows) with an enlarged section (orange border) showing colocalisation with the basal actin cytoskeleton. Scale bar = 5 mm.

D. Western immunoblots (IB) with either an anti-meckelin Ct antibody or anti-β-actin (a loading control) to show loss of full-length meckelin A expression following transfection of mouse IMCD3 cells with *Mks3* siRNA duplexes but not scrambled (scr.) siRNA control.

E. Co-immunocytostaining and confocal microscopy of IMCD3 confluent epithelial monolayers transfected with scrambled (scr.) or *Mks3* siRNAs and stained for actin (green) and DAPI (blue), showing gaps in the confluent cell monolayer indicating disruption of cell-cell contacts (*),and loss of baso-lateral actin (arrow). A 3μm baso-lateral projection is shown. Scale bar = 5 mm

F. Co-immunocytostaining and confocal microscopy of IMCD3 confluent epithelial monolayers transfected with scrambled (scr.) or *Mks3* siRNAs and stained for actin (green) and acetylated (Ac) α-tubulin, showing disruption of cell-cell contacts (*), loss of basal actin and disruption of baso-lateral actin, concurrent with cilia loss. A single confocal x-y planar projection (plan. projn.) and x-z side projection are shown for cells treated with scrambled siRNA. Scale bar = 5 mm

Figure S3: Actin cytoskeleton and filamin localization in *FLNA*-mutated fibroblasts, loss of filamin A expression following siRNA knockdown and distribution of filamin B in IMCD3 cells

A. Co-immunostaining and confocal microscopy of serum-starved immortalized dermal fibroblasts (fibs) from a female patient with periventricular heterotopia (PVH) carrying the *FLNA* frameshift mutation c.1587delG p.K529fs. Stainings are

for filamin A (green), filamin B (red) and actin (blue), showing apparent mosaic loss of expression of filamin A due to random X-inactivation and no apparent disruption of the actin cytoskeleton. Scale bar = 10 mm.

B. Western immunoblots (IB) with either an anti-filamin A monoclonal antibody or anti-histone H3 (a loading control) to show loss of filamin A expression following transfection of mouse IMCD3 cells with two separate filamin A (*Flna*) siRNA duplexes (dup.) but not scrambled (scr.) siRNA control.

C. Immunostaining and confocal microscopy of ciliated IMCD3 cells for MKS1 (basal body marker; green) and filamin B (red). A 2μm x-y apical projection is shown in the upper panels demonstrating localisation of filamin at the basal body (arrow; enlarged inset). Lower panels show the mid cell distribution of filamin B at the baso-lateral and basal surfaces. A x-z side projection also demonstrates filamin B localization tto the basal body (arrow). Scale bar = 5 mm.

Figure S4: Control experiments for Wnt signalling assays in *MKS3*-mutated fibroblasts

The TOP Flash reporter assay was used to measure levels of activated β-catenin and hence canonical Wnt signalling in normal immortalized control dermal fibroblasts (control fibs, blue bars) and *MKS3*-mutated dermal fibroblasts (*MKS3* fibs, red bars; see Figure 4E). Activity is expressed as ratios of transfected TOP Flash or negative control FOP Flash luciferase reporter constructs expression, normalized for loading by measurement of a *Renilla* construct expression. The responses are shown to 0.5 x L cell control conditioned media (control), and either 0.5 x or 1.0 x conditioned media containing expressed Wnt3A or Wnt5A. Values shown are means of two independent replicates.

Figure S5: Meckelin is required for development of notochord, eye, ear and kidney in zebrafish embryos following morpholino oligonucleotide knockdown of *mks3*.

A. Schematic representation of *Danio rerio* meckelin protein with predicted transmembrane domains (TM) marked and length 982 amino acids (aa). The *mks3* splice-site morpholino oligonucleotide (MO) was directed towards the exon-intron site of exon 4 of the *Danio rerio mks3* gene. Following RT-PCR of *mks3* in MO-injected embryos, direct sequencing confirmed insertion of an 165bp intronic sequence after exon 4 (data not shown). This leads to an alternative reading frame after amino acid 125, a premature stop codon reached after amino acid 144, and a predicted truncated protein.

B. RT-PCR of mRNA from wild-type and *mks3* MO-injected embryos at 48 hpf demonstrates a splicing defect, with inclusion of intronic sequence into the mRNA (arrow), confirmed by direct sequencing (data not shown).

C. Examples of minor disruption of myotome and fin layers, representative of human meningoceles (panels a to c, indicated by arrows), following *mks3* MO injection and seen in embryos at 72 hpf.

D. Examples of severe notochord defects (panels a to c) following *mks3* MO injection and seen in embryos at 72 hpf.

E. Abnormal eye formation with unilateral micropthalmia (arrow)

F. Single otic placode (arrow)

G. Detail of severe notochord defects (arrow)

H. Renal cyst formation (arrow)

I. Axial section through Zebrafish controls (a & c) and following *mks3* MO injection (b & d). Brain sections are shown in panels a & b with the arrow highlighting encephalocele. Glomerulus and pronephrotic duct shown in panels c & d with

arrowheads showing moderately dilated pronephrotic ducts in *mks3* MO. The black pigmented tissue is neural crest cells forming part of the ventral stripe.

J. Percentage incidence and range of morphant phenotypes at 72hpf following *mks3* MO injection with 3.0 and 1.5 ng doses. Numbers of embryos were 254 for 3ng and 438 for 1.5ng.

K. Coinjection of 100 pg of human *MKS3* mRNA (n=132) almost completely rescues the morphant phenotype of the *mks3* MO (3 ng dose; n=254). Injection of *MKS3* mRNA alone (n=168) has minimal effect on embryo phenotype. The y-axis represents the percentage of embryos displaying severe (black), moderate (dark grey), mild (light grey) and normal (white) phenotypes.

L. Dose-dependant effect on mortality at 24 hpf seen with increasing dose (0.04 to 4 ng) of *mks3* MO.

Figure S6: Developmental defects in zebrafish embryos following morpholino oligonucleotide knockdown of *flna*.

A. Example of otic placode defects (arrowhead) seen with *flna* MO injection in embryos at 72hpf.

B. otic placode defect as in A)

C. Example of severe eye defects (arrowhead) seen with *flna* MO injection in embryos at 72hpf.

D. severe eye defect as in C)

Frequency and range of phenotypes at 72 hpf following *mks3*, *flna* MO and combination injection. Numbers of embryos were 438 for *mks3*, 129 for *flna* and 50 for the co-injection. Combining low dose *mks3* MO (1.5ng) and low dose *flna* MO (0.04ng) increased the frequency of tail defects, notochord abnormalities, hydrocephalus, renal cysts and otic placode/eye defects. Meningoceole-like abnormalities of the notochord were specific to *mks3* MO treatment.

A

Meckelin amino acid sequence from transcript NM_153704.5
this represents the longest transcript and encodes the meckelin isoform 1 protein NP_714915.3

MATRGGAGVAMAVWSLLSARAVTAFLLLFLPRFLQAQTFSFPFQQPEKCDNNQYFDI
SALSCVPCGANQRQDARGTSCVCLPGFQMISNNGGPAIICKKCPENMKGVTEDGWN
CISCPSDLTAEGKCHCPIGHILVERDINGTLLSQATCELCDGNENSFMVVNALGDRCV
RCEPTFVNTSRSCACSEPNILTGGLCFSSTGNFPLRRISAARYGEVGMSLTSEWFAKY
LQSSAAACWVYANLTSCQALGNMCVMNMNSYDFATFDACGLFQFIFENTAGLSTVH
SISFWRQNLPWLFYGDQLGLAPQVLSSTSLPTNFSFKGENQNTKLKFVAASYDIRGNF
LKWQTLEGGVLQLCPDTETRLNAAYSFGTTYQQNCEIPISKILIDFPTPIFYDVYLEYTD
ENQHQYILAVPVLNLNLQHNKIFVNQDSNSGKWLLTRRIFLVDAVSGRENDLGTQPRV
IRVATQISLSVHLVPNTINGNIYPPLITIAYSDIDIKDANSQSVKVSFSV**T**YEMDHGEAHV
QTDIALGVLGGLAVLASLLKTAGWKRRIGSPMIDLQTVVKFLVYYAGDLANVFFIITVGT
GLYWLIFFKAQKSVSVLLPMPIQEERFVTYVGCAFALKALQFLHKLISQITIDVFFIDWE
RPKGKVLKAVEGEGGVRSATVPVSIWRTYFVANEWNEIQTVRKINSLFQVLTVLFFLE
VVGFKNLALMDSSSSLSRNPPSYIAPYSCILRYAVSAALWLAIGIIQVVFFAVFYERFIED
KIRQFVDLCSMSNISVFLLSHKCFGYYIHGRSVHGH**ADTNMEEMNMNLKREAENLCS**
QRGLVPNTDGQTFEIAISNQMRQHYDRIHETLIRKNGPARLLSSSASTFEQSIKAYHM
MNKFLGSFIDHVHKEMDYFIKDKLLLERILGMEFMEPMEKSIFYNDEGYSFSSVLYYGN
EATLLIFDLLFFCVVDLACQNFILASFLTYLQQEIFRYIRNTVGQKNLASKTLVDQRFLI

Meckelin motifs:

signal peptide (predicted by SignalP--HMM)

transmembrane domains (predicted by TMHMM v2)

transmembrane domains (predicted by HMMTOP v2.0)

coiled coil domain A798 to R820 (predicted by COILS)

meckelin intracellular C--terminal domain D761 to Y925, used as the bait for the yeast two hybrid assay

peptide for antibody Nt Ab

peptide for antibody Ct Ab

F *MKS3* mutation (p.919delF)

B

Filamin A (*FLNA*) amino acid sequence for the meckelin interacting domain (6531--7017 nt) from transcript NM_001456.3
this represents the predominant transcript and encodes the filamin A isoform 1 protein NP_001447

TSPSGKTHEAEIVEGENHTYCIRFVPAEMGTHTVSVKYKGQHVPGSPFQFTVGPLGE
GGAHKVRAGGPGLERAEAGVPAEFSIWTREAGAGGLAIAVEGPSKAEISFEDRKDGS
CGVAYVVQEPGDYEVSVKFNEEHIPDSPFVVPVASPSGDARRLTVSSLQESGLK

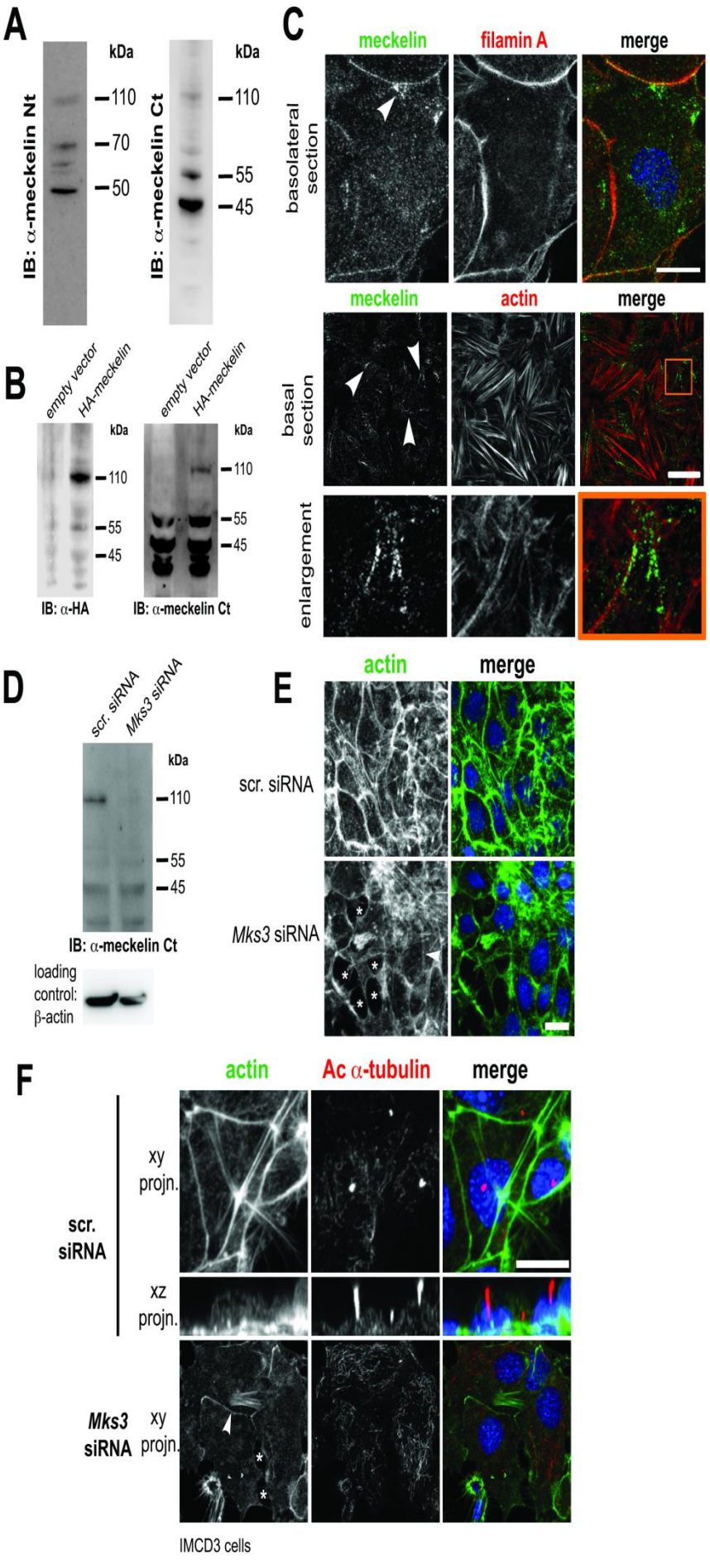
A
kDa
110
70
50
IB: α-meckelin Nt
kDa
110
55
45
IB: α-meckelin Ct
B
empty vector
HA-meckelin
kDa
110
55
45
IB: α-HA
empty vector
HA-meckelin
kDa
110
55
45
IB: α-meckelin Ct
C
meckelin
filamin A
merge
basolateral section
meckelin
actin
merge
basal section
enlargement
D
scr. siRNA
Mks3 siRNA
kDa
110
55
45
IB: α-meckelin Ct
loading control: β-actin
E
actin
merge
scr. siRNA
Mks3 siRNA
F
actin
Ac α-tubulin
merge
scr. siRNA
xy projn.
xz projn.
Mks3 siRNA
xy projn.
IMCD3 cells

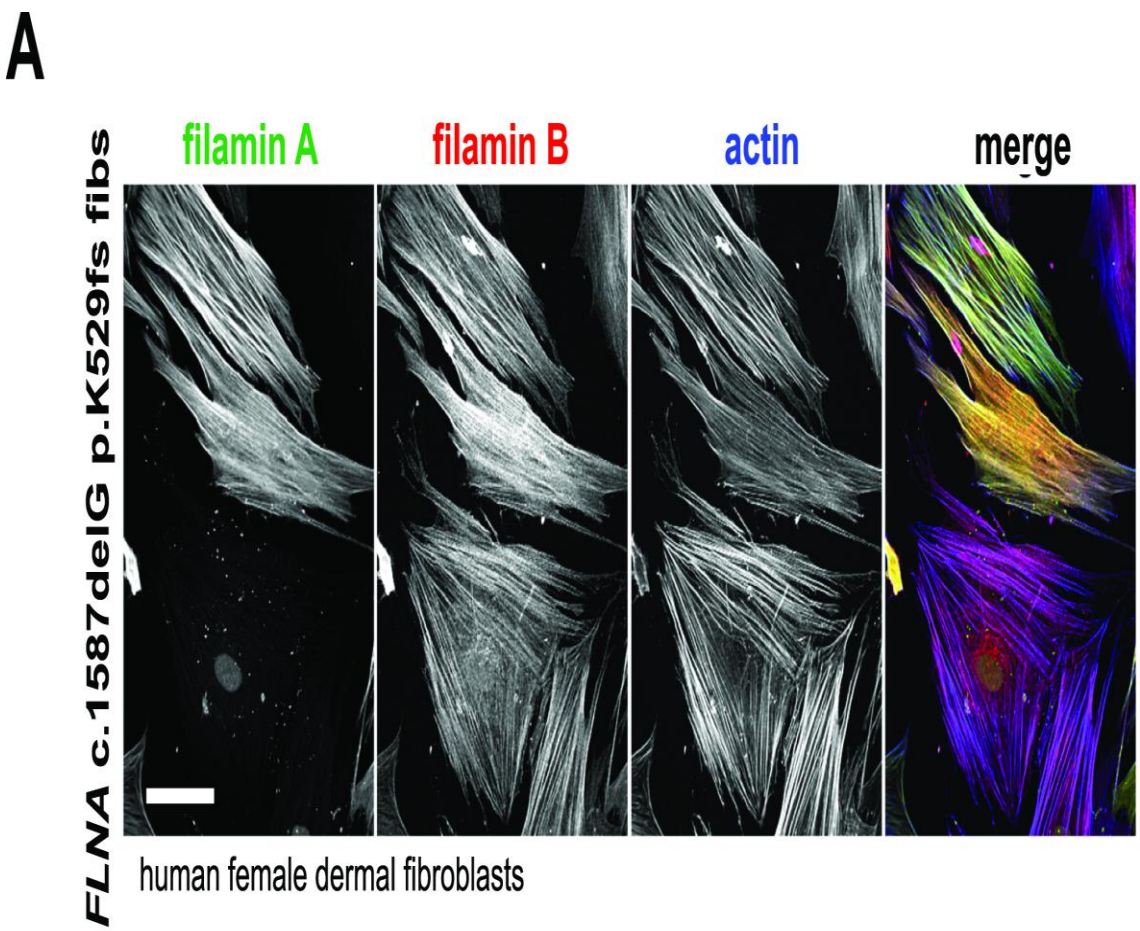
A
filamin A
filamin B
actin
merge
FLNA c.1587delG p.K529fs fibs
human female dermal fibroblasts
B
scr. siRNA
Flna siRNA
dup. 1
dup. 2
filamin A
280 kDa
IB: α-filamin A
loading control
(histone H3)
C
MKS1
filamin B
merge
xy
apical
xy
mid-cell.
xz
projn.

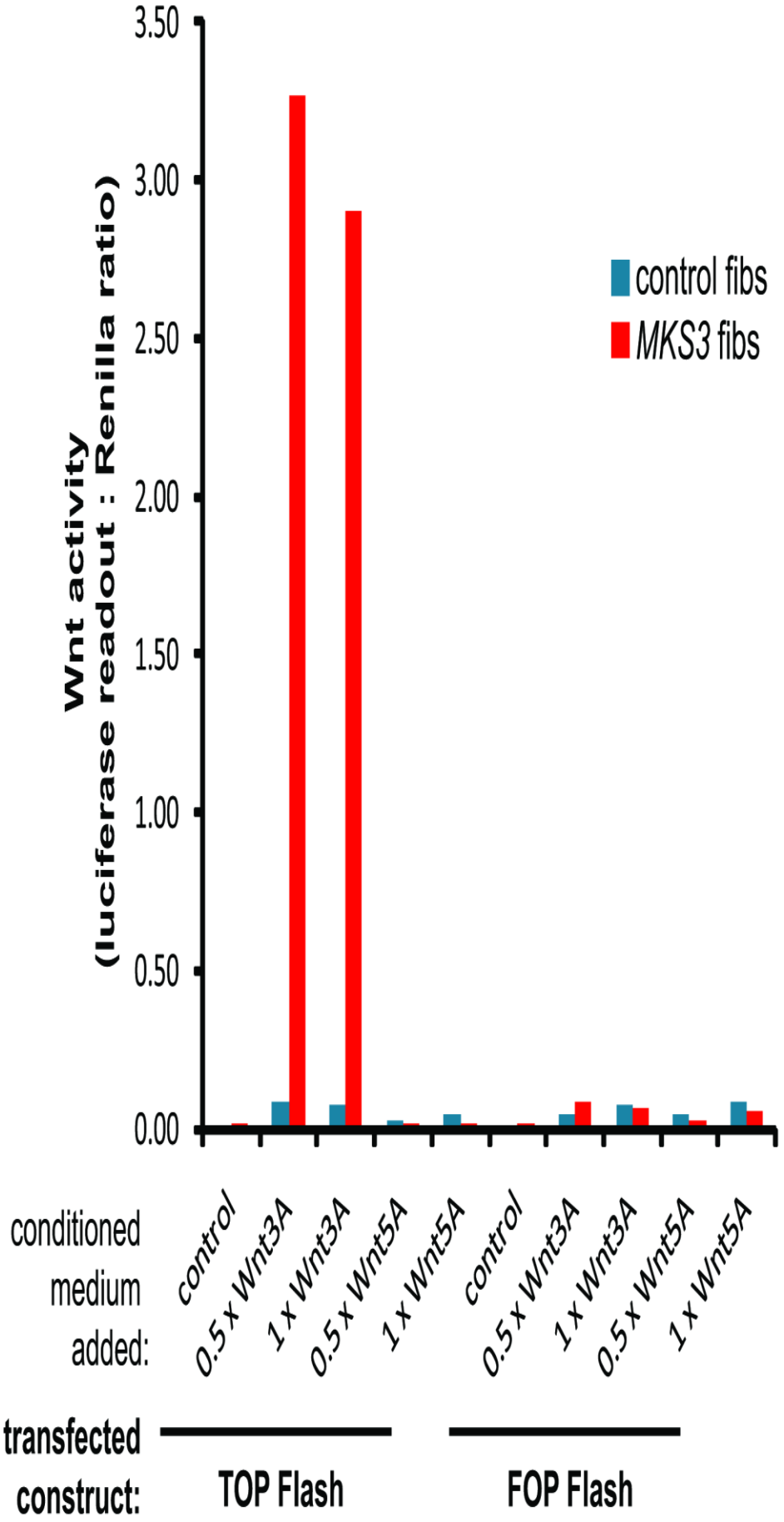
Wnt activity
(luciferase readout : Renilla ratio)
3.50
3.00
2.50
2.00
1.50
1.00
0.50
0.00
control fibs
MKS3 fibs
conditioned medium added:
control
0.5 x Wnt3A
1 x Wnt3A
0.5 x Wnt5A
1 x Wnt5A
control
0.5 x Wnt3A
1 x Wnt3A
0.5 x Wnt5A
1 x Wnt5A
transfected construct:
TOP Flash
FOP Flash

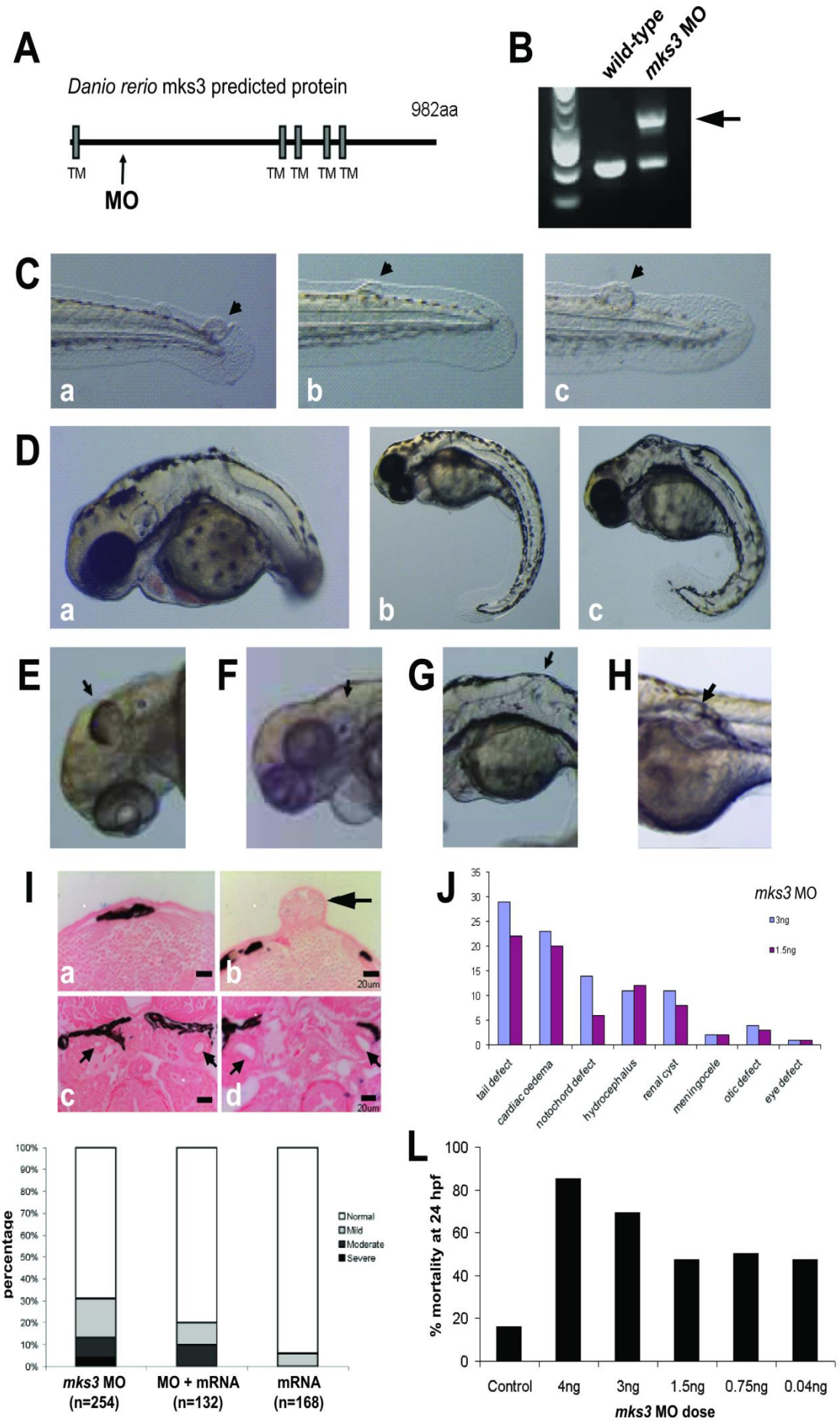
A
Danio rerio mks3 predicted protein
982aa
TM
MO
TM TM TM TM
B
wild-type
mks3 MO
C
a
b
c
D
a
b
c
E
F
G
H
I
a
b
20um
c
d
20um
J
mks3 MO
3ng
1.5ng
tail defect
cardiac oedema
notochord defect
hydrocephalus
renal cyst
meningocele
otic defect
eye defect
K
percentage
Normal
Mild
Moderate
Severe
mks3 MO (n=254)
MO + mRNA (n=132)
mRNA (n=168)
L
% mortality at 24 hpf
Control
4ng
3ng
1.5ng
0.75ng
0.04ng
mks3 MO dose

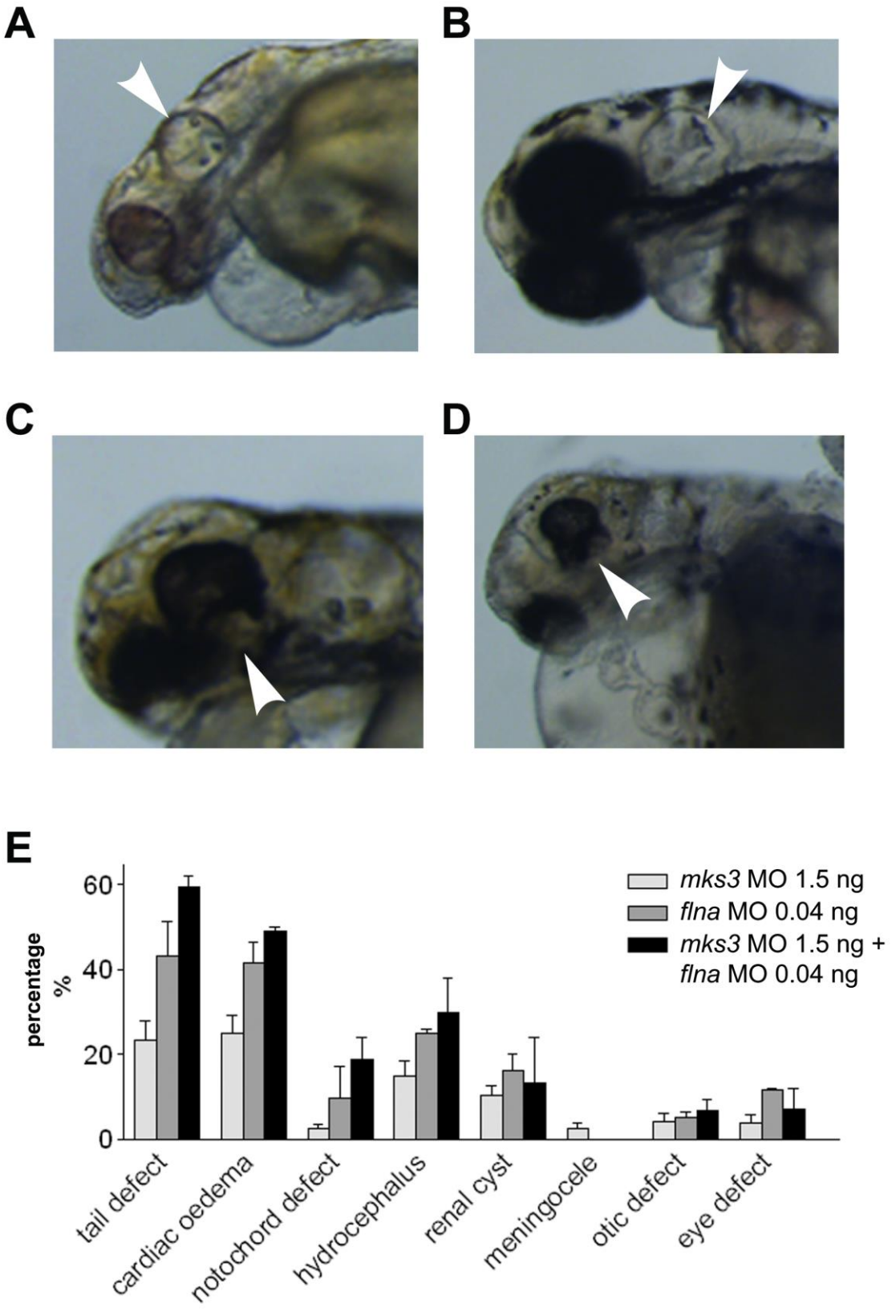
A
B
C
D
E
percentage %
60
40
20
0
mks3 MO 1.5 ng
flna MO 0.04 ng
mks3 MO 1.5 ng +
flna MO 0.04 ng
tail defect
cardiac oedema
notochord defect
hydrocephalus
renal cyst
meningocele
otic defect
eye defect

References

Adalat, S., A.S. Woolf, K.A. Johnstone, A. Wirsing, L.W. Harries, D.A. Long, R.C. Hennekam, S.E. Ledermann, L. Rees, W. van't Hoff, S.D. Marks, R.S. Trompeter, K. Tullus, P.J. Winyard, J. Cansick, I. Mushtaq, H.K. Dhillon, C. Bingham, E.L. Edghill, R. Shroff, H. Stanescu, G.U. Ryffel, S. Ellard, and D. Bockenhauer. 2009. HNF1B mutations associate with hypomagnesemia and renal magnesium wasting. J Am Soc Nephrol. 20:1123-1131.

Adams, M., R.J. Simms, Z. Abdelhamed, H.R. Dawe, K. Szymanska, C.V. Logan, G. Wheway, E. Pitt, K. Gull, M.A. Knowles, E. Blair, S.H. Cross, J.A. Sayer, and C.A. Johnson. 2012. A meckelin-filamin A interaction mediates ciliogenesis. Hum Mol Genet. 21:1272-1286.

Adams, N.A., A. Awadein, and H.S. Toma. 2007. The retinal ciliopathies. Ophthalmic Genet. 28:113-125.

Ahmad, N., S. Long, and M. Rebagliati. 2004. A southpaw joins the roster: the role of the zebrafish nodal-related gene southpaw in cardiac LR asymmetry. Trends Cardiovasc Med. 14:43-49.

Aitman, T.J., C. Boone, G.A. Churchill, M.O. Hengartner, T.F. Mackay, and D.L. Stemple. 2011. The future of model organisms in human disease research. Nat Rev Genet. 12:575-582.

Ala-Mello, S., S.M. Kivivuori, K.A. Ronnholm, O. Koskimies, and M.A. Siimes. 1996. Mechanism underlying early anaemia in children with familial juvenile nephronophthisis. Pediatr Nephrol. 10:578-581.

Ala-Mello, S., E.M. Sankila, O. Koskimies, A. de la Chapelle, and H. Kaariainen. 1998. Molecular studies in Finnish patients with familial juvenile nephronophthisis exclude a founder effect and support a common mutation causing mechanism. J Med Genet. 35:279-283.

Alexiev, B.A., X. Lin, C.C. Sun, and D.S. Brenner. 2006. Meckel-Gruber syndrome: pathologic manifestations, minimal diagnostic criteria, and differential diagnosis. Arch Pathol Lab Med. 130:1236-1238.

Amack, J.D., X. Wang, and H.J. Yost. 2007. Two T-box genes play independent and cooperative roles to regulate morphogenesis of ciliated Kupffer's vesicle in zebrafish. Dev Biol. 310:196-210.

Amack, J.D., and H.J. Yost. 2004. The T box transcription factor no tail in ciliated cells controls zebrafish left-right asymmetry. Curr Biol. 14:685-690.

Amsterdam, A., and N. Hopkins. 2006. Mutagenesis strategies in zebrafish for identifying genes involved in development and disease. Trends Genet. 22:473-478.

Anderson, C., S.J. Bartlett, J.M. Gansner, D. Wilson, L. He, J.D. Gitlin, R.N. Kelsh, and J. Dowden. 2007. Chemical genetics suggests a critical role for lysyl oxidase in zebrafish notochord morphogenesis. Mol Biosyst. 3:51-59.

Ansley, S.J., J.L. Badano, O.E. Blacque, J. Hill, B.E. Hoskins, C.C. Leitch, J.C. Kim, A.J. Ross, E.R. Eichers, T.M. Teslovich, A.K. Mah, R.C. Johnsen, J.C. Cavender, R.A. Lewis, M.R. Leroux, P.L. Beales, and N. Katsanis. 2003. Basal body dysfunction is a likely cause of pleiotropic Bardet-Biedl syndrome. Nature. 425:628-633.

Anzenberger, U., N. Bit-Avragim, S. Rohr, F. Rudolph, B. Dehmel, T.E. Willnow, and S. Abdelilah-Seyfried. 2006. Elucidation of megalin/LRP2-dependent endocytic transport processes in the larval zebrafish pronephros. J Cell Sci. 119:2127-2137.

Arts, H.H., D. Doherty, S.E. van Beersum, M.A. Parisi, S.J. Letteboer, N.T. Gorden, T.A. Peters, T. Marker, K. Voesenek, A. Kartono, H. Ozyurek, F.M. Farin, H.Y. Kroes, U. Wolfrum, H.G. Brunner, F.P. Cremers, I.A. Glass, N.V. Knoers, and R. Roepman. 2007. Mutations in the gene encoding the basal body protein RPGRIP1L, a nephrocystin-4 interactor, cause Joubert syndrome. Nat Genet. 39:882-888.

Attanasio, M., N.H. Uhlenhaut, V.H. Sousa, J.F. O'Toole, E. Otto, K. Anlag, C. Klugmann, A.C. Treier, J. Helou, J.A. Sayer, D. Seelow, G. Nurnberg, C. Becker, A.E. Chudley, P. Nurnberg, F. Hildebrandt, and M. Treier. 2007. Loss of GLIS2 causes nephronophthisis in humans and mice by increased apoptosis and fibrosis. Nat Genet. 39:1018-1024.

Baala, L., S. Audollent, J. Martinovic, C. Ozilou, M.C. Babron, S. Sivanandamoorthy, S. Saunier, R. Salomon, M. Gonzales, E. Rattenberry, C. Esculpavit, A. Toutain, C. Moraine, P. Parent, P. Marcorelles, M.C. Dauge, J. Roume, M. Le Merrer, V. Meiner, K. Meir, F. Menez, A.M. Beaufrere, C. Francannet, J. Tantau, M. Sinico, Y. Dumez, F. MacDonald, A. Munnich, S. Lyonnet, M.C. Gubler, E. Genin, C.A. Johnson, M. Vekemans, F. Encha-Razavi, and T. Attie-Bitach. 2007a. Pleiotropic effects of CEP290 (NPHP6) mutations extend to Meckel syndrome. Am J Hum Genet. 81:170-179.

Baala, L., S. Romano, R. Khaddour, S. Saunier, U.M. Smith, S. Audollent, C. Ozilou, L. Faivre, N. Laurent, B. Foliguet, A. Munnich, S. Lyonnet, R. Salomon, F. Encha-Razavi, M.C. Gubler, N. Boddaert, P. de Lonlay, C.A. Johnson, M. Vekemans, C. Antignac, and T. Attie-Bitach. 2007b. The Meckel-Gruber syndrome gene, MKS3, is mutated in Joubert syndrome. Am J Hum Genet. 80:186-194.

Bachmann-Gagescu, R., G.E. Ishak, J.C. Dempsey, J. Adkins, D. O'Day, I.G. Phelps, M. Gunay-Aygun, A.D. Kline, K. Szczaluba, L. Martorell, A. Alswaid, S. Alrasheed, S. Pai, L. Izatt, A. Ronan, M.A. Parisi, H. Mefford, I. Glass, and D. Doherty. 2012. Genotype-phenotype correlation in CC2D2A-related Joubert syndrome reveals an association with ventriculomegaly and seizures. J Med Genet. 49:126-137.

Bachmann-Gagescu, R., I.G. Phelps, G. Stearns, B.A. Link, S.E. Brockerhoff, C.B. Moens, and D. Doherty. 2011. The ciliopathy gene cc2d2a controls zebrafish photoreceptor outer segment development through a role in Rab8-dependent vesicle trafficking. Hum Mol Genet. 20:4041-4055.

Badano, J.L., S.J. Ansley, C.C. Leitch, R.A. Lewis, J.R. Lupski, and N. Katsanis. 2003. Identification of a novel Bardet-Biedl syndrome protein, BBS7, that shares structural features with BBS1 and BBS2. Am J Hum Genet. 72:650-658.

Badano, J.L., C.C. Leitch, S.J. Ansley, H. May-Simera, S. Lawson, R.A. Lewis, P.L. Beales, H.C. Dietz, S. Fisher, and N. Katsanis. 2006a. Dissection of epistasis in oligogenic Bardet-Biedl syndrome. Nature. 439:326-330.

Badano, J.L., N. Mitsuma, P.L. Beales, and N. Katsanis. 2006b. The ciliopathies: an emerging class of human genetic disorders. Annu Rev Genomics Hum Genet. 7:125-148.

Baker, K., and P.L. Beales. 2009. Making sense of cilia in disease: the human ciliopathies. Am J Med Genet C Semin Med Genet. 151C:281-295.

Barr, M.M., J. DeModena, D. Braun, C.Q. Nguyen, D.H. Hall, and P.W. Sternberg. 2001. The Caenorhabditis elegans autosomal dominant polycystic kidney disease gene homologs lov-1 and pkd-2 act in the same pathway. Curr Biol. 11:1341-1346.

Beales, P., Jackson, P.K. 2012. Cilia - the prodigal organelle. Cilia. 1.

Beales, P.L., N. Elcioglu, A.S. Woolf, D. Parker, and F.A. Flinter. 1999. New criteria for improved diagnosis of Bardet-Biedl syndrome: results of a population survey. J Med Genet. 36:437-446.

Bedell, V.M., S.E. Westcot, and S.C. Ekker. 2011. Lessons from morpholino-based screening in zebrafish. Briefings in functional genomics. 10:181-188.

Bellomo, D., A. Lander, I. Harragan, and N.A. Brown. 1996. Cell proliferation in mammalian gastrulation: the ventral node and notochord are relatively quiescent. Dev Dyn. 205:471-485.

Benzing, T., and B. Schermer. 2012. Clinical spectrum and pathogenesis of nephronophthisis. Curr Opin Nephrol Hypertens. 21:272-278.

Berbari, N.F., A.K. O'Connor, C.J. Haycraft, and B.K. Yoder. 2009. The primary cilium as a complex signaling center. Curr Biol. 19:R526-535.

Bergmann, C. 2012. Educational paper : Ciliopathies. Eur J Pediatr. 171:1285-1300.

Bergmann, C., M. Fliegauf, N.O. Bruchle, V. Frank, H. Olbrich, J. Kirschner, B. Schermer, I. Schmedding, A. Kispert, B. Kranzlin, G. Nurnberg, C. Becker, T. Grimm, G. Girschick, S.A. Lynch, P. Kelehan, J. Senderek, T.J. Neuhaus, T. Stallmach, H. Zentgraf, P. Nurnberg, N. Gretz, C. Lo, S. Lienkamp, T. Schafer, G. Walz, T. Benzing, K. Zerres, and H. Omran. 2008. Loss of nephrocystin-3 function can cause embryonic lethality, Meckel-Gruber-like syndrome, situs inversus, and renal-hepatic-pancreatic dysplasia. Am J Hum Genet. 82:959-970.

Bielas, S.L., J.L. Silhavy, F. Brancati, M.V. Kisseleva, L. Al-Gazali, L. Sztriha, R.A. Bayoumi, M.S. Zaki, A. Abdel-Aleem, R.O. Rosti, H. Kayserili, D. Swistun, L.C. Scott, E. Bertini, E. Boltshauser, E. Fazzi, L. Travaglini, S.J. Field, S. Gayral, M. Jacoby, S. Schurmans, B. Dallapiccola, P.W. Majerus, E.M. Valente, and J.G. Gleeson. 2009. Mutations in INPP5E, encoding inositol polyphosphate-5-phosphatase E, link phosphatidyl inositol signaling to the ciliopathies. Nat Genet. 41:1032-1036.

Bill, B.R., A.M. Petzold, K.J. Clark, L.A. Schimmenti, and S.C. Ekker. 2009. A primer for morpholino use in zebrafish. Zebrafish. 6:69-77.

Bloodgood, R.A. 2010. Sensory reception is an attribute of both primary cilia and motile cilia. J Cell Sci. 123:505-509.

Borovina, A., S. Superina, D. Voskas, and B. Ciruna. 2010. Vangl2 directs the posterior tilting and asymmetric localization of motile primary cilia. Nat Cell Biol. 12:407-412.

Brancati, F., B. Dallapiccola, and E.M. Valente. 2010. Joubert Syndrome and related disorders. Orphanet J Rare Dis. 5:20.

Bredrup, C., S. Saunier, M.M. Oud, T. Fiskerstrand, A. Hoischen, D. Brackman, S.M. Leh, M. Midtbo, E. Filhol, C. Bole-Feysot, P. Nitschke, C. Gilissen, O.H. Haugen, J.S. Sanders, I.

Stolte-Dijkstra, D.A. Mans, E.J. Steenbergen, B.C. Hamel, M. Matignon, R. Pfundt, C. Jeanpierre, H. Boman, E. Rodahl, J.A. Veltman, P.M. Knappskog, N.V. Knoers, R. Roepman, and H.H. Arts. 2011. Ciliopathies with skeletal anomalies and renal insufficiency due to mutations in the IFT-A gene WDR19. Am J Hum Genet. 89:634-643.

Bubenshchikova E., I.K., Fukuyo Y., Powell R., Hsu C., Morrical S.O., Sedor J.R., Sakai T., Obara T. 2012. Wtip and Vangl2 are required for mitotic spindle orientation and cloaca morphogenesis Biology Open. 1:588-596.

Bukanov, N.O., L.A. Smith, K.W. Klinger, S.R. Ledbetter, and O. Ibraghimov-Beskrovnaya. 2006. Long-lasting arrest of murine polycystic kidney disease with CDK inhibitor roscovitine. Nature. 444:949-952.

Burckle, C., H.M. Gaude, C. Vesque, F. Silbermann, R. Salomon, C. Jeanpierre, C. Antignac, S. Saunier, and S. Schneider-Maunoury. 2011. Control of the Wnt pathways by nephrocystin-4 is required for morphogenesis of the zebrafish pronephros. Hum Mol Genet. 20:2611-2627.

Burkhard, P., J. Stetefeld, and S.V. Strelkov. 2001. Coiled coils: a highly versatile protein folding motif. Trends Cell Biol. 11:82-88.

Byrne, C., R. Steenkamp, C. Castledine, D. Ansell, and J. Feehally. 2010. UK Renal Registry 12th Annual Report (December 2009): chapter 4: UK ESRD prevalent rates in 2008: national and centre-specific analyses. Nephron Clin Pract. 115 Suppl 1:c41-67.

C Nusslein-Volhard, R.D. 2002. Zebrafish (Practical Approach Series). OUP.

Cantagrel, V., J.L. Silhavy, S.L. Bielas, D. Swistun, S.E. Marsh, J.Y. Bertrand, S. Audollent, T. Attie-Bitach, K.R. Holden, W.B. Dobyns, D. Traver, L. Al-Gazali, B.R. Ali, T.H. Lindner, T. Caspary, E.A. Otto, F. Hildebrandt, I.A. Glass, C.V. Logan, C.A. Johnson, C. Bennett, F. Brancati, E.M. Valente, C.G. Woods, and J.G. Gleeson. 2008. Mutations in the cilia gene ARL13B lead to the classical form of Joubert syndrome. Am J Hum Genet. 83:170-179.

Cardenas-Rodriguez, M., D.P. Osborn, F. Irigoin, M. Grana, H. Romero, P.L. Beales, and J.L. Badano. 2012. Characterization of CCDC28B reveals its role in ciliogenesis and provides insight to understand its modifier effect on Bardet-Biedl syndrome. Hum Genet.

Caridi, G., M. Dagnino, A. Rossi, E.M. Valente, E. Bertini, E. Fazzi, F. Emma, L. Murer, E. Verrina, and G.M. Ghiggeri. 2006. Nephronophthisis type 1 deletion syndrome with neurological symptoms: prevalence and significance of the association. Kidney Int. 70:1342-1347.

Carney, T.J., N.M. Feitosa, C. Sonntag, K. Slanchev, J. Kluger, D. Kiyozumi, J.M. Gebauer, J. Coffin Talbot, C.B. Kimmel, K. Sekiguchi, R. Wagener, H. Schwarz, P.W. Ingham, and M. Hammerschmidt. 2010. Genetic analysis of fin development in zebrafish identifies furin and hemicentin1 as potential novel fraser syndrome disease genes. PLoS Genet. 6:e1000907.

Caspary, T., C.E. Larkins, and K.V. Anderson. 2007. The graded response to Sonic Hedgehog depends on cilia architecture. Dev Cell. 12:767-778.

Chaki, M., R. Airik, A.K. Ghosh, R.H. Giles, R. Chen, G.G. Slaats, H. Wang, T.W. Hurd, W. Zhou, A. Cluckey, H.Y. Gee, G. Ramaswami, C.J. Hong, B.A. Hamilton, I. Cervenka, R.S. Ganji, V. Bryja, H.H. Arts, J. van Reeuwijk, M.M. Oud, S.J. Letteboer, R. Roepman, H. Husson, O.

Ibraghimov-Beskrovnaya, T. Yasunaga, G. Walz, L. Eley, J.A. Sayer, B. Schermer, M.C. Liebau, T. Benzing, S. Le Corre, I. Drummond, S. Janssen, S.J. Allen, S. Natarajan, J.F. O'Toole, M. Attanasio, S. Saunier, C. Antignac, R.K. Koenekoop, H. Ren, I. Lopez, A. Nayir, C. Stoetzel, H. Dollfus, R. Massoudi, J.G. Gleeson, S.P. Andreoli, D.G. Doherty, A. Lindstrad, C. Golzio, N. Katsanis, L. Pape, E.B. Abboud, A.A. Al-Rajhi, R.A. Lewis, H. Omran, E.Y. Lee, S. Wang, J.M. Sekiguchi, R. Saunders, C.A. Johnson, E. Garner, K. Vanselow, J.S. Andersen, J. Shlomai, G. Nurnberg, P. Nurnberg, S. Levy, A. Smogorzewska, E.A. Otto, and F. Hildebrandt. 2012. Exome Capture Reveals ZNF423 and CEP164 Mutations, Linking Renal Ciliopathies to DNA Damage Response Signaling. Cell. 150:533-548.

Chaki, M., J. Hoefele, S.J. Allen, G. Ramaswami, S. Janssen, C. Bergmann, J.R. Heckenlively, E.A. Otto, and F. Hildebrandt. 2011. Genotype-phenotype correlation in 440 patients with NPHP-related ciliopathies. Kidney Int. 80:1239-1245.

Chang, B., H. Khanna, N. Hawes, D. Jimeno, S. He, C. Lillo, S.K. Parapuram, H. Cheng, A. Scott, R.E. Hurd, J.A. Sayer, E.A. Otto, M. Attanasio, J.F. O'Toole, G. Jin, C. Shou, F. Hildebrandt, D.S. Williams, J.R. Heckenlively, and A. Swaroop. 2006. In-frame deletion in a novel centrosomal/ciliary protein CEP290/NPHP6 perturbs its interaction with RPGR and results in early-onset retinal degeneration in the rd16 mouse. Hum Mol Genet. 15:1847-1857.

Chang, M.Y., and A.C. Ong. 2012. Mechanism-based therapeutics for autosomal dominant polycystic kidney disease: recent progress and future prospects. Nephron Clin Pract. 120:c25-34; discussion c35.

Chen, J.N., F.J. van Eeden, K.S. Warren, A. Chin, C. Nusslein-Volhard, P. Haffter, and M.C. Fishman. 1997. Left-right pattern of cardiac BMP4 may drive asymmetry of the heart in zebrafish. Development. 124:4373-4382.

Cheng, Y.Z., L. Eley, A.M. Hynes, L.M. Overman, R.J. Simms, A. Barker, H.R. Dawe, S. Lindsay, and J.A. Sayer. 2012. Investigating Embryonic Expression Patterns and Evolution of AHI1 and CEP290 Genes, Implicated in Joubert Syndrome. PLoS One. 7:e44975.

Cheung, H.O., X. Zhang, A. Ribeiro, R. Mo, S. Makino, V. Puviindran, K.K. Law, J. Briscoe, and C.C. Hui. 2009. The kinesin protein Kif7 is a critical regulator of Gli transcription factors in mammalian hedgehog signaling. Sci Signal. 2:ra29.

Chiang, A.P., J.S. Beck, H.J. Yen, M.K. Tayeh, T.E. Scheetz, R.E. Swiderski, D.Y. Nishimura, T.A. Braun, K.Y. Kim, J. Huang, K. Elbedour, R. Carmi, D.C. Slusarski, T.L. Casavant, E.M. Stone, and V.C. Sheffield. 2006. Homozygosity mapping with SNP arrays identifies TRIM32, an E3 ubiquitin ligase, as a Bardet-Biedl syndrome gene (BBS11). Proc Natl Acad Sci U S A. 103:6287-6292.

Chin, A.J., M. Tsang, and E.S. Weinberg. 2000. Heart and gut chiralities are controlled independently from initial heart position in the developing zebrafish. Dev Biol. 227:403-421.

Choi, K.S., and B.D. Harfe. 2011. Hedgehog signaling is required for formation of the notochord sheath and patterning of nuclei pulposi within the intervertebral discs. Proc Natl Acad Sci U S A. 108:9484-9489.

Christodoulou, K., M. Tsingis, C. Stavrou, A. Eleftheriou, P. Papapavlou, P.C. Patsalis, P. Ioannou, A. Pierides, and C. Constantinou Deltas. 1998. Chromosome 1 localization of a gene for autosomal dominant medullary cystic kidney disease. Hum Mol Genet. 7:905-911.

Coene, K.L., R. Roepman, D. Doherty, B. Afroze, H.Y. Kroes, S.J. Letteboer, L.H. Ngu, B. Budny, E. van Wijk, N.T. Gorden, M. Azhimi, C. Thauvin-Robinet, J.A. Veltman, M. Boink, T. Kleefstra, F.P. Cremers, H. van Bokhoven, and A.P. de Brouwer. 2009. OFD1 is mutated in X-linked Joubert syndrome and interacts with LCA5-encoded lebercilin. Am J Hum Genet. 85:465-481.

Colantonio, J.R., J. Vermot, D. Wu, A.D. Langenbacher, S. Fraser, J.N. Chen, and K.L. Hill. 2009. The dynein regulatory complex is required for ciliary motility and otolith biogenesis in the inner ear. Nature. 457:205-209.

Concordet, J.P., K.E. Lewis, J.W. Moore, L.V. Goodrich, R.L. Johnson, M.P. Scott, and P.W. Ingham. 1996. Spatial regulation of a zebrafish patched homologue reflects the roles of sonic hedgehog and protein kinase A in neural tube and somite patterning. Development. 122:2835-2846.

Consort. 1994. The polycystic kidney disease 1 gene encodes a 14 kb transcript and lies within a duplicated region on chromosome 16. The European Polycystic Kidney Disease Consortium. Cell. 78:725.

Cook, S.A., G.B. Collin, R.T. Bronson, J.K. Naggert, D.P. Liu, E.C. Akeson, and M.T. Davisson. 2009. A mouse model for Meckel syndrome type 3. J Am Soc Nephrol. 20:753-764.

Coppieters, F., S. Lefever, B.P. Leroy, and E. De Baere. 2010. CEP290, a gene with many faces: mutation overview and presentation of CEP290base. Hum Mutat. 31:1097-1108.

Corey, D.R., and J.M. Abrams. 2001. Morpholino antisense oligonucleotides: tools for investigating vertebrate development. Genome Biol. 2:REVIEWS1015.

Coutinho, P., M.J. Parsons, K.A. Thomas, E.M. Hirst, L. Saude, I. Campos, P.H. Williams, and D.L. Stemple. 2004. Differential requirements for COPI transport during vertebrate early development. Dev Cell. 7:547-558.

Cui, C., B. Chatterjee, D. Francis, Q. Yu, J.T. SanAgustin, R. Francis, T. Tansey, C. Henry, B. Wang, B. Lemley, G.J. Pazour, and C.W. Lo. 2011. Disruption of Mks1 localization to the mother centriole causes cilia defects and developmental malformations in Meckel-Gruber syndrome. Dis Model Mech. 4:43-56.

Curatolo, P., R. Bombardieri, and S. Jozwiak. 2008. Tuberous sclerosis. Lancet. 372:657-668.

Dafinger, C., M.C. Liebau, S.M. Elsayed, Y. Hellenbroich, E. Boltshauser, G.C. Korenke, F. Fabretti, A.R. Janecke, I. Ebermann, G. Nurnberg, P. Nurnberg, H. Zentgraf, F. Koerber, K. Addicks, E. Elsobky, T. Benzing, B. Schermer, and H.J. Bolz. 2011. Mutations in KIF7 link Joubert syndrome with Sonic Hedgehog signaling and microtubule dynamics. J Clin Invest. 121:2662-2667.

Dahan, K., A. Fuchshuber, S. Adamis, M. Smaers, S. Kroiss, G. Loute, J.P. Cosyns, F. Hildebrandt, C. Verellen-Dumoulin, and Y. Pirson. 2001. Familial juvenile hyperuricemic nephropathy

and autosomal dominant medullary cystic kidney disease type 2: two facets of the same disease? J Am Soc Nephrol. 12:2348-2357.

Danos, M.C., and H.J. Yost. 1996. Role of notochord in specification of cardiac left-right orientation in zebrafish and Xenopus. Dev Biol. 177:96-103.

Davenport, J.R., and B.K. Yoder. 2005. An incredible decade for the primary cilium: a look at a once-forgotten organelle. Am J Physiol Renal Physiol. 289:F1159-1169.

Davis, E.E., and N. Katsanis. 2012. The ciliopathies: a transitional model into systems biology of human genetic disease. Curr Opin Genet Dev. 22:290-303.

Davis, E.E., Q. Zhang, Q. Liu, B.H. Diplas, L.M. Davey, J. Hartley, C. Stoetzel, K. Szymanska, G. Ramaswami, C.V. Logan, D.M. Muzny, A.C. Young, D.A. Wheeler, P. Cruz, M. Morgan, L.R. Lewis, P. Cherukuri, B. Maskeri, N.F. Hansen, J.C. Mullikin, R.W. Blakesley, G.G. Bouffard, N.C.S. Program, G. Gyapay, S. Rieger, B. Tonshoff, I. Kern, N.A. Soliman, T.J. Neuhaus, K.J. Swoboda, H. Kayserili, T.E. Gallagher, R.A. Lewis, C. Bergmann, E.A. Otto, S. Saunier, P.J. Scambler, P.L. Beales, J.G. Gleeson, E.R. Maher, T. Attie-Bitach, H. Dollfus, C.A. Johnson, E.D. Green, R.A. Gibbs, F. Hildebrandt, E.A. Pierce, and N. Katsanis. 2011. TTC21B contributes both causal and modifying alleles across the ciliopathy spectrum. Nat Genet. 43:189-196.

Davis, R.E., R.E. Swiderski, K. Rahmouni, D.Y. Nishimura, R.F. Mullins, K. Agassandian, A.R. Philp, C.C. Searby, M.P. Andrews, S. Thompson, C.J. Berry, D.R. Thedens, B. Yang, R.M. Weiss, M.D. Cassell, E.M. Stone, and V.C. Sheffield. 2007. A knockin mouse model of the Bardet-Biedl syndrome 1 M390R mutation has cilia defects, ventriculomegaly, retinopathy, and obesity. Proc Natl Acad Sci U S A. 104:19422-19427.

Dawe, H.R., U.M. Smith, A.R. Cullinane, D. Gerrelli, P. Cox, J.L. Badano, S. Blair-Reid, N. Sriram, N. Katsanis, T. Attie-Bitach, S.C. Afford, A.J. Copp, D.A. Kelly, K. Gull, and C.A. Johnson. 2007. The Meckel-Gruber Syndrome proteins MKS1 and meckelin interact and are required for primary cilium formation. Hum Mol Genet. 16:173-186.

Delous, M., L. Baala, R. Salomon, C. Laclef, J. Vierkotten, K. Tory, C. Golzio, T. Lacoste, L. Besse, C. Ozilou, I. Moutkine, N.E. Hellman, I. Anselme, F. Silbermann, C. Vesque, C. Gerhardt, E. Rattenberry, M.T. Wolf, M.C. Gubler, J. Martinovic, F. Encha-Razavi, N. Boddaert, M. Gonzales, M.A. Macher, H. Nivet, G. Champion, J.P. Bertheleme, P. Niaudet, F. McDonald, F. Hildebrandt, C.A. Johnson, M. Vekemans, C. Antignac, U. Ruther, S. Schneider-Maunoury, T. Attie-Bitach, and S. Saunier. 2007. The ciliary gene RPGRIP1L is mutated in cerebello-oculo-renal syndrome (Joubert syndrome type B) and Meckel syndrome. Nat Genet. 39:875-881.

den Hollander, A.I., R.K. Koenekoop, S. Yzer, I. Lopez, M.L. Arends, K.E. Voesenek, M.N. Zonneveld, T.M. Strom, T. Meitinger, H.G. Brunner, C.B. Hoyng, L.I. van den Born, K. Rohrschneider, and F.P. Cremers. 2006. Mutations in the CEP290 (NPHP6) gene are a frequent cause of Leber congenital amaurosis. Am J Hum Genet. 79:556-561.

Diep, C.Q., and A.J. Davidson. 2011. Transplantation of cells directly into the kidney of adult zebrafish. Journal of visualized experiments : JoVE.

Dixon-Salazar, T., J.L. Silhavy, S.E. Marsh, C.M. Louie, L.C. Scott, A. Gururaj, L. Al-Gazali, A.A. Al-Tawari, H. Kayserili, L. Sztriha, and J.G. Gleeson. 2004. Mutations in the AHI1 gene,

encoding jouberin, cause Joubert syndrome with cortical polymicrogyria. Am J Hum Genet. 75:979-987.

Dobell, C. 1932. Antony van Leeuwenhoek and his "little animals". John Bale, Sons & Danielsson, [S.l.].

Doering, J.E., K. Kane, Y.C. Hsiao, C. Yao, B. Shi, A.D. Slowik, B. Dhagat, D.D. Scott, J.G. Ault, P.S. Page-McCaw, and R.J. Ferland. 2008. Species differences in the expression of Ahi1, a protein implicated in the neurodevelopmental disorder Joubert syndrome, with preferential accumulation to stigmoid bodies. J Comp Neurol. 511:238-256.

Doherty, D., M.A. Parisi, L.S. Finn, M. Gunay-Aygun, M. Al-Mateen, D. Bates, C. Clericuzio, H. Demir, M. Dorschner, A.J. van Essen, W.A. Gahl, M. Gentile, N.T. Gorden, A. Hikida, D. Knutzen, H. Ozyurek, I. Phelps, P. Rosenthal, A. Verloes, H. Weigand, P.F. Chance, W.B. Dobyns, and I.A. Glass. 2010. Mutations in 3 genes (MKS3, CC2D2A and RPGRIP1L) cause COACH syndrome (Joubert syndrome with congenital hepatic fibrosis). J Med Genet. 47:8-21.

Dowdle, W.E., J.F. Robinson, A. Kneist, M.S. Sirerol-Piquer, S.G. Frints, K.C. Corbit, N.A. Zaghloul, G. van Lijnschoten, L. Mulders, D.E. Verver, K. Zerres, R.R. Reed, T. Attie-Bitach, C.A. Johnson, J.M. Garcia-Verdugo, N. Katsanis, C. Bergmann, and J.F. Reiter. 2011. Disruption of a ciliary B9 protein complex causes Meckel syndrome. Am J Hum Genet. 89:94-110.

Driever, W., L. Solnica-Krezel, A.F. Schier, S.C. Neuhauss, J. Malicki, D.L. Stemple, D.Y. Stainier, F. Zwartkruis, S. Abdelilah, Z. Rangini, J. Belak, and C. Boggs. 1996. A genetic screen for mutations affecting embryogenesis in zebrafish. Development. 123:37-46.

Drummond, I. 2003. Making a zebrafish kidney: a tale of two tubes. Trends Cell Biol. 13:357-365.

Drummond, I.A. 2000. The zebrafish pronephros: a genetic system for studies of kidney development. Pediatr Nephrol. 14:428-435.

Drummond, I.A. 2005. Kidney development and disease in the zebrafish. J Am Soc Nephrol. 16:299-304.

Drummond, I.A., and A.J. Davidson. 2010. Zebrafish kidney development. Methods Cell Biol. 100:233-260.

Drummond, I.A., A. Majumdar, H. Hentschel, M. Elger, L. Solnica-Krezel, A.F. Schier, S.C. Neuhauss, D.L. Stemple, F. Zwartkruis, Z. Rangini, W. Driever, and M.C. Fishman. 1998. Early development of the zebrafish pronephros and analysis of mutations affecting pronephric function. Development. 125:4655-4667.

Duldulao, N.A., S. Lee, and Z. Sun. 2009. Cilia localization is essential for in vivo functions of the Joubert syndrome protein Arl13b/Scorpion. Development. 136:4033-4042.

Dutton, K., L. Abbas, J. Spencer, C. Brannon, C. Mowbray, M. Nikaido, R.N. Kelsh, and T.T. Whitfield. 2009. A zebrafish model for Waardenburg syndrome type IV reveals diverse roles for Sox10 in the otic vesicle. Dis Model Mech. 2:68-83.

Edghill, E.L., C. Bingham, S. Ellard, and A.T. Hattersley. 2006. Mutations in hepatocyte nuclear factor-1beta and their related phenotypes. J Med Genet. 43:84-90.

Edghill, E.L., R.A. Oram, M. Owens, K.L. Stals, L.W. Harries, A.T. Hattersley, S. Ellard, and C. Bingham. 2008. Hepatocyte nuclear factor-1beta gene deletions--a common cause of renal disease. Nephrol Dial Transplant. 23:627-635.

Edvardson, S., A. Shaag, S. Zenvirt, Y. Erlich, G.J. Hannon, A.L. Shanske, J.M. Gomori, J. Ekstein, and O. Elpeleg. 2010. Joubert syndrome 2 (JBTS2) in Ashkenazi Jews is associated with a TMEM216 mutation. Am J Hum Genet. 86:93-97.

Eisen, J.S., and J.C. Smith. 2008. Controlling morpholino experiments: don't stop making antisense. Development. 135:1735-1743.

Eley, L., C. Gabrielides, M. Adams, C.A. Johnson, F. Hildebrandt, and J.A. Sayer. 2008. Jouberin localizes to collecting ducts and interacts with nephrocystin-1. Kidney Int. 74:1139-1149.

Elizondo, M.R., B.L. Arduini, J. Paulsen, E.L. MacDonald, J.L. Sabel, P.D. Henion, R.A. Cornell, and D.M. Parichy. 2005. Defective skeletogenesis with kidney stone formation in dwarf zebrafish mutant for trpm7. Curr Biol. 15:667-671.

Essner, J.J., J.D. Amack, M.K. Nyholm, E.B. Harris, and H.J. Yost. 2005. Kupffer's vesicle is a ciliated organ of asymmetry in the zebrafish embryo that initiates left-right development of the brain, heart and gut. Development. 132:1247-1260.

Essner, J.J., K.J. Vogan, M.K. Wagner, C.J. Tabin, H.J. Yost, and M. Brueckner. 2002. Conserved function for embryonic nodal cilia. Nature. 418:37-38.

European Chromosome 16 Tuberous Sclerosis, C. 1993. Identification and characterization of the tuberous sclerosis gene on chromosome 16. Cell. 75:1305-1315.

Fanconi, G., E. Hanhart, A.A. von, E. Uhlinger, G. Dolivo, and A. Prader. 1951. [Familial, juvenile nephronophthisis (idiopathic parenchymal contracted kidney)]. Helv Paediatr Acta. 6:1-49.

Fath, M.A., R.F. Mullins, C. Searby, D.Y. Nishimura, J. Wei, K. Rahmouni, R.E. Davis, M.K. Tayeh, M. Andrews, B. Yang, C.D. Sigmund, E.M. Stone, and V.C. Sheffield. 2005. Mkks-null mice have a phenotype resembling Bardet-Biedl syndrome. Hum Mol Genet. 14:1109-1118.

Ferland, R.J., W. Eyaid, R.V. Collura, L.D. Tully, R.S. Hill, D. Al-Nouri, A. Al-Rumayyan, M. Topcu, G. Gascon, A. Bodell, Y.Y. Shugart, M. Ruvolo, and C.A. Walsh. 2004. Abnormal cerebellar development and axonal decussation due to mutations in AHI1 in Joubert syndrome. Nat Genet. 36:1008-1013.

Ferrante, M.I., L. Romio, S. Castro, J.E. Collins, D.A. Goulding, D.L. Stemple, A.S. Woolf, and S.W. Wilson. 2009. Convergent extension movements and ciliary function are mediated by ofd1, a zebrafish orthologue of the human oral-facial-digital type 1 syndrome gene. Hum Mol Genet. 18:289-303.

Ferrante, M.I., A. Zullo, A. Barra, S. Bimonte, N. Messaddeq, M. Studer, P. Dolle, and B. Franco. 2006. Oral-facial-digital type I protein is required for primary cilia formation and left-right axis specification. Nat Genet. 38:112-117.

Fischer, E., E. Legue, A. Doyen, F. Nato, J.F. Nicolas, V. Torres, M. Yaniv, and M. Pontoglio. 2006. Defective planar cell polarity in polycystic kidney disease. Nat Genet. 38:21-23.

Flinn, L., H. Mortiboys, K. Volkmann, R.W. Koster, P.W. Ingham, and O. Bandmann. 2009. Complex I deficiency and dopaminergic neuronal cell loss in parkin-deficient zebrafish (Danio rerio). Brain. 132:1613-1623.

Floege, J., R.J. Johnson, and J. Feehally. 2010. Comprehensive clinical nephrology. Elsevier Mosby, St. Louis, Mo. ; London.

Fogelgren, B., S.Y. Lin, X. Zuo, K.M. Jaffe, K.M. Park, R.J. Reichert, P.D. Bell, R.D. Burdine, and J.H. Lipschutz. 2011. The exocyst protein Sec10 interacts with Polycystin-2 and knockdown causes PKD-phenotypes. PLoS Genet. 7:e1001361.

Forsythe, E., and P.L. Beales. 2012. Bardet-Biedl syndrome. Eur J Hum Genet.

Fukui, H., D. Shiba, K. Asakawa, K. Kawakami, and T. Yokoyama. 2012. The ciliary protein Nek8/Nphp9 acts downstream of Inv/Nphp2 during pronephros morphogenesis and left-right establishment in zebrafish. FEBS Lett. 586:2273-2279.

Garcia-Gonzalo, F.R., K.C. Corbit, M.S. Sirerol-Piquer, G. Ramaswami, E.A. Otto, T.R. Noriega, A.D. Seol, J.F. Robinson, C.L. Bennett, D.J. Josifova, J.M. Garcia-Verdugo, N. Katsanis, F. Hildebrandt, and J.F. Reiter. 2011. A transition zone complex regulates mammalian ciliogenesis and ciliary membrane composition. Nat Genet. 43:776-784.

Gascue, C., N. Katsanis, and J.L. Badano. 2011. Cystic diseases of the kidney: ciliary dysfunction and cystogenic mechanisms. Pediatr Nephrol. 26:1181-1195.

Gerdes, J.M., E.E. Davis, and N. Katsanis. 2009. The vertebrate primary cilium in development, homeostasis, and disease. Cell. 137:32-45.

Germino, G.G. 2005. Linking cilia to Wnts. Nat Genet. 37:455-457.

Gilbert, S.F. 2000. Developmental biology. Sinauer Associates ; Basingstoke : Macmillan, Sunderland, Mass.

Goetz, S.C., and K.V. Anderson. 2010. The primary cilium: a signalling centre during vertebrate development. Nat Rev Genet. 11:331-344.

Gorden, N.T., H.H. Arts, M.A. Parisi, K.L. Coene, S.J. Letteboer, S.E. van Beersum, D.A. Mans, A. Hikida, M. Eckert, D. Knutzen, A.F. Alswaid, H. Ozyurek, S. Dibooglu, E.A. Otto, Y. Liu, E.E. Davis, C.M. Hutter, T.K. Bammler, F.M. Farin, M. Dorschner, M. Topcu, E.H. Zackai, P. Rosenthal, K.N. Owens, N. Katsanis, J.B. Vincent, F. Hildebrandt, E.W. Rubel, D.W. Raible, N.V. Knoers, P.F. Chance, R. Roepman, C.B. Moens, I.A. Glass, and D. Doherty. 2008. CC2D2A is mutated in Joubert syndrome and interacts with the ciliopathy-associated basal body protein CEP290. Am J Hum Genet. 83:559-571.

Grantham, J.J. 1991. Acquired cystic kidney disease. Kidney Int. 40:143-152.

Greenwood, M.P., G. Flik, G.F. Wagner, and R.J. Balment. 2009. The corpuscles of Stannius, calcium-sensing receptor, and stanniocalcin: responses to calcimimetics and physiological challenges. Endocrinology. 150:3002-3010.

Gunay-Aygun, M. 2009. Liver and kidney disease in ciliopathies. Am J Med Genet C Semin Med Genet. 151C:296-306.

Haas, P., and D. Gilmour. 2006. Chemokine signaling mediates self-organizing tissue migration in the zebrafish lateral line. Dev Cell. 10:673-680.

Haffter, P., M. Granato, M. Brand, M.C. Mullins, M. Hammerschmidt, D.A. Kane, J. Odenthal, F.J. van Eeden, Y.J. Jiang, C.P. Heisenberg, R.N. Kelsh, M. Furutani-Seiki, E. Vogelsang, D. Beuchle, U. Schach, C. Fabian, and C. Nusslein-Volhard. 1996. The identification of genes with unique and essential functions in the development of the zebrafish, Danio rerio. Development. 123:1-36.

Harris, P.C. 2009. 2008 Homer W. Smith Award: insights into the pathogenesis of polycystic kidney disease from gene discovery. J Am Soc Nephrol. 20:1188-1198.

Harris, P.C., and V.E. Torres. 2009. Polycystic kidney disease. Annu Rev Med. 60:321-337.

Hart, T.C., M.C. Gorry, P.S. Hart, A.S. Woodard, Z. Shihabi, J. Sandhu, B. Shirts, L. Xu, H. Zhu, M.M. Barmada, and A.J. Bleyer. 2002. Mutations of the UMOD gene are responsible for medullary cystic kidney disease 2 and familial juvenile hyperuricaemic nephropathy. J Med Genet. 39:882-892.

Hashimoto, H., M. Rebagliati, N. Ahmad, O. Muraoka, T. Kurokawa, M. Hibi, and T. Suzuki. 2004. The Cerberus/Dan-family protein Charon is a negative regulator of Nodal signaling during left-right patterning in zebrafish. Development. 131:1741-1753.

Hayashi, T., T. Mochizuki, D.M. Reynolds, G. Wu, Y. Cai, and S. Somlo. 1997. Characterization of the exon structure of the polycystic kidney disease 2 gene (PKD2). Genomics. 44:131-136.

Heidet, L., S. Decramer, A. Pawtowski, V. Moriniere, F. Bandin, B. Knebelmann, A.S. Lebre, S. Faguer, V. Guigonis, C. Antignac, and R. Salomon. 2010. Spectrum of HNF1B mutations in a large cohort of patients who harbor renal diseases. Clin J Am Soc Nephrol. 5:1079-1090.

Hentschel, D.M., K.M. Park, L. Cilenti, A.S. Zervos, I. Drummond, and J.V. Bonventre. 2005. Acute renal failure in zebrafish: a novel system to study a complex disease. Am J Physiol Renal Physiol. 288:F923-929.

Hildebrandt, F. 2010. Genetic kidney diseases. Lancet. 375:1287-1295.

Hildebrandt, F., M. Attanasio, and E. Otto. 2009a. Nephronophthisis: disease mechanisms of a ciliopathy. J Am Soc Nephrol. 20:23-35.

Hildebrandt, F., T. Benzing, and N. Katsanis. 2011. Ciliopathies. N Engl J Med. 364:1533-1543.

Hildebrandt, F., S.F. Heeringa, F. Ruschendorf, M. Attanasio, G. Nurnberg, C. Becker, D. Seelow, N. Huebner, G. Chernin, C.N. Vlangos, W. Zhou, J.F. O'Toole, B.E. Hoskins, M.T. Wolf, B.G. Hinkes, H. Chaib, S. Ashraf, D.S. Schoeb, B. Ovunc, S.J. Allen, V. Vega-Warner, E. Wise, H.M. Harville, R.H. Lyons, J. Washburn, J. Macdonald, P. Nurnberg, and E.A. Otto.

2009b. A systematic approach to mapping recessive disease genes in individuals from outbred populations. PLoS Genet. 5:e1000353.

Hildebrandt, F., and E. Otto. 2000. Molecular genetics of nephronophthisis and medullary cystic kidney disease. J Am Soc Nephrol. 11:1753-1761.

Hildebrandt, F., and E. Otto. 2005. Cilia and centrosomes: a unifying pathogenic concept for cystic kidney disease? Nat Rev Genet. 6:928-940.

Hildebrandt, F., E. Otto, C. Rensing, H.G. Nothwang, M. Vollmer, J. Adolphs, H. Hanusch, and M. Brandis. 1997. A novel gene encoding an SH3 domain protein is mutated in nephronophthisis type 1. Nat Genet. 17:149-153.

Hildebrandt, F., and W. Zhou. 2007. Nephronophthisis-associated ciliopathies. J Am Soc Nephrol. 18:1855-1871.

Hodges, M.E., N. Scheumann, B. Wickstead, J.A. Langdale, and K. Gull. 2010. Reconstructing the evolutionary history of the centriole from protein components. J Cell Sci. 123:1407-1413.

Hoefele, J., R. Sudbrak, R. Reinhardt, S. Lehrack, S. Hennig, A. Imm, U. Muerb, B. Utsch, M. Attanasio, J.F. O'Toole, E. Otto, and F. Hildebrandt. 2005. Mutational analysis of the NPHP4 gene in 250 patients with nephronophthisis. Hum Mutat. 25:411.

Hoefele, J., M.T. Wolf, J.F. O'Toole, E.A. Otto, U. Schultheiss, G. Deschenes, M. Attanasio, B. Utsch, C. Antignac, and F. Hildebrandt. 2007. Evidence of oligogenic inheritance in nephronophthisis. J Am Soc Nephrol. 18:2789-2795.

Hoey, D.A., M.E. Downs, and C.R. Jacobs. 2012. The mechanics of the primary cilium: an intricate structure with complex function. J Biomech. 45:17-26.

Holmes, L.B., S.G. Driscoll, and L. Atkins. 1976. Etiologic heterogeneity of neural-tube defects. N Engl J Med. 294:365-369.

Hong, K.W., and B. Oh. 2010. Overview of personalized medicine in the disease genomic era. BMB Rep. 43:643-648.

Hopp, K., C.M. Heyer, C.J. Hommerding, S.A. Henke, J.L. Sundsbak, S. Patel, P. Patel, M.B. Consugar, P.G. Czarnecki, T.J. Gliem, V.E. Torres, S. Rossetti, and P.C. Harris. 2011. B9D1 is revealed as a novel Meckel syndrome (MKS) gene by targeted exon-enriched next-generation sequencing and deletion analysis. Hum Mol Genet. 20:2524-2534.

Hsiao, Y.C., Z.J. Tong, J.E. Westfall, J.G. Ault, P.S. Page-McCaw, and R.J. Ferland. 2009. Ahi1, whose human ortholog is mutated in Joubert syndrome, is required for Rab8a localization, ciliogenesis and vesicle trafficking. Hum Mol Genet. 18:3926-3941.

Hsu, C.H., Z.H. Wen, C.S. Lin, and C. Chakraborty. 2007. The zebrafish model: use in studying cellular mechanisms for a spectrum of clinical disease entities. Current neurovascular research. 4:111-120.

Huang, C.J., C.T. Tu, C.D. Hsiao, F.J. Hsieh, and H.J. Tsai. 2003. Germ-line transmission of a myocardium-specific GFP transgene reveals critical regulatory elements in the cardiac myosin light chain 2 promoter of zebrafish. Dev Dyn. 228:30-40.

Huang, L., K. Szymanska, V.L. Jensen, A.R. Janecke, A.M. Innes, E.E. Davis, P. Frosk, C. Li, J.R. Willer, B.N. Chodirker, C.R. Greenberg, D.R. McLeod, F.P. Bernier, A.E. Chudley, T. Muller, M. Shboul, C.V. Logan, C.M. Loucks, C.L. Beaulieu, R.V. Bowie, S.M. Bell, J. Adkins, F.I. Zuniga, K.D. Ross, J. Wang, M.R. Ban, C. Becker, P. Nurnberg, S. Douglas, C.M. Craft, M.A. Akimenko, R.A. Hegele, C. Ober, G. Utermann, H.J. Bolz, D.E. Bulman, N. Katsanis, O.E. Blacque, D. Doherty, J.S. Parboosingh, M.R. Leroux, C.A. Johnson, and K.M. Boycott. 2011. TMEM237 is mutated in individuals with a Joubert syndrome related disorder and expands the role of the TMEM family at the ciliary transition zone. Am J Hum Genet. 89:713-730.

Huangfu, D., A. Liu, A.S. Rakeman, N.S. Murcia, L. Niswander, and K.V. Anderson. 2003. Hedgehog signalling in the mouse requires intraflagellar transport proteins. Nature. 426:83-87.

Hurd, T.W., and F. Hildebrandt. 2011. Mechanisms of nephronophthisis and related ciliopathies. Nephron Exp Nephrol. 118:e9-14.

Ibanez-Tallon, I., N. Heintz, and H. Omran. 2003. To beat or not to beat: roles of cilia in development and disease. Hum Mol Genet. 12 Spec No 1:R27-35.

Israel, G.M., and M.A. Bosniak. 2005. An update of the Bosniak renal cyst classification system. Urology. 66:484-488.

Jacoby, M., J.J. Cox, S. Gayral, D.J. Hampshire, M. Ayub, M. Blockmans, E. Pernot, M.V. Kisseleva, P. Compere, S.N. Schiffmann, F. Gergely, J.H. Riley, D. Perez-Morga, C.G. Woods, and S. Schurmans. 2009. INPP5E mutations cause primary cilium signaling defects, ciliary instability and ciliopathies in human and mouse. Nat Genet. 41:1027-1031.

Jaffe, K.M., S.Y. Thiberge, M.E. Bisher, and R.D. Burdine. 2010. Imaging cilia in zebrafish. Methods Cell Biol. 97:415-435.

Jennette, J.C., Olson, J. L., Schwartz, M. M., Silva, F. G. 2007. Heptinstall's Pathology of the Kidney. Vol. 1.

Jiang, S.T., Y.Y. Chiou, E. Wang, H.K. Lin, S.P. Lee, H.Y. Lu, C.K. Wang, M.J. Tang, and H. Li. 2008. Targeted disruption of Nphp1 causes male infertility due to defects in the later steps of sperm morphogenesis in mice. Hum Mol Genet. 17:3368-3379.

Jiang, X., Z. Hanna, M. Kaouass, L. Girard, and P. Jolicoeur. 2002. Ahi-1, a novel gene encoding a modular protein with WD40-repeat and SH3 domains, is targeted by the Ahi-1 and Mis-2 provirus integrations. J Virol. 76:9046-9059.

Joerger, M., D. Koeberle, H.P. Neumann, and S. Gillessen. 2005. Von Hippel-Lindau disease--a rare disease important to recognize. Onkologie. 28:159-163.

Jones, C., V.C. Roper, I. Foucher, D. Qian, B. Banizs, C. Petit, B.K. Yoder, and P. Chen. 2008. Ciliary proteins link basal body polarization to planar cell polarity regulation. Nat Genet. 40:69-77.

Jopling, C., E. Sleep, M. Raya, M. Marti, A. Raya, and J.C. Izpisua Belmonte. 2010. Zebrafish heart regeneration occurs by cardiomyocyte dedifferentiation and proliferation. Nature. 464:606-609.

Joubert, M., J.J. Eisenring, and F. Andermann. 1968. Familial dysgenesis of the vermis: a syndrome of hyperventilation, abnormal eye movements and retardation. Neurology. 18:302-303.

Kaelin, W.G. 2007. Von Hippel-Lindau disease. Annu Rev Pathol. 2:145-173.

Kaelin, W.G., Jr. 2008. The von Hippel-Lindau tumour suppressor protein: O2 sensing and cancer. Nature reviews. Cancer. 8:865-873.

Katabathina, V.S., G. Kota, A.K. Dasyam, A.K. Shanbhogue, and S.R. Prasad. 2010. Adult renal cystic disease: a genetic, biological, and developmental primer. Radiographics. 30:1509-1523.

Katsanis, N. 2004. The oligogenic properties of Bardet-Biedl syndrome. Hum Mol Genet. 13 Spec No 1:R65-71.

Katsanis, N., S.J. Ansley, J.L. Badano, E.R. Eichers, R.A. Lewis, B.E. Hoskins, P.J. Scambler, W.S. Davidson, P.L. Beales, and J.R. Lupski. 2001. Triallelic inheritance in Bardet-Biedl syndrome, a Mendelian recessive disorder. Science. 293:2256-2259.

Katsanis, N., P.L. Beales, M.O. Woods, R.A. Lewis, J.S. Green, P.S. Parfrey, S.J. Ansley, W.S. Davidson, and J.R. Lupski. 2000. Mutations in MKKS cause obesity, retinal dystrophy and renal malformations associated with Bardet-Biedl syndrome. Nat Genet. 26:67-70.

Khanna, H., E.E. Davis, C.A. Murga-Zamalloa, A. Estrada-Cuzcano, I. Lopez, A.I. den Hollander, M.N. Zonneveld, M.I. Othman, N. Waseem, C.F. Chakarova, C. Maubaret, A. Diaz-Font, I. Macdonald, D.M. Muzny, D.A. Wheeler, M. Morgan, L.R. Lewis, C.V. Logan, P.L. Tan, M.A. Beer, C.F. Inglehearn, R.A. Lewis, S.G. Jacobson, C. Bergmann, P.L. Beales, T. Attie-Bitach, C.A. Johnson, E.A. Otto, S.S. Bhattacharya, F. Hildebrandt, R.A. Gibbs, R.K. Koenekoop, A. Swaroop, and N. Katsanis. 2009. A common allele in RPGRIP1L is a modifier of retinal degeneration in ciliopathies. Nat Genet.

Kim, S.K., A. Shindo, T.J. Park, E.C. Oh, S. Ghosh, R.S. Gray, R.A. Lewis, C.A. Johnson, T. Attie-Bittach, N. Katsanis, and J.B. Wallingford. 2010. Planar cell polarity acts through septins to control collective cell movement and ciliogenesis. Science. 329:1337-1340.

Kim, Y.S., H.S. Kang, R. Herbert, J.Y. Beak, J.B. Collins, S.F. Grissom, and A.M. Jetten. 2008. Kruppel-like zinc finger protein Glis2 is essential for the maintenance of normal renal functions. Mol Cell Biol. 28:2358-2367.

Kimmel, C.B., W.W. Ballard, S.R. Kimmel, B. Ullmann, and T.F. Schilling. 1995. Stages of embryonic development of the zebrafish. Dev Dyn. 203:253-310.

Kimmel, C.B., R.M. Warga, and T.F. Schilling. 1990. Origin and organization of the zebrafish fate map. Development. 108:581-594.

Kolatsi-Joannou, M., C. Bingham, S. Ellard, M.P. Bulman, L.I. Allen, A.T. Hattersley, and A.S. Woolf. 2001. Hepatocyte nuclear factor-1beta: a new kindred with renal cysts and diabetes and gene expression in normal human development. J Am Soc Nephrol. 12:2175-2180.

Kramer-Zucker, A.G., F. Olale, C.J. Haycraft, B.K. Yoder, A.F. Schier, and I.A. Drummond. 2005. Cilia-driven fluid flow in the zebrafish pronephros, brain and Kupffer's vesicle is required for normal organogenesis. Development. 132:1907-1921.

Krishnan, R., L. Eley, and J.A. Sayer. 2008. Urinary concentration defects and mechanisms underlying nephronophthisis. Kidney Blood Press Res. 31:152-162.

Kroes, H.Y., P.H. van Zon, D. Fransen van de Putte, M.R. Nelen, R.J. Nievelstein, D. Wittebol-Post, O. van Nieuwenhuizen, G.M. Mancini, M.S. van der Knaap, M.L. Kwee, S.M. Maas, J.M. Cobben, J.E. De Nef, D. Lindhout, and R.J. Sinke. 2008. DNA analysis of AHI1, NPHP1 and CYCLIN D1 in Joubert syndrome patients from the Netherlands. Eur J Med Genet. 51:24-34.

Kudryashova, E., A. Struyk, E. Mokhonova, S.C. Cannon, and M.J. Spencer. 2011. The common missense mutation D489N in TRIM32 causing limb girdle muscular dystrophy 2H leads to loss of the mutated protein in knock-in mice resulting in a Trim32-null phenotype. Hum Mol Genet. 20:3925-3932.

Kudryashova, E., J. Wu, L.A. Havton, and M.J. Spencer. 2009. Deficiency of the E3 ubiquitin ligase TRIM32 in mice leads to a myopathy with a neurogenic component. Hum Mol Genet. 18:1353-1367.

Kulaga, H.M., C.C. Leitch, E.R. Eichers, J.L. Badano, A. Lesemann, B.E. Hoskins, J.R. Lupski, P.L. Beales, R.R. Reed, and N. Katsanis. 2004. Loss of BBS proteins causes anosmia in humans and defects in olfactory cilia structure and function in the mouse. Nat Genet. 36:994-998.

Kumar, S., M. Adeva, B.F. King, P.S. Kamath, and V.E. Torres. 2006. Duodenal diverticulosis in autosomal dominant polycystic kidney disease. Nephrol Dial Transplant. 21:3576-3578.

Kyttala, M., J. Tallila, R. Salonen, O. Kopra, N. Kohlschmidt, P. Paavola-Sakki, L. Peltonen, and M. Kestila. 2006. MKS1, encoding a component of the flagellar apparatus basal body proteome, is mutated in Meckel syndrome. Nat Genet. 38:155-157.

Lagos, J.C., and M.R. Gomez. 1967. Tuberous sclerosis: reappraisal of a clinical entity. Mayo Clin Proc. 42:26-49.

Lancaster, M.A., D.J. Gopal, J. Kim, S.N. Saleem, J.L. Silhavy, C.M. Louie, B.E. Thacker, Y. Williams, M.S. Zaki, and J.G. Gleeson. 2011. Defective Wnt-dependent cerebellar midline fusion in a mouse model of Joubert syndrome. Nat Med. 17:726-731.

Lancaster, M.A., C.M. Louie, J.L. Silhavy, L. Sintasath, M. Decambre, S.K. Nigam, K. Willert, and J.G. Gleeson. 2009. Impaired Wnt-beta-catenin signaling disrupts adult renal homeostasis and leads to cystic kidney ciliopathy. Nat Med. 15:1046-1054.

Langenau, D.M., D. Traver, A.A. Ferrando, J.L. Kutok, J.C. Aster, J.P. Kanki, S. Lin, E. Prochownik, N.S. Trede, L.I. Zon, and A.T. Look. 2003. Myc-induced T cell leukemia in transgenic zebrafish. Science. 299:887-890.

Latif, F., K. Tory, J. Gnarra, M. Yao, F.M. Duh, M.L. Orcutt, T. Stackhouse, I. Kuzmin, W. Modi, L. Geil, and et al. 1993. Identification of the von Hippel-Lindau disease tumor suppressor gene. Science. 260:1317-1320.

Latta, H., A.B. Maunsbach, and S.C. Madden. 1961. Cilia in different segments of the rat nephron. The Journal of biophysical and biochemical cytology. 11:248-252.

Lee, J.E., J.L. Silhavy, M.S. Zaki, J. Schroth, S.L. Bielas, S.E. Marsh, J. Olvera, F. Brancati, M. Iannicelli, K. Ikegami, A.M. Schlossman, B. Merriman, T. Attie-Bitach, C.V. Logan, I.A. Glass, A. Cluckey, C.M. Louie, J.H. Lee, H.R. Raynes, I. Rapin, I.P. Castroviejo, M. Setou, C. Barbot, E. Boltshauser, S.F. Nelson, F. Hildebrandt, C.A. Johnson, D.A. Doherty, E.M. Valente, and J.G. Gleeson. 2012a. CEP41 is mutated in Joubert syndrome and is required for tubulin glutamylation at the cilium. Nat Genet. 44:193-199.

Lee, J.H., J.L. Silhavy, J.E. Lee, L. Al-Gazali, S. Thomas, E.E. Davis, S.L. Bielas, K.J. Hill, M. Iannicelli, F. Brancati, S.B. Gabriel, C. Russ, C.V. Logan, S.M. Sharif, C.P. Bennett, M. Abe, F. Hildebrandt, B.H. Diplas, T. Attie-Bitach, N. Katsanis, A. Rajab, R. Koul, L. Sztriha, E.R. Waters, S. Ferro-Novick, C.G. Woods, C.A. Johnson, E.M. Valente, M.S. Zaki, and J.G. Gleeson. 2012b. Evolutionarily assembled cis-regulatory module at a human ciliopathy locus. Science. 335:966-969.

Leitch, C.C., N.A. Zaghloul, E.E. Davis, C. Stoetzel, A. Diaz-Font, S. Rix, M. Alfadhel, R.A. Lewis, W. Eyaid, E. Banin, H. Dollfus, P.L. Beales, J.L. Badano, and N. Katsanis. 2008. Hypomorphic mutations in syndromic encephalocele genes are associated with Bardet-Biedl syndrome. Nat Genet. 40:443-448.

Lenhart, K.F., S.Y. Lin, T.A. Titus, J.H. Postlethwait, and R.D. Burdine. 2011. Two additional midline barriers function with midline lefty1 expression to maintain asymmetric Nodal signaling during left-right axis specification in zebrafish. Development. 138:4405-4410.

Lessman, C.A. 2012. Centrosomes in the zebrafish (Danio rerio): a review including the related basal body. Cilia. 1:9.

Letamendia, A., C. Quevedo, I. Ibarbia, J.M. Virto, O. Holgado, M. Diez, J.C. Izpisua Belmonte, and C. Callol-Massot. 2012. Development and validation of an automated high-throughput system for zebrafish in vivo screenings. PLoS One. 7:e36690.

Lewis, M., J. Shaw, C. Reid, J. Evans, N. Webb, and K. Verrier-Jones. 2007. Demography and management of childhood established renal failure in the UK (chapter 13). Nephrol Dial Transplant. 22 Suppl 7:vii165-175.

Lewis, M.A., J. Shaw, M. Sinha, S. Adalat, F. Hussain, and C. Inward. 2009. UK Renal Registry 11th Annual Report (December 2008): Chapter 13 Demography of the UK paediatric renal replacement therapy population. Nephron Clin Pract. 111 Suppl 1:c257-267.

Li, J.B., J.M. Gerdes, C.J. Haycraft, Y. Fan, T.M. Teslovich, H. May-Simera, H. Li, O.E. Blacque, L. Li, C.C. Leitch, R.A. Lewis, J.S. Green, P.S. Parfrey, M.R. Leroux, W.S. Davidson, P.L. Beales, L.M. Guay-Woodford, B.K. Yoder, G.D. Stormo, N. Katsanis, and S.K. Dutcher. 2004. Comparative genomics identifies a flagellar and basal body proteome that includes the BBS5 human disease gene. Cell. 117:541-552.

Liem, K.F., Jr., M. He, P.J. Ocbina, and K.V. Anderson. 2009. Mouse Kif7/Costal2 is a cilia-associated protein that regulates Sonic hedgehog signaling. Proc Natl Acad Sci U S A. 106:13377-13382.

Limb, L., Nutt, S. . 2011. Improving Lives Optimising Resources: A Vision for the UK Rare Disease Strategy

Limb, L., Nutt, S., Sen, A. 2010. Experiences of Rare Diseases: An Insight from Patients and Families. In Rare Disease UK.

Liu, C., X. Zhang, J. Deng, M. Hecker, A. Al-Khedhairy, J.P. Giesy, and B. Zhou. 2011. Effects of prochloraz or propylthiouracil on the cross-talk between the HPG, HPA, and HPT axes in zebrafish. Environ Sci Technol. 45:769-775.

Liu, S., W. Lu, T. Obara, S. Kuida, J. Lehoczky, K. Dewar, I.A. Drummond, and D.R. Beier. 2002. A defect in a novel Nek-family kinase causes cystic kidney disease in the mouse and in zebrafish. Development. 129:5839-5846.

Logan, C.V., Z. Abdel-Hamed, and C.A. Johnson. 2011. Molecular genetics and pathogenic mechanisms for the severe ciliopathies: insights into neurodevelopment and pathogenesis of neural tube defects. Molecular neurobiology. 43:12-26.

Long, S., N. Ahmad, and M. Rebagliati. 2003. The zebrafish nodal-related gene southpaw is required for visceral and diencephalic left-right asymmetry. Development. 130:2303-2316.

Lopes, S.S., R. Lourenco, L. Pacheco, N. Moreno, J. Kreiling, and L. Saude. 2010. Notch signalling regulates left-right asymmetry through ciliary length control. Development. 137:3625-3632.

Lopez-Schier, H., C.J. Starr, J.A. Kappler, R. Kollmar, and A.J. Hudspeth. 2004. Directional cell migration establishes the axes of planar polarity in the posterior lateral-line organ of the zebrafish. Dev Cell. 7:401-412.

Louie, C.M., G. Caridi, V.S. Lopes, F. Brancati, A. Kispert, M.A. Lancaster, A.M. Schlossman, E.A. Otto, M. Leitges, H.J. Grone, I. Lopez, H.V. Gudiseva, J.F. O'Toole, E. Vallespin, R. Ayyagari, C. Ayuso, F.P. Cremers, A.I. den Hollander, R.K. Koenekoop, B. Dallapiccola, G.M. Ghiggeri, F. Hildebrandt, E.M. Valente, D.S. Williams, and J.G. Gleeson. 2010. AHI1 is required for photoreceptor outer segment development and is a modifier for retinal degeneration in nephronophthisis. Nat Genet. 42:175-180.

Makky, K., J. Tekiela, and A.N. Mayer. 2007. Target of rapamycin (TOR) signaling controls epithelial morphogenesis in the vertebrate intestine. Dev Biol. 303:501-513.

Mangos, S., P.Y. Lam, A. Zhao, Y. Liu, S. Mudumana, A. Vasilyev, A. Liu, and I.A. Drummond. 2010. The ADPKD genes pkd1a/b and pkd2 regulate extracellular matrix formation. Dis Model Mech. 3:354-365.

Mani, R., R.P. St Onge, J.L.t. Hartman, G. Giaever, and F.P. Roth. 2008. Defining genetic interaction. Proc Natl Acad Sci U S A. 105:3461-3466.

Maria, B.L., K.B. Hoang, R.J. Tusa, A.A. Mancuso, L.M. Hamed, R.G. Quisling, M.T. Hove, E.B. Fennell, M. Booth-Jones, D.M. Ringdahl, A.T. Yachnis, G. Creel, and B. Frerking. 1997. "Joubert syndrome" revisited: key ocular motor signs with magnetic resonance imaging correlation. J Child Neurol. 12:423-430.

Maria, B.L., R.G. Quisling, L.C. Rosainz, A.T. Yachnis, J. Gitten, D. Dede, and E. Fennell. 1999. Molar tooth sign in Joubert syndrome: clinical, radiologic, and pathologic significance. J Child Neurol. 14:368-376.

Marion, V., F. Stutzmann, M. Gerard, C. De Melo, E. Schaefer, A. Claussmann, S. Helle, V. Delague, E. Souied, C. Barrey, A. Verloes, C. Stoetzel, and H. Dollfus. 2012. Exome sequencing identifies mutations in LZTFL1, a BBSome and smoothened trafficking regulator, in a family with Bardet--Biedl syndrome with situs inversus and insertional polydactyly. J Med Genet. 49:317-321.

Marshall, W.F. 2008. Basal bodies platforms for building cilia. Curr Top Dev Biol. 85:1-22.

Marszalek, J.R., P. Ruiz-Lozano, E. Roberts, K.R. Chien, and L.S. Goldstein. 1999. Situs inversus and embryonic ciliary morphogenesis defects in mouse mutants lacking the KIF3A subunit of kinesin-II. Proc Natl Acad Sci U S A. 96:5043-5048.

Mason, J.M., and K.M. Arndt. 2004. Coiled coil domains: stability, specificity, and biological implications. Chembiochem. 5:170-176.

May-Simera, H.L., M. Kai, V. Hernandez, D.P. Osborn, M. Tada, and P.L. Beales. 2010. Bbs8, together with the planar cell polarity protein Vangl2, is required to establish left-right asymmetry in zebrafish. Dev Biol. 345:215-225.

Mayer, B.J. 2001. SH3 domains: complexity in moderation. J Cell Sci. 114:1253-1263.

McGrath, J., S. Somlo, S. Makova, X. Tian, and M. Brueckner. 2003. Two populations of node monocilia initiate left-right asymmetry in the mouse. Cell. 114:61-73.

Mollet, G., R. Salomon, O. Gribouval, F. Silbermann, D. Bacq, G. Landthaler, D. Milford, A. Nayir, G. Rizzoni, C. Antignac, and S. Saunier. 2002. The gene mutated in juvenile nephronophthisis type 4 encodes a novel protein that interacts with nephrocystin. Nat Genet. 32:300-305.

Mollet, G., F. Silbermann, M. Delous, R. Salomon, C. Antignac, and S. Saunier. 2005. Characterization of the nephrocystin/nephrocystin-4 complex and subcellular localization of nephrocystin-4 to primary cilia and centrosomes. Hum Mol Genet. 14:645-656.

Montserrat, A., Freese K. 2009, June. Council Recommendation on an action in the field of rare diseases. E.R.D. Policy, editor.

Mougou-Zerelli, S., S. Thomas, E. Szenker, S. Audollent, N. Elkhartoufi, C. Babarit, S. Romano, R. Salomon, J. Amiel, C. Esculpavit, M. Gonzales, E. Escudier, B. Leheup, P. Loget, S. Odent, J. Roume, M. Gerard, A.L. Delezoide, S. Khung, S. Patrier, M.P. Cordier, R. Bouvier, J. Martinovic, M.C. Gubler, N. Boddaert, A. Munnich, F. Encha-Razavi, E.M. Valente, A. Saad, S. Saunier, M. Vekemans, and T. Attie-Bitach. 2009. CC2D2A mutations in Meckel and Joubert syndromes indicate a genotype-phenotype correlation. Hum Mutat. 30:1574-1582.

Moyer, J.H., M.J. Lee-Tischler, H.Y. Kwon, J.J. Schrick, E.D. Avner, W.E. Sweeney, V.L. Godfrey, N.L. Cacheiro, J.E. Wilkinson, and R.P. Woychik. 1994. Candidate gene associated with a mutation causing recessive polycystic kidney disease in mice. Science. 264:1329-1333.

Müller, O.F., and O.t.Y.B. Fabricius. 1786. Animalcula infusoria fluviatilia et marina, quæ detexit, systematice descripsit et ad vivum delineari curavit O. F. M. Opus cura O. Fabricii. Hanniæ.

Mullor, J.L., P. Sanchez, and A. Ruiz i Altaba. 2002. Pathways and consequences: Hedgehog signaling in human disease. Trends Cell Biol. 12:562-569.

Murcia, N.S., W.G. Richards, B.K. Yoder, M.L. Mucenski, J.R. Dunlap, and R.P. Woychik. 2000. The Oak Ridge Polycystic Kidney (orpk) disease gene is required for left-right axis determination. Development. 127:2347-2355.

Mykytyn, K., T. Braun, R. Carmi, N.B. Haider, C.C. Searby, M. Shastri, G. Beck, A.F. Wright, A. Iannaccone, K. Elbedour, R. Riise, A. Baldi, A. Raas-Rothschild, S.W. Gorman, D.M. Duhl, S.G. Jacobson, T. Casavant, E.M. Stone, and V.C. Sheffield. 2001. Identification of the gene that, when mutated, causes the human obesity syndrome BBS4. Nat Genet. 28:188-191.

Mykytyn, K., R.F. Mullins, M. Andrews, A.P. Chiang, R.E. Swiderski, B. Yang, T. Braun, T. Casavant, E.M. Stone, and V.C. Sheffield. 2004. Bardet-Biedl syndrome type 4 (BBS4)-null mice implicate Bbs4 in flagella formation but not global cilia assembly. Proc Natl Acad Sci U S A. 101:8664-8669.

Mykytyn, K., D.Y. Nishimura, C.C. Searby, M. Shastri, H.J. Yen, J.S. Beck, T. Braun, L.M. Streb, A.S. Cornier, G.F. Cox, A.B. Fulton, R. Carmi, G. Luleci, S.C. Chandrasekharappa, F.S. Collins, S.G. Jacobson, J.R. Heckenlively, R.G. Weleber, E.M. Stone, and V.C. Sheffield. 2002. Identification of the gene (BBS1) most commonly involved in Bardet-Biedl syndrome, a complex human obesity syndrome. Nat Genet. 31:435-438.

Nasevicius, A., and S.C. Ekker. 2000. Effective targeted gene 'knockdown' in zebrafish. Nat Genet. 26:216-220.

Nauli, S.M., F.J. Alenghat, Y. Luo, E. Williams, P. Vassilev, X. Li, A.E. Elia, W. Lu, E.M. Brown, S.J. Quinn, D.E. Ingber, and J. Zhou. 2003. Polycystins 1 and 2 mediate mechanosensation in the primary cilium of kidney cells. Nat Genet. 33:129-137.

Nichane, M., C. Van Campenhout, H. Pendeville, M.L. Voz, and E.J. Bellefroid. 2006. The Na+/PO4 cotransporter SLC20A1 gene labels distinct restricted subdomains of the developing pronephros in Xenopus and zebrafish embryos. Gene Expr Patterns. 6:667-672.

Nishimura, D.Y., M. Fath, R.F. Mullins, C. Searby, M. Andrews, R. Davis, J.L. Andorf, K. Mykytyn, R.E. Swiderski, B. Yang, R. Carmi, E.M. Stone, and V.C. Sheffield. 2004. Bbs2-null mice have neurosensory deficits, a defect in social dominance, and retinopathy associated with mislocalization of rhodopsin. Proc Natl Acad Sci U S A. 101:16588-16593.

Nishimura, D.Y., C.C. Searby, R. Carmi, K. Elbedour, L. Van Maldergem, A.B. Fulton, B.L. Lam, B.R. Powell, R.E. Swiderski, K.E. Bugge, N.B. Haider, A.E. Kwitek-Black, L. Ying, D.M. Duhl, S.W. Gorman, E. Heon, A. Iannaccone, D. Bonneau, L.G. Biesecker, S.G. Jacobson, E.M. Stone, and V.C. Sheffield. 2001. Positional cloning of a novel gene on chromosome 16q causing Bardet-Biedl syndrome (BBS2). Hum Mol Genet. 10:865-874.

Nishimura, D.Y., R.E. Swiderski, C.C. Searby, E.M. Berg, A.L. Ferguson, R. Hennekam, S. Merin, R.G. Weleber, L.G. Biesecker, E.M. Stone, and V.C. Sheffield. 2005. Comparative genomics and gene expression analysis identifies BBS9, a new Bardet-Biedl syndrome gene. Am J Hum Genet. 77:1021-1033.

Nonaka, S., Y. Tanaka, Y. Okada, S. Takeda, A. Harada, Y. Kanai, M. Kido, and N. Hirokawa. 1998. Randomization of left-right asymmetry due to loss of nodal cilia generating leftward flow of extraembryonic fluid in mice lacking KIF3B motor protein. Cell. 95:829-837.

Noor, A., C. Windpassinger, M. Patel, B. Stachowiak, A. Mikhailov, M. Azam, M. Irfan, Z.K. Siddiqui, F. Naeem, A.D. Paterson, M. Lutfullah, J.B. Vincent, and M. Ayub. 2008. CC2D2A, encoding a coiled-coil and C2 domain protein, causes autosomal-recessive mental retardation with retinitis pigmentosa. Am J Hum Genet. 82:1011-1018.

Norris, D.P., and D.T. Grimes. 2012. Mouse models of ciliopathies: the state of the art. Dis Model Mech. 5:299-312.

Nyengaard, J.R., and T.F. Bendtsen. 1992. Glomerular number and size in relation to age, kidney weight, and body surface in normal man. Anat Rec. 232:194-201.

O'Brien, L.L., M. Grimaldi, Z. Kostun, R.A. Wingert, R. Selleck, and A.J. Davidson. 2011. Wt1a, Foxc1a, and the Notch mediator Rbpj physically interact and regulate the formation of podocytes in zebrafish. Dev Biol. 358:318-330.

O'Dea, D., P.S. Parfrey, J.D. Harnett, D. Hefferton, B.C. Cramer, and J. Green. 1996. The importance of renal impairment in the natural history of Bardet-Biedl syndrome. Am J Kidney Dis. 27:776-783.

Obara, T., S. Mangos, Y. Liu, J. Zhao, S. Wiessner, A.G. Kramer-Zucker, F. Olale, A.F. Schier, and I.A. Drummond. 2006. Polycystin-2 immunolocalization and function in zebrafish. J Am Soc Nephrol. 17:2706-2718.

Oh, E.C., and N. Katsanis. 2012. Cilia in vertebrate development and disease. Development. 139:443-448.

Oishi, I., Y. Kawakami, A. Raya, C. Callol-Massot, and J.C. Izpisua Belmonte. 2006. Regulation of primary cilia formation and left-right patterning in zebrafish by a noncanonical Wnt signaling mediator, duboraya. Nat Genet. 38:1316-1322.

Olbrich, H., M. Fliegauf, J. Hoefele, A. Kispert, E. Otto, A. Volz, M.T. Wolf, G. Sasmaz, U. Trauer, R. Reinhardt, R. Sudbrak, C. Antignac, N. Gretz, G. Walz, B. Schermer, T. Benzing, F. Hildebrandt, and H. Omran. 2003. Mutations in a novel gene, NPHP3, cause adolescent nephronophthisis, tapeto-retinal degeneration and hepatic fibrosis. Nat Genet. 34:455-459.

Omran, H., G. Sasmaz, K. Haffner, A. Volz, H. Olbrich, R. Melkaoui, E. Otto, T.F. Wienker, R. Korinthenberg, M. Brandis, C. Antignac, and F. Hildebrandt. 2002. Identification of a gene locus for Senior-Loken syndrome in the region of the nephronophthisis type 3 gene. J Am Soc Nephrol. 13:75-79.

Ong, A.C., and B. Wagner. 2005. Detection of proximal tubular motile cilia in a patient with renal sarcoidosis associated with hypercalcemia. Am J Kidney Dis. 45:1096-1099.

Oteiza, P., M. Koppen, M. Krieg, E. Pulgar, C. Farias, C. Melo, S. Preibisch, D. Muller, M. Tada, S. Hartel, C.P. Heisenberg, and M.L. Concha. 2010. Planar cell polarity signalling regulates cell adhesion properties in progenitors of the zebrafish laterality organ. Development. 137:3459-3468.

Ott, E.B., N.M. van den Akker, P.A. Sakalis, A.C. Gittenberger-de Groot, A.J. Te Velthuis, and C.P. Bagowski. 2008. The lim domain only protein 7 is important in zebrafish heart development. Dev Dyn. 237:3940-3952.

Otto, E., J. Hoefele, R. Ruf, A.M. Mueller, K.S. Hiller, M.T. Wolf, M.J. Schuermann, A. Becker, R. Birkenhager, R. Sudbrak, H.C. Hennies, P. Nurnberg, and F. Hildebrandt. 2002. A gene mutated in nephronophthisis and retinitis pigmentosa encodes a novel protein, nephroretinin, conserved in evolution. Am J Hum Genet. 71:1161-1167.

Otto, E.A., T.W. Hurd, R. Airik, M. Chaki, W. Zhou, C. Stoetzel, S.B. Patil, S. Levy, A.K. Ghosh, C.A. Murga-Zamalloa, J. van Reeuwijk, S.J. Letteboer, L. Sang, R.H. Giles, Q. Liu, K.L. Coene, A. Estrada-Cuzcano, R.W. Collin, H.M. McLaughlin, S. Held, J.M. Kasanuki, G. Ramaswami, J. Conte, I. Lopez, J. Washburn, J. Macdonald, J. Hu, Y. Yamashita, E.R. Maher, L.M. Guay-Woodford, H.P. Neumann, N. Obermuller, R.K. Koenekoop, C. Bergmann, X. Bei, R.A. Lewis, N. Katsanis, V. Lopes, D.S. Williams, R.H. Lyons, C.V. Dang, D.A. Brito, M.B. Dias, X. Zhang, J.D. Cavalcoli, G. Nurnberg, P. Nurnberg, E.A. Pierce, P.K. Jackson, C. Antignac, S. Saunier, R. Roepman, H. Dollfus, H. Khanna, and F. Hildebrandt. 2010. Candidate exome capture identifies mutation of SDCCAG8 as the cause of a retinal-renal ciliopathy. Nat Genet. 42:840-850.

Otto, E.A., B. Loeys, H. Khanna, J. Hellemans, R. Sudbrak, S. Fan, U. Muerb, J.F. O'Toole, J. Helou, M. Attanasio, B. Utsch, J.A. Sayer, C. Lillo, D. Jimeno, P. Coucke, A. De Paepe, R. Reinhardt, S. Klages, M. Tsuda, I. Kawakami, T. Kusakabe, H. Omran, A. Imm, M. Tippens, P.A. Raymond, J. Hill, P. Beales, S. He, A. Kispert, B. Margolis, D.S. Williams, A. Swaroop, and F. Hildebrandt. 2005. Nephrocystin-5, a ciliary IQ domain protein, is mutated in Senior-Loken syndrome and interacts with RPGR and calmodulin. Nat Genet. 37:282-288.

Otto, E.A., G. Ramaswami, S. Janssen, M. Chaki, S.J. Allen, W. Zhou, R. Airik, T.W. Hurd, A.K. Ghosh, M.T. Wolf, B. Hoppe, T.J. Neuhaus, D. Bockenhauer, D.V. Milford, N.A. Soliman, C. Antignac, S. Saunier, C.A. Johnson, and F. Hildebrandt. 2011. Mutation analysis of 18 nephronophthisis associated ciliopathy disease genes using a DNA pooling and next generation sequencing strategy. J Med Genet. 48:105-116.

Otto, E.A., B. Schermer, T. Obara, J.F. O'Toole, K.S. Hiller, A.M. Mueller, R.G. Ruf, J. Hoefele, F. Beekmann, D. Landau, J.W. Foreman, J.A. Goodship, T. Strachan, A. Kispert, M.T. Wolf, M.F. Gagnadoux, H. Nivet, C. Antignac, G. Walz, I.A. Drummond, T. Benzing, and F. Hildebrandt. 2003. Mutations in INVS encoding inversin cause nephronophthisis type 2, linking renal cystic disease to the function of primary cilia and left-right axis determination. Nat Genet. 34:413-420.

Otto, E.A., K. Tory, M. Attanasio, W. Zhou, M. Chaki, Y. Paruchuri, E.L. Wise, M.T. Wolf, B. Utsch, C. Becker, G. Nurnberg, P. Nurnberg, A. Nayir, S. Saunier, C. Antignac, and F. Hildebrandt. 2009. Hypomorphic mutations in meckelin (MKS3/TMEM67) cause nephronophthisis with liver fibrosis (NPHP11). J Med Genet. 46:663-670.

Otto, E.A., M.L. Trapp, U.T. Schultheiss, J. Helou, L.M. Quarmby, and F. Hildebrandt. 2008. NEK8 mutations affect ciliary and centrosomal localization and may cause nephronophthisis. J Am Soc Nephrol. 19:587-592.

Owens, K.N., F. Santos, B. Roberts, T. Linbo, A.B. Coffin, A.J. Knisely, J.A. Simon, E.W. Rubel, and D.W. Raible. 2008. Identification of genetic and chemical modulators of zebrafish mechanosensory hair cell death. PLoS Genet. 4:e1000020.

Papon, J.F., I. Perrault, A. Coste, B. Louis, X. Gerard, S. Hanein, L. Fares-Taie, S. Gerber, S. Defoort-Dhellemmes, A.M. Vojtek, J. Kaplan, J.M. Rozet, and E. Escudier. 2010. Abnormal respiratory cilia in non-syndromic Leber congenital amaurosis with CEP290 mutations. J Med Genet. 47:829-834.

Parisi, M.A. 2009. Clinical and molecular features of Joubert syndrome and related disorders. Am J Med Genet C Semin Med Genet. 151C:326-340.

Parisi, M.A., D. Doherty, P.F. Chance, and I.A. Glass. 2007. Joubert syndrome (and related disorders) (OMIM 213300). Eur J Hum Genet. 15:511-521.

Parisi, M.A., D. Doherty, M.L. Eckert, D.W. Shaw, H. Ozyurek, S. Aysun, O. Giray, A. Al Swaid, S. Al Shahwan, N. Dohayan, E. Bakhsh, O.S. Indridason, W.B. Dobyns, C.L. Bennett, P.F. Chance, and I.A. Glass. 2006. AHI1 mutations cause both retinal dystrophy and renal cystic disease in Joubert syndrome. J Med Genet. 43:334-339.

Parkin, C.A., C.E. Allen, and P.W. Ingham. 2009. Hedgehog signalling is required for cloacal development in the zebrafish embryo. Int J Dev Biol. 53:45-57.

Parng, C., W.L. Seng, C. Semino, and P. McGrath. 2002. Zebrafish: a preclinical model for drug screening. Assay and drug development technologies. 1:41-48.

Patton, E.E., and L.I. Zon. 2005. Taking human cancer genes to the fish: a transgenic model of melanoma in zebrafish. Zebrafish. 1:363-368.

Pazour, G.J., B.L. Dickert, Y. Vucica, E.S. Seeley, J.L. Rosenbaum, G.B. Witman, and D.G. Cole. 2000. Chlamydomonas IFT88 and its mouse homologue, polycystic kidney disease gene tg737, are required for assembly of cilia and flagella. J Cell Biol. 151:709-718.

Pazour, G.J., and G.B. Witman. 2003. The vertebrate primary cilium is a sensory organelle. Curr Opin Cell Biol. 15:105-110.

Pedersen, L.B., and J.L. Rosenbaum. 2008. Intraflagellar transport (IFT) role in ciliary assembly, resorption and signalling. Curr Top Dev Biol. 85:23-61.

Pineda, R., C.E. Beattie, and C.W. Hall. 2011. Recording the adult zebrafish cerebral field potential during pentylenetetrazole seizures. J Neurosci Methods. 200:20-28.

Pirson, Y. 2010. Extrarenal manifestations of autosomal dominant polycystic kidney disease. Adv Chronic Kidney Dis. 17:173-180.

Poss, K.D., L.G. Wilson, and M.T. Keating. 2002. Heart regeneration in zebrafish. Science. 298:2188-2190.

Pretorius, P.R., L.M. Baye, D.Y. Nishimura, C.C. Searby, K. Bugge, B. Yang, R.F. Mullins, E.M. Stone, V.C. Sheffield, and D.C. Slusarski. 2010. Identification and functional analysis of the vision-specific BBS3 (ARL6) long isoform. PLoS Genet. 6:e1000884.

Pyati, U.J., M.S. Cooper, A.J. Davidson, A. Nechiporuk, and D. Kimelman. 2006. Sustained Bmp signaling is essential for cloaca development in zebrafish. Development. 133:2275-2284.

Qiagen. 2008. QIAquick Spin Handbook.

Ravanelli, A.M., and J. Klingensmith. 2011. The actin nucleator Cordon-bleu is required for development of motile cilia in zebrafish. Dev Biol. 350:101-111.

Ravine, D., R.N. Gibson, J. Donlan, and L.J. Sheffield. 1993. An ultrasound renal cyst prevalence survey: specificity data for inherited renal cystic diseases. Am J Kidney Dis. 22:803-807.

Reimschuessel, R. 2001. A fish model of renal regeneration and development. ILAR journal / National Research Council, Institute of Laboratory Animal Resources. 42:285-291.

Reiter, J.F., and W.C. Skarnes. 2006. Tectonic, a novel regulator of the Hedgehog pathway required for both activation and inhibition. Genes Dev. 20:22-27.

Roach, E.S., M.R. Gomez, and H. Northrup. 1998. Tuberous sclerosis complex consensus conference: revised clinical diagnostic criteria. J Child Neurol. 13:624-628.

Robu, M.E., J.D. Larson, A. Nasevicius, S. Beiraghi, C. Brenner, S.A. Farber, and S.C. Ekker. 2007. p53 activation by knockdown technologies. PLoS Genet. 3:e78.

Rodat-Despoix, L., and P. Delmas. 2009. Ciliar functions in the nephron. Pflugers Arch. 458:179-187.

Rohatgi, R., L. Milenkovic, and M.P. Scott. 2007. Patched1 regulates hedgehog signaling at the primary cilium. Science. 317:372-376.

Rosen, J.N., Sweeney, M. F., Mably, J. D. . 2009. Microinjection of Zebrafish Embryos to Analyze Gene Function. In J. Vis. Exp. Vol. 25. e1115

Ross, A.J., H. May-Simera, E.R. Eichers, M. Kai, J. Hill, D.J. Jagger, C.C. Leitch, J.P. Chapple, P.M. Munro, S. Fisher, P.L. Tan, H.M. Phillips, M.R. Leroux, D.J. Henderson, J.N. Murdoch, A.J. Copp, M.M. Eliot, J.R. Lupski, D.T. Kemp, H. Dollfus, M. Tada, N. Katsanis, A. Forge, and P.L. Beales. 2005. Disruption of Bardet-Biedl syndrome ciliary proteins perturbs planar cell polarity in vertebrates. Nat Genet. 37:1135-1140.

Saburi, S., I. Hester, E. Fischer, M. Pontoglio, V. Eremina, M. Gessler, S.E. Quaggin, R. Harrison, R. Mount, and H. McNeill. 2008. Loss of Fat4 disrupts PCP signaling and oriented cell division and leads to cystic kidney disease. Nat Genet. 40:1010-1015.

Salomon, R., S. Saunier, and P. Niaudet. 2009. Nephronophthisis. Pediatr Nephrol. 24:2333-2344.

Salonen, R., and R. Norio. 1984. The Meckel syndrome in Finland: epidemiologic and genetic aspects. Am J Med Genet. 18:691-698.

Sanders, L.H., and K.E. Whitlock. 2003. Phenotype of the zebrafish masterblind (mbl) mutant is dependent on genetic background. Dev Dyn. 227:291-300.

Sang, L., J.J. Miller, K.C. Corbit, R.H. Giles, M.J. Brauer, E.A. Otto, L.M. Baye, X. Wen, S.J. Scales, M. Kwong, E.G. Huntzicker, M.K. Sfakianos, W. Sandoval, J.F. Bazan, P. Kulkarni, F.R. Garcia-Gonzalo, A.D. Seol, J.F. O'Toole, S. Held, H.M. Reutter, W.S. Lane, M.A. Rafiq, A. Noor, M. Ansar, A.R. Devi, V.C. Sheffield, D.C. Slusarski, J.B. Vincent, D.A. Doherty, F. Hildebrandt, J.F. Reiter, and P.K. Jackson. 2011. Mapping the NPHP-JBTS-MKS protein network reveals ciliopathy disease genes and pathways. Cell. 145:513-528.

Sarmah, B., V.P. Winfrey, G.E. Olson, B. Appel, and S.R. Wente. 2007. A role for the inositol kinase Ipk1 in ciliary beating and length maintenance. Proc Natl Acad Sci U S A. 104:19843-19848.

Satir, P., L.B. Pedersen, and S.T. Christensen. 2010. The primary cilium at a glance. J Cell Sci. 123:499-503.

Saunier, S., J. Calado, R. Heilig, F. Silbermann, F. Benessy, G. Morin, M. Konrad, M. Broyer, M.C. Gubler, J. Weissenbach, and C. Antignac. 1997. A novel gene that encodes a protein with a putative src homology 3 domain is a candidate gene for familial juvenile nephronophthisis. Hum Mol Genet. 6:2317-2323.

Sayer, J.A., E.A. Otto, J.F. O'Toole, G. Nurnberg, M.A. Kennedy, C. Becker, H.C. Hennies, J. Helou, M. Attanasio, B.V. Fausett, B. Utsch, H. Khanna, Y. Liu, I. Drummond, I. Kawakami, T. Kusakabe, M. Tsuda, L. Ma, H. Lee, R.G. Larson, S.J. Allen, C.J. Wilkinson, E.A. Nigg, C. Shou, C. Lillo, D.S. Williams, B. Hoppe, M.J. Kemper, T. Neuhaus, M.A. Parisi, I.A. Glass, M. Petry, A. Kispert, J. Gloy, A. Ganner, G. Walz, X. Zhu, D. Goldman, P. Nurnberg, A. Swaroop, M.R. Leroux, and F. Hildebrandt. 2006. The centrosomal protein nephrocystin-6 is mutated in Joubert syndrome and activates transcription factor ATF4. Nat Genet. 38:674-681.

Schafer, T., M. Putz, S. Lienkamp, A. Ganner, A. Bergbreiter, H. Ramachandran, V. Gieloff, M. Gerner, C. Mattonet, P.G. Czarnecki, J.A. Sayer, E.A. Otto, F. Hildebrandt, A. Kramer-Zucker, and G. Walz. 2008. Genetic and physical interaction between the NPHP5 and NPHP6 gene products. Hum Mol Genet. 17:3655-3662.

Schilling, T.F., J.P. Concordet, and P.W. Ingham. 1999. Regulation of left-right asymmetries in the zebrafish by Shh and BMP4. Dev Biol. 210:277-287.

Schneider, I., P.N. Schneider, S.W. Derry, S. Lin, L.J. Barton, T. Westfall, and D.C. Slusarski. 2010. Zebrafish Nkd1 promotes Dvl degradation and is required for left-right patterning. Dev Biol. 348:22-33.

Scolari, F., D. Puzzer, A. Amoroso, G. Caridi, G.M. Ghiggeri, R. Maiorca, P. Aridon, M. De Fusco, A. Ballabio, and G. Casari. 1999. Identification of a new locus for medullary cystic disease, on chromosome 16p12. Am J Hum Genet. 64:1655-1660.

Seller, M.J. 1978. Meckel syndrome and the prenatal diagnosis of neural tube defects. J Med Genet. 15:462-465.

Serra, A.L., A.D. Kistler, D. Poster, M. Struker, R.P. Wuthrich, D. Weishaupt, and F. Tschirch. 2007. Clinical proof-of-concept trial to assess the therapeutic effect of sirolimus in patients with autosomal dominant polycystic kidney disease: SUISSE ADPKD study. BMC Nephrol. 8:13.

Serra, A.L., D. Poster, A.D. Kistler, F. Krauer, S. Raina, J. Young, K.M. Rentsch, K.S. Spanaus, O. Senn, P. Kristanto, H. Scheffel, D. Weishaupt, and R.P. Wuthrich. 2010. Sirolimus and kidney growth in autosomal dominant polycystic kidney disease. N Engl J Med. 363:820-829.

Sheffield, V.C., R. Carmi, A. Kwitek-Black, T. Rokhlina, D. Nishimura, G.M. Duyk, K. Elbedour, S.L. Sunden, and E.M. Stone. 1994. Identification of a Bardet-Biedl syndrome locus on

chromosome 3 and evaluation of an efficient approach to homozygosity mapping. Hum Mol Genet. 3:1331-1335.

Shillingford, J.M., N.S. Murcia, C.H. Larson, S.H. Low, R. Hedgepeth, N. Brown, C.A. Flask, A.C. Novick, D.A. Goldfarb, A. Kramer-Zucker, G. Walz, K.B. Piontek, G.G. Germino, and T. Weimbs. 2006. The mTOR pathway is regulated by polycystin-1, and its inhibition reverses renal cystogenesis in polycystic kidney disease. Proc Natl Acad Sci U S A. 103:5466-5471.

Shmukler, B.E., C.E. Kurschat, G.E. Ackermann, L. Jiang, Y. Zhou, B. Barut, A.K. Stuart-Tilley, J. Zhao, L.I. Zon, I.A. Drummond, D.H. Vandorpe, B.H. Paw, and S.L. Alper. 2005. Zebrafish slc4a2/ae2 anion exchanger: cDNA cloning, mapping, functional characterization, and localization. Am J Physiol Renal Physiol. 289:F835-849.

Simms, R.J., A.M. Hynes, L. Eley, D. Inglis, B. Chaudhry, H.R. Dawe, and J.A. Sayer. 2012. Modelling a ciliopathy: Ahi1 knockdown in model systems reveals an essential role in brain, retinal, and renal development. Cell Mol Life Sci. 69:993-1009.

Siroky, B.J., M.F. Czyzyk-Krzeska, and J.J. Bissler. 2009. Renal involvement in tuberous sclerosis complex and von Hippel-Lindau disease: shared disease mechanisms? Nat Clin Pract Nephrol. 5:143-156.

Siroky, B.J., and L.M. Guay-Woodford. 2006. Renal cystic disease: the role of the primary cilium/centrosome complex in pathogenesis. Adv Chronic Kidney Dis. 13:131-137.

Slanchev, K., M. Putz, A. Schmitt, A. Kramer-Zucker, and G. Walz. 2011. Nephrocystin-4 is required for pronephric duct-dependent cloaca formation in zebrafish. Hum Mol Genet. 20:3119-3128.

Slavotinek, A.M., E.M. Stone, K. Mykytyn, J.R. Heckenlively, J.S. Green, E. Heon, M.A. Musarella, P.S. Parfrey, V.C. Sheffield, and L.G. Biesecker. 2000. Mutations in MKKS cause Bardet-Biedl syndrome. Nat Genet. 26:15-16.

Smart, E.J., R.A. De Rose, and S.A. Farber. 2004. Annexin 2-caveolin 1 complex is a target of ezetimibe and regulates intestinal cholesterol transport. Proc Natl Acad Sci U S A. 101:3450-3455.

Smith, C.G., J. 1945. Congenital medullary cysts of the kidneys with severe refractory anaemia. Am J Dis Child. 69:369-377.

Smith, H.W. 1953. From Fish to Philosopher. CIBA, Pharmaceutical products.

Smith, U.M., M. Consugar, L.J. Tee, B.M. McKee, E.N. Maina, S. Whelan, N.V. Morgan, E. Goranson, P. Gissen, S. Lilliquist, I.A. Aligianis, C.J. Ward, S. Pasha, R. Punyashthiti, S. Malik Sharif, P.A. Batman, C.P. Bennett, C.G. Woods, C. McKeown, M. Bucourt, C.A. Miller, P. Cox, L. Algazali, R.C. Trembath, V.E. Torres, T. Attie-Bitach, D.A. Kelly, E.R. Maher, V.H. Gattone, 2nd, P.C. Harris, and C.A. Johnson. 2006. The transmembrane protein meckelin (MKS3) is mutated in Meckel-Gruber syndrome and the wpk rat. Nat Genet. 38:191-196.

Sohara, E., Y. Luo, J. Zhang, D.K. Manning, D.R. Beier, and J. Zhou. 2008. Nek8 regulates the expression and localization of polycystin-1 and polycystin-2. J Am Soc Nephrol. 19:469-476.

Sorokin, S.P. 1968. Reconstructions of centriole formation and ciliogenesis in mammalian lungs. J Cell Sci. 3:207-230.

Srour, M., F.F. Hamdan, J.A. Schwartzentruber, L. Patry, L.H. Ospina, M.I. Shevell, V. Desilets, S. Dobrzeniecka, G. Mathonnet, E. Lemyre, C. Massicotte, D. Labuda, D. Amrom, E. Andermann, G. Sebire, B. Maranda, F.C. Consortium, G.A. Rouleau, J. Majewski, and J.L. Michaud. 2012a. Mutations in TMEM231 cause Joubert syndrome in French Canadians. J Med Genet. 49:636-641.

Srour, M., J. Schwartzentruber, F.F. Hamdan, L.H. Ospina, L. Patry, D. Labuda, C. Massicotte, S. Dobrzeniecka, J.M. Capo-Chichi, S. Papillon-Cavanagh, M.E. Samuels, K.M. Boycott, M.I. Shevell, R. Laframboise, V. Desilets, F.C. Consortium, B. Maranda, G.A. Rouleau, J. Majewski, and J.L. Michaud. 2012b. Mutations in C5ORF42 cause Joubert syndrome in the French Canadian population. Am J Hum Genet. 90:693-700.

Stavrou, C., M. Koptides, C. Tombazos, E. Psara, C. Patsias, I. Zouvani, K. Kyriacou, F. Hildebrandt, T. Christofides, A. Pierides, and C.C. Deltas. 2002. Autosomal-dominant medullary cystic kidney disease type 1: clinical and molecular findings in six large Cypriot families. Kidney Int. 62:1385-1394.

Stemple, D.L. 2005. Structure and function of the notochord: an essential organ for chordate development. Development. 132:2503-2512.

Stoetzel, C., V. Laurier, E.E. Davis, J. Muller, S. Rix, J.L. Badano, C.C. Leitch, N. Salem, E. Chouery, S. Corbani, N. Jalk, S. Vicaire, P. Sarda, C. Hamel, D. Lacombe, M. Holder, S. Odent, S. Holder, A.S. Brooks, N.H. Elcioglu, E.D. Silva, B. Rossillion, S. Sigaudy, T.J. de Ravel, R.A. Lewis, B. Leheup, A. Verloes, P. Amati-Bonneau, A. Megarbane, O. Poch, D. Bonneau, P.L. Beales, J.L. Mandel, N. Katsanis, and H. Dollfus. 2006. BBS10 encodes a vertebrate-specific chaperonin-like protein and is a major BBS locus. Nat Genet. 38:521-524.

Stoetzel, C., J. Muller, V. Laurier, E.E. Davis, N.A. Zaghloul, S. Vicaire, C. Jacquelin, F. Plewniak, C.C. Leitch, P. Sarda, C. Hamel, T.J. de Ravel, R.A. Lewis, E. Friederich, C. Thibault, J.M. Danse, A. Verloes, D. Bonneau, N. Katsanis, O. Poch, J.L. Mandel, and H. Dollfus. 2007. Identification of a novel BBS gene (BBS12) highlights the major role of a vertebrate-specific branch of chaperonin-related proteins in Bardet-Biedl syndrome. Am J Hum Genet. 80:1-11.

Streisinger, G., C. Walker, N. Dower, D. Knauber, and F. Singer. 1981. Production of clones of homozygous diploid zebra fish (Brachydanio rerio). Nature. 291:293-296.

Sukhatme, V.P. 2003. The Kidney: From Normal Development to Congenital Disease. The New England Journal of Medicine. 349:2176-2177.

Sullivan-Brown, J., J. Schottenfeld, N. Okabe, C.L. Hostetter, F.C. Serluca, S.Y. Thiberge, and R.D. Burdine. 2008. Zebrafish mutations affecting cilia motility share similar cystic phenotypes and suggest a mechanism of cyst formation that differs from pkd2 morphants. Dev Biol. 314:261-275.

Summerton, J., and D. Weller. 1997. Morpholino antisense oligomers: design, preparation, and properties. Antisense & nucleic acid drug development. 7:187-195.

Sun, Z., A. Amsterdam, G.J. Pazour, D.G. Cole, M.S. Miller, and N. Hopkins. 2004. A genetic screen in zebrafish identifies cilia genes as a principal cause of cystic kidney. Development. 131:4085-4093.

Sun, Z., and N. Hopkins. 2001. vhnf1, the MODY5 and familial GCKD-associated gene, regulates regional specification of the zebrafish gut, pronephros, and hindbrain. Genes Dev. 15:3217-3229.

Sutton, R.B., and S.R. Sprang. 1998. Structure of the protein kinase Cbeta phospholipid-binding C2 domain complexed with Ca2+. Structure. 6:1395-1405.

Swanhart, L.M., C.C. Cosentino, C.Q. Diep, A.J. Davidson, M. de Caestecker, and N.A. Hukriede. 2011. Zebrafish kidney development: basic science to translational research. Birth Defects Res C Embryo Today. 93:141-156.

Sweeney, W.E., Jr., and E.D. Avner. 2011. Diagnosis and management of childhood polycystic kidney disease. Pediatr Nephrol. 26:675-692.

Tadenev, A.L., H.M. Kulaga, H.L. May-Simera, M.W. Kelley, N. Katsanis, and R.R. Reed. 2011. Loss of Bardet-Biedl syndrome protein-8 (BBS8) perturbs olfactory function, protein localization, and axon targeting. Proc Natl Acad Sci U S A. 108:10320-10325.

Tallila, J., E. Jakkula, L. Peltonen, R. Salonen, and M. Kestila. 2008. Identification of CC2D2A as a Meckel syndrome gene adds an important piece to the ciliopathy puzzle. Am J Hum Genet. 82:1361-1367.

Tao, Y., J. Kim, R.W. Schrier, and C.L. Edelstein. 2005. Rapamycin markedly slows disease progression in a rat model of polycystic kidney disease. J Am Soc Nephrol. 16:46-51.

Thisse, C., and B. Thisse. 2008. High-resolution in situ hybridization to whole-mount zebrafish embryos. Nature protocols. 3:59-69.

Tickoo, S.K., M.N. dePeralta-Venturina, L.R. Harik, H.D. Worcester, M.E. Salama, A.N. Young, H. Moch, and M.B. Amin. 2006. Spectrum of epithelial neoplasms in end-stage renal disease: an experience from 66 tumor-bearing kidneys with emphasis on histologic patterns distinct from those in sporadic adult renal neoplasia. Am J Surg Pathol. 30:141-153.

Tobin, J.L., and P.L. Beales. 2008. Restoration of renal function in zebrafish models of ciliopathies. Pediatr Nephrol. 23:2095-2099.

Torban, E., C. Kor, and P. Gros. 2004. Van Gogh-like2 (Strabismus) and its role in planar cell polarity and convergent extension in vertebrates. Trends Genet. 20:570-577.

Torres, P.C.H.a.V.E. 2009. Polycystic kidney disease. The Annual Review of Medicine. 60:321-337.

Torres, V.E. 2008. Role of vasopressin antagonists. Clin J Am Soc Nephrol. 3:1212-1218.

Torres, V.E., and P.C. Harris. 2009. Autosomal dominant polycystic kidney disease: the last 3 years. Kidney Int. 76:149-168.

Tory, K., T. Lacoste, L. Burglen, V. Moriniere, N. Boddaert, M.A. Macher, B. Llanas, H. Nivet, A. Bensman, P. Niaudet, C. Antignac, R. Salomon, and S. Saunier. 2007. High NPHP1 and

NPHP6 mutation rate in patients with Joubert syndrome and nephronophthisis: potential epistatic effect of NPHP6 and AHI1 mutations in patients with NPHP1 mutations. J Am Soc Nephrol. 18:1566-1575.

Town, T., J.J. Breunig, M.R. Sarkisian, C. Spilianakis, A.E. Ayoub, X. Liu, A.F. Ferrandino, A.R. Gallagher, M.O. Li, P. Rakic, and R.A. Flavell. 2008. The stumpy gene is required for mammalian ciliogenesis. Proc Natl Acad Sci U S A. 105:2853-2858.

Tran, P.V., C.J. Haycraft, T.Y. Besschetnova, A. Turbe-Doan, R.W. Stottmann, B.J. Herron, A.L. Chesebro, H. Qiu, P.J. Scherz, J.V. Shah, B.K. Yoder, and D.R. Beier. 2008. THM1 negatively modulates mouse sonic hedgehog signal transduction and affects retrograde intraflagellar transport in cilia. Nat Genet. 40:403-410.

Truong, L.D., Y.J. Choi, S.S. Shen, G. Ayala, R. Amato, and B. Krishnan. 2003. Renal cystic neoplasms and renal neoplasms associated with cystic renal diseases: pathogenetic and molecular links. Adv Anat Pathol. 10:135-159.

Tse, C.A., Drummond, I.A. 2012. Ciliated cell-type specific functions of Cep290/NPHP6. In Cilia 2012, University College London. 55.

Ullmann, J.F., G. Cowin, N.D. Kurniawan, and S.P. Collin. 2010. A three-dimensional digital atlas of the zebrafish brain. Neuroimage. 51:76-82.

Utsch, B., J.A. Sayer, M. Attanasio, R.R. Pereira, M. Eccles, H.C. Hennies, E.A. Otto, and F. Hildebrandt. 2006. Identification of the first AHI1 gene mutations in nephronophthisis-associated Joubert syndrome. Pediatr Nephrol. 21:32-35.

Valente, E.M., F. Brancati, and B. Dallapiccola. 2008. Genotypes and phenotypes of Joubert syndrome and related disorders. Eur J Med Genet. 51:1-23.

Valente, E.M., F. Brancati, J.L. Silhavy, M. Castori, S.E. Marsh, G. Barrano, E. Bertini, E. Boltshauser, M.S. Zaki, A. Abdel-Aleem, G.M. Abdel-Salam, E. Bellacchio, R. Battini, R.P. Cruse, W.B. Dobyns, K.S. Krishnamoorthy, C. Lagier-Tourenne, A. Magee, I. Pascual-Castroviejo, C.D. Salpietro, D. Sarco, B. Dallapiccola, and J.G. Gleeson. 2006a. AHI1 gene mutations cause specific forms of Joubert syndrome-related disorders. Ann Neurol. 59:527-534.

Valente, E.M., C.V. Logan, S. Mougou-Zerelli, J.H. Lee, J.L. Silhavy, F. Brancati, M. Iannicelli, L. Travaglini, S. Romani, B. Illi, M. Adams, K. Szymanska, A. Mazzotta, J.E. Lee, J.C. Tolentino, D. Swistun, C.D. Salpietro, C. Fede, S. Gabriel, C. Russ, K. Cibulskis, C. Sougnez, F. Hildebrandt, E.A. Otto, S. Held, B.H. Diplas, E.E. Davis, M. Mikula, C.M. Strom, B. Ben-Zeev, D. Lev, T.L. Sagie, M. Michelson, Y. Yaron, A. Krause, E. Boltshauser, N. Elkhartoufi, J. Roume, S. Shalev, A. Munnich, S. Saunier, C. Inglehearn, A. Saad, A. Alkindy, S. Thomas, M. Vekemans, B. Dallapiccola, N. Katsanis, C.A. Johnson, T. Attie-Bitach, and J.G. Gleeson. 2010. Mutations in TMEM216 perturb ciliogenesis and cause Joubert, Meckel and related syndromes. Nat Genet. 42:619-625.

Valente, E.M., J.L. Silhavy, F. Brancati, G. Barrano, S.R. Krishnaswami, M. Castori, M.A. Lancaster, E. Boltshauser, L. Boccone, L. Al-Gazali, E. Fazzi, S. Signorini, C.M. Louie, E. Bellacchio, E. Bertini, B. Dallapiccola, and J.G. Gleeson. 2006b. Mutations in CEP290, which encodes a centrosomal protein, cause pleiotropic forms of Joubert syndrome. Nat Genet. 38:623-625.

van Slegtenhorst, M., R. de Hoogt, C. Hermans, M. Nellist, B. Janssen, S. Verhoef, D. Lindhout, A. van den Ouweland, D. Halley, J. Young, M. Burley, S. Jeremiah, K. Woodward, J. Nahmias, M. Fox, R. Ekong, J. Osborne, J. Wolfe, S. Povey, R.G. Snell, J.P. Cheadle, A.C. Jones, M. Tachataki, D. Ravine, J.R. Sampson, M.P. Reeve, P. Richardson, F. Wilmer, C. Munro, T.L. Hawkins, T. Sepp, J.B. Ali, S. Ward, A.J. Green, J.R. Yates, J. Kwiatkowska, E.P. Henske, M.P. Short, J.H. Haines, S. Jozwiak, and D.J. Kwiatkowski. 1997. Identification of the tuberous sclerosis gene TSC1 on chromosome 9q34. Science. 277:805-808.

Vierkotten, J., R. Dildrop, T. Peters, B. Wang, and U. Ruther. 2007. Ftm is a novel basal body protein of cilia involved in Shh signalling. Development. 134:2569-2577.

Vihtelic, T.S., and D.R. Hyde. 2000. Light-induced rod and cone cell death and regeneration in the adult albino zebrafish (Danio rerio) retina. J Neurobiol. 44:289-307.

Vize, P.D., A.S. Woolf, and J. Bard. 2003. The kidney : from normal development to congenital disease. Academic, Amsterdam ; London.

Waldherr, R., T. Lennert, H.P. Weber, H.J. Fodisch, and K. Scharer. 1982. The nephronophthisis complex. A clinicopathologic study in children. Virchows Arch A Pathol Anat Histol. 394:235-254.

Walz, G., K. Budde, M. Mannaa, J. Nurnberger, C. Wanner, C. Sommerer, U. Kunzendorf, B. Banas, W.H. Horl, N. Obermuller, W. Arns, H. Pavenstadt, J. Gaedeke, M. Buchert, C. May, H. Gschaidmeier, S. Kramer, and K.U. Eckardt. 2010. Everolimus in patients with autosomal dominant polycystic kidney disease. N Engl J Med. 363:830-840.

Wang, N., Y.H. Sun, J. Liu, Y.P. Wang, and Z.Y. Zhu. 2007. Molecular characterization of common carp (Cyprinus carpio) Sonic Hedgehog and discovery of its maternal expression. Dev Genes Evol. 217:299-305.

Waters, A.M., and P.L. Beales. 2011. Ciliopathies: an expanding disease spectrum. Pediatr Nephrol. 26:1039-1056.

Weatherbee, S.D., L.A. Niswander, and K.V. Anderson. 2009. A mouse model for Meckel syndrome reveals Mks1 is required for ciliogenesis and Hedgehog signaling. Hum Mol Genet. 18:4565-4575.

Webber, W.A., and J. Lee. 1975. Fine structure of mammalian renal cilia. Anat Rec. 182:339-343.

Westerfield, M. 1995. The Zebrafish Book. A guide for the Laboratory Use of Zebrafish (Danio rerio). Eugene: University of Oregon Press.

Westfall, J.E., C. Hoyt, Q. Liu, Y.C. Hsiao, E.A. Pierce, P.S. Page-McCaw, and R.J. Ferland. 2010. Retinal degeneration and failure of photoreceptor outer segment formation in mice with targeted deletion of the Joubert syndrome gene, Ahi1. J Neurosci. 30:8759-8768.

Wheatley, D.N. 1995. Primary cilia in normal and pathological tissues. Pathobiology. 63:222-238.

Williams, C.L., C. Li, K. Kida, P.N. Inglis, S. Mohan, L. Semenec, N.J. Bialas, R.M. Stupay, N. Chen, O.E. Blacque, B.K. Yoder, and M.R. Leroux. 2011. MKS and NPHP modules cooperate to

establish basal body/transition zone membrane associations and ciliary gate function during ciliogenesis. J Cell Biol. 192:1023-1041.

Wilson, C.W., and D.Y. Stainier. 2010. Vertebrate Hedgehog signaling: cilia rule. BMC biology. 8:102.

Wingert, R.A., and A.J. Davidson. 2008. The zebrafish pronephros: a model to study nephron segmentation. Kidney Int. 73:1120-1127.

Wingert, R.A., R. Selleck, J. Yu, H.D. Song, Z. Chen, A. Song, Y. Zhou, B. Thisse, C. Thisse, A.P. McMahon, and A.J. Davidson. 2007. The cdx genes and retinoic acid control the positioning and segmentation of the zebrafish pronephros. PLoS Genet. 3:1922-1938.

Winyard, P., and L.S. Chitty. 2008. Dysplastic kidneys. Semin Fetal Neonatal Med. 13:142-151.

Wolf, M.T., and F. Hildebrandt. 2011. Nephronophthisis. Pediatr Nephrol. 26:181-194.

Wolf, M.T., S. Saunier, J.F. O'Toole, N. Wanner, T. Groshong, M. Attanasio, R. Salomon, T. Stallmach, J.A. Sayer, R. Waldherr, M. Griebel, J. Oh, T.J. Neuhaus, U. Josefiak, C. Antignac, E.A. Otto, and F. Hildebrandt. 2007. Mutational analysis of the RPGRIP1L gene in patients with Joubert syndrome and nephronophthisis. Kidney Int. 72:1520-1526.

Won, J., C. Marin de Evsikova, R.S. Smith, W.L. Hicks, M.M. Edwards, C. Longo-Guess, T. Li, J.K. Naggert, and P.M. Nishina. 2011. NPHP4 is necessary for normal photoreceptor ribbon synapse maintenance and outer segment formation, and for sperm development. Hum Mol Genet. 20:482-496.

Wythe, J.D., M.J. Jurynec, L.D. Urness, C.A. Jones, M.K. Sabeh, A.A. Werdich, M. Sato, H.J. Yost, D.J. Grunwald, C.A. Macrae, and D.Y. Li. 2011. Hadp1, a newly identified pleckstrin homology domain protein, is required for cardiac contractility in zebrafish. Dis Model Mech. 4:607-621.

Yang, H.W., J.L. Kutok, N.H. Lee, H.Y. Piao, C.D. Fletcher, J.P. Kanki, and A.T. Look. 2004. Targeted expression of human MYCN selectively causes pancreatic neuroendocrine tumors in transgenic zebrafish. Cancer Res. 64:7256-7262.

Yen, H.J., M.K. Tayeh, R.F. Mullins, E.M. Stone, V.C. Sheffield, and D.C. Slusarski. 2006. Bardet-Biedl syndrome genes are important in retrograde intracellular trafficking and Kupffer's vesicle cilia function. Hum Mol Genet. 15:667-677.

Yoder, B.K., X. Hou, and L.M. Guay-Woodford. 2002. The polycystic kidney disease proteins, polycystin-1, polycystin-2, polaris, and cystin, are co-localized in renal cilia. J Am Soc Nephrol. 13:2508-2516.

Yokoyama, T., N.G. Copeland, N.A. Jenkins, C.A. Montgomery, F.F. Elder, and P.A. Overbeek. 1993. Reversal of left-right asymmetry: a situs inversus mutation. Science. 260:679-682.

Zerres, K., G. Mucher, L. Bachner, G. Deschennes, T. Eggermann, H. Kaariainen, M. Knapp, T. Lennert, J. Misselwitz, K.E. von Muhlendahl, and et al. 1994. Mapping of the gene for autosomal recessive polycystic kidney disease (ARPKD) to chromosome 6p21-cen. Nat Genet. 7:429-432.

Zerres, K., G. Mucher, J. Becker, C. Steinkamm, S. Rudnik-Schoneborn, P. Heikkila, J. Rapola, R. Salonen, G.G. Germino, L. Onuchic, S. Somlo, E.D. Avner, L.A. Harman, J.M. Stockwin, and L.M. Guay-Woodford. 1998. Prenatal diagnosis of autosomal recessive polycystic kidney disease (ARPKD): molecular genetics, clinical experience, and fetal morphology. Am J Med Genet. 76:137-144.

Zhang, Q., S. Seo, K. Bugge, E.M. Stone, and V.C. Sheffield. 2012. BBS proteins interact genetically with the IFT pathway to influence SHH-related phenotypes. Hum Mol Genet. 21:1945-1953.

Zhou, J. 2009. Polycystins and primary cilia: primers for cell cycle progression. Annu Rev Physiol. 71:83-113.

Zhou, W., R.C. Boucher, F. Bollig, C. Englert, and F. Hildebrandt. 2010a. Characterization of mesonephric development and regeneration using transgenic zebrafish. Am J Physiol Renal Physiol. 299:F1040-1047.

Zhou, W., J. Dai, M. Attanasio, and F. Hildebrandt. 2010b. Nephrocystin-3 is required for ciliary function in zebrafish embryos. Am J Physiol Renal Physiol. 299:F55-62.

Zimmerman, K. 1898. Beitrage zur Kenntniss einiger drusen and epithelien (English translation: Contributions to knowledge of some glands and epithelium). Arch Mikr Anat. 52:552-706.

Zollinger, H.U., M.J. Mihatsch, A. Edefonti, F. Gaboardi, E. Imbasciati, and T. Lennert. 1980. Nephronophthisis (medullary cystic disease of the kidney). A study using electron microscopy, immunofluorescence, and a review of the morphological findings. Helv Paediatr Acta. 35:509-530.

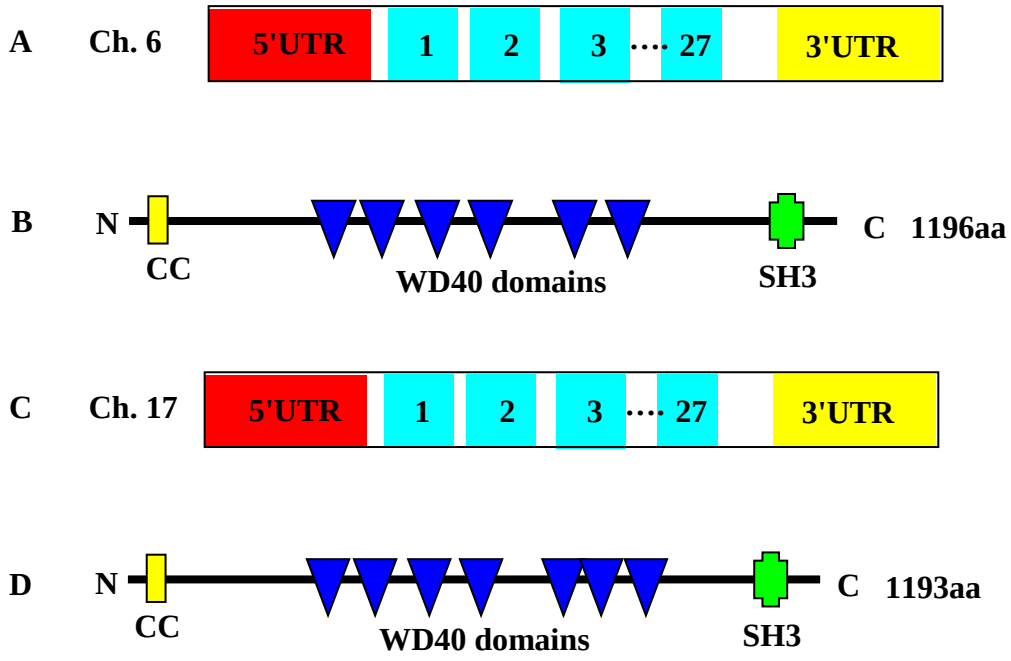

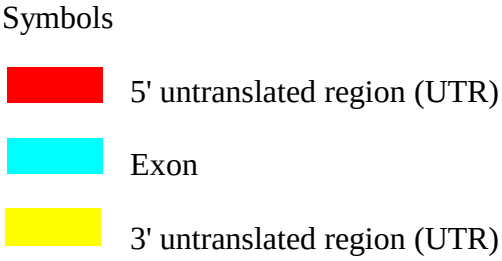

Figure 3.1 *AHI1* gene transcript and partial protein product (Jouberin) structure in humans and zebrafish
(**A**) *AHI1* transcript in humans (OTTHUMT00000391948) and schematic representation of encoded protein product, Jouberin (**B**). (**C**) *ahi1* transcript in zebrafish (OTTDART00000049821) and schematic representation of encoded protein product, Jouberin (**D**). aa, amino acids; CC, coiled coil; Ch., chromosome; WD40 repeats; SH3, Src homology domain.

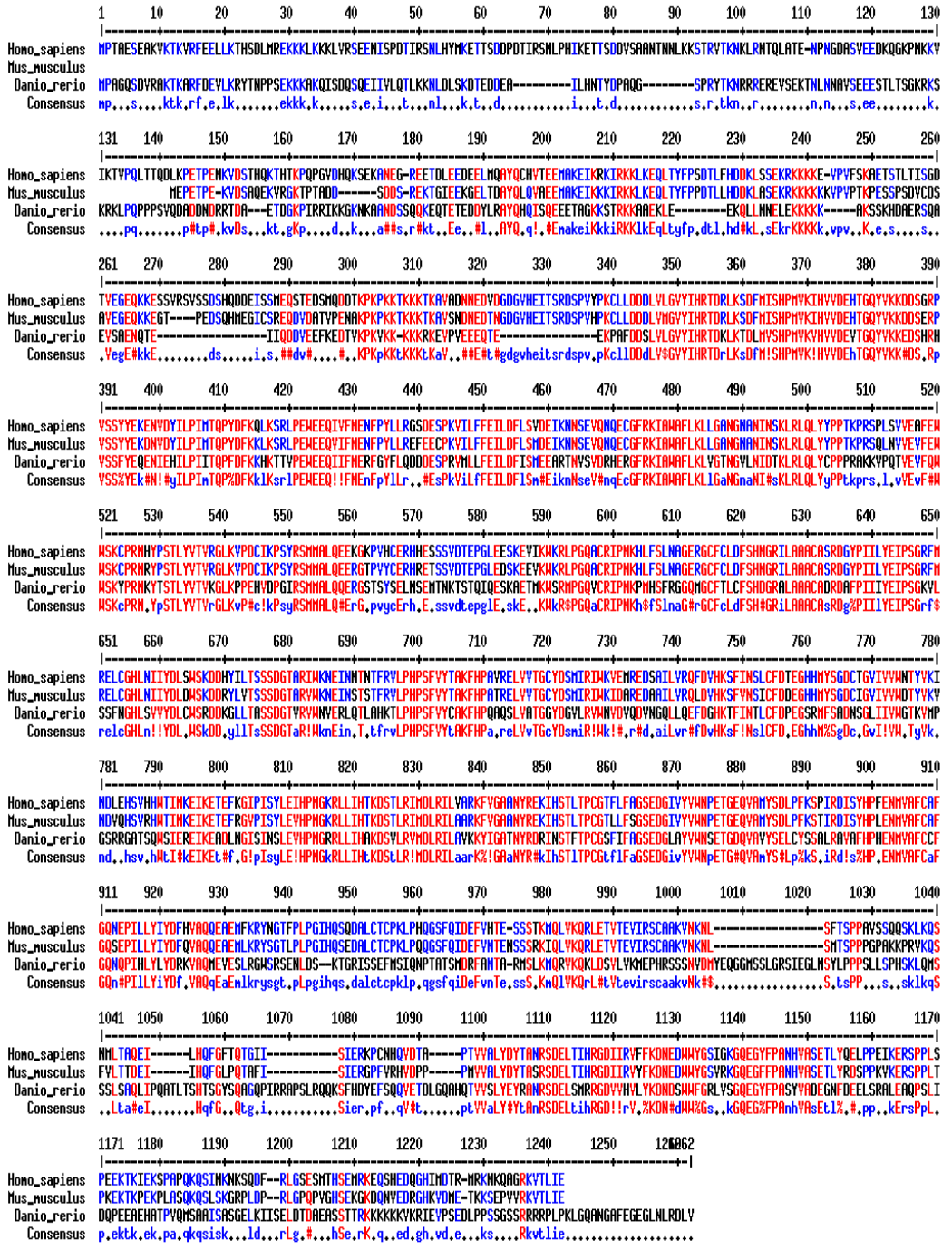

Figure 3.2 Evolutionary conservation of Ahi1 (Jouberin) in humans, mice and zebrafish

Jouberin peptide sequence alignment in humans (homo sapiens, OTTHUMP00000234456), mice (mus musculus, ENSMUSP00000101164) and zebrafish (danio rerio, OTTDARP00000039088). Conservation of amino acid alignment (red font).

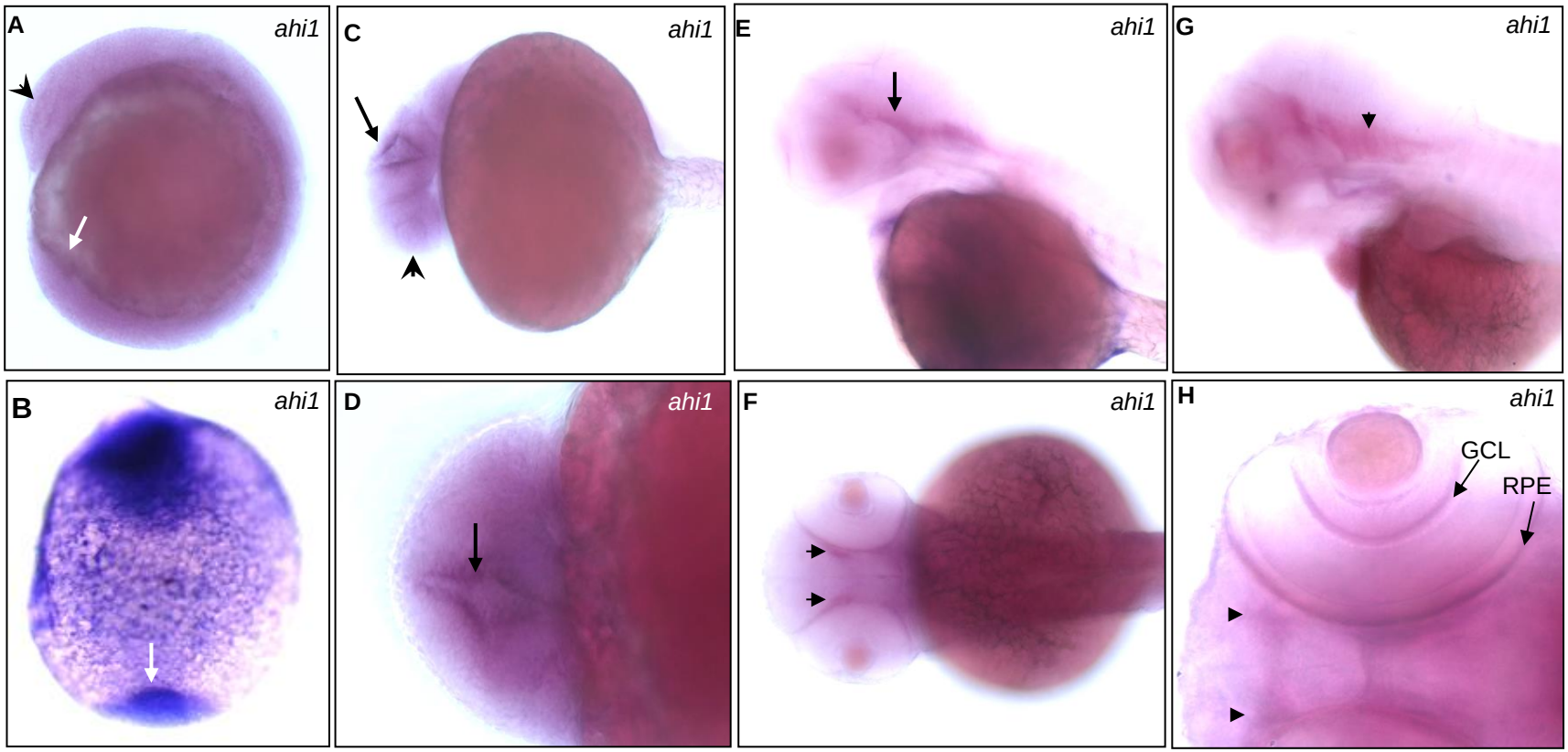

Figure 3.3 Expression of *ahi1* during zebrafish embryogenesis

Lateral (A, C, E, G) and dorsal (B, D, F, H) images of whole-mount *in situ* hybridisation using an *ahi1* antisense riboprobe on golden, wild type embryos at 8 somites (8s) (**A**, **B**), 24hpf (**C**, **D**), 48hpf (**E**, **F**) and 72hpf (**G**, **H**). *ahi1* is expressed at: 8s in the eye (black arrowhead, **A**), the notochord and in Kupffer's vesicle (white arrow, **A**, **B**); 24hpf in the midbrain, hindbrain (arrows, **C**, **D**) and retina (arrowhead, **C**); 48hpf in the retina, hypothalamus (arrow, **E**, **F**) and inner ear; 72hpf in the inner ear (arrowhead, **G**), olfactory bulbs (arrowheads, **H**), and specific retinal layers (GCL and RPE, **H**). GCL, ganglion cell layer; hpf, hours post fertilisation; RPE, retinal pigmented epithelium.

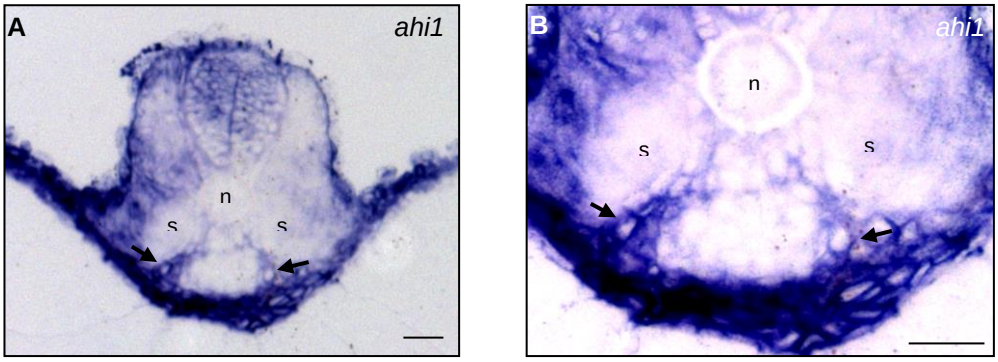

Figure 3.4 Expression of *ahi1* in zebrafish pronephros
Transverse section at the level of the medial tubules of the pronephros following whole-mount *in situ* hybridisation using an *ahi1* antisense riboprobe on golden, wild type embryos at 48 hpf. In both images, the arrows demonstrate *ahi1* expression in the pronephros. Images were taken with a 20x (**A**) and 40x (**B**) objective lens. Scale bars are 20µm. n, notochord; s, somites.

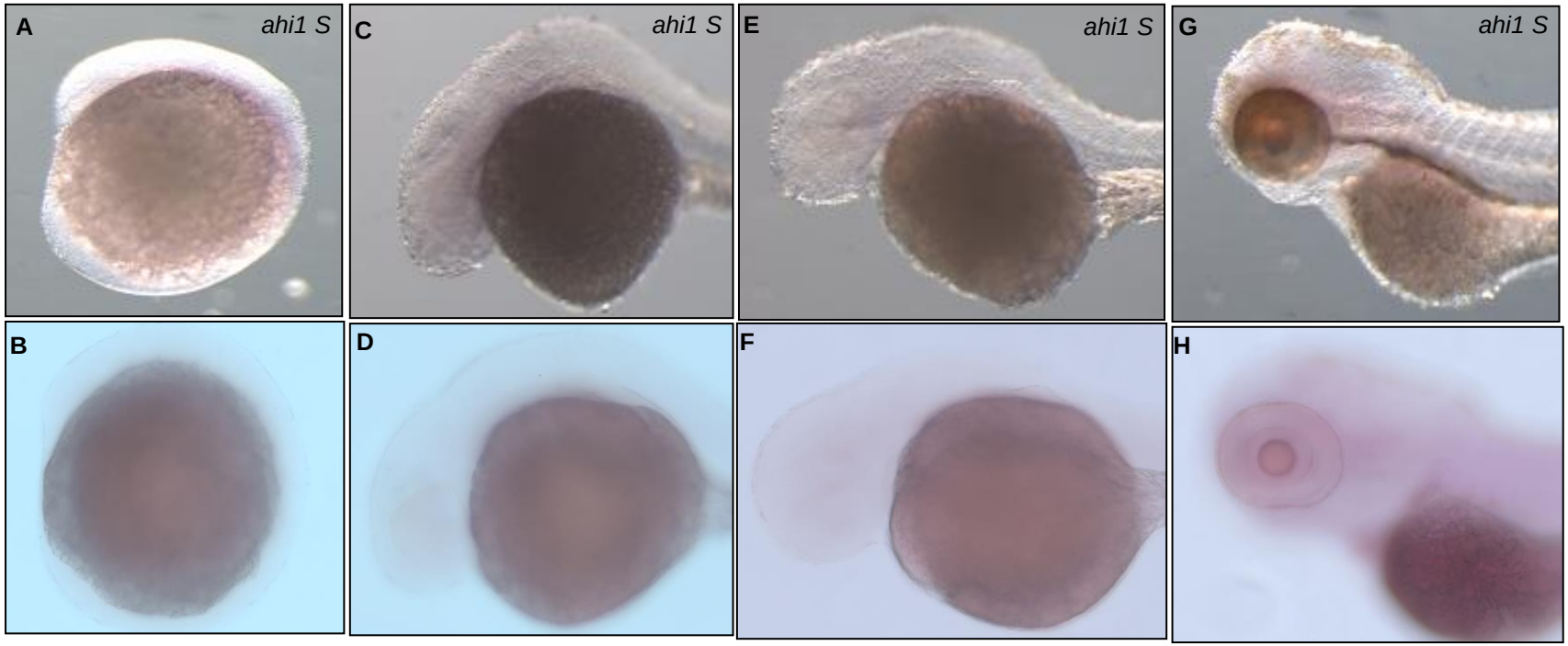

Figure 3.5 *In situ* hybridisation controls for *ahi1* antisense riboprobe during zebrafish embryogenesis
Lateral views of whole-mount *in situ* hybridisation using *ahi1* sense riboprobe (A, C, E, G) and no probe (B, D, F, H) on golden, wild type embryos at 8 somites (8s) (**A**, **B**), 24hpf (**C**, **D**), 48hpf (**E**, **F**) and 72hpf (**G**, **H**). hpf, hours post fertilisation.

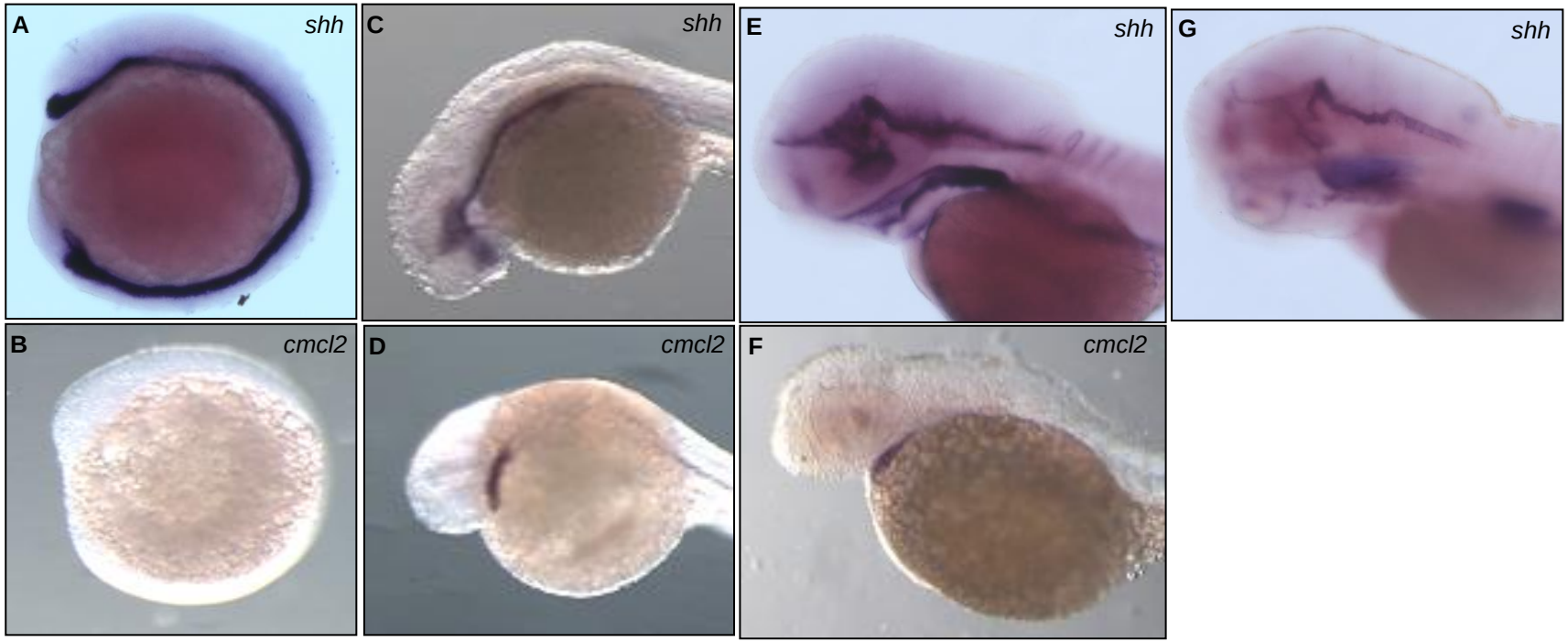

Figure 3.6 *In situ* hybridisation positive controls for *ahi1* antisense riboprobe during zebrafish embryogenesis
Lateral views of whole-mount *in situ* hybridisation using s*hh* antisense (**A**, **C**, **E**, **G**) and *cmcl2* antisense (**B**, **D**, **F**, **H**) riboprobes on golden, wild type embryos at 8 somites (8s) (**A**, **B**), 24hpf (**C**, **D**), 48hpf (**E**, **F**) and 72hpf (**G**). s*hh* is expressed in the notochord (**A**) at the 8s stage; in the eye and floorplate at 24hpf (**C**); additionally in the telencephalon, diencephalon, hypothalamus and pharyngeal arches at 48hpf (**E**) and 72hpf (**G**). *cmcl2* expression is not detectable at the 8s stage (**B**), however at 24hpf (**D**) and 48hpf (**F**) it is evident specifically in the single ventricle. *cmcl2*, *cardiac myosin light chain 2*; hpf, hours post fertilisation; *shh*, *sonic hedgehog*.

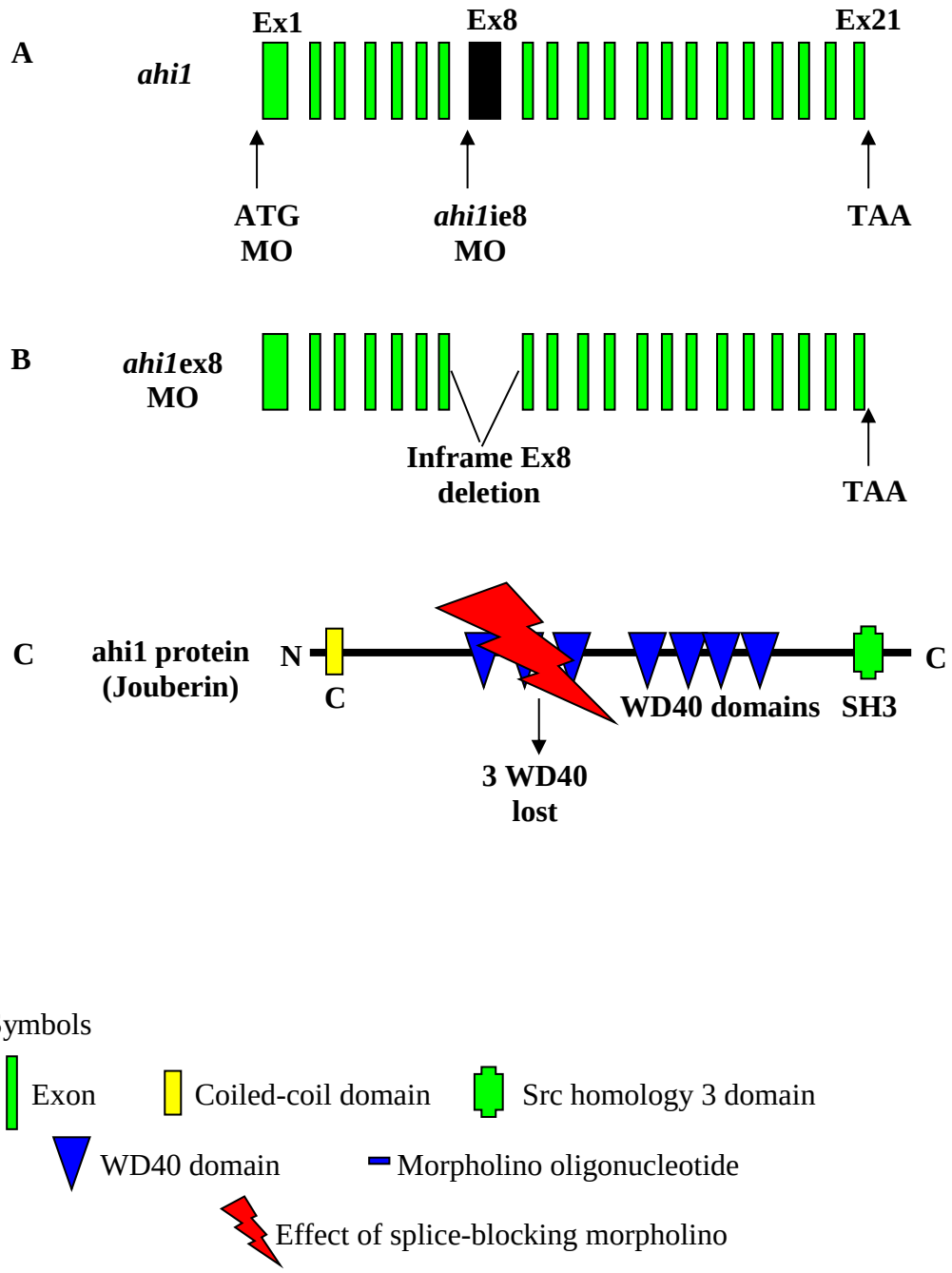

Figure 3.7 *ahi1* morpholino oligonucleotide design
(**A**) Schematic representation of zebrafish *ahi1*showing target sites of translation (ATG) and splice (*ahi1*iex8) blocking morpholino oligonucleotides (MO). (**B**) Schematic representation of the effect of the splice blocking MO designed to target exon 8, leading to an inframe deletion and loss of 3 WD40 repeats from the protein product, Jouberin (**C**).

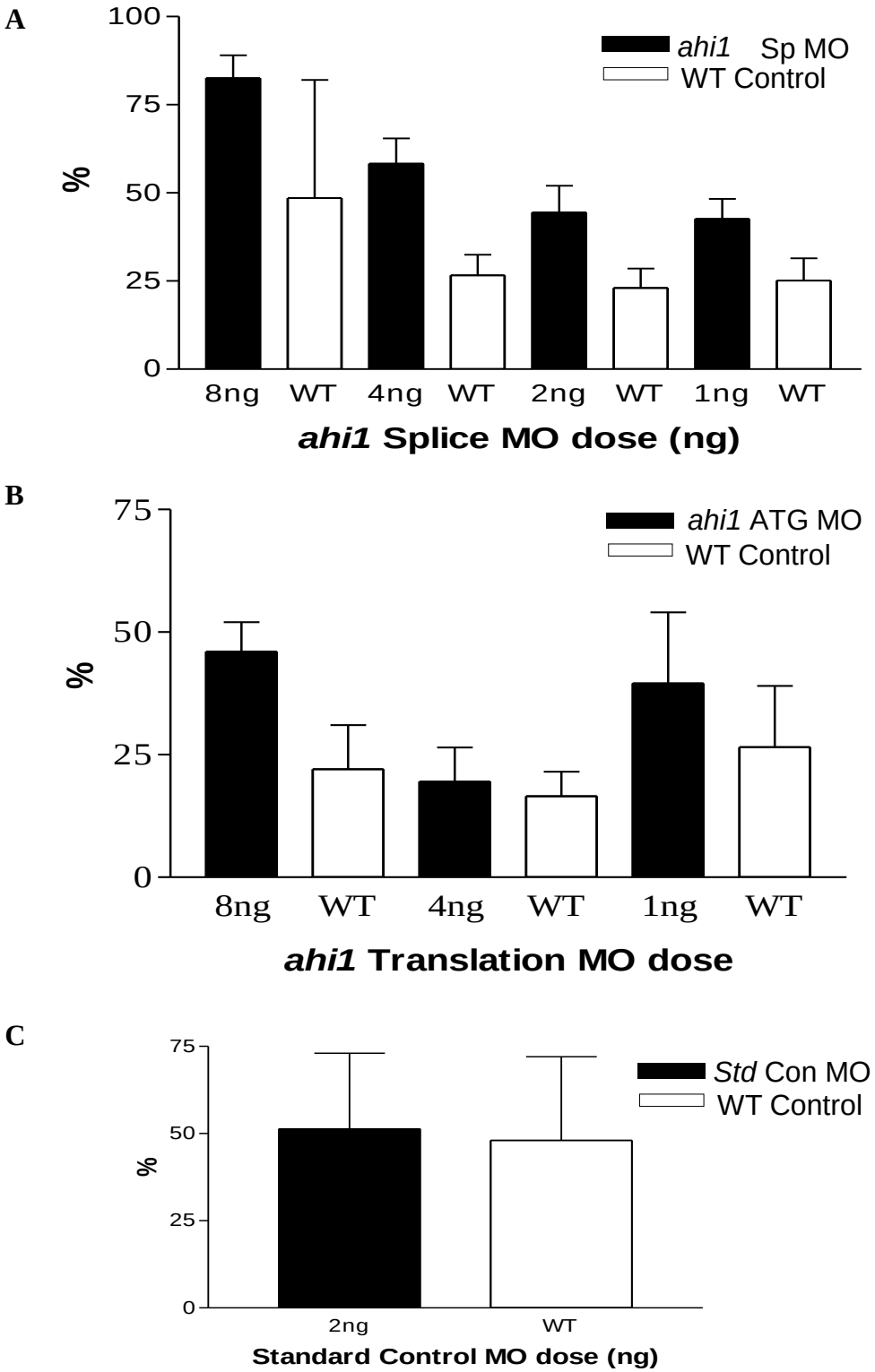

Figure 3.8 Mortality at 24hpf following MO injection

Mortality at 24 hours post fertilisation (hpf) is shown as mean percentage (%) and standard error of the mean (where appropriate) in zebrafish embryos injected with morpholino oligonucleotide (MO) compared to matched uninjected wild type (WT) controls. (**A**) *ahi1* splice (Sp) MO induces a dose dependent effect on mortality. (**B**) *ahi1* translation (ATG) blocking MO has a more variable effect on mortality. (**C**) Injection of a standard control (Std Con) MO induced no significant difference (p=0.92, unpaired t-test) in mortality at 24hpf compared to uninjected WT controls.


A
WT
B
Std Con MO
C
ahi1 Sp MO
*
D
ahi1 Sp MO
*
E
ahi1 ATG MO
*
F
ahi1 ATG MO
*

Figure 3.9 Phenotype following *ahi1* MO knockdown at 72 hpf
Lateral views show wild type uninjected (**A**) zebrafish embryos and those following injection with a standard negative control MO (Std Con MO, **B**) were morphologically normal. Injection of *ahi1* splice (Sp, **C, D**) and translation (ATG, **E, F**) blocking MOs leads to curved body axis, hydrocephalus (arrows), cardiac oedema (*), pronephric cysts and altered number of otoliths (single in **F** (arrowhead). hpf, hours post fertilisation; MO, morpholino oligonucleotide.

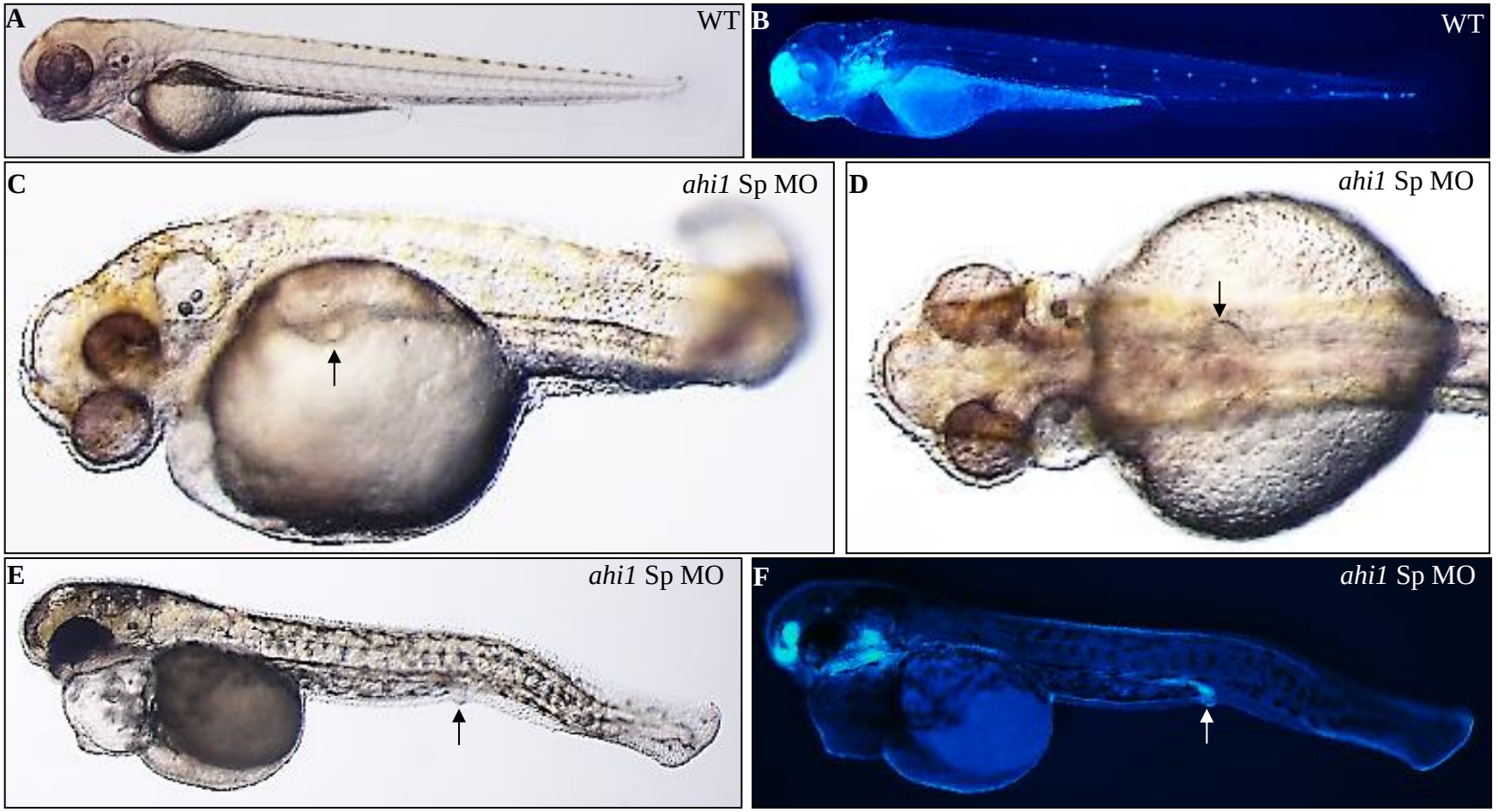

Figure 3.10 *ahi1* knockdown induces pronephric cysts in zebrafish embryos

Light and fluorescent microscopy images of pronephric cysts in golden (**A**, **C**-**E**) and *claudin-b:lyn-gfp* transgenic (**B**, **F**) zebrafish embryos at 72hpf. Lateral views of wild type, uninjected embryos were morphologically normal (**A**, **B**). 1-4ng of *ahi1* splice blocking MO induces proximal (lateral and dorsal views, arrowed, **C**, **D**) and distal (at the cloaca, arrowed **E**, **F**) pronephric cysts. MO=morpholino oligonucleotide

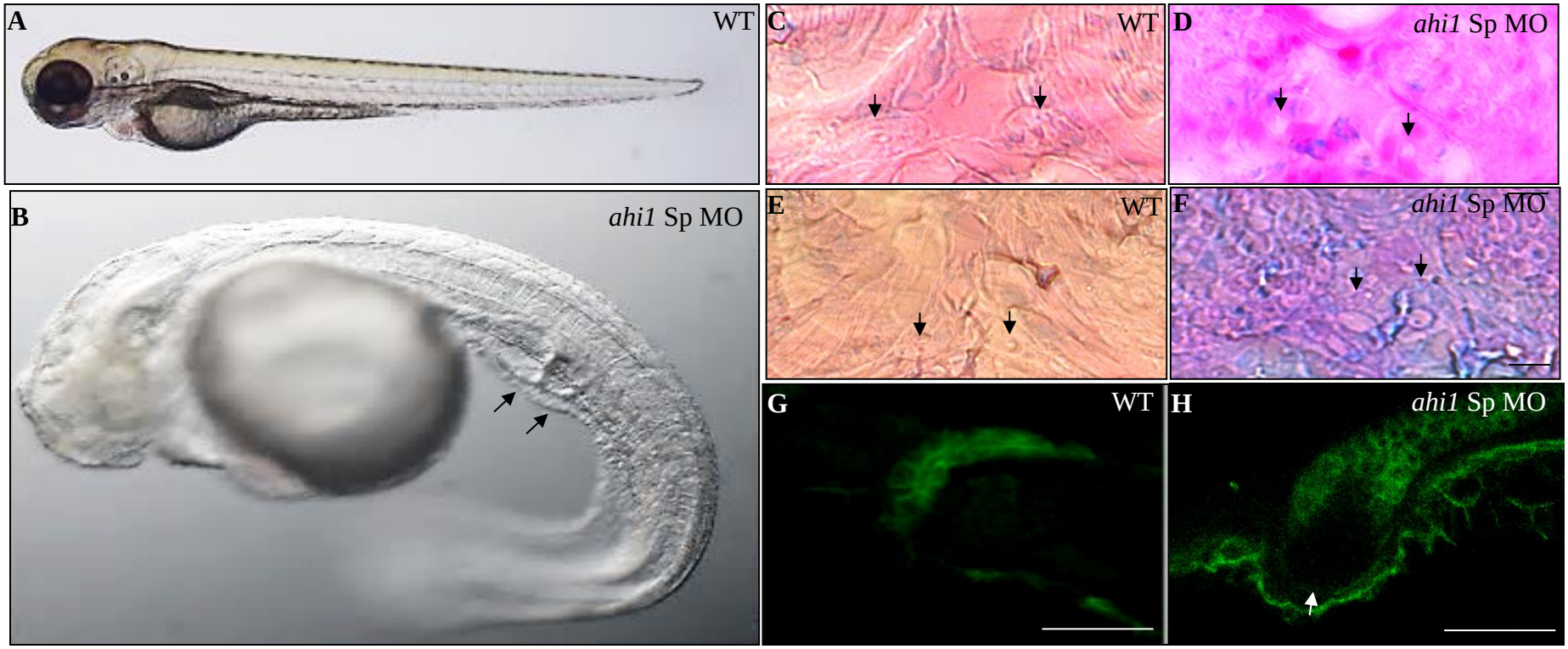

Figure 3.11 *ahi1* knockdown induces cystic dilatation, cloacal dilatation and obstruction in zebrafish embryos

Light microscopy images of distal pronephric cysts (arrows) leading to cloacal obstruction in golden *ahi1* morphant (*ahi1* Sp MO) embryo at 72hpf (**B**), compared to uninjected wild type (WT) control (**A**). Resin histology 5μm sections through the pronephros (arrows) in embryos at 72hpf, stained with methylene blue-basic fuchsin stain. Images taken with a 40x objective lens at the level of the posterior pronephric tubules (arrows, **C-D**) and the cloaca (**E-F**). In *ahi1* morphants, the posterior tubules are modestly dilated (**D**, diameter 5μm), compared to WT controls (**C**, diameter 3μm). This pronephric dilatation becomes more pronounced in *ahi1* morphants at the level of the cloaca (**F**, diameter 10μm), compared to WT controls (**E**, diameter 2μm). Scale bar = 10μm. Fluorescent images of the cloaca (**G**,**H**) using the *claudinb:*Lyn-GFP transgenic line, taken with a 20x objective. *ahi1* morphants have cystic dilatation of the cloaca (**H**, arrow), compared to WT controls (**G**). Scale bar = 50μm.

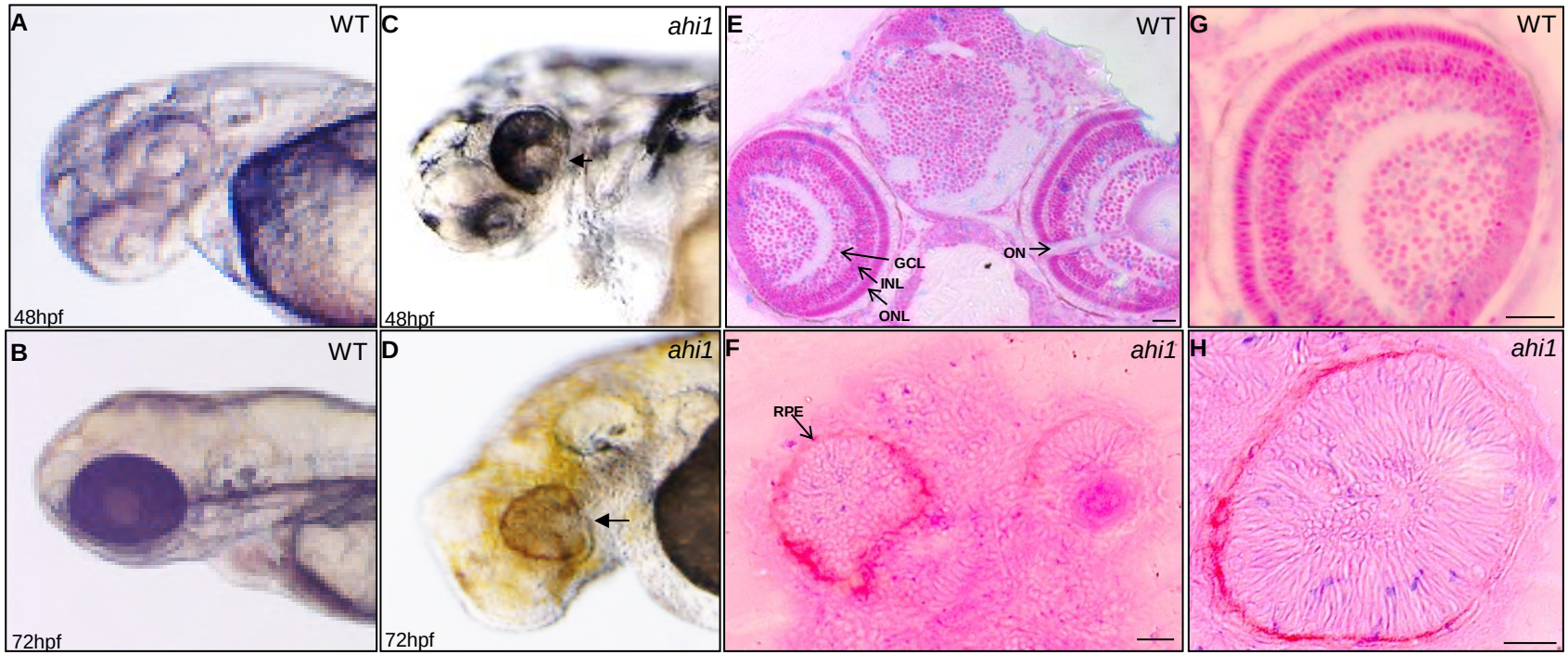

Figure 3.12 *ahi1* knockdown induces coloboma formation and retinal dystrophy in zebrafish embryos
Light microscopy images comparing the eyes of uninjected wild type (WT) embryos (**A**, **B**) and *ahi1* morphants (**C**, **D**) at 48hpf and 72hpf. In *ahi1* morphants there is abnormal eye development with coloboma formation (arrowed, **C**, **D**). Resin histology of eyes at 72hpf, sectioned at 5-7µm and stained with methylene blue-basic fuchsin stain. Images taken with a 20x (**E**, **F**) and 40x (**G**, **H**) objective lens, scale bars = 20µm. In WT control embryos (**E**, **G**), there is normal retinal lamination (arrowed, **E**) including formation of the ganglion cell layer (GCL), inner nuclear layer (INL) and outer nuclear layer (ONL). In *ahi1* morphants (**F**, **H**) there is severe disruption to normal retinal development, with failure of discrete retinal layer formation, however, the outer retinal pigmented epithelium (RPE, arrowed in **F**) remains present. hpf, hours post fertilisation.

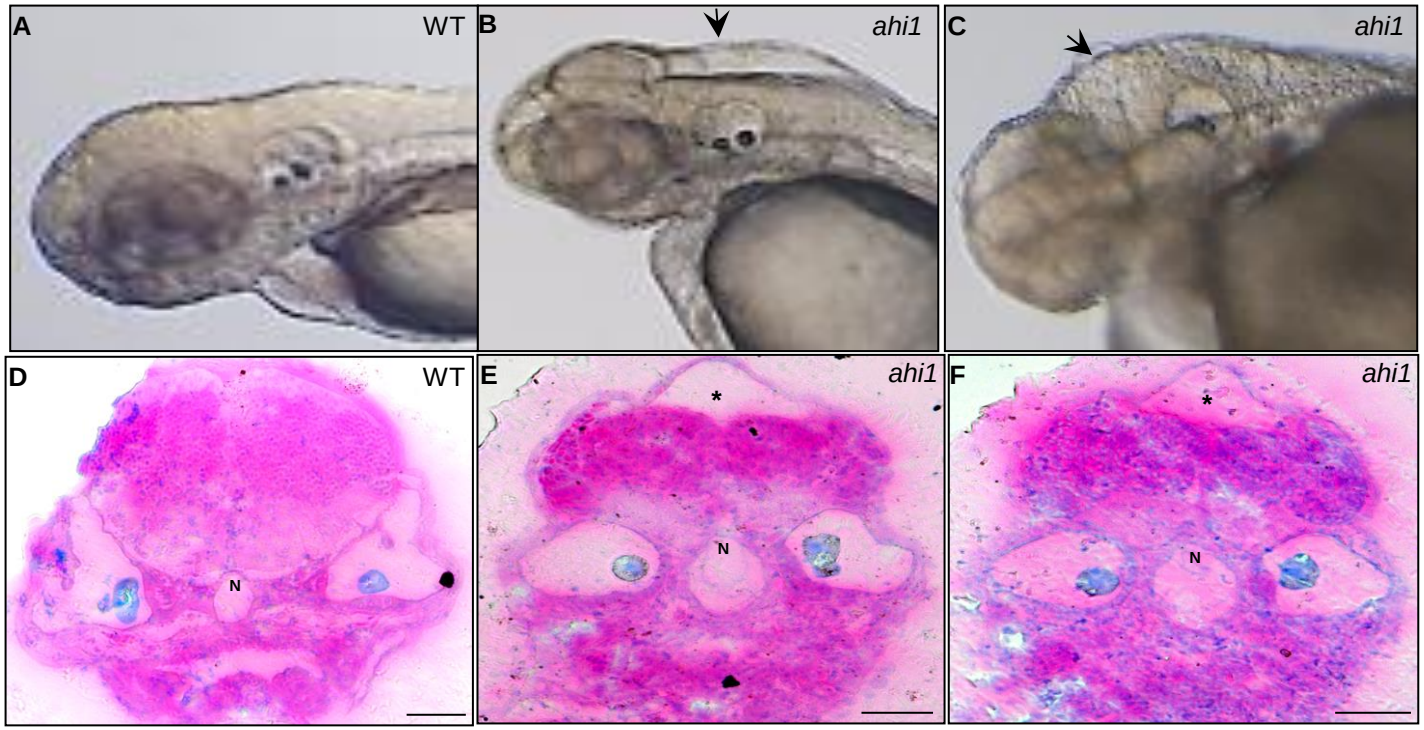

Figure 3.13 *ahi1* knockdown induces hydrocephalus and abnormal brain development in zebrafish embryos
Light microscopy images demonstrating hydrocephalus (arrowed, **B**, **C**) and abnormal hindbrain development in *ahi1* morphant zebrafish embryos, compared to normal brain development in uninjected wild type (WT) control embryos (**A**) at 72hpf. Resin histology cross sections (5-7μm) through the brain at the level of the otoliths in WT controls (**D**) and *ahi1* morphants (**E**, **F**) at 72hpf. In *ahi1* morphants there is hydrocephalus (asterisk, **E**, **F**) and expanded notochord (midline diameter 52μm in *ahi1* morphants, compared to 34μm in WT controls. Scale bar = 50μm. hpf, hours post fertilisation; N, notochord.

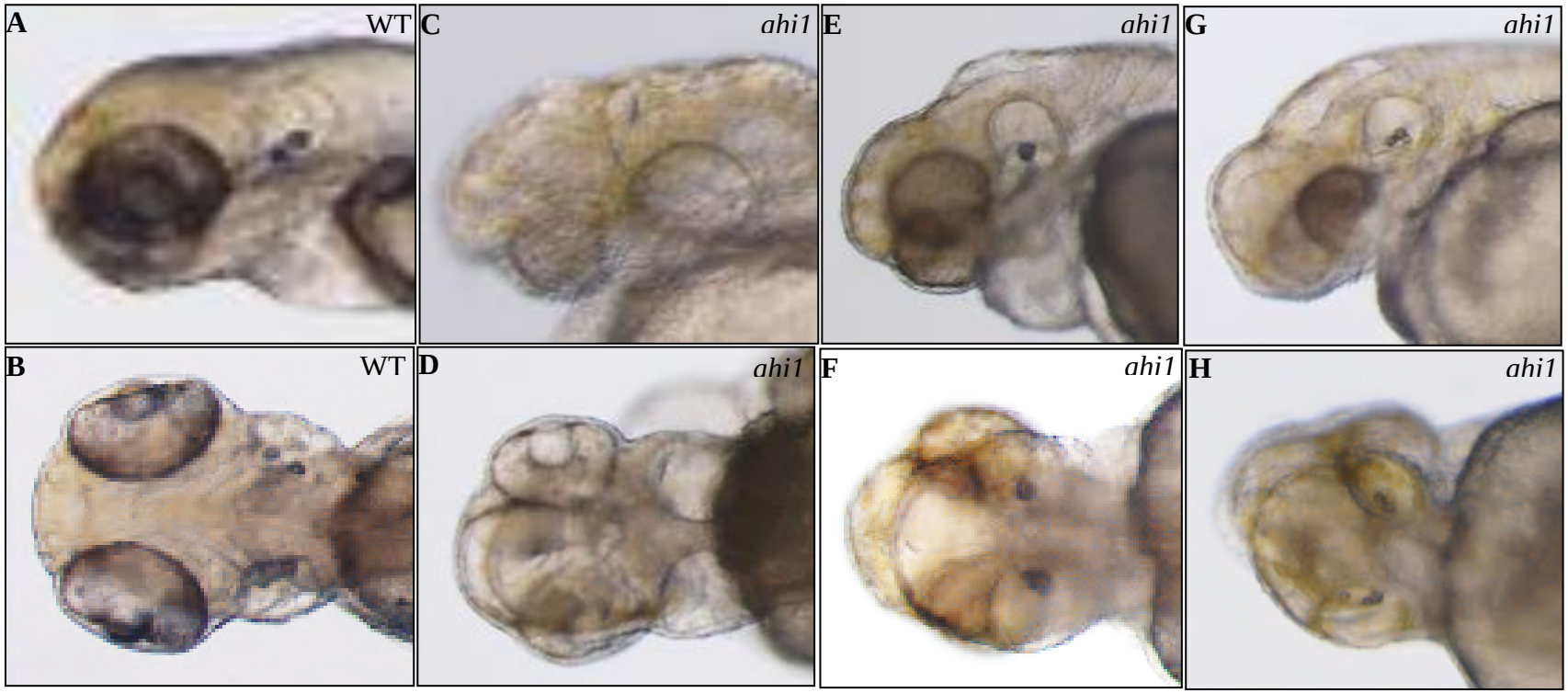

Figure 3.14 *ahi1* knockdown induces abnormal ear development with altered number of otoliths in the otic vesicle of zebrafish embryos

Light microscopy lateral (**A**, **C**, **E**, **G**) and dorsal (**B**, **D**, **F**, **H**) images of the head of zebrafish embryos focusing on the otic vesicles (developmental ear) at 72hpf. Uninjected wild type (WT) control embryos have 2 otoliths in each otic vesicle (**A**, **B**), whilst *ahi1* morphants have either no otoliths and an empty otic vesicle (**C**, **D**), a single otolith (**E**, **F**), or three otoliths (left otic vesicle **G**, **H**). hpf, hours post fertilisation.

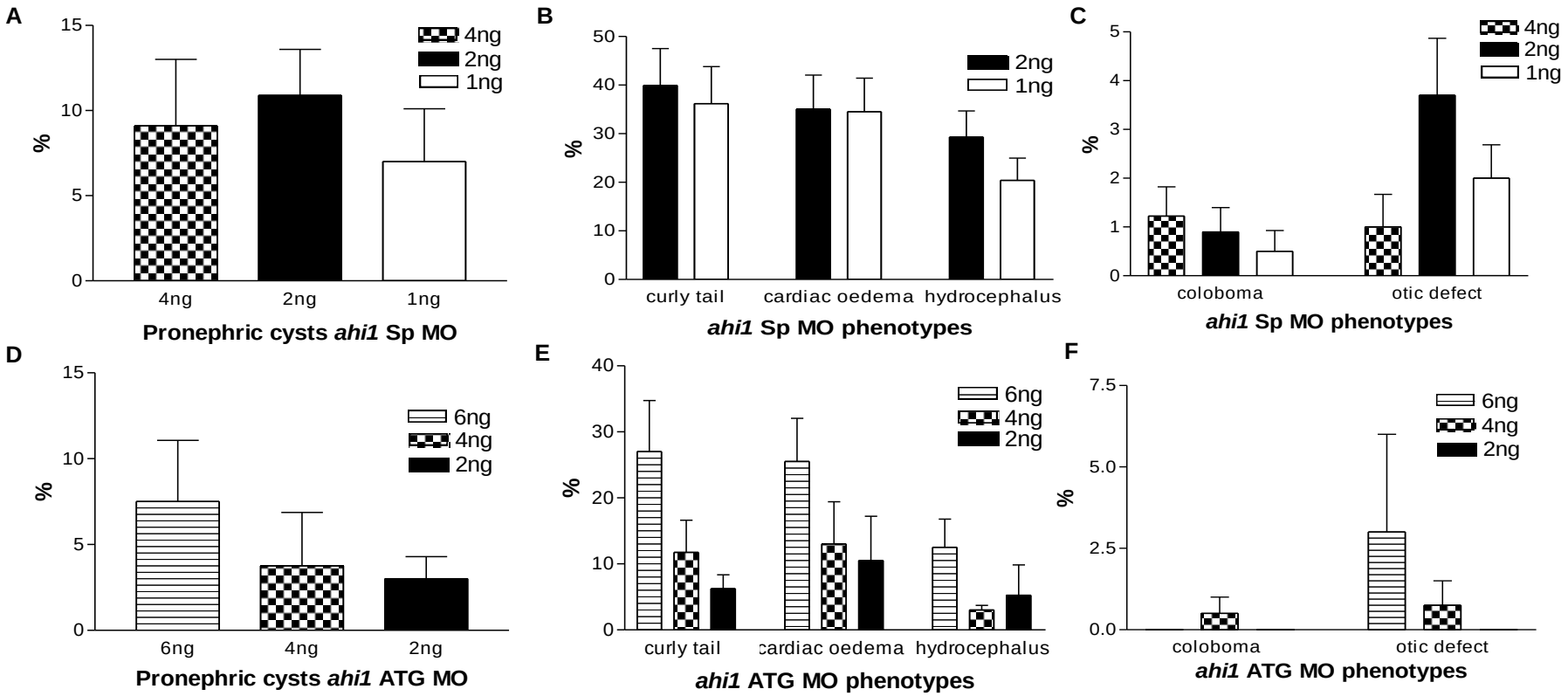

Figure 3.15 Quantification of abnormal phenotypes at 72hpf following injection with *ahi1* splice or translation blocking MO
Data are displayed as mean ± SEM. The percentage frequency of each abnormal phenotype was higher following injection of a lower dose of *ahi1* splice (Sp) MO (**A**-**C**), compared to following injection of an equivalent dose of *ahi1* translation (ATG) MO (**D**-**F**). With *ahi1* Sp MO knockdown, there was a dose dependent effect on the frequency of curly tail, cardiac oedema, hydrocephalus and coloboma (**B**, **C**). Following *ahi1* ATG MO knockdown, there was a dose dependent effect on the frequency of pronephric cysts, curly tail, cardiac odema and otic defects (**D**-**F**). The total number of zebrafish embryos phenotyped at 72hpf following *ahi1* Sp MO were 1498 and following *ahi1* ATG MO were 458. hpf, hours post fertilisation; MO, morpholino oligonucleotide.

Figure 3.16 Exclusion of off-target effects and confirmation of specificity of phenotype with *ahi1* MO knockdown

Lateral views of zebrafish embryos 72 hours post fertilisation. Wild type (WT) uninjected (**A**), embryos injected with *p53* MO alone (**B**) and embryos injected with mouse *Ahi1* mRNA alone (**E**), were morphologically normal. Embryos co-injected with *p53* MO and *ahi1* splice (**C**) or translation blocking (**D**) MOs continued to develop a morphant phenotype including hydrocephalus (**C**, (*)), pronephric cysts (**D**, arrowhead) and altered number of otoliths (**C**, arrow), and excludes the possibility of off-target effects. Co-injecting mouse *ahi1* mRNA with *ahi1* splice blocking MO rescued embryos to a normal phenotype (**F**), confirming the specificity of targeted *ahi1* MO knockdown. MO, morpholino oligonucleotide.

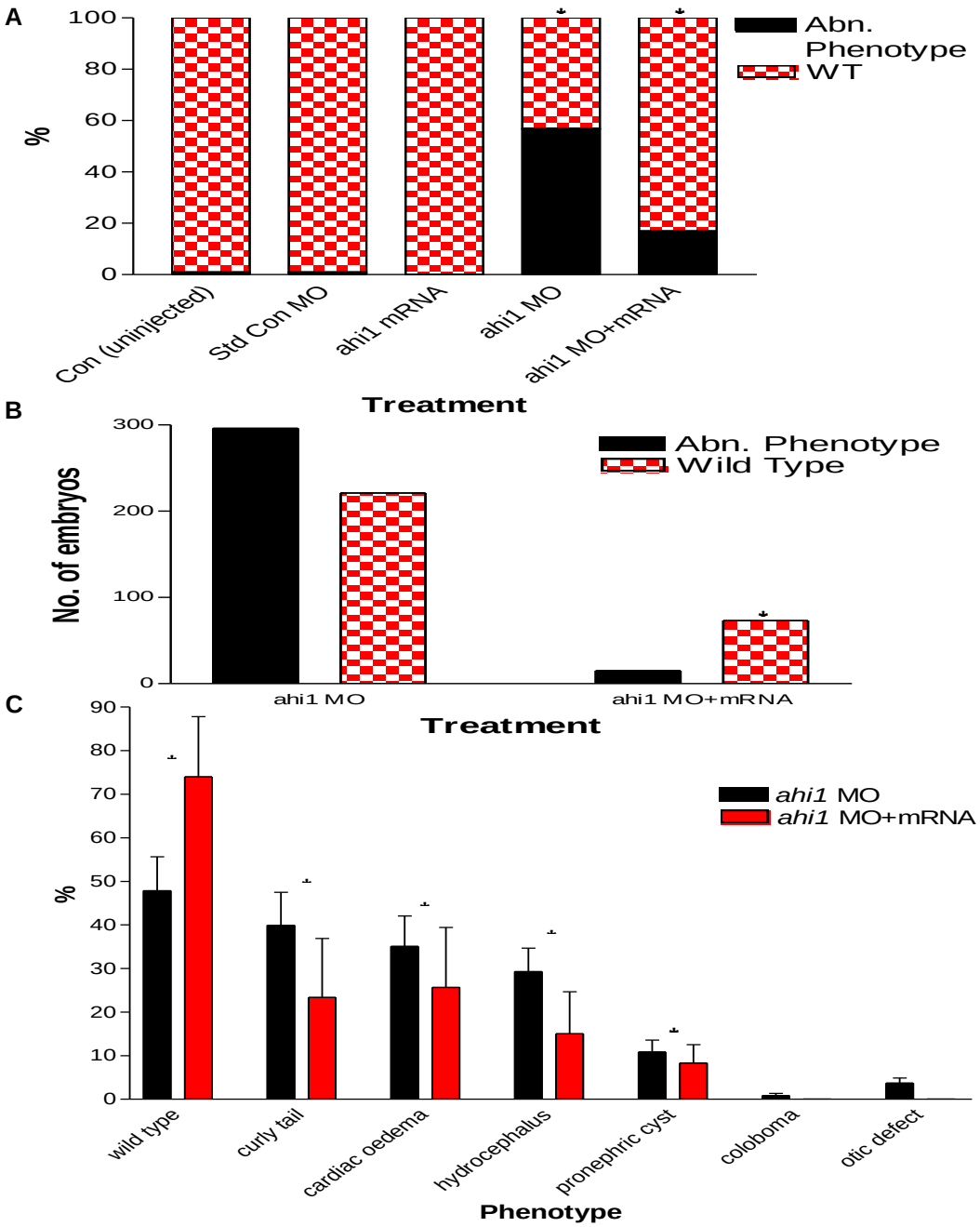

Figure 3.17 Rescue of *ahi1* morphant phenotype following co-injection with murine *Ahi1* mRNA

(**A**) Percentage of normal wild type (WT) and abnormal morphant phenotype of embryos: uninjected (n=2699); 2ng standard control MO (n=197); 100pg murine *Ahi1* mRNA (n=117); 2-4ng *ahi1* MO (n=517); coinjection of murine *Ahi1* mRNA and 2-4ng *ahi1* MO (n=88). Rescue to WT phenotype by coinjection with 100pg murine *Ahi1* mRNA was statistically significant (*, $p < 0.0001$, chi-squared test). (**B**) Raw quantification of overall rescue from *ahi1* morphant to WT phenotype after co-injection with 100pg murine *Ahi1* mRNA was statistically significant (*, $p < 0.0001$, chi-squared test). (**C**) There was a statistically significant rescue of *ahi1* morphants to the WT phenotype, and reduced frequency of anomalies (curly tail, cardiac oedema, hydrocephalus, pronephric cysts) after co-injection with murine *Ahi1* mRNA (*, $p < 0.0001$, chi-squared test). Data are % mean ± SEM. MO, morpholino oligonucleotide.

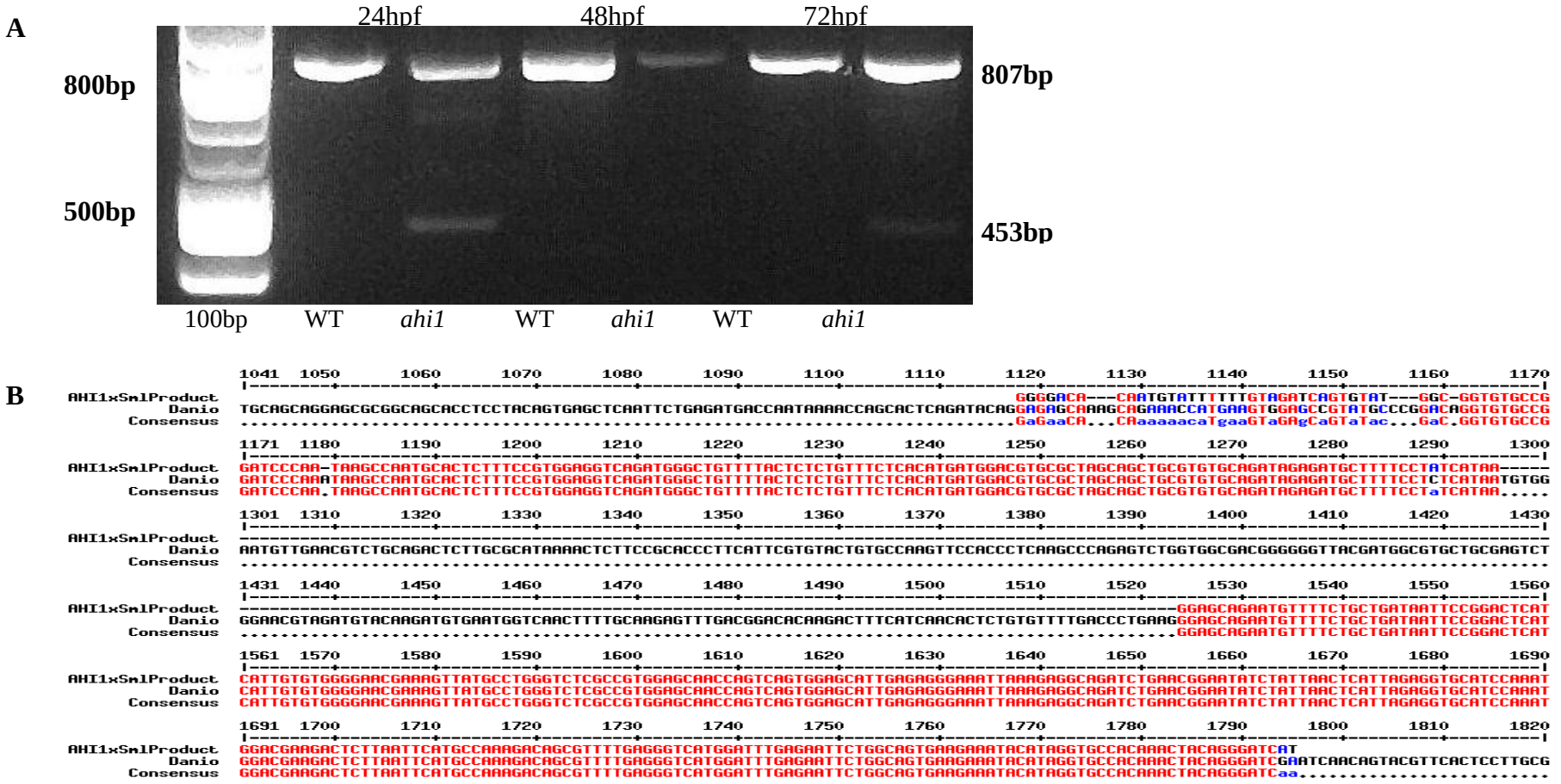

Figure 3.18 Evidence of *ahi1* splice MO knockdown by RT-PCR and direct sequencing

(**A**) RT-PCR of single embryos at 24, 48 and 72hpf following *ahi1* splice MO knockdown reveals a smaller RT-PCR product (white arrowhead) compared to uninjected wild type (WT) control embryos. The normal RT-PCR product of 807bp is maximally reduced in *ahi1* morphants at 48hpf, with recovery at 72hpf. (**B**) Direct sequencing of the smaller product (453bp) in *ahi1* morphants identifies direct skipping of exon 8 and introduction of a premature stop codon. bp, base pairs; hpf, hours post fertilisation.

C

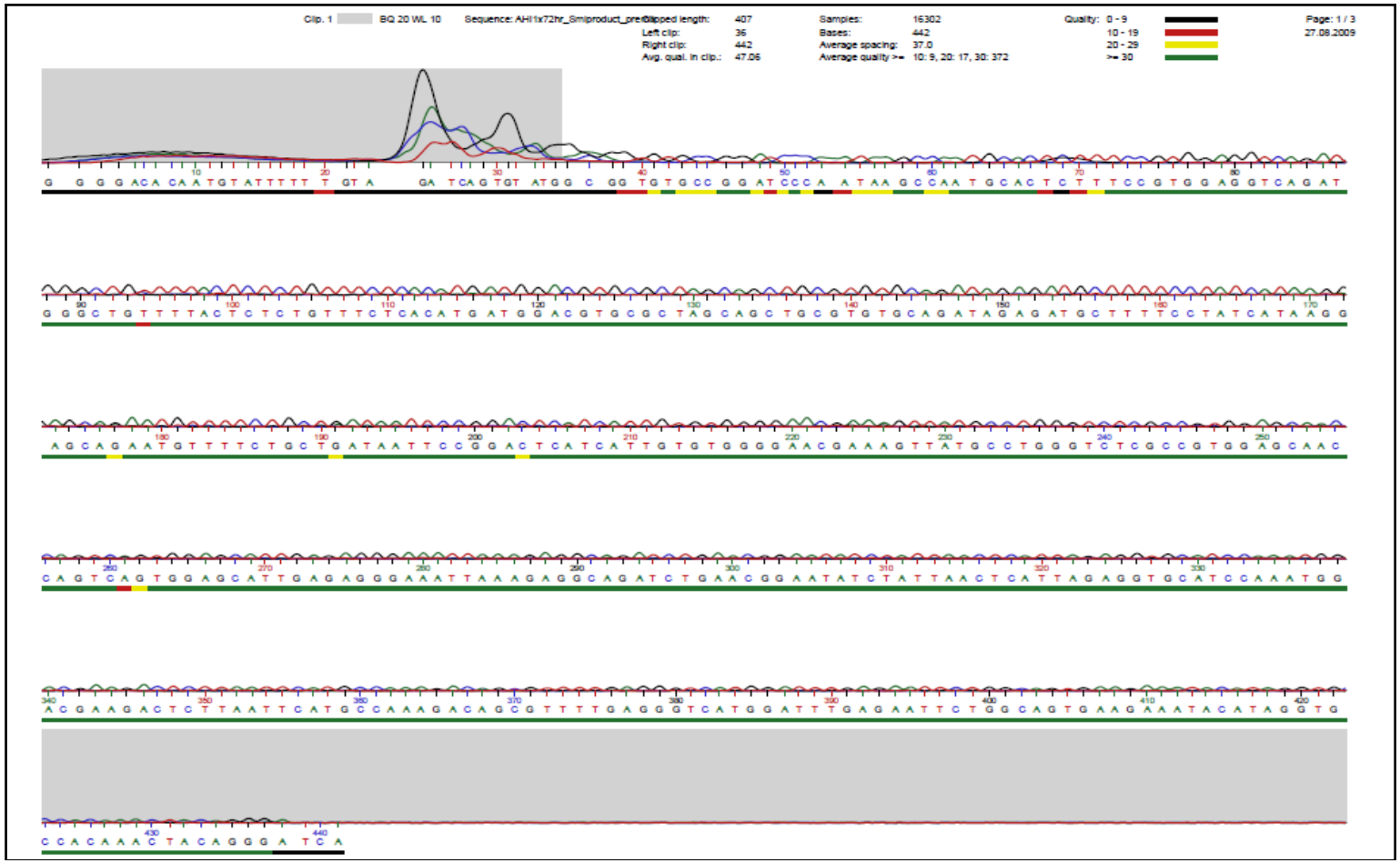

Figure 3.18 continued (C) Evidence of *ahi1* splice MO knockdown by direct sequencing
Chromatogram showing good quality of sequencing of smaller *ahi1* product at 72hpf. hpf, hours post fertilisation; MO, morpholino oligonucleotide.

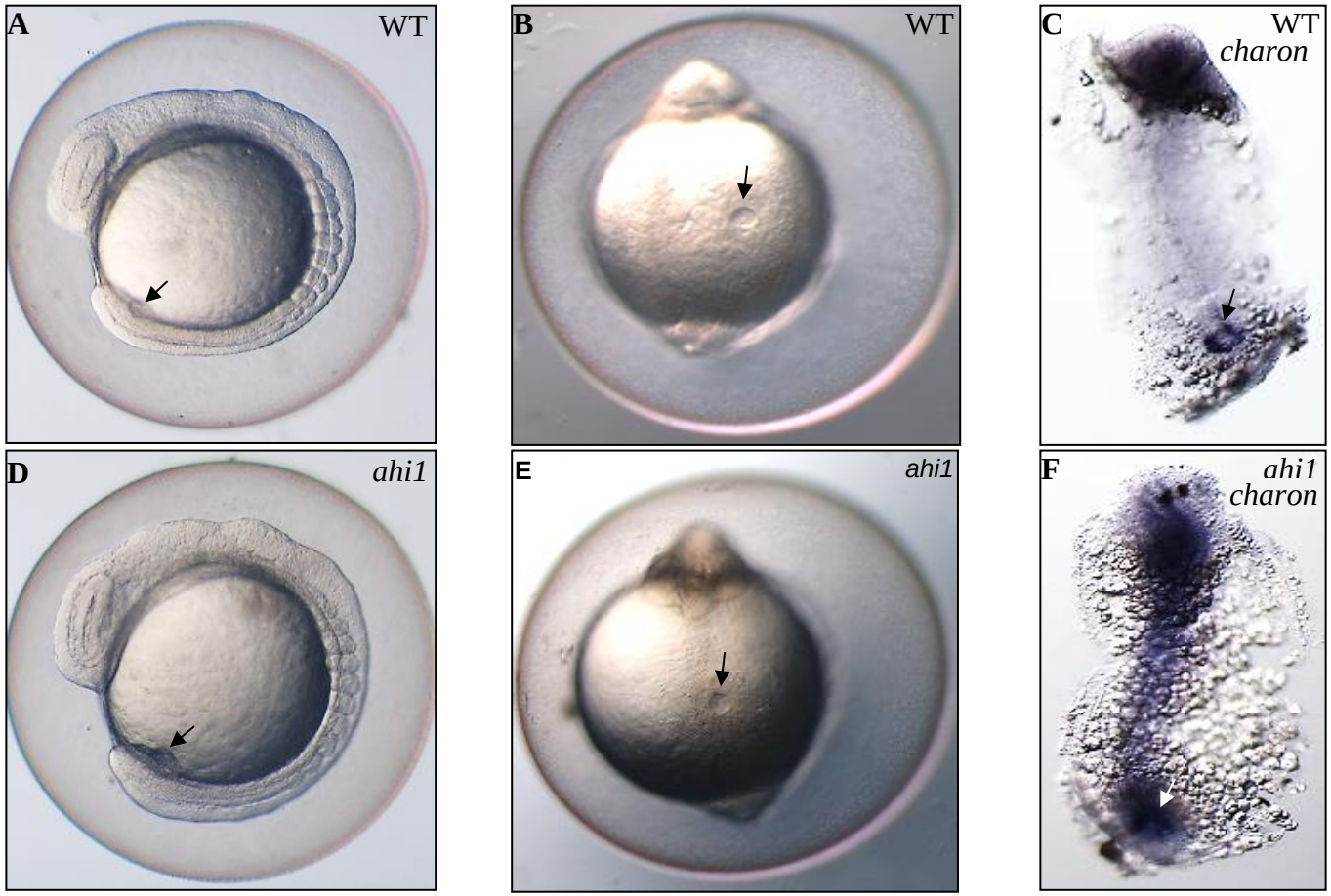

Figure 3.19 The gross morphology of Kupffer's vesicle is preserved in *ahi1* MO injected embryos
Images of uninjected wild type (WT) control (**A**-**C**) and *ahi1* MO injected (**D**-**F**) golden zebrafish embryos at the 8-10 somite stage to illustrate Kupffer's vesicle (KV, arrowed). Both lateral (**A**, **D**) and dorsal (**B**, **E**) light microscopy images of live embryos at the 8-10 somite stage confirm the presence of KV in both WT (**A**, **B**) and *ahi1* MO injected (**D**, **E**) embryos. A *charon in situ* hybridisation probe is expressed in the region around KV, confirming its presence in both WT controls (**C**) and *ahi1* MO injected embryos (**F**). MO, morpholino oligonucleotides.

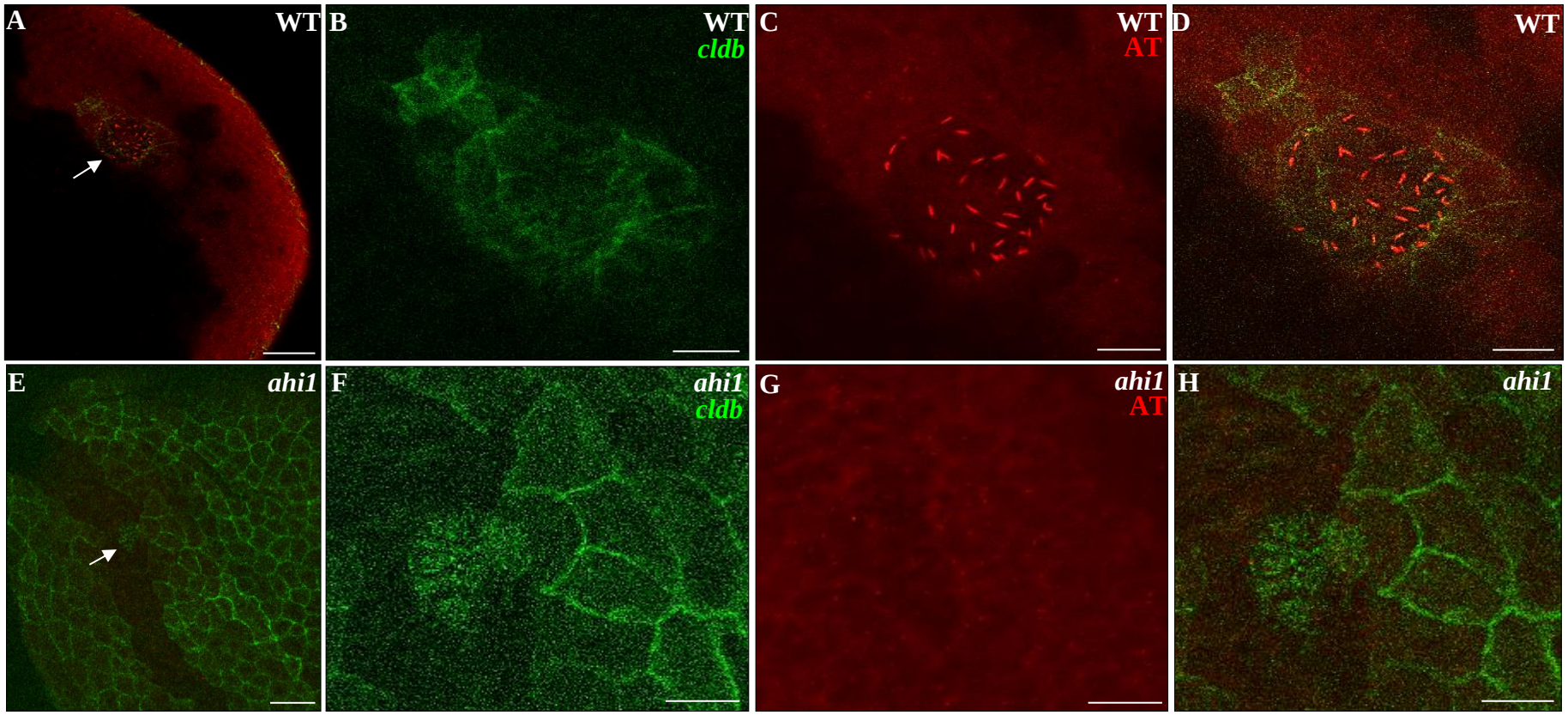

Figure 3.20 Loss of cilia from Kupffer's vesicle in *ahi1* MO injected embryos

Confocal microscopy images of *cldnb*:Lyn-GFP zebrafish embryos following fixation at the 8-10 somite stage and fluorescent immunostaining using anti-acetylated tubulin (AT, red) to study cilia in Kupffer's vesicle (KV). Overlay images using 20x objective (KV arrowed, **A**, **E**, scale bar = 50µm) and higher magnification (zoom of 3) showing individual (**B**, **C**, **F**, **G**, scale bars = 20µm) and overlay (**D**, **H**, scale bars = 20µm) images. Uninjected wild type (WT, **A-D**) control embryos show *cldnb*:Lyn-GFP expression in an organised pattern at epithelial cell-cell junctions within KV (**B**) and apical cilia (red, **C**) extending from cells lining KV. *ahi1* MO injected embryos (**E-H**) have disorganised expression of *cldnb*:Lyn-GFP (**F**) and loss of cilia (**G**) from KV. MO, morpholino oligonucleotide.

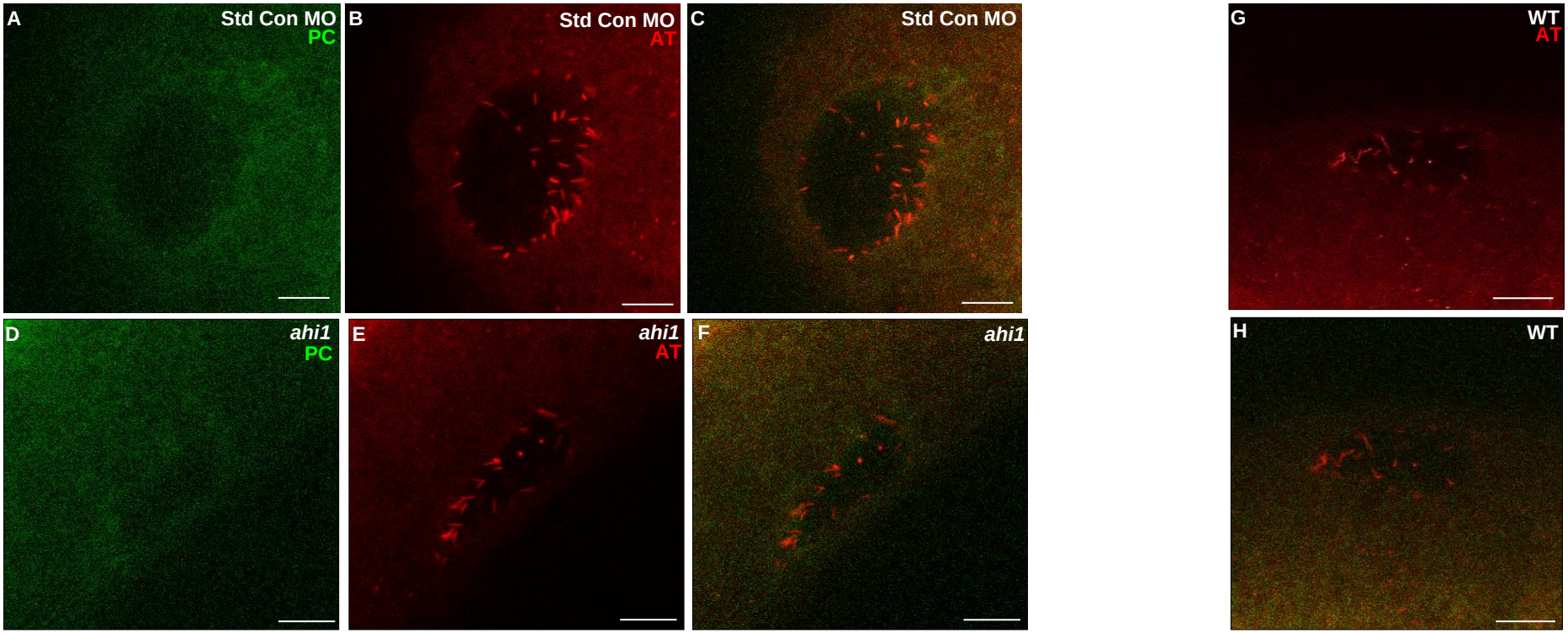

Figure 3.21 Cilia remain present in Kupffer's vesicle in Standard Control MO injected embryos and some *ahi1* MO injected embryos
Confocal microscopy images of *cldnb*:Lyn-GFP zebrafish embryos following fixation at the 8-10 somite stage and double fluorescent immunostaining using anti-acetylated tubulin (AT, red) and pericentrin (PC, green) to study cilia and centrosomes respectively in Kupffer's vesicle (KV). Images are standard control MO injected (Std Con, **A**-**C**), *ahi1* MO injected (**D**-**F**) and uninjected wild type (WT, **G**, **H**) for comparison. Individual green channel images (**A**, **D**) fail to show discrete centrosome staining, KV is represented as a dark lumen. Individual red channel images (**B**, **E**, **G**) show staining of cilia at KV in Std Con (**B**), some *ahi1* (**E**) MO injected embryos and WT (**G**). Overlay fluorescent images (**C**, **F**, **H**) are shown. All images were taken using a 20x objective and zoom of 3, scale bars = 20µm. GFP, green fluorescent protein; MO, morpholino oligonucleotide.

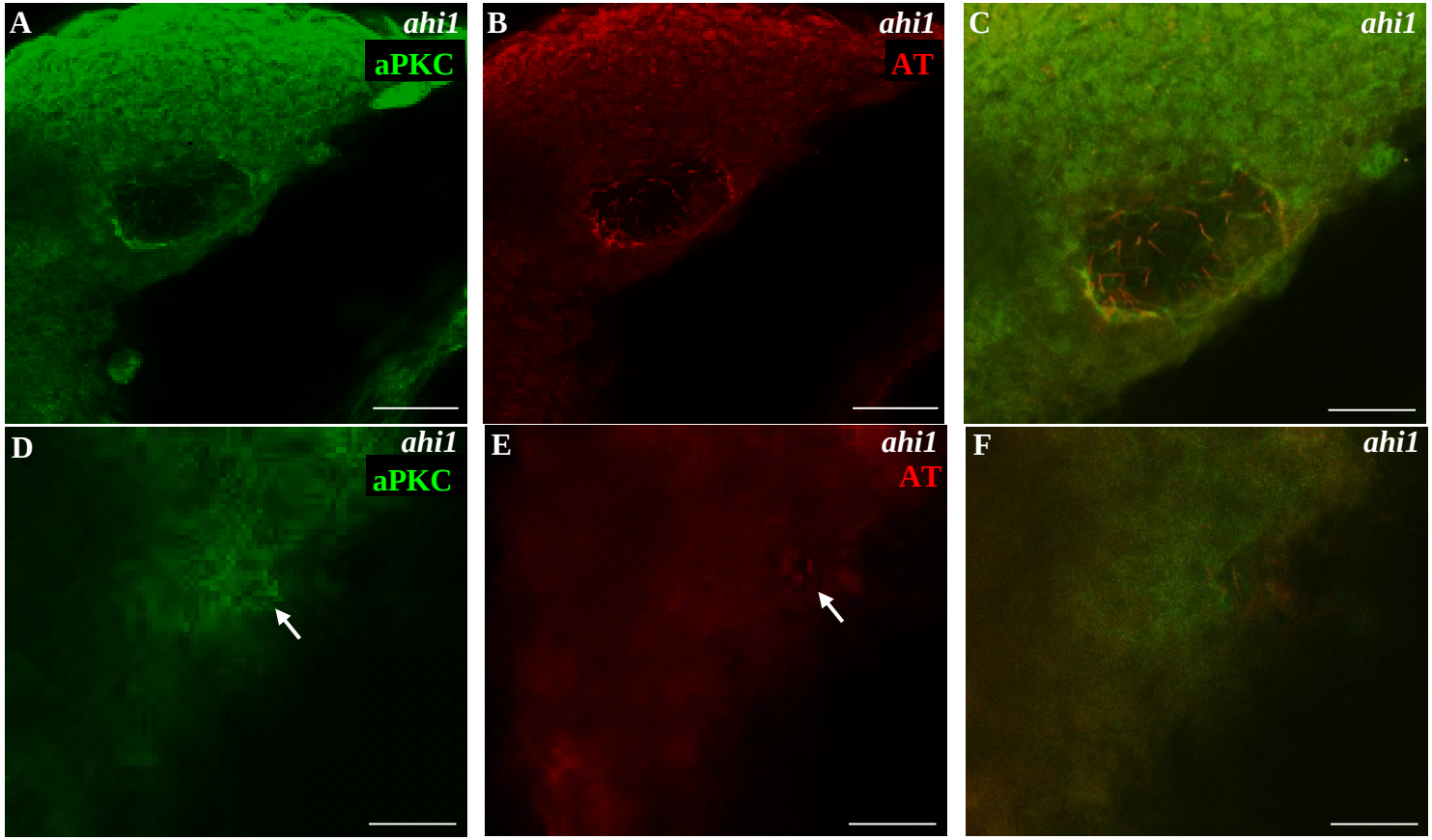

Figure 3.22 Variable spectrum of disruption to the development of Kupffer's Vesicle in *ahi1* MO injected zebrafish
Confocal microscopy images of golden zebrafish embryos injected with *ahi1* MO following fixation at the 8-10 somite stage and double fluorescent immunostaining using atypical protein kinase C (aPKC, green, **A**, **D**) antibody to label the apical membrane of KV cells and anti-acetylated tubulin (AT,red, **B**, **E**) antibody to label cilia. Whilst the development of KV appears normal in some *ahi1* MO-injected embryos (**A**-**C**), in others there is marked disruption of the KV (white arrow, **D**), with reduction in the number of cilia (white arrow, **E**). Images were taken with a 20x objective and zoom of 3. Scale bars = 20 µm. MO, morpholino oligonucleotide.

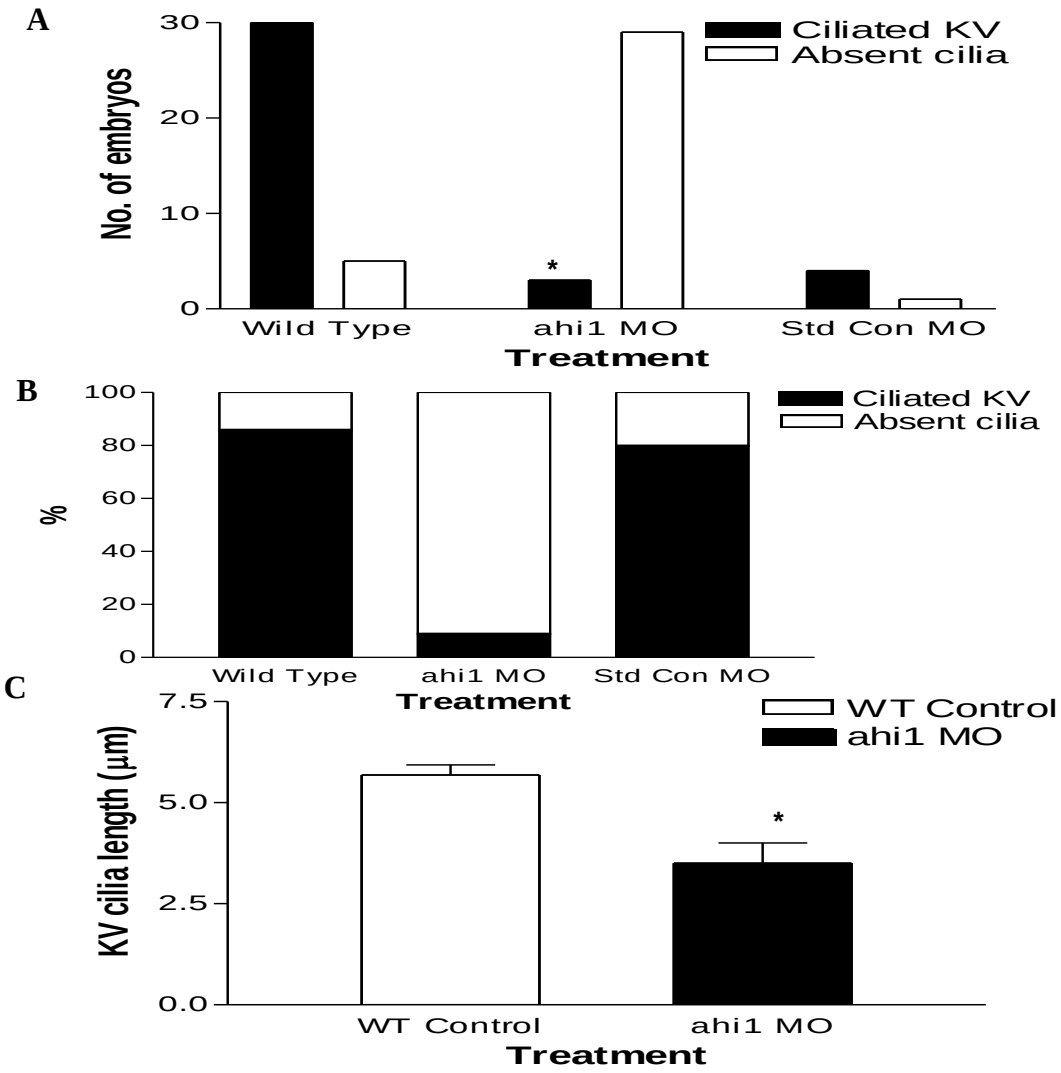

Figure 3.23 Analysis of cilia in Kupffer's vesicle of *ahi1* MO injected embryos

(**A**) Quantification of KV phenotype, whether ciliated or not, as determined by confocal microscopy of embryos fixed at 8-10 somite stage and labelled with anti-acetylated tubulin antibody to detect cilia. *ahi1* MO injected embryos (n=32) had a statistically significant reduction in the number of embryos with cilia in KV (*, $p < 0.0001$ chi-squared test), compared to uninjected wild type (WT) control embryos (n=35) and embryos injected with a standard control (Std Con) MO (n=5). (**B**) Stacked bar chart showing the percentage reduction in KV with cilia in *ahi1* morphants, compared to uninjected and Std Con MO injected embryos. (**C**) Data are shown as mean ± SEM of length of cilia in in KV. Cilia in KV were significantly shorter, when present, in *ahi1* MO injected embryos (n=2, 3.50± 0.50µm), compared to uninjected WT controls (n=6, 5.68± 0.25µm) (*, p=0.0057, unpaired t-test). Simple neurite tracer (Fiji software) was used to measure the length of cilia from confocal z-stack images of embryos labelled with anti-acetylated tubulin antibody. Approximately 20 cilia in KV were measured per embryo. MO, morpholino oligonucleotide.

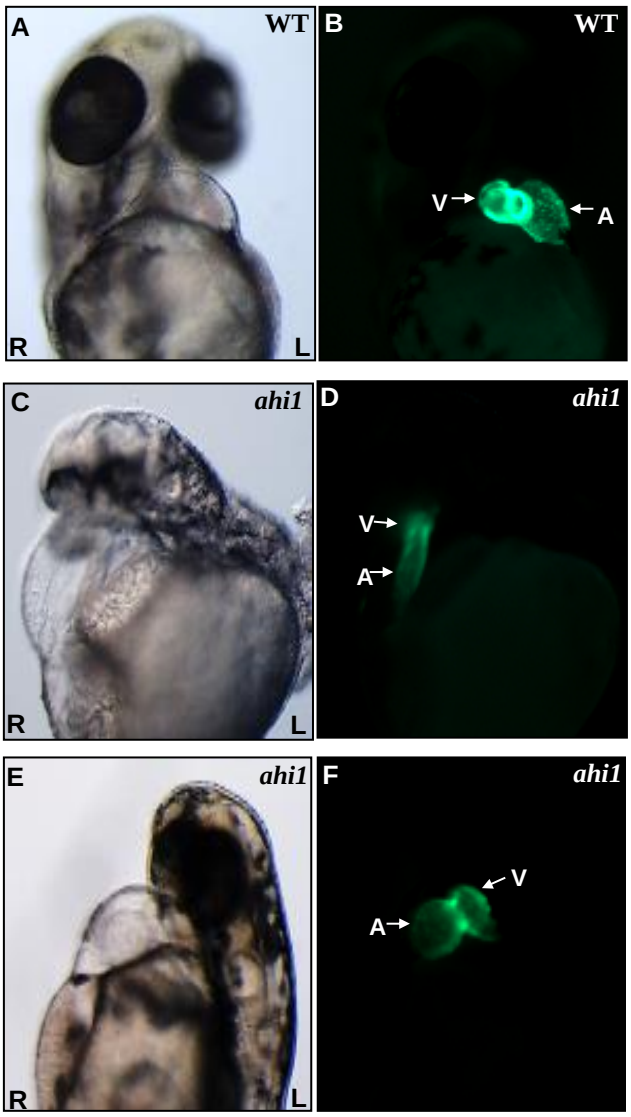

Figure 3.24 Defects in heart laterality after *ahi1* knockdown in *cmcl2*-GFP zebrafish embryos

Paired light and fluorescent microscopy ventral images of *cardiac myosin light chain 2* (*cmcl2*-GFP) zebrafish embryos at 56 hours post fertilisation (hpf) to assess cardiac looping. The normal rightward looping (D-looping) of the zebrafish heart tube leads to positioning of the single ventricle (V) to the right of the single atrium (A) as seen in uninjected wild type (WT) control embryos (**A**, **B**). In contrast, in *ahi1* morphant embryos there is either no looping of the heart tube (**C**, **D**) or a reversal of the normal pattern with leftward looping (L-looping, **E** , **F**).

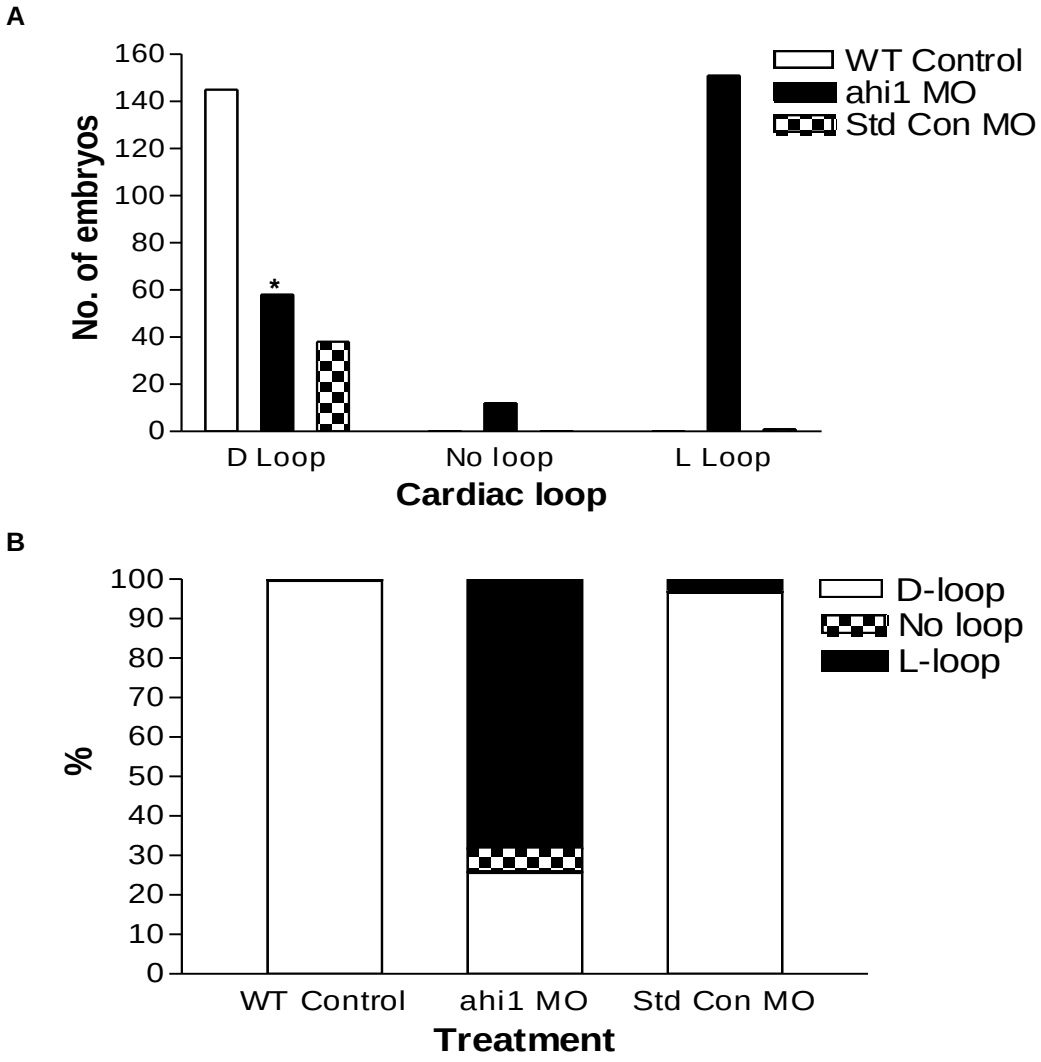

Figure 3.25 Analysis of cardiac looping reveals laterality defects in *ahi1* MO injected embryos

(**A**) Quantification of orientation of cardiac looping at 56hpf in cardiac myosin light chain 2 (*cmcl2*-GFP) embryos. Normal looping is to the right (D-looping), alternatives are no looping or looping to the left. There is a significant reduction in frequency of normal cardiac D-looping in *ahi1* MO injected embryos (n=221) (*, $p < 0.0001$, chi squared test), compared to uninjected wild type (WT) controls (n=145) and embryos injected with a standard control (Std Con) MO (n=39). (**B**) Stacked bar chart showing the percentage frequency of each cardiac looping orientation in each experimental group (D-loop, white; no loop, checked; L-loop, black). hpf, hours post fertilisation; MO, morpholino oligonucleotide.

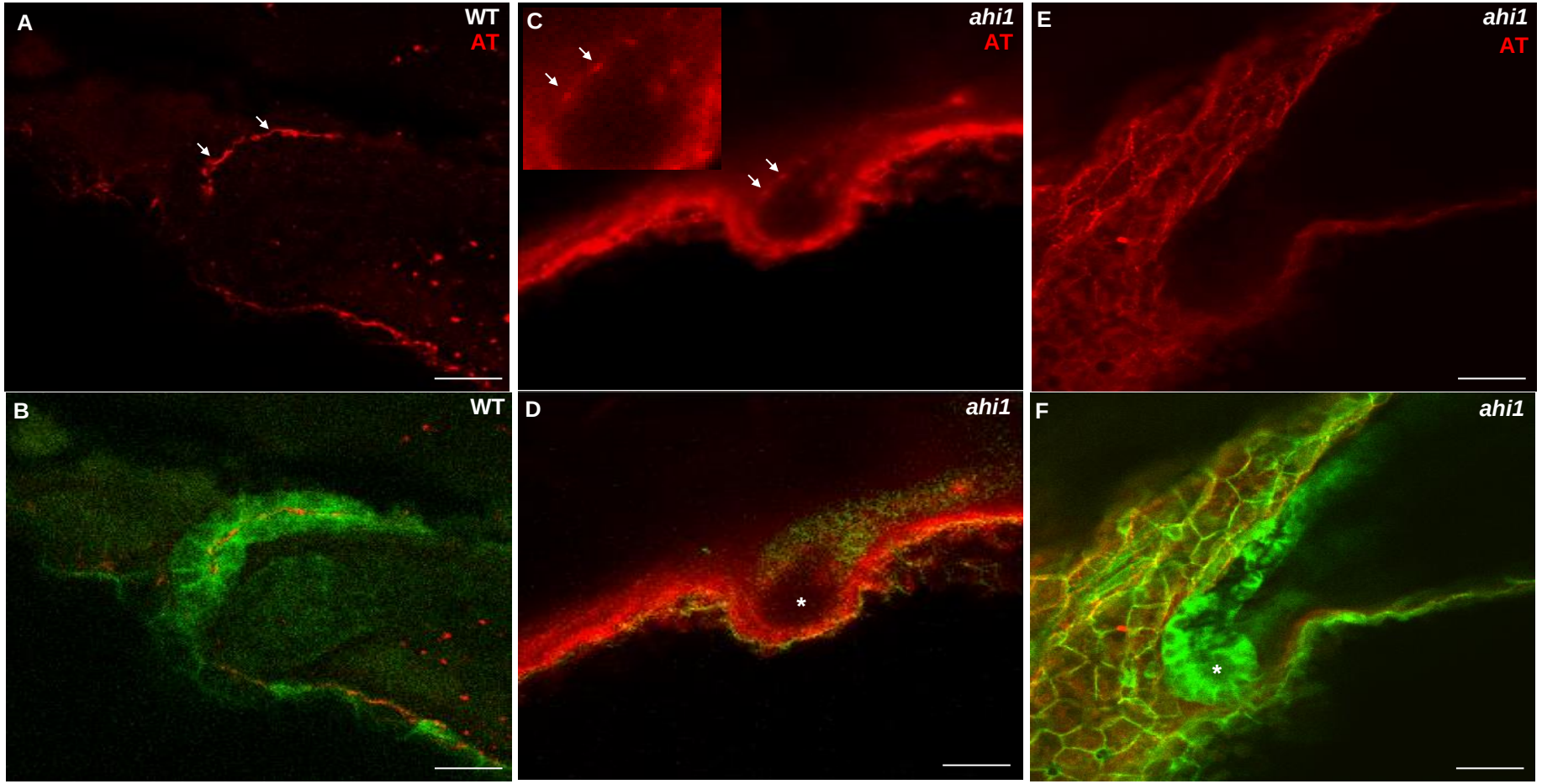

Figure 3.26 Variable spectrum of disruption to cilia at the cloaca in *ahi1* morphant zebrafish embryos

Confocal microscopy images of *claudinb:*Lyn GFP zebrafish embryos fixed at 72hpf and immunostained with anti-acetylated tubulin antibody (AT, red, **A**-**C**) to identify cilia. Uninjected wild type controls (WT, **A**, **B**) have cilia (arrows, **A**) lining the pronephros which meets at the cloaca (**B**). In *ahi1* morphants, the pronephric ducts are dilated at the cloaca (star, **D**, **F**), with variable preservation of cilia (enlarged image, arrows, **C**) or complete absence of cilia (**E**). Images were taken with a 20x objective and zoom of 3. Scale bars = 50 µm.

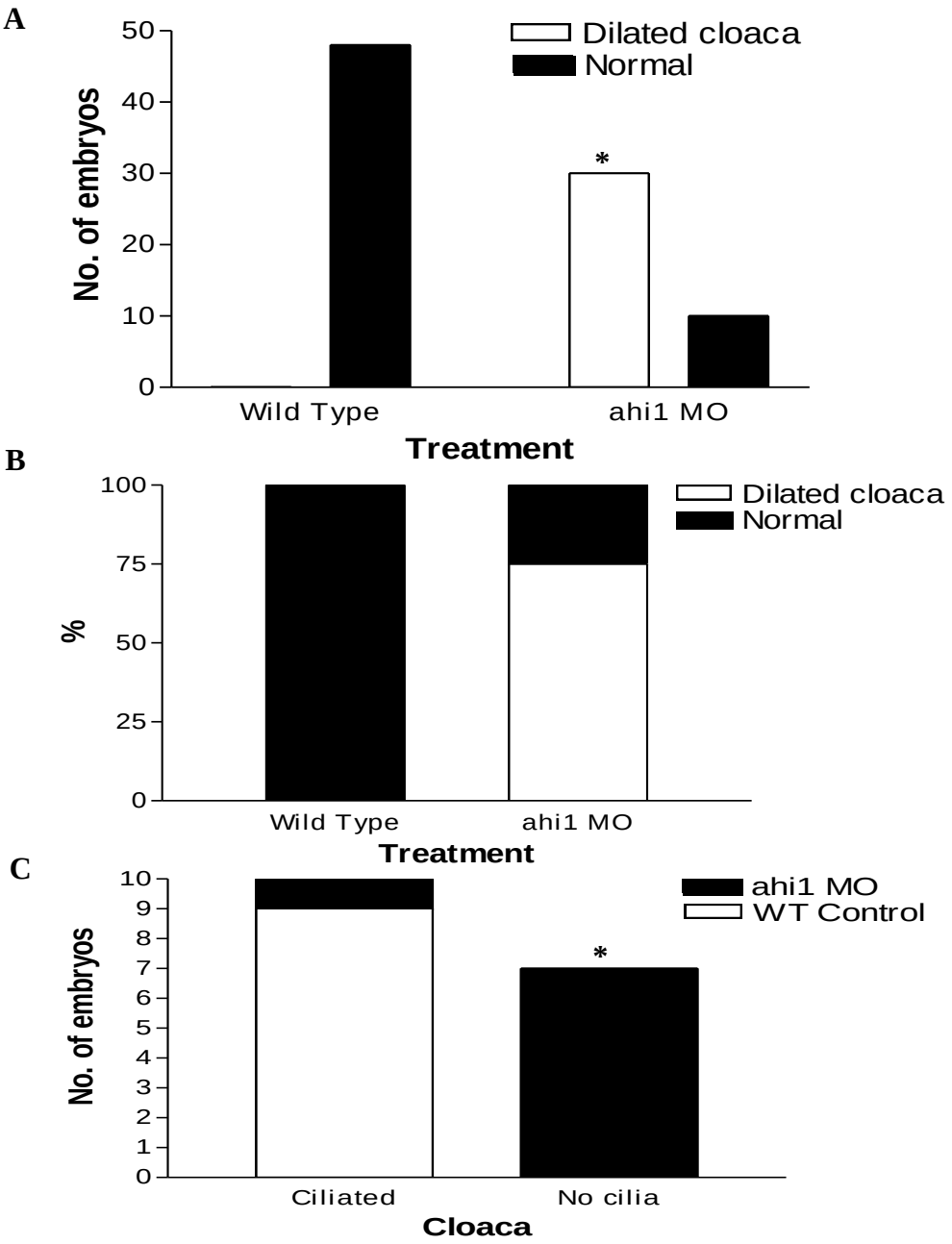

Figure 3.27 Analysis of cloaca for dilatation and cilia in *ahi1* MO injected zebrafish embryos

(**A**) Quantification of cloaca phenotype in *claudinb*:Lyn GFP zebrafish embryos at 72 hours post fertilisation (hpf) reveals that there was a statistically significant difference between *ahi1* morphants, which mostly have a dilated cloaca (n=30), compared to the normal apposed appearance of the cloaca in uninjected wild type (WT) controls (n=48, *, $p < 0.0001$ chi-squared test). (**B**) Stacked bar chart showing the percentage difference in the cloaca phenotype between *ahi1* morphants and WT zebrafish embryos. (**C**) Cilia were mainly absent from the cloaca in *ahi1* morphant (n=7) zebrafish embryos compared to WT controls (n=9, *, $p < 0.0003$ chi-squared test).

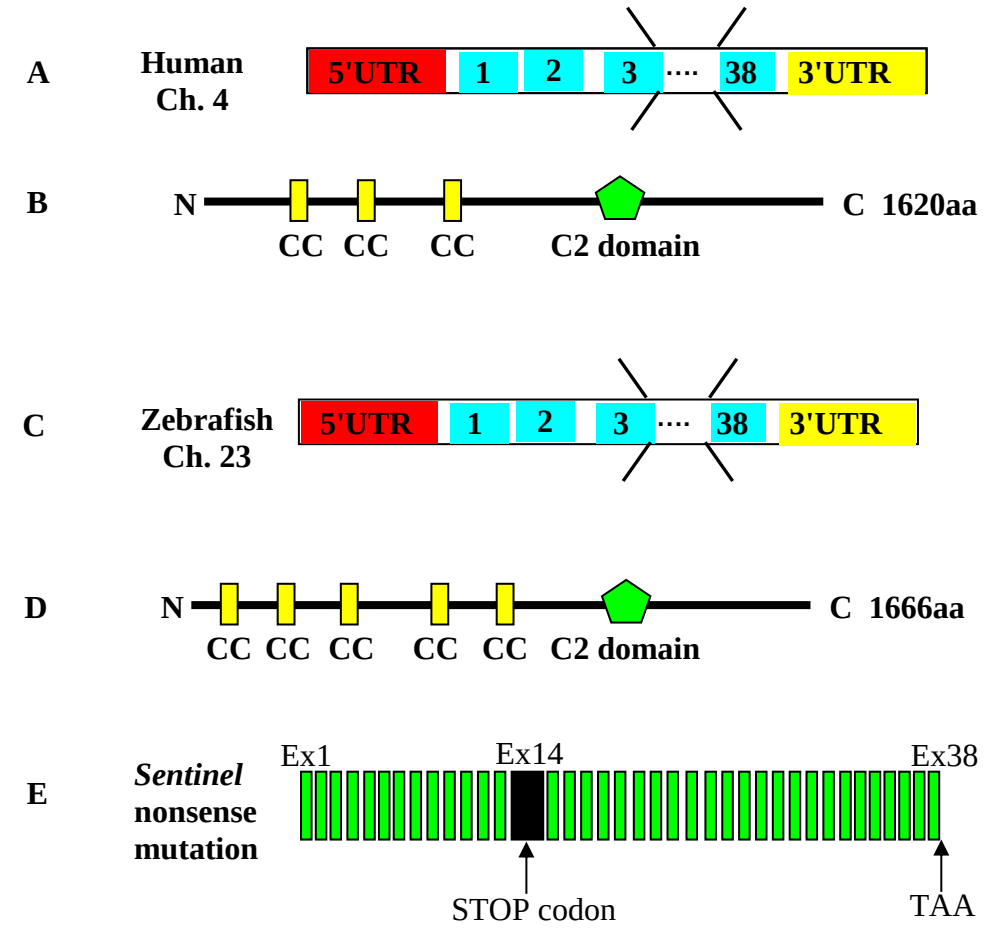

Figure 4.1 *CC2D2A* gene transcript and partial protein product structure in humans and zebrafish

(**A**) *CC2D2A* gene transcript in humans (OTTHUMT00000359906) and schematic representation of encoded protein product, coiled coil domain containing protein 2A (CC2D2A), with 3 coiled-coil domains and 1 C2 domain, consisting of 1620 amino acids (OTTHUMP00000217873) (**B**). (**C**) *cc2d2a* transcript in zebrafish (ENDSDART00000126768) and schematic representation of encoded protein product, cc2d2a (ENDSDARP00000107405) (**D**). (**E**) Schematic representation of zebrafish *cc2d2a* showing the nonsense mutation, a stop codon present in exon 14. aa, amino acids; CC, coiled coil; Ch., chromosome; C2 domain.

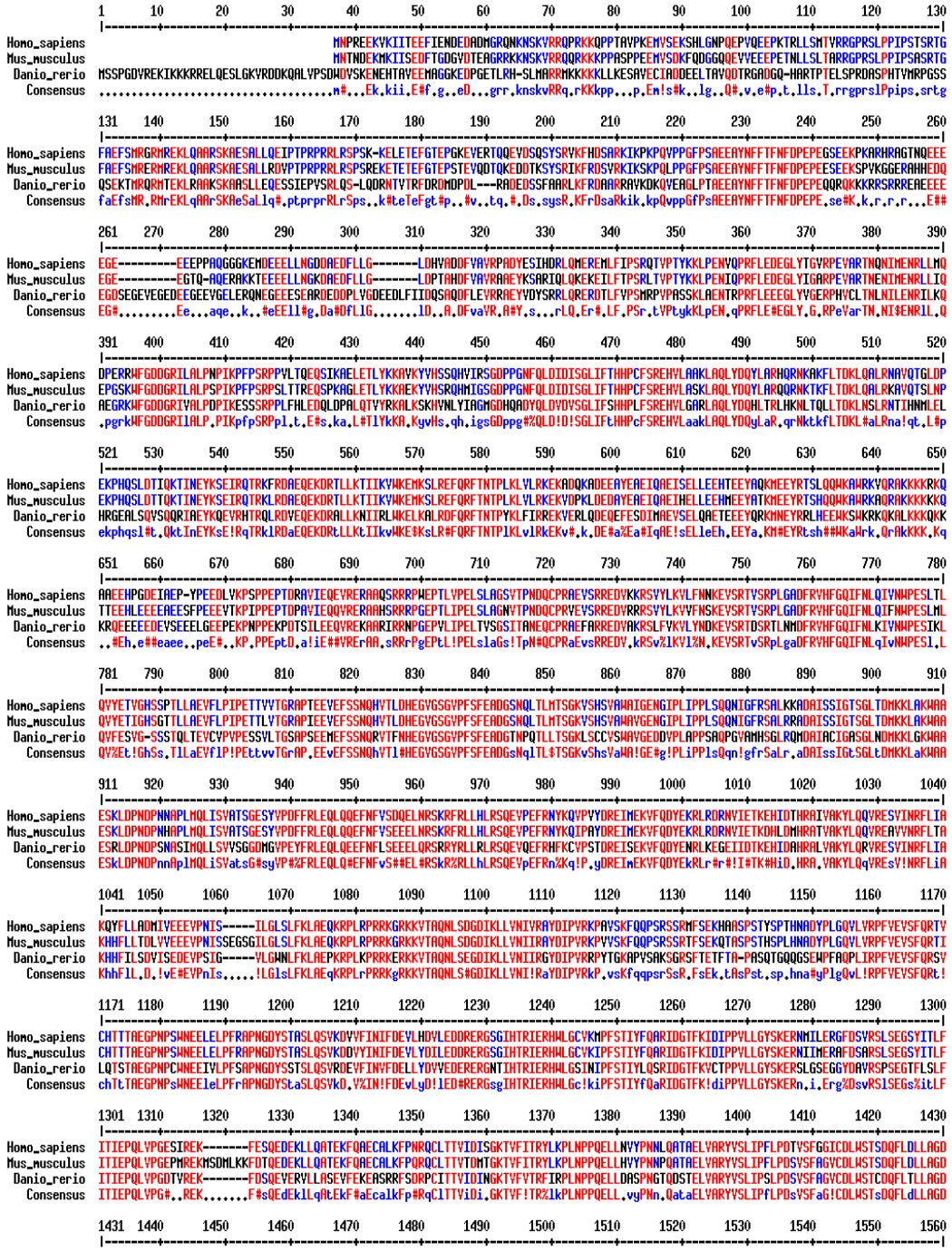

Figure 4.2 Evolutionary conservation of Cc2d2a in humans, mice and zebrafish

Cc2d2a peptide sequence alignment in humans (homo sapiens, OTTHUMP00000217873), mice (mus musculus, ENSMUSP00000048320), zebrafish (danio rerio, ENSDASP00000107405) and consensus sequence is shown (Multalin). Conservation of amino acid alignment (red font).

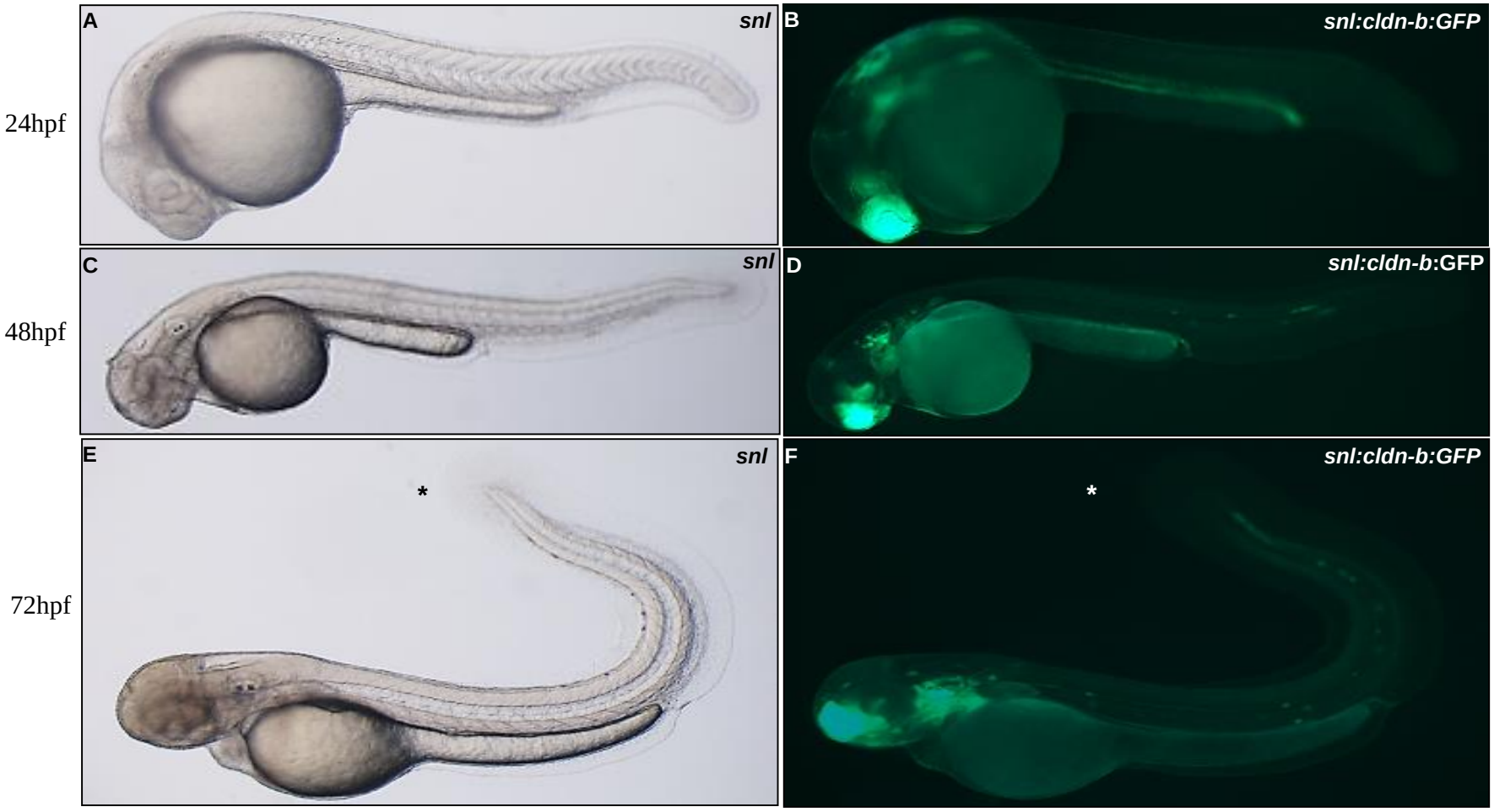

Figure 4.3 Development of *sentinel* and transgenic *sentinel:claudin-b:*Lyn-GFP zebrafish embryos
Lateral views of *sentinel* (*snl*) (**A,C,E**) and *snl:cldn-b:*GFP (**B,D,F**) zebrafish embryos at 24, 48 and 72 hours post fertilisation (hpf). The characteristic sine wave shaped tail (*****, **E-F**) of *snl* homozygous zebrafish embryos is evident at 72hpf.

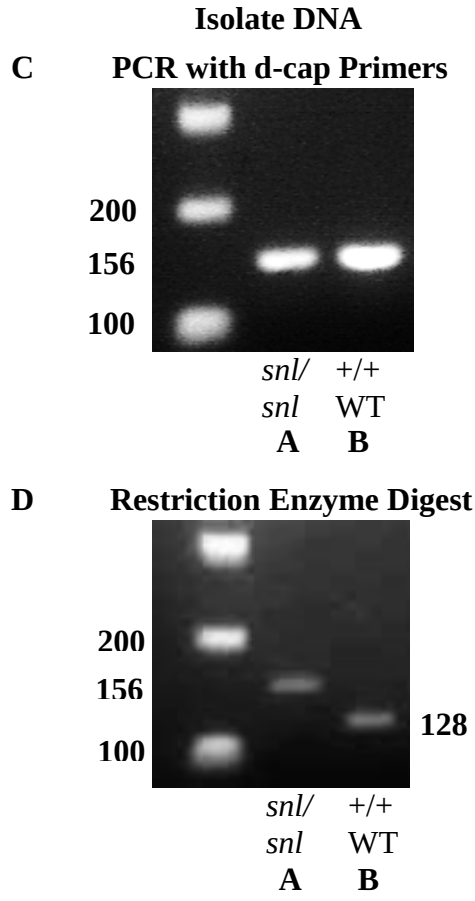

Figure 4.4 Genotyping of *sentinel* zebrafish embryos
Lateral views of presumed homozygote *sentinel* (*snl/snl*) with sine wave shaped tail (**A**) and golden uninjected wild type control (+/+ WT) (**B**) zebrafish embryos at 72hpf. DNA was isolated from each single embryo and PCR performed with dCAP primers, which introduce a restriciton enzyme recognition site into WT embryos. The agarose gel (**C**) confirms sufficient DNA for each sample (156 bp). Following a restriction enzyme digest, the gel (**D**) shows the *snl* homozygotes have a product of 156bp, whereas WT embryos are cut and have a smaller product of 128bp. This confirms the phenotype. bp, base pairs; hpf, hours post fertilisation.

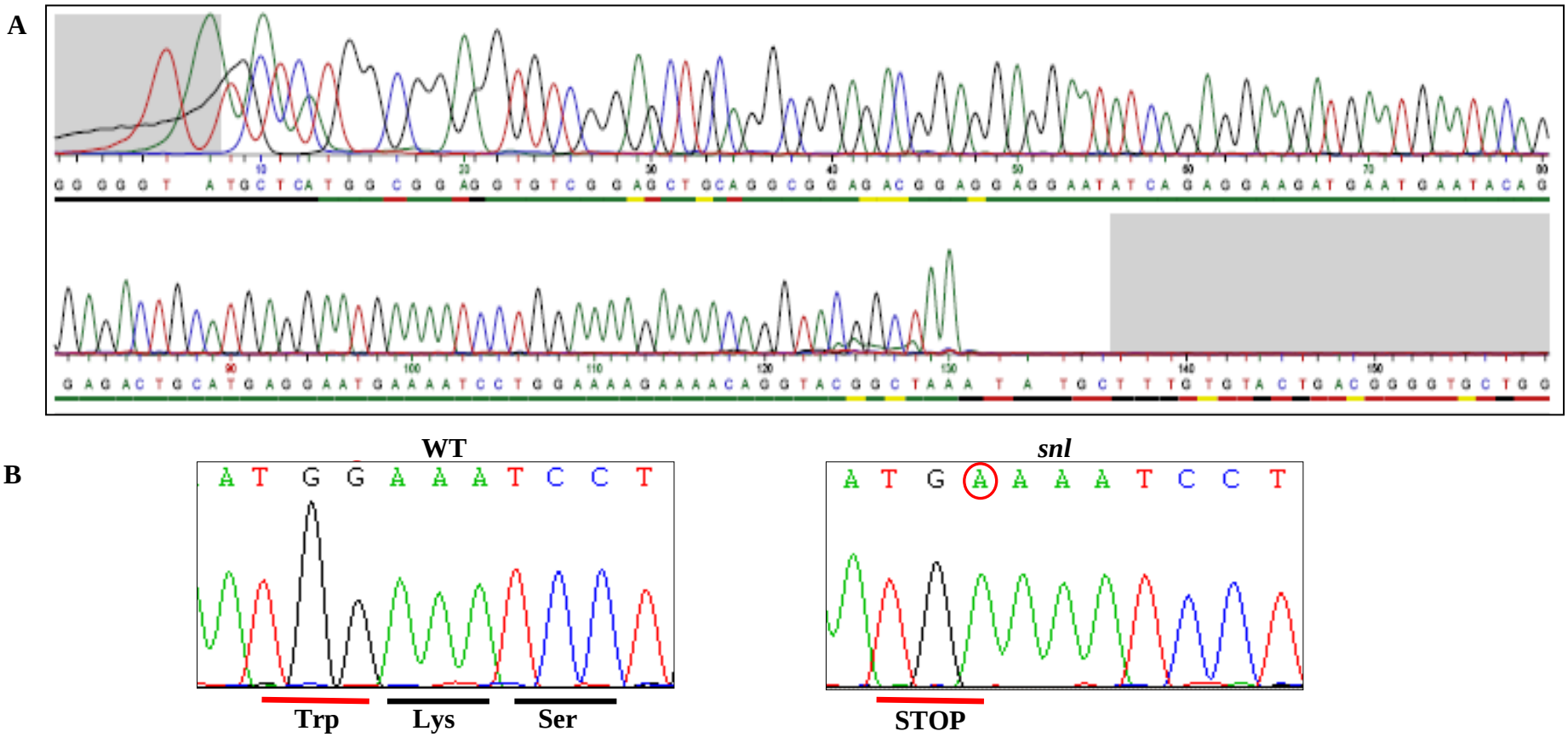

Figure 4.5 Sequencing of *sentinel* (*snl*) and uninjected wild type (WT) zebrafish embryos at 72hpf
(**A**) Chromatogram of PCR product across predicted point mutation in *snl* mutant obtained by RT-PCR of RNA at 72 hpf. Zoomed view of WT and *snl* mutant cDNA sequencing (**B**) shows there was a nonsense mutation (G>A), (circled in red in each sequence), in the *snl* homozygous embryos resulting in a trytophan changing to a premature stop codon and truncation at 498 amino acids, compared to the WT controls. hpf, hours post fertilisation; Lys, lysine; Ser, serine; STOP, stop codon; Trp, tryptophan.

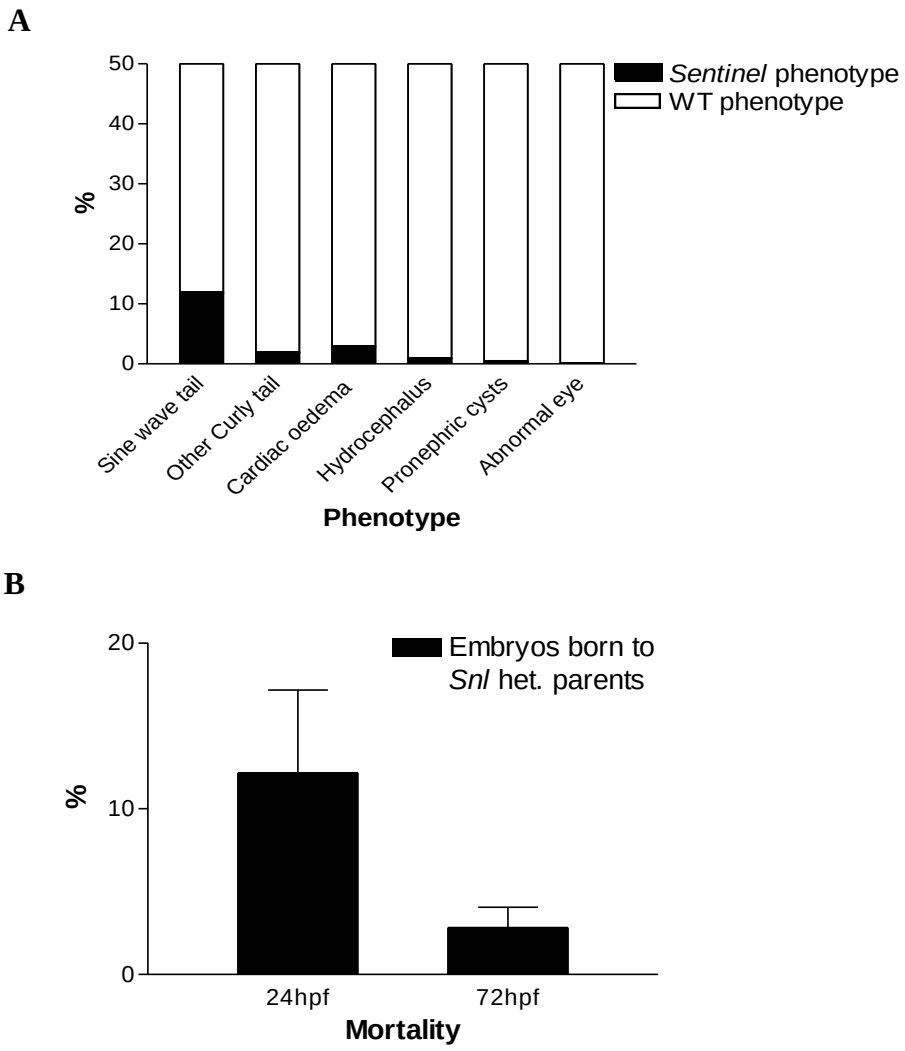

Figure 4.6 Phenotypes & Mortality rates of *sentinel* zebrafish embryos
(**A**) Quantification of the percentage (%) frequency of abnormal phenotypes at 72hpf in embryos born from two *sentinel* (*snl*) heterozygous (het) parents (n=1254). A sine wave tail phenotypically defines a *snl* embryo, however only 12% (n=153) of clutches of embryos were identified with this appearance. The low percentage of *snl* homozygotes may account for the overall low percentage of abnormal phenotypes. 2% (n=24) had a non-sine wave curly tail, 3% (n=32) had cardiac oedema, 1% (n=12) had hydrocephalus, 0.5% (n=6) had pronephric cysts and 0.2% had an abnormal eye (either coloboma or unilateral micropthalmia, n=2). A cyclops appearance was not identified in any embryos. (**B**) The percentage mortality rates at 24 (n=178) and 72 (n=35) hpf are shown as mean and standard error of the mean in embryos born from *snl* het parents. hpf, hours post fertilisation.

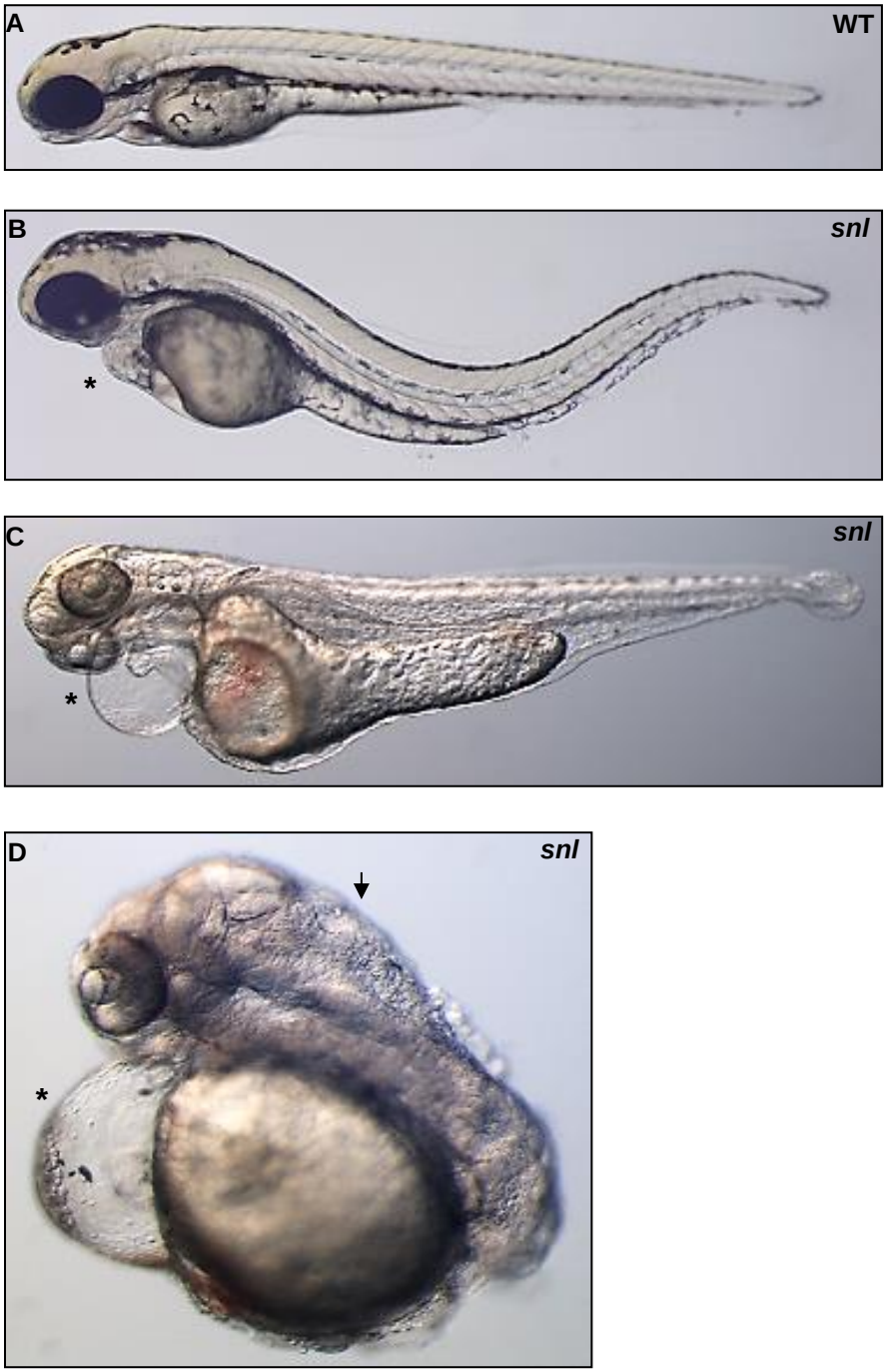

Figure 4.7 Phenotypes (Tail, Cardiac, Brain) in *sentinel* zebrafish embryos at 72hpf
The characteristic sine wave shaped tail of *sentinel* (*snl*) mutant zebrafish is shown in (**B**), compared to the normal appearance of uninjected wild type (WT) controls (**A**). The variable spectrum of severity of cardiac anomalies and oedema are highlighted (*) in **B**-**D**. Hydrocephalus is arrowed in **D**.

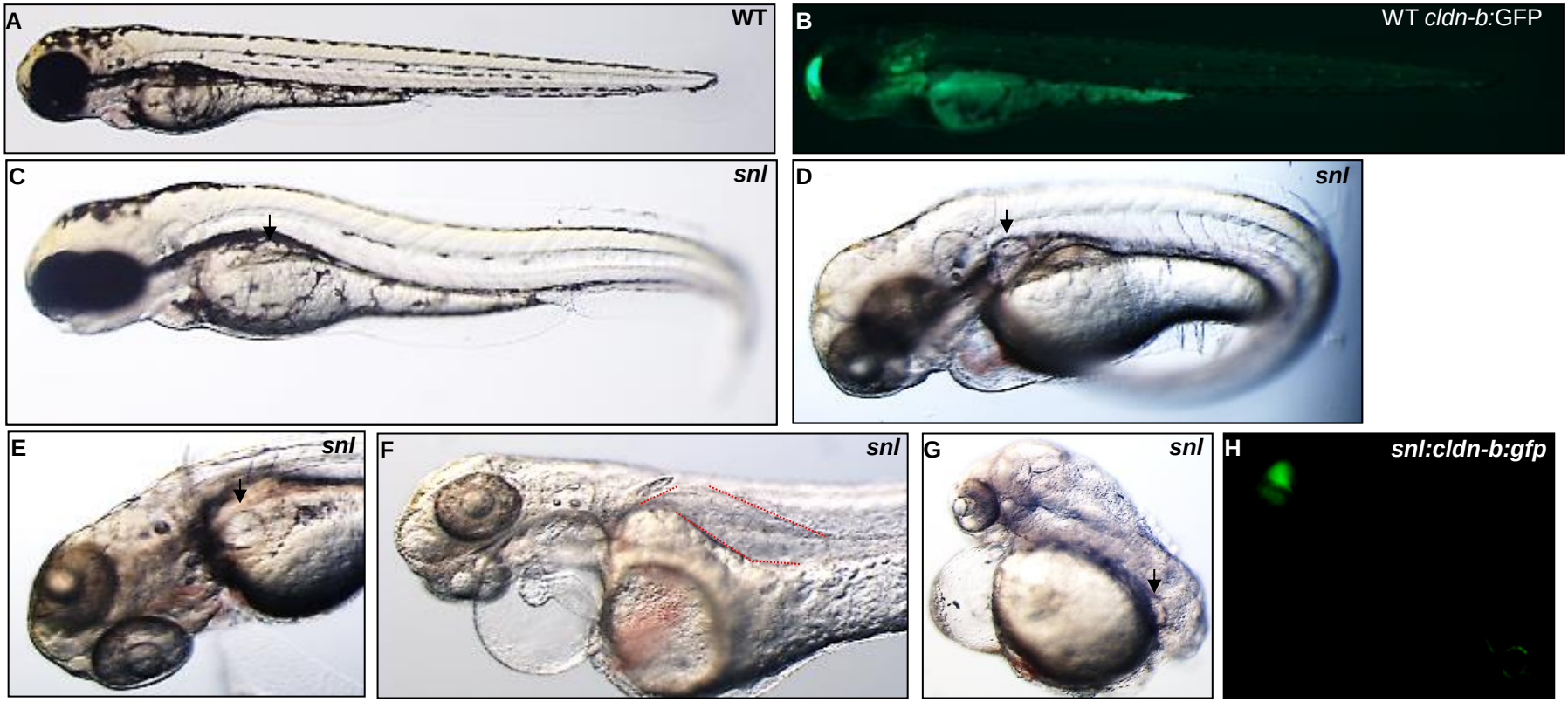

Figure 4.8 Pronephric cysts in *sentinel* and *sentinel:claudin-b:*Lyn-GFP zebrafish embryos at 72hpf
Light and fluorescent microscopy images of the normal appearance of uninjected wild type (WT) *claudin-b:*Lyn-GFP (*cldn-b:*GFP) controls (**A**, **B**), compared to *sentinel* (*snl)* and *sentinel:claudin-b:*Lyn-GFP (*snl:cldn-b:*GFP) zebrafish mutant embryos. Some *snl* mutants display proximal pronephric cysts (arrowed, lateral view (**C**, **D**), dorsal view (**E**); large cysts at the level of the proximal convuluted/straight tubule (red dotted line, **F**); distal pronephros (arrowed, **G**, **H**). The variable severity of developmental deformities in the *snl* mutants is evident.

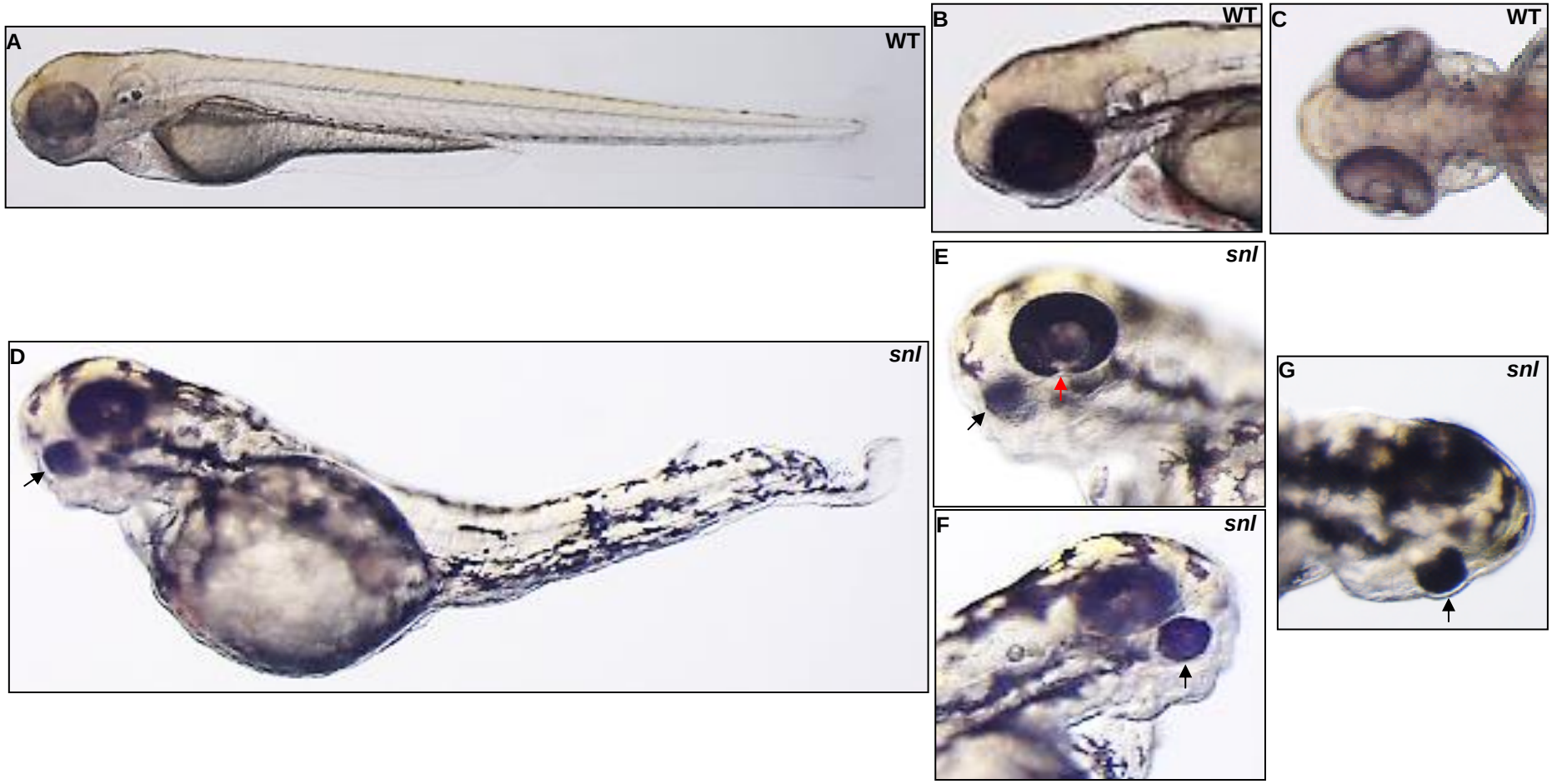

Figure 4.9 Abnormal eye development in *sentinel* zebrafish embryos at 72hpf
Light microscopy, lateral and dorsal, images focusing on the eyes of an uninjected wild type (WT, **A**-**C**) and a *sentinel* (*snl*, **D**-**G**) mutant zebrafish embryo. In the *snl* mutant embryo, there is abnormal eye development with both unilateral microphthalmia (black arrows, **D**-**G**) and a coloboma (red arrow, **E**).

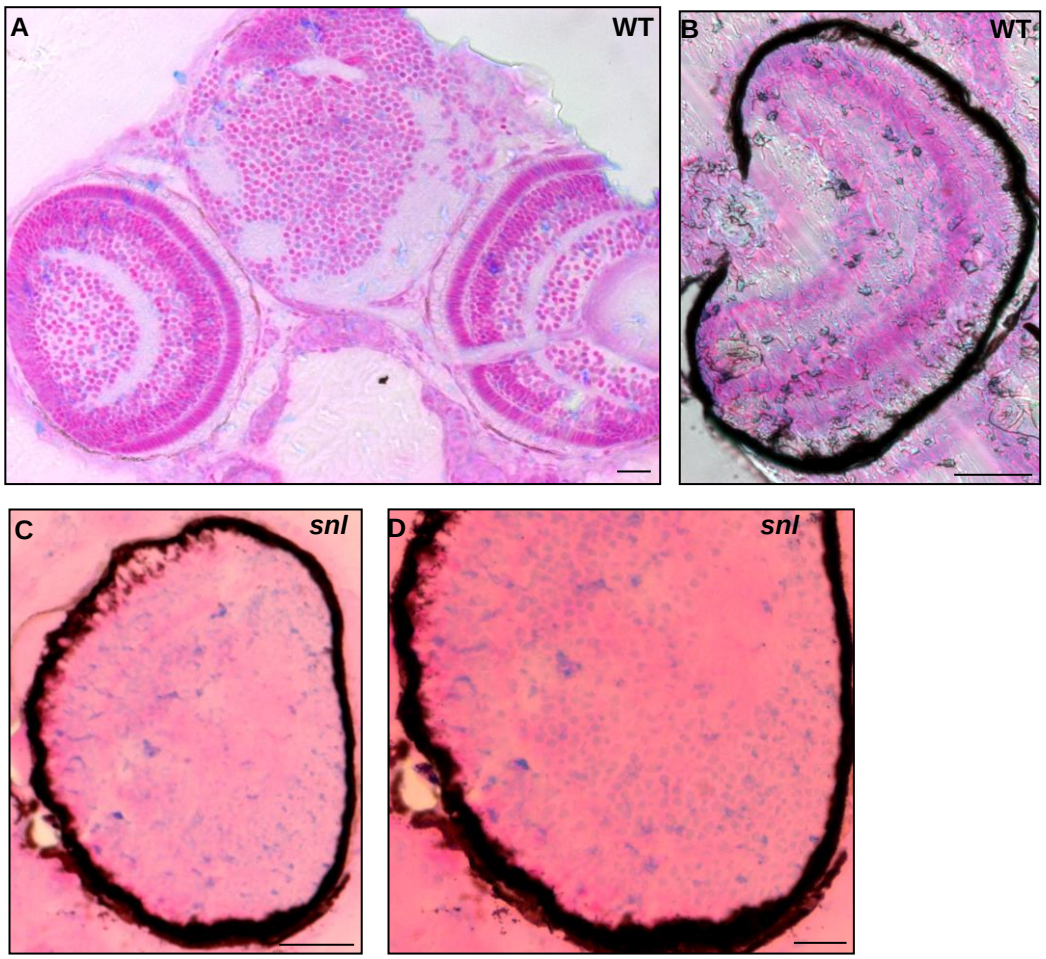

Figure 4.10 Abnormal retinal histology in *sentinel* zebrafish embryos Resin histology 5µm sections of the eyes of uninjected wild type (WT, **A**, **B**) and *sentinel* (*snl*, **C**, **D**) mutant zebrafish embryos, stained with methylene blue-basic fuchsin stain. **A** shows overview of the normal retina, with formation of discrete retinal layers from 72 hours post fertilisation. **B**-**D** show that at 5 days post fertilisation, whilst the retinal pigmented epithelial layer is preserved in *snl* mutants (**C**, **D**), there is disorganisation of retinal development, with loss of definition of retinal layers. Images are taken with 20x objective (**A**-**C**) and 40x objective (**D**). Scale bars = 20µm.

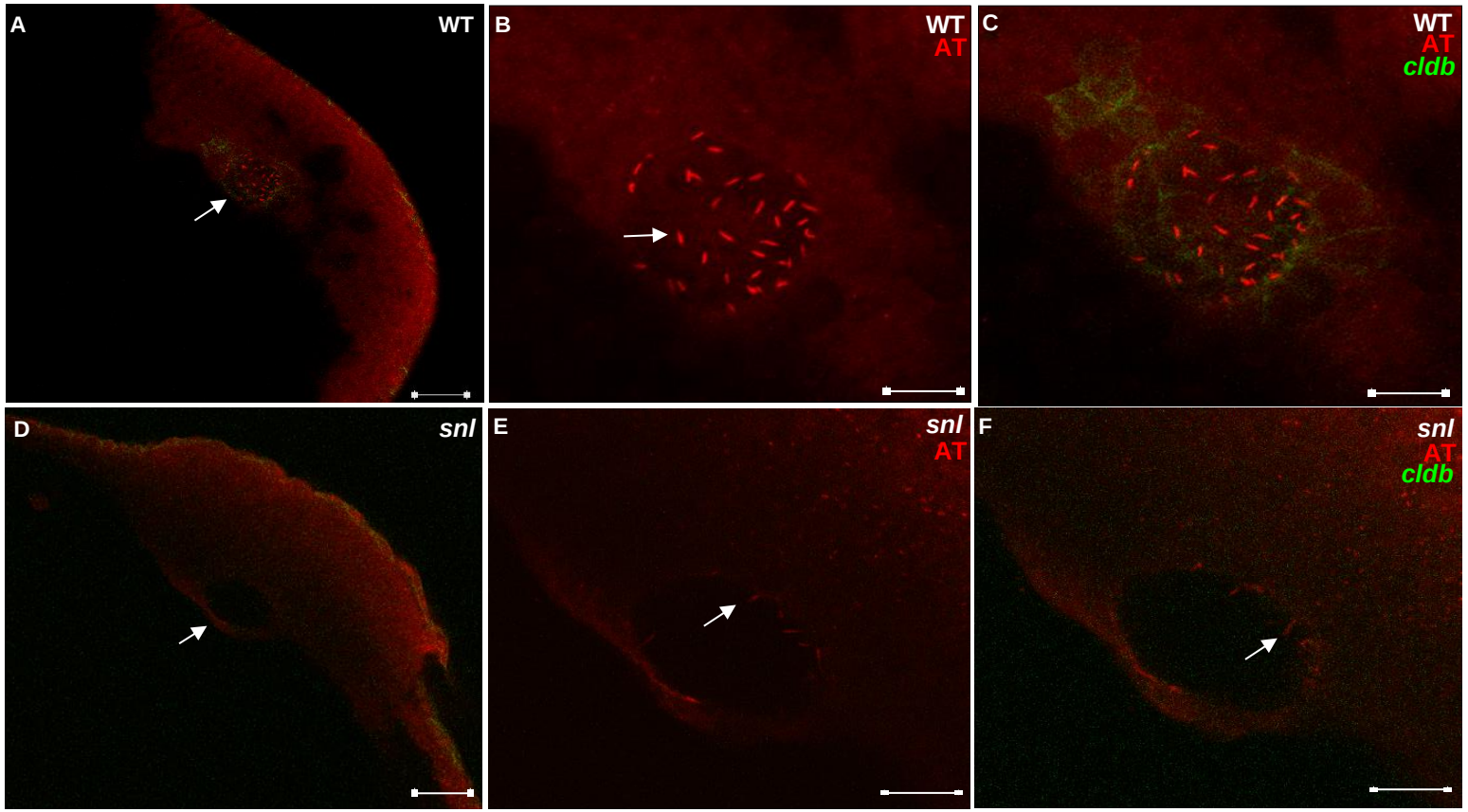

Figure 4.11 Reduction in number of cilia in Kupffer's vesicle in embryo from heterozygous *snl* zebrafish parents

Confocal microscopy images of *cldnb*:Lyn-GFP wild type (WT, **A**-**C**) and those born to heterozygous *sentinel:cldnb:*Lyn-GFP (*snl*, **D**-**F**) parents, following fixation at the 8-10 somite stage and fluorescent immunostaining using anti-acetylated tubulin (red) to study cilia in Kupffer's vesicle (KV). Overlay images of KV (arrowed, scale bar = 50µm, 20x objective) in WT (**A**) and *snl* (**D**) embryos. Higher magnification images **B, C, E, F** (zoom of 3, scale bar = 20µm). Red laser shows a normally ciliated (arrowed) KV in WT (**B**), whilst a sparse number of cilia are apparent in *snl* (**E**) embryos. In WT (**C**) expression of *cldnb*:Lyn-GFP at epithelial cell-cell junctions within KV is organised (**C**). In this *snl* (**F**) there is no distinct delineation of KV epithelium (*cldnb*:Lyn-GFP), cilia are sparse (arrow).

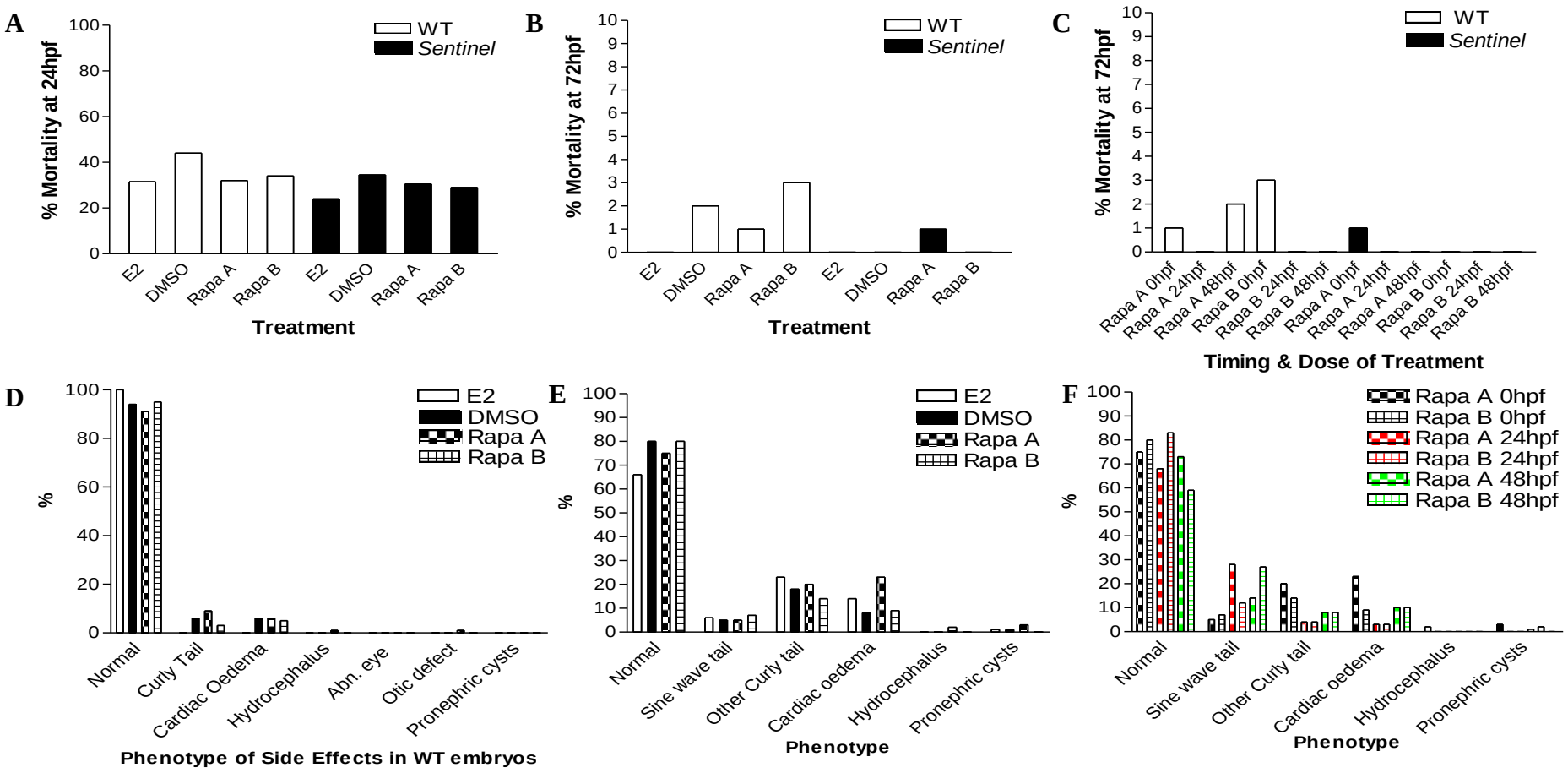

Figure 4.12 Safety and Efficacy of Rapamycin therapy for use in zebrafish embryos

Wild type (WT) and *sentinel* (*snl*, born to heterozygous *snl* parents) embryos were selected from the same parental pairs and exposed to four different media: E2, 0.05% DMSO (a solvent vehicle for Rapamycin), Rapa A (0.1µM), Rapa B (0.05µM). There was no significant difference (chi-squared test) in the mortality rates of WT and *snl* embryos at 24 (**A**) and 72 (**B**) hpf following 24 or 72 hours exposure to the four different media. (continued next page)

Figure 4.12 (cont.) Safety and Efficacy of Rapamycin therapy for use in zebrafish embryos
The delayed introduction of Rapamycin therapy to 24 and 48hpf (C) did not alter mortality rates. The side effect profile of each media was evaluated at 72hpf in WT embryos exposed from 0hpf (**D**). All embryos exposed to standard E2 media were phenotypically normal. There was no significant difference in the frequency of abnormal phenotypes in WT embryos exposed to different media, however some developmental anomalies occurred in embryos exposed to 0.05% DMSO and increasing concentrations of Rapamycin therapy (dose-dependent). All WT embryos exposed to Rapa A or B from 24hpf and 48hpf were phenotypically normal, suggesting any toxicity is associated with early exposure (prior to 24hpf). No WT embryos developed an abnormal eye phenotype or pronephric cysts. The efficacy of two doses of Rapamycin therapy was evaluated in *snl* embryos exposed from fertilisation (0hpf, **E**). The timing of initiation of Rapamycin was also evaluated, in *snl* embryos exposed from 24hpf and 48hpf (**F**). There was no significant difference in the percentage frequency of abnormal phenotypes of *snl* embryos treated with different doses of Rapamycin therapy and no difference introduced by varying the timing of initiation of therapy. DMSO, dimethyl sulfoxide; E2, standard zebrafish embryo media; hpf, hours post fertilisation; Rapa, Rapamycin.

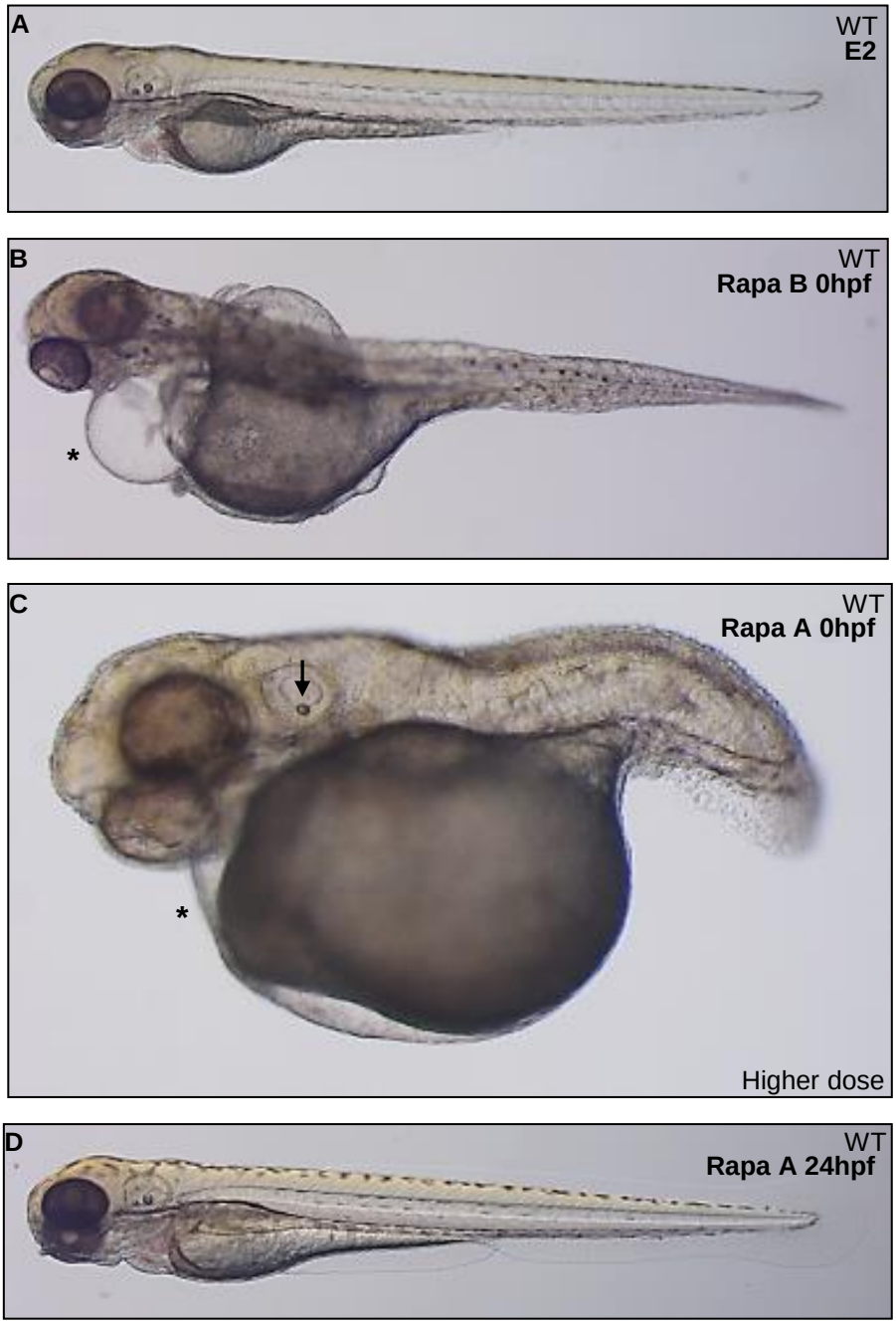

Figure 4.13 Phenotypes of wild type zebrafish embryos exposed to Rapamycin: toxicity associated with dose and timing of onset of exposure
Light microscopy images of wild type (WT) zebrafish embryos at 72hpf. (**A**) shows a normal WT embryo maintained in the standard embryo media (E2) from 0hpf. (**B**, **C**) show WT embryos maintained in two different doses of Rapamycin (Rapa B= 0.05µM, Rapa A=0.1µM) from 0hpf, the media was replaced every 24hpf. **B** has developed gross cardiac odema (*), whilst exposure to a higher dose of Rapamycin (0.1µM) from 0hpf can lead to more severe developmental anomalies (**C**) including growth arrest (short tail) and a single otolith (arrow, **C**). **D** is a WT embryo maintained in E2 for the first 24hpf prior to exposure to high dose Rapamycin (Rapa A, 0.1µM) from 24hpf. **D** has a normal appearance (n=85), suggesting any toxicity associated with Rapamycin occurs during early exposure, in the inital 24hrs of development.

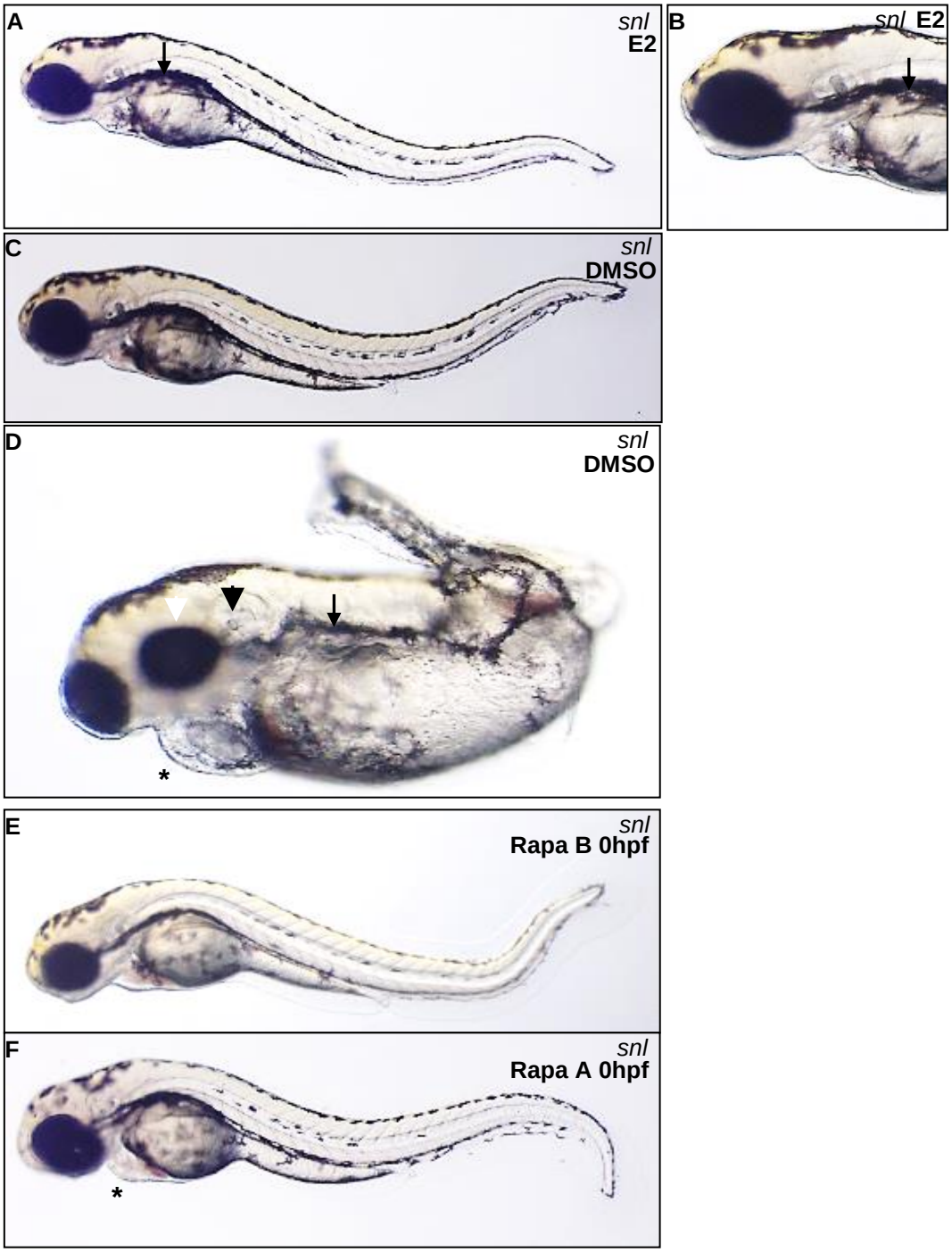

Figure 4.14 Phenotypes of *sentinel* zebrafish embryos exposed to Rapamycin from 0hpf

Light microscopy images of *sentinel* zebrafish embryos at 72hpf. (**A**, **B**) shows a *sentinel* (*snl*) embryo maintained in the standard embryo media (E2). The characteristic sine wave tail is evident and a pronephric cyst is arrowed (**A**, **B**). **C**, **D** show *snl* embryos maintained in 0.05% DMSO (the solvent vehicle for Rapamycin). **D** shows a *snl* which has developed cardiac oedema (*), a pronephric cyst (black arrow), a single otolith (black arrowhead) and unilateral microphthalmia (white arrow). **E**,**F** show *snl* embryos which have been maintained in two different doses of Rapamycin (**E**, Rapa B= 0.05µM) and (**F**, Rapa A=0.1µM) from 0hpf, the media was replaced every 24hpf. In addition to the characteristic sine wave shaped tail, **F** has developed cardiac odema (*). DMSO, dimethyl sulfoxide; Rapa, Rapamycin.

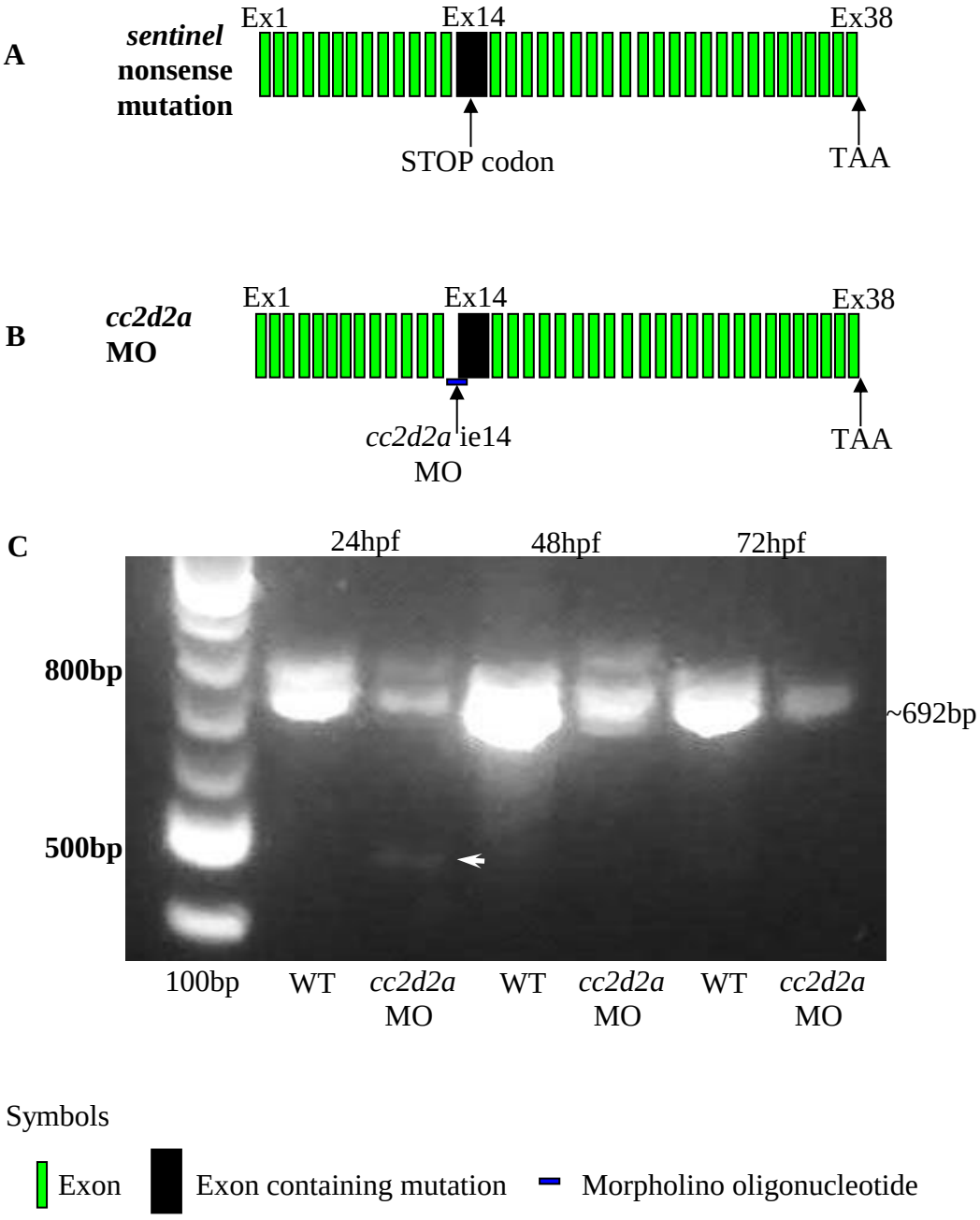

Figure 4.15 *cc2d2a* morpholino design
(**A**) Schematic representation of zebrafish *cc2d2a* showing the spontaneous nonsense mutation, a stop codon, present in exon 14 of *sentinel* mutants. (**B**) Schematic representation of the splice blocking (*cc2d2a* ie14) morpholino oligonucleotide (MO) designed to mimic the spontaneous mutation in *sentinels*, by targeting the same exon (14). (**C**) RT-PCR of single embryos at 24-72hpf following *cc2d2a* splice MO knockdown reveals maximal reduction of the normal 692bp product at 24hpf and an additional smaller product in *cc2d2a* morphants measuring approximately 500bp (white arrow). The larger band at 800bp in all 24-48hpf embryos does not appear relevant. hpf, hours post fertilisation; MO, morpholino oligonucleotide; WT, wild type.

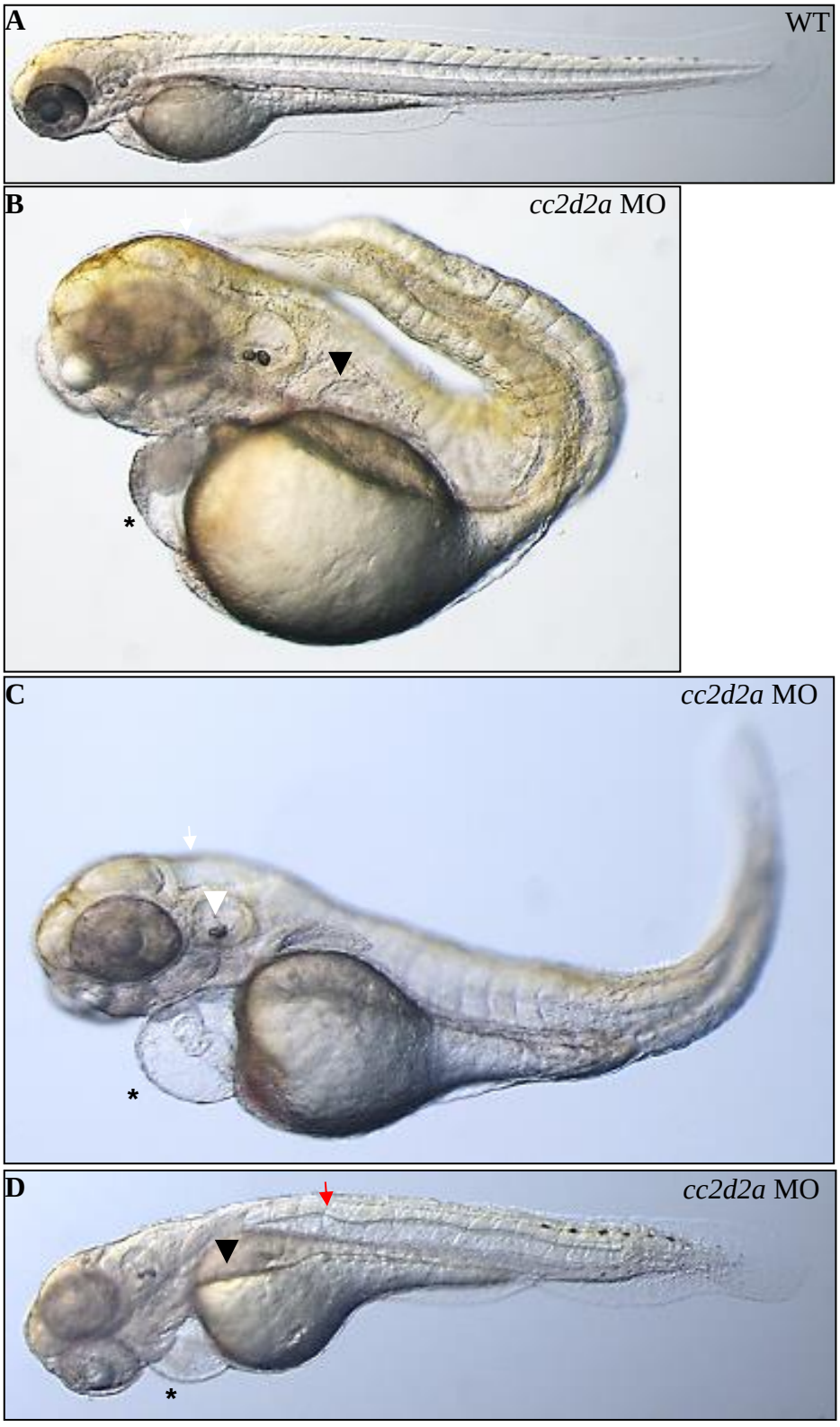

Figure 4.16 Phenotype with *cc2d2a* MO knockdown
Lateral views of zebrafish embryos 72 hours post fertilisation. **A** is an uninjected wild type control (WT) and is phenotypically normal. Embryos injected with 6ng of *cc2d2a* splice MO develop a range of anomalies including: cardiac oedema (*); hydrocephalus (white arrows, **B**, **C**); pronephric cysts (**B**, **D**), altered number of otoliths (single in **C**, white arrowhead) and a wavy notochord (red arrow, **D**). MO, morpholino oligonucleotide.

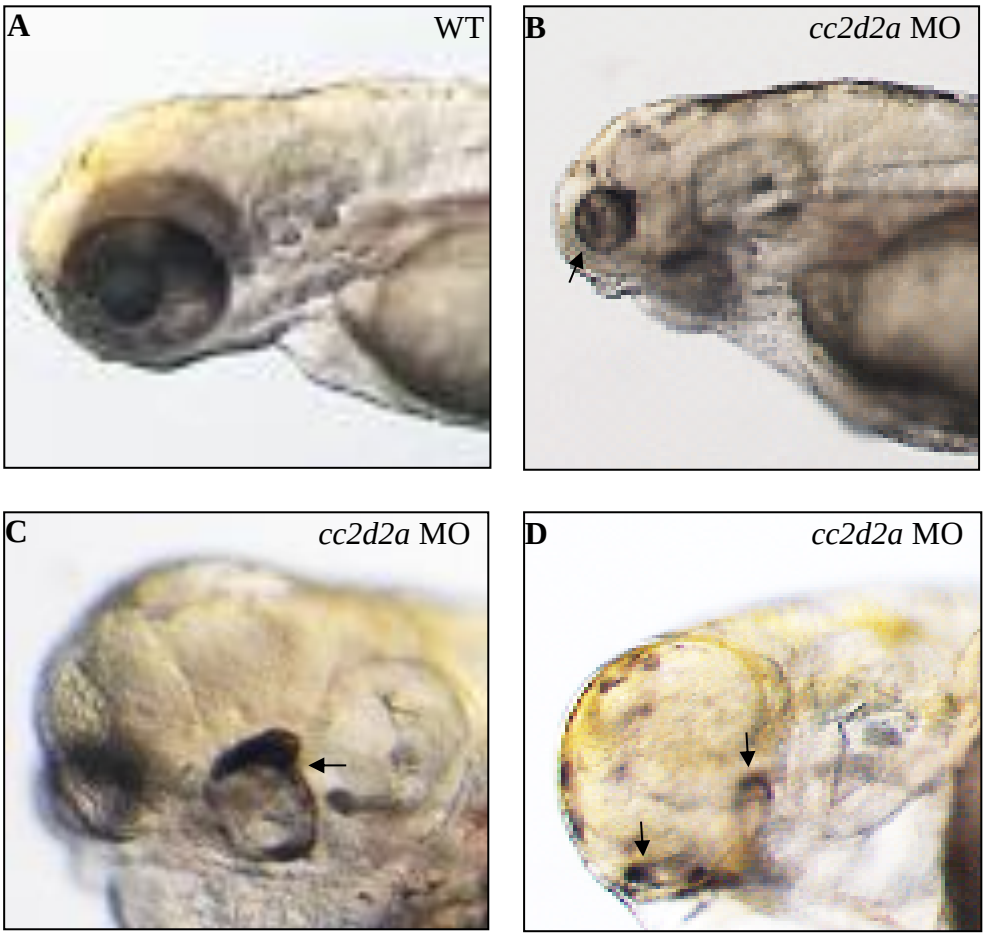

Figure 4.17 Abnormal eye development in zebrafish embryos injected with *cc2d2a* MO

Lateral views of the head of zebrafish embryos 72 hours post fertilisation. **A** is an uninjected wild type control (WT) and is phenotypically normal. Embryos injected with *cc2d2a* splice MO (arrows, **B**-**D**) have abnormal eye development including microphthalmia or coloboma formation. MO, morpholino oligonucleotide.

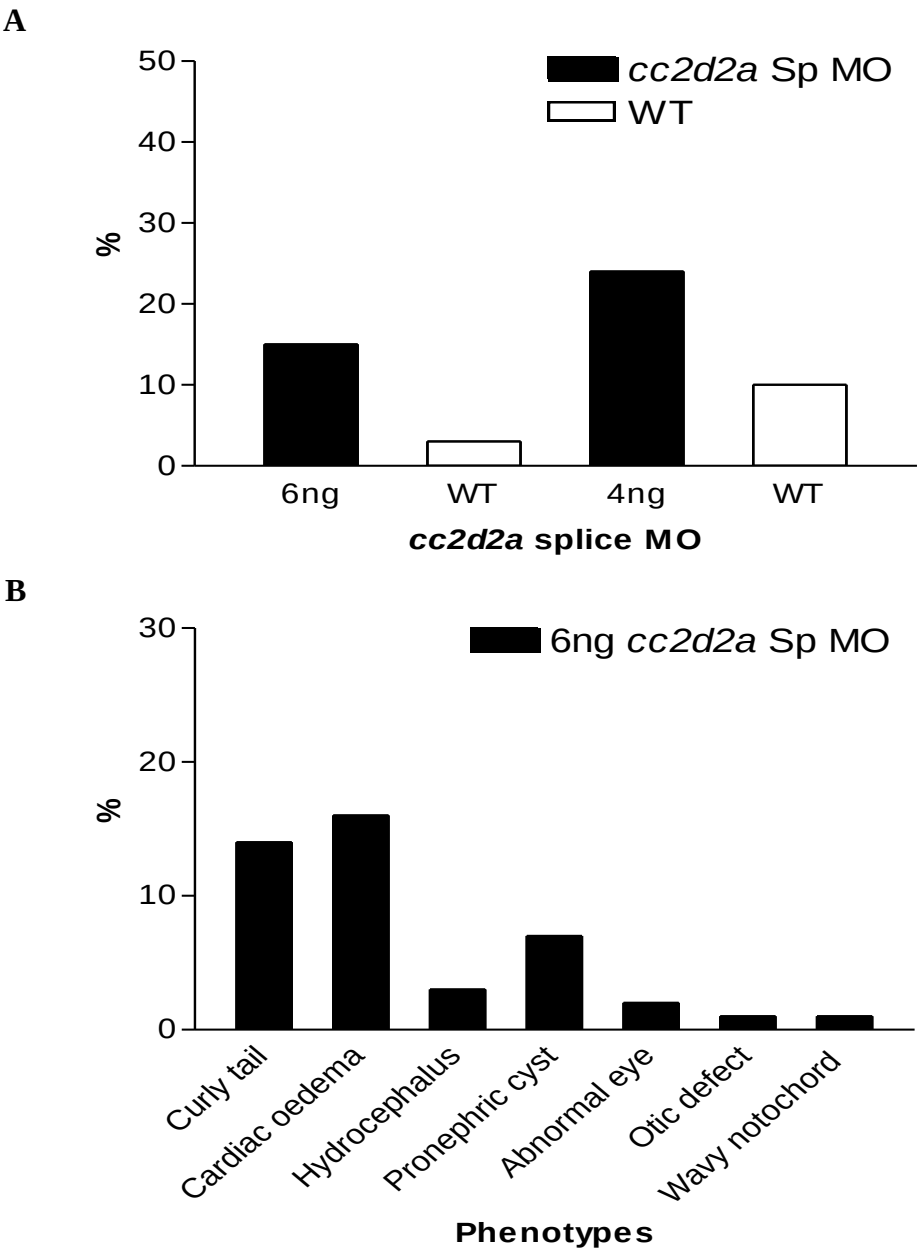

Figure 4.18 Mortality at 24hpf and phenotypes at 72hpf of zebrafish embryos following *cc2d2a* MO injection

Mortality at 24hpf (**A**) is not significantly higher in embryos injected with *cc2d2a* MO (n=234), compared to uninjected wild type controls (n=85, p=0.31, chi-squared test). The percentage mortality rises in both *cc2d2a* MO injected embryos from 15% (6ng, n=151) to 24% (4ng, n=83) and from 3% to 10% in matched WT embryos, however the mortality ratio of *cc2d2a* MO injected embryos relative to WT embryos falls from 5:1 (6ng) to 2.4:1 (4ng), confirming the dose dependent effect of increasing MO dose on mortality. Graph **B** shows the percentage frequency of abnormal phenotypes at 72hpf in embryos injected with 6ng (n=150) of *cc2d2a* MO. 7% of embryos developed pronephric cysts following 6ng of *cc2d2a* MO. hpf, hours post fertilisation; MO, morpholino oligonucleotide.

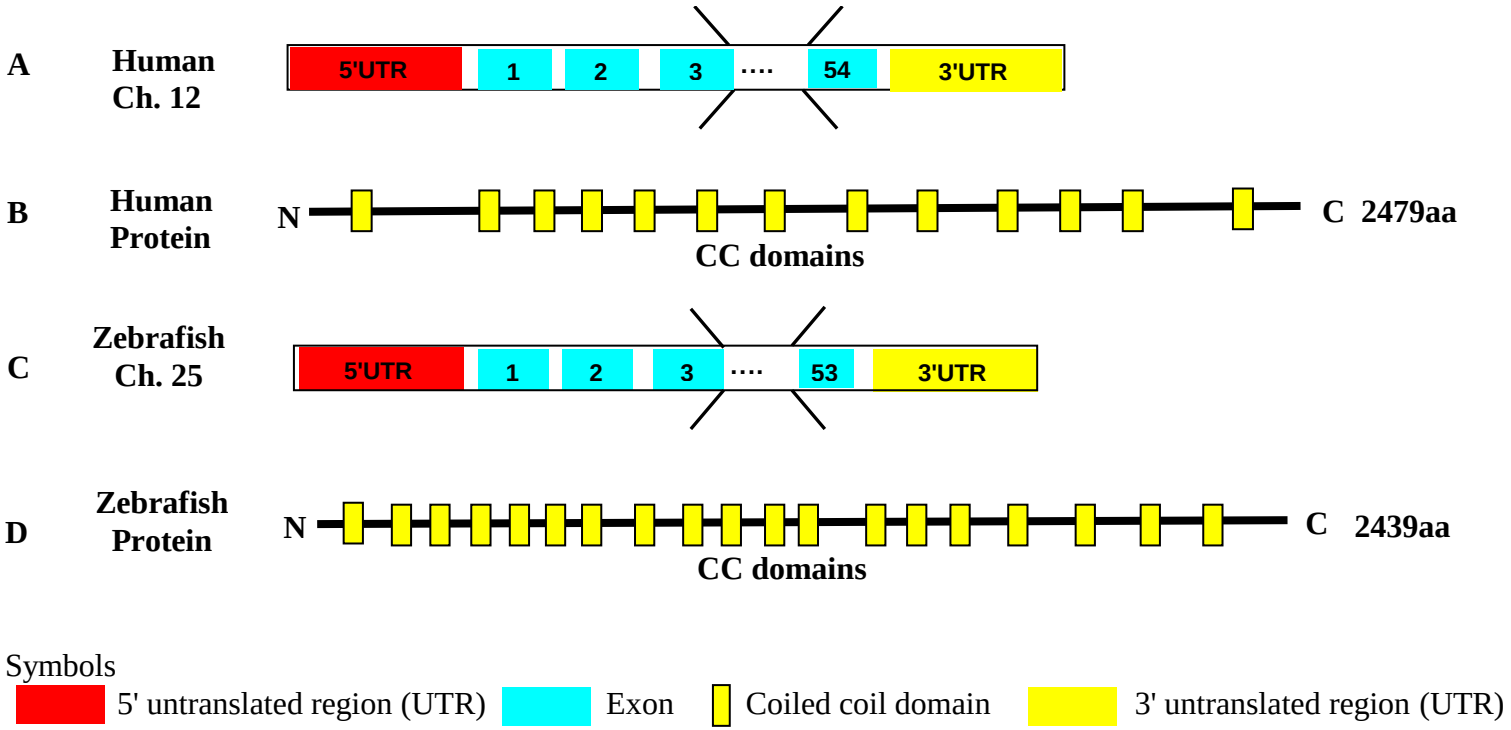

Figure 4.19 *NPHP6* gene transcript and partial protein product structure in humans and zebrafish
(**A**) *NPHP6* gene transcript in humans (OTTHUMT00000406344) and schematic representation of encoded protein product, centrosomal protein of 290kDa (CEP290) which includes 13 coiled-coil domains (CC) and has 2479 amino acids (OTTHUMP00000242341) (**B**). (**C**) *nphp6* gene transcript in zebrafish (OTTDART00000051136) and schematic representation of encoded protein product, cep290 (OTTDARP00000040195), which includes 19 CC domains and has 2439 amino acids (**D**). aa, amino acids; Ch., chromosome.

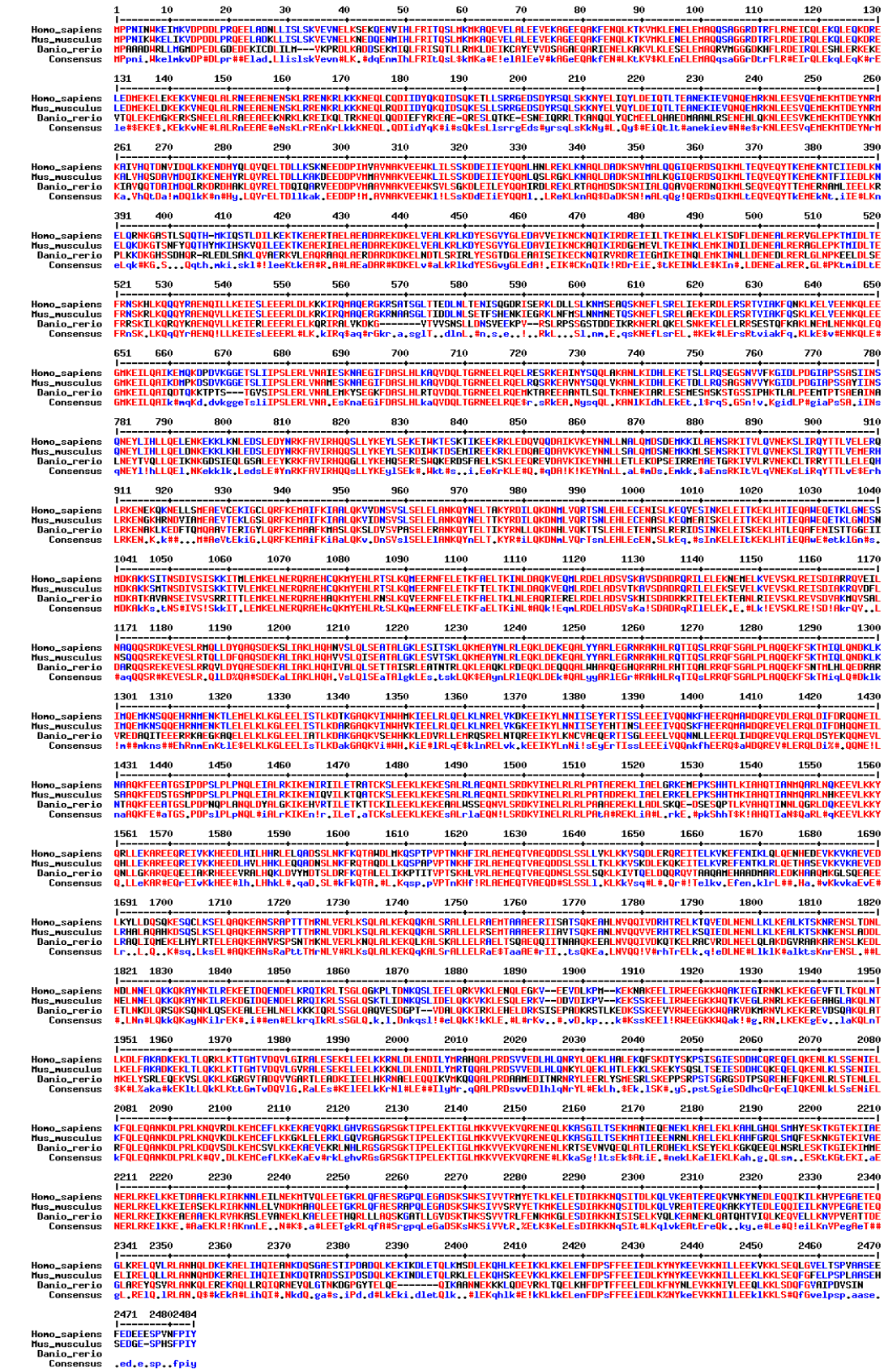

Figure 4.20 Evolutionary conservation of Nphp6 (CEP290) in humans, mice and zebrafish

Nphp6 (CEP290) peptide sequence alignment in humans (homo sapiens, OTTHUMP00000242341), mouse (mus musculus, ENSMUSP00000130899) and zebrafish (danio rerio, OTTDARP00000040195). Conservation of amino acid alignment (red font).

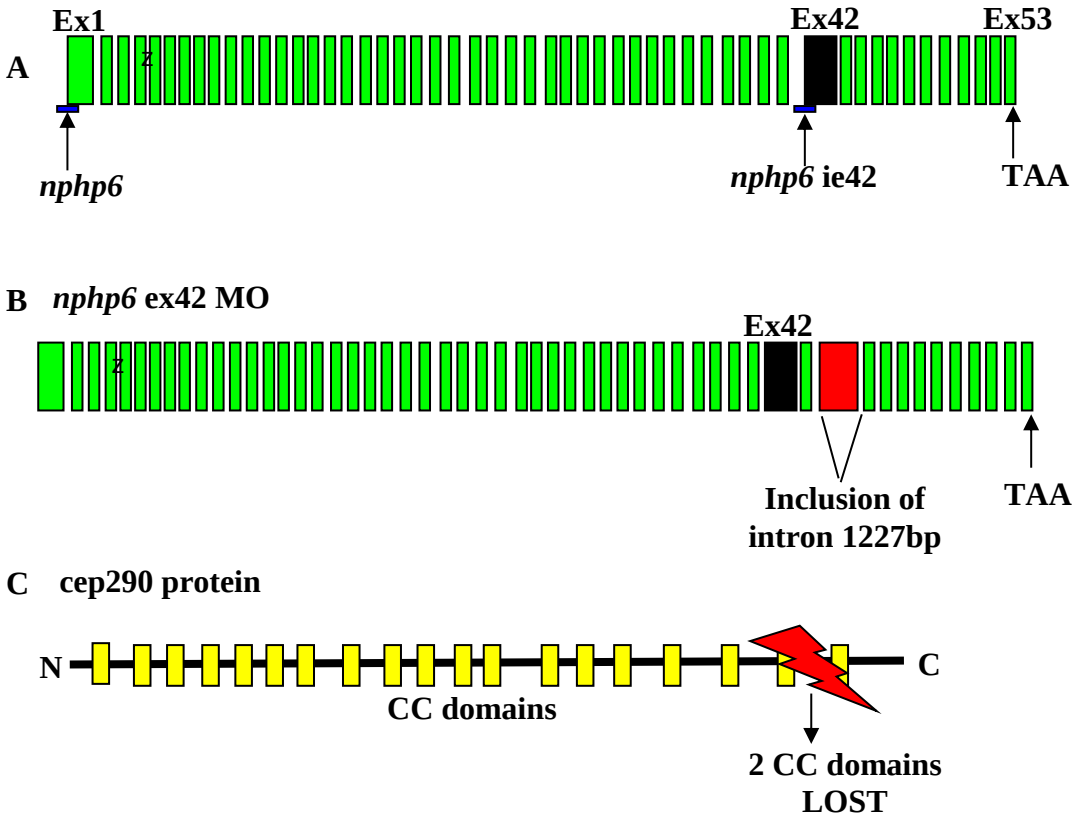

Figure 4.21 Design of *nphp6* MO and the effect of the splice blocking MO at the protein level

(**A**) Schematic representation of zebrafish *nphp6* showing target sites of translation (ATG) and splice (*nphp6*iex42) blocking morpholino oligonucleotides (MO). (**B**) The splice blocking MO, *nphp6*iex42, designed to target exon 42, leads to abnormal splicing with inclusion of a 1227bp intron (red) after exon 43. At the protein level, the intron is included after 2029 amino acids and results in loss of 2 coiled coil domains (**C**).

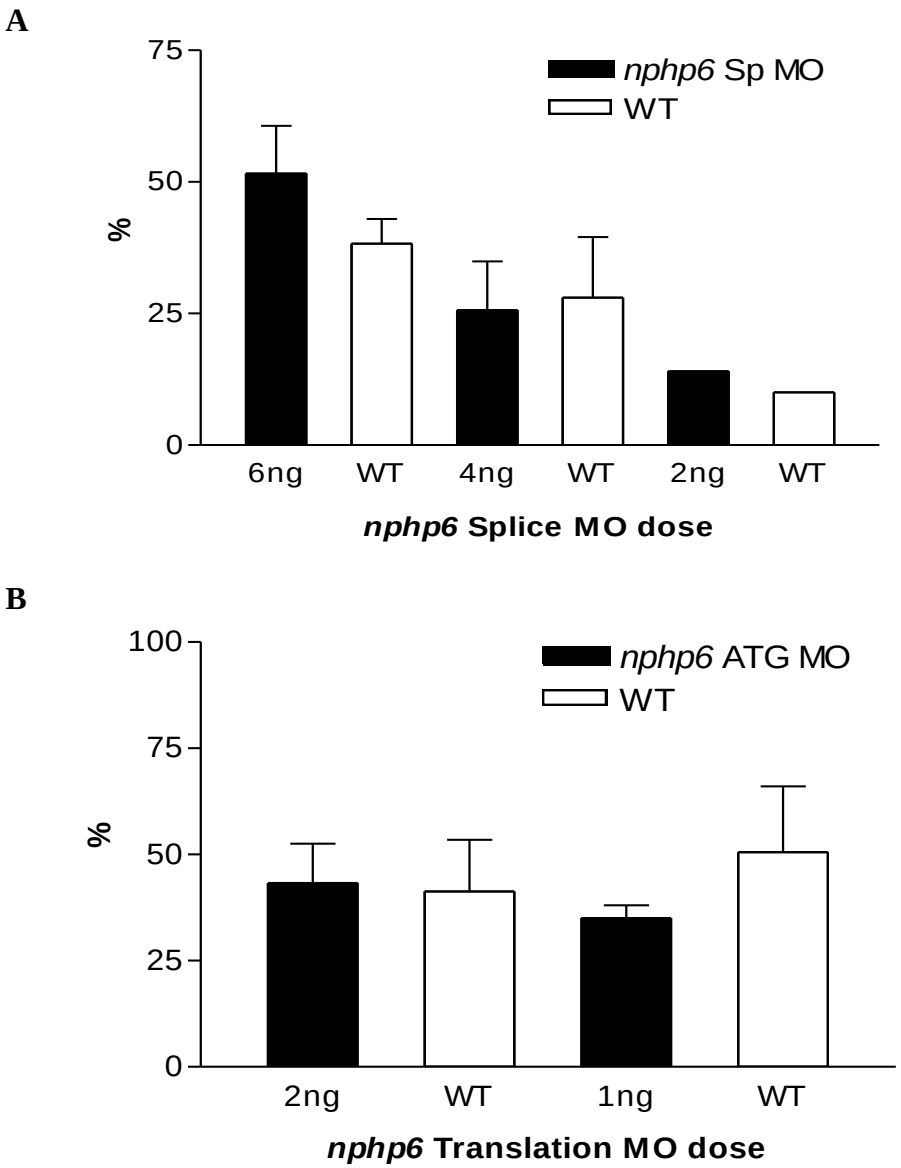

Figure 4.22 Mortality at 24hpf following *nphp6* MO injection
Mortality at 24 hours post fertilisation (hpf) is shown as mean percentage (%) and standard error of the mean (where appropriate) in zebrafish embryos injected with a range of morpholino oligonucleotide (MO) doses. Matched uninjected wild type (WT) controls are shown. Both *nphp6* splice (**A**) and *nphp6* translation blocking (**B**) MO induce a dose dependent effect on mortality. For the splice blocking MO (**A**), total numbers of embryos at 24hpf were 547 from 7 pairs (6ng), 342 from 3 pairs (4ng) and 73 from 1 pair (2ng). For the translation blocking MO (**B**), total numbers of embryos at 24hpf were 430 from 4 pairs (2ng) and 303 from 2 pairs (1ng).

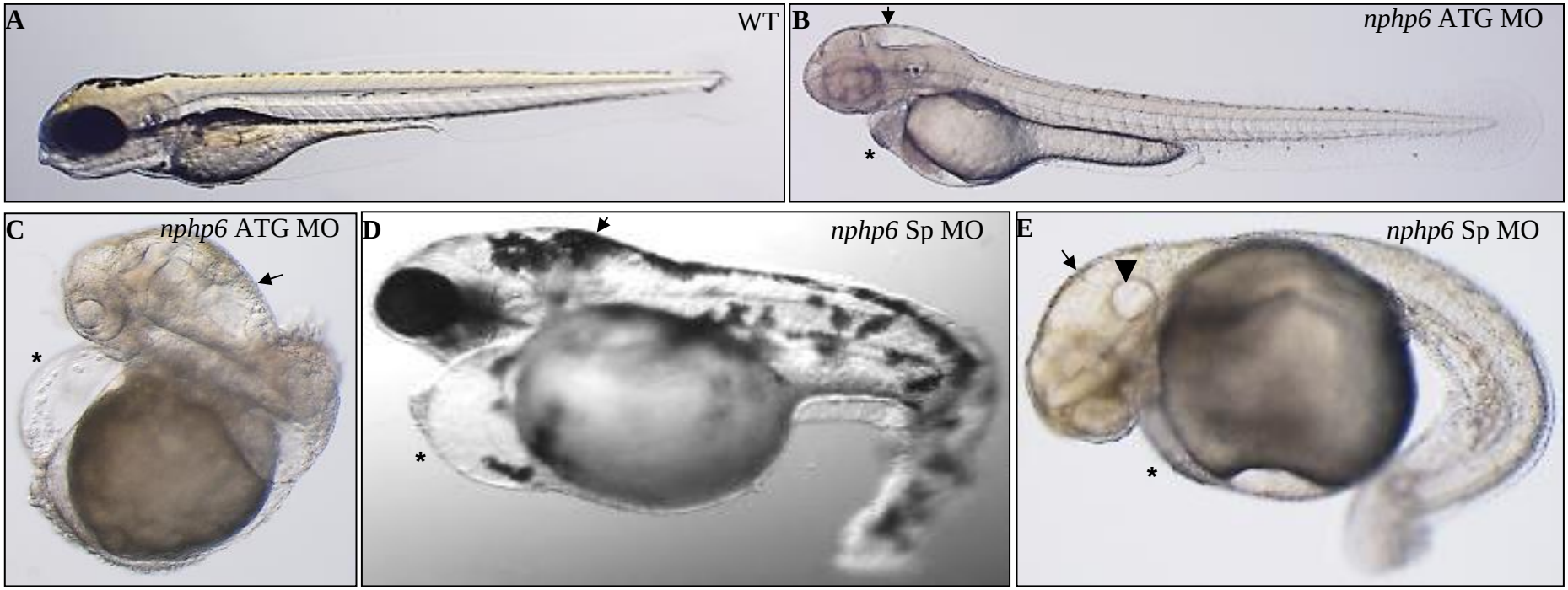

Figure 4.23 Phenotype with *nphp6* MO knockdown
Lateral views of zebrafish embryos 72 hours post fertilisation. Wild type (WT) uninjected control embryos are phenotypically normal (**A**). Embryos injected with *nphp6* translation (**B**, **C**) and splice (**D**, **E**) blocking MO develop hydrocephalus (black arrows), cardiac oedema (*), curved body axis (**C**-**E**) and altered number of otoliths (none, black arrowhead, **E**). MO, morpholino oligonucleotide.

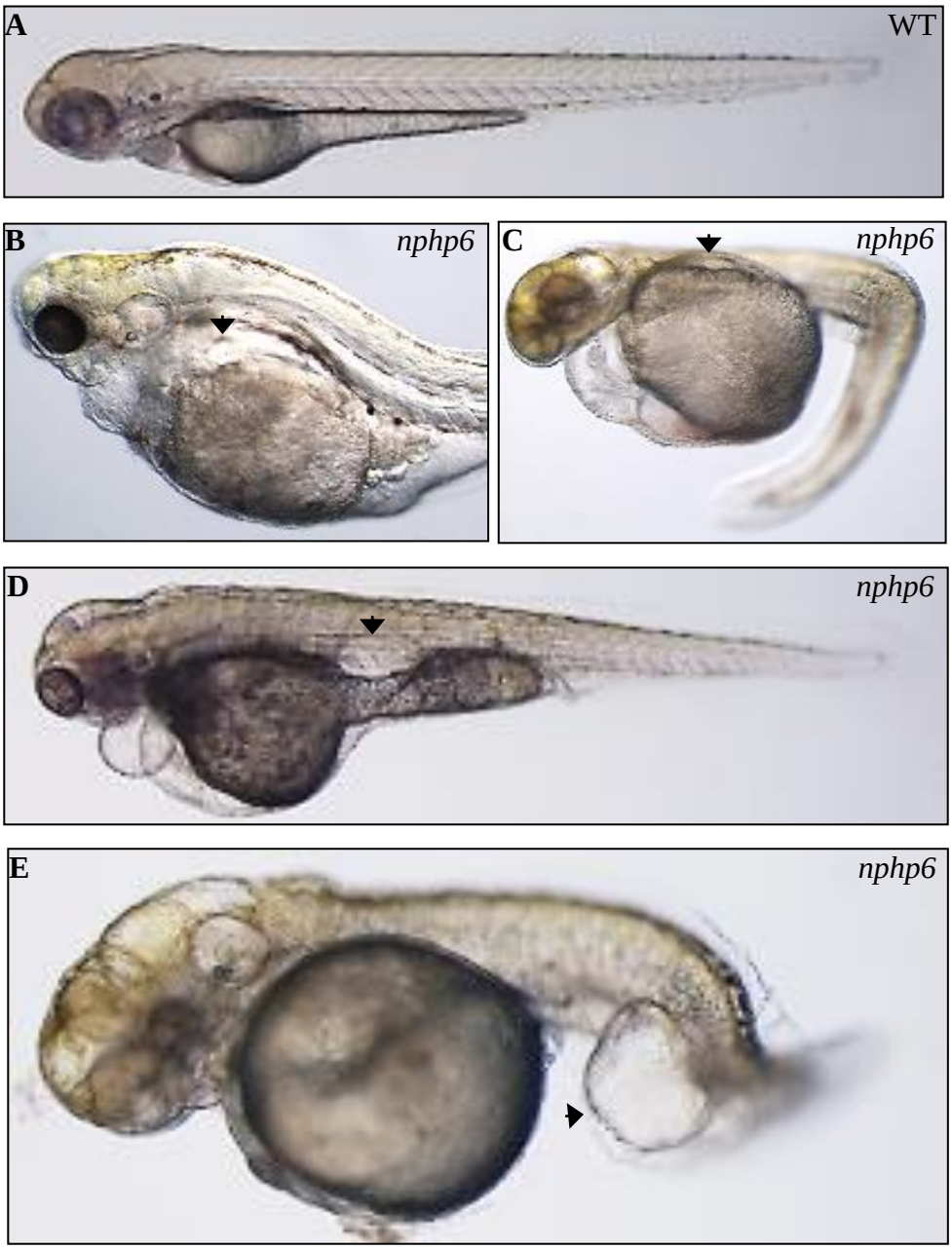

Figure 4.24 *nphp6* MO knockdown induces pronephric cysts in zebrafish embryos

Lateral views of pronephric cysts (black arrowheads) in *nphp6* morphants at 72 hours post fertilisation (**B**-**E**). (**A**) is a phenotypically normal uninjected wild type (WT) control embryo. *nphp6* morphants develop proximal (**B**-**C**), distal (**D**) and cloacal (**E**) pronephric cysts. The cloaca in **E** is very dilated and distorted, this embryo also has hydrocephalus and a single otolith.

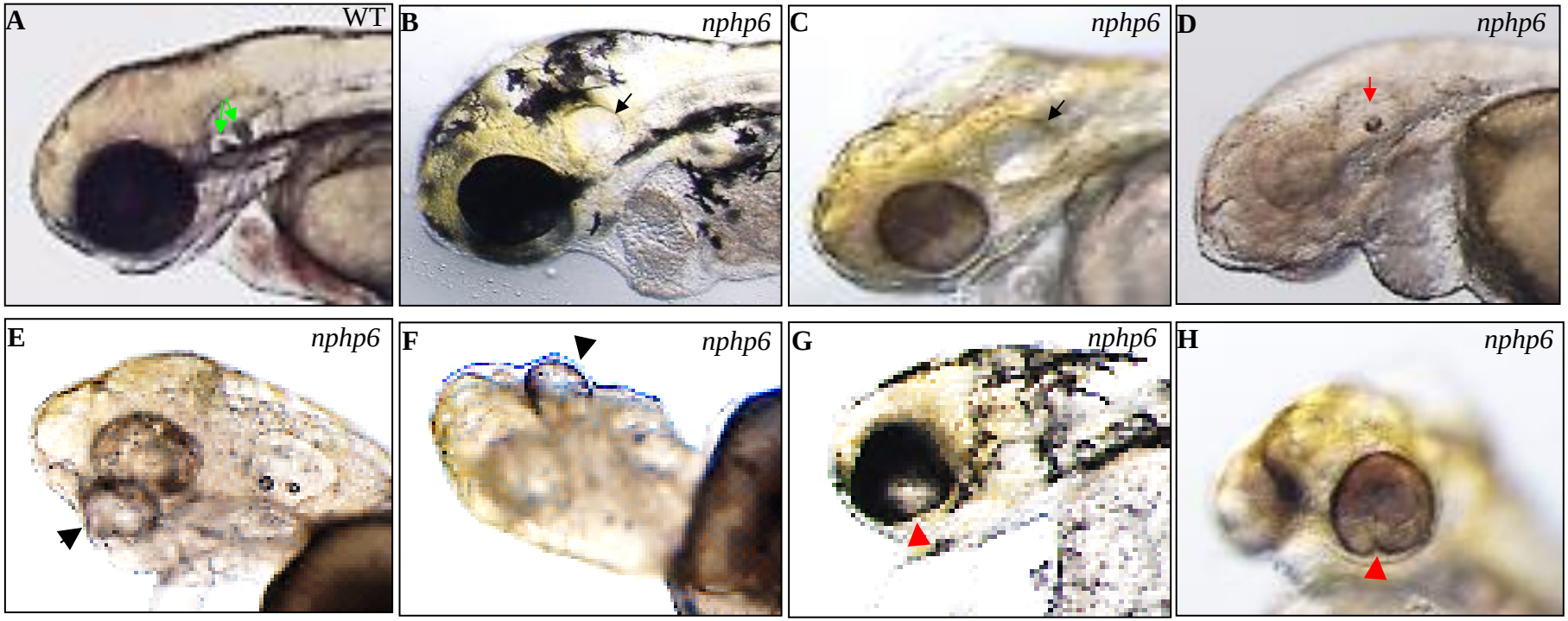

Figure 4.25 Abnormal eye and ear development following *nphp6* MO knockdown
Views of the head of zebrafish embryos at 72 hours post fertilisation, focusing on the otic vesicles (**A**-**D**) and eyes (**A**, **E**-**H**). Wild type (WT) uninjected control embryos have normal eyes of equal size and two otoliths in each otic vesicle (green arrows, **A**). Lateral views of embryos injected with *nphp6* MO show abnormal ear development with either an empty otic vesicle (black arrow, **B**-**C**) or a single otolith (red arrow, **D**). Abnormal eye development includes unilateral microphthalmia (black arrowheads, lateral (**E**) and dorsal (**F**) views) and coloboma formation (red arrowheads, lateral (**G**) and ventral (**H**) views) in *nphp6* morphants. MO, morpholino oligonucleotide.

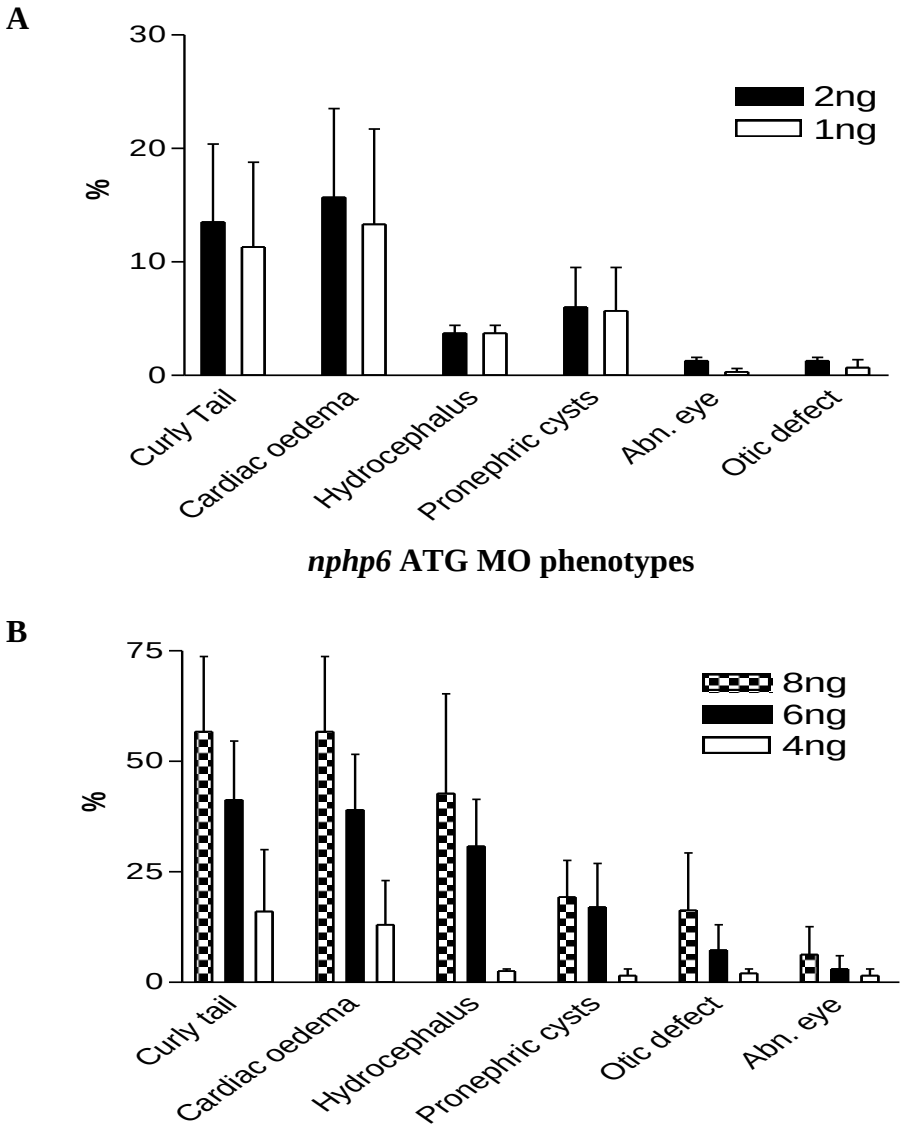

Figure 4.26 Quantification of abnormal phenotypes at 72hpf following injection with *nphp6* splice or translation blocking MO

Data are displayed as mean ± SEM. The percentage frequency of each abnormal phenotype was higher following *nphp6* splice (Sp) MO (**B**) knockdown, compared to following *nphp6* translation (ATG) MO (**A**) knockdown. There was a dose dependent effect on the frequency of each abnormal phenotype. The total number of zebrafish embryos phenotyped at 72hpf following each dose of *nphp6* ATG MO was 236 (2ng) and 158 (1ng) (**A**). The total number of zebrafish embryos phenotyped at 72hpf following each dose of *nphp6* Sp MO were 84 (8ng), 216 (6ng) and 261 (4ng). MO, morpholino oligonucleotide.

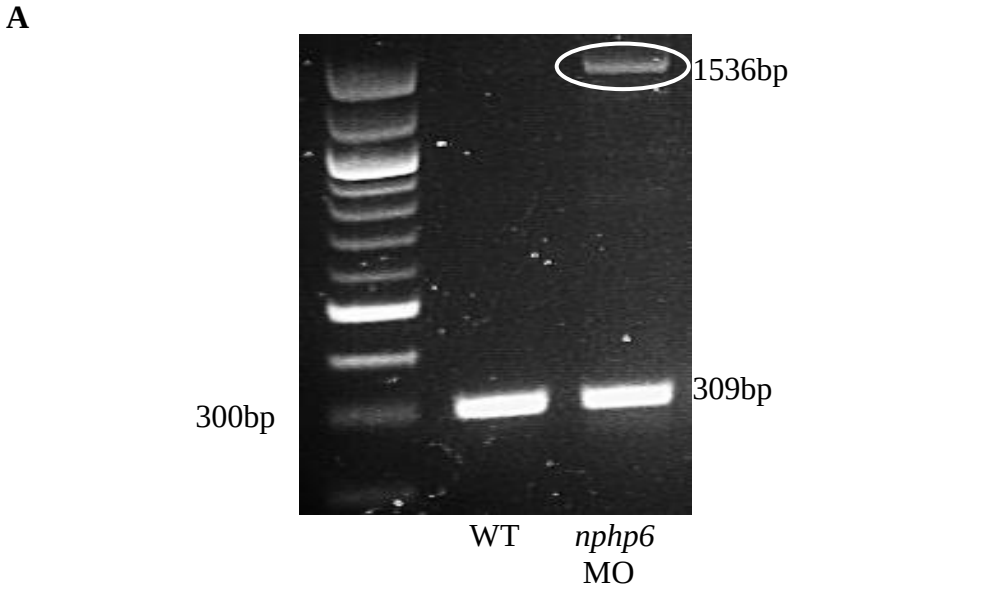

Figure 4.27 Evidence of *nphp6* splice MO knockdown by RT-PCR and direct sequencing

(**A**) RT-PCR of single embryos at 24hpf following *nphp6* splice MO knockdown reveals an additional larger RT-PCR product (circled in white), compared to uninjected wild type (WT) control embryos, which only have the normal RT-PCR product of 309bp. (**B**) Direct sequencing (data not shown) confirmed the identity of the larger product in *nphp6* morphants which included intronic sequence after exon 43, confirming abnormal splicing. hpf, hours post fertilisation.

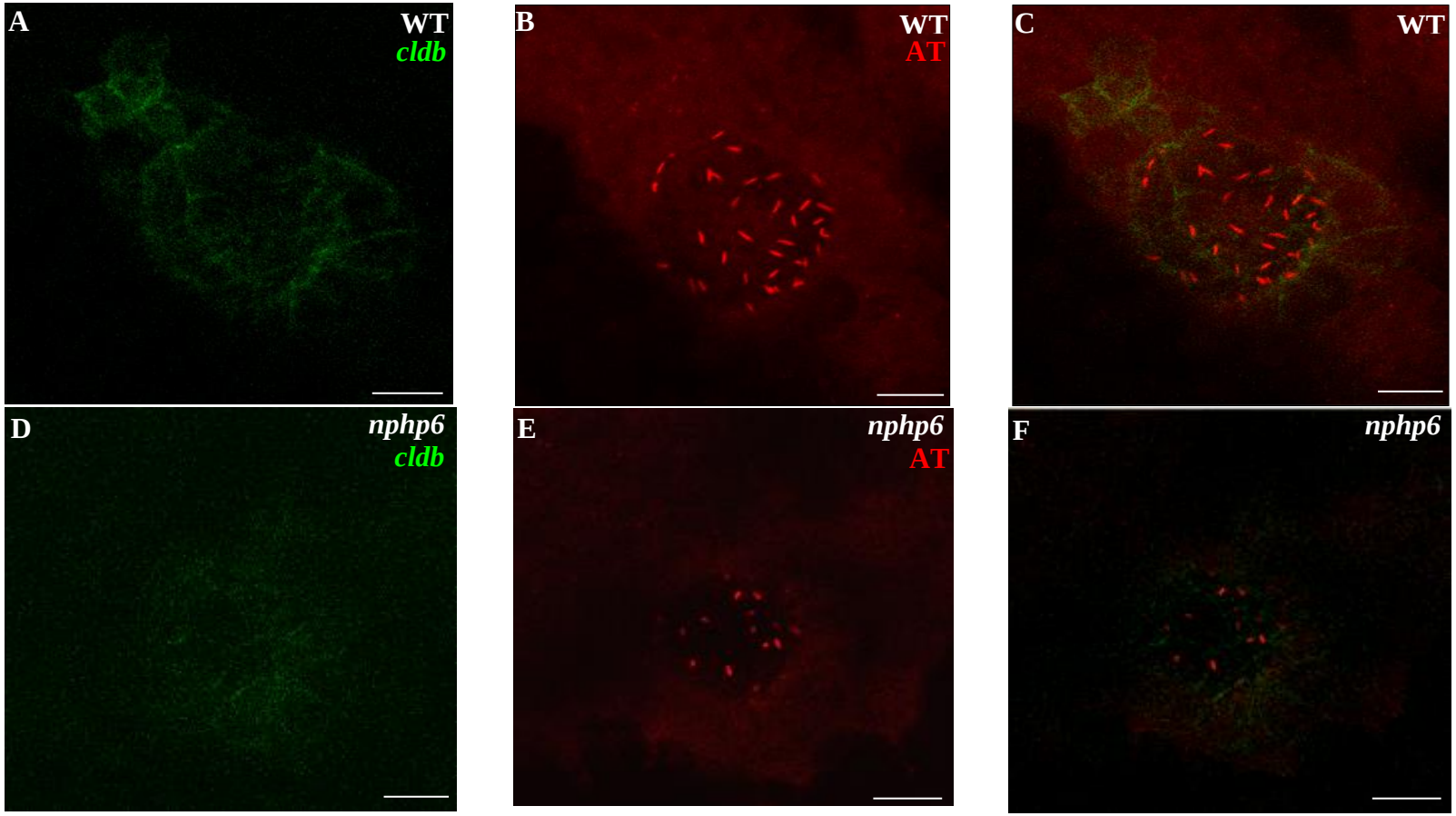

Figure 4.28 Shorter cilia in Kupffer's Vesicle of *nphp6* MO injected zebrafish embryos

Confocal microscopy images of *cldb*:Lyn-GFP wild type (WT, **A**-**C**) and *nphp6* MO injected (**D**-**F)** zebrafish embryos following fixation at the 8-10 somite stage and fluorescent immunostaining using anti-acetylated tubulin (AT, red, **B**, **E**) antibody to label cilia. Cilia appear shorter and of a reduced number in KV of *nphp6* MO injected embryos (**E**-**F**), compared to uninjected WT (**B**-**C**). Images were taken with a 20x objective, zoom of 3. Scale bars = 20 µm. KV, Kupffer's vesicle; MO, morpholino oligonucleotide.

A

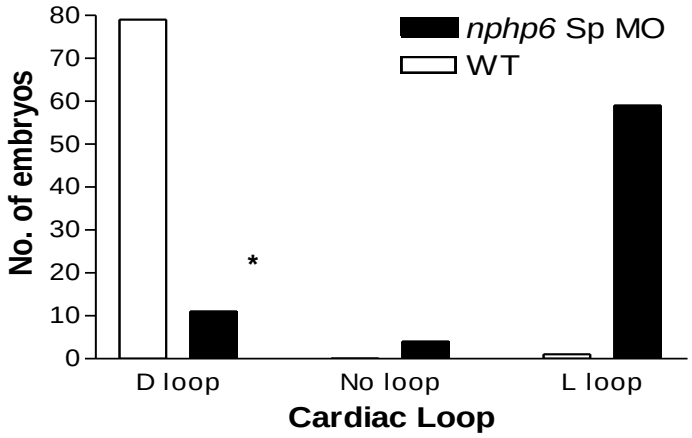

B

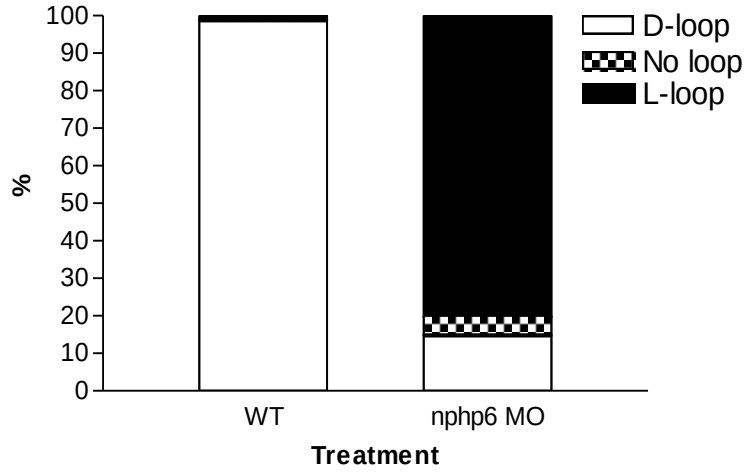

Figure 4.29 Analysis of cardiac looping reveals laterality defects in *nphp6* morphants at 56hpf

Quantification of orientation of cardiac looping at 56hpf in zebrafish embryos (**A**) reveals there is a significant reduction in the normal rightward cardiac looping (D-looping) in *nphp6* morphants (n=11, *, $p < 0.0001$, chi squared test), compared to uninjected wild type (WT) controls (n=79). (**B**) Stacked bar chart showing the percentage frequency of cardiac looping orientation in each experimental group. In the WT embryos, 99% (n=79) have D-looping and 1% (n=1) L-looping, compared to *nphp6* morphants in which 15% (n=11) have D-looping, 5% (n=4) have No looping and 80% (n=59) have L-looping. hpf, hours post fertilisation.

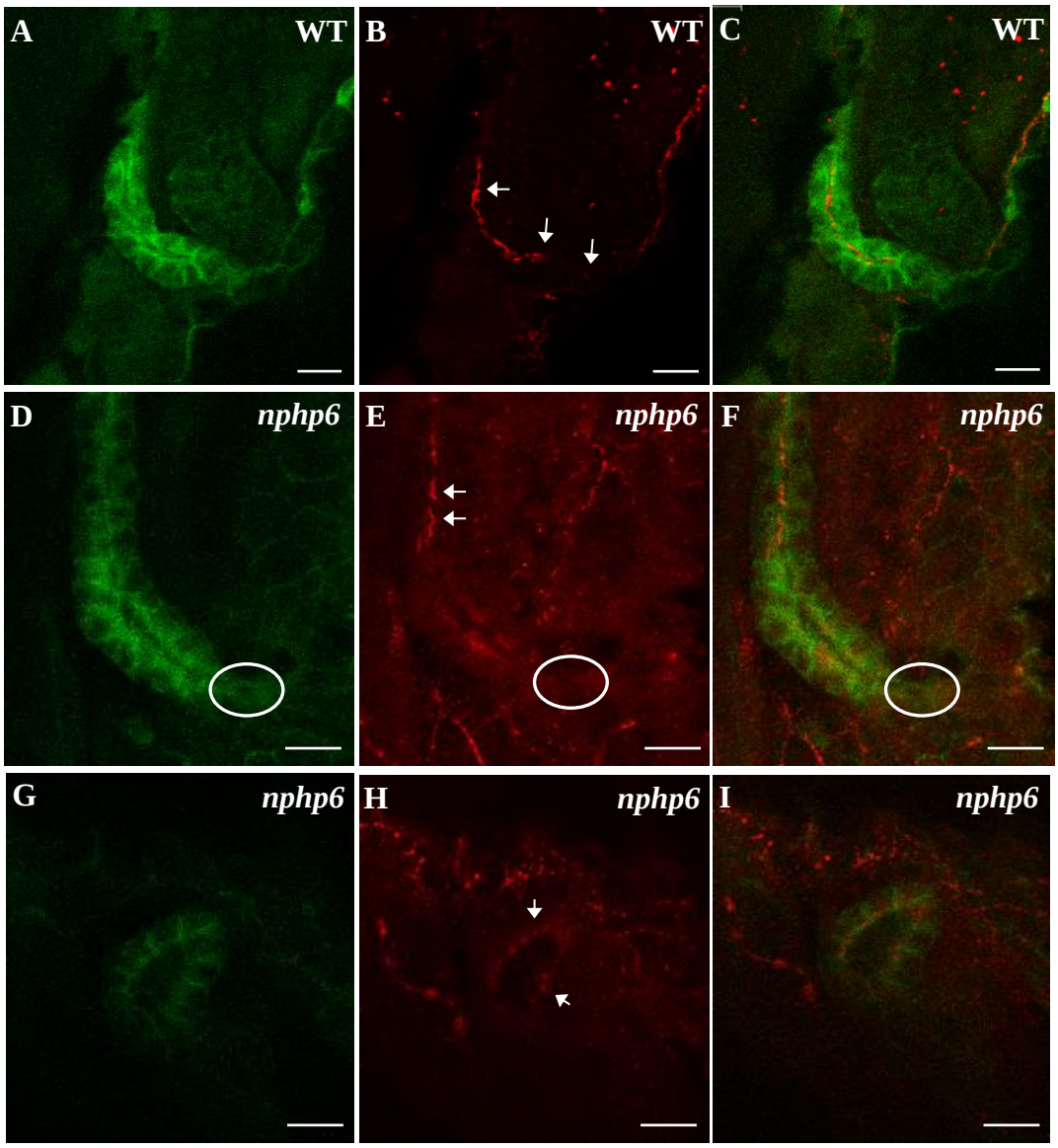

Figure 4.30 Cilia in the distal pronephros and cloaca of *nphp6* morphant zebrafish embryos

Confocal microscopy images of *claudinb:*Lyn GFP zebrafish embryos following fixation at 72hpf and immunostaining with anti-acetylated tubulin antibody (AT, red) to identify cilia. Uninjected wild type control (WT, **A**-**C**) embryos have cilia (white arrows, **B**) lining the pronephros which meet in apposition at the cloaca (**A**, **C**). In *nphp6* morphants, cilia are present in the distal pronephros, however reduce in number/disappear as the cloaca is approached (white circle, **E**, **F**). **G**-**I** show a cross sectional view of a dilated cloaca in an *nphp6* morphant with what appears to be short cilia. Images were taken with a 20x objective and zoom of 3. Scale bars = 20 µm.

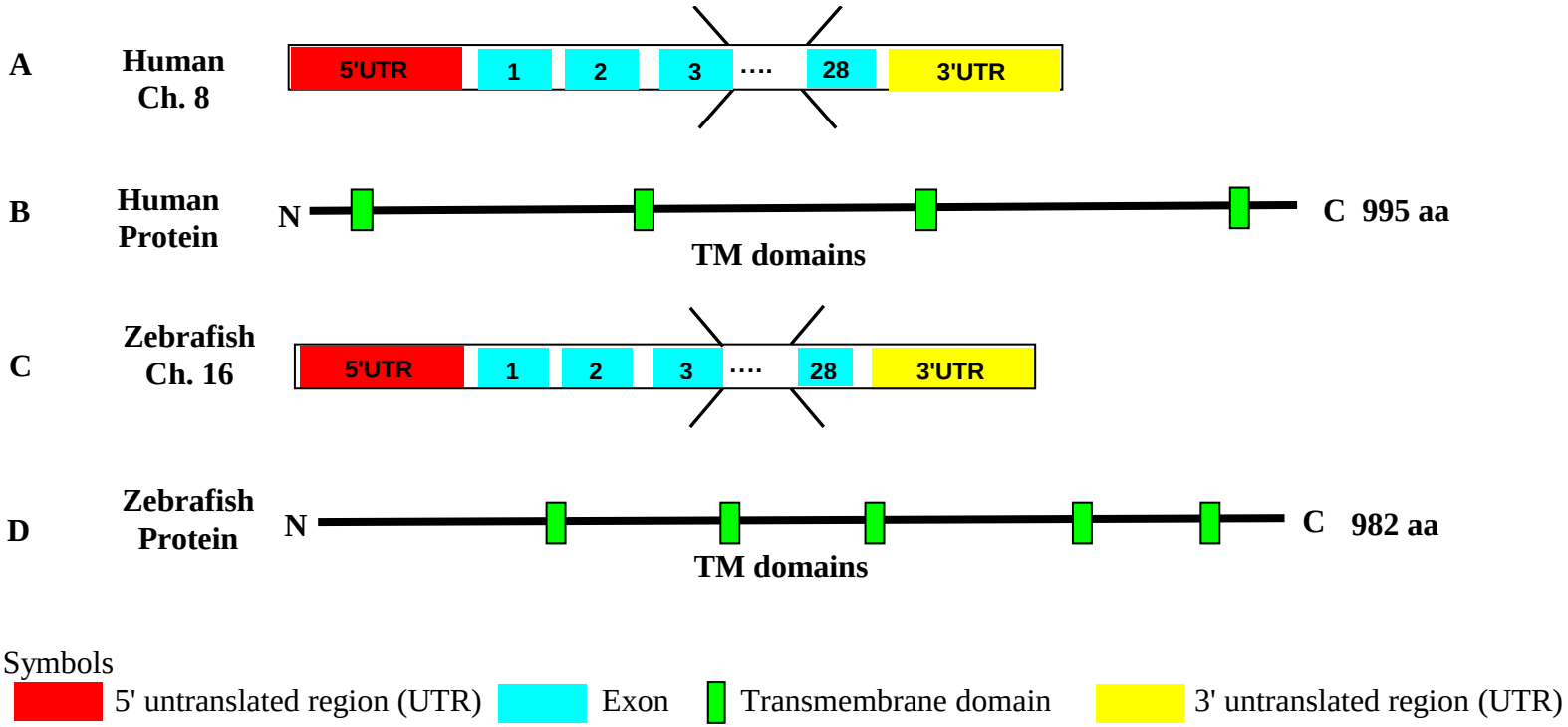

Figure 4.31 *MKS3* gene transcript and partial protein product structure in humans and zebrafish
(**A**) *MKS3* gene transcript in humans (OTTHUMT00000329641) has 28 exons and schematic representation of encoded protein product, Meckelin which includes 4 transmembrane domains (TM) and has 995 amino acids (OTTHUMP00000203157) (**B**). (**C**) *mks3* gene transcript in zebrafish (OTTDART00000042166) has 28 exons and schematic representation of encoded protein product, meckelin (OTTDARP00000033569), which has 5 TM domains and 982 amino acids (**D**). aa, amino acids; Ch., chromosome.

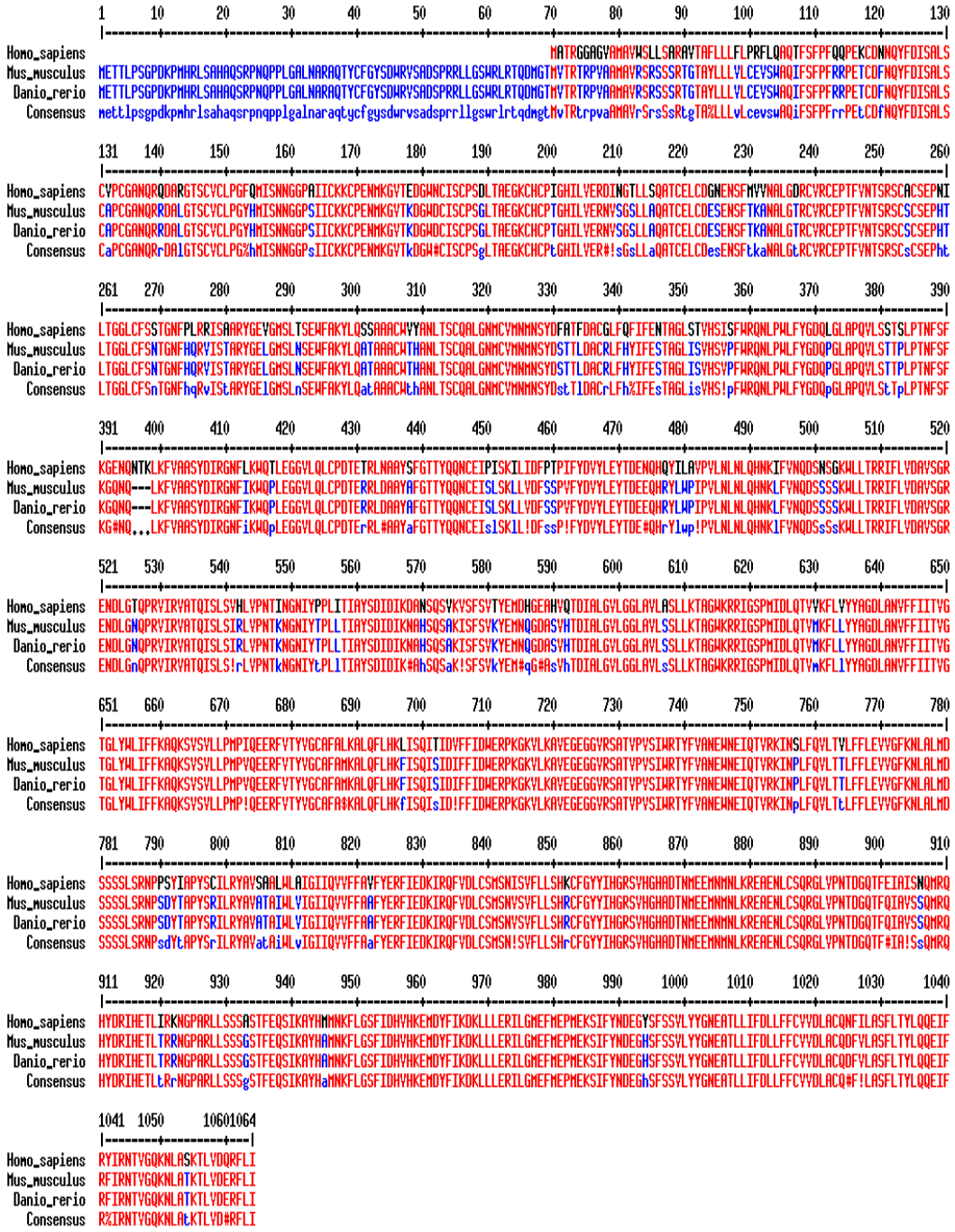

Figure 4.32 Evolutionary conservation of Mks3 protein, Meckelin, in humans, mice and zebrafish

Meckelin peptide sequence alignment in humans (homo sapiens, ENSP00000389998), mice (mus musculus, ENSMUSP00000103928) and zebrafish (danio rerio, ENSDARP00000116688). Conservation of amino acid alignment (red font).

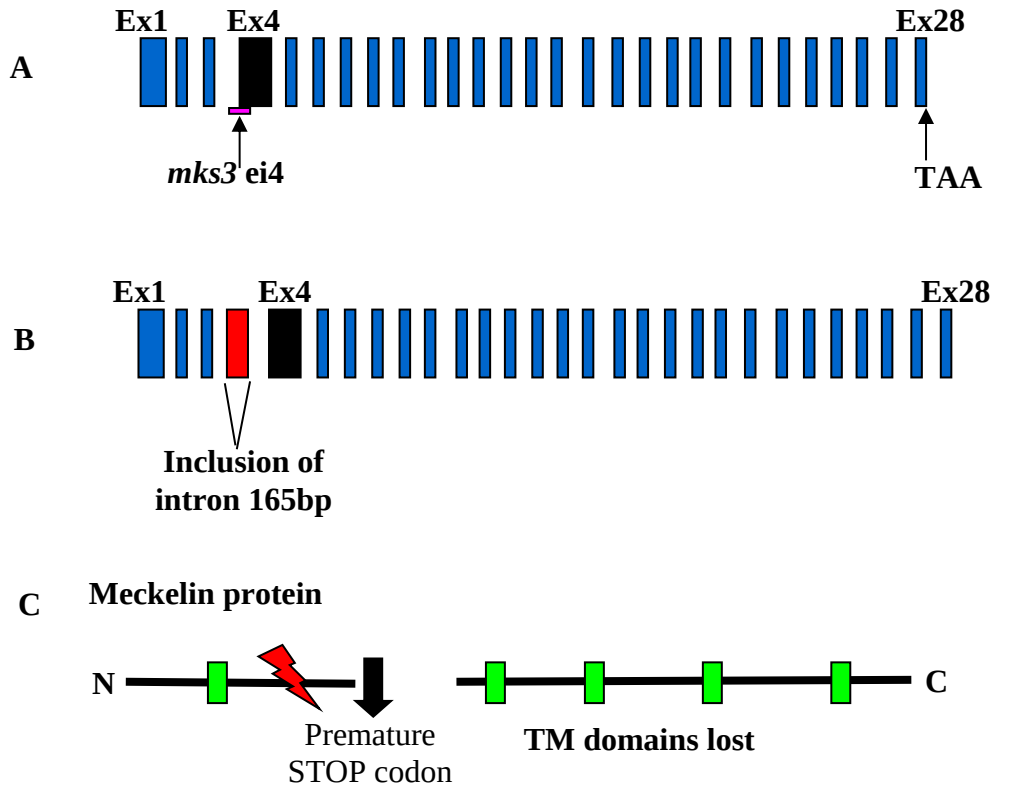

Figure 4.33 Design of *mks3* splice blocking MO and the effect at the protein level

(**A**) Schematic representation of zebrafish *mks3* showing the target site of the splice blocking MO is exon 4 (*mks3*ei4). Knockdown with *mks3* MO leads to abnormal splicing with inclusion of a 165bp intron (red) after exon 3 (**B**). At the protein level, this leads to an alternative reading frame after 125 amino acids and a premature stop codon after 144 amino acids, resulting in a truncated protein with loss of 4 transmembrane domains (**C**). MO, morpholino oligonucleotide.

A

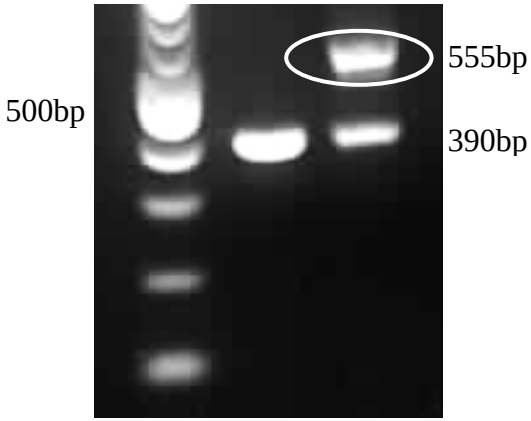

B

```
                131       140       150       160       170       180       190       200       210       220       230       240       250       260
                |---------+---------+---------+---------+---------+---------+---------+---------+---------+---------+---------+---------+---------|
mks3MO          TTTGATATTTCGAGCCTGTCTTGCGTGAAATGCGGGTCAAATCAAGTCAGCAGCAAATCAGGACTGGCATGTGAGTGTCAGGCTGGTTCCAGAGTGCTGGTCAGTAATGGGGTGTCTATCTTGTGCCAGC
mks3 cDNA             TGAGCCTGTCTTGCGTGAAATGCGGGTCAAATCAAGTCAGCAGCAAATCAGGACTGGCATGTGAGTGTCAGGCTGGTTCCAGAGTGCTGGTCAGTAATGGGGTGTCTATCTTGTGCCAGC
Consensus       ..........cGAGCCTGTCTTGCGTGAAATGCGGGTCAAATCAAGTCAGCAGCAAATCAGGACTGGCATGTGAGTGTCAGGCTGGTTCCAGAGTGCTGGTCAGTAATGGGGTGTCTATCTTGTGCCAGC

                261       270       280       290       300       310       320       330       340       350       360       370       380       390
                |---------+---------+---------+---------+---------+---------+---------+---------+---------+---------+---------+---------+---------|
mks3MO          AGTGTCCTGATGCTGATCAGGTGGTCACCCAGGATGGATATGAATGTATTCGTTGTCCTGGAACTGTGGGGAAGGATGGCAAGTGTCAGTGTCCTGAGGGAAGTGTGCTGGTGGAGAGAGATGGGAATGG
mks3 cDNA       AGTGTCCTGATGCTGATCAGGTGGTCACCCAGGATGGATATGAATGTATTCGTTGTCCTGGAACTGTGGGGAAGGATGGCAAGTGTCAGTGTCCTGAGGGAAGTGTGCTGGGTAGGCGC-TTGTCATTTT
Consensus       AGTGTCCTGATGCTGATCAGGTGGTCACCCAGGATGGATATGAATGTATTCGTTGTCCTGGAACTGTGGGGAAGGATGGCAAGTGTCAGTGTCCTGAGGGAAGTGTGCTGGggaaGaGa.aTGgcAaTgg

                391       400       410       420       430       440       450       460       470       480       490       500       510       520
                |---------+---------+---------+---------+---------+---------+---------+---------+---------+---------+---------+---------+---------|
mks3MO          CAATCCCTTAATTGAAGCAAGGTGTCAA-GCATGTAGTGCAACAGATCCTGCTTTTCTGCCCCAGATATGAAAGGCAACAGTTAGGTGTGAGAGATGTGGGGACTCATTCATTAACTCATCTCAGTCTT
mks3 cDNA       TACTAAAAACAAAAAATACATGCATTAATTGGACAGACTATATAAAGACTTAGTTATTTTCCTGAAAGCTATAATTCAAACATGTGCAATTTGGGTAGATGGTTAAGAATTACTTAATATTTGATGGCAT
Consensus       cAaTaaaacAAaaaAaaCAaGcagTaAa.GcAcagAcTacAaaAaaaCcTacTTaTTcTgCCccAaAgaTaaAAggCAAaaaTgaGcaaTgaGaGaaGagGGgaaacAaTcAcTaAaTaaTcgaaGgCaT

                521       530       540       550       560       570       580       590       600       610       620       630       640       650
                |---------+---------+---------+---------+---------+---------+---------+---------+---------+---------+---------+---------+---------|
mks3MO          GTGTTTGCGGCACTTCGAATACGCTGGCAGGAGGAATGTGCTTCCCTGCGAACAGTCTGCCTACCTCAGTTGCCTCAAGTGTTATTTTTAGCCAACTGACTCTCCCTGTCCAGTCAGCATGGTTTTCAAG
mks3 cDNA       CTGATTGT---TTTTTGTAGTGGAGAGAGATGGGAATGGCAATCCCTTAATTGAAGCAAGGTGTCAA----GCATGTAGTGC
Consensus       cTGaTTGc...acTTcGaAgacGagaGaaagaGGAATGgcaaTCCCTgaaaacAagCaaccTacCaa....GCaTcaAGTGc.....................................................
```

Figure 4.34 Evidence of *mks3* splice MO knockdown by RT-PCR and direct sequencing

(**A**) RT-PCR of single zebrafish embryos at 24hpf following *mks3*splice MO knockdown reveals an additional larger RT-PCR product (circled in white), compared to uninjected wild type (WT) control embryos, which only have the normal RT-PCR product of 390bp. (**B**) Direct sequencing of the larger product (555bp) in *mks3* morphants identifies that it includes the intron (165bp) situated after exon 3, as a result of abnormal splicing. bp, base pairs; hpf, hours post fertilisation; *mks3*cDNA, reference *mks3* cDNA sequence; MO, morpholino oligonucleotide.

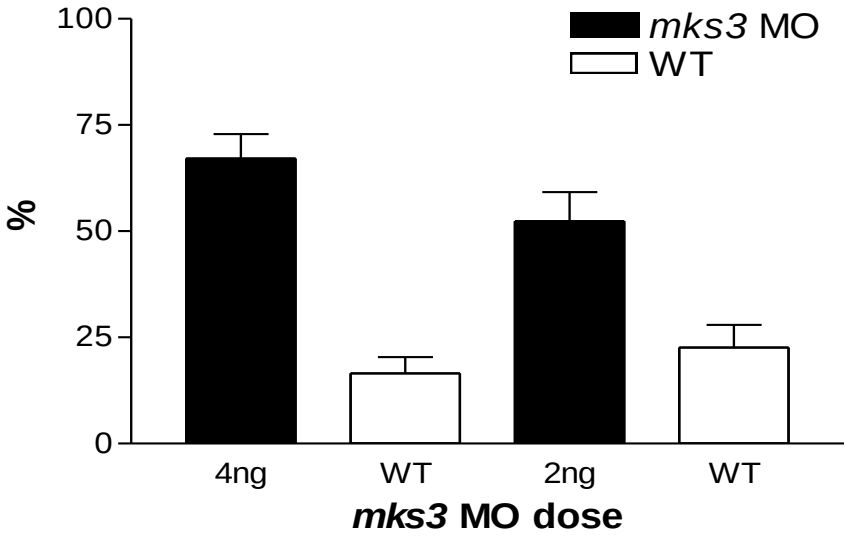

Figure 4.35 Mortality at 24hpf following *mks3* MO injection
Mortality at 24 hours post fertilisation (hpf) is shown as mean percentage (%) and standard error of the mean in zebrafish embryos injected with two different doses of morpholino oligonucleotide (MO). Matched uninjected wild type (WT) controls are shown. There is a dose dependent effect on mortality associated with *mks3* MO injection. The total numbers of embryos at 24hpf were 837 from 12 pairs (4ng) and 968 from 16 pairs (2ng).

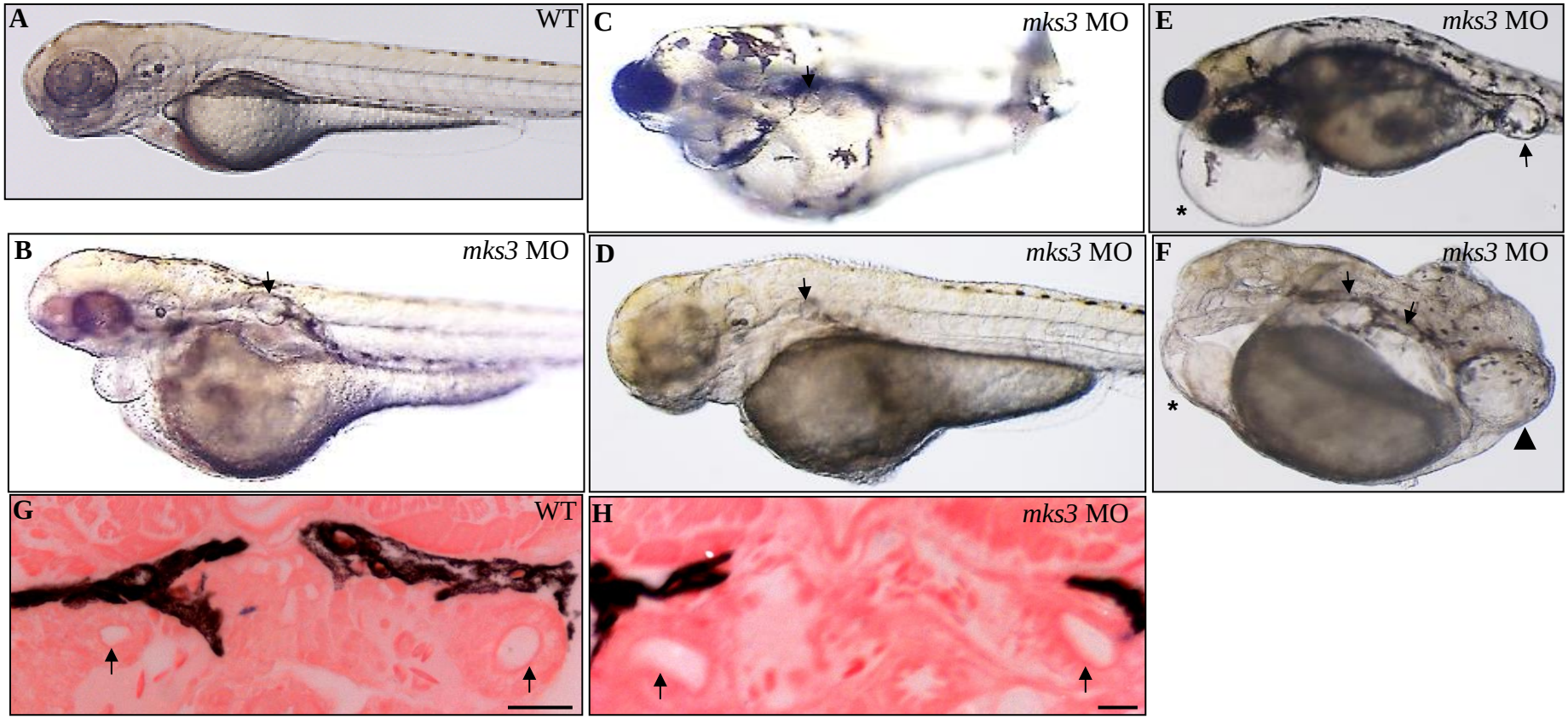

Figure 4.36 *mks3* knockdown induces pronephric and cloacal cysts leading to obstruction of the cloaca

Lateral views of zebrafish embryos 72 hours post fertilisation (**A**-**F**). Wild type (WT) uninjected control embryos are normal (**A**). Embryos injected with *mks3* MO develop pronephric cysts both proximally (arrow, **B**-**D**) and distally at the cloaca (arrow **E**, arrowhead **F**). The cloacal cyst (**E**) appears to cause outflow obstruction as there is marked associated cardiac oedema (*). The large cloacal cyst (arrowhead **F**) leads to proximal cystic dilatation of the pronephros (arrows). Resin histology 5μm sections through the pronephros (arrows) at 5 days (**G**-**H**) reveals dilatation in *mks3* morphants (diameter 29.2-29.7μm, **H**), compared to WT controls (diameter 9.7-13.6μm, **G**). Scale bars = 20μm. Stained with methylene blue-basic fuchsin stain. MO, morpholino oligonucleotide.

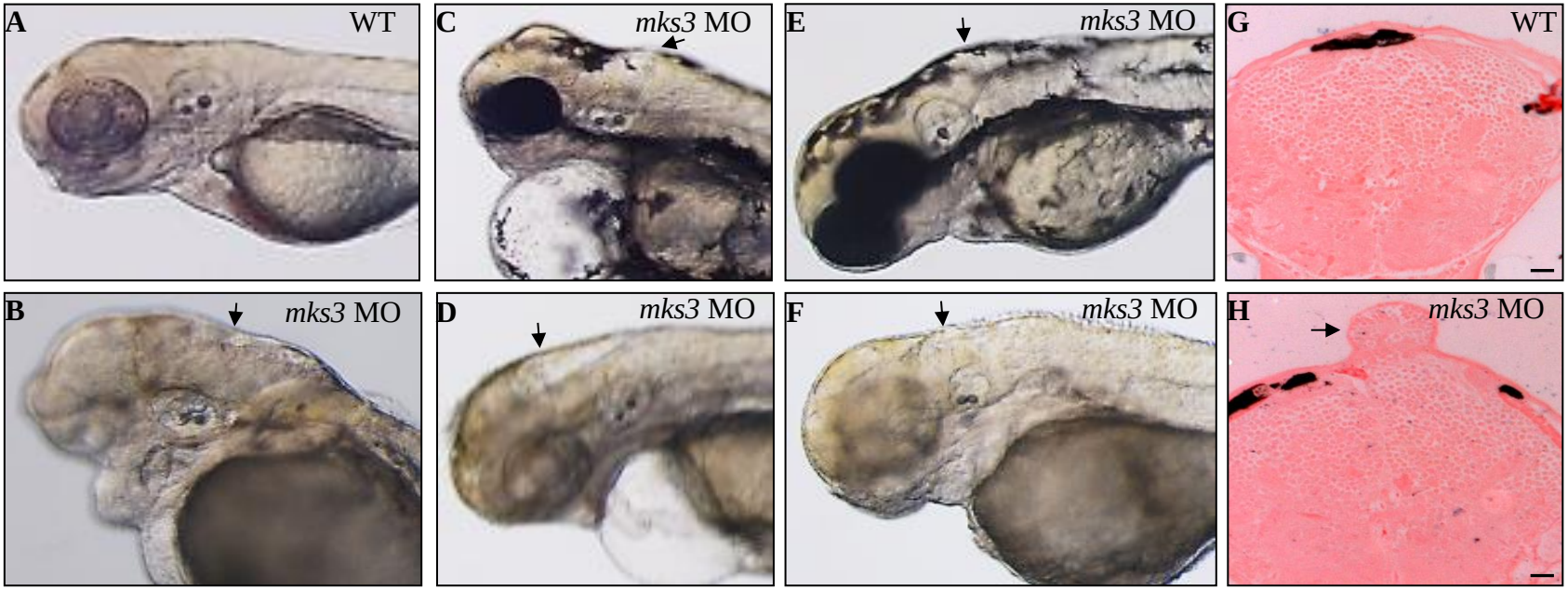

Figure 4.37 *mks3* knockdown induces hydrocephalus and abnormal brain development in zebrafish embryos
Lateral views of zebrafish embryos at 72hpf (**A-F**). Wild type (WT) uninjected control embryos are normal (**A**). Embryos injected with *mks3* MO develop hydrocephalus (arrows, **B-F**). Resin histology 5µm sections through the brain at 5dpf (**G-H**) reveals an encephalocele in *mks3* morphants (arrow, **H**) compared to WT controls (**G**). Scale bars = 20µm. Stained with methylene blue-basic fuchsin stain. dpf, days post fertilisation; hpf, hours post fertilisation; MO, morpholino oligonucleotide.

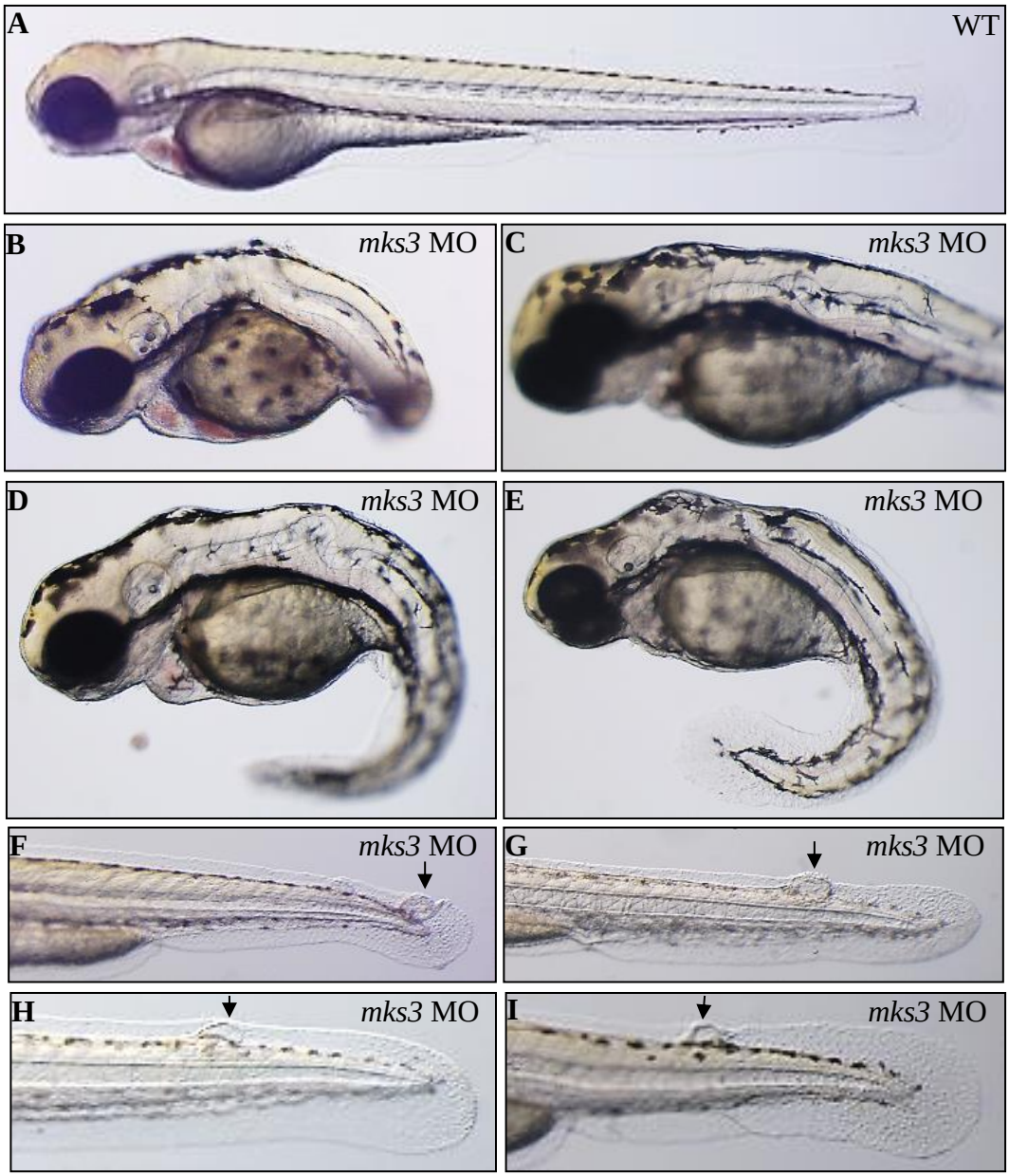

Figure 4.38 *mks3* knockdown induces notochord defects and abnormal tail development in zebrafish embryos

Lateral views of zebrafish embryos 72hpf (**A**-**F**). Wild type (WT) uninjected control embryos are normal (**A**). Embryos injected with *mks3* MO (**B**-**I**) develop abnormal, wavy notochords (**B**-**E**), in severe cases the notochord projects dorsally to the skin surface (**B**). *mks3* morphants also have abnormal tail development (**F**-**I**), with disruption of myotome and fin layers (arrows), possibly representative of human meningoceles. hpf, hours post fertilisation; MO, morpholino oligonucleotide.

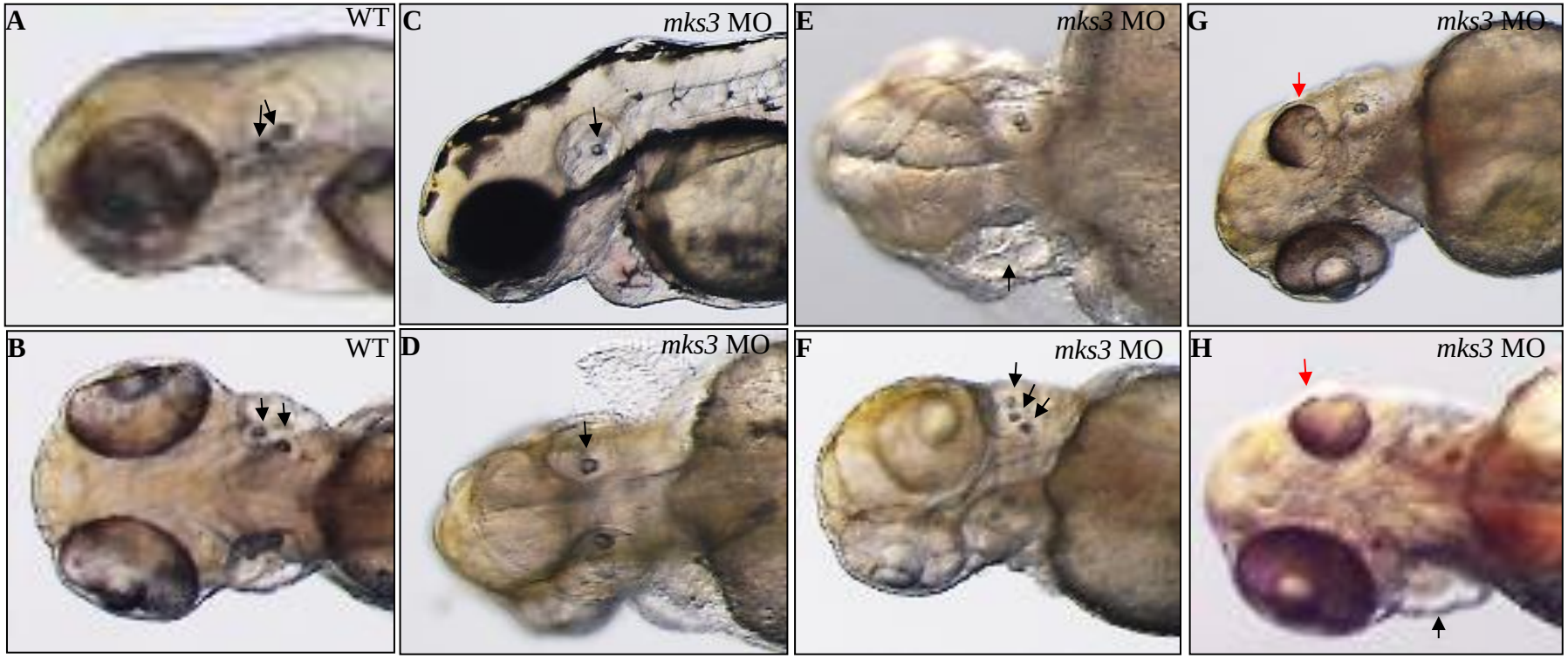

Figure 4.39 Abnormal ear and eye development following *mks3* MO knockdown
Views of the head of zebrafish embryos at 72 hours post fertilisation, focusing on the otic vesicles (**A**-**F**) and eyes (**A**, **B**, **G**, **H**). Wild type (WT) uninjected control embryos have normal eyes of equal size and two otoliths in each otic vesicle (black arrows, **A**, **B**). *mks3* morphants show abnormal ear development with either a single otolith (black arrow, lateral and dorsal views, **C**-**D**), unilateral empty otic vesicle (black arrow, **E**, **H**) or 3 otoliths in an otic vesicle (black arrows, **F**). Abnormal eye development with unilateral microphthalmia (red arrows, **G**-**H**) is also seen in *mks3* morphants. MO, morpholino oligonucleotide.

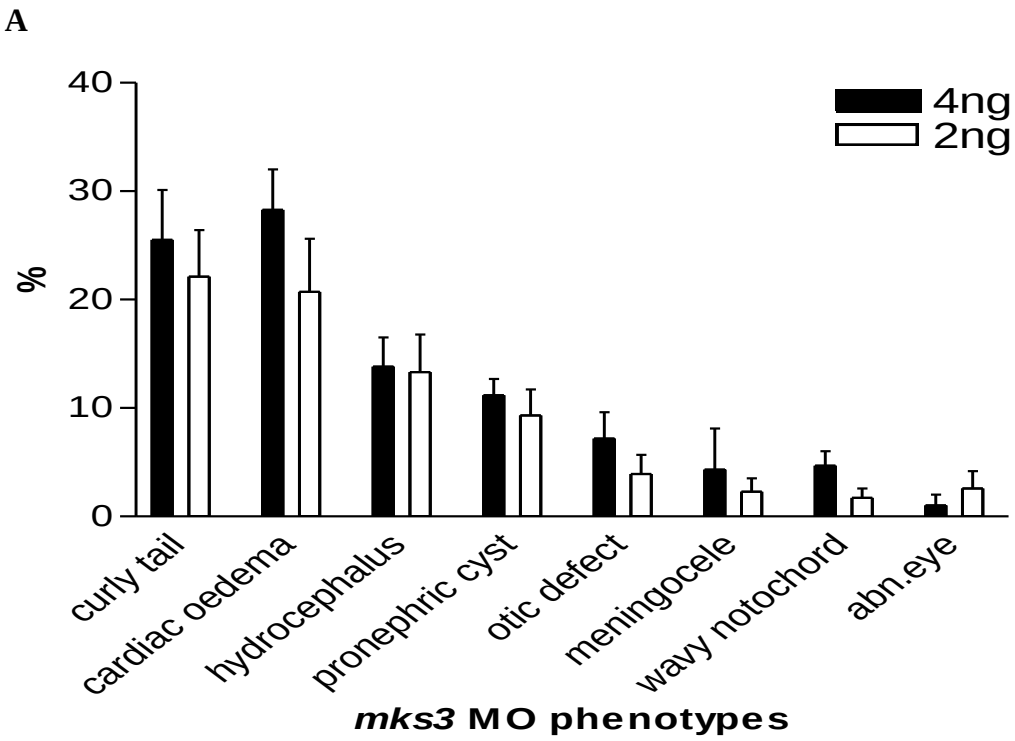

Figure 4.40 Quantification of abnormal phenotypes at 72hpf following injection with *mks3* splice blocking MO

Data are displayed as mean ± SEM. Following injection with 2-4ng of *mks3* splice blocking MO, there was a dose dependent effect on the percentage frequency of each abnormal phentoype (**A**). The total number of zebrafish embryos phenotyped at 72hpf following *mks3* MO injection of: 2ng was 325 and 4ng was 233. hpf, hours post fertilisation; MO, morpholino oligonucleotide.

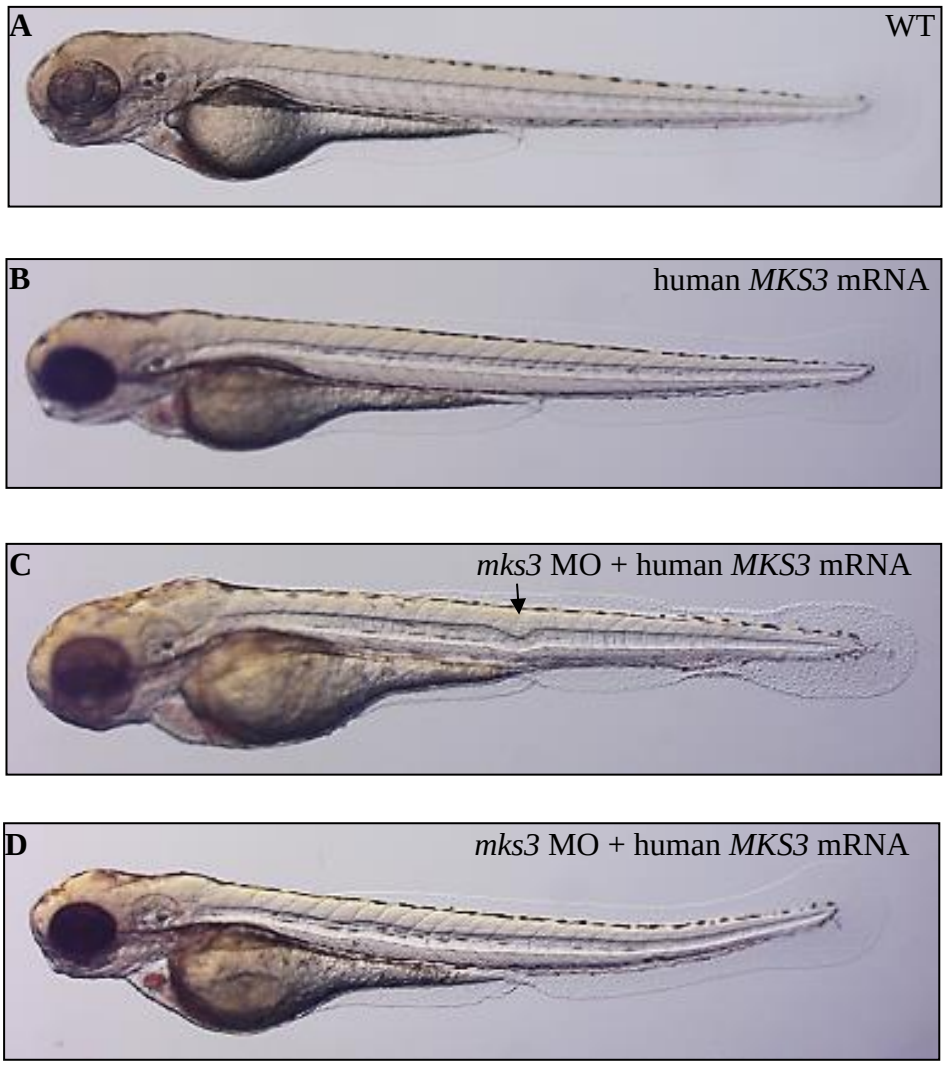

Figure 4.41 Rescue of *mks3* morphant phenotype by co-injection of *mks3* MO with human *MKS3* mRNA

Lateral views of zebrafish embryos 72 hours post fertilisation. Wild type uninjected (**A**) and embryos injected with 50-100pg of human *MKS3* mRNA alone (**B**) were morphologically normal. Partial (**C**) and complete (**D**) rescue of embryos co-injected with *mks3* MO and 50-100pg of human *MKS3* mRNA. A small notochord defect is arrowed in **C**. MO, morpholino oligonucleotide.

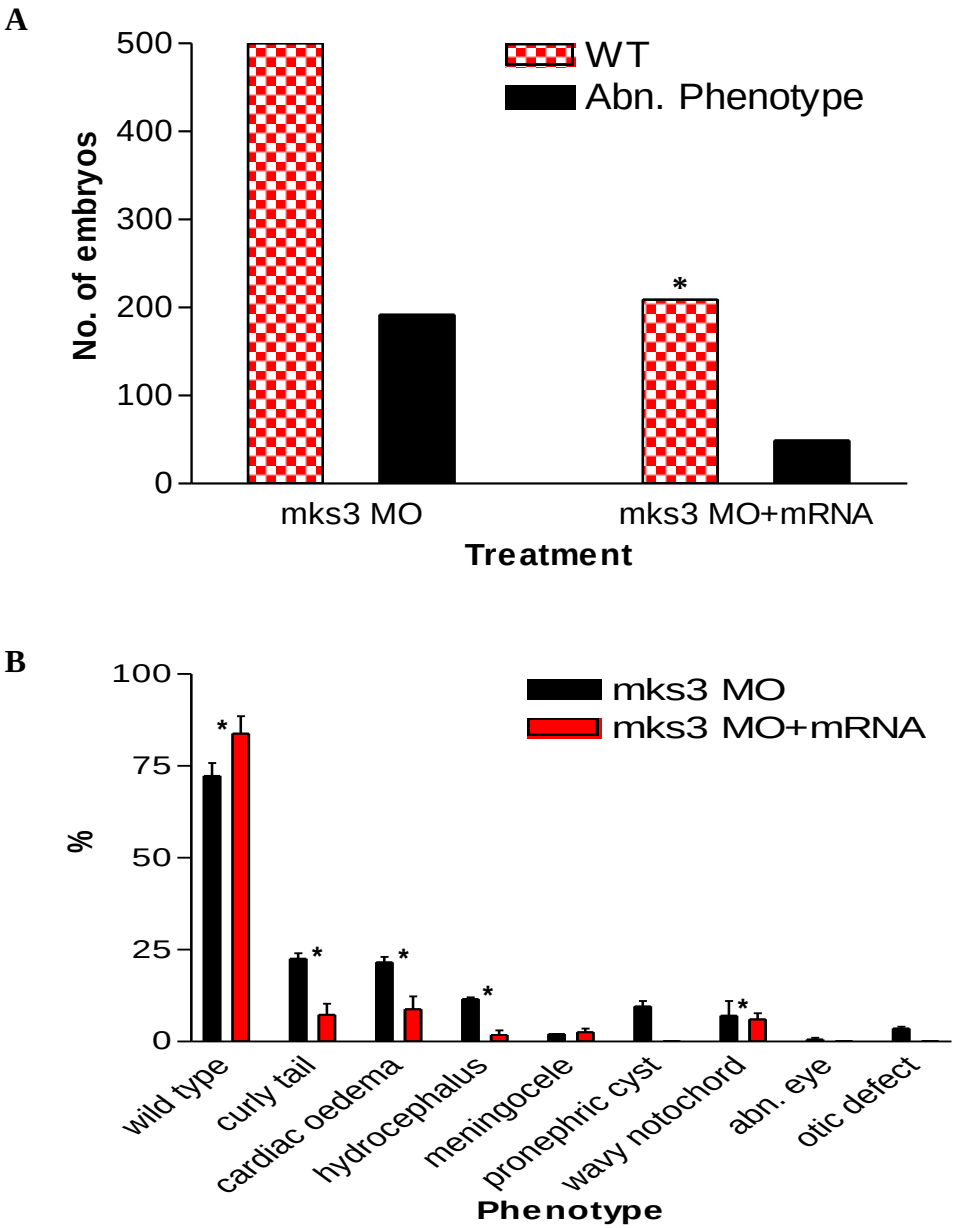

Figure 4.42 Quantification of Rescue of *mks3* morphant phenotype
(**A**) Raw quantification of overall rescue from a morphant phenotype to a normal, wild type appearance in embryos co-injected with 50-100pg of human *MKS3* mRNA and 2-4ng of *mks3* MO (n=318). The degree of rescue to the normal wild type phenotype was just significant (*, p=0.052, chi-squared test). The total number of embryos injected with 2-4ng of *mks3* MO alone was 691. (**B**) Percentage of each phenotype shown as mean ± SEM, in embryos injected with 2-4ng of *mks3* MO alone, compared to those co-injected with 50-100pg human *MKS3* mRNA. There was a significant degree of rescue to the wild type phenotype and reduction of each abnormal phenotype following co-injection with *MKS3* mRNA (*, p=0.0058, chi-squared test). MO, morpholino oligonucleotide.

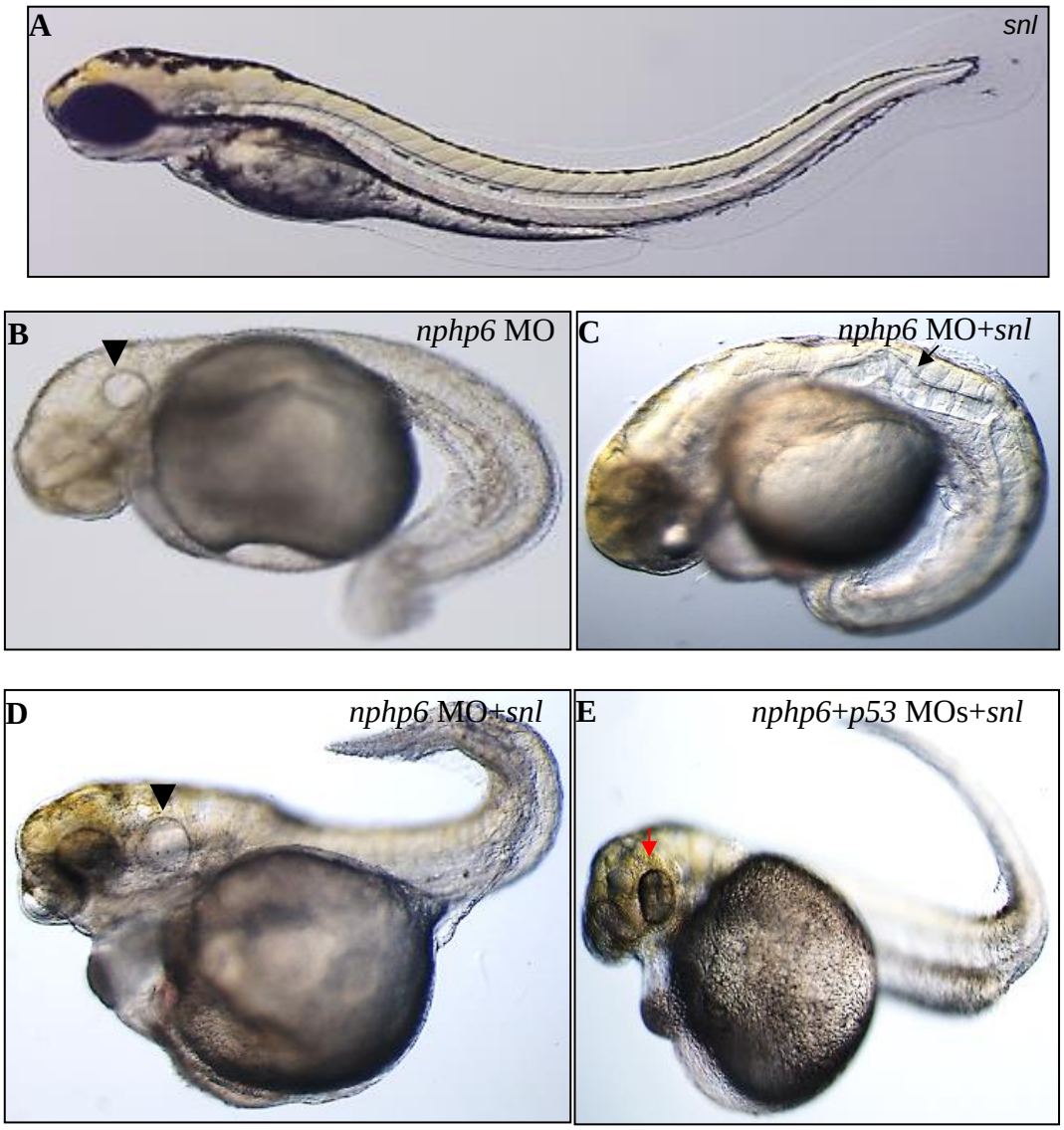

Figure 5.1 Phenotypes following combination of *nphp6* MO knockdown in *sentinel* (*snl*) zebrafish embryos

Lateral views of zebrafish embryos at 72 hours post fertilisation. Uninjected *sentinel* (*snl*, **A**) zebrafish embryos have a characteristic sine wave shaped tail. **B** is a wild type (not *snl*) embryo injected with *nphp6* MO which has a ventrally curved tail, hydrocephalus, cardiac oedema and empty otic vesicle (black arrowhead). Combination of *nphp6* MO knockdown in *snl* embryos (**C**, **D**) induces a range of abnormal phenotypes including wavy notochord (**C**), cardiac oedema, hydrocephalus, dorsal curly tail (**D**) and delayed development of otoliths in the otic vesicle (black arrowhead, **D**). *snl* embryos additionally co-injected with *nphp6* and *p53* MOs (**E**) continue to develop an aberrant phenotype with dorsal curly tail, cardiac oedema, hydrocephalus and unilateral microphthalmia (red arrow), excluding the possibility of the combination resulting from an off-target effect. MO, morpholino oligonucleotide.

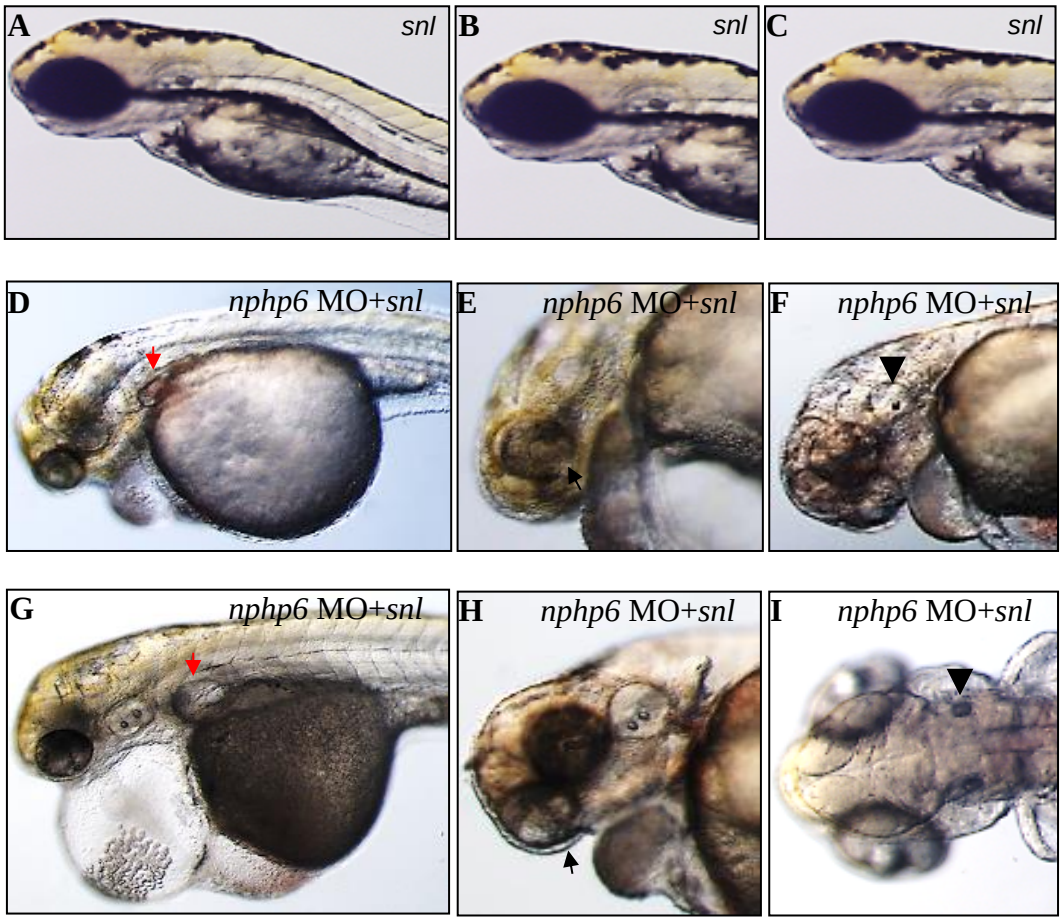

Figure 5.2 Pronephric cysts and abnormal eye and ear development following combination of *nphp6* MO knockdown in *sentinel (snl)* zebrafish embryos

Cropped views of *snl* zebrafish embryos at 72 hours post fertilisation, focusing on the proximal pronephros (**A**, **D**, **G**), eyes (**B**, **E**, **H**) and otic vesicles (**C**, **F**, **I**). Compared to uninjected *snl* embryos (**A**-**C**), *snl* embryos injected with *nphp6* MO develop pronephric cysts (red arrows, **D**, **G**), colobomas (black arrows, **E**, **H**) and fewer otoliths in the otic vesicle (single, black arrowhead, **F**, **I**(dorsal view)). MO, morpholino oligonucleotide.

A

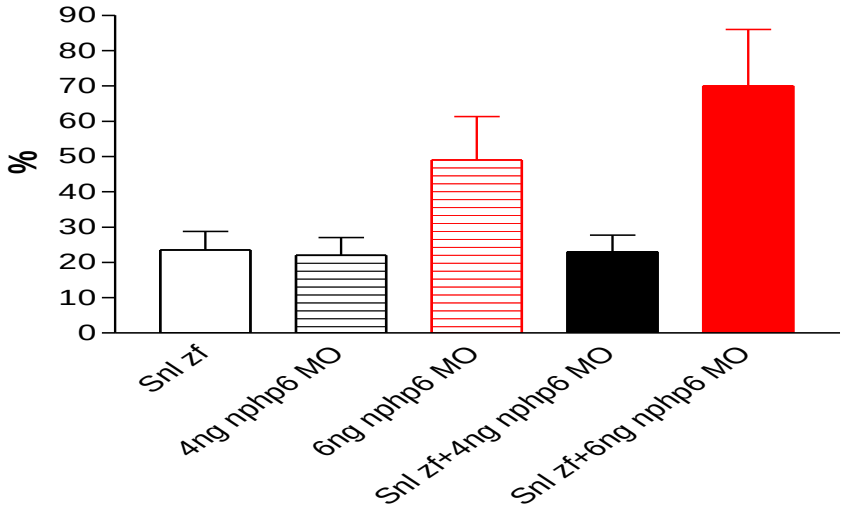

Figure 5.3 Mortality at 24hpf following combination of *nphp6* MO knockdown in *sentinel* (*snl*) zebrafish embryos

Mortality at 24hpf is shown as mean percentage (%) and standard error of the mean in *snl* zebrafish embryos alone, wild type zebrafish embryos injected with 4-6ng *nphp6* MO alone and *snl* embryos injected with 4-6ng *nphp6* MO (**A**). The mean 24hpf mortality is similar in *snl* zebrafish embryos alone (24%), wild type embryos injected with 4ng *nphp6* MO alone (22%) and *snl* embryos injected with 4ng *nphp6* MO (23%). Injection of 6ng of *nphp6* MO alone is associated with a much higher 24hpf mortality of 49% and in *snl* embryos this rises to 70%. hpf, hours post fertilisation. MO, morpholino oligonucleotide.

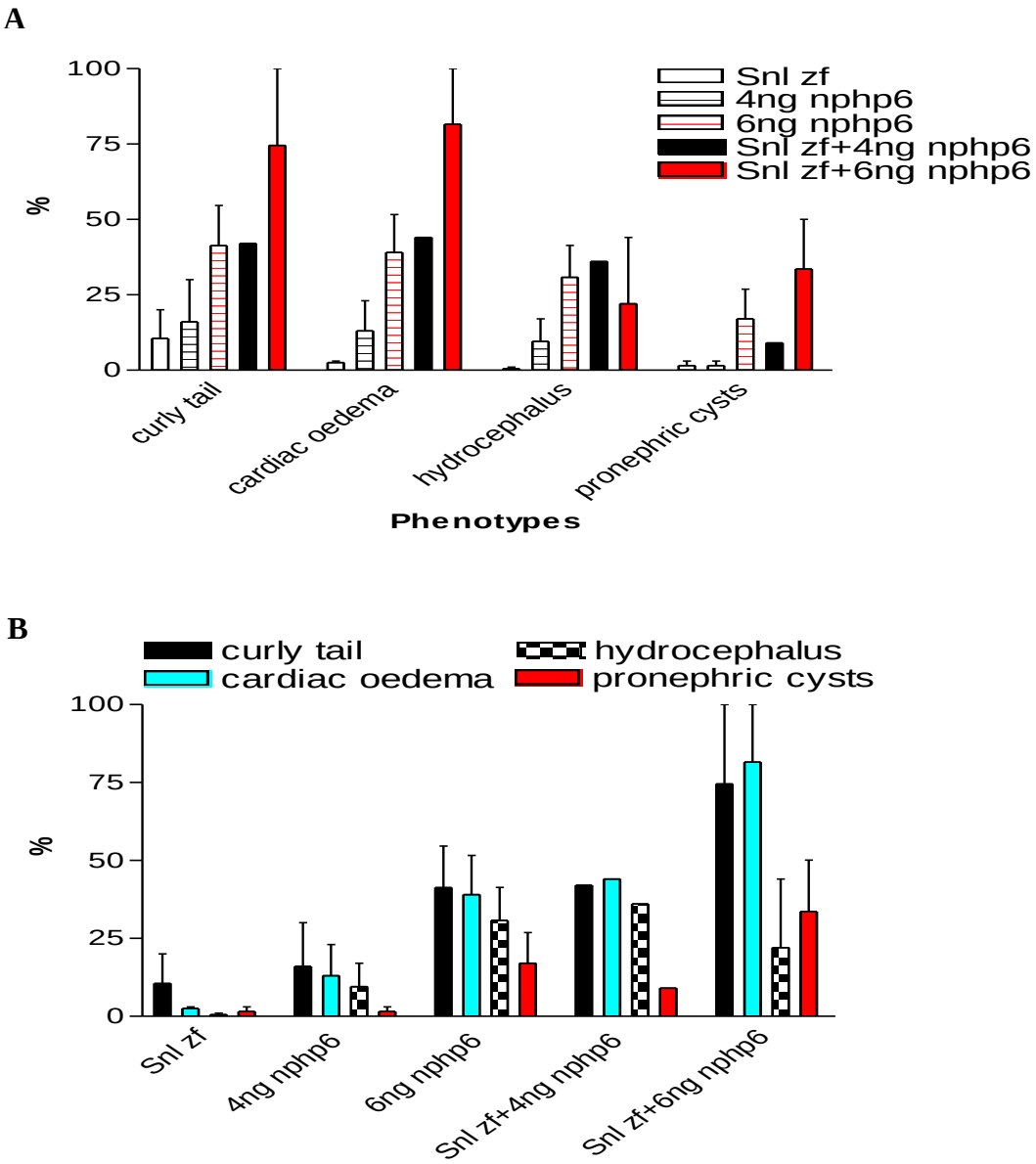

Figure 5.4 Percentage frequency of abnormal phenotypes at 72hpf following combination of *nphp6* MO knockdown in *sentinel* (*snl*) zebrafish embryos

Data are displayed as mean ± SEM. **A** emphasises the range of phenotypes in each group of zebrafish embryos. **B** highlights the effect of the individual genes (*cc2d2a* in *snl*; *nphp6* MO) and gene combinations on the frequency of abnormal phenotypes. The percentage frequency of each abnormal phenotype increases in a dose dependent manner following 4-6ng of *nphp6* MO knockdown alone (2-42%) and is generally low (1-11%) in *snl* embryos alone (**A**). The frequency of abnormal phenotypes following 6ng of *nphp6* MO alone is similar to the cumulative effect of 4ng of *nphp6* MO in *snl* embryos (**B**). The cumulative effect of 4 or 6ng of *nphp6* MO in *snl* zebrafish embryos has a synergistic effect on each abnormal phenotype except for hydrocephalus in *snl* embryos injected with 6ng of *nphp6* MO (**B**). The total numbers of embryos were 321 (*snl* zf), 261 (4ng *nphp6* MO), 216 (6ng *nphp6* MO), 144 (*snl* zf+4ng *nphp6* MO) 43 (*snl* zf+6ng *nphp6* MO). hpf, hours post fertilisation; SEM, standard error of the mean; zf, zebrafish. MO, morpholino oligonucleotide.

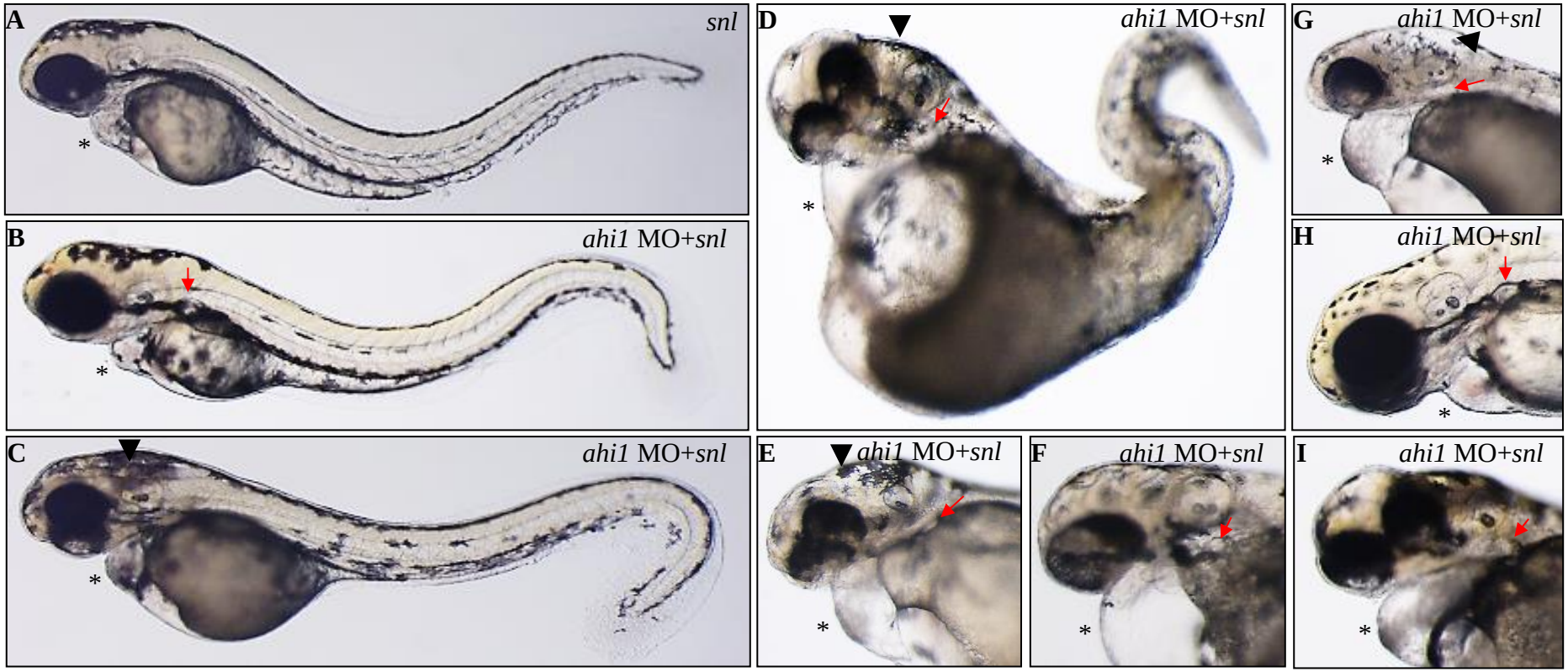

Figure 5.5 Hydrocephalus and pronephric cysts following combination of *ahi1* MO knockdown in *sentinel* (*snl*) zebrafish embryos
Lateral views of zebrafish embryos at 72 hours post fertilisation. Uninjected *sentinel* (*snl*, **A**) zebrafish embryo with cardiac oedema (*) and characteristic sine wave shaped tail. **B-I** are *snl* embryos injected with *ahi1* MO and display a range of abnormal phenotypes including hydrocephalus (black arrowhead **C-E**, **G**) and pronephric cysts (red arrow **B**, **D-I**). A pronounced dorsal sine wave shaped tail is seen in **D**. MO, morpholino oligonucleotide.

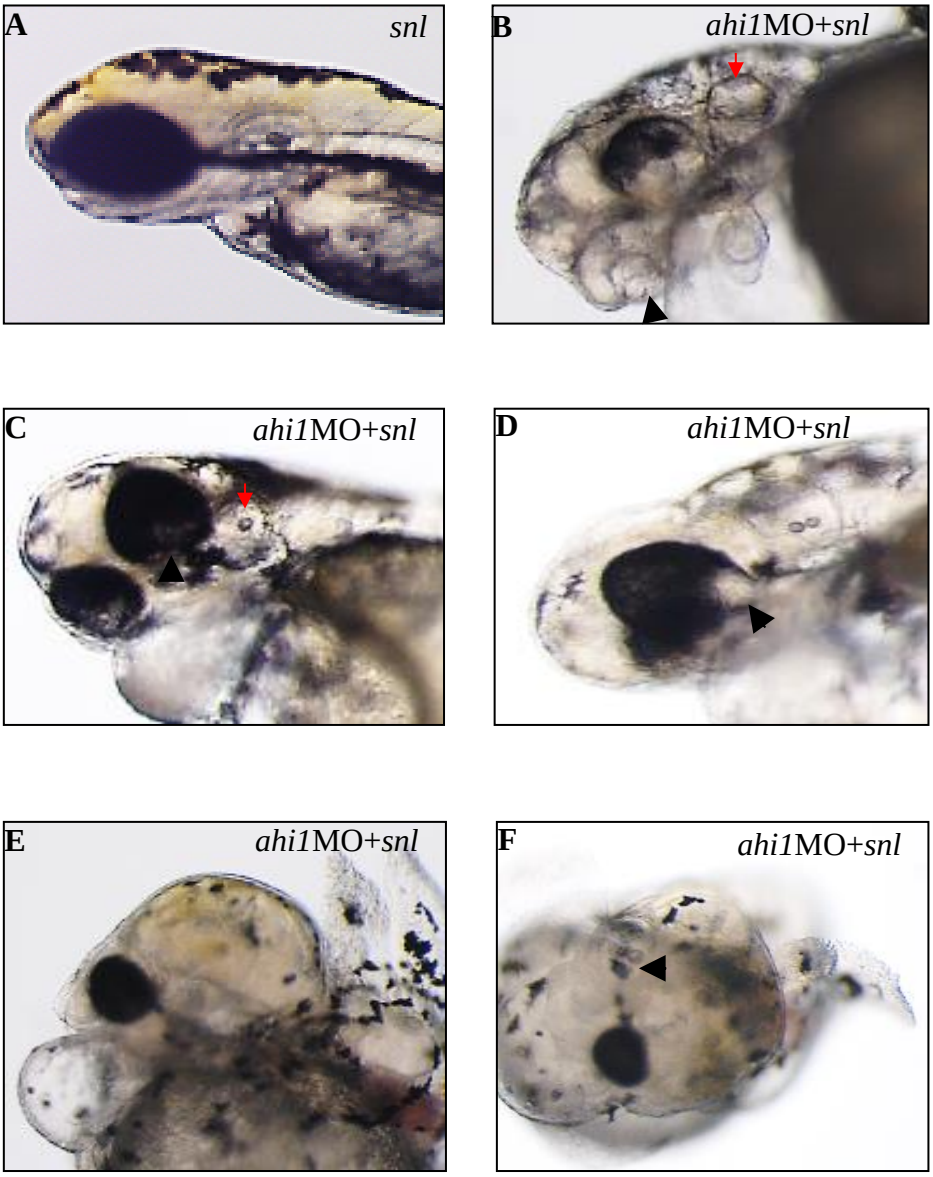

Figure 5.6 Abnormal eye and ear development following combination of *ahi1* MO knockdown in *sentinel* (*snl*) zebrafish embryos
Cropped views of *snl* zebrafish embryos at 72 hours post fertilisation, focusing on the eyes and otic vesicles. Compared to uninjected *snl* embryos which predominantly have normal eyes and 2 otoliths in each otic vesicle (**A**), *snl* embryos injected with *ahi1* MO have abnormal development of the eyes (black arrowheads) and rudimentary ear (red arrow) (**B-F**). (**B**) A coloboma and empty otic vesicle, (**C**) coloboma and single otolith, (**D**) coloboma. **E** and **F** are lateral and dorsal views of an embryo with unilateral microphthalmia of the right eye (black arrowhead, **F**). MO, morpholino oligonucleotide.

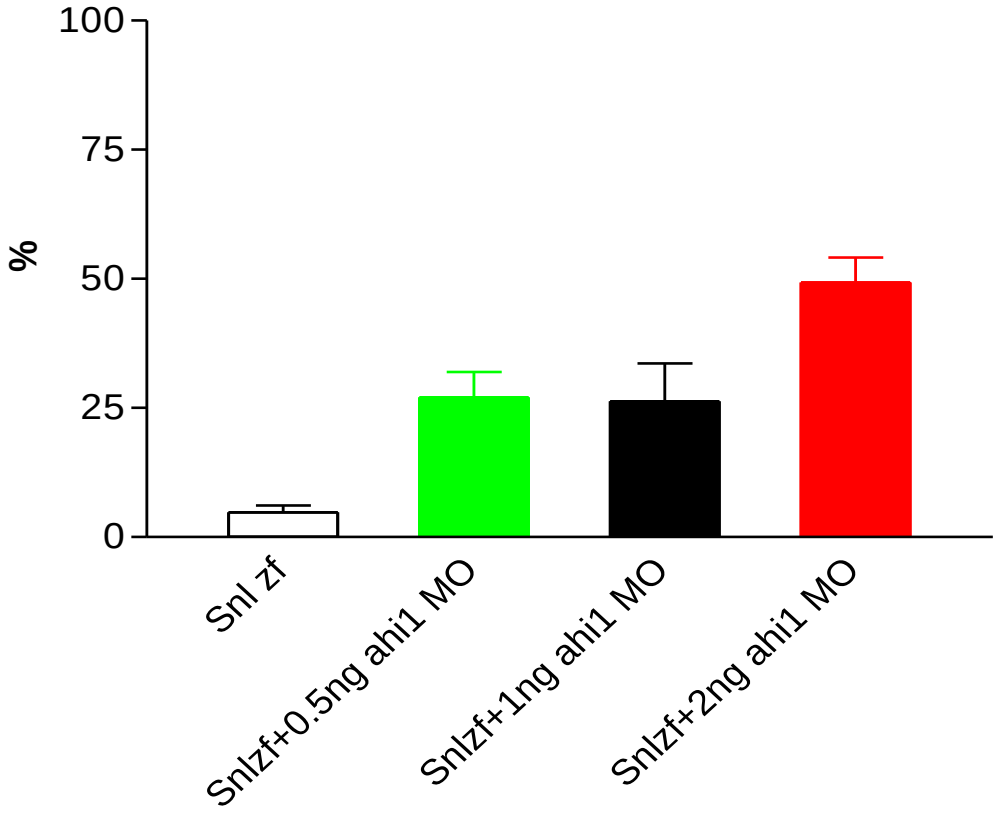

Figure 5.7 Mortality at 24hpf following combination of *ahi1* MO knockdown in *sentinel* (*snl*) zebrafish embryos

Mortality at 24hpf is shown as mean percentage (%) and standard error of the mean (SEM) in *snl* zebrafish embryos alone and *snl* embryos injected with 0.5-2ng of *ahi1* MO (**A**). The mean 24hpf mortality is only 4.8% ± 1.4% in *snl* zebrafish embryos alone and rises in a predominantly dose dependent manner when *snl* embryos are injected with: 0.5ng *ahi1* MO (27% ± 4.9%), 1ng *ahi1* MO (26.3% ± 7.4%) and 2ng *ahi1* MO (49.3% ± 4.8%). MO, morpholino oligonucleotide.

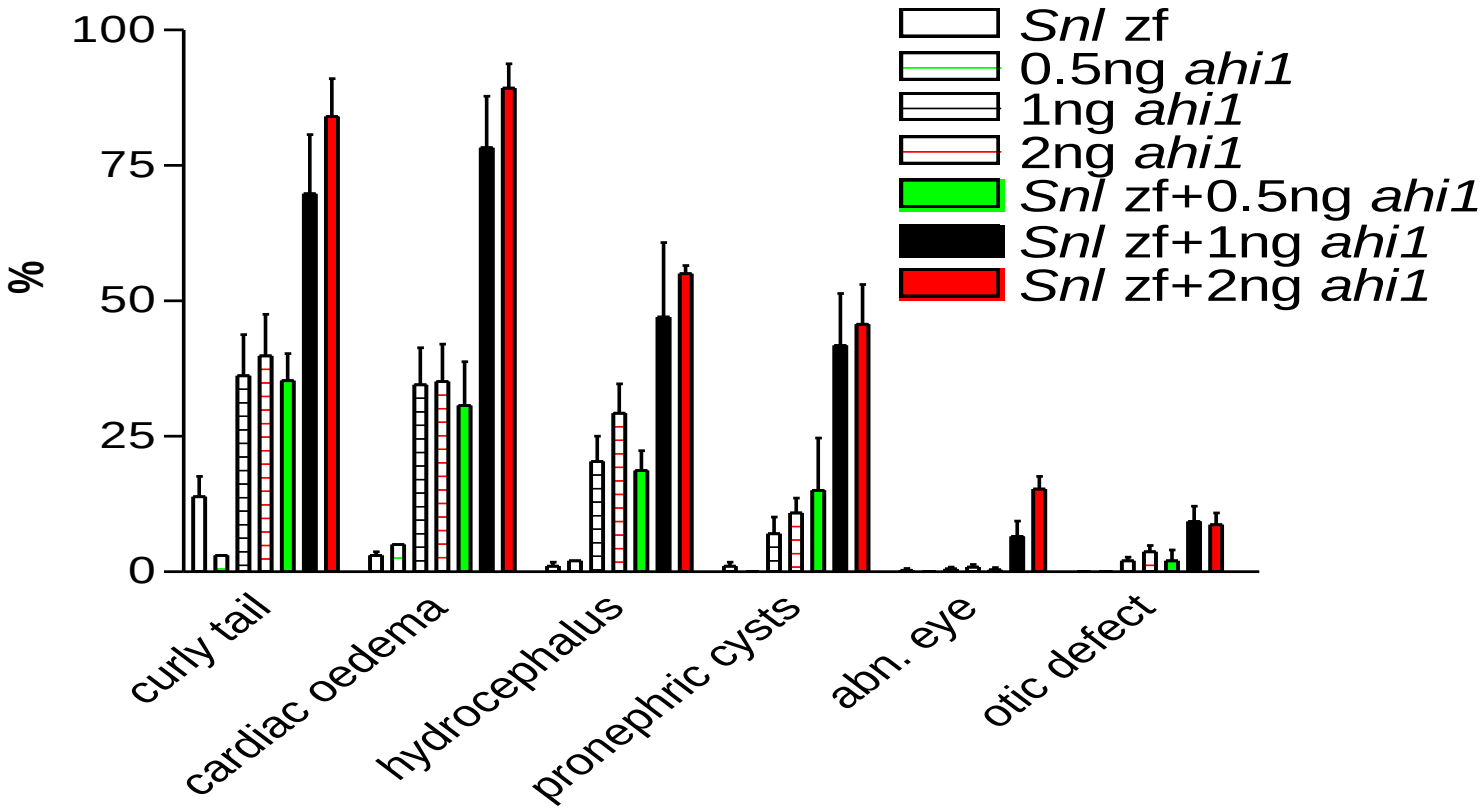

Figure 5.8 Percentage frequency of abnormal phenotypes following combination of *ahi1* MO knockdown in *sentinel* (*snl*) zebrafish embryos

The mean and SEM frequency of abnormal phenotypes for *snl* zebrafish embryos alone (white bars, n=933), wild type (WT) embryos injected with 0.5ng *ahi1* MO alone (green striped bars, n=58), 1ng *ahi1* MO alone (black striped bars, n=793), 2ng *ahi1* MO alone (red striped bars, n=517) and the combination of *snl* embryos injected with 0.5ng *ahi1* MO (green bars, n=246), 1ng *ahi1* MO (black bars, n=291) and 2ng *ahi1* MO (red bars, n=105) are shown. The mean frequency of abnormal phenotypes is low (0-14%) in *snl* embryos alone (white bars) and WT embryos injected with 0.5ng *ahi1* MO alone (green striped bars). There is a synergistic and dose dependent increase in abnormal phenotypes when 0.5-2ng of *ahi1* MO is injected into *snl* embryos. MO, morpholino oligonucleotide.

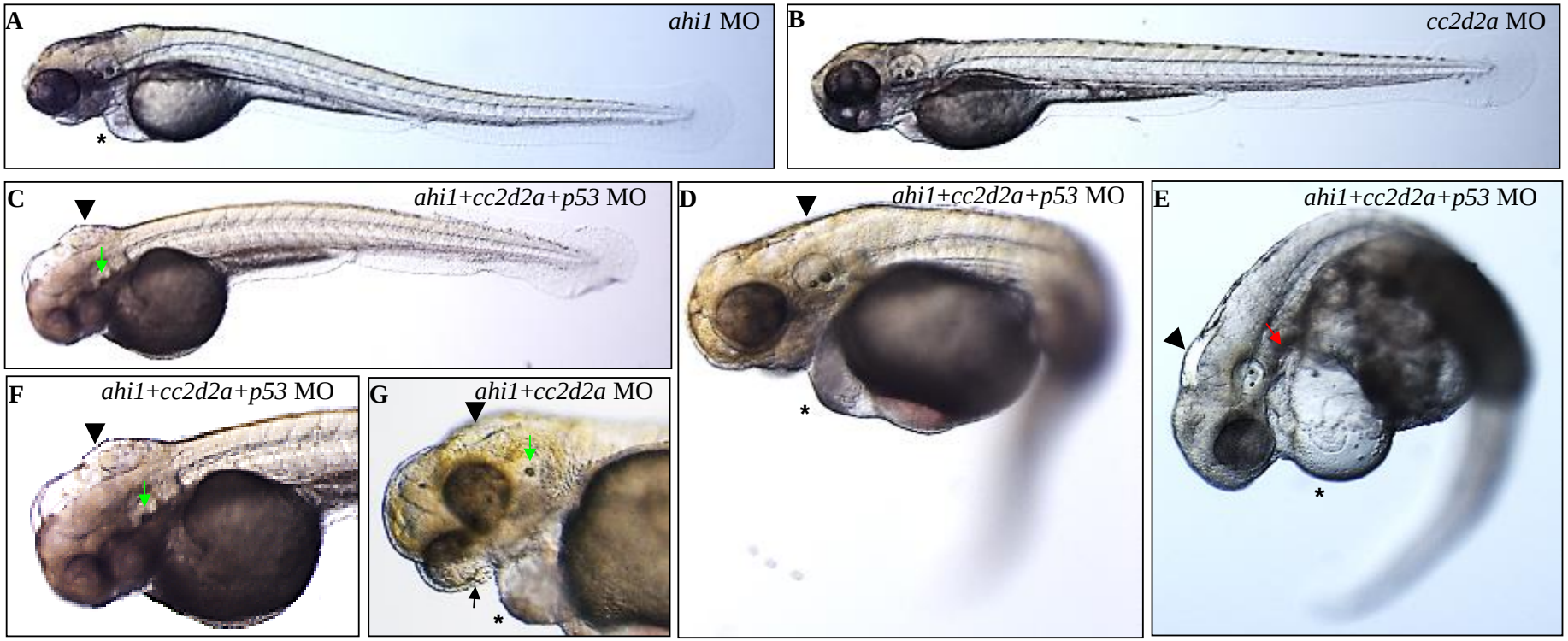

Figure 5.9 Phenotypes following combination of low dose *ahi1* and *cc2d2a* MO knockdown in zebrafish embryos
Lateral views of zebrafish embryos at 72 hours post fertilisation. Wild type (WT) zebrafish embryos injected with a low dose of *ahi1* MO (0.5ng, **A**) and *cc2d2a* MO (4ng, **B**) alone showed minimal cardiac oedema (*, **A**) or were phenotypically normal. WT zebrafish embryos co-injected with low dose *ahi1* (0.5ng) and *cc2d2a* (2ng) MOs develop abnormal phenotypes, which persist when also co-injected with *p53* MO (to exclude off-target effects, **C**-**F**). The range of abnormal phenotypes following co-injection of low dose *ahi1* and *cc2d2a* MOs includes: cardiac oedema (*, **D**, **E**); hydrocephalus (black arrowhead, **C**-**F**); curved body axis (**D**, **E**); pronephric cysts (red arrow **E**); coloboma (black arrow, **G**); single otolith (green arrow, **F**, **G**). MO, morpholino oligonucleotide.

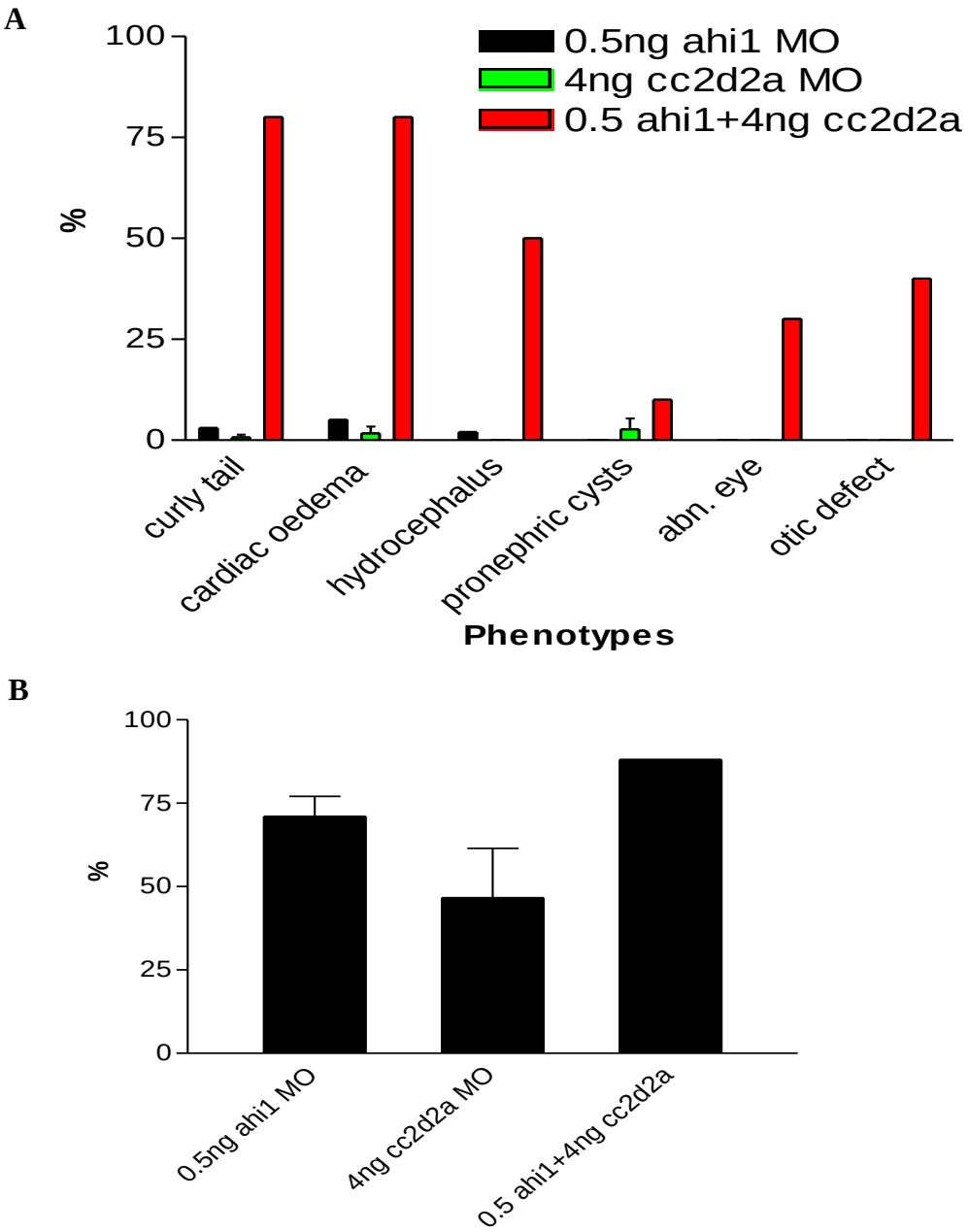

Figure 5.10 Percentage frequency of abnormal phenotypes following combined MO knockdown using 0.5ng *ahi1* and 4ng *cc2d2a* in zebrafish embryos and associated mortality at 24hpf

Low dose (0.5ng) *ahi1* MO alone (black bars, n=58) and 4ng *cc2d2a* MO alone (green bars, n=96) induce a low frequency (≤5%) of abnormal phenotypes (**B**). The combined MO knockdown of 0.5ng *ahi1* and 4ng *cc2d2a* (red bars, n=10) leads to a synergistic increase in the frequency of development of each abnormal phenotype (**B**). Mortality at 24hpf (**A**) is shown as mean percentage (%) and standard error of the mean (where possible) in zebrafish embryos following: 0.5ng of *ahi1* MO alone, 4ng *cc2d2a* MO alone and co-injection of 0.5ng *ahi1* MO + 4ng *cc2d2a* MO. hpf, hours post fertilisation; MO, morpholino oligonucleotide.

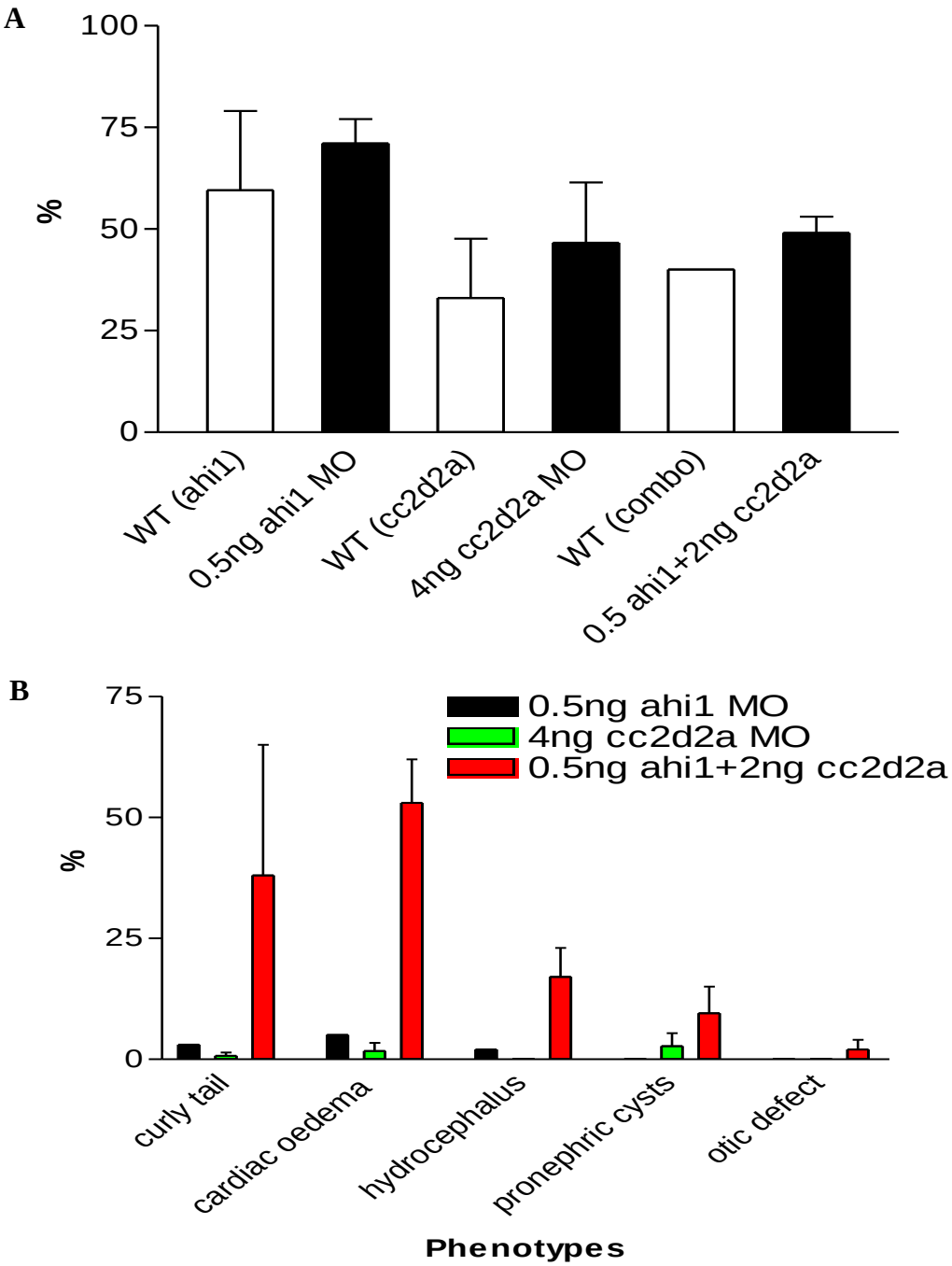

Figure 5.11 Mortality at 24hpf and percentage frequency of abnormal phenotypes following combined *ahi1*, *cc2d2a* and *p53* MO knockdown in zebrafish embryos

(**A**) Mortality at 24hpf is shown as mean percentage (%) and standard error of the mean (where possible) in zebrafish embryos following: 0.5ng of *ahi1* MO alone, 4ng *cc2d2a* MO alone and co-injection of 0.5ng *ahi1* MO, 2ng *cc2d2a* MO and 2ng *p53* MO. Mortality in uninjected WT matched for each MO experiment are shown (white bars). Low dose (0.5ng) *ahi1* MO alone (black bars, n=58) and 4ng *cc2d2a* MO alone (green bars, n=96) induce a low frequency (<5%) of abnormal phenotypes (**B**). The combined MO knockdown of 0.5ng *ahi1*, 2ng *cc2d2a* and 2ng *p53* MO leads to a synergistic increase in the frequency of each abnormal phenotype (**B**, red bars, n=53). hpf, hours post fertilisation; MO, morpholino oligonucleotide; WT, wild type.

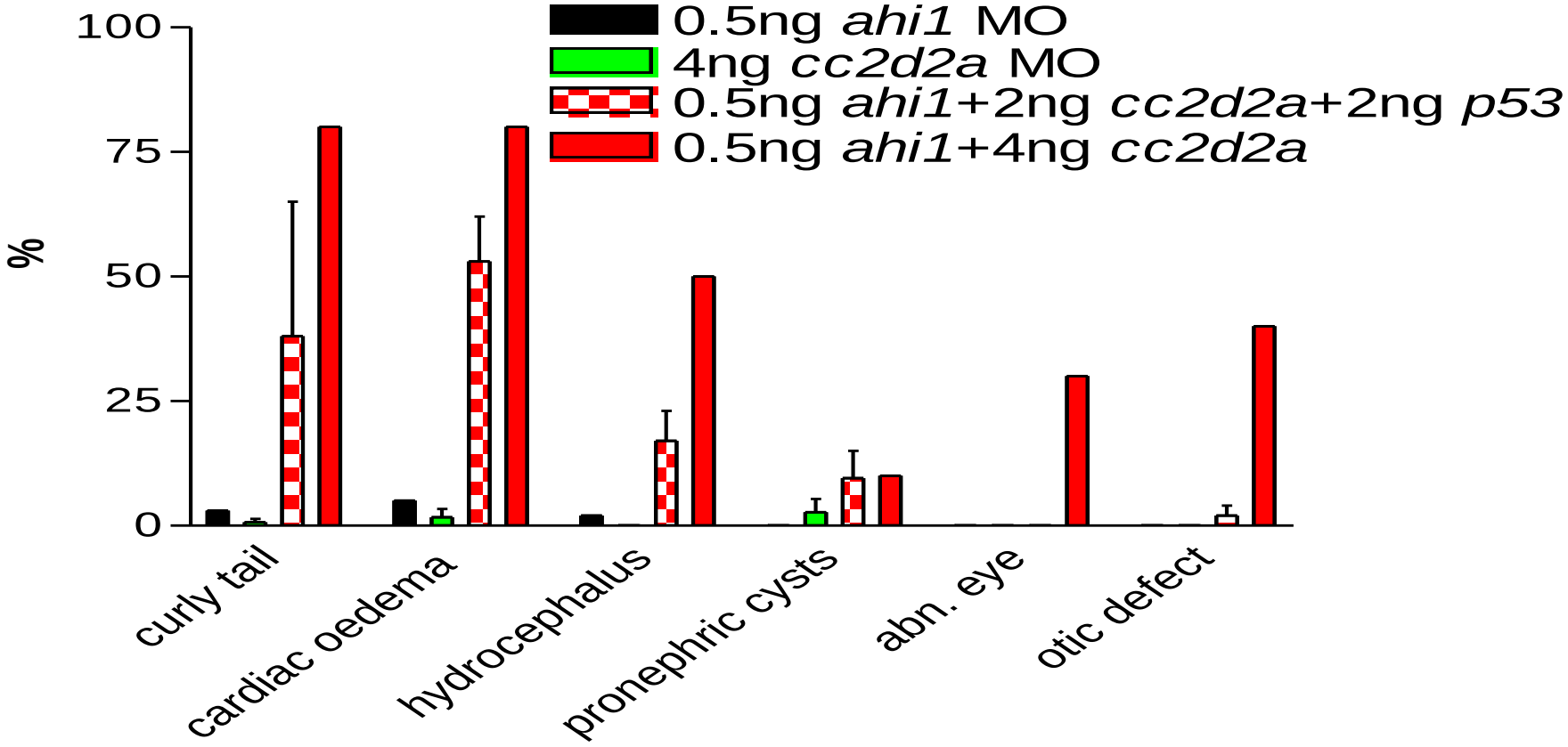

Figure 5.12 Effect of gene dosage on the frequency of abnormal phenotypes following combined *ahi1* and *cc2d2a* MO knockdown in wild type zebrafish embryos

Low dose (0.5ng) *ahi1* MO alone (black bars, n=58) and 4ng *cc2d2a* MO alone (green bars, n=96) induce a low frequency (≤5%) of abnormal phenotypes. Combination of 0.5ng *ahi1*, with a lower dose (2ng) *cc2d2a* and 2ng *p53* MO leads to a synergistic increase in the frequency of abnormal phenotypes (red checked bars, n=53). Combination injection with an additional 2ng *cc2d2a* MO and without *p53* MO further increases the frequency of aberrant phenotypes (red bars, n=10). MO, morpholino oligonucleotide.

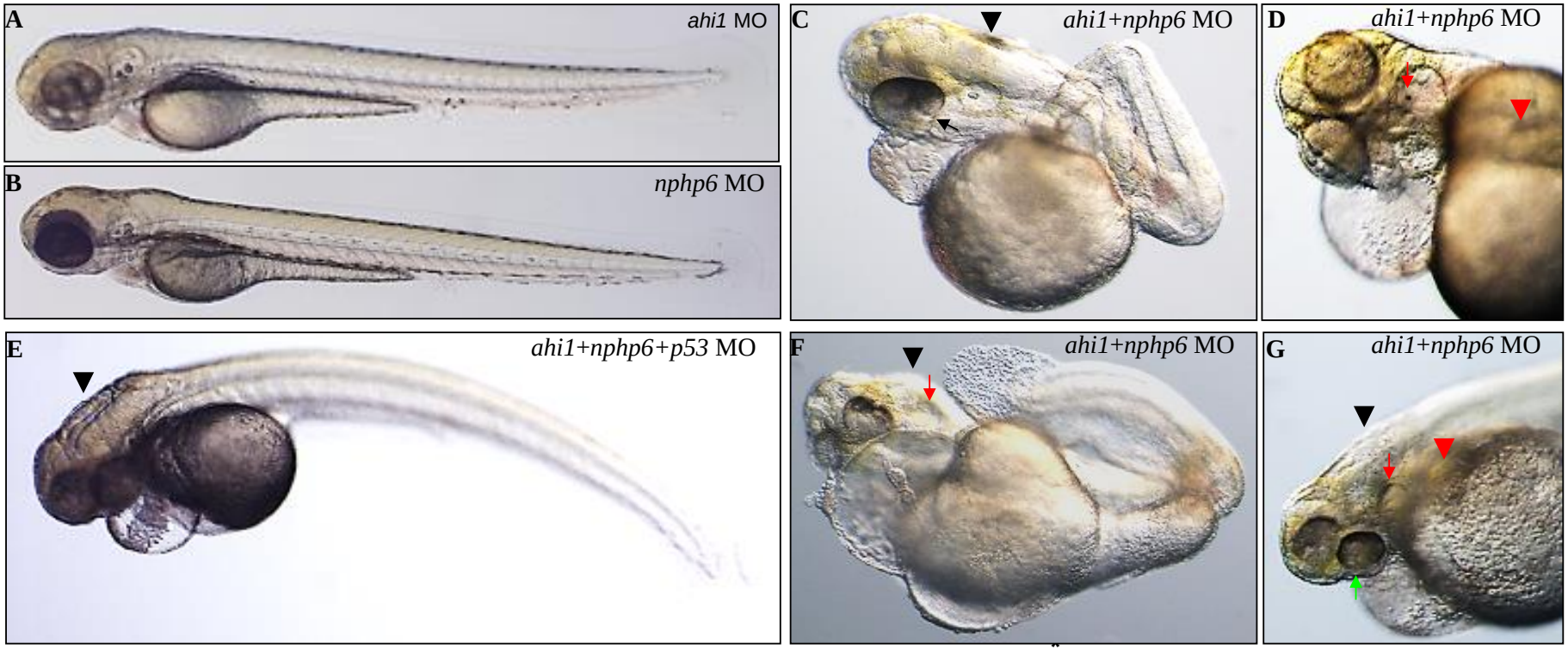

Figure 5.13 Phenotypes following combination of low dose *ahi1* and *nphp6* MO knockdown in zebrafish embryos
Lateral views of zebrafish embryos at 72 hours post fertilisation. Golden zebrafish embryos injected with a low dose of *ahi1* MO (0.5ng, **A**) and *nphp6* MO (2ng, **B**) alone were phenotypically normal. Golden zebrafish embryos co-injected with low dose *ahi1* and *nphp6* MOs (**C**, **D**, **F**, **G**) develop abnormal phenotypes, which persist when also co-injected with *p53* MO (to exclude off-target effects, **E**). The range of abnormal phenotypes seen following co-injection of *ahi1* and *nphp6* MOs includes: hydrocephalus (black arrowhead **C**, **E**, **F**, **G**); curved body axis (**C**, **E**, **F**); cardiac oedema (**C**-**G**); pronephric cysts (red arrowhead **D**, **G**); coloboma (black arrow **C**); unilateral microphthalmia (green arrow **G**); empty otic vesicle (red arrow **F**, **G**) and single otolith (red arrow **D**). MO, morpholino oligonucleotide.

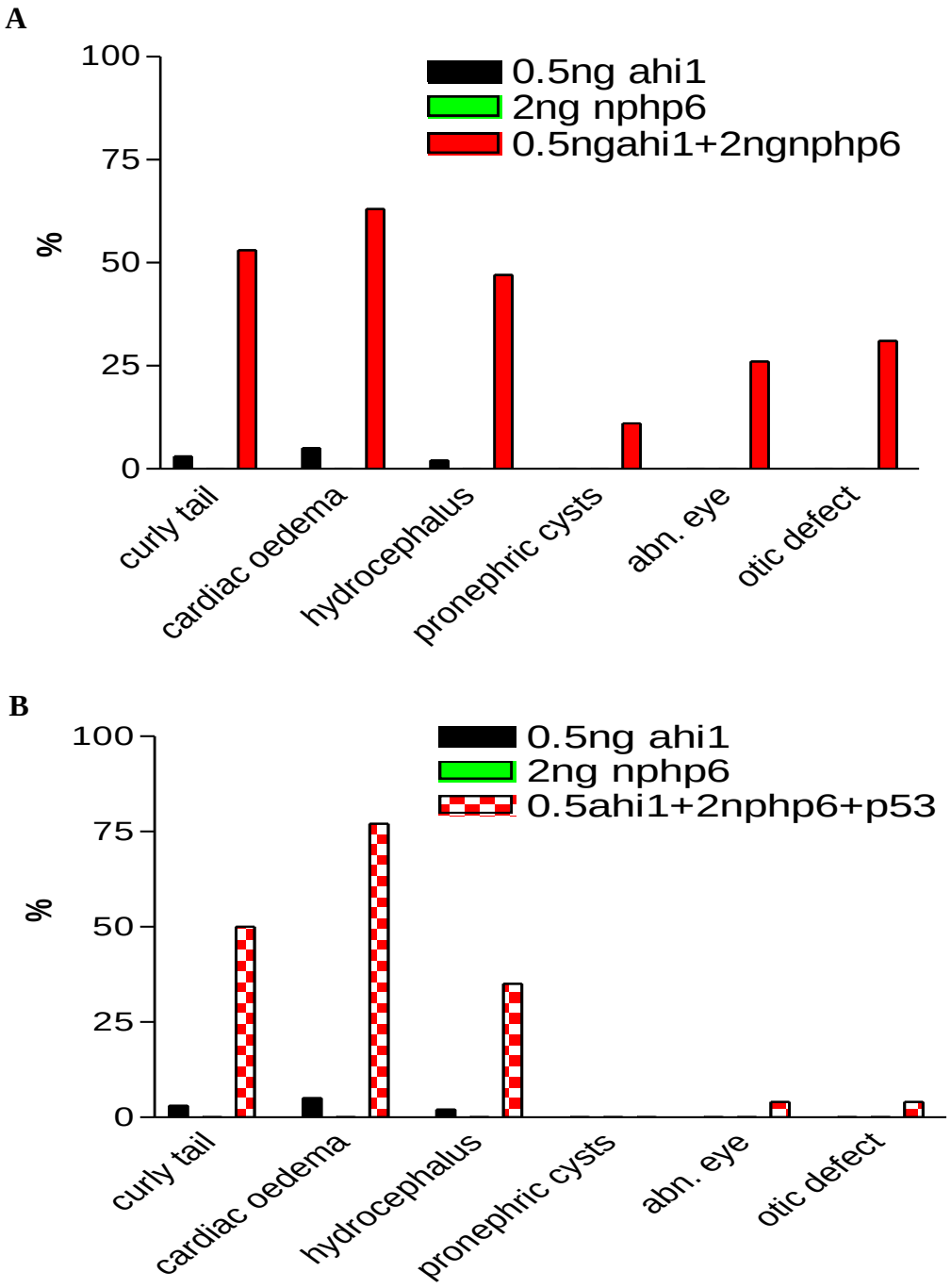

Figure 5.14 Percentage frequency of abnormal phenotypes following individual and combined *ahi1* and *nphp6* (±*p53*) MO knockdown in zebrafish embryos

0.5ng *ahi1* MO alone induces a low frequency of abnormal phenotypes and no pronephric cysts, developmental eye or ear abnormalties (black bars, **A-B**, n=58). 2ng of *nphp6* MO alone does not induce any developmental anomalies (green bars, **A-B**, n=64). Combined MO knockdown using 0.5ng *ahi1* and 2ng *nphp6* leads to a synergistic increase in the frequency of each abnormal phenotype (red bars, **A**, n=19). **B** shows the synergistic increase in the frequency of abnormal phenotypes when 2ng *p53* MO is combined with 0.5ng *ahi1* and 2ng *nphp6* MOs (red/white checked bars, n=26). MO, morpholino oligonucleotide.

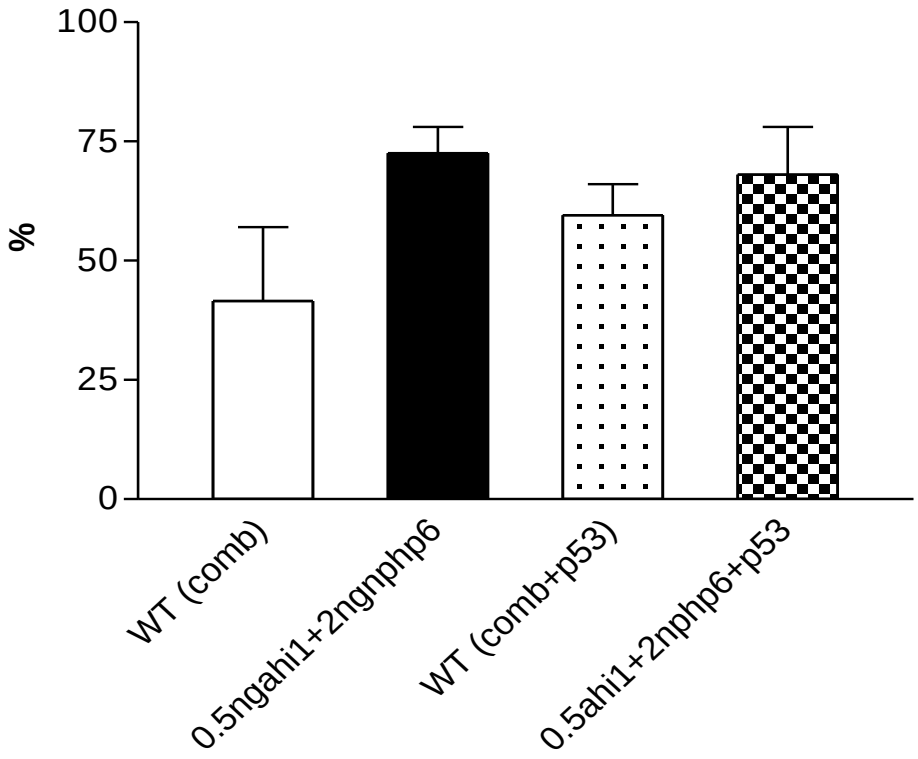

Figure 5.15 Mortality rates at 24hpf following combined *ahi1* and *nphp6* ± *p53* MO knockdown compared to matched uninjected zebrafish embryos
Data are shown as mean percentage (%) and standard error of the mean. Mortality rates are increased following combined MO injections. Mortality at 24hpf following injection of 0.5ng *ahi1* and 2ng *nphp6* MO (black bar) is 72.5% (1.7 times) compared to 41.5% in matched uninjected WT embryos (white bar). Mortality at 24hpf following injection of 2ng *p53* MO in combination with 0.5ng *ahi1* and 2ng *nphp6* MO (black/white checked bar) is 68% (1.1 times) compared to 59.5% in matched uninjected WT embryos (white spotted bar). comb, 0.5ng *ahi1*+2ng *nphp6*; MO, morpholino oligonucleotide; WT, wild type.

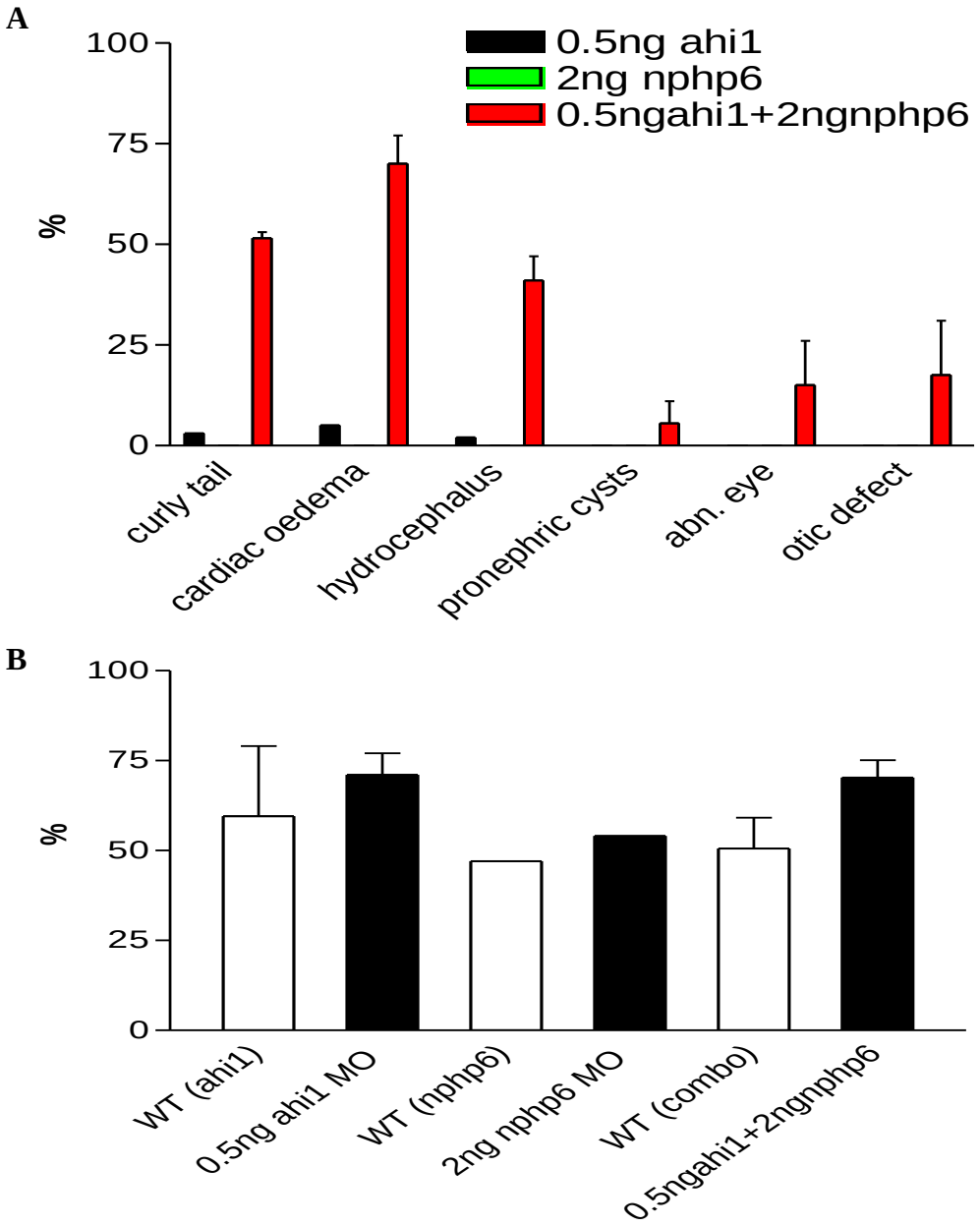

Figure 5.16 Percentage frequency of abnormal phenotypes and mortality at 24hpf following combined *ahi1* and *nphp6* MO knockdown in zebrafish embryos

Injection of 0.5ng *ahi1* MO alone induces a low frequency of abnormal phenotypes and no pronephric cysts, developmental eye or ear abnormalties (black bars, **A**, n=58). 2ng of *nphp6* MO alone does not induce any developmental anomalies (green bars, **A**, n=64). Combined MO knockdown using 0.5ng *ahi1* and 2ng *nphp6* ±2ng *p53* MO (red bars, **A**, n=45) leads to a synergistic increase in the frequency of each abnormal phenotype. Mortality at 24hpf is shown (**B**) as mean percentage (%) and standard error of the mean in zebrafish embryos following: 0.5ng of *ahi1* MO alone, 2ng *nphp6* MO alone and co-injection of 0.5ng *ahi1* MO + 2ng *nphp6* MO ± 2ng *p53* MO (**B**). Mortality rates in uninjected WT embryos matched for each group (white bars). MO injections are associated with a relative increase in 24hpf mortality rates. hpf, hours post fertilisation; MO, morpholino oligonucleotide; WT, wild type.